2010

Influence of retinal states on the development and maintenance of retinofugal projections

Duncan Morhardt
Virginia Commonwealth University

INFLUENCE OF RETINAL STATES ON THE DEVELOPMENT AND MAINTENANCE OF RETINOFUGAL PROJECTIONS

A dissertation in partial fulfillment of the requirements for the degree of Doctor of Philosophy in Biochemistry and Molecular and Cell Biology at Virginia Commonwealth University

By

Duncan R. Morhardt
B.A. University of California, Berkeley, 2001

Advisor: Ching-Kang Jason Chen, Ph.D.
Associate Professor
Department of Biochemistry and Molecular and Cell Biology

Co-advisor: William Guido, Ph.D.
Professor
Department of Anatomy and Neurobiology

Virginia Commonwealth University
Richmond, Virginia
June 21, 2010

ACKNOWLEDGEMENTS

I first met Ching-Kang Jason Chen for a lab in the summer of 2004. I was interested in vision science and thought that I could find a home in the biochemistry department studying photoreceptor biology. My first encounter with Dr. Chen was frightening: an ensemble of rigor and skepticism that stirred my thoughts about science. At the same time, William Guido arrived at VCU to restart his lab after the unprecedented damage of Hurricane Katrina. John Bigbee said that I would benefit from any interactions with Dr. Guido, a well-established neuroscientist in vision, and would further benefit from a PhD under his tutelage.

In a Frostian dilemma, I debated the strengths of each lab and advisor until I reached indecision. Resolving this, both Dr. Chen and Dr. Guido agreed to take me into their labs as a more-or-less shared student. For this, I am very grateful. It gave me the opportunity to personally explore several aspects of vision science while at the same time affording me the protected environment of my advisors expertise. Though much of my work was a combination of efforts between these labs, ultimately my primary work was in the Chen Lab. In this area, Jason provided me with ample opportunities to investigate different question in the retina, particularly those that required more advanced calculation and were, at the time, beyond the scope of his expertise. This "loosening of the reigns" made for harrowing and rewarding learning experience for which I am eternally grateful. By allowing me to work rather independently of the lab, he sacrificed working hands for my intellectual satisfaction. I can only hope he enjoyed this even half as much as I did. When things became swampy and difficult, I would look for a guideline. Balancing the openness of Jason's style was the structure of Bill's style. I need to be grounded occasionally and Bill was more than happy to spend hours upon hours going over data or outlining the directions that may prove fruitful. And when the time came to "reign me in," both Bill and Jason did their parts to ensure I was not lost forever. Without their help, I would have been able to find my way through this body of work and generate this product of which I am extremely proud. Thank you Jason. Thank you Bill.

Indeed the other members of the Chen-Guido collaborations have changed over the years. I hope their contributions to my experience as positive and uplifting. In particular, Yen-Ling Chen, Kevin Fu, and Tania Seabrook were instrumental in executing some of the experiments contained within.

I am grateful, specifically, to Dr. Thomas Krahe who was a steadfast collaborator and friend throughout this process, even before I met Bill and Jason.

I would like to thank the other members of my graduate committee, Babette Fuss, Scott Henderson, and Carmen Sato-Bigbee, for their participation in my education. Together, they kept me on my toes throughout this process.

I would like to thank the support of my family: My parents, Jeffrey and Francia, my brother Connor, his wife Liz, and their son Connor; Mary Greene and Albert Hazen Smith; and my Aunt Kate.

I would like to thank the MD/PhD program Director, Gordon Archer, for initiating this process by allowing me to attend medical school. Furthermore, the MD/PhD students and other PhD students were a great source of support throughout.

Lastly, I would like to thank Tina Lung. She stuck it out with me for the last two, and difficult, years as I struggled through my graduate work. She has been the beacon for much of this journey.

TABLE OF CONTENTS

List of Tables……..vi

List of Figures……vii

List of Abbreviations……...x

Abstract…….……xiv

Chapter 1: Introduction……1

Retina and Gβ5……1
Photoreceptors, G-protein signaling and phototransduction……....1
Gβ5 and the R7RGS family……8

Spontaneous retinal activity……...22
Development of the eye……27
Developmental spontaneous retinal activity……..28

Activity in visual development and retinogeniculate synapse……...39
Forming connections in the visual system…….……39
Retinal activity and the retinogeniculate development……..42
Reinforcing synapses with activity: The Hebbian hypothesis……...49

Abstract for Chapters 2 and 3: Abnormal retinal activity in Gβ5-/- mice correlates with disruptions in eye-specific segregation in the dorsal lateral geniculate nucleus …….……..…….55

Chapter 2: Gβ5 is required for normal spontaneous retinal activity……..57

Introduction ……...57

Methods……..62
Animals and genotyping……62
Immunohistochemistry……..…66
Western blot analysis……66
Multielectrode array recordings……67
Spike sorting and analysis…….....68
Statistics……70

Results……70

Conclusions……..113
Gβ5 is required for normal stage II retinal activity……113

Role of Gβ5 in glutamatergic waves……...119
Gβ5 is required for normal RGC firing, but not for rhythmic *nob* firing……123

Chapter 3: Gβ5 is required for normal retinogeniculate development ……...127

Introduction…….....127
Methods……132
Animals and genotyping……..132
Anatomical tracing……...132
Imaging and analysis……133
Statistics……...134
Results……..134

Conclusions……..146
Gβ5-/- has both induction and maintenance phenotypes in the dLGN…147
Source of LGN phenotype in Gβ5-/- mice……..148
Comparison of *nob* and Gβ5-/- phenotypes in maintenance……...150
Maintenance program does not require a normal eye-specific segregation program……150

Discussion- Activity and retinogeniculate development ……152
Retinal activity and retinogeniculate refinement……152
No b-wave phenotype correlates with maintenance failure…….154
Abnormal-normal-abnormal retinal activity correlates with eye-specific segregation in dLGN……157

Chapter 4: State of retinofugal projections in mice with retinal remodeling after photoreceptor degeneration……..……159

Abstract……159

Introduction……..160
Animal models of retinal degeneration and mechanisms of photoreceptor death...……..160
Photoreceptor loss is a model of deafferentation……163
Central retinal projections have not been compared in mice with differing degrees of retinal remodeling……...167

Methods……170
Animals and Genotyping……170
Immunohistochemistry..……..……171
Anterograde tracing……172
Quantification of retinogeniculate projections……173
Consensual pupillary light responses...……...174
Electrophysiology…...……175

Statistics……...……175

Results……..177

Conclusions……..196
Retinal remodeling does not grossly affect retinofugal projections……196
Alterations in ΔCT and TG9N mice are restricted to the retina……..202
Retinal remodeling in retina based therapies……...204

Chapter 5: Discussion ……205
Eye-specific maintenance of projections may have a critical period…..…….205
The ceiling of maintenance and preserved projections in degenerated animals underscore the stability of established retinofugal circuits……..211

List of References……214

Appendices……...……227

Vita……...……398

LIST OF TABLES

Table 1.1 - Locations of Gβ5 and R7RGS proteins in the visual system……16

Table 2.1 - Numerical burst parameters of RGCs…….……..85

LIST OF FIGURES

Figure 1.1- G-protein signaling and Gβ5…….3

Figure 1.2- Phototransduction, and R7RGS function in photoreceptor and ON bipolar cells.…….6

Figure 1.3- R7RGS/Gβ5 expression in retina……11

Figure 1.4-The murine visual system ……14

Figure 1.5- Gβ5 increases over development from P0 – P14 in retina. ……21

Figure 1.6-Spontaneous retinal activity during development .....…..……..24

Figure 1.7-Spontnaoues retinal wave stages and mechanisms…....…….26

Figure 1.8- Normal retinogeniculate development ……...38

Figure 1.9- β2-/- and *nob* retinal activity and LGN phenotypes……47

Figure 2.1- Genotyping methods ……..64

Figure 2.2- Retinal activity is decreased in Gβ5-/- mice at P7. ……72

Figure 2.3- Gβ5 +/- retinas have reduced Gβ5 and lower overall retinal activity at P7…77

Figure 2.4- Gβ5 -/- and Gβ5 +/- retinas have an increased interwave interval.……79

Figure 2.5- Gβ5 -/- and +/- RGCs bursts have altered firing parameters at P7…….81

Figure 2.6- RGS11 -/-, SG7 mutant, and RGS6 -/- retinas have normal IWI and wave duration.…….…83

Figure 2.7- Normal pharmacological sensitivity in Gβ5 -/- retinas……...…87

Figure 2.8- Global retinal activity in Gβ5-/- and +/- is less correlated at near neighbor distances at P12.…….90

Figure 2.9- Coherence analysis approximations of IWI. ……..92

Figure 2.10- Gβ5 -/- and +/- RGCs bursts have altered firing parameters at P12...…..…94

Figure 2.11- Gβ5-/- retinas have persistent wave activity at p14 reminiscent of *nob* mice……..……..99

Figure 2.12- P14 coherence spectra illustrate periodic firing of Gβ5 -/-, *nob*xGβ5 -/- and *nob* retinas but underlying *nob*-like rhythmicity does not require Gβ5. …….101

Figure 2.13- In animals without Gβ5, P14 RGCs exhibit more bursting than Gβ5 +/+ and Gβ5+/-, but less than *nob*xGβ5 +/+……103

Figure 2.14- Wave-like activity persists in Gβ5-/-, *nob*xGβ5 +/+, and *nobxGb5* -/- retinas..…….……106

Figure 2.15- Underlying rhythmic activity emerges in Gβ5-/- retinas at P28 yet diminishes in *nobx*Gβ5+/+ and *nobx*Gβ5-/- retinas. ……...…108

Figure 2.16- Normalized RGC burst firing parameters in Gβ5-/-, Gβ5+/-, *nob, and nob*xGβ5-/- retinas……...110

Figure 2.17- Summary of spontaneous activity in Gβ5-/- and Gβ5+/- is shown……115

Figure 2.18- Rhythmicity at P14 is exclusive of rhythmicity at P28……...…123

Figure 3.1- Gβ5-/- retinogeniculate projections have limited refinement and an impaired maintenance phase.……..……134

Figure 3.2- Gβ5 and RGS7 are reduced in Gβ5+/- dLGNs at P7……137

Figure 3.3- Retinogeniculate refinement in Gβ5+/- mice is similar to Gβ5+/+……..140

Figure 3.4- Assessment of retinal projections at extreme ages in Gβ5-/- and early eye-specific segregation in SG7 and *nobx*Gβ5-/- mice…….....143

Figure 3.5- Gβ5-/- mice have an abnormal-normal-abnormal activity-segregation profile……...154

Figure 4.1- Retinal degeneration leads to retinal remodeling……..164

Figure 4.2- ΔCT and TG9N retinas remodel to a different degree after photoreceptor death. ……...……177

Figure 4.3- Gross morphology of retinofugal projections is intact in ΔCT and TG9N mice.……179

Figure 4.4- Fine retinogeniculate terminal patterning is intact in ΔCT and TG9N mice……..185

Figure 4.5-Whole-cell Current clamp intracellular recordings identify physiologically intact retinogeniculate synapses in TG9N dLGNs. ……188

Figure 4.6-Cell-attached and Field Potential Extracellular Recordings survey Excitatory Postsynaptic Activity in ΔCT and TG9N LGNs…….191

Figure 4.7-ΔCT and TG9N mice exhibit pupillary light responses……196

LIST OF ABBREVIATIONS

18-GA	18 alpha-glycyrrhetinic acid
2-APB	R-2-amino5-phosphopentanoate
A2A, A2	A2 subtype Adenosine receptor
ABCA	ABC transporter
AC	Adenlyate cyclase
ACh	Acetylcholine
ACSF	Artificial cerebrospinal fluid
AIPL	Aryl hydrocarbon interacting-like
AMPA	Alpha-amino-3-hydroxyl-5methyl-4isoxazole-propionate
AP-1	Activator protein
APB	2-amino-4 phosphobutyrate
ATP	Adenosine triphosphate
β2	Cholinergic Receptor subunit beta 2
BDNF	Brain derived neurotrophic factor
BP	Binding protein
C	Correlation
C-	Carboxy terminus
C1q	Complement protein 1q
C3	Complement protein 3
Ca^{2+}	Calcium
CaCl2	Calcium chloride
cAMP	cyclic adenosine monophosphate
CCW	Counter clockwise
ChAT	Choline acetyl transferase
ChOP	Channel opsin
Chx10	Homeobox transcription factor Chromosome 10
CI	Correlation index
CMP	Computerized morphological phenotyping
CMV	Cytomegalovirus
CNG	Cyclic nucleotide gated
CNQX	6-cyano-7nitroquinoxaline-2,3-dinone
CO2	Carbon dioxide
CSNB	Congenital Stationary Night Blindness
CTB	Cholera toxin B
CX36	Connexin 36
D1	Dopamine receptor subtype 1
D2R, D2	Dopamine receptor subtype 2
DAG	Diacylglycerol
DAPI	Diaminino phenylindole

ΔCT	C-terminal deleted Rhodospin
DEP	Desheveled, Egl-10, Pleckstrin homology
DHβE	Dihydro-beta-erythroidine
dLGN	dorsal lateral geniculate nucleus
DNA	Deoxyribonucleic acid
DNQX	6,7-Dinitroquinoxaline-2,3-dione
DOPA	Dihydroxyphenylalanine
Dp	Distribution of probability
DSCAM	Down syndrome associated cell adhesion molecule
E	Glutamate
EYFP	Enhanced yellow fluorescent protein
EphA	Ephrin A receptor
EPSP	Excitatory postsynaptic potential
ERG	Electroretinogram
EWN	Edinger-Wesphal nucleus
Gα	G-protein alpha (beta, gamma) subunit
GABA	Gamma amino butyric acid
$GABA_A$	GABA receptor subtype a
GABAcρ	GABA c-type rho subunit
Gαi/o	G protein alpha inhibitory type
GAP	GTPase accelerating protein
GAP-43	Growth associated protein 43
GAPDH	Gluteraldehyde 3-phosphate dehydrogenase
Gαq	G protein alpha q
GαT	Tranducin
Gβ1	G-protein beta 1
Gβ5	G-protein beta 5 (short form implied)
Gβ5L	Long form of G-protein beta 5
Gβγ	G-protein beta gamma heterodimer
GC	Guanylate cyclase
GCAP	Guanylate cyclase activating protein
GCL	Ganglion cell layer
GDP	Guanosine diphosphate
GGL	G-protein Gamma-like
Gi/o	G protein inhibitory type
GIRK	G-protein coupled inward rectifying potassium channel
GLM	Generalized linear model
GMP	Guanosine monophosphate
GPCR	G-protein coupled receptor
GTP	Guanosine triphosphate
HSD	Honest significant difference
Hz	Hertz

IBI	Interburst interval
IGL	Intergeniculate leaflet
IP3	Inositol Tris-phosphate
IPL	Inner plexiform layer
ipRGC	intrinsically photosensitive retinal ganlion cells
IS	Inner segment
IWI	Interwave interval
K1/2	half-maximal activation concentration
KCC2	Potassium Chloride exchanger 2
KCl	Potassium Chloride
L296	Lysine 296
LCA	Leber congenital amaurosis
LGN	Lateral genicualate nucleus
MAPK	Mitogen-activated protein kinase
MEA	Multi-electrode array
MEF2D	Myocyte specific enhancer factor 2D
MgCl	Magnesium chloride
mGluR6	metabotropic glutamate receptor type 6
MHC	Major histocompatility complex
N	Number
N-	amino terminus
NaCl	Sodium Chloride
NMDA	N-methyl aspartic acid
*nob_*	No b wave (animal number)
NT	Neurotropin
Nyx	Nycaloptin gene
O2	Oxygen
ONL	Outer nuclear layer
OPL	Outer plexiform layer
OPN	Olivary pretectal nucleus
OPN4	Opsin 4 Melanopsin
OS	Outer segment
OT	Optic tract
PBS	Phosphate buffered saline
PCR	Polymerase chain reaction
PD	Photoreceptor degeneration
PDE6αβ	Phosphodiesterase alpha beta heterodimer
PDE6β	Phosphodiesterase beta subunit
PDE6γ	Phosphodiesterase gamma subunit
PFA	Paraformaldehyde
PFH	Population firing histogram
Pi	Inorganic Phosphate
PKA	Protein kinase A

PLC	Phospholipase C
PLR	Pupillary light response
R*	Metarhodopsin II
R7BP	RGS7 binding protein
R7RGS	R7 family of regulators of G-protein signaling
R9AP	RGS9 anchor protein
Rd	"rodless"
RdCVF	Rod-derived cone viability factor
RF	Receptive field
RGC	Retinal ganglion cell
RGS	Regulator of G-protein signaling
R	Rhodopsin
RNA	Ribonucleic acid
ROI	Region of interest
RP	Retinitis Pigmentosa
RPC	Retinal precursor cell
RPE	Retinal pigment epithelium
Rvar	R variance
S	Spectra
S.E.M.	Standard error of the means
S1-S5	Substrata of inner plexiform layer
SAC	Starburst amacrine cell
SC	Superior colliculus
SCN	Suprachiasmatic nucleus
SG7	Steve Gold RGS7 mutant
SMI-32	Heavy Neurofilament antibody
ST	Spatial-temporal
T	Time bin
TBS	Tris buffered saline
TG9N	N-terminal RGS9
TTX	Tetrodotoxin
VEP	Visual evoked potential
vLGN	ventral lateral geniculate nucleus
WT	Wild type
XIAP	X-linked inhibitor of apoptosis protein
YFP	Yellow fluorescent protein

ABSTRACT
INFLUENCE OF RETINAL STATES ON THE DEVELOPMENT AND MAINTENANCE OF RETINOFUGAL PROJECTIONS

By Duncan R. Morhardt

A dissertation in partial fulfillment of the requirements for the degree of Doctor of Philosophy in Biochemistry and Molecular and Cell Biology at Virginia Commonwealth University

Advisor: Ching-Kang Jason Chen, Ph.D., Associate Professor, Department of Biochemistry and Molecular and Cell Biology

Co-advisor: William Guido, Ph.D., Professor, Department of Anatomy and Neurobiology

Vision provides a critical interface with the physical world. This work examines visual development and vision loss in mice to glean the influence of the retinal state on visual connections. I first assessed the impact of retinal activity on the eye-specific segregation of retinal afferents in the lateral geniculate nucleus (LGN) of young Gβ5 -/- mice. Gβ5 is the fifth member of the β subfamily of heterotrimeric G proteins. Gβ5 binds and stabilizes the R7 family of regulators of G-protein signaling (RGS), which accelerate Gi/o GTP hydrolysis. Gβ5 -/- mice, which lack R7RGS activity, have malformed synapses in the outer plexiform layer (OPL) and impaired OPL transmission. Altered spontaneous retinal activity in Gβ5-/- mice at P7, P12, P14, and P28 correlates with impaired eye-specific segregation of retinal afferents in the LGN at corresponding timepoints. However, Gβ5-/- mice exhibit a normal transition from cholinergic to glutamatergic drive that corresponds with a temporary recovery of refinement at P10. Thus the abnormal-normal-abnormal pattern of activity in the retina is coupled with

abnormal-normal-abnormal segregation. This activity-segregation profile suggests activity may instruct early retinogeniculate development. *nob* mice, which also exhibit impaired OPL transmission, have aberrant retinal waves that align with loss of segregation. *nob*xGβ5-/- mice have similar levels of segregation as Gβ5-/- at P21, but activity only similar P14 *nob*xGβ5-/- and Gβ5-/- RGCs. This suggests that the critical period of eye-specific segregation closes shortly after P14 and that R7RGS activity is critically important to postnatal RGCs. Next, I investigated the aged visual system via the retinofugal projections of mice with retinal remodeling after photoreceptor degeneration (PD). ΔCT mice, with mild remodeling, and TG9N mice, with aggressive remodeling, retain gross anatomical and physiological connectivity in the presence of attenuated visual activity compounded by organic remodeling. However, the magnitude of pupillary light responses in PD mice was diminished. Reduced melanopsin signal in the retina, not downstream anomalies, explains this functional deficiency. These observations suggest that changes to eye-specific segregation are limited once projections are established, regardless of retinal activity or remodeling. These observations bode well for future retina-based treatments of vision loss.

CHAPTER 1

Introduction

Our visual system provides a critical, tangible means of interacting with our environment. When we do not see properly, we miss essential information in our surroundings that is important for survival, whether prey, predator, cliff or car, and suffer the evolutionary consequences. Vision is a cherished sense to all humans and science has made great efforts to understand its development, normal function, and diseased states.

The Retina and Gβ5

Photoreceptors, G-protein signaling and photoreception

Light is electromagnetic radiation of varying energy, designated by wavelength, and carried by photons. Human photoreceptors can detect a narrow (400 nanometer wavelength (nm) – 700nm) yet useful range of the light spectrum. Light travels first through the cornea and strikes the retina after being focused by the curvature of the lens. Light then passes through all the layers of the retina until it finally reaches photosensitive pigment. Photoreceptors are neurons with a large specialized dendrite filled with this pigment. There are three classes of photoreceptive cells, each with a particular class of photo-pigment apoproteins sensitive to various ranges of light, which serve different roles in vision. Rods contain rhodopsin, cones contain a variety of opsins (Yau and Hardie, 2009), and photosenstive ganglion cells, which are not classical photoreceptors, contain melanopsin (Hankins et al., 2008; Lucas et al., 2001).

Figure 1.1-G-protein signaling and Gβ5- Activated seven transmembrane receptor catalyses GDP→GTP exchange followed by dissociation of Gα and Gβγ. Gα and Gβγ perform respective secondary signaling actions depending on subtype (Gα) or subtype combination (Gβγ). Duration of Gα signaling can be regulated by speeding up hydrolysis of GTP, rendering Gα inactive. Hydrolysis of GTP (releasing inorganic Phosphate, Pi) by Gαi/o can be accelerated in vivo by R7RGS proteins that couple to Gβ5, shortening the period of the G-protein cycle. The R7RGS complex consists of one R7RGS (RGS6, 7,9,11), either Gβ5L or the short isoform, and may also include a binding protein (BP, R7BP or R9AP).

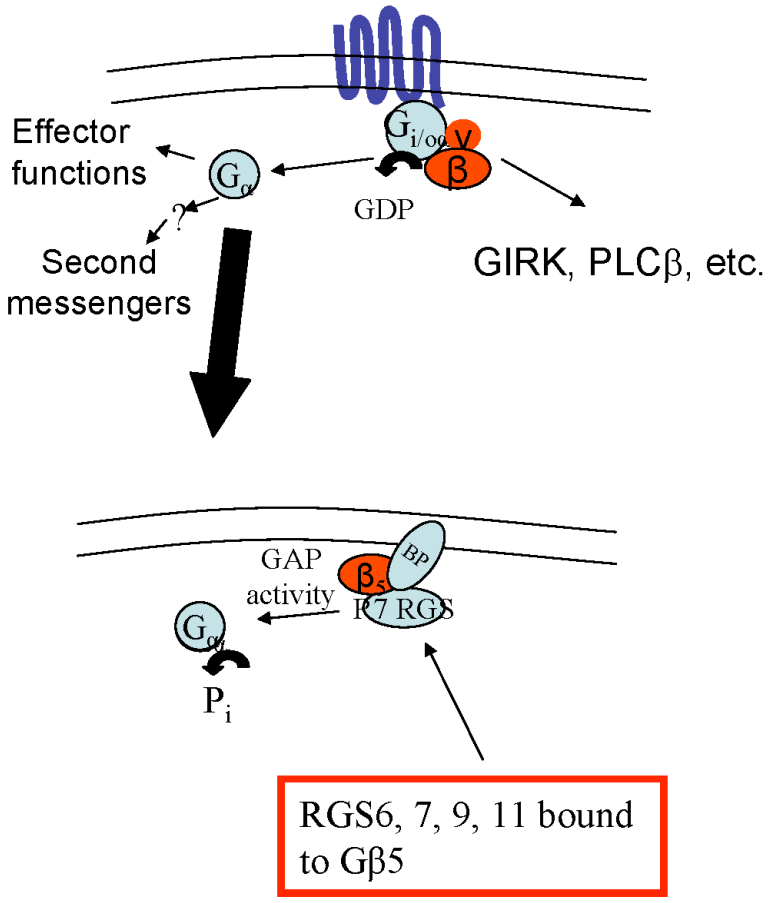
Effector
functions
G_α
?
Second
messengers
$G_{i/o\alpha}$
γ
β
GDP
GIRK, PLCβ, etc.
GAP
activity
β_5
Bp
R7 RGS
G_α
P_i
RGS6, 7, 9, 11 bound
to Gβ5

Figure 1.1

Photopigments are receptors in the traditional sense: bound ligand changes conformation of the receptor and initiates the internal transduction of an external signal. Photopigments, however, do not themselves interact with the incident photons from the outside world. Instead, photopigments bind a light sensitive derivative of vitamin A, the chromophore 11-*cis* retinal. 11-cis-retinal binds rhodopsin at a lysine 296 residue via a Schiff base linkage. The supporting retinal pigment epithelium maintains a supply of this chromophore through the visual cycle (Young and Bok 1969; Bok 1993). Before the energy from photons straightens this crooked molecule, 11-*cis* retinal acts as an inverse agonist for rhodopsin in rods, locking rhodopsin in a stable inactive state. Upon light exposure, the 11-*cis* double bond isomerizes to 11-*trans*. All-t*rans* retinal acts is a strong agonist to activate rhodopsin (Burns and Baylor, 2001). Activated rhodopsin, in the form of Metarhodopsin II (R*), is now capable of phototransduction and initiates a heterotrimeric G-protein pathway (Chen, 2005).

Heterotrimeric G-protein signaling conventionally starts from a deactivated state where a G-protein coupled receptor, an integral protein with seven transmembrane domains, is bound to a heterotrimer (Figure 1.1). This heterotrimer consists of a Gα, bound to the nucleotide Guanosine Diphosphate (GDP), and a Gβγ dimer. The GPCR is activated by ligand-induced conformational change and then catalyzes Gα's exchange of GDP for Guanosine Triphosphate (GTP). Gα, now GTP bound and activated, dissociates from Gβγ and interacts with downstream effectors. Such effectors amplify the initial signal by altering the concentration of second messengers, like cyclic adenosine monophosphate or calcium. Gβγ can also interact with effectors. For example, Gβγ

Figure 1.2-Phototransduction, and R7RGS function in Photoreceptor and ON Bipolar Cells - Activation: In rod photoreceptors, G-protein activation occurs in the light when a photon isomerizes 11-*cis* retinal to all-*trans* retinal thereby converting Rhodopsin GPCR, to Meta-Rhodopsin II (R*, purple, step 1). By interacting with R*, transducin (GαT) exchanges GDP for GTP and dissociates from the Gβγ dimer (step 2). GαT then binds phosphodiesterase 6 γ (PDE6γ, step 3) and permits PDE6αβ to hydrolyze cGMP to GMP (step 4). The subsequent drop in cGMP concentration (step 5) closes the cyclic nucleotide gated (CNG) channel (step 6), hyperpolarizes the rod photoreceptor, and stops glutamate release onto bipolar cells. At the tips of ON-bipolar cells (Chang et al.), the resident G-protein pathway, mGluR6, is active in the dark when glutamate (E) is abundant (step 1). Glutamate-bound mGluR6 catalyzes the exchange of GTP for GDP on Gαo1 (step 2). Gαo1 then dissociates from Gβγ (step 3). In the mGluR6 pathway, neither the downstream targets for Gαo1 or Gβγ nor the subsequent effectors have been confirmed. Ultimately, these events trigger the closure of a non-selective cation channel (step 4). Deactivation (Bottom): In rods (left), phosphorylation and arrestin binding quickly render R* deactivated. The hydrolysis of GTP to GDP deactivates GαT. This is a slower step and therefore rate-limits the deactivation of phototransduction. The GTPase accelerating protein (GAP) complex consists of regulator of protein signaling 9 (RGS9), a Gβ homologue Gβ5L, and RGS9 anchor protein (R9AP). The GAP complex catalyzes faster GTP hydrolysis. When bound to PDE6γ, GαT temporarily associates with the GAP complex, hydrolyzes GTP, and dissociates from PDE6γ. PDE6γ bind and inhibits PDE6αβ thereby preventing further hydrolysis of cGMP. Now unopposed guanlyate cyclase (GC) activity increases the cGMP concentration, the CNG channel opens, and the rod resumes a slightly depolarized "dark current". In bipolar cells (Chang et al.), mGluR6 can deactivate when extracellular glutamate concentration drops. Gαo1 hydrolyzes GTP to GDP and re-associates with Gβγ. Unknown downstream events follow, open a non-selective cation channel that depolarizes the cell, and generate the positive deflection ("b-wave") shown on the representative electroretinogram (ERG). RGS11 and RGS7, in complex with Gβ5 and other proteins, provide redundant GAP activity for Gαo1.

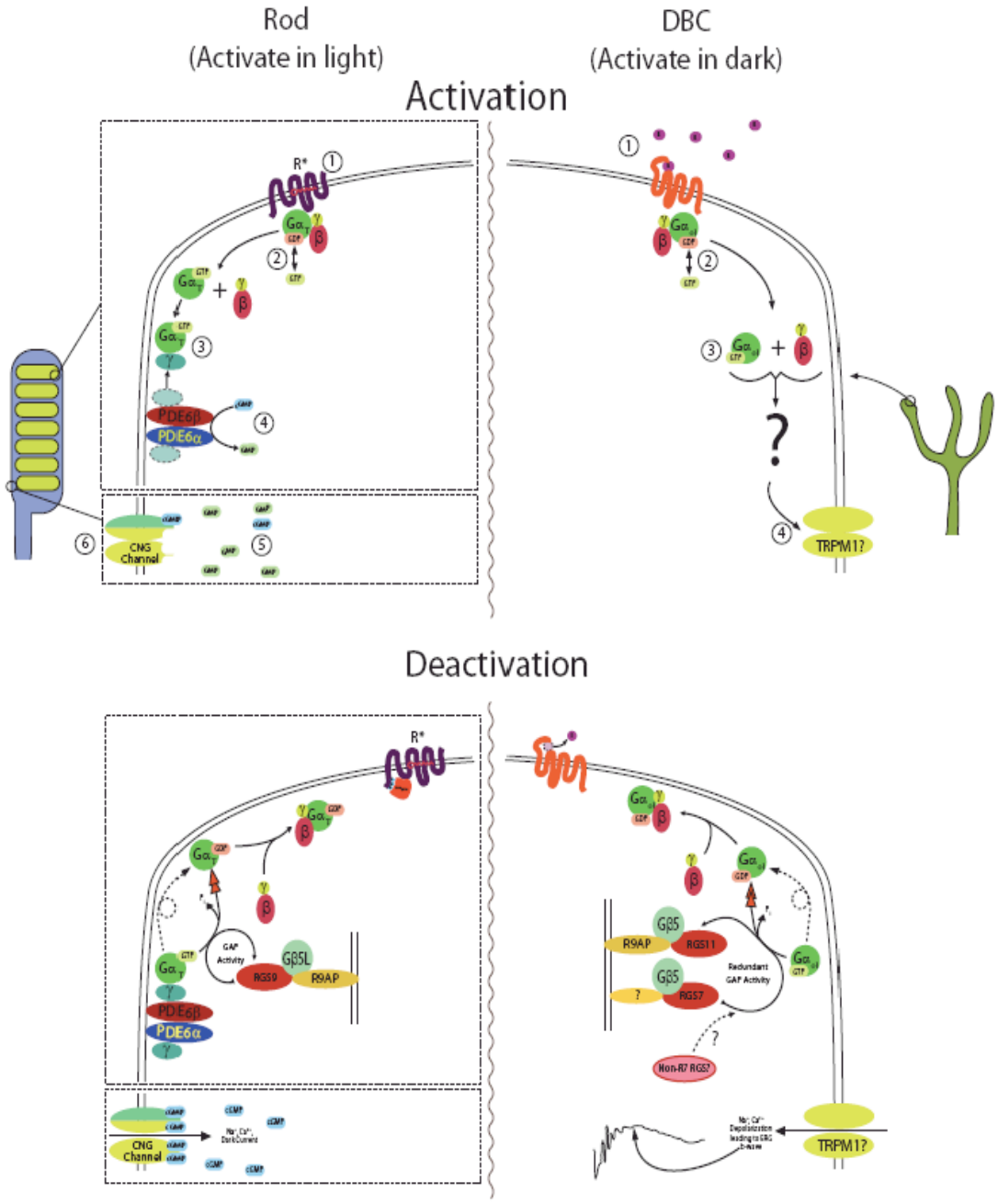
Rod
(Activate in light)
DBC
(Activate in dark)
Activation
R*
PDE6β
PDE6α
CNG Channel
TRPM1?
Deactivation
GAP Activity
RGS9
Gβ5L
R9AP
Gβ5
RGS11
RGS7
Redundant GAP Activity
Non-R7 RGS?
TRPM1?

Figure 1.2

activates G-protein coupled inward rectifying potassium (K+) channels (GIRKs) (Wickman et al., 1994), which dampen the cellular response to ligand when open. Among its other effecters are PLC β1, β2 and β3, which generate IP3 and DAG, and adenlyate cyclases (AC), which produce cAMP from ATP (Clapham and Neer, 1997). Simplifying the shut-off steps for now, we shall state that amplification halts when the Gα subunit hydrolyses the bound GTP to GDP and returns to quiescence.

Phototransduction in rods is a canonical G-protein cascade (Luo et al., 2008; Figure 1.2). To date, the activation of phototransduction in rods, from light onset to channel closing, is well understood in vertebrate with regard to the main activation players (Palczewski 1994; Chen 2005; Lamb and Pugh 2006). The rod phototransduction GPCR is rhodopsin (R). As described before, phototransduction begins with activation of R to R*. Upon catalysis at R*, transducin (GαT) loads GTP and subsequently binds the inhibitory phosphodieserase subunit gamma (PDEγ), disinhibiting the catalytic dimer called PDEαβ. In the dark, high cGMP concentration (Fesenko, Kolesnikov et al. 1985; Yau and Nakatani 1985) permits the opening of cyclic nucleotide gated (CNG) cation channels. The cGMP concentration required to half-maximally activate CNG channels is $K_{1/2}$ = 30 - 80μM in excised rod outer segments (Fesenko, Kolesnikov et al. 1985; Yau and Nakatani 1985). The free cGMP concentration is thought to be far less *in vivo* (4-6 μM; Pugh and Lamb, 1993) but is sufficient to activate CNG channels to pass the "dark current" of unstimulated photoreceptors (Nakatani and Yau, 1988). PDEαβ cleaves the phosphodiester bond of cyclic GMP (cGMP), reducing its concentration. The drop in cGMP stops the dark current and hyperpolarizes the photoreceptor. Hyperpolarization stops the presynaptic release of glutamate across the outer plexiform layer (OPL) onto

postsynaptic bipolar cells (responding to either increases, ON, or decreases, OFF, in light) and horizontal cells. The details of this pathway will be discussed later.

Gβ5 and R7RGS Activity

Rod photoreceptors can report the absorption of a single photon (Baylor et al., 1979). The timely deactivation of this report is essential for resolution of visual events and allows accurate encoding of light responses (Mendez et al., 2000; Burns et al., 2002). In contrast to phototransduction activation, *deactivation* has proven a challenge to understand because deactivation of all steps must be simultaneous, rather than sequential (Chen 2005; Yau and Hardie 2009; Figure 1.2). Calcium feedback was ruled out as the rate-limiting step because it shortened the lifetime of a *non*dominant, or fast, component of the cascade (Nikonov et al., 1998). Theoretical analysis of these experiments implicated disc-associated intermediates (activated R, GαT, or PDE) as the determinants of the response decay. Consequently, the debate over the rate-limiting step had two camps based on experimental evidence: rhodopsin shutoff (Pepperberg et al., 1992; Rieke and Baylor 1998) or transducin deactivation (Sagoo and Lagnado 1997; Nikonov et al. 1998; Krispel et al., 2003). Settling this controversy, Krispel, et al (2006) determined the rate-limiting step was transducin deactivation, an event controlled by an R7RGS/Gβ5 complex.

Gβ5 is the fifth member of the Gβ protein family. The primary structural homology of Gβ5 diverges from other Gβ subunits, e.g. Gβ1, and modest differences can be gleaned from its crystal structures (Cheever et al., 2008). Gβ5 has a conserved face that allows it to bind to gamma subunits like other Gβs. However, this face is a more suitable scaffold for another class of proteins. Gβ5 binds and stabilizes the R7 Regulators

of G protein signaling (RGS) at a Gγ-like (GGL) domain (Chen et al., 2003; Figure 1.3A), unique to R7RGS proteins (Snow et al., 1998), and is critical for their *in vitro* functions (Kovoor et al., 2000). The R7RGS proteins (RGS6, RGS7, RGS9, and RGS11) have an RGS domain that accelerates GTP hydrolysis in Gα thereby shortening the duration of the G-protein cycle *in vitro* (Posner et al., 1999; Hooks et al., 2003; Hooks and Harden 2004). Proteins that provide GTPase acceleration are called GAPs and are said to have "GAPing" activity. RGS proteins have a DEP domain, homologous to Desheveled, Egl-10 and Pleckstrin motifs, allowing them to bind anchor proteins, R9AP and R7BP, which can localize RGS activity (Martemyanov et al., 2003; Drenan et al., 2005; Song et al., 2006; Song et al., 2007; Jayaraman et al., 2009).

In rod phototransduction deactivation, the RGS complex consists of the short retina-specific RGS9 isoform, RGS9-1, the long isoform of Gβ5, Gβ5L, and R9AP. In adults, R9AP concentration limits the overall concentration of the RGS9-1/Gβ5L/R9AP complex (Keresztes et al., 2004; Krispel et al., 2006). By varying the degree of R9AP expression, it was found that the *in vivo* concentration of the RGS9-l/Gβ5L/R9AP complex critically regulates transducin shutoff (Figure 1.2). Put another way, the timing of transducin (GαT) signaling period is regulated by the R7RGS complex. This finding in photoreceptors provides a standpoint from which R7RGS physiological function in other parts of the visual system may be understood. Consequently, additional studies investigating the *in vivo* roles of R7RGS function have looked in other retinal cell types.

Bipolar cells act as conduits of visual information from photoreceptors. R7RGS/Gβ5 function is critical for their *in vivo* function (Mojumder et al., 2009; Chen et al., 2010; Zhang et al., 2010). ON-bipolar cells (sensing light increments) have a sign-

Figure 1.3- R7RGS/ Gβ5 expression in retina- A. Retinal extracts have been blotted for R7RGS proteins. All R7RGS proteins (RGS6, 7, 9, and 11) considerably reduced in Gβ5-/- retinas or absent altogether (RGS7, 11). This figure was published in (Chen, 2003). B. Schematic of retina shows laminar structure. Layers are defined by structural features, resident cell nuclei, or neurite plexi from top to bottom: Outer segments of photoreceptors (OS), Inner segments of photoreceptors (IS), outer nuclear layer (ONL) containing photoreceptor nuclei, outer plexiform layer (OPL) containing photoreceptor, bipolar, and horizontal cell processes and their synapses, inner nuclear layer containing ON and OFF bipolar cell nuclei, and amacrine cell nuclei, inner plexiform layer, containing bipolar, amacrine and retinal ganglion cell neurites and respective synapses, and ganglion cell layer (GCL) containing ganglion cell and displaced amacrine cell layers. The IPL can be further defined by ON (above) and OFF (below) layering, five (5) lamina based on calbindin stain demarcation, and further subdivided into 10 parallel layers. C. Immunostaining for Gβ5 details its locations throughout the retina, particularly in the OS, IPL, and INL. Figure was published in (Rao, 2007). D. Immunstaining for R7RGS proteins reveals RGS6 and RGS7 are notably in the IPL, RGS7 and RGS11 in the OPL and RGS9 is largely restricted to OS. Figure was published in (Song, 2007).

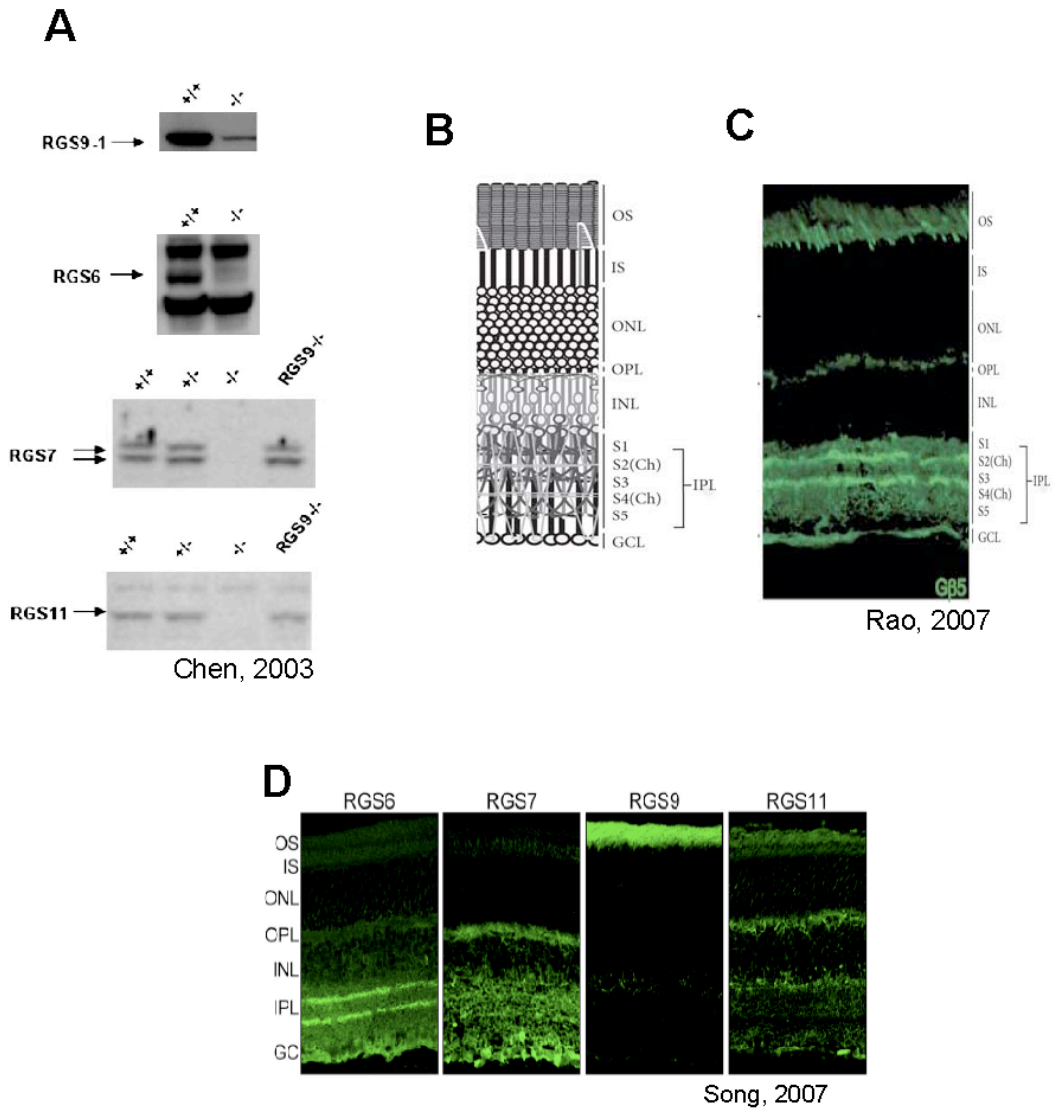
A
RGS9-1
RGS6
RGS7
RGS11
+/+
-/-
RGS9-/-
Chen, 2003
B
OS
IS
ONL
OPL
INL
S1
S2(Ch)
S3
S4(Ch)
S5
IPL
GCL
C
Rao, 2007
D
RGS6
RGS7
RGS9
RGS11
OS
IS
ONL
OPL
INL
IPL
GC
Song, 2007

Figure 1.3

reversing response and depolarize in the absence of glutamate because photoreceptors paradoxically *stop* releasing glutamate when they are activated. Conversely, OFF bipolar cells depolarize to light decrements because they are gated by ionotropic glutamate receptors (AMPA and kainite; DeVries and Schwartz, 1999) and activate when light shuts off. The metabotropic glutamate receptor type 6 (mGluR6) is found specifically in dendritic tips of ON-bipolar cells (Masu et al., 1995; Morgans et al., 2007; Rao et al., 2007; Song et al., 2007; Cao, et al., 2008; Sampath and Reike, 2004). In dark (Figure 1.2), glutamate released from photoreceptors activates mGluR6, followed by Gαo1 activation (Nawy, 1999; Dhingra et al., 2002). After an unidentified sequence of events, a cation channel closes and hyperpolarizes the cell, possibly TRPM1 (Shen et al., 2009). In ON-bipolar cells this channel closure stops the release of glutamate from their terminals, thereby achieving the polarity switch of the light responses. This allows ON retinal ganglion cells, which will carry the signal forth into the visual system, to activate upon rhodopsin activation. Hence ON RGCs effectively excite in the presence of light.

Gβ5/R7RGS activity is involved in the normal OPL transmission and bipolar signaling. In the outer plexiform layer, photoreceptors, bipolar cells, and the laterally communicating horizontal cells form triadic synapses. Animals without Gβ5 have a no b-wave phenotype on electroretinogram (ERG) (Rao et al., 2007), indicating an improperly functioning OPL (Stockton and Slaughter 1989; Peachey and Ball 2003). Gβ5-/- mice have poorly formed triadic synapses (Rao et al., 2007) that would certainly predetermine the no b-wave phenotype. However, the true origin of the synaptic malformation, and its impact on OPL signaling, is still a source of speculation and is not well understood. Another possibility is that Gβ5 -/- mice do not turn off Goα1 in a timely manner. In this

Figure 1.4-The murine visual system A*, Eye, Optic Nerve, and Sagittal Section of the Brian*. Retinal Ganglion Cells (RGCs) at the vitreal border of the retina project to the optic disc within the eye and become the optic nerve (ON). The ON then projects to central targets: the suprachiasmatic nucleus (SCN) in hypothalamus; the lateral geniculate nucleus with the dorsal LGN (dLGN,), intergeniculate leaflet (IGL), and ventral LGN (vLGN) in thalamus; the olivary pretectal nucleus of the pretectal nuclei (OPN); and the superior colliculus (SC) in midbrain. For simplicity, paths to central targets are shown as dotted lines. B: *Coronal Sections of Brain*: Images correspond to section levels in figure A. Section 1: Level of the SCN (yellow) where lateral and third ventricles shown in black for reference. Section 2: Level of the LGN where dLGN (red), vLGN (orange), IGL (between dLGN and vLGN) and PTN (green, OPN medial and superior, anterior pretectal nucleus, which does not receive direct ON input, medial and inferior). Section 3: Level of the SC (blue) with visual cortex expanded to show orientation and layering. In sections 2 and 3, dashed lines represent hippocampus.

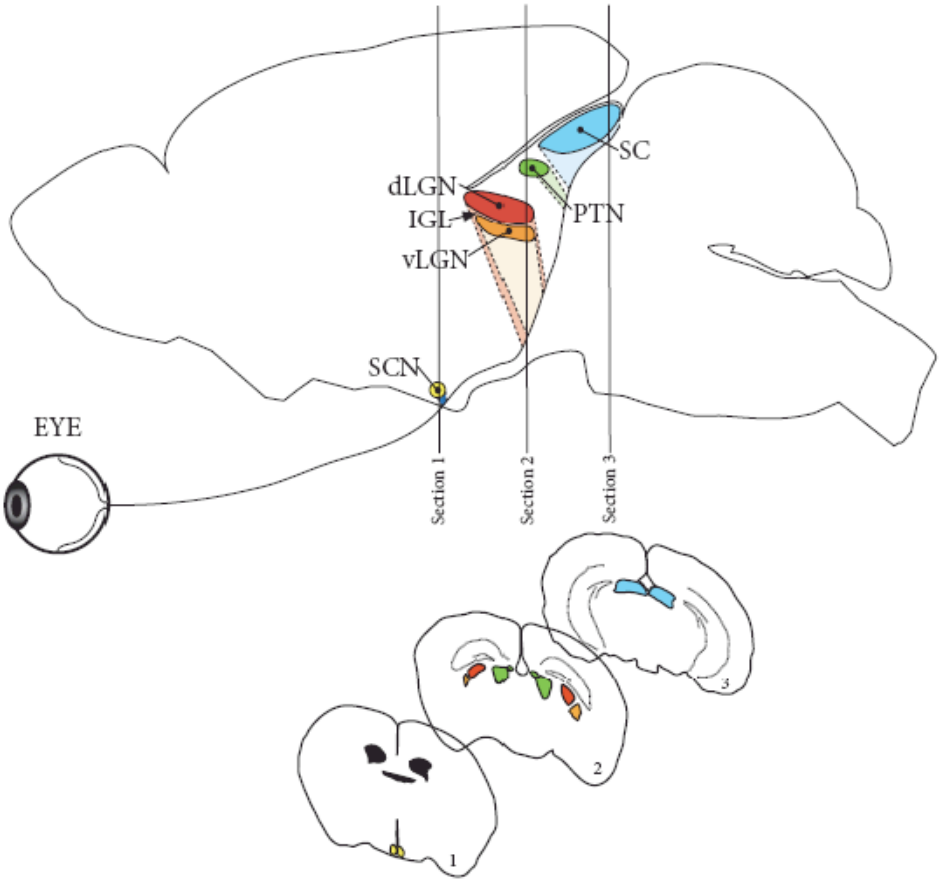

Figure 1.4

Table 1.1- Locations of Gβ5 and R7RGS in the visual system.

Location of Gβ5 and R7 RGS protein expression in the visual system

Location	Gβ5	RGS7	RGS9	RGS6	RGS11
Retina					
-Photoreceptor outer segment	+++(5,7)	- (5)	++++(6)	-(6)	+/-(6)
-Photoreceptor inner segment	++(5,7)	- (5)	-(6)	-(6)	+/-(6)
-Outer nuclear layer	-(5), +/-(6)	- (6)	-(6)	-(6)	+/-(6)
-Outer plexiform layer	++(5,7)	++(5)	-(6)	-(6)	++(5), ++(6)
-Inner nuclear layer	-(5), -(6)	-(6)	-(6)	-(6)	-(6)
-Inner plexiform layer					
-Cholinergic strata (s2,4)	++++(5,7)	++++(5), ++(6)	-(6)	+++(6)	+/-(6)
-Other strata (s1,3,5)	+++(5,7)	+++(5), ++(6)	+(6)[e]	++(6)	+/-(6)
-Ganglion cell layer	+++(5,7), +++(6)	+++ (6)	-(6)	+(6)	+/-(6)
Optic Nerve	+++[IB](n.p.)	n.r.	n.r.	n.r.	n.r.
Hypothalamus	+(3)[b]	+(3)			
-Suprachiasmatic Nucleus	++(8)	+(1), +++(8)	+++(1), +++ (8)	-(1), -(8)	-(1), +(8)
-Arcuate Nucleus	+++(2)	++(1),+++(8)	++++(1), + (8)	-(1), -(8)	-(1), +(8)
Thalamus		+++ (4)			
-Lateral Geniculate			-(1)		-(1)
-Dorsal LGN (dLGN)	+(3)[c], ++(8)	+++(1)[a], +++(3), +++(8)	-(8)	-(8)	-(8)
-Intergeniculate Leaflet	+(8)	++(8)	-(8)	-(8)	-(8)
-Ventral LGN (vLGN)	+(8)	+++(8)	-(8)	-(8)	-(8)
-Reticular nuclei	+(3)[c]	+(1), ++(3), +++(8)	-(1)	++++(1), +++(8)	-(1)
Pretectal Nuclei					
-Olivary Pretectal Nucleus	+(8)	++(8)	-(8)	-(8)	-(8)
-Anterior Pretectal Nucleus	++(8)	++(8)	-(8)	++(8)	-(8)
-Posterior Pretectal Nucleus	+(8)	++(8)	-(8)	-(8)	-(8)
Lateral Habenula	+(8)	+(1), ++(8)	-(8)	-(8)	-(8)
Superior Colliculus	+(3)[b]	+++(1), ++(3), +++(8)	-(1), +(8)	+(1), +(8)	-(1), -(8)
Cortex					
-Layer 1	+/-(2)	-(1), ++ (3), -(8)[f]	-(1), -(8)[f]	-(1), -(8)[f]	-(1), +(8)[f]
-Layer 2/3	+++(2), ++ (3)[b], +++(8)[f]	+++(1), ++++(4)[d], ++++(8)[f]	-(1), -(8)[f]	+(1), +(8)[f]	-(1), +(8)[f]
-Layer 4	++(2), +++(8)[f]	+(1), ++++(4)[d], +++(8)[f]	-(1), -(8)[f]	+(1), -(8)[f]	-(1), +(8)[f]
-Layer 5	+(2), ++(8)[f]	+(1), +++(4)[d], +++(8)[f]	-(1), -(8)[f]	+(1), -(8)[f]	-(1), +(8)[f]
-Layer 6	+(2), ++(8)[f]	+(1), +++(4)[d], +++(8)[f]	+(1), +(8)[f]	+(1), -(8)[f]	-(1), +(8)[f]

Very intense ++++, Moderately intense +++, Light ++, Faint +, difficult to distinguish +/-, no signal -, not reported n.r., not published n.p., Immunoblot, IB.

a: Principle relay nuclui include dLGN

b: Does not colocalize with RGS7

c: Does colocalize with RGS7

d: At developmental expression at P2, decreasing in intensity at ages P10, P18, and adult

e: Limited to strata 1

f: Refers specifically to visual cortex

g: Sources (cited on chart, *in situ:* * , immunohistochemistry:†)

1.Gold, S.J., et al., *Regulators of G-protein signaling (RGS) proteins: region-specific expression of nine subtypes in rat brain.* J Neurosci1997. **17** (20): p. 8024-37. *

2.Zhang, J.H., Z. Lai, and W.F. Simonds, *Differential expression of the G protein beta(5) gene: analysis of mouse brain, peripheral tissues, and cultured cell lines.* J. Neurochem, 2000. **75**(1): p. 393-403. *

3.Liang, J.J., et al., *RGS7 complex formation and colocalization with the Gbeta5 subunit in the adult rat brain and influence on Gbeta5gamma2-mediated PLCbeta signaling.* J Neurosci Res, 2000. **60**(1): p. 58-64. †

4.Ingi, T. and Y. Aoki, *Expression of RGS2, RGS4 and RGS7 in the developing postnatal brain.* Eur J Neurosci, 2002. **15**(5): p. 929-36.*

5.Rao, A., et al., *Gbeta5 is required for normal light responses and morphology of retinal ON-bipolar cells.* J Neurosci, 2007. **27**(51): p. 14199-204. †

6.Song, J.H., et al., *Localization and differential interaction of R7 RGS proteins with their membrane anchors R7BP and R9AP in neurons of vertebrate retina.* Mol Cell Neurosci, 2007. **35**(2): p. 311-9. †

7.Cao, Y., et al., *Targeting of RGS7/Gbeta5 to the dendritic tips of ON-bipolar cells is independent of its association with membrane anchor R7BP.* J Neurosci, 2008. **28**(41): p. 10443-9. †

8.Allen Institute of Brain Science, http://mouse.brain-map.org. Expression results based on "expression analysis" function.*

scenario, the ON bipolar cells would remain depolarized and the unknown downstream events would never close the cation channel nor register a positive deflection on an ERG.

In spite of the Gβ5 -/- morphological phenotype, *in vivo* manipulations of R7RGS proteins have provided insights into the particular role of Gβ5 in bipolar cell signaling. RGS7 and RGS11 are the predominant R7RGS proteins found at bipolar cell tips (Morgans et al., 2007; Rao et al., 2007; Song et al., 2007). Targeted deletion of exon 10 in RGS7 creates a truncated mutant of RGS7. Mice homozygous for this mutant protein (SG7) do not present a significant phenotype in the b-wave. RGS11-/- mice, on the other hand, have a moderately delayed b-wave even though RGS7 is upregulated (Chen et al., 2010). Furthermore, mice lacking both normal RGS7 and RGS11 (SG711) have a more pronounced delay in b-wave. This suggests RGS7 and 11, both missing in Gβ5-/- mice, provide redundant GAP activity at the ON bipolar cell dendritic tips (Mojumder et al., 2009; Chen et al., 2010; Zhang et al., 2010). These findings, however, do not recapitulate the Gβ5-/- no b-wave phenotype suggesting that Gβ5 is critical for OPL synaptic formation and *then* photoreceptor-bipolar cell transmission through RGS7 and 11. Gβ5 has a structural capacity to bind gamma subunits (Cheever et al., 2008) that invites the possibility it may interact with Gγ13 (Blake et al., 2001) to achieve any of its non-RGC phenotypes. Therefore, developmental studies in the Gβ5-/- animal may uncover potential mechanisms that contribute its constellation of phenotypes.

The ON and OFF pathways in the retina represent parallel streams of information that are processed and perceived by higher centers (Chalupa and Gunhan, 2004). Beginning at bipolar cells, these pathways generate the beginning of a center-surround receptive field that is seen in retinal ganglion cells. RGCs are classified as ON, OFF, or

ON/OFF if they respond to both increments and decrements of light. From these receptive fields arise the building blocks of visual representation (Kandel et al., 2000). In normal mature animals, ON and OFF pathways interact through a network of feed-forward inhibitory responses where ON bipolar cells temporarily quell OFF bipolar cell glutamatergic release (Renteria et al., 2006). This permits clear delineation of ON and OFF responses. This same circuitry is dysfunctional in some no "b-wave" mice. The no ERG b-wave phenotype can originate from presynaptic, postsynaptic, or other sources (as in the case of the Gβ5-/- synaptic malformation), and is found in clinical cases of Congenital Stationary Night Blindness (CSNB)(Miyake et al., 1986). Presynaptic sources prevent the release of glutamate and are exemplified by *nob2* mice, with a mutated voltage dependant calcium channel alpha1F subunit. Postsynaptic no b-wave mice usually have loss of bipolar cell function. The gene for the extracellular glycoprotein nyctalopin, *Nyx*, is mutated in *nob* mice (Pardue et al., 1998), and restoration of nyctalopin in ON-bipolar cells rescues function. MGluR6, also specific to ON-bipolar cells, is mutated in *nob3* (Pinto et al, 2007) and *nob4* (Maddox et al., 2008). Loss of Goα1-/-, which is responsible for normal ON-bipolar cell signaling (Dhingra et al., 2000, 2002), results in a "no b-wave" phenotype. Of course, mice without Gβ5-/-, which is presumptively involved in bipolar signaling and certainly involved in OPL synaptic formation, also lack a b-wave. In post synaptic b-wave models, ON responses are either unobservable *(*as in *nob;* Demas et al., 2006) or reveal dysfunctional ON-OFF feed-forward inhibition (like *nob3;* Renteria et al., 2006). Because of the fundamental role of these pathways, "no b-wave" animals will be instrumental in understanding the visual function. Furthermore, these abnormal signaling pathways have provided (Demas et al.,

2006), and may continue to provide, insights into neural development that will be discussed later.

Beyond the retina, R7RGS proteins have been investigated in the brain, particularly volitional and addictive centers. For example, RGS9-/- mice exhibit DOPA-induced dyskinesias, a hallmark Parkinson's disease treatment side-effect (Kovoor, et al., 2005). In the striatum, RGS9-2, the long RGS9 isoform, regulates Ca^{2+} channels in cholinergic neurons (Cabrera-Vera et al., 2004). In both cases, these functions are mediated through D2 dopamine receptors, which couple to Gαi/o. In ventral tegmental area, which mediates addiction, RGS9-2 is increased after cocaine exposure and acts as a compensatory mechanism that decreases drug responsiveness (Rahman et al., 2003). These findings underscore the subtle regulatory roles for RGS proteins in neural signaling. Similarly, retinal phenotypes (with the obvious exception of the no b-wave in Gβ5-/- mice) in animals with absent R7RGS activity reveal altered regulation, but not overt obliteration of function. Thus, further functional examination into R7RGS roles in the retina and visual system (Table 1.1) could provide valuable fodder for understanding central R7RGS function.

What other roles are there for Gβ5 in the retina? In adults, R7RGS proteins (Figures 1.3B, C, and D) colocalize with cholinergic strata of the inner plexiform layer (Rao, Dallman et al. 2007; Song, Song et al. 2007) and are found diffusely about the inner plexiform and ganglion cell layers (GCL). Cholinergic strata contain process extensions of starburst amacrine cells that are important for periodic waves of retinal activity during development and other mature visual processing (Masland 2005; Petit-

Figure 1.5- Gβ5 increases over development from P0 – P14 in retina. Immunoblot of Gβ5 retinal extracts shows Gβ5S as early as P0 and Gβ5L can be detected at P7. Bottom row is GAPDH loading control. This figure was published in (Rao, 2007).

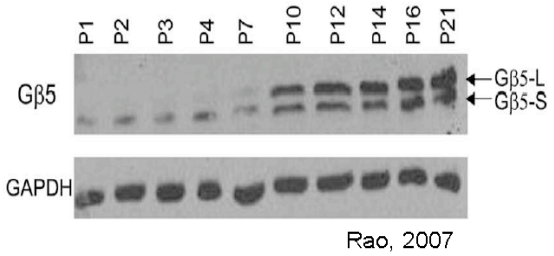

Figure 1.5

Jacques et al., 2005; Petit-Jacques and Bloomfield 2008). Gβ5 is also found in early postnatal retina (Figure 1.5; Rao et al., 2007). Therefore, these may be a particularly fruitful location and age span to look for novel defects in Gβ5-/- mice. Such experiments could reveal where Gβ5 may have developmental roles and identify periodic processes that Gβ5/R7RGS regulates. As will be described later, these manipulations could also provide a means to examine the role of activity in formation of visual circuits (Figure 1.4).

Spontaneous Retinal Activity

Before normal connectivity is achieved, developing sensory system cells utilize coarse electrical and chemical signals to communicate with their neighbors. For example in the auditory system, the developing cochlea, the hearing organ analogous to vision's retina, exhibits episodic waves of ATP that excite nearby cells before the onset of hearing (Tritsch et al., 2007). Similar phenomena have been investigated in the developing somatosensory system, spinal cord, hippocampus, and particularly in the retina (Blankenship and Feller, 2010). In each case this patterned activity is periodic and can drive gene expression (Flavell and Greenberg 2008; Lin, Bloodgood et al. 2008), report relative cell positions through spatially and temporally correlated firing (Feller, Butts et al. 1997; DeVries 1999; Weliky 2000; Huberman, Wang et al. 2003; McLaughlin, Torborg et al. 2003; O'Leary and McLaughlin 2005; Shah and Crair 2008), and facilitate the formation of local circuits (Bodnarenko and Chalupa 1993; Tian and Copenhagen 2003; Kerschensteiner, Morgan et al. 2009). In the retina, retinal cell development is followed by the emergence of spontaneous activity before the onset of normal vision.

Figure 1.6-Spontaneous Retinal Waves and time course of transitions A. Retinal activity is assessed by multi-electrode array extracellular recordings of RGCs in live peripheral retina. B. Pattern of spontaneous retinal activity changes through development. *Top to bottom* MEA recordings can be visualized with raster plots of several individual RGC spike trains. Rasters can be represented as population firing histograms (PFH) that show average firing rates of all RGCS. P7 raster matches P7 PFH. Note changes in timescale. Frequency of waves increases at P12 and regularity diminishes as P14, and eye opening, approach.

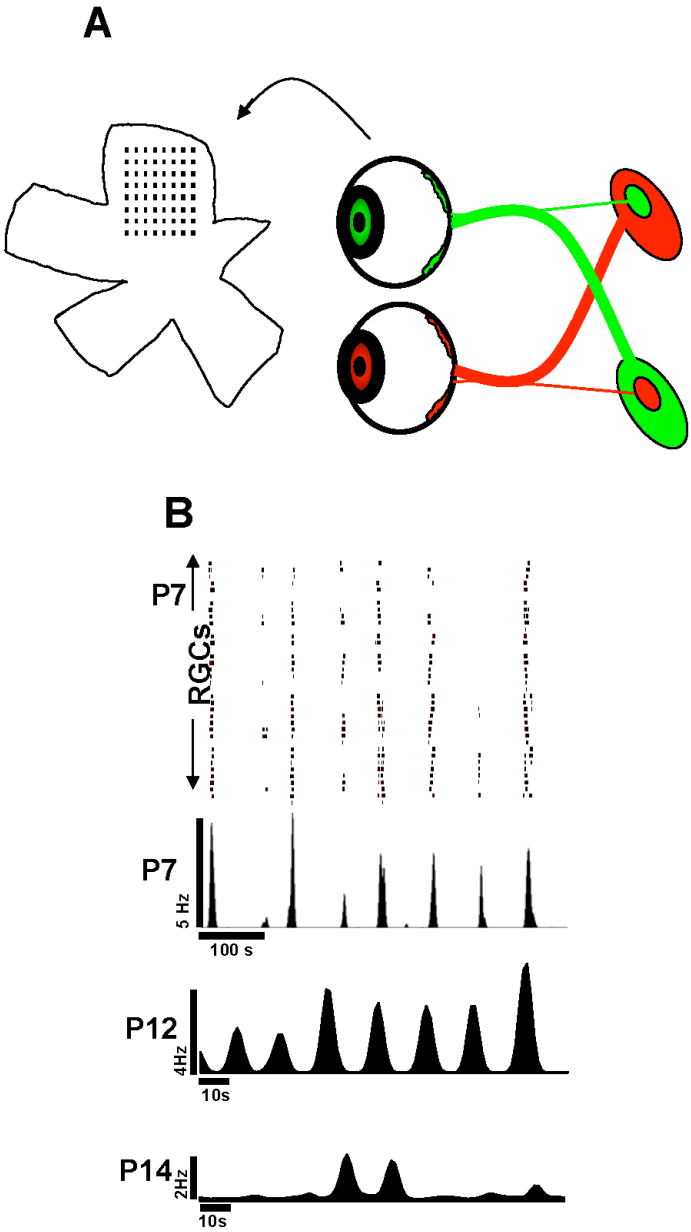

Figure 1.6

Figure 1.7 Spontaneous retinal wave stages and mechanisms A. In mice, Stage I-connexin mediated waves are followed by Stage II- acetylcholine mediated waves, which exist from P2-P10. Stage III-glutamate mediated waves emerge sometime between P8 and P12 and eventually subside as normal visual activity appears around P14. B. Stage II waves generate action potentials in RGCs (blue) and are thought to be driven by a transient network of spiking cholinergic starburst amacrine cells (green). *Bottom* Stage III waves are thought to arise from maturing bipolar cells that release glutamate onto RGCs. *Inset* Immature bipolar cell terminals permit indiscriminate spill-over of glutamate onto RGC dendrites.

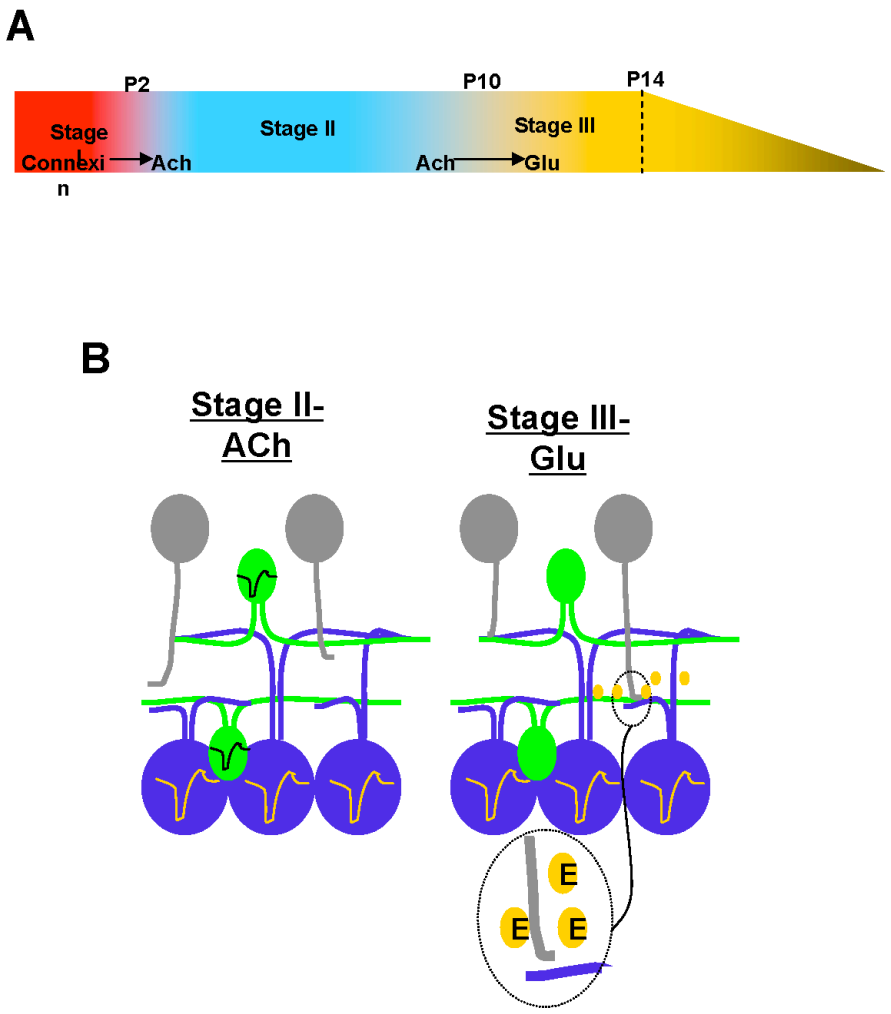
A
P2
P10
P14
Stage
Connexin
Ach
Stage II
Stage III
Ach
Glu
B
Stage II-
ACh
Stage III-
Glu
E
E
E

Figure 1.7

Development of the eye

Early in embryonic development, basic cell classifications emerge from one of three primordial ectoplasmic sources: the endoderm, mesoderm, and ectoderm (Kandel et al., 2000). Neural cells, including those that will become the retina, are the progeny of ectodermal cells that migrate into what is known as the neural tube. Cells at the rostral, or head end, of the developing vertebrate neural crest form the proencephalon, gives way to the diencephalon, eye stalks, and finally the neural retina. After a structure develops that resembles the eye, nascent retina forms as a single layer of primordial cells that will differentiate into multiple retinal cell types. When newborn mice are injected with tritiated thymidine, mitotic multipotent retinal progenitor cells (RPCs) (Turner and Cepko, 1987) that take up the tracer can be followed until they terminally differentiate in their respective layers (Young, 1985b). RGCs are mitotic as early as E10 and cease mitosis as late as P3. Horizontal cells are only briefly mitotic from E10 to E14. Amacrine cells have a broad period of mitosis between E10 and P4 (Young 1985a; Marquardt and Gruss, 2002). Cones divide from E10 to E18, whereas rods begin division at E12 and still divide as late as P14 (Carter-Dawson and LaVail, 1979). Bipolar cells are the last neurons to differentiate (E14-P11) and divide almost concurrently with Muller glial cells (E16-P11; Young, 1985a), as both cell types see peak division at P3.5. Between E15 and P2, all retinal cell types can be seen dividing. After birth, these cells migrate, form proper connections, and eventually establish a functional retina prepared for vision.

Retinal cells see many kinds of activity throughout their lifetime. Activity is found before the eyes open and prior when photoreceptors report the visual world to the brain. The mammalian retina exhibits periodic waves of spontaneous retinal activity

among its cell types during development (Maffei and Galli-Resta 1990; Meister, Wong et al. 1991).

Developmental Spontaneous Retinal Activity

In 1988, Galli and Maffei recorded robust spontaneous activity in the developing rat retinal cells. *In vivo* studies in retina also showed near-neighbor retinal cells were more likely to fire together (Maffei and Galli-Resta, 1990). Later, using *in vitro* ensemble recording methods (Figure 1.6A), Meister (1991) and Wong (1993) (Demas et al., 2003) would go on to rigorously quantify the spatial-temporal aspects of spontaneous retinal activity. The cells in the first relay of the image-forming pathway, the lateral geniculate nucleus, respond to spontaneous retinal activity (Mooney et al., 1996). Therefore, the early visual system is privy to the activity generated in the developing retina. Such correlated activity could hypothetically drive the formation of maps in the brain. The mechanisms of this development will be discussed later in greater detail. This flurry of evidence for spontaneous retinal activity compelled investigators to uncover its underlying mechanisms. To date there are three stages of spontaneous activity before eye opening. The following uses rat and mouse ages (Blankenship and Feller, 2010). These three stages (Figures 1.6B and 1.7A) and the underlying mechanisms are largely conserved across mammalian species.

Stage I waves are seen as early as E16 and subside around P2. Stage I waves cover relatively small patches of the retina compared to later stages and occur relatively infrequently (every 30 seconds to 2 minutes or 0.03-0.008Hz). Because this stage is predominantly before birth, relatively little is known about the underlying mechanism. In rabbits (Syed et al., 2004) it is clear that stage I spontaneous activity is carried through

gap junctions. Gap junctions are pores formed by connexin proteins that electrically couple cells (Penn et al., 1994; Hansen et al., 2005). In mice, late stage I wave propagation is also thought to occur via gap junctions (Torborg and Feller 2005; Blankenship and Feller 2010). Interestingly, Bansal et. al (2000) observed that some stage I waves could be diminished by cholinergic blockade with curare at P2. Consistent with these findings, β2 and α3 acetylcholine receptor subunit null mice have altered waves size at P0 (Bansal et al., 2000). These observations are subject to debate, however, because the ages of the mice were close to the transition into cholinergic stage II waves.

As cholinergic circuits emerge, stage II waves overtake stage I waves (Figure 1.7A). A transient network forms (Zheng et al., 2006) among cholinergic starburst amacrine cells (SACs)(Famiglietti, 1983) and provides periodic surges of acetylcholine approximately every minute (0.16Hz) (Feller et al., 1996). Developing SACs exhibit propagating calcium waves with calcium spikes (Zhou and Fain, 1996), generating the release of acetylcholine onto 10-30 other SACs (Zheng et al., 2006). SAC-released ACh in the IPL can also drive RGCs depolarization (Zhou, 1998; Figure 1.7B). This network of SACs is thought to generate periodic oscillatory activity, however the mechanism of periodicity is unclear. Increasing cAMP with forskolin treatment increases frequency of cholinergic waves (Torborg et al., 2005). Conversely, the AC inhibitor SQ22536 decreases wave frequency when tested in ferrets (Stellwagen et al., 1999). Dual patch recordings of adjacent SACs suggest that a 'pacemaker' current, regulated by cAMP, is responsible for this firing (Zheng et al., 2006).

At roughly P8-P11, stage II cholinergic waves subside (Figure 1.7A). Glutamatergic neurotransmission, provided by bipolar cells, sets the stage for stage III

waves. Stage III waves are the last epoch of wave activity before eye opening and the onset of normal visual activity. These waves are blocked with concurrent application of AMPA/Kainate specific antagonists, 6,7-Dinitroquinoxaline-2,3-dione (DNQX) or 6-cyano-7nitroquinoxaline-2,3-dinone (CNQX), and NMDA-specific antagonist R-2-amino5-phosphopentanoate (2-APB) (Demas et al., 2006). The stage III waves are shorter in duration, occurring as frequently as once every 10 seconds (0.1Hz) in normal conditions, yet still cover most of the retina (Blankenship et al., 2009). Like photoreceptors, bipolar cells employ glutamate to transmit visual information to amacrine cells and RGCs. At immature synapses, neurotransmitter is not yet restricted to postsynaptic targets, allowing a spillover of glutamate (Figure 1.7B). Feller and colleagues demonstrated that this glutamate spillover from bipolar cells terminals regulates the propagation speed and initiation of stage III waves (Blankenship et al., 2009). At the time of eye opening at P14, the maturation of photoreceptor–bipolar cell synapses allows transmission of patterned visual information. Stage III retinal waves subside and yield to normal visual activity coincident with these events.

GABA also plays a significant role in retinal waves and mature retinal function. Early in development, intracellular chloride levels are high. $GABA_A$ passes chloride down its chemo-electric gradient and as the negative charge moves outside of the cell, the cell depolarizes. Consequently in stage I and II, $GABA_A$ activation is capable of depolarizing RGCs (Fischer et al., 1998; Stellwagen et al., 1999; Johnson et al., 2003; Zheng et al., 2006). One study by Feller and colleagues (Wang, Blankenship et al. 2007) offers some explanation for its complex role in early retinal development. Gabazine, which blocks extra-synaptic and synaptic $GABA_A$ receptors, increases the interwave

interval of stage II waves (Wang, Blankenship et al. 2007). This is a surprising outcome because the prediction from the cell-level GABA activity would be that $GABA_A$ blockade would disquiet retinal activity. Gabazine application also increases the degree of spatial-temporal correlation in stage II waves. This action runs somewhat contrary to the expectation that a decreased inhibitory drive would also decrease correlated firing, which is what is seen in mature circuits. These conflicting local and global results may be explained by phasic GABA activation versus tonic GABA activation. GABA has different affects on SACs and RGCs. Tonic $GABA_A$ hyperpolarizes SACs. And whereas phasic GABA depolarizes RGCs, tonic $GABA_A$ acts as an electrical shunt that reduces the driving force of depolarization. Furthermore, responses in RGCs may be due to postsynaptic receptors whereas GABA influences in SACs are likely due to extrasynaptic receptors (Wang et al., 2007). However, a reconciliation of the discrepancies in GABAergic effects in stage II waves has not been fully achieved and awaits further study. Sometime after P7, the potassium chloride channel (KCC2) is expressed and extrudes chloride out of the cell (Fischer, et al., 1998; Blankenship and Feller 2010). Intracellular chloride drops and GABA activation become inhibitory. Interestingly, this switch from stage I to stage II is mediated by a $GABA_A$ activity itself (Leitch et al., 2005) because blockade of $GABA_A$ prevents the eventual extrusion of intracellular chloride. By P12, GABAergic inhibition, as well as glycinergic inhibition, mediates the ordered firing of ON then OFF RGCs during stage III waves (Wong and Oakley 1996; Kerschensteiner and Wong 2008). This firing may have implications on ON/OFF circuit development and will be discussed later.

Adenosine signaling and exogenous dopamine (Stellwagen et al., 1999) can also

regulate the dynamics of stage II waves but has ambiguous roles. Aminophilline is an adenosine receptor antagonist. At high concentrations (>200μM), it hyperpolarizes RGCs and blocks retinal waves, presumably by direct $GABA_A$ activation (Wang et al., 2007). At low concentrations (<2μM) it increases retinal wave frequency either by deactivating a potassium channel linked to A1 receptors or via A2A receptor activation. A2 receptors antagonists increase wave frequency yet adenosine deaminase treatment, which decreases extracellular adenosine concentration, dramatically slows waves. Blocking PKA prevents the adenosine-mediated wave changes (Stellwagen et al., 1999). The activity of PKA and the level of its upstream regulatory mediators, Ca^{2+} and several group I adenylate cyclases (Watts and Neve 2005; Dunn et al., 2009) increase after RGC depolarization. In addition to regulating wave dynamics, PKA signaling in during RGC axonal ingrowth may also mediate axonal repulsion responses to ephrinAs (Nicol et al., 2006; Nicol et al., 2006; Nicol et al., 2007).

Exogenous dopamine application increases wave frequency even though endogenous dopamine does not seem to be critical for retinal wave dynamics (Stellwagen et al., 1999). This exogenous application effect on retinal waves is though to be mediated by the Gs-coupled D1 receptor (Stellwagen et al., 1999; Wang et al., 2007). D1 message is found in prenatal RGCs (Schambra et al., 1994) and early in postnatal rat INL (Koulen, 1999). That dopamine increases wave frequency is consistent with the fact that D1 receptor activation increases cAMP. D2 and D2-like receptors are also found in the retina. Gαi/o coupled D2-like receptor expression is detectable in the postnatal retinal as early as P6 (Klitten et al., 2008). Though D2 receptors have not been directly localized in early postnatal retina, in adult rat retina D2 receptors are reported across the entire retina

(Tran and Dickman, 1992). Interestingly, A2A and D2 receptors can interact at the receptor level as well as at their effectors levels by oppositely regulating ACs (Ferre et al., 2008; Zezula and Freissmuth 2008). This suggests the possibility that dopamine and adenosine receptors can also interact in the retina, thereby indirectly regulating stage II waves. Experiments that explicitly rule in or rule out D2 activity would provide insights into additional retinal wave mechanisms.

Several mouse models with abnormal spontaneous retinal activity have provided additional insights into the underlying mechanisms at different stages. Stage I waves cease in the presence of gap junction blockade with 18α-glycyrrhetinic acid (18-GA) (Syed et al., 2004). Unfortunately, no recordings have been reported in mice with altered or absent connexins before P4 that could isolate particular connexin proteins involved. Interestingly, stage II waves have less spatial-temporal correlation in connexin 36 -/- mice (Torborg et al., 2005), suggesting an extended role for gap junctions beyond stage I.

Targeted deletion of nicotinic cholinergic receptor subunits β2 and α4 prevents normal stage II waves (Bansal et al., 2000). The de-correlated activity in the nicotinic β2 receptor knockout (β2 -/-) mouse retina has been exhaustively studied (Figure 1.9B). The β2 -/- mouse model has implications on activity-dependent synaptic refinement and will be discussed in detail later. In the absence of normal stage II waves in β2-/- mice, gap junctions can provide a backup route for wave transmission (Sun et al., 2008b). However, the waves are still de-correlated and overly frequent (Figure 1.9B). Mice without choline acetyl transferase (ChAT), the enzyme that synthesizes ACh in SACs, exhibit gap junction mediated waves at P5 (Stacy et al., 2005). In wild-type mice, the potentiation of L-type calcium channels with pharmacological agents (FPL-64176) also

reveals calcium waves (Singer, Mirotznik et al. 2001), which are attenuated by with 18-GA. This same phenomenon exists in nicotinic receptor β2 -/- mice, although the overall spontaneous retinal activity is still weak and fails to rescue central projection problems seen in these animals (Torborg and Feller, 2004). Therefore, mechanisms found in stage I waves can compensate for improper stage II waves.

Similarly, stage II waves can compensate for stage III waves. In VGLUT2 knockout mice, which lack functional glutamatergic terminals, stage III waves are absent and cholinergic activity continues (Blankenship, Ford et al. 2009). β2 -/- mice also experience an earlier onset of glutamatergic activity by postnatal day 8 compared to postnatal day 10-12 (Bansal, Singer et al. 2000). These results suggest there is an interaction of cholinergic and glutamatergic drives in wave transition. Interestingly, muscarinic AChR antagonists also block stage III waves in rabbits (Syed et al., 2004), but these results have not been recapitulated in mice.

Finally, the naturally occurring no b-wave (*nob*) mutant mouse, with an 85-bp deletion in the nyctalopin gene, exhibits rapid and rhythmic glutamatergic waves after eye opening (Demas, Sagdullaev et al. 2006; Huberman 2006)(Figure 8B). Gregg and colleagues bred *nob* mice with mice expressing a transgenic GABAcρ−driven nyctalopin-EYFP in an effort to rescue the *nob* retinal phenotypes (Gregg, Kamermans et al. 2007). In these animals, nycaloptin only localizes in the OPL and particularly in ON-bipolar cells. Retinal activity in the *nob*x*nyx-EYFP* mice was indistinguishable from WT, suggesting that the OPL is locus of dysfunction in the *nob* mouse. However, the mechanism of this abnormal phenotype is still not understood. It is unclear if these phenomena are positively compensatory for the retina (or activity-dependant targets of

the retina) through homeostatic mechanisms (Maffei and Fontanini 2009; Blankenship and Feller 2010), detrimental, or simply a consequence of improper formations. Animals without b-waves have impaired OPL transmission. The Gβ5-/- mouse, which also lacks a b-wave, is likely to have other signaling anomalies in the retina. A survey of Gβ5-/- developmental retinal activity may provide insights into these mechanisms.

At the local scale, retina development orchestrates synaptic connectivity through several mechanisms. ON and OFF bipolar cells synapse onto their respective RGCs to form distinct ON and OFF sublamina in the IPL. In this way, they preserve two fundamental parallel pathways in the visual system. The IPL can be further subdivided into S1-S5 substrata or even 10 substrata (Wassle 2004; Yamagata and Sanes 2008). Subsets of amacrine, bipolar and retinal ganglion cells synapse within each using adhesion molecules. In chicks, homophilic contacts of immunoglobulin superfamily adhesion molecules are required for proper laminar specification of S1 (DSCAML1), S5 (DSCAM), S2 (Sidekick2), and S4 (Sidekick1)(Yamagata and Sanes, 2008). This presents the possibility that similar subsets of cells would identify each other via such homotypic interactions. However, in mice, DSCAM and DSCAML1 are not required for normal synaptic function (Fuerst et al., 2009). The positioning of RGC soma and their dendritic fields has also been explored. In some melanopsin and SMI-32 containing RGCs, somatic mosaicism, the even distribution of somas across the retina, does not require homotypic interactions (Lin et al., 2004). In other RGCs, DSCAMs are certainly involved in the dendritic layout and self-avoidance of cells and axons (Fuerst et al., 2009).

Retinal synaptic development also critically relies on synaptic activity (Tian, 2008). Bodnarenko (1993) and colleagues treated prenatal kitten retinas with APB, which blocks depolarization of ON cone and rod bipolar cells. APB application prevented normal ON and OFF lamination of RGC dendrites (Bodnarenko and Chalupa, 1993) and revealed a role for glutamatergic activity in retinal development. Normal visual activity also drives proper synaptic connectivity after eye opening. ON and OFF sublamina, as well as ON/OFF lamination, are disrupted in dark-rearing (Tian and Copenhagen 2001; Tian and Copenhagen 2003). β2−/− mice, which exhibit de-correlated (Sun et al., 2008b) and mis-oriented stage II waves (Stafford et al., 2009), also have delayed ON/OFF laminar refinement (Bansal, Singer et al. 2000). However, mosaic patterning of direction selective RGCs are indifferent to abnormal spontaneous retinal waves (Elstrott, Anishchenko et al. 2008) or visual activity (Anishchenko et al., 2010). Beyond activity alone, activity-related BDNF expression can increase laminar refinement (Liu et al., 2007). Finally, lamination is not the only indicator of proper synaptic formation. The presynaptic release of glutamate from ON bipolar cells directs the proper formation of ON-bipolar cell/ON RGC synapses (Kerschensteiner et al., 2009), which can be abnormal even in conjunction with normal stratification. So it is clear that activity is one of many important contributors to retinal development and synaptic specification. Further examination of spontaneous activity will provide insights into these mechanisms.

On the larger scale, when spontaneous developmental activity is registered by projection neurons, e.g. RGCs, local information can be relayed to the brain where early maps of the sensory organ are established. Therefore, local activity is critical beyond the retinal neighborhood and can direct the formation of systemic neural pathways and neural

Figure 1.8-Normal Retinogeniculate development A. Different colored fluorophores are intravitreally injected and transported by RGCs to terminals in the dLGN. Terminals can then be visualized simultaneously to determine eye-specific projection features. B. After eye-specific segregation of afferents, inputs are pruned to monocular preference (in this case the green eye refined, red eye is eliminated) followed by fine-scale refinement of retinal input onto geniculate relay cells (dark blue synaptic contacts). C. Time course of course eye-specific segregation shows ipsilateral (red in inset binarized images), contralateral (green), and overlapping terminals (yellow). Inset are examples of normal P7 (left) and adult (right) eye-specific retinogeniculate projections. Data for figure courtesy of W. Guido and adapted from Jaubert-Miazza, 2005.

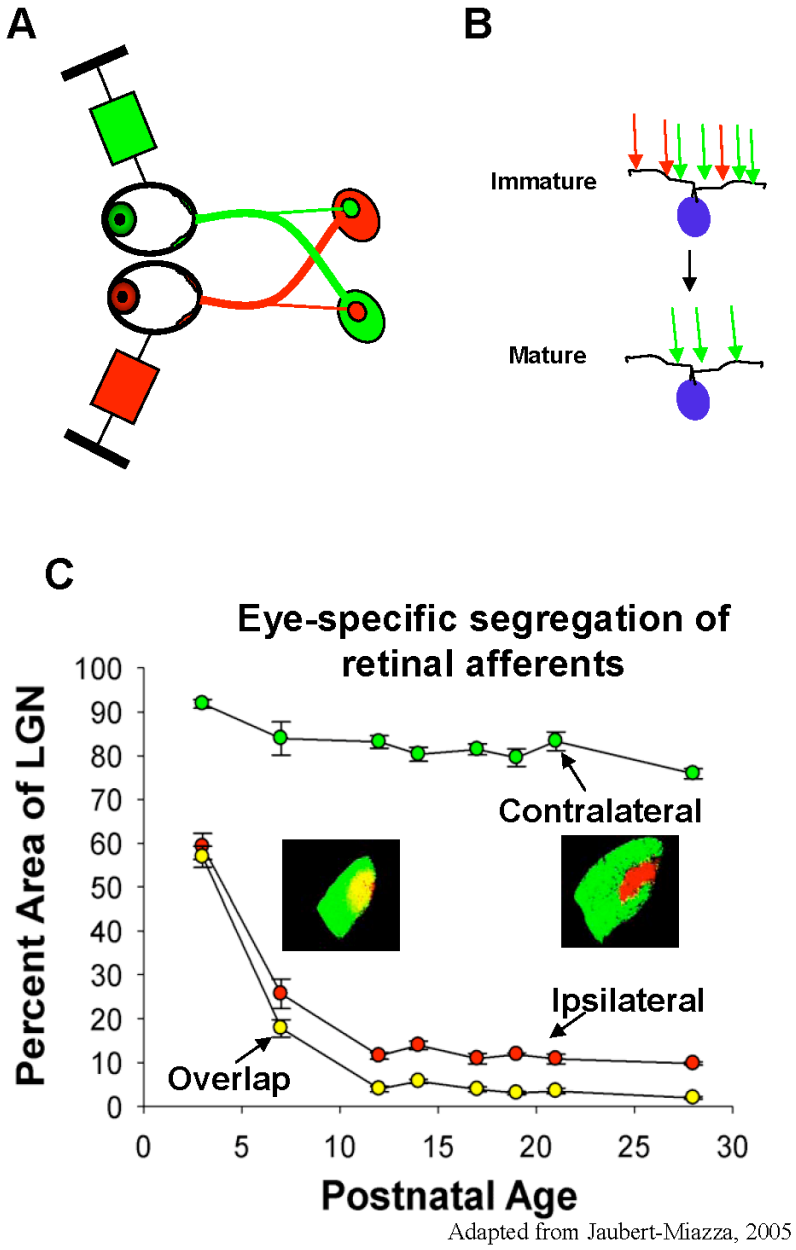

Adapted from Jaubert-Miazza, 2005

Figure 1.8

map formation. The developing visual system has been a canonical model for illuminating these important processes.

Activity in visual development and the retinogeniculate synapse

The mature visual system is a remarkable entity. Consider a lion in the Sahara or a cab driver navigating New York's 42nd street. Both must identify relevant objects: the lion sees a grazing antelope in tall grass; the cabbie spots his next fair among hundreds of pedestrians. To act, both the lion and the cabbie must pinpoint the position of their object else miss the opportunity to preserve their respective livelihoods. And to close the chase, the velocity and position of the object must coincide with the calculation to pounce or pull over. Their survival depends on visual systems that can resolve fine details (opponency), precise position (retinotopy), and rate of movement of objects within a scene (directional sensitivity). Faithful transmission the information to brain structures (Kandel et al., 2000) then allows processing of these events for immediate action. If the visual system is not working correctly, either by development or injury, the results can range from devastating, in the case of complete blindness, to relatively subtle loss of visual acuity, as in the case of amblyopia (Moseley et al., 2009).

Forming connections in the visual system

Sensory systems, from auditory (Lee and Winer, 2005) to somatosensory modalities (Petersen, 2007), display several examples of precise synaptic connections. The visual system too has been a model for studying synaptic formation and maintenance. The first modern evidence of the precision of connections in the nervous system was reported in the visual system, specifically in the retina. At the end of the 19th century, using a Golgi stain that labeled only a few cells at a time, Ramon y Cajal teased

out the exquisite and regular arrangement of photoreceptors, bipolar cells, amacrine cells, and RGCs (Kandel et al., 2000). For this work, Ramon y Cajal and Golgi received a Nobel Prize in Medicine and Physiology in 1906. Over the next several decades, numerous investigators clarified the functional significance of these connections. By the 1960s, visual cortex functional organization (Hubel, 1959; Hubel and Wiesel, 2009), the importance of activity in this organization (Wiesel and Hubel 1963; Constantine-Paton 1990), and chemo-attractive mechanisms of synaptic specificity (Sperry, 1963) were emerging. For pioneering this work to resolve neural organization and development, Hubel, Wiesel, and Sperry were awarded the Nobel Prize in 1981. Since that time, several investigators have uncovered critical steps and mechanisms in the development of the visual system.

In mammals, RGCs send axons to structures deep within the brain. The major RGC targets can be grouped by function, which include non-image forming (NIF) and image forming (containing discrete retinotopic maps, IF) structures (Figure 1.4). The first non-image forming target is the Suprachiasmatic Nucleus (SCN), which is responsible for circadian rhythms, and sits superior to the crossing of RGC axons at the optic chiasm (Hattar, Kumar et al. 2006). Another chief non-image forming target is the Olivary Pretectal Nucleus (OPN), which is responsible for the pupillary light reflex (PLR). The Superior Colliculus, known as the optic tectum in non-mammalian vertebrates (Debski and Cline, 2002), is image forming and involved in coordinating head, neck, and eye movements. The last major RGC target in mammals is the Lateral Geniculate Nucleus (LGN). The ventral LGN (vLGN) and intergeniculate leaflet (IGL), have some non-image forming function particularly in circadian rhythms (Harrington, 1997). The dLGN

is image forming and acts as a regulating gateway to the visual cortex. In cats, the receptive fields (RFs) of dLGN relays cells closely reproduce RGC RFs (Mastronarde, 1987): stimulus-activated centers sharpened by a concentrically-arranged suppressing surround. This design helps achieve a pinpoint faithful reproduction of the visual world for the cortex. Not simply a relay, slight differences between these RFs may represent further visual information processing (Alonso and Swadlow 2005; Alonso, Yeh et al. 2006). The dLGN itself assimilates input from the layer 6 of the visual cortex and brainstem sources (Sherman and Guillery, 2002). Paired physiological recording of RGC and dLGN RFs have not directly compared visual representations in mouse. However, mouse RGC RFs are similar to cat (Stone and Pinto 1993; Sagdullaev and McCall 2005). Furthermore, murine dLGN possess ultrastructural synaptic organization and inhibitory circuitry elements similar to previously characterized mammals, including cat (Bickford, Slusarczyk et al. 2010). Therefore, studies that clarify the process of connectivity in the murine retinogeniculate pathway may reflect similar processes in other mammals.

For a synapse to form, two soma or processes must come into close apposition. This contact requires at least one cell to extend processes towards the other. When these processes traverse great distances, extracellular proteins bind to receptors at the axonal growth cone, trigger an intracellular signal, and facilitate navigation. Sperry (1963) first proposed chemical gradients existent in tissues and provide a chemoaffinity-based "decision" for the growth cone to advance, retract, or turn. A vast array of molecular cues have been shown to be important at different regions, but are similar in that they involve receptors binding to ligands expressed in a gradient or at an anatomical limit (O'Leary and McLaughlin, 2005). Slit1 and EphrinBs guide decussation, or crossing, of RGC

axons at the optic chiasm (Petros et al., 2008). Immunological proteins like neural pentraxins (Bjartmar et al., 2006), complement C1q and C3 proteins (Stevens et al., 2007), and MHC class 1 proteins (Datwani et al., 2009) are involved in initial synaptic refinements. For instance, loss of multiple neural pentraxins alters retinal activity and reduces eye-specific segregation of retinogeniculate afferents. EphrinsAs are expressed in a gradient across the LGN and SC (Huberman et al., 2005; Feldheim et al., 2000) This gradient repels incoming RGC axons (Reber et al., 2007) that express a complementary gradient of EphA receptors. These events direct early coarse topographic arrangement in conjunction with spontaneous retina activity (Pfeiffenberger et al., 2006). Interestingly, PKA oscillations, driven by the periodic electrical activity of spontaneous waves, are required for normal EphA responses to ephrinAs (Nicol et al., 2007; Nicol et. al, 2006). As mentioned, molecular cues and activity influences often commingle. Generally, however, molecular guidance cues tend to dominate early visual development, whereas activity appears to exert a greater influence after coarse target-finding is complete.

Retinal activity and the retinogeniculate development

Once RGC axons reach the vicinity of their postsynaptic targets, visual development utilizes activity to refine and specify connections. For our purposes, activity is defined as an measured event, much like what is seen in spontaneous retinal waves, which results in the membrane depolarization of a cell. The precise role of activity in development is not fully understood and depending on the location in the visual system and the species evidence for the role of activity varies (Chalupa, 2009; Huberman et al., 2008). Nevertheless, many experiments have determined that it is critical for the normal form and function of the visual system (Huberman et al., 2008; Feller 2009). In the

cortex, patching or sewing the eye closed reduces cortical responses to the visually deprived eye (Hubel and Wiesel, 1970). Subsequent experiments in mammals further determined a critical period during development of such a plastic event (Hooks and Chen, 2007). These findings led to numerous experiments in visual development and piqued interest in examining direct retinal targets namely the lateral geniculate nucleus (LGN), before the cortex in mammals and optic tectum in lower vertebrates. In *Xenopus*, extra eyes transplanted during development carve out their own map in tectum among the maps of the two other eyes. Because the same eye has roughly the same molecular cues, this experiment suggested that the activity of the retina, the only unique trait, was sufficient to drive eye-specific segregation (Constantine-Paton and Law, 1978; Constantine-Paton et al., 1990). In mammals, blocking activity in the retina or brain resulted in unrefined RGC axonal arbors in the LGN (Sretavan et al., 1988), suggesting activity is important for normal refinement of axons. Furthermore, altered spontaneous retinal waves, and not simply blockade, can disrupt refinement of projections in LGN (Torborg et al., 2005) and SC (McLaughlin et al., 2003) or retinotopy in the cortex (Triplett et al., 2009; Cang et al., 2005; Cang et al., 2008). Collectively with other observations that will be described later, these findings suggest not only that activity is necessary, but also that particular aspects of activity may be more critical than others for normal visual development.

An excellent system for testing the particular roles of activity on visual circuit development is the aforementioned retinogeniculate pathway (Figures 1.4 and diagrammed in Figure 1.8A). First, the primary players, the retina and the LGN, are relatively easy to access for anatomical, pharmacological, and electrophysiological experimentation. Anatomical tracing techniques can be used to visualize the eye-specific

segregation of the retinal afferents into discrete zones and the spontaneous and evoked electrical properties of the retina can be recorded in vitro to assess activity. The use of laboratory mice, which have a relatively simple layout of eye-specific segregation in dLGN (Jaubert-Miazza et al., 2005), provides additional experimental advantages by enabling transgenic and targeted genetic manipulations to examine molecular mechanisms of activity-dependent refinement.

Guido and colleagues have investigated the normal anatomical and physiological development of the mouse dLGN in detail (Bickford et al., 2010; Demas et al., 2006; Jaubert-Miazza et al., 2005; Lo et al., 2002; Ziburkus et al., 2009; Ziburkus and Guido, 2006; Ziburkus et al., 2003). When retinal projections initially reach the lateral border of the dLGN before P3, contralateral axons penetrate the tissue followed by ipsilateral axons (Godement et al. 1984). Anatomical tracing at this age—performed by injecting recombinant cholera toxin B conjugated with different colored fluorescent dyes into each eye (Figure 1.8A)—shows ipsilateral projections almost completely overlapping with contralateral projections (Figure 1.8B). These overlapped projections then segregate into eye-specific regions during the induction phase of refinement, before P14, and remain segregated during the maintenance phase, after P14. In adult mice, the ipsilateral, or uncrossed, retinal projections occupy a central tube of the dLGN. Contralateral, or crossed, projections reside in the remaining dLGN within its cytoarchtechtonic limit (Guido, 2008). Once these connections are established, it is assumed that they are consistently maintained, barring any RGC cell death (Mazzoni et al. 2008).

Manipulations that interfere with the stage II cholinergic spontaneous retinal activity (~P2-P9) prevent normal eye-specific patterning in the dLGN. Chief among these

models is the β2 knockout (β2 -/-) mice whose RGCs fire bursts less synchronously than normal (Torborg et al., 2005). Eye-specific afferents fail to segregate in a timely fashion (Rossi et al., 2001; Muir-Robinson et al., 2002) in β2 -/- mice, never fully achieving normal eye-specific patterns as late as P60. Similarly, intraocular injection of slowly released TTX into ferret eye delays fine eye-specific refinement of afferents in dLGN (Cook et al., 1999). Though these dLGNs appear to recover, they still have abnormal synaptic responses. Epibatidine is a cholinergic agonist that paradoxically down-regulates AChRs thus disrupting spontaneous retinal activity (Sun et al., 2008a) (Figure 1.9B). In ferrets, intravitreal epibatidine injection prevents eye-specific segregation (Huberman et al., 2003; Penn et al., 1998). Activity between the two eyes may provide a basis for competitive occupancy of LGN territories. Monocular epibatadine injection places the treated retinal projection at a disadvantage. The projections from the untreated eye completely replace those from the treated eye (Penn et al., 1998). Forskolin, which increases the frequency of spontaneous retinal waves, can also increase the competitive advantage of one eye and increase the percentage of dLGN territory it occupies (Penn et al., 1998; Stellwagen and Shatz, 2002). Together, these data suggest retinal activity has a potentially instructive role in retinogeniculate eye-specific refinement.

After eye-specific projections refine through P12, they must be maintained (Figure 1.9A). This maintenance of segregation is susceptible to disruption in activity. Altering ON visual pathway with the mGluR6 agonist APB (Chapman, 2000) generates abnormal activity. Retinal APB treatment also induces the loss of maintenance of eye-specific segregation. Similarly, this is largely recapitulated in the *nob* mouse, in which ON visual pathway is not functional. Persistent abnormal retinal activity in *nob* mice

Figure 1.9-β2-/- and *nob* retinal activity and LGN phenotypes A. Eye-specific refinement of retinogeniculate afferents has two known stages: induction and maintenance. β2 ACh -/- mice and *nob* mutant mice exemplify these stages. B. β2 ACh -/- have lower spatial and temporal correlation of retinal waves at P7 and fail to segregate eye-specific projections in LGN at P8. After normal stage III waves, LGNs recover somewhat but are still relatively unrefined at P28. C. *nob* mutants have normal retinal waves at P7 and P12 but exhibit persistent, rhythmic firing after P15. *nob* LGNs refine normally until P12 but fail to maintain segregation at P15 coinciding with aberrant activity.

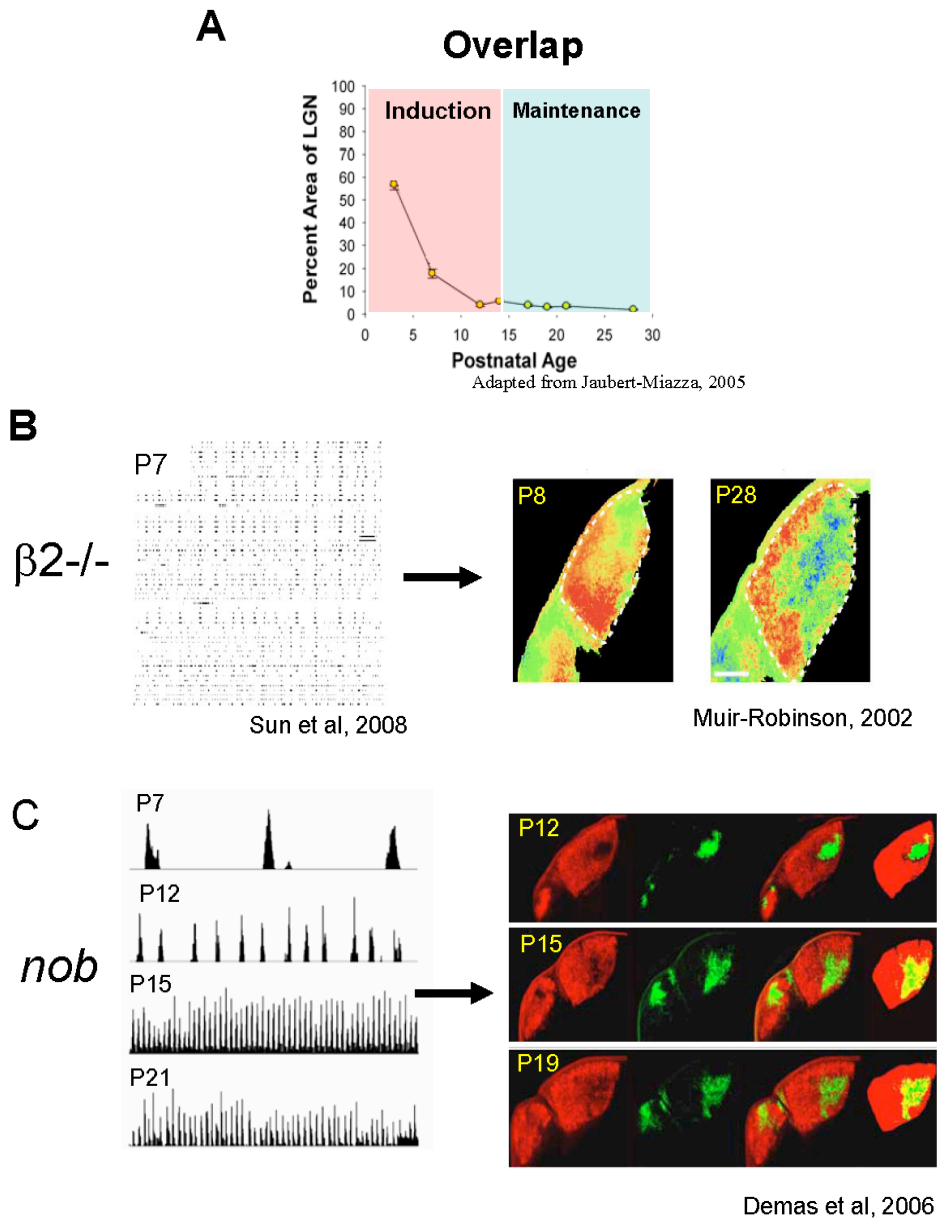
A
Overlap
Induction
Maintenance
Percent Area of LGN
Postnatal Age
Adapted from Jaubert-Miazza, 2005
B
P7
β2-/-
Sun et al, 2008
P8
P28
Muir-Robinson, 2002
C
P7
P12
nob
P15
P21
P12
P15
P19
Demas et al, 2006

Figure 1.9

(Demas et al., 2006) hinders maintenance of segregated retinal afferents. In both cases, normal refinement occurs during the induction phase, but is interrupted after eye opening. Furthermore, whereas APB blocks normal patterned activity, *nob* mice fail to refine even in the dark, strongly suggesting that it is the abnormal activity itself, and not the disruption of normal visually patterned activity, drives desegregation (Figure 1.9B). However, all the necessary elements of activity that drive segregation failure are undetermined. Interestingly, eye-specific segregation proceeds normally in chronically dark-reared (Demas et al., 2006) animals. Both of these studies also indicate that maintenance is an active process, yet only observable when it is disrupted, e.g. loss of maintenance, intuitively, constitutes a functional maintenance stage. The precise window of the maintenance phase is also unclear. It is assumed maintenance begins when eye-specific refinements are complete at P12 (Demas et al., 2006), but its end is not known. This work will specifically examine eye-specific segregation, not the fine synaptic contacts of RGC terminals onto geniculate cells. However, eye-specific segregation is linked to these refinements and is a useful tool for understanding visual development.

Eye-specific segregation in mice parallels early retinogeniculate refinement at the synaptic level. In normal mice, the bulk of coarse eye-specific segregation (P7-P15) roughly corresponds to the reduction in the geniculate relay cell binocularity (Ziburkus and Guido, 2006). Over the same time period, the total number of inputs refine from >10 to 2-4 (Guido, 2008; Jaubert-Miazza et al., 2005; schematized in Figure 1.8C). Further refinement and strengthening of these inputs occurs after eye-opening (Chen and Regehr, 2000; Hooks and Chen, 2006). Other manipulations of retinal activity indicate a close relationship between eye-specific and synaptic level refinement. Interestingly, chronic

dark rearing elicits only modest change in retinogeniculate synaptic refinements (Hooks and Chen, 2006) and no change in eye-specific refinement (Demas et al., 2006). However, if mice are reared in normal light-dark cycles and then held in the dark shortly *after* eye opening, the so-called "delayed dark rearing" paradigm, the retinal inputs onto geniculate cells regress by increasing number and decreasing strength (Hooks and Chen, 2006, 2008). Unfortunately, eye-specific segregation was not assessed in these mice. However, examining the eye-specific segregation of aged mice with complete photoreceptor loss after eye-opening would constitute a similar scenario. Moreover, this experiment may help outline the critical period of eye-specific maintenance. Work in ferrets also indicates a correlation between eye-specific segregation and synaptic refinement. TTX treatment just before eye opening weakens normal refinement and development of retinogeniculate synapses (Hooks and Chen, 2006). Chronic TTX treatment delays the bulk of projection refinement (Cook et al., 1999). Furthermore, after TTX geniculate relay cells exhibit decreased NMDAR subunit composition switching, a hallmark of retinogeniculate synaptic maturation (Ramoa and Prusky, 1997). Even without the influence of altered activity, eye-specific segregation reflects synaptic maturation. In complement protein C3-/- mice, with normal retinal activity, impaired eye-specific segregation is clearly associated with limited synaptic refinement (Stevens et al., 2007). Thus it appears that eye-specific segregation patterning not only sets the stage for synaptic level refinements, it also mirrors them. Furthermore, both are sensitive to manipulations that perturb retinal activity. In this way, eye-specific segregation of early afferents be can used a means to understand what factors direct early synaptic refinement.

Reinforcing synapses with activity: The Hebbian hypothesis

How can a particular aspect of activity be important for synaptic refinement, and in particular something like map formation in the visual system? Donald Hebb first proposed the theory of activity-driven reinforcement as a model of associative learning in the 1940s (Hebb, 1946). The Hebbian mechanism posits that if a presynaptic cell frequently excites a postsynaptic cell, that connection will be strengthened. Conversely, if a presynaptic cell does not excite a postsynaptic cell, that connection will deteriorate. Thirty years later, Gunter Stent (1976)(Constantine-Paton et al., 1990) framed the "Hebbian" mechanism for the visual system: synchronous inputs onto a single cell will be reinforced whereas asynchronous inputs will be eliminated. In short, correlated inputs that *fire together* will eventually *wire together*. In the case of the LGN, RGCs from the same eye will reinforce and thus specify synapses on the same cells. Spatial-temporal correlated activity provides a very accessible method of reporting relative spatial locations to central targets. Spontaneous waves of activity traverse the retina and concurrently excite near-neighbor cells. Such activity would telegraph the relative position of RGCs in the retina and sharpen retinotopic maps in retinofugal targets. If, for instance, waves are sufficiently isolated in time, as they are in stage II waves, the probability that two eyes would fire simultaneously is very small. RGCs from the same eye are far more likely to synchronize their firing onto geniculate relay cells (Meister et al., 1991; Wong et al., 1993). Therefore, in theory spontaneous retinal activity can drive map formation, synaptic refinement, and specificity.

In practice, however, an ongoing debate has formed regarding whether activity is indeed "instructional", where the Hebbian mechanism prevails (Crowley and Katz, 2000), or simply "permissive", thus necessary but not sufficient. In one extreme, the

instructive retinal activity could be modulated in a dose dependent fashion to proportionately modulate segregation of eye-specific afferents (Feller, 2009). At the other extreme, the presence of activity is only coincidental with several activity-independent biological events that determine eye-specific segregation (favored by (Chalupa, 2009), a permissive role. Indeed this is a feasible explanation for delayed refinement followed by recovery (Warland et al., 2006; Muir-Robinson et al., 2002; Cook et al., 1999). An effective counterpoint to this argument would be to alter activity after refinement, as in the *nob* mouse (Demas et al., 2006). More convincing would be to tightly correlate improper activity with improper eye-specific segregation across several time points, but with a temporary eye-specific recovery accompanied by normal activity. In this way, the normal progression of cellular events would be decoupled from activity modulation. Activity would then be the critical driver of eye-specific segregation. Given the preponderance of evidence in support of the role of activity it is also possible that a particular kind of activity, when titrated, could drive an organic mechanism (Nicol et al., 2007). That particular activity parameter, or combination thereof, has not been clearly identified.

During a retinal wave, RGCs fire in a spatially correlated manner (Wong et al., 1993; Meister et al., 1991). Therefore, an RGC is more likely to fire with near neighbor RGCs, thereby exciting the same region of retina. Retinal wave impulses have been shown to transmit from retina to LGN (Mooney et al., 1996). In an *in vitro* preparation that preserves the optic tract and retinogeniculate synapses (Chen and Regehr, 2000), stimulation of the optic tract elicits postsynaptic currents in geniculate cells. As early as P3, relay cells exhibit strong depolarization after OT stimulation (Jaubert-Miazza et al.,

2005). These depolarizing responses consist of a sodium upstroke, a T-type calcium current, and a "plateau potential" generated by L-type calcium channels (Lo et al., 2002). This plateau potential generates an influx of Ca^{2+}, which is capable of transducing several intracellular signaling cascades. These cascades could directly modulate cellular events, such as channel insertion or phosphorylation (Barish, 1998), or activate transcriptional regulatory elements like CREB (Kornhauser et al., 2002). Indeed decrements of CREB lead to severely impaired eye-specific refinement (Pham et al., 2001). Other possible candidates for transcriptional binding include the Ca^{2+} channel (Cav2.1) terminals themselves (Gomez-Ospina et al., 2006). While direct intracellular cascades are thought to be important, the expression of Npas4, a determinant of inhibitory cell fate, is directly linked to depolarization and independent of known intracellular activators (Lin et al., 2008b)

The Hebbian mechanism suggests that synchronous activity is critical for synapse specification. Surprisingly, manipulations that abolish strictly correlated activity indicate the correlation alone is not necessary for eye-specific segregation in ferrets (Huberman et al., 2003). Therefore, the search for refinement-critical activity patterns now focuses on parameters that can sufficiently depolarize postsynaptic cells. For example, Torborg (2005) demonstrated that high frequency firing (>10Hz) coupled with immediately synchronous (within 1ms) firing of two cells corresponds to normal eye-specific refinement in mice. In this case, the exact correlation is not critical, rebutting Huberman (2003), and rather a Hebbian substrate is still present. However, even the 10Hz threshold is not steadfast and has been scrutinized by Chalupa (Sun et al., 2008b). Other suggested parameters provide a means of synchronous firing (Sun et al., 2008b). The high percent

of total spikes within in a burst increases the likelihood that two cells will fire together in a wave. The peak burst frequency reflects the potential for exciting postsynaptic cells during a wave. The overall firing frequency and firing frequency within a burst also increase the probability of sufficiently and synchronously depolarizing a postsynaptic cell. Finally, the degree of correlation may provide a threshold of spatially and temporally correlated activity necessary for refinement.

Further complicating matters is that at any stage in segregation, the type of activity that is responsible for proper developmental progress may be different. Indeed, there are qualitative changes in spontaneous retinal activity (Demas et al., 2003) suggesting the activity parameters vary across all stages of eye-specific refinement. Interestingly, stages of retinal activity appear to roughly match stages in retinogeniculate refinement. Stage I waves correspond to the inward growth of RGC axons toward central targets. Consistent with a role for activity during axonal ingrowth, periodic depolarization of RGCs *in vitro* is required for EphA mediated repulsion (Nicol et al., 2007). Stage II waves correspond to the eye-specific segregation phases in the LGN of both the mouse and ferret. Stage III waves correspond to ON-OFF laminar segregation in ferret LGN (Myhr et al., 2001; Wong and Oakley, 1996) and fine synaptic refinement at the retinogeniculate synapse (Hooks and Chen, 2006). Though mice do not have laminar ON/OFF segregation in the LGN, they do possess ON center and OFF center receptive fields with center-surround opponency (Stone et al. 1993). This design of receptive fields sharpens responses in the visual system and improves acuity. Stage II waves may supply activity impulses to oligodendrocytes for myelination (Demerens et al., 1996). In stage III waves, ON RGCs fire before OFF RGCs (Kerschensteiner and Wong, 2008). This pattern

of firing separately reports ON and OFF circuitry and may reinforce the ON and OFF pathway development (Lee et al., 2002). Amazingly, β2-/- mice with early onset of stage III waves develop ON/OFF laminae in the LGN (Grubbs et al., 2003). Finally, the maintenance phase corresponds to the onset of normal visual activity sometime after P12. Alterations in normal developmental activity timing or quality may perturb segregation (Demas et al., 2006), lengthen the critical window synaptic refinement (Hooks and Chen, 2006, 2008), or perhaps do nothing at all (Huberman et al., 2003; Torborg et al., 2005).

These issues surrounding activity, activity timing, and activity-organic interactions remain unresolved for eye-specific development. Therefore, studies that can tightly correlate activity phenotypes to eye-specific phenotypes, perhaps across several ages, would reveal stage-critical features of activity. The roles of vision or activity have not been addressed at all in aged animals. For development and aging, understanding how activity influences retinofugal pathways will be valuable in evaluating the underlying mechanisms of circuit formation and maintenance.

ABSTRACT FOR CHAPTERS 2 AND 3

Abnormal retinal activity in Gβ5-/- mice correlates with disruptions in eye-specific segregation in the dorsal lateral geniculate nucleus

Eye-specific segregation of retinal axon terminals is a model for topographic specificity in sensory systems. In the mouse retinogeniculate pathway, RGC axon terminals from each eye occupy distinct eye-specific region in the dLGN. Alterations in retinal activity disrupt segregation and maintenance of established segregation. β2-/- mice, which lack normal cholinergic retinal activity, have abnormal refinement of eye-specific projections. *nob* mice, with abnormal rhythmic activity after eye-opening, fail to maintain eye-specific segregation. Whereas both β2-/- and *nob* studies correlate abnormal activity with abnormal segregation in single stages of retinogeniculate development, there has been no report of abnormal-normal-abnormal segregation in the face of abnormal-normal-abnormal retinal activity. Such an observation would strongly suggest activity is instructive for eye-specific refinement. We assessed the retinal activity of Gβ5-/- mice, which are deficient in R7RGS protein. Gβ5-/- mice have a lower frequency of stage II spontaneous retinal waves, *normal* transition from stage II to stage III waves, and less correlated stage III waves. Gβ5-/- mice also exhibit a no b-wave phenotype, indicative of abnormal visual transmission, and abnormal retinal activity after P14. With intravitreal injections of fluorescent dye-conjugated cholera toxin B, we can simultaneously visualized projections from both eyes. We show that Gβ5-/- mice have both refinement and maintenance phenotypes. Though similar to Gβ5+/+ at P3, by P7 Gβ5-/- mice exhibit elevated overlap of eye-specific projections. By P10, animals refine to Gβ5+/+ levels. At P12, however, Gβ5-/- mice halt refinement and remain de-segregated as late as P28,

similar to *nob* mice. Crossing *nob* mice with Gβ5-/- does not increase the overlapping areas, suggesting there is a limit to the degree of desegregation in animals with maintenance failure. Refinement and maintenance of Gβ5+/- dLGNs is normal, even in the face of early abnormal activity. First, these results suggest that Gβ5 is critical for normal function of RGCs after postnatal development. Second, these results support an instructive role for activity in eye-specific refinement and early maintenance, but do not identify a particular parameter responsible. Based on the titration of Gβ5+/- activity, it appears a threshold of activity may be necessary to achieve an instructive role.

CHAPTER 2

Gβ5 is required for normal spontaneous retinal activity

Introduction

During development, spatially and temporally correlated activity, called spontaneous retinal waves, traverses the retina and depolarizes retinal ganglion cells (RGCs). This activity is critical for normal visual development. Improper retinal activity during development can interfere with normal eye-specific segregation of retinal inputs (Bansal et al., 2000; Rossi et al., 2001), receptive field formation (Grubbs et al., 2003), and maintenance of proper connections in lateral geniculate nucleus (Demas et al., 2006). In other regions abnormal retinal activity during development alters retinotopic arrangements in both the superior colliculus (Triplett et al., 2009; McLaughlin et al., 2003) and visual cortex (Cang et al., 2005).

Normal spontaneous retinal activity passes through three stages and each stage is characterized by the dominant neurotransmitter (Huberman et al., 2008; Syed et al., 2004). Before P2, gap junctions mediate stage I retinal waves. Between P2 and P10, acetylcholine from cholinergic starburst amacrine cells (SACs) drives stage II retinal waves. After P12, glutamate drives stage III waves until photoreceptor-driven visual activity emerges at P14, approximately eye-opening, and waves subside. Although not restricted to any particular stage, synaptic regulation by GABAergic influences also shapes activity over development (Syed et al., 2004). In stage I and early stage II, GABA activates a depolarizing current. In stage II, tonic GABA hyperpolarizes SACs (Wang et al., 2007). However in RGCs, GABA conductance can shunt activating currents,

decreasing excitability, as well as decrease correlative firing (Wang, 2007). As the retina matures, chloride reversal potential eventually flips, rendering GABA activation inhibitory. As an inhibitory influence, $GABA_A$ regulates the precise timing of ON and OFF cell firing in stage III waves (Kerschensteiner and Wong, 2008) and provides inhibition for normal retinal processing (Ackert et al., 2009; Eggers et al., 2007; Renteria et al., 2006).

Efforts to elucidate the molecular mechanisms that generate and regulate stage II waves have established a foothold on some dominant driving forces and modulators. Raising cAMP concentration by activating adenylate cyclase (AC) with forskolin decreases the interwave interval (increases the frequency of waves) (Stellwagen et al., 1999; Torborg et al., 2005). Conversely, inhibiting AC with SQ22536 increases the interwave interval (Stellwagen et al., 1999). In ferrets, inhibition of PKA with Rp-cAMP also increases interwave intervals, implicating PKA in the intracellular machinery of stage II waves (Stellwagen et al., 1999). Furthermore, in rats separate dopamine, adenosine, and forskolin application induce increases in PKA activity (Dunn et al., 2006). Zheng et al (2006) showed that SACs form a transient network that oscillates and drives RGC firing during stage II waves. Consistent with the notion that PKA is an intracellular mediator of retinal waves, they further demonstrated that cAMP levels regulate the rate of oscillations in developing SACs (Zheng et al., 2006). While cAMP dynamics regulate spontaneous retinal waves, PKA oscillations also drive normal eprhinA repulsion responses in RGC axons and may be critical for other developmental processes (Nicol et al. 2007).

However, new avenues to investigate spontaneous retinal waves are scarce because studies in the inner retina present major challenges. In particular, complex circuitry and multiple cell types limit the resolution of studies of inner retinal activity. First, pharmacological manipulations are coarse and rely on the specific localization of receptors, reagent specificity for receptors, and reagent purity to arrive at interpretable data and firm conclusions. For example, pharmacological studies with reagents targeting adenosine receptors produce conflicting results in our understanding of stage II waves. Application of aminophilline, an A2 adenosine receptor antagonist, varies in its effects depending on the concentration used. At high concentrations (>200μM), it hyperpolarizes RGCs and blocks retinal waves, presumably by direct $GABA_A$ activation (Wang et al., 2007). At low concentrations (<2μM) it makes RGCs more excitable and increases retinal wave frequency, presumably by activation of AC through A2 receptors. A2 receptor antagonists increase wave frequency yet adenosine deaminase treatment, which decreases extracellular adenosine concentration, blocks waves. Second, in the developing retina there are many cell types (Ohsawa and Kageyama, 2008). Of these cells, two are known to participate in spontaneous retinal activity in stage II: RGCs and SACs. Many pharmacological treatments are not restricted to a particular region or cell type. Therefore, the above manipulations that modulate cAMP or adenosine do so in RGCs, SACs, and likely other retinal cell subtypes. Third, while many pharmacological reagents exist, such studies can only assess roles at targets for which there are specific reagents. Alternatively, targeted genetic manipulations offer a useful means to discover other relevant players spontaneous retinal activity, notably in regard to cAMP. AC1 and AC8 *barrelless* knockout mice have already uncovered the possibility that multiple ACs

regulate cAMP levels in RGCs during spontaneous waves (Dunn et al., 2009). Therefore, we propose a similar approach to address new potential players, this time targeting a downstream regulator of G-protein signal timing: Gβ5.

The fifth member of the heterotrimeric G-protein beta family, Gβ5, is unique because its structure allows it to bind and stabilize R7RGS proteins (consisting of RGS6, 7, 9, 11) that regulate Gαi/o signaling. By accelerating GTP hydrolysis, R7RGS proteins control the timing of certain G-protein coupled processes *in vivo* (Krispel et al., 2006) and *in vitro* (Hooks et al., 2003). R7RGS activity has been shown to regulate signaling in modified dendrites (the outer segment of rod photoreceptors) and dendritic processes. One member of the R7RGS family, RGS9-1, is necessary for normal rod photoreceptor responses, while two other members, RGS7 and RGS11, for bipolar cell light responses (Chen et al., 2010; Mojumder et al., 2009; Zhang et al., 2010). It is possible that R7RGS proteins mediate other activity in additional locations in the retina, particularly the inner plexiform layer (Rao et al., 2007; Song et al., 2007), which has high synaptic density. Gβ5 binds R7RGS proteins at a G-gamma like domain and this protein/protein interaction is crucial for their intracellular stability. The loss of Gβ5 destabilizes R7RGS proteins but not their messenger RNAs, presumably through a post-transcriptional mechanism involving protein degradation (Chen et al., 2003). Interestingly, Gβ5-/- mice exhibit malformed triadic synapses in the OPL and the absence of b-waves on ERG (Rao, 2007). Gβ5 is found in the early postnatal retina (Rao et al., 2007). Moreover, Gβ5-/- mice can be used to survey the role of R7RGS activity, particularly periodic activity such as what is seen in spontaneous retinal waves. R7RGS activity regulates D2R signaling in the striatum (Cabrera-Vera et al., 2004) and cAMP levels in ventral tegmentum (Rahman

et al., 2003). R7RGS activity has not been tested in the inner retina during postnatal development.

Another model germane to spontaneous retinal activity is the *nob* mouse. *nob* mice are particularly interesting with respect to Gβ5 -/- mice because they also have a no b-wave phenotype. The first to be discovered in a screen for ERG no b-wave mutants, they exhibit the no b-wave phenotype seen in human congenital stationary night blindness (Pardue et al., 1998). The *nob* mouse has a naturally occurring 85 bp deletion in the *Nyx* gene (Gregg et al., 2003), encoding a large extracellular protein called nyctalopin, and is found at the tips of bipolar cell dendrites (Demas et al., 2006; Gregg et al., 2007). The *Nyx* mutation prevents normal outer plexiform layer signaling, resulting in the no b-wave ERG phenotype. *nob* mice have persistent spontaneous retinal activity after eye-opening (Demas et al., 2006). The activity is notably rhythmic and robust relative to wild-type activity after eye-opening. Finally, adult *nob* mice also have abnormal ON and OFF retinal responses (Demas et al., 2006; Gregg et al., 2007). Nyctalopin is found in bipolar cells and the inner plexiform layer in the retina (Gregg et al., 2007). Transgenic expression of EYFP-tagged nyctalopin using GABAcρ promoter directs the expression of the fusion protein to outer plexiform layer and specifically to dendritic terminals of depolarizing bipolar cells. When this transgenic line is mated into the *nob* background, it rescues all observed phenotypes (Demas et al., 2006; Gregg et al., 2007), thus identifying the cellular locus critical for the observed *nob* phenotypes. However, the exact reason why *nob* mice have persistent and robust retinal waves remains unclear.

Using multielectrode array recordings, we investigated the role of Gβ5 in spontaneous retinal activity during postnatal development. Stage II waves in Gβ5 knockout mice are Ach-mediated but have a prolonged interwave interval. This phenotype is also seen in Gβ5 +/- retinas. Animals lacking individual R7RGS proteins were also tested (RGS6, 7, 11) and do not exhibit the IWI phenotype. In Stage III waves, Gβ5 -/- and Gβ5+/- were de-correlated at P12. Gβ5 +/- retinas approach wild-type activity by P14. Gβ5 -/- retinas retained abnormal activity as late as P28. Given the resemblance of their no b-wave ERG phenotype to the *nob* mouse, we predicted that Gβ5 knockout mouse retinal functions would provide clues into the abnormal function of *nob* retinas. Therefore, in an effort to uncover other roles for Gβ5 in inner retinal activity we crossed *nob* and Gβ5-/- mice. We find that Gβ5 is not responsible for the persistent periodic firing seen in *nob* retinas. Instead, Gβ5 appears critical for RGC firing properties. Furthermore, at P28 Gβ5-/- retinas begin to exhibit their own rhythmic activity as rhythmic activity in *nob* and *nobx*Gβ5-/- retinas diminish. We conclude that Gβ5 plays a critical role in inner retinal signaling during postnatal development and is required for normal spontaneous retinal activity. Moreover, by comparing Gβ5-/-, *nob*, and *nobx*Gβ5-/- activity patterns, we speculate that persistent rhythmic activity may be a hallmark of animals with no ERG b-waves.

Methods

Animals and Genotyping

Gβ5-/- mice were bred by mating Gβ5+/- x Gβ5+/- to ensure littermate heterozygote alleles and wt controls. *nob* mice were produced with a similar mating scheme on a *nob* background. Mice were maintained in 12hr/12hr light/dark conditions

Figure 2.1- Genotyping Methods are shown. *Above:* Conditions, primers, and sequences were used for all genotyping for experiments in this dissertation. *Below:* Representative genotyping gels for Gβ5, *nob*, ΔCT, P35, and TG9N. Ladders indicate sizing.

Genotype	Conditions and Comments	Primer	Sequence
Gβ5	JC64	Neo3	cggcgaggatctccgtcgtga
		Gb5WT10	actctcttcgtggttagaggc
		Gb5SA1	aagagggacaggcggtagag
nob	JC62 and precipitated DNA	Nob- f	cggccttcgacaatctcttcc
		Nob-r	aggaagaaacctggctgggaaa
P35	JC64	Rh1.1	tcagtgcctggagttgcgctgtggg
		P35-r1	cgctgccatttggcaacttacccg
TG9N	JC64	Rgs9-1	atgacgatccgacaccaagg
		3ms9	ggcgtctgaaatcggtagag
ΔCT	JC64	Rh2	tgggagatgacgacgcctaa
		Rh3	tgagggaggggtacagatcc

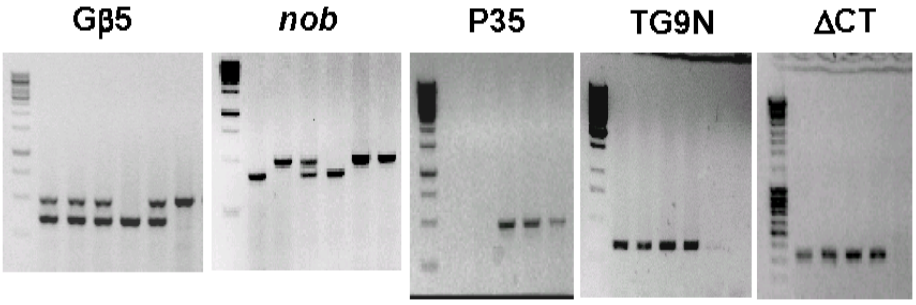

Figure 2.1

and all experiments followed VCU IACUC protocols for safety and humane animal care. Animal tails, digested in ddH20:DirectDigest (Los Angeles, CA, 1:1), were the DNA source for genotyping (described above). DNA for *nob* genotyping was digested in proteinase K: SDS tail buffer (1:1). DNA was precipitated using 1:10, high salt (8M acetate):digest followed by 1:2, digest:alcohol. Preciptiated DNA was removed with a burnt pipette and stored in TAE/EDTA buffer. Animals were considered P0 on the day of their birth.

Genetic manipulations can be grouped into three general categories, all of which are used in the following studies: spontaneous mutations, transgenic expression, and targeted mutation. Spontaneous mutations occur naturally and can contain a single mutation, as seen nycaloptin (*Nyx)* gene in the *nob* mouse. Transgenic expression requires a construct of the gene of interest driven by a promoter that can either globally overexpress the transcript (perhaps a CMV promoter) or expresses foreign protein in a particular cell type. The latter requires the promoter for a protein/gene that is restricted to a particular cell type, like rhodopsin in rods. After injection into embryonic stem cells, this construct then randomly incorporates into the DNA, presenting the possibility of multiple gene copies within a cell and a subsequent increase in the protein of interest. Targeted mutations are far more difficult to obtain. In these a gene can be deleted or replaced in the natural locus using a construct where wild-type DNA sequences flank a region of modified DNA. The homology of the wild-type sequence allows the construct to preferentially incorporate in the natural locus. For instance, a knockout animal can have a targeted Neomycin cassette replace a particular exon. Ideally, this could create 1) a missense or nonsense transcript in the gene of interest, which may not be translated, or

2) abnormal translation product, which would be quickly degraded. A knock-in construct would replace the wild-type gene with some of other construct, perhaps a specifically mutated gene. In contrast to the transgenically regulated genes, which are artificially driven, the endogenous transcriptional machinery regulate targeted genes.

In each genetic manipulation, genotyping can be used to amplify specified stretches of DNA that are unique to each animal allele. In this way one can identify an animal with a spontaneous allele, a transgenic incorporation (P35, or ΔCT under the Rho1.1 promoter specifying rods), or a knockout allele (as with Gβ5). The genotyping conditions are listed (Figure 2.1) as well as representative genotyping gels.

Immunohistochemistry

Animals were euthanized by CO_2. The superior aspect of the cornea marked with a heated needle and the whole eye removed. Eyes were then fixed in 4%PFA/PBS for 1hr and then cryoprotected in 30% sucrose/PBS. After embedding in TBS (Triangle, NC), eyes were section at 10-15mm on a cryostat at -24C. Sections were dried overnight, rehydrated, and prepared for indirect immunohistochemistry. Sections were incubated overnight with primary antibodies, washed 3x with PBS, incubated for 2-4 hours in secondary, washed 5x with PBS, and sealed with Prolong Gold with DAPI (Invitrogen). Primary and secondary incubations were in secondary host specific stock solutions (.03%Triton, 5% Normal Serum in PBS). Primary antibodies used: anti-ChAT (1:100 in mouse), anti-Gβ5 (1:500 in goat). Secondary antibodies used: Anti-mouse (1:1000), anti-Goat (1:2000). Fluorescent images were taken with Spot camera on an Olympus E600 microscope.

Western blot analysis

Eyes were removed from euthanized animals and cornea and lens removed to create an eyecup. Eyecup was transferred to PBS solution and the retina separated from the retinal pigment epithelium. Retina samples were homogenized, denatured at 100˚ with denaturing dye, and loaded into a %10 polyacrylamide gel. After samples were resolved by electrophoresis, they were transferred to nitrocellulose membrane and blotted for protein content with the following primary antibodies: anti-Gβ5 (1:500), anti-RGS7/6 (7RC-1,1:500), anti-GAPDH (1:10,000). After 3x PBS wash, membranes were incubated in secondary antibodies conjugated to horseradish peroxidase for 2 hrs: anti-goat (1:2000) and anti-mouse (1:2000). Stock solution was 10% dry non-fat milk/1% Tween/PBS. Blots were visualized using peroxidase developer (Dura, CA) and exposed on Kodak 10.4 developer system (Rochester, New York). Bands were quantified with K10.4 developer system software. The ROI was identified and its area was maintained within each blot. Intensity of each band was normalized to the adjacent background.

Multielectrode Recordings

Mice were dark-adapted for more than 30 minutes before experiments. Mice were then euthanized with halothane, and the eye removed. The retina was extracted in oxygenated (95%/5% O2/CO2) artificial cerebrospinal fluid (ACSF) with glucose (140mM NaCl, 2.5mM KCl, 5 mM CaCl2, 2 mM MgCl2) and maintained by a steady perfusion (1-2ml/min) throughout the experiment. The retina was placed on an 8X8 ITO 60 electrode array (Multichannel Systems, Tubingin, Germany) and secured with a lightly weighted insert filter (Corning, Corning, NY). Retina were allowed to settle for ~1hr before recordings. Recordings were taken for approximately 1.5 hours and electronic raw data was sampled at 25kHz. Drugs (DNQX, APV, and DHβE, Tocris,

Ellesville, MO) were applied through the perfusion system. Light responses (~12,000cd/m2) were manually triggered using an electronic shutter (Orien, Newport, CT). At P7, retinas were considered usable if more than 30 channels (50%) responded over the course of the recording. At later ages, retinas were much quieter (Demas, 2003)(Demas et al., 2006) and the criteria was relaxed to >5 responding cells.

Spike Sorting and Analysis

Spike Sorting: Responding channels were identified during the recording and used as a guideline for available channels. Raw data was band pass filtered 80-3000Hz. Spikes were first identified by threshold (>6σ above noise), where at time 0 their amplitude equal threshold. Individual waveform traces were 1ms before 3ms after meeting threshold amplitude. Spikes were sorted using MCRack window method, which separates cells along several wave components including upstroke, amplitude, decay, and trough. Waveforms with a positive-negative-positive deflection pattern were considered axons and discarded. Consistently identifiable waveforms, between 5-100 per retina depending on age, were then selected for analysis. Spike timestamps and cell locations were then analyzed. *Filtering:* Occasional mechanical noise, occurring on all channels within 2ms, was filtered from coincident timestamp data using Neuroexplorer 4.0 (Plexon, Denton, TX) and custom NexScript program. *Wave counting:* Retinal waves were defined was 4 cells, or 3 adjacent cells, firing more than 1 spike (essentially a burst) after 10 seconds of no wave activity. Waves were counted blind to genotype for continuous, stable 40 minute recording periods. Stability selection within recording was determined by the longest average wave duration during the recording. *Burst Analysis:* Bursts were identified using the surprise method (surprise = 4, bin = 0.1s). At P7, bursts consistently identified waves

(Legendy and Salcman, 1985). Briefly, the surprise method assumes all spikes are Poisson (independent of each other), thereby establishing a distribution of normal interspike intervals, a Dp-mean. The surprise parameter reflects a selected threshold of interspike interval over which spikes are considered outside of a burst. When a spike appears, the program searches for the next spike until the Dp-mean determines no more spikes will likely occur based on the "surprise" parameter. If a spike appears within that interval, it is added to the burst. From spike two, the algorithm begins again. If the interspike interval is greater than what is predicted by the surprise parameter, the burst is at an end and the algorithm searches for the beginning of the next burst. *Correlation Analysis:* Spatial and temporal correlation, CI, between two cells A and B was calculated with the following formula: CI = Nab x T/(Nat x Nbt x 2 x b)(See (Wong, 1993; Demas, 2003); where CI is the correlation coefficient, Nat is the number of spikes cell A (the reference cell) fires in time t, Nbt is the number of spikes cell B fires in time T, T is the window of observation for which cell a fires a spike, b is the bin time (10ms), and Nab is number of spikes B fires in a window time b from a given spike in A. Neuroexplorer calculated these values iteratively. The values were then averaged across all time bins for that cell to get the CI. This CI was paired with a distance relative to the reference cell. *Coherenece Analysis:* Coherence analysis was performed with Neuroexplorer and custom Matlab software. Briefly, the coherence, Cxy, between two cells is the product of their power spectra normalized to spectra of auto-comparison, thereby amplifying frequencies with high power in the spectra of both cells. Where Sxy is the power spectra of x over a frequency domain, Syx is the power spectrum of y over the same frequency domain, and SxxSyy is the "auto-spectra" $Cxy = |Sxy|^2/Sxx\ Syy$ (Demas et al., 2006).

Statistics

Statistical tests were performed with JMP 7.0. A variety of statistics were used to match the appropriate statistical test for the comparison conditions. Measurements comparing animals (interwave interval, wave duration, quantification of immunoblots, peak coherence) employed standard non-parametric tests (Mann-Whitney, Kruskal-Wallis) because of small sample size, and pair-wise comparisons using a Tukey-HSD post-hoc. ST correlation analyses were compared using a generalized linear model (GLM) to compare effects of genotype, distance, and their interactions. Tukey-HSD post hoc tests were performed for pair-wise comparisons between animals. A GLM was again analysis of RGC parameters across all cells within each age group with Tukey-HSD post hoc tests. Differences were considered significant at $p < 0.05$.

Results

P7 mouse retinal activity has been described previously (Demas et al., 2003; Demas et al., 2006; Wong et al., 1993). At P7, Gβ5-/- retinas exhibit spontaneous retinal activity with markedly diminished overall frequency compared to WT (Figure 2.2, shown in spike rasters and population average firing histograms), a striking observation we wanted to quantify. We assessed the global wave properties of interwave interval and wave duration (Figure 2.4A) by visually inspecting and counting waves over recording sessions. We chose visual inspection for three reasons. First, though stage II waves are periodic, they are not rhythmic in the sense that inter-event times vary up to 20 seconds even in relatively regular firing. This prevents us from effectively employing a tool like coherence analysis, which quantifies rhythmic processes and will be described later. Second, P7 retinal waves occur with duration of 10-15 seconds yet occur less than once

Figure 2.2- Retinal activity is decreased in Gβ5-/- mice at P7. Raster plots of multielectrode array recordings show simultaneously recorded individual cell spike trains. A. Rasters of Gβ5+/+ and Gβ5-/- retinas are shown over 1500 seconds. Condensed rasters use color to indicate firing frequency (black is low, yellow intermediate, red high). B. Raster plots for individual cells over 700 seconds are matched in time with population firing histograms (PFH) representing the average firing of all cells.

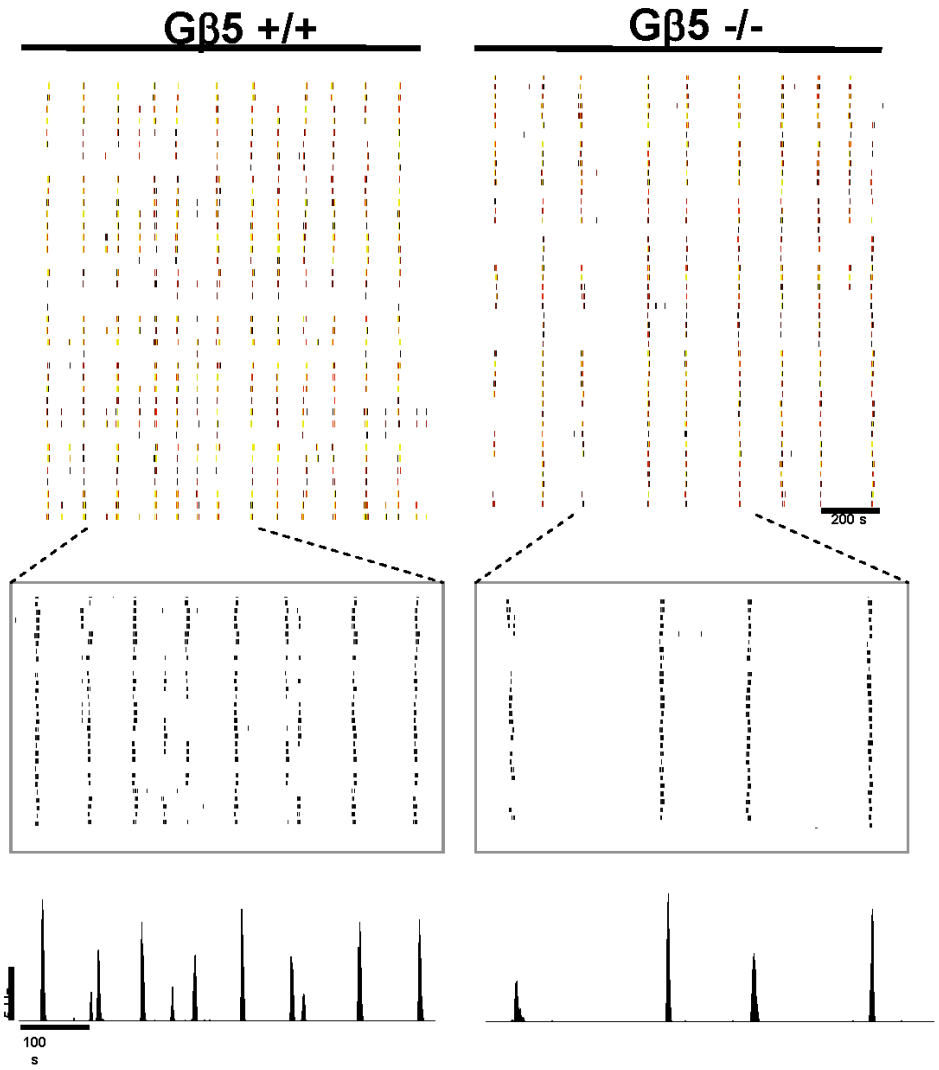

Figure 2.2

per minute, making them temporally sparse. Lastly, stage II waves are robust and identifiable as distinct events (Demas et al., 2003; Demas et al., 2006; Wong et al., 1993). Gβ5-/- retinas exhibit increased interwave intervals (Figure 2.4B, 175s, 77-597 seconds, 9 retinas) compared to Gβ5+/+ (Figure 2.4B, 68s, 59-81 seconds, 5 retinas). Wave duration is not different between groups (Figure2.4). Early in our work, we also examined Gβ5+/+ (n=3) and Gβ5-/- (n=3) retinas at P5 and found a similar increased interwave interval in Gβ5-/- retinas (Figure A11). We did not pursue this avenue because little has been reported in the literature at this age that was useful for comparison and animals were scarce.

Normal retinal circuitry exhibits correlative firing (Pillow et al., 2008; Shlens et al., 2009; Shlens et al., 2008) and can be used to assess retinal function (Meister et al., 1991; Wong et al., 1993). Spatial-temporal (ST) correlation of firing measures the likelihood a pairs of cells would fire together in a given window of time (10ms) as a function of their distance from each other. Distances between cells were approximated by the separation of their respective electrode location. The degree of ST correlation in Gβ5-/- and Gβ5+/+ retinas were not different at any distance (Figure 2.4C). Also activity in each condition shows a distance effect and "falls off" within genotypes ($P<0.05$). This fall off indicates a high correlation of near-neighbor cell firing.

We then examined individual retinal ganglion cell (RGC) burst firing statistics, which quantify specific firing parameters. A 'surprise' algorithm (Legendy and Salcman, 1985; described in methods), which incrementally parses spike timestamps and includes them in a burst based on a probability distribution established by the mean frequency of firing for each cell, identified bursts. Bursts were examined by parameters based on

previous studies (Demas et al., 2006; Sun et al., 2008b; Torborg et al., 2005) that would provide clues about retinal circuitry and relate to Hebbian mechanisms. For example, interburst interval intuitively approximates (Figure 2.5A) the interwave interval and can be used to validate our global findings. Percent of spikes in burst elaborates on the source of correlative firing between cells. Several other parameters describe the rates of activity of the RGCs within (mean peak burst frequency or mean burst frequency) or among the bursts (mean frequency and bursts per second). To improve text clarity, numerical values for all burst parameters, all conditions, and at all ages are listed in Table 2.1. Gβ5-/- RGCs have fewer bursts per second and a lower mean frequency of firing compared to Gβ5+/+ RGCs. Both parameters are consistent with the decreased activity measured by visual inspection (Figure 2.5B). Gβ5-/- retinas have an increased interburst interval, which is also congruent with global findings (Figure 2.4B and C). Mean burst duration, peak frequency within a burst, mean interspike interval, percent of spikes in burst, mean frequency in burst, and mean spikes in burst are not different from Gβ5+/+.

As adults, Gβ5+/- mice are similar to Gβ5+/+ in all reported literature (Chen et al., 2003; Krispel et al., 2003). Retinal Gβ5 increases over development (Rao et al., 2007), allowing us to consider the possibility that Gβ5 levels in Gβ5+/- mice may be reduced during development relative to Gβ5+/+. If true, Gβ5+/- retinas could be a useful manipulation to titrate the IWI phenotype seen in Gβ5-/- retinas. In homogenized P7 Gβ5+/- retinas (prepared and quantified by C.K. Chen, n = 3 mice per group, Figure 2.3A), quantitative western blot analysis demonstrates a 39% drop in Gβ5 protein when normalized to total cellular content (GAPDH). Surprisingly, RGS6 and RGS7 were not significantly reduced. The level of Gβ5 remains lower in the Gβ5+/- as late as P14

(Figure 2.3C, Figure A13). Because Gβ5+/- mice have intermediate amounts of Gβ5 at P7, we tried to exploit this 'dosing' as a manipulation in our P7 wave recordings. Indeed, Gβ5+/- retinas also have an increased interwave interval (132s, 73-198seconds, 8 retinas, Figures 2.3C and 2.4B). Like Gβ5-/-, global changes are mirrored by diminished RGC overall activity (mean frequency) and bursts per minute (Table 2.1 and Figure 2.5B). However, Gβ5+/- retinas did not have a statistically increased interburst interval. This phenomenon can be explained by occasional multiple bursts within a wave (seen in third wave of Figure 2.3C). Interesting, Gβ5+/- retinas also have and increased mean frequency of firing within a burst when compared to Gβ5+/+. ST correlation of cell pair firing in Gβ5+/- was also similar to Gβ5+/+ at all interelectrode distances (Figure 2.4C). Together these data indicate that P7 spontaneous activity is altered with decrements of Gβ5.

In an effort to identify the source of the prolonged interwave interval in Gβ5-/- and Gβ5+/- retinas, we tested mutants that lack the individual coupling partners of Gβ5: RGS6, RGS7, RGS11. RGS6 (n = 6 retinas), RGS7 (n = 7) and RGS11 (n = 3) have been reported in the inner retina by our lab and others (Rao et al., 2007; Song et al., 2007; Cao et al., 2008). None manifested the significantly prolonged IWI or increased RGC interburst interval (Figure 2.6 and Table 2.1) seen in Gβ5-/- or Gβ5+/- retinas. However, many mutants exhibited a different cohort of bursting alterations (Table 2.1), possibly reflecting other sources of fine R7RGS regulatory control. In particular, notable increases were seen in the activity of RGS11-/- mice. Though RGS11 is questionably present in the IPL (Song et al., 2007), RGS11-/- RGCs displayed increased mean frequency, peak frequency, spikes in burst, and bursts per second and decreased interspike interval and

Figure 2.3- Gβ5 +/- retinas have reduced Gβ5 and lower overall retinal activity at P7. For this figure all retina were removed, probed and quantified by C-K. Chen A. Immunoblots for this figure were fully performed by C-K. Chen. Immunoblots of homogenized dLGN (1 retina per lane, Gβ5+/- n = 6 animals, Gβ5+/+ n = 8 animals) were probed with antibodies specific for Gβ5 (Gβ5S) and RGS6/7 (7RC-1) epitopes. Loading control is GAPDH and genotypes are indicated above Gβ5S band. *B*. Quantification of Gβ5, RGS6, and RGS7 amount in retina are normalized to GAPDH loading control. Asterisks indicate significant difference between groups (Wilkoxon Rank-Sum, $p<0.05$). C. Raster plot of spontaneous activity in a Gβ5+/- retina.

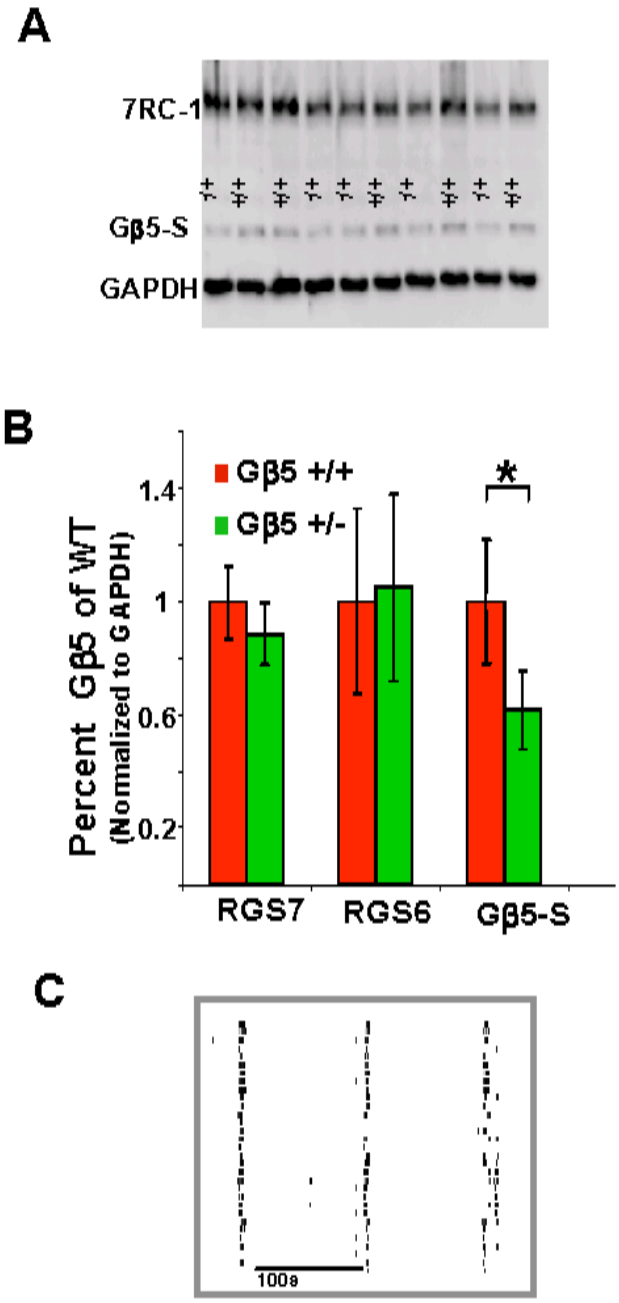
A
7RC-1
Gβ5-S
GAPDH
B
Gβ5 +/+
Gβ5 +/-
*
Percent Gβ5 of WT
(Normalized to GAPDH)
1.4
1
0.6
0.2
RGS7
RGS6
Gβ5-S
C
100s

Figure 2.3

Figure 2.4- Gβ5 -/- and Gβ5 +/- retinas have an increased interwave interval. A. IWI was measured from end of wave to the start of the next wave and wave duration from wave start to wave end. B. Bar graphs of interwave interval and wave duration Gβ5 +/+, Gβ5 +/-, Gβ5 -/-. Each bar represents the mean ± S.E.M for each respective measurement. C. Spatiotemporal correlation measures the likelihood a cell with fire relative to another cell within a narrow time window (100ms) as a function of intracellular distance, here approximated as intra-electrode distance. Each point represents the average cell pair correlation of all retinas within a genotype. Error bars represent ± S.E.M. Asterisks indicate significant differences from Gβ5 +/+. Number of retinas used at P7 are: Gβ5 +/+, n=5; Gβ5 +/-, n=8; Gβ5 -/-, n=9; RGS11 -/-, n=3; SG7, n=7; RGS6 -/-, n=6.

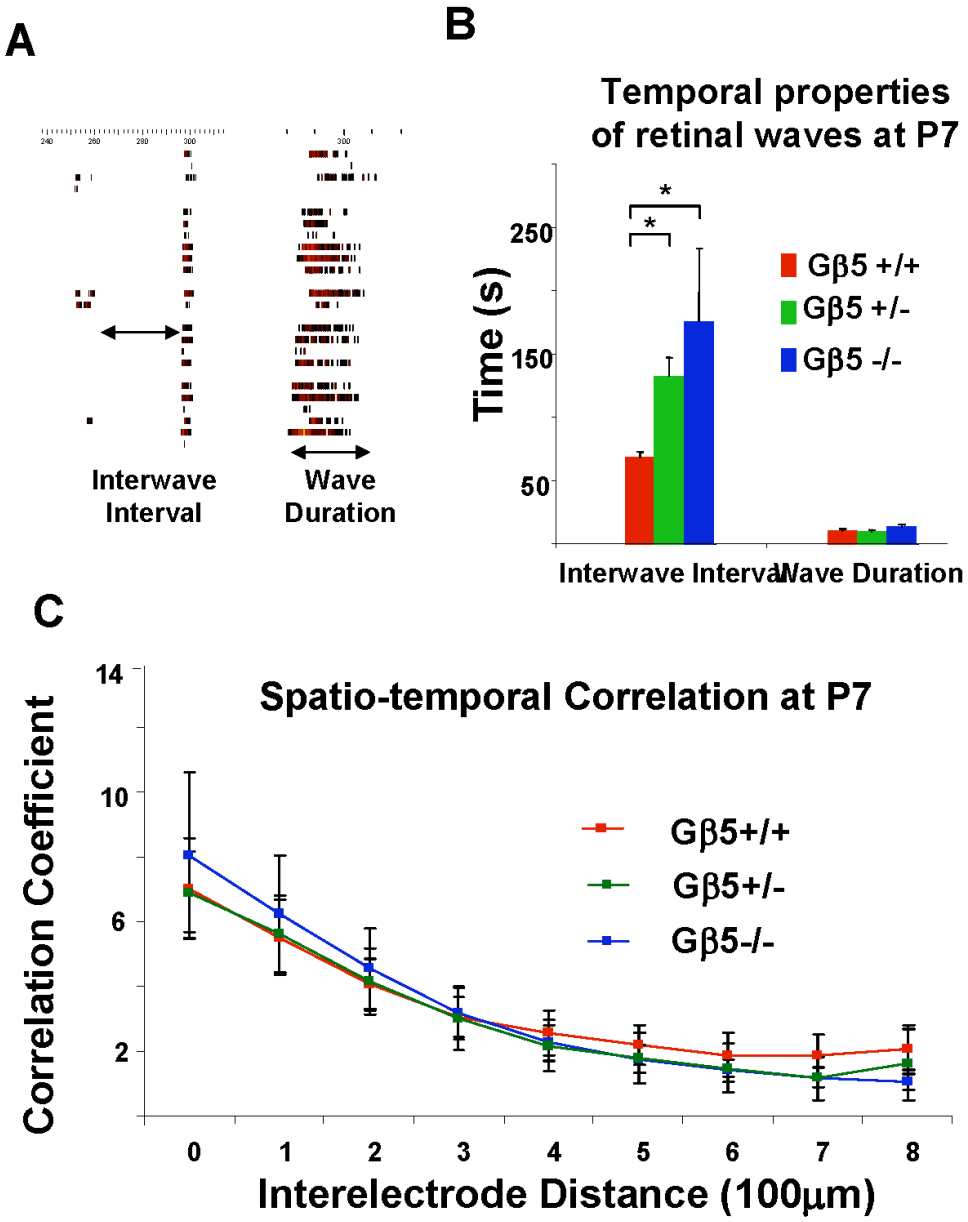
A
B
Temporal properties of retinal waves at P7
Interwave Interval
Wave Duration
Time (s)
250
150
50
*
*
Gβ5 +/+
Gβ5 +/-
Gβ5 -/-
Interwave Interval
Wave Duration
C
Spatio-temporal Correlation at P7
Correlation Coefficient
14
10
6
2
Gβ5+/+
Gβ5+/-
Gβ5-/-
0
1
2
3
4
5
6
7
8
Interelectrode Distance (100μm)

Figure 2.4

Figure 2.5- Gβ5 -/- and +/- RGCs bursts have altered firing parameters at P7. A. Bursts are identified using surprise method and highlighted by blue lines across spikes. Schematic representation of "within burst" parameters are shown in actual burst examples. Peak frequency in burst reflects the maximum instantaneous frequency within a burst. Mean frequency in burst averages the instantaneous frequencies between spikes. B. Global burst statistics are schematically represented. Interburst interval is between bursts of the same RGC. Mean frequency of a single RGC is the sum of all spike timestamps divided by the total recording time. C. Sorted single RGC spike trains were analyzed for burst parameters. Gβ5 -/- and +/- parameters were averaged within genotype and are shown as a percentage of respective average P7 Gβ5 +/+ parameters. Dotted line indicates 100% level of Gβ5 +/+. Asterisks indicate significant difference from Gβ5 +/+. Cells numbers are indicated in Table 2.1 and are from the same number of retinas noted in Figure 2.4.

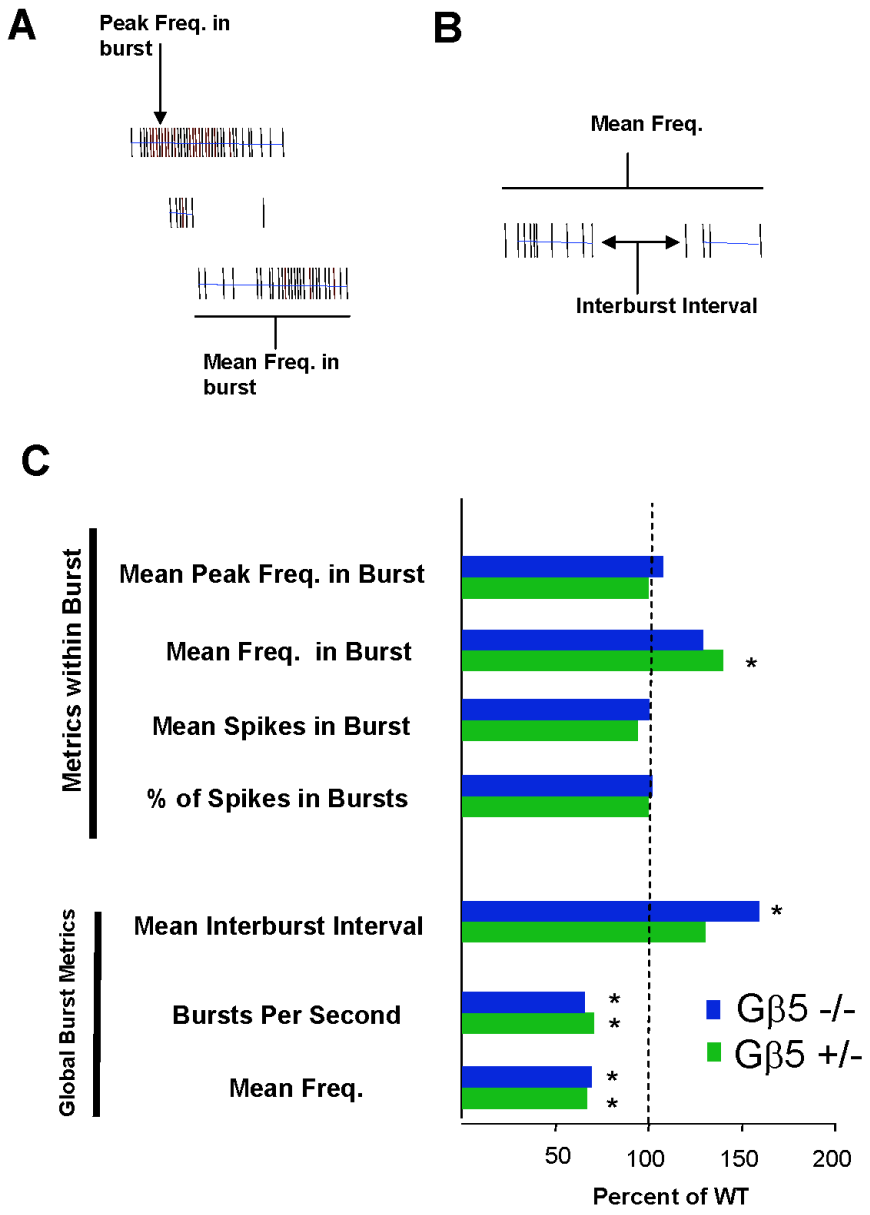
A
Peak Freq. in burst
Mean Freq. in burst
B
Mean Freq.
Interburst Interval
C
Metrics within Burst
Mean Peak Freq. in Burst
Mean Freq. in Burst
Mean Spikes in Burst
% of Spikes in Bursts
Global Burst Metrics
Mean Interburst Interval
Bursts Per Second
Mean Freq.
Gβ5 -/-
Gβ5 +/-
50
100
150
200
Percent of WT

Figure 2.5

Figure 2.6- RGS11 -/-, SG7 mutant, and RGS6 -/- retinas have normal IWI and wave duration. Error bar represents the mean ± S.E.M for each respective measurement. RGS11 -/-, n=3; SG7, n=7; RGS6 -/-, n=6.

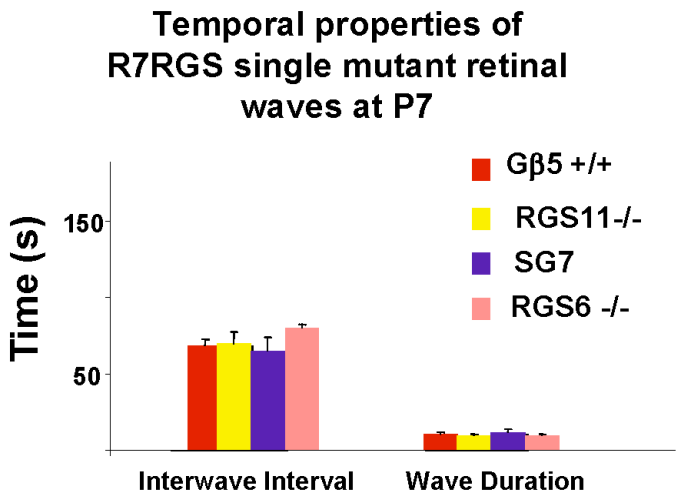
Temporal properties of
R7RGS single mutant retinal
waves at P7
Gβ5 +/+
RGS11-/-
SG7
RGS6 -/-
Time (s)
150
50
Interwave Interval
Wave Duration

Figure 2.6

Table 2.1- Burst Statistics of all measurements are represented as mean ± S.E.M. Parameters statistically different from Gβ5 +/+ are shaded blue. Additional comparisons within age groups are shown.

Burst Parameters of Spontaneously Firing RGCs

P7	Mean Freq.	Bursts Per Second	% of Spikes in Bursts	Mean Burst Duration	Mean Spikes in Burst	Mean ISI in Burst	Mean Freq. in Burst	Mean Peak Freq. in Burst	Mean Interburst Interval	Correl.	Cohere.
Gβ5+/+ (221)	0.207 ± 0.014	0.0058 ± 0.0002	72.77 ± 2.26	2.27 ± 0.88	24.49 ± 1.51	0.141 ± 0.009	9.41 ± 0.45	125.48 ± 7.88	157.95 ± 13. 73		n.t.
Gβ5+/- (304)	0.138 ± 0.009^{e,g}	0.0040 ± 0.0001^{e,f,g}	72.75 ± 1.88^{e,f}	2.60 ± 0.24^{b,f}	23.11 ± 1.30,^{fg}	0.166 ± 0.020^{g}	13.15 ± 1.25^{f}	125.46 ± 6.22^{e,f,g}	205.74 ± 11. 62^{g}	-	n.d
Gβ5-/- (343)	0.143 ± 0.011^{e,g}	0.0038 ± 0.0001^{e,f,g}	74.00 ± 1.60^{e,f}	1.92 ± 0.06^{a,e}	24.59 ± 1.44^{fg}	0.137 ± 0.007	12.15 ± 0.56^{fg}	135.05 ± 6.62,^{f}	251.32 ± 16.82^{e,fg}		n.d
RGS11 -/- (144)	0.410 ± 0.035^{a,b,e,f}	0.0091 ± 0.0003^{a,b,e,f}	79.79 ± 2.24^{f}	1.94 ± 0.08	34.50 ± 2.76^{a,b,e,f}	0.093 ± 0.006^{a}	15.54 ± 0.87^{a,b,e,f}	157.73 ± 9.77^{a,f}	97.84 ± 5.24^{a,b,e,f}	n.d	n.d
SG7 (328)	0.143 ± 0.205	0.0049 ± 0.0044^{a,b,g}	61.45 ± 37.79^{a,b,e,g}	1.70 ± 2.88^{b,f}	16.27 ±18.87^{a,b,e,g}	0.144 ± 0.238	7.96 ± 6.65^{e}	76.68 ± 86.02^{a,b,e,g}	172.18 ± 208.96^{b,g}	n.d.	n.d
RGS6-/- (344)	0.194 ± 0.010^{a,b,e,g}	0.0054 ± 0.0001^{a,b,g}	81.90 ± 1.28^{a,b,f}	2.50 ± 0.10	26.99 ± 1.2^{fg}	0.133 ± 0.006	11.51 ± 0.34^{a,b,fg}	153.34 ± 5.63^{a,f}	186.20 ± 9.47^{b,g}	n.d.	n.d

P12	Mean Freq.	Bursts Per Second	% of Spikes in Bursts	Mean Burst Duration	Mean Spikes in Burst	Mean ISI in Burst	Mean Freq. in Burst	Mean Peak Freq. in Burst	Mean Interburst Interval	Correl.	Cohere.
Gβ5 +/+ (241)	0.726 ± 0.05	0.019 ± 0.001	76.08 ± 1.38	2.078 ± 0.12	25.22 ± 1.23	0.114 ± 0.006	15.63 ± 0.63	183.0 ± 7.5	108.8 ± 7.0	-	-
Gβ5 +/- (272)	0.321 ± 0.02	0.013 ± 0.009	42.84 ± 1.92^{a}	5.912 ± 2.36	9.98 ± 0.53^{a}	0.301 ± 0.072	9.62 ± 0.43	78.0 ± 4.2	123.1 ± 17.0		
Gβ5 -/- (351)	0.327 ± 0.02	0.011 ± 0.001	28.92 ± 1.51^{b}	3.193 ± 1.32	7.04 ± 0.41^{b}	0.206 ± 0.063	10.55 ± 0.51	77.3 ± 4.1	88.1 ± 10.0		

P14	Mean Freq.	Bursts Per Second	% of Spikes in Bursts	Mean Burst Duration	Mean Spikes in Burst	Mean ISI in Burst	Mean Freq. in Burst	Mean Peak Freq. in Burst	Mean Interburst Interval	Correl.	Cohere.
Gβ5 +/+ (213)	0.130 ± 0.05	0.003 ± 0.0002	60.53 ± 2.45	5.11 ± 2.60	12.35 ± 0.99	0.228 ± 0.075	19.84 ± 1.23	126.8 ± 6.74	224.9 ± 18.9	-	-
Gβ5 +/- (132)	0.152 ± 0.02	0.004 ± 0.0005	48.65 ± 0.39^{b,c,d}	2.14 ± 0.74	12.63 ± 1.18^{b}	0.131 ± 0.021	17.66 ± 1.35^{d}	126.2 ± 9.39^{b,c,d}	200.7 ± 22.6^{b,c,d}	d	b,c,d
Gβ5-/- (218)	0.259 ± 0.02	0.008 ± 0.0010	20.78 ± 1.51^{a}	7.56 ± 2.08	6.68 ± 0.55^{a,d}	0.387 ± 0.091	16.28 ± 1.15^{d}	76.2 ± 4.91^{d}	124.5 ± 16.1^{a,c,d}	d	a
nobx Gβ5-/- (145)	0.411 ± 0.14	0.010 ± 0.0039	18.14 ± 3.45^{a}	16.80 ± 6.81	9.30 ± 1.69	1.048 ± 0.494^{a,b,d}	9.97 ± 1.94^{d}	57.6 ± 9.92^{d}	165.3 ± 53.7^{a,b,d}	d	a
nobx Gβ5+/+ (106)	3.178 ± 0.30^{a,b,c}	0.049 ± 0.0057^{a,b,c}	17.74 ± 1.49^{a}	0.42 ± 0.07	11.98 ± 0.70^{b}	0.037 ± 0.007	45.16 ± 1.86^{a,b,c}	211.0 ± 9.31^{a,b,c}	88.1 ± 12.7^{a,b,c}	a,b,c	a

P28	Mean Freq.	Bursts Per Second	% of Spikes in Bursts	Mean Burst Duration	Mean Spikes in Burst	Mean ISI in Burst	Mean Freq. in Burst	Mean Peak Freq. in Burst	Mean Interburst Interval	Correl.	Cohere.
Gβ5+/+ (55)	0.191 ± 0.057	0.004 ± 0.0018	10.59 ± 2.46	15.48 ± 8.35	5.37 ± 1.64	0.485 ± 0.245	9.69 ± 2.40	31.80 ± 7.28	47.9 ± 14.9	-	-
Gβ5+/- (83)	0.101 ± 0.042^{c,d}	0.002 ± 0.0014^{c,d}	33.51 ±3.64^{c,d}	29.29 ± 9.62	16.50 ± 6.23	1.0264 ± 0.264^{c}	17.23 ± 2.47^{d}	74.09 ± 8.80^{b,c,d}	139.8 ± 24. 1^{b,d}		
Gβ5-/- (142)	0.267 ± 0.057^{c,d}	0.005 ± 0.0015^{c,d}	24.21 ± 2.53^{d}	27.62 ± 6.64	11.27 ± 2.32	1.036 ± 0.223^{c}	19.58 ± 2.75^{d}	86.19 ± 8.65^{a,d}	57.8 ± 8.8^{a}		
nobx Gβ5-/- (150)	0.995 ± 0.136^{a,b}	0.015 ± 0.0024^{a,b}	20.25 ± 1.97^{a}	11.47 ± 3.07	13.96 ± 2.14	0.506 ± 0.144^{a,b,d}	32.56 ± 2.80^{d}	119.85 ± 8.43^{a,d}	111.0 ± 16.3		
nobx Gβ5+/+ (112)	1.081 ± 0.174^{a,b}	0.018 ± 0.0040^{a,b}	21.63 ± 2.55^{a,b}	13.73 ± 4.95	16.39 ± 3.10	0.392 ± 0.161^{c}	33.07 ± 3.86^{a,b,c}	103.34 ± 9.20^{a,b,c}	95.0 ± 16.2^{a}		

Averages and S.E.Ms reported were used in the RGC burst parameter bar graphs.
Though these are not normally distributed, averages are reported as to demonstrate relative trends in bursting statistics as median values of the normalizing quantity, Gβ5+/+, are often zero at P28. Therefore averages are used for consistency.
Blue lettering denotes differences from Gβ5+/+ ($p<0.05$).
a, different from Gβ5+/-.
b, different from Gβ5-/-.
c, different from *nobx* Gβ5-/-.
d, different from *nobx* Gβ5+/+.
e, different from RGS6-/-.
f, different from SG7.
g, different from RGS11-/-.
n.d., not determined.

Figure 2.7- Normal pharmacological sensitivity in Gβ5 -/- retinas. Population firing histograms of Gβ5 -/- retinal recordings show cessation of activity after application of pharmacological agents. Frequency scale bar is on the left and horizontal scale bar indicates time. Lines with drug name and concentration represent application. Washout occurs after the line disappears. A. Cholinergic antagonists (DHβE, 20μM) were used at P7. B. Glutamatergic antagonists AMPA (DNQX, 20μM) and NMDA (D-APV) 20μM were applied at P12. At both ages, waves return after washout.

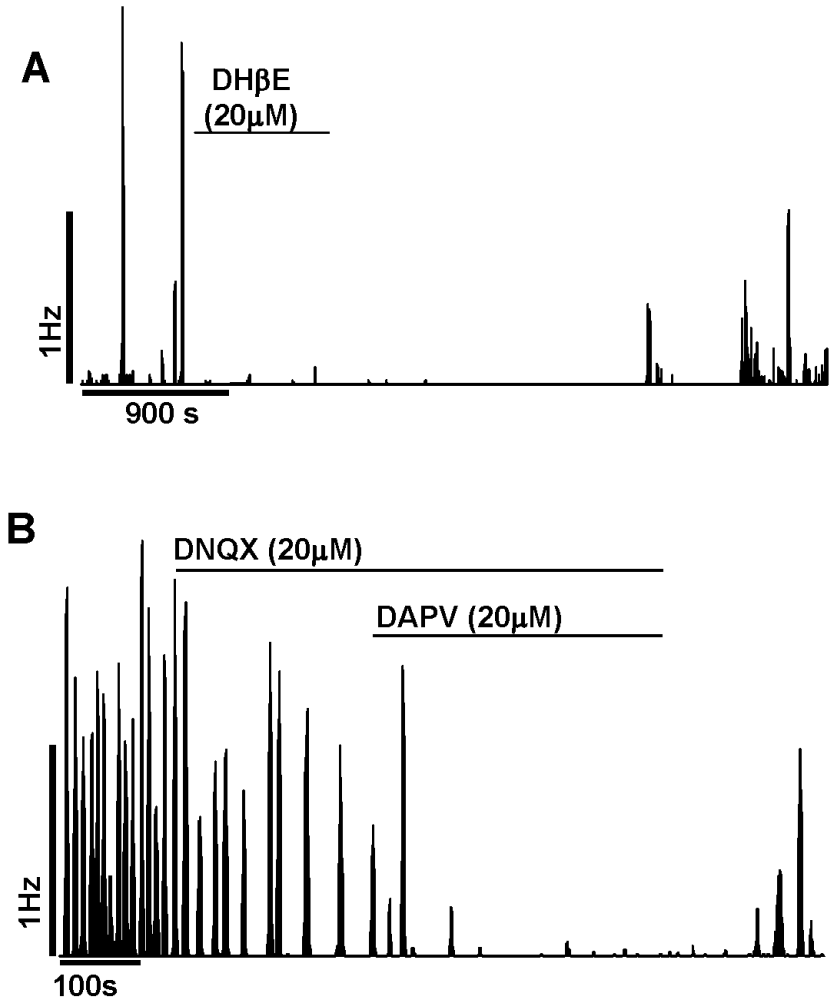

Figure 2.7

interburst interval. Collectively, these results suggest more than one R7RGS is responsible for the interwave interval phenotype seen in retinas lacking Gβ5.

Other models of abnormal spontaneous retinal activity have additional anomalies where gap junction mediated transmission of stage II waves (Stacy et al., 2005; Sun et al., 2008b; Torborg et al., 2004). We asked whether Gβ5-/- retinas had the appropriate pharmacological sensitivities, cholinergic at P7 and glutamatergic at P12, and whether they undergo a timely transmission from stage II to stage III waves. At P7, spontaneous retina waves were blocked by acetylcholine antagonist dihydro-β-erythroidine (DHβE, 20μm) and returned after washout (Figure 2.7A). Similarly, at P12, spontaneous retinal activity is blocked by concurrent application of glutamatergic antagonists for AMPA, 6,7-Dinitroquinoxaline-2,3-dione (DNQX, 20μm), and NMDA, D-(-)-2-Amino-5-phosphonopentanoic acid (APV, 20μm). Again, activity returns after sufficient washout of pharmacological agents (Figure 2.7B). From these experiments, we conclude that Gβ5-/- retinas retain a relatively normal timeline of stage transition and mechanism of neurotransmission for stage II and stage III retinal waves.

We continued to investigate spontaneous activity in Gβ5 alleles at P12, P14, and P28 in an effort to uncover any subsequent changes in retinal activity. At P12, Gβ5-/- retinas (n = 5) have periodic waves that are visibly different from Gβ5+/+ (n = 5 retinas), yet consist of very regular waves of activity (Figure 2.8A). Globally, Gβ5-/- retinas do exhibit a striking phenotype (Figure 2.8B): decreased ST correlation at near-neighbor distances (≤ 300μm interelectrode distances, GLM, Tukey-HSD, $p < 0.05$). We find P12 waves were the result of periodic bursting, with greater rhythmicity than P7, yet too frequent to distinguish one wave from another (Figure 2.8A). Coherence analysis

Figure 2.8- Global retinal activity in Gβ5-/- and +/- is less correlated at near neighbor distances at p12. A. Raster plots of P12 retinal recordings for Gβ5+/+, +/- and -/- show individual cell spike trains. Time scale bar is 20 seconds. B. Spatiotemporal correlation is shown as a function of interelectrode distance. Each point represents the average cell pair correlation of all retinas within a genotype. Error bars represent ± S.E.M. Asterisks indicate significant differences from Gβ5 +/+. Number of retinas used at P12 are: Gβ5 +/+, n=5; Gβ5 +/-, n=5; Gβ5 -/-, n=5.

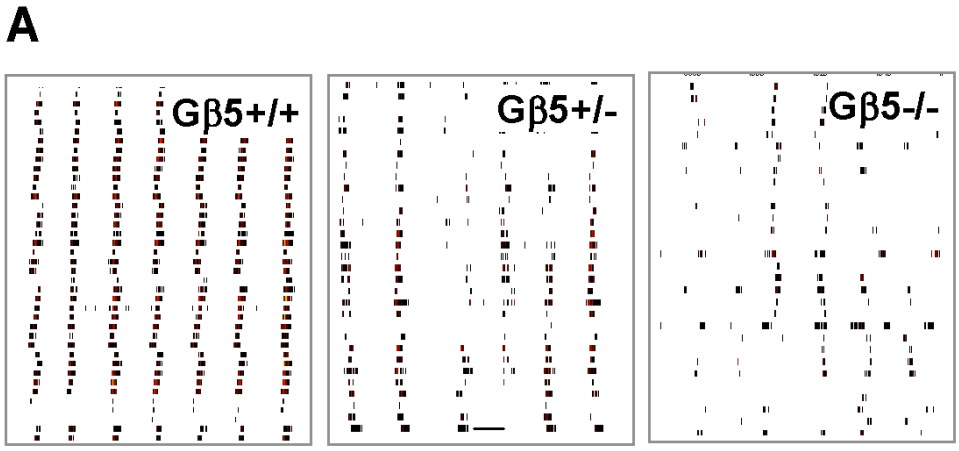
A
Gβ5+/+
Gβ5+/-
Gβ5-/-

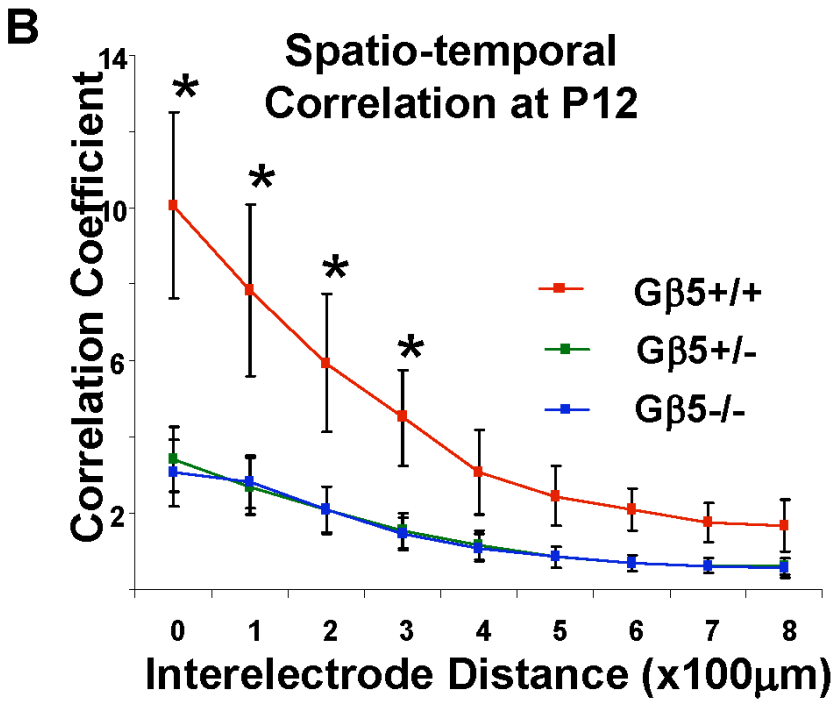
B
Spatio-temporal
Correlation at P12
Correlation Coefficient
14
10
6
2
*
*
*
*
Gβ5+/+
Gβ5+/-
Gβ5-/-
0
1
2
3
4
5
6
7
8
Interelectrode Distance (x100μm)

Figure 2.8

Figure 2.9- Coherence analysis approximations of IWI. Coherence analysis exhibits peaks of firing at frequencies where two cells share high power of firing frequency. Lower abscissa ranges (0.01-1.5Hz) can be used identify slower rhythmic firing frequencies in a retina. We approximate the IWI by determining the frequency at which a peak coherence signal (power/Hz) arises. A. Averaged coherence spectra of Gβ5 +/+, Gβ5 +/-, and Gβ5 -/- at P12 show high power (in watts, W) if two cells fire at a given frequency, independent of phase. Plots are binned at 0.01Hz. B. Peak frequencies, determined by identifying the frequency bin in which the maximum power occurs, are displayed as the mean± S.E.M. No differences were found among the groups (Kruskal-Wallis, Tukey HSD Test, $p<0.05$). This analysis was done on the same retinas as reported in Figure 2.9.

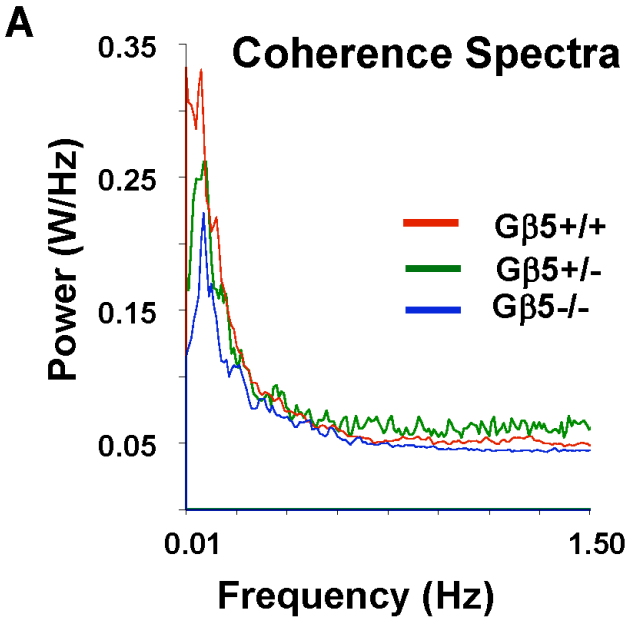
A
Coherence Spectra
0.35
0.25
0.15
0.05
Power (W/Hz)
Gβ5+/+
Gβ5+/-
Gβ5-/-
0.01
1.50
Frequency (Hz)

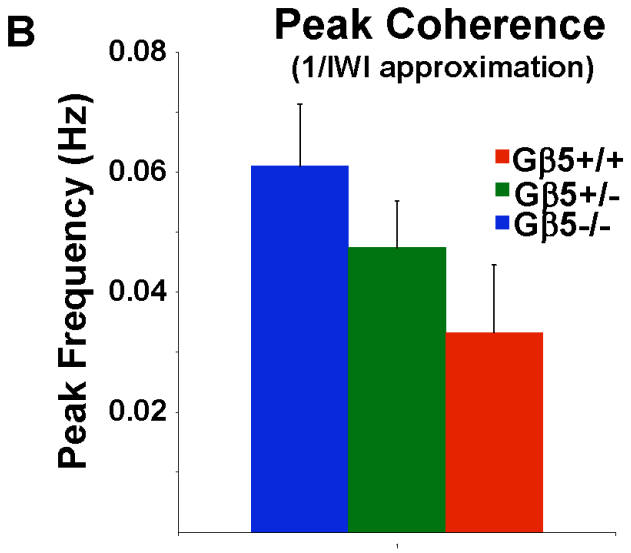
B
Peak Coherence
(1/IWI approximation)
0.08
0.06
0.04
0.02
Peak Frequency (Hz)
Gβ5+/+
Gβ5+/-
Gβ5-/-

Figure 2.9

Figure 2.10- Gβ5 -/- and +/- RGCs bursts have altered firing parameters at P12. Sorted single RGC spike trains were analyzed for burst parameters. Gβ5 -/- and +/- parameters are averaged within genotype and shown as a percentage of respective average P7 Gβ5 +/+ parameters. Dotted line indicates 100% level of Gβ5 +/+. Single asterisks denote significant difference from Gβ5 +/+ and double asterisks indicate differences between each group. Cells numbers are indicated in Table 2.1 and are from the same number of retinas noted in Figure 2.9.

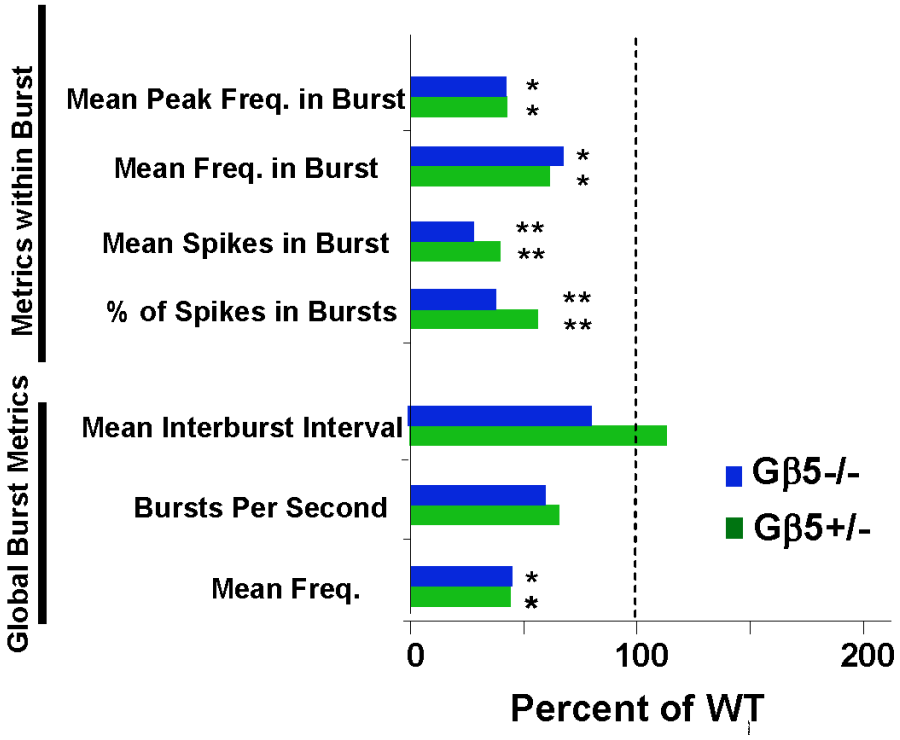
Metrics within Burst
Global Burst Metrics
Mean Peak Freq. in Burst
Mean Freq. in Burst
Mean Spikes in Burst
% of Spikes in Bursts
Mean Interburst Interval
Bursts Per Second
Mean Freq.
*
*
*
*
**
**
**
**
*
*
Gβ5-/-
Gβ5+/-
0
100
200
Percent of WT

Figure 2.10

compares the frequency spectra of cell pairs and exhibits high-power peaks (greater amplitude) at frequencies where the two cells fire at the same frequency. Coherence analysis identifies matched frequencies between cells regardless of phase, i,e, two cells need not fire the same frequency at the same time. Therefore, low-frequency range coherence analysis was employed to approximate the interwave interval and identify any underlying rhythmic activity (Demas et al., 2006). Peak frequencies, reflecting the IWI, are normal in Gβ5-/- mice (Figure 2.9). Single Gβ5-/- RGC activity bears out these observations. Though Gβ5-/- RGCs exhibit a lower mean frequency of firing, their interburst intervals are similar to Gβ5 +/+ RGCs (Figure 2.10). Gβ5-/- RGCs have lower percentage of spikes within a burst, fewer spikes within each burst, and a corresponding decrease in the mean frequency within a burst. Bursts per second, though numerically lower, were not significantly different because of a broad distribution of responses (Figure A14). These features reduce the probability two cells will fire at the same time, corroborating the observed decrease in ST correlation in Gβ5-/- retinas.

Gβ5+/- retinas (n = 5) exhibit spontaneous retinal activity intermediate to Gβ5+/+ and Gβ5+/-. Upon visual inspection, P12 waves in Gβ5+/- retina rasters have qualities of both Gβ5+/+ and -/- (Figure 2.8A). ST correlation analysis, however, reveals that the degree to which cells fire together in Gβ5+/- retinas is reduced in a similar fashion to Gβ5-/- retinas (>300 μm, Figure 2.8B). Peak frequencies in coherence analysis, reflecting the IWI, show a Gβ5 dose-dependant trend but are not statistically different (Figure 2.9B), in contrast to P7 where the IWI is greater in Gβ5-/- and +/- retinas. Single RGC bursting parameters show that Gβ5+/- RGCs have decreased mean frequency and mean frequency in burst, like Gβ5-/- RGCs (Figure 2.10). Interestingly, the percent of spikes in

bursts and mean spikes in a burst correspond to Gβ5 -/- allele dose (Figure 2.10). The salient feature of P12 retinas is that both Gβ5+/- and Gβ5-/- retinas have a drastically reduced near neighbor firing correlation.

By P14, eyes open and permit the onset of normal visual activity. Robust spontaneous glutamatergic activity concurrently subsides in normal animals (Figure 2.11A). Global activity patterns in Gβ5-/- retinas (n = 3) are still somewhat robust (Figure 2.11A) and exhibit coherence spectra peaks at higher frequencies from Gβ5 +/+ retinas (n = 5, Figure 2.12, Kruskal-Wallis, Tukey-HSD, $p < 0.05$). Overall, ST correlation of firing, though somewhat decreased, is not different from Gβ5+/+ (Figure 2.11B). RGC firing parameters indicate that Gβ5-/- RGCs have a smaller percent of spikes in burst and fewer spikes in each burst compared to Gβ5 +/+ (Figure 2.13), suggesting Gβ5 -/- waves are somewhat de-correlated even at P14. Also underscoring the bursting in Gβ5 -/- retinas, there is a relatively decreased interburst interval compared to Gβ5 +/+ (Figure 2.13) that reflects more frequent bursts. However, there is no significant increase in mean frequency. By this age, Gβ5+/- retinas (n = 5) appear to have normal spontaneous retinal activity (Figures 2.11A and 2.13) and only exhibit a slight decrease in the percent of spikes within bursts compared to Gβ5+/+ (Figure 2.13), consistent with the presence of an ERG b-wave and normal protein levels of Gβ5. ST correlation and coherence analyses show spatiotemporal wave properties and pair-wise firing coherence in Gβ5-/- and Gβ5+/- retinas are similar to Gβ5+/+ (Figures 2.11B and 2.12).

Robust spontaneous retinal activity persists, indeed augments, in another animal with a post-synaptically derived no b-wave ERG phenotype: the *nob* mouse (Gregg et al., 2003). *nob* mice have exuberant rhythmic firing at P14-15 (Figure 2.11A) (Demas et al.,

2006). Because Gβ5-/- mice also have a no b-wave phenotype, we wanted to know how the rhythmic firing compared to what is seen in Gβ5-/- mice and if Gβ5 was involved in *nob* rhythmic firing. To this end, we crossed *nob* mice with Gβ5-/- and examined their spontaneous retinal activity. Sibling *nob*xGβ5+/+ (n = 3) retinas exhibit robust and rapidly bursting spontaneous activity (Figure 2.11A), as previously described (Demas et al., 2006), and were used as a second basis of comparison for *nob*xGβ5-/- retinas. Globally, *nob*xGβ5-/- retinas (n = 5) have a marked decrease in activity compared to *nob*xGβ5+/+ as well as a lesser degree of correlated firing, often resembling Gβ5-/- retinas (Figure 2.11B, Tukey-HSD $p < 0.05$). We also find that *nob*xGβ5+/+ have an *increase* in correlation compared to all genotypes.

Coherence analysis revealed *nob*-like rhythmic firing is still present in the *nob*xGβ5-/- retinas, as seen by harmonic-like peaks at approximately every 0.3Hz (Figure 2.12A). At the RGC level, mean peak frequency of bursting, mean frequency within a burst, mean interspike interval, mean burst duration, and interburst interval are similar to Gβ5-/- RGCs and reduced compared to *nob*xGβ5+/+ levels (Tukey-HSD, $p < 0.05$, Figure 2.13). Surprisingly, in most parameters (mean peak burst frequency, mean interspike interval, mean frequency in burst, mean burst duration, and mean interburst interval), *nob*xGβ5-/- retinas have activity that was even more attenuated than Gβ5-/-. In the same way, when Gβ5-/- retinas have increased mean burst duration, *nob*xGβ5-/- retinas are also augmented compared to *nob*xGβ5+/+. The number of spikes per burst are also similarly diminished in *nob*xGβ5-/- and the Gβ5-/- RGCs (Tukey-HSD, $p<0.05$). Finally, *nob*xGβ5-/- overall retinal activity (mean frequency) reflects a similar quieting effect for Gβ5 loss (Figures 2.11A and 2.13). These results juxtapose the importance of

Figure 2.11- Gβ5-/- retinas have persistent wave activity at p14 reminiscent of *nob* mice. A. *above* Raster plots of P14 retinal recordings for Gβ5+/+, +/- and -/- show individual cell spike trains. *below* Raster plots of *nobx*Gβ5+/+ and *nobx*Gβ5-/- retinas are shown. Time scale bar is 20 seconds. B. Spatiotemporal correlation is plotted as a function of interelectrode distance. Each point represents the average cell pair correlation of all retinas within a genotype. Error bars represent ± S.E.M. Asterisks indicate significant differences from Gβ5 +/+. Number of retinas used at P12 are: Gβ5 +/+, n=3; Gβ5 +/-, n=5; Gβ5 -/-, n=5; *nobx*Gβ5+/+, n=3; *nobx*Gβ5-/- n=5.

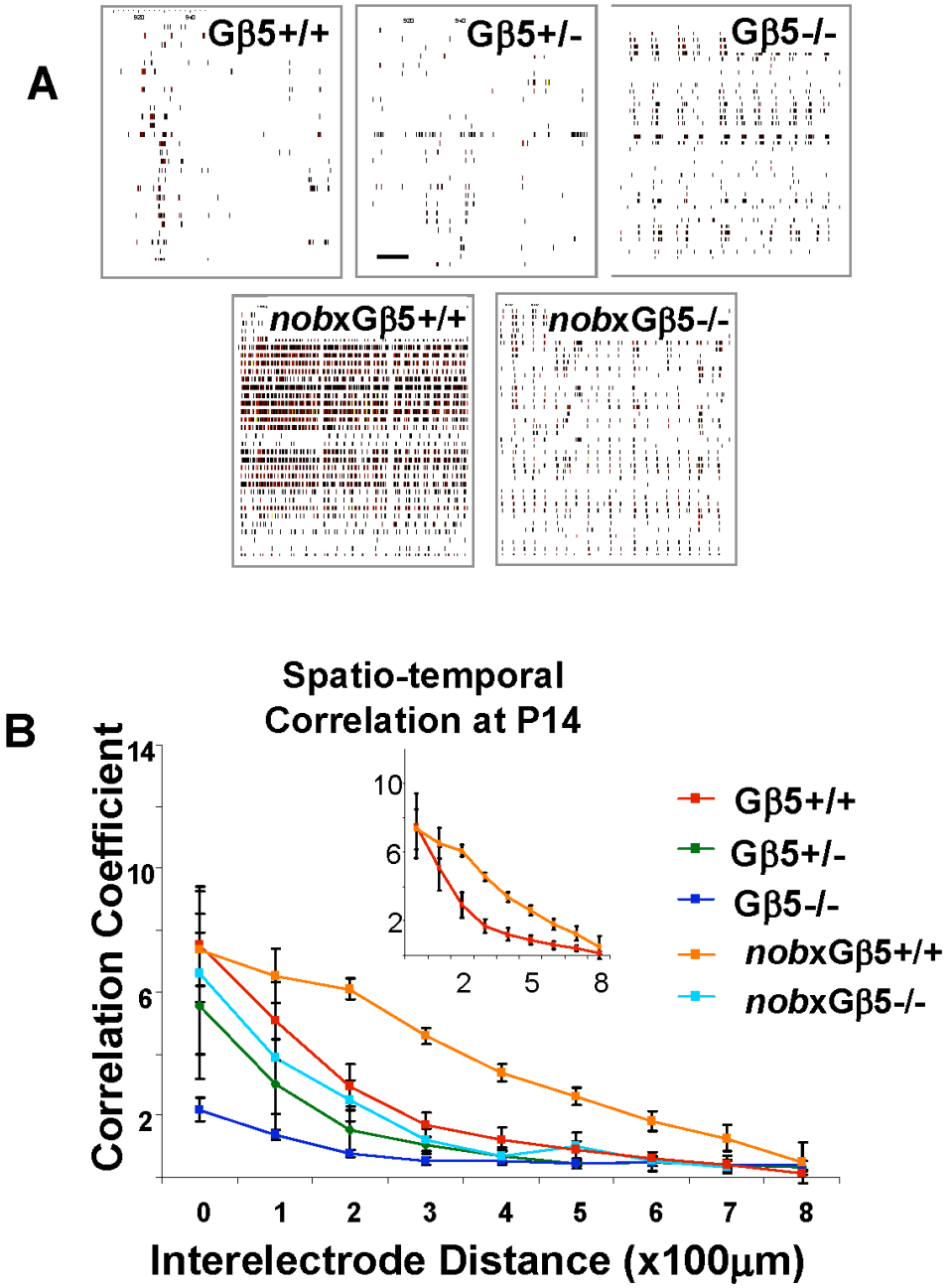
A
Gβ5+/+
Gβ5+/-
Gβ5-/-
nobxGβ5+/+
nobxGβ5-/-
B
Spatio-temporal
Correlation at P14
Correlation Coefficient
Interelectrode Distance (x100μm)
Gβ5+/+
Gβ5+/-
Gβ5-/-
nobxGβ5+/+
nobxGβ5-/-

Figure 2.11

Figure 2.12- P14 coherence spectra illustrate periodic firing of Gβ5 -/-, *nob*xGβ5 -/- and *nob* retinas but underlying *nob*-like rhythmicity does not require Gβ5. A. Averaged coherence spectra of Gβ5 +/+, Gβ5 +/-, Gβ5 -/-, *nob*xGβ5 +/+ and *nob*xGβ5 -/- show the power (in watts, W) of two cells firing at a given frequency. Plots are binned at 0.01Hz. B. Peak frequencies, determined by identifying the frequency bin in which the maximum power occurs, are displayed as the mean± S.E.M. Asterisks indicate significant differences from Gβ5 +/+,. This analysis was done on the same retinas as reported in Figure 2.11.

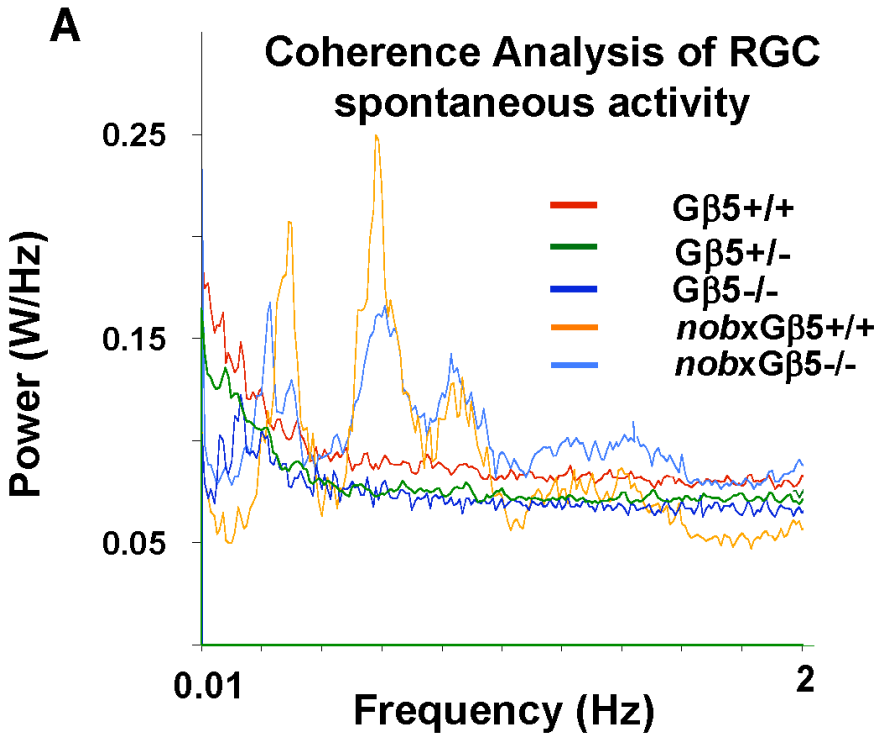
A
Coherence Analysis of RGC spontaneous activity
Power (W/Hz)
0.25
0.15
0.05
0.01
2
Frequency (Hz)
Gβ5+/+
Gβ5+/-
Gβ5-/-
*nob*xGβ5+/+
*nob*xGβ5-/-

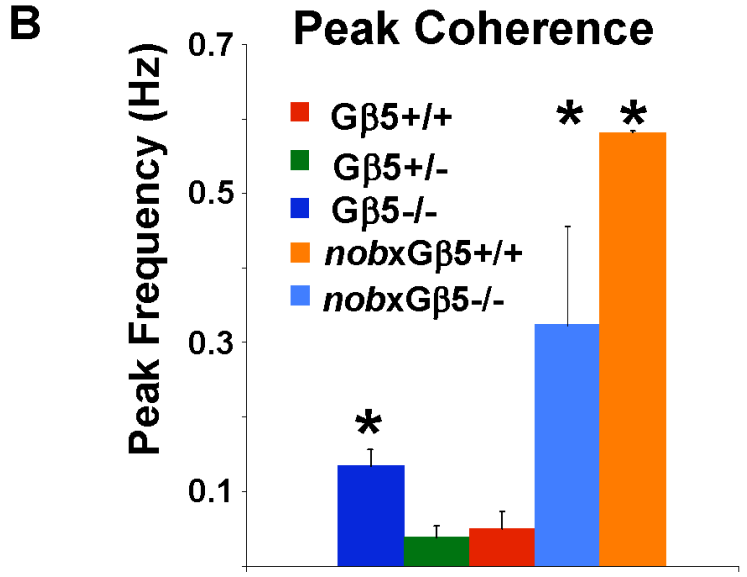
B
Peak Coherence
Peak Frequency (Hz)
0.7
0.5
0.3
0.1
Gβ5+/+
Gβ5+/-
Gβ5-/-
*nob*xGβ5+/+
*nob*xGβ5-/-
*
*
*

Figure 2.12

Figure 2.13- Animals without Gβ5, P14 RGCs exhibit more bursting than Gβ5 +/+ and Gβ5+/-, but less than *nob*xGβ5 +/+. RGC burst firing parameters in Gβ5-/-, Gβ5+/-, *nob, and nob*xGβ5-/- retinas are shown. Sorted single RGC spike trains were analyzed for burst parameters. Normalized Parameters are averaged within genotype and are shown as a percentage of respective average Gβ5 +/+ parameters. Dotted line indicates 100% level of Gβ5 +/+. A line above a particular genotype parameter denotes significant differences from Gβ5 +/+. Cells numbers are indicated in Table 2.1 and are from the same number of retinas noted in figure 2.11.

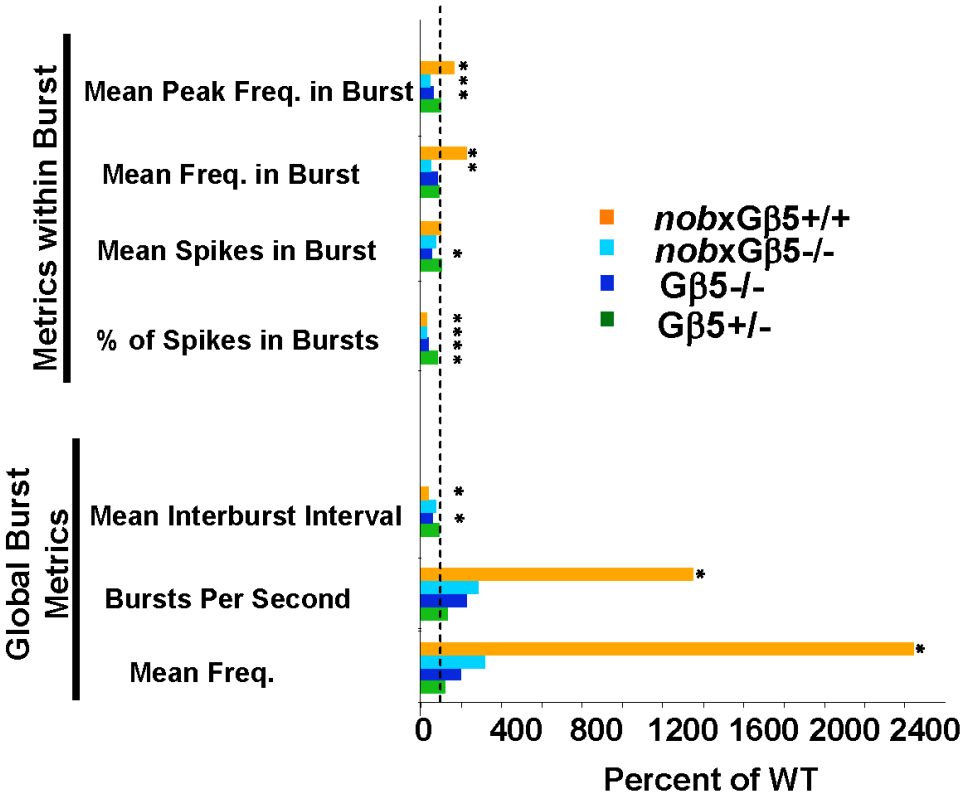
Metrics within Burst
Mean Peak Freq. in Burst
Mean Freq. in Burst
Mean Spikes in Burst
% of Spikes in Bursts
Global Burst Metrics
Mean Interburst Interval
Bursts Per Second
Mean Freq.
nobxGβ5+/+
nobxGβ5-/-
Gβ5-/-
Gβ5+/-
0
400
800
1200
1600
2000
2400
Percent of WT

Figure 2.13

Gβ5 in the RGC firing properties and correlation against its dispensability in *nob* rhythmic activity at P14.

At P28, retinal activity profiles in all alleles are quieter (Table 2.1, Figure 2.14A) and diverge from their P14 trends. Compared to Gβ5+/+ (n = 4 retinas), Gβ5-/- retinas (n = 5) still exhibit unusual periodic activity but a similar degree of ST correlation. Indeed, the degree of ST correlation is very low (correlation index < 3) in all tested alleles and only "fall off" significantly in *nob* genotype animals (GLM, Tukey post-hoc test, $p<0.05$). Gβ5+/+ spectra are virtually flat at P28 (Figure 2.15B), indicating no notable rhythmic activity. Therefore their spectral peaks are not truly comparable to those seen by Gβ5-/- or the *nob* allele retinas, which have distinctive peaks above noise. Interestingly, the most striking feature of Gβ5-/- retinas is a broad dominant peak and a smaller peak at a higher frequency, both at 0.4Hz intervals (Figure 2.15A). These features report the emergence of robust underlying rhythmic activity Gβ5-/- retinas not seen at P14.

Gβ5+/- retinas (n = 5), on the other hand, remain similar to Gβ5+/+ retinas in many respects at P28. Visual inspection does not glean any particular pattern of activity, similar to Gβ5+/+ (Figure 2.14A). At this stage, fewer RGCs respond in most Gβ5+/+ and Gβ5+/- recordings (Figure 2.14A), as expected (Demas et al., 2003). ST correlations in Gβ5+/- retinas are no different from Gβ5+/+. However, they do appear to "fall off" at closer interelectrode distances (Figure 2.15B) more than other genotypes. Interestingly, single RGC burst parameter analysis indicate Gβ5+/- RGCs fire more percent of spikes within bursts and have an increased mean peak frequency within a burst (Figure 2.16). This may effectively reflect packing more spikes into a burst, which could suggest highly auto-correlated firing or may reinforce correlative firing in mature retina cells. Both can

Figure 2.14- Wave-like activity persists in Gβ5-/-, *nob*xGβ5 +/+, and *nobxGb5* -/- retinas. A. *above* Raster plots of P28 retinal recordings for Gβ5+/+, +/- and -/-show individual cell spike trains. *below* Raster plots of *nobx*Gβ5+/+ and *nobx*Gβ5-/- retinas are shown. Time scale bar is 20 seconds. B. Spatiotemporal correlation is plotted as a function of interelectrode distance. Each point represents the average cell pair correlation of all retinas within a genotype. Error bars represent ± S.E.M. Asterisks indicate statistical differences from Gβ5 +/+. Number of retinas used at P12 are: Gβ5 +/+, n=4; Gβ5 +/-, n=5; Gβ5 -/-, n=5; *nobx*Gβ5+/+, n=5; *nobx*Gβ5-/- n=5.

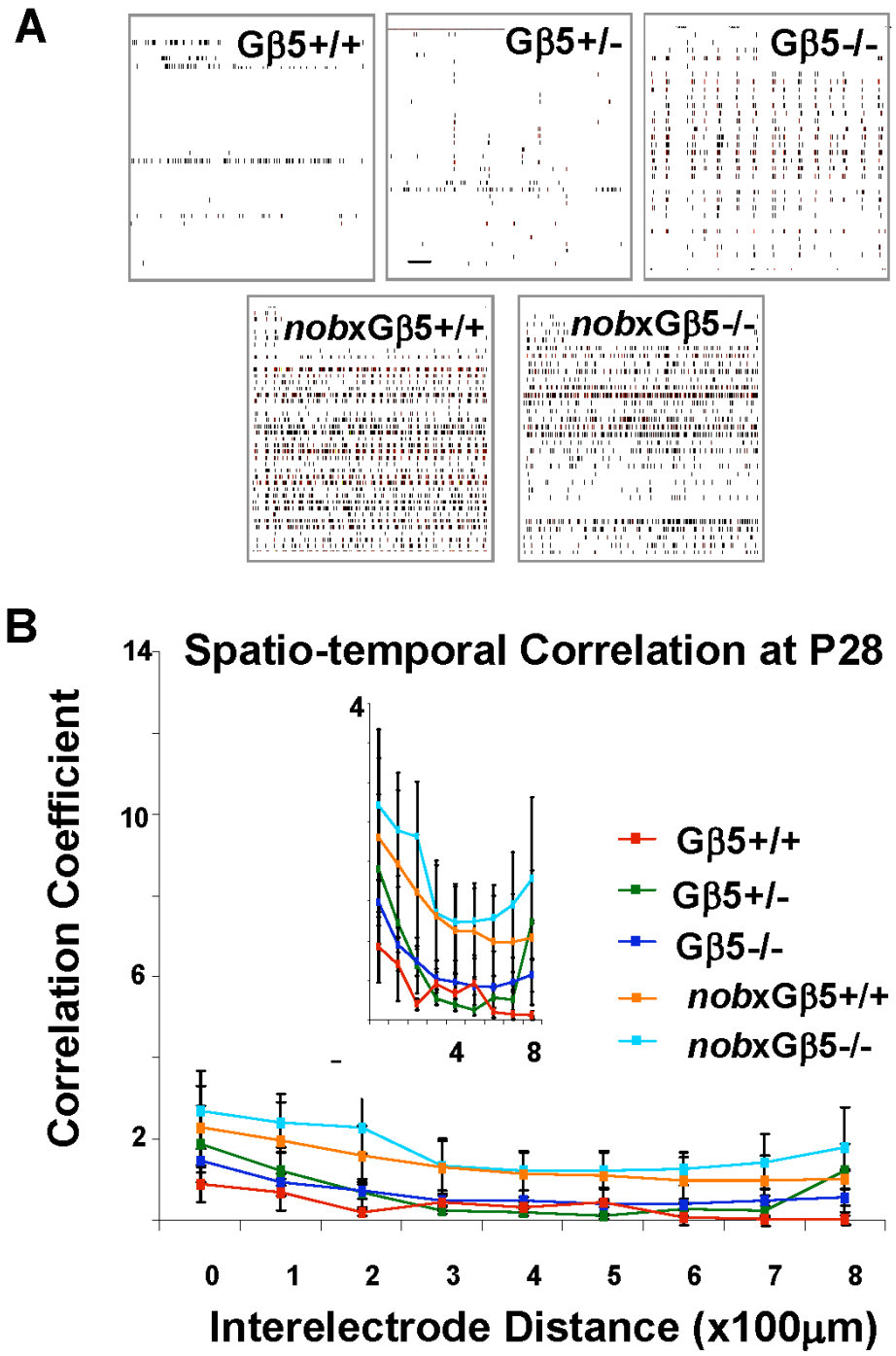
A
Gβ5+/+
Gβ5+/-
Gβ5-/-
nobxGβ5+/+
nobxGβ5-/-
B
Spatio-temporal Correlation at P28
Correlation Coefficient
14
10
6
2
4
4
8
Gβ5+/+
Gβ5+/-
Gβ5-/-
nobxGβ5+/+
nobxGβ5-/-
0
1
2
3
4
5
6
7
8
Interelectrode Distance (x100μm)

Figure 2.14

Figure 2.15- Underlying rhythmic activity emerges in Gβ5-/- retinas at P28 yet diminishes in *nobx*Gβ5+/+ and *nobx*Gβ5-/- retinas. A. Averaged coherence spectra of Gβ5 +/+, Gβ5 +/-, Gβ5 -/-, *nob*xGβ5 +/+ and *nob*xGβ5 -/- show high power (wattage, W) if two cells fire at a given frequency, independent of phase. Plots are binned at 0.01Hz. B. Peak frequencies, determined by identifying the frequency bin in which the maximum power occurs, are displayed as the mean± S.E.M. Asterisks indicate significant differences from WT. This analysis was done on the same retinas as reported in figure 12.

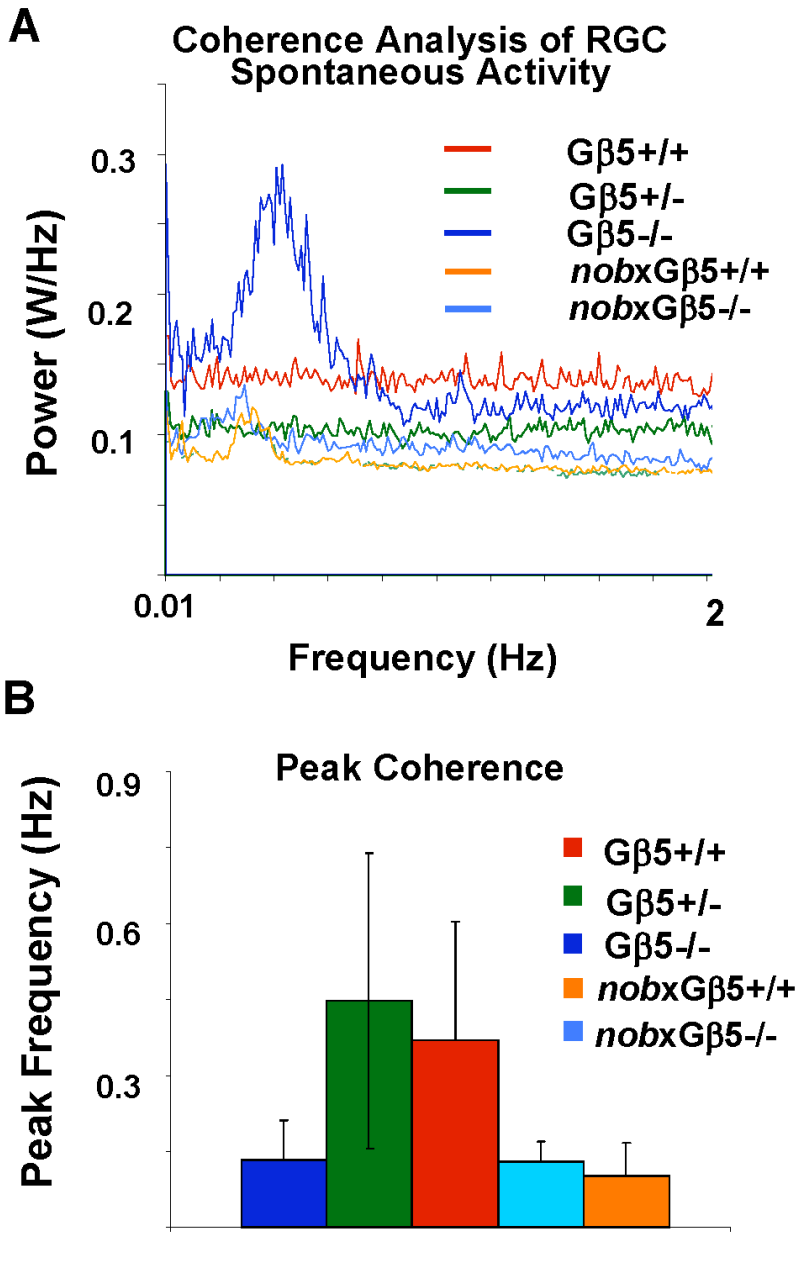
A
Coherence Analysis of RGC Spontaneous Activity
Power (W/Hz)
0.3
0.2
0.1
0.01
2
Frequency (Hz)
Gβ5+/+
Gβ5+/-
Gβ5-/-
nobxGβ5+/+
nobxGβ5-/-
B
Peak Coherence
Peak Frequency (Hz)
0.9
0.6
0.3
Gβ5+/+
Gβ5+/-
Gβ5-/-
nobxGβ5+/+
nobxGβ5-/-

Figure 2.15

Figure 2.16- Normalized RGC burst firing parameters in Gβ5-/-, Gβ5+/-, *nob, and nob*xGβ5-/- retinas are shown. Normalized parameters are averaged within genotype and are shown as a percentage of respective average P7 Gβ5 +/+ parameters. Dotted line indicates 100% level of Gβ5 +/+. A line above a particular genotype parameter denotes significant differences from Gβ5 +/+. Cells numbers are indicated in Table 2.1 and are from the same number of retinas noted in figure 2.13.

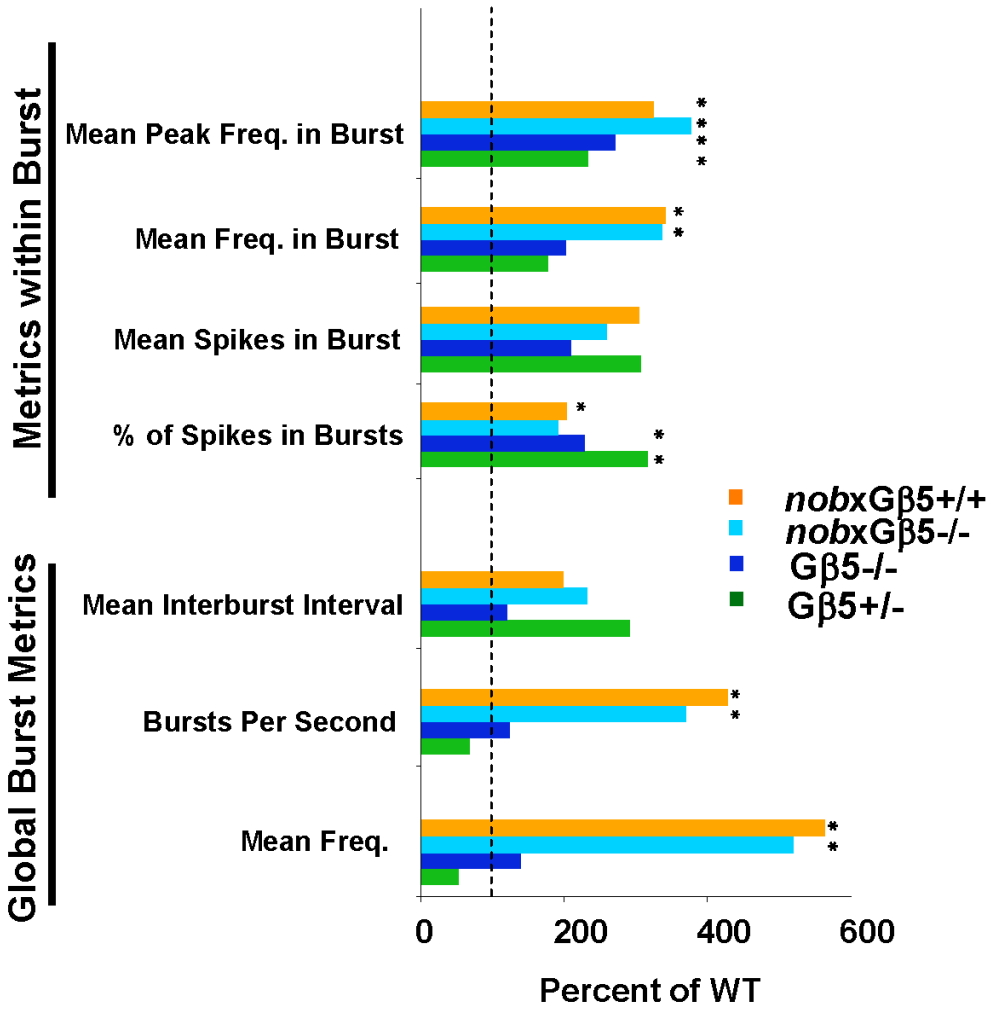
Metrics within Burst
Mean Peak Freq. in Burst
Mean Freq. in Burst
Mean Spikes in Burst
% of Spikes in Bursts
Global Burst Metrics
Mean Interburst Interval
Bursts Per Second
Mean Freq.
nobxGβ5+/+
nobxGβ5-/-
Gβ5-/-
Gβ5+/-
0
200
400
600
Percent of WT

Figure 2.16

contribute to normal behavior in several mammalian retinas (Mastronarde, 1983; Pillow et al., 2008; Shlens et al., 2009).

At P28, *nob*xGβ5+/+ retinal activity is reduced compared to P14 but still increased relative Gβ5+/+. Coherence spectra display greatly diminished harmonic peaks for rhythmic activity (Figure 2.15A), as previously reported (Demas et al., 2006), as do *nob*xGβ5-/- retinas. In addition to similar coherence spectra (Figure 2.15A), P28 *nob*xGβ5-/- retinas (n = 5) now share more activity features in common with *nob*xGβ5+/+ retinas (n = 5). Overall activity (mean frequency), burst frequency, mean frequency within bursts, and mean peak frequency within bursts (Figure 2.16) in P28 *nob*xGβ5-/- retinas resemble *nob*xGβ5+/+ retinas more than at P14.

Conclusions

We explored the role of Gβ5 and R7RGS activity in spontaneous retinal activity during over 4 weeks of postnatal development. There are six main findings in this study: (1) At P7, retinas with sufficiently low Gβ5, but not the loss of single R7RGS proteins, have a decrease in activity largely linked to an increase in their interwave interval. (2) At P12, retinas lacking Gβ5 have decreased near neighbor RGC firing during Stage III waves. (3) Gβ5 +/- retinas are largely normal by P14. (4) Gβ5 -/- retinas have persistent spontaneous retinal waves at P14 but no significant underlying rhythmic activity. (5) Gβ5-/- retinas show an increase in activity and emergent rhythmic activity at P28. (6) Gβ5 has a quieting effect on *nob* retinas but is dispensable for the characteristic P14 *nob* rhythmicity.

Gβ5 is required for normal stage II waves

Our preliminary experimental objective was to identify additional roles for Gβ5 in periodic activity in the retina. Stage II waves appeared to be a suitable beginning because of the underlying cAMP dynamic drive (Feller et al., 1996; Stellwagen et al., 1999) and easily accessible periodic events (Demas et al., 2006; Syed MM, 2004; Wong et al., 1993) that may be governed by intracellular periodic events like after-hyperpolarization refractory periods (Godfrey and Swindale, 2007; Hennig et al., 2009). Both Gβ5 -/- and +/-, which have less Gβ5 than Gβ5+/+ retinas, exhibit longer interwave intervals. There are two likely sources for this phenotype: developmental calamity, such as malformed synapses, or prolonged intracellular signaling. In the OPL, loss of Gβ5 is catastrophic to synapse formation (Rao et al., 2007). We expected a similar "no spontaneous wave" phenotype if Gβ5 grossly affected the synapses necessary for cholinergic waves. Gβ5 -/- mice have both cholinergic waves (Figure 2.6A) and normal cholinergic strata suggesting intact synapses (Figure 2.4, 2.3). Although this does not completely discount the possibility of synaptic problems, this suggests that synaptic malformation is not likely to be the primary source of the IWI phenotype. Loss of ON bipolar cell presynaptic release does not lead to overt morphological phenotypes, just fewer formed ON bipolar cell-RGC synapses in the IPL (Kershensteiner, 2009). Such a phenomenon may govern some aspects of the Gβ5 IWI phenotype in the transient cholinergic network (Zheng, 2005). Morphological assessment of fine synaptic contacts in the Gβ5-/- IPL can exclude this possibility.

The altered global properties we see differ mostly in the interwave interval (approximately 2 fold), which closely corresponds to the 50% drop in overall activity (Figures 2.4 and 2.17). This suggests that this preliminary circuitry in the IPL is largely

intact and that the prolonged IWI is the result of some slowed intracellular regulation. This conclusion would be greatly reinforced with data demonstrating 1) intact synapses in cholinergic strata or 2) the precise localization of R7RGS proteins, or Gβ5, at the bipolar/RGC synapse at the EM level (Zhang and Diamond, 2009). Antagonizing glutamate receptors in stage III waves increases interwave interval (Blankenship et al., 2009). Therefore, an effective drop in ACh may contribute to the increased interwave interval, suggesting Gβ5 may be involved in pre-synaptic release in SACs or post-synaptic sensitivity in RGCs.

In mammalian retinas (specifically rabbit, ferret, and mouse), spontaneous activity has many similarities, particularly the influence of the cholinergic network and cAMP dynamics in stage II retinal activity (Feller et al., 1996; Stellwagen et al., 1999; Torborg et al., 2004; Torborg et al., 2005). However, we find there are no single R7 proteins (Figure 2.6) responsible for Gβ5-/- phenotype.. It is important to mention the SG7 animal is not a true null and we await the production of a true RGS7 -/- to verify the role RGS7. However, the SG7 mouse does produce a retinal phenotype in conjunction with the RGS11-/- mouse (Chen et al., 2010) and is therefore capable of exhibiting a functional deficit. Also, R7RGS activity may have redundant players as seen in bipolar cells (Chen et al., 2010; Mojumder et al., 2009; Zhang et al., 2010). Only animals lacking the correct complement of R7RGS proteins (by location likely RGS7 and RGS6) will recapitulate the phenotype. If the known partners have been exhausted the conclusion must be that Gβ5 acts with a gamma subunit (Blake et al., 2001) or with an entirely different RGS protein. Lastly, an interesting possibility supported by the sole drop in Gβ5 (Figure

Figure 2.17 –Summary of spontaneous activity in Gβ5-/- and Gβ5+/- is shown. Arrows indicate increases or decreases in numerical parameters. Parameters are interwave interval (IWI), interburst interval (IBI) and mean frequency (activity) for P7. Correlation parameters and dose parameters included for P12. Normalization of Gβ5 +/- is based on bulk of parameters. At P14 each age displays a selection of parameters and is not a complete list. % Spikes is percent of spikes in burst. "Spikes" is mean spikes in burst. Rhythmicity indicates multiple harmonic peaks on coherence analysis. "Peak freq." is peak frequency in burst. "Mean Freq" is mean frequency in burst.

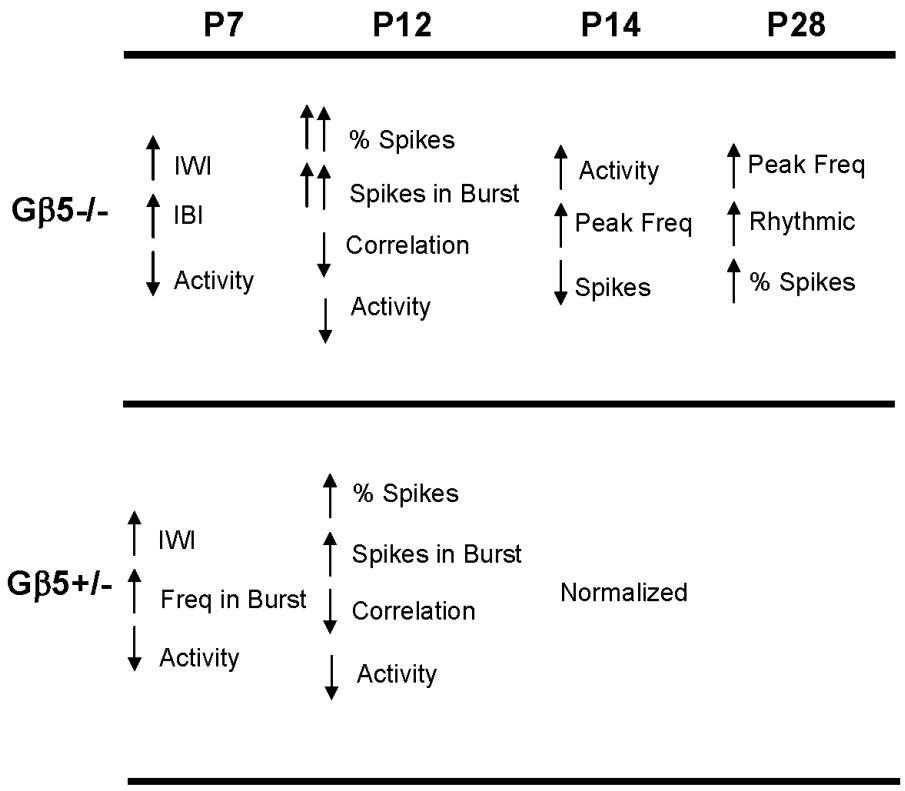
P7
P12
P14
P28
Gβ5-/-
IWI
IBI
Activity
% Spikes
Spikes in Burst
Correlation
Activity
Activity
Peak Freq
Spikes
Peak Freq
Rhythmic
% Spikes
Gβ5+/-
IWI
Freq in Burst
Activity
% Spikes
Spikes in Burst
Correlation
Activity
Normalized

Figure 2.17

2.3A), is that Gβ5 acts alone. But currently no evidence supporting that role has been reported.

Other locations may contribute to Gβ5's role in stage II waves. In adults, Gβ5 is strongly detected in the cholinergic strata of the IPL inner plexiform layer. Gαi/o can regulate cAMP signaling through adenylate cyclase (AC (Watts and Neve, 2005) and multiple ACs are thought to be responsible for regulation of stage II waves in mice (Dunn et al., 2009). In striatum, Gαi/o-coupled D2 receptors (D2R) and Gs-coupled A2A receptors can antagonize each other's signaling when activated, possibly though AC dynamics (Ferre et al., 2008). A2A (Kvanta et al., 1997) and D2R (Tran and Dickman, 1992) receptor message is found in the inner nuclear, inner plexiform and ganglion cell layers of rat retina. Dopamine signaling during retinal waves is assumed to activate D1 receptors on RGCs or SACs (Dunn et al., 2006) but D2 receptors on dopaminergic amacrine cells could contribute to these dynamics (Schambra et al., 1994). R7RGS proteins are critical partners for Gβ5 in the retina (Chen et al., 2010; Krispel et al., 2003; Krispel et al., 2006). Functioning as regulators of Gαi/o signaling, they could direct the tempo of AC1 activation in certain RGCs (Dunn et al., 2006; Nicol et al., 2006). The increased interwave interval seen in the RGS11-/- mouse suggests another contribution of Gβ5 activity in stage II waves. RGS11 is primarily located in bipolar cells and acts with RGS7 to regulate ERG b-wave timing. Therefore, increasing levels of Gβ5/RGS11 may be important for stage II wave dynamics. Testing loci outside of the usual SACs and RGCs may elucidate additional players in stage II retinal waves.

There are additional experimental avenues for understanding the Gβ5 phenotype, namely cell-specific deletion of Gβ5 in SACs. This manipulation will help tease apart the

roles of network drivers (Zheng et al., 2006 and partially addressed in Stacy et al., 2005) versus RGC refractory mechanisms in spontaneous retinal activity, a question previously addressable by modeling alone (Godfrey and Swindale, 2007). In the event this does not recapitulate the Gβ5 -/- phenotype, further levels of regulation in the retina may be utilized. For instance, R7RGS proteins may be localized to different compartments within the cell (Grabowska et al., 2008). Coupling to binding proteins R7BP or R9AP (Jayaraman et al., 2009), whose cytosolic localization is regulated by palmitoylation (Drenan et al., 2005; Drenan et al., 2006), presents one level of spatial regulation. It is possible that R7RGSs do not bind anchoring proteins as RGS7 does in mature ON-bipolar cells (Cao et al., 2008). Furthermore, it is not known if other binding partners exist that would add dimensions of regulation. Cell-specific elimination of these players in a piecewise fashion would certainly reproduce the Gβ5 -/- phenotype as well as improve our understanding of the underlying components responsible for spontaneous retinal activity. Perhaps the best approach to determine the potential locus of Gβ5 involvement would be to patch-clamp RGCs and SACs separately during stage II waves under both pharmacologically coupled and decoupled conditions (similar to Zheng et al., 2006).

Role of Gβ5 in Glutamatergic waves

At P12, Gβ5-/- retinas have transitioned to stage III waves (Figure 2.7). Both Gβ5 -/- and +/- exhibit differences from Gβ5+/+ (Figure 2.8A). The key feature of Gβ5-deficient retinas at this age is greatly reduced ST correlation (Figures 2.8B and 2.17). De-correlation of wave activity could be the result of less concerted glutamate release and subsequent spillover from glutamatergic terminals (Blankenship et al., 2009). Gβ5 may

ultimately regulate glutamate release in developing ON-bipolar cells (Morgan et al., 2006), which dramatically upregulate their VGlut1 expression after P12 (Sherry et al., 2003), thus sharpening differences between Gβ5-/- and Gβ5 +/-. This phenotype would predict more spikes outside of bursts and fewer spikes within bursts (Figure 2.10) that may "loosen" normally tight bursts. Though both genotypes are different from Gβ5 +/+, the compactness of spiking is Gβ5 dose-dependent (Figure 2.11C). This may arise from an intracellular threshold of activity where Gβ5 levels are increasing to wild-type levels in the Gβ5 +/-. This would also explain why Gβ5 +/- retinas are functionally normal at P14 (Figures 2.11, 2.12, and 2.13) and as adults (Krispel et al., 2003). Outside-out patching experiments across all Gβ5-/- alleles could answer whether the ON bipolar cell terminal glutamate release is increased relative to Gβ5 dose, but still may not be conclusive. It is important to note that whereas the source of the single IWI phenotype at P7 can conceivably be attributed to Gβ5 signaling, as mice age, observed phenotypes in Gβ5-/- and +/- mice are considerably more susceptible to developmental derailment.

Some have observed that abnormal stage II activity (Bansal et al., 2000) or SAC disruptions (Speer and Chapman, 2009) alter glutamatergic wave properties. Although the specific mechanism is not known, activity itself is critical for proper retinal connections (Bodnarenko and Chalupa, 1993; Tian, 2008; Tian and Copenhagen, 2001, 2003) and normal cholinergic activity can be linked to maturing GABAergic activity through SACs (Zheng JJ, 2004). Indeed, stage II waves are disrupted in both Gβ5-/- and +/- retinas, setting the stage for a similar anomaly (Figure 2.5). GABAergic circuits provide an appealing and testable candidate to explain the de-correlated stage III phenotypes in Gβ5 +/- and Gβ5 -/-. GABA is critical for all stages of retinal waves, but

plays a variety of roles that often change depending on the stage or receptor (Blankenship and Feller, 2010; Fischer et al., 1998; Syed MM, 2004). In the developing retina, $GABA_A$ receptors act to stimulate activity early RGCs (Sernagor et al., 2003), specifically in mice at P5 (Wang, Blankenship et al. 2007). GABA is required for orderly firing in spontaneous activity at P12 (Kerschensteiner and Wong, 2008). In adults, light-evoked responses reveal that $GABA_A$ is critical for the timing of ON and OFF responses at the bipolar cell level of *nob3* and *nob4* mice (Renteria et al., 2006; Maddox et al., 2006; 2008; McCall and Gregg 2008). These, in turn, may contribute to direction selective RGC processing (Ackert et al., 2009) and differential regulation of bipolar cell responses (Eggers, McCall et al. 2007). Therefore, assessing light responses after application of picrotoxin or bicuculine in a P12 or adult Gβ5 -/- retina may unmask potential GABAergic anomalies.

We were surprised by the Gβ5+/- phenotypes at P7 and P12 because previous reports failed to detect anomalies (Chen et al., 2003; Krispel et al., 2003). By P14, Gβ5+/- retinas are indistinguishable from Gβ5 +/+ in all measurements (Figures 2.12, 2.13, and 2.14). The pressing question emerges: what allows Gβ5 +/-'s to recover? First, Gβ5 +/- mice have a b-wave (internal communication, C.K.Chen), confirming a functional photoreceptor-bipolar cell transmission through the OPL. Presumably, this also heralds the transmission of normal light activity to the inner retina, a critical step in normal activity-dependant retinal development (Tian and Copenhagen, 2001). APB, which disrupts ON-pathway via mGluR6, also leads prevents ON/OFF segregation of afferents in kitten retinas (Bodnarenko and Chalupa, 1993), reinforcing the importance of visual activity. Second, Gβ5 +/- retinas approach wild-type Gβ5 levels (Figure A15) and

restore any Gβ5-dependant processes in the inner retina. While not exhaustive, both observations reflect a function normalization of the Gβ5 +/- retina. Lastly, these events may constitute a "threshold" pardoning of missed developmental milestones by achieving a very important one: visual transmission. Both spontaneous RGC activity and OPL transmission are intact, suggesting much of the retina is normal. Indeed, R7RGS single mutant/knockout mice also have some abnormal activity parameters at P7, but still manage to achieve visual transmission (Chen et al., 2010, personal communication with C.K. Chen for RGS6). Given the tolerance for abnormal activity, in the Gβ5-/- multiple factors mount to prevent normal function. Further study, particularly the characterization of visual responses and bipolar cell membrane properties, will help clarify the precise dysfunction in Gβ5-/-.

Activity-dependant formation of retinal circuits invites additional explanations for the OPL malformation in the Gβ5-/-. This is a singular phenotype among animals with no b-wave (McCall and Gregg, 2008). Restoring Gβ5 in Gβ5-/- rods improves rod photoreceptor recovery and normal presynaptic activity (Rao et al., 2007) in Gβ5-/- retinas. This manipulation failed to rescue the morphological phenotype suggesting other sources of activity may be responsible. Early spontaneous calcium retinal waves, though synaptically downstream, have been shown to propagate to the ventricular zone of nascent retinas (Syed MM, 2004). Ventricular waves correlate with the timing of spontaneous retinal waves across RGCs (Syed, Lee et al. 2004). This activity can affect migration of cells through release of glutamate or GABA (Manent et al., 2005) or neuronal process motility (Poo and Zheng, 2006). Postsynaptic activity whose source is both proximal, in the IPL, and distant from the OPL, RGCs, is altered in Gβ5-/- retinas.

Thus there are many sources of activity to be explored. Experiments that selectively disrupt or rescue these sources of abnormal activity may provide valuable insights into the role of Gβ5 in OPL synaptic development.

Gβ5 is required for normal RGC firing, but not for rhythmic *nob* firing

nob mice exhibit a rhythmic wave phenotype during after eye opening. *nob* mice have a high wave frequency coupled with harmonics in their coherence spectra (Figure 2.11A) (Demas et al., 2006). However, non-responsive, spontaneously active RGCs have been reported in two other post-synaptic no b-wave mutants (Renteria et al., 2006; Maddox et al., 2008). These are thought to arise through dysfunctional ON pathways (McCall and Gregg, 2008). Gβ5-/- mice, while still displaying abnormal spontaneous activity, do not exhibit this exuberant *nob* firing at P14. Therefore, the *nob* rhythmic activity is not a consequence of a no-b wave phenotype. Furthermore, Gβ5 is not required for the rhythmic firing in the *nob* mouse, suggesting unique factors drives the *nob* activity phenotype.

Gβ5 -/- retinas do eventually exhibit dominant rhythmic activity at P28 (Figures 2.15 and 2.18). Given the extent of this study, and the dynamic nature of retinal development, it is difficult to pinpoint to mechanism through with Gβ5 exerts its influence by P28. Ultimately, any abnormalities should be considered relative heavily influenced developmental anomalies. Interestingly, the *nob*xGβ5-/- retinas, which possess increased peak frequency in coherence, have drastically less robust firing than *nobx*Gβ5+/+ retinas at P14. Across all burst metrics, except burst duration (elevated) and interspike interval (elevated and related), *nob*xGβ5-/-mice resemble Gβ5-/-s. Yet by P28, *nobx*Gβ5-/- retinas are similar to *nobx*Gβ5+/+ retinas in both RGC firing and reduced

Figure 2.18- Rhythmicity at P14 is exclusive of rhythmicity at P28. Arrows reflect relative changes in either activity (mean frequency) or rhythmic firing (harmonics on coherence analysis). *nob*xGβ5-/- resembles Gβ5-/- at P14, but retains rhythmic firing. Gβ5-/-, the only condition without P14 rhythmicity, exhibits augmented rhythmicity at P28. *nob*-like activity is indicated in orange.

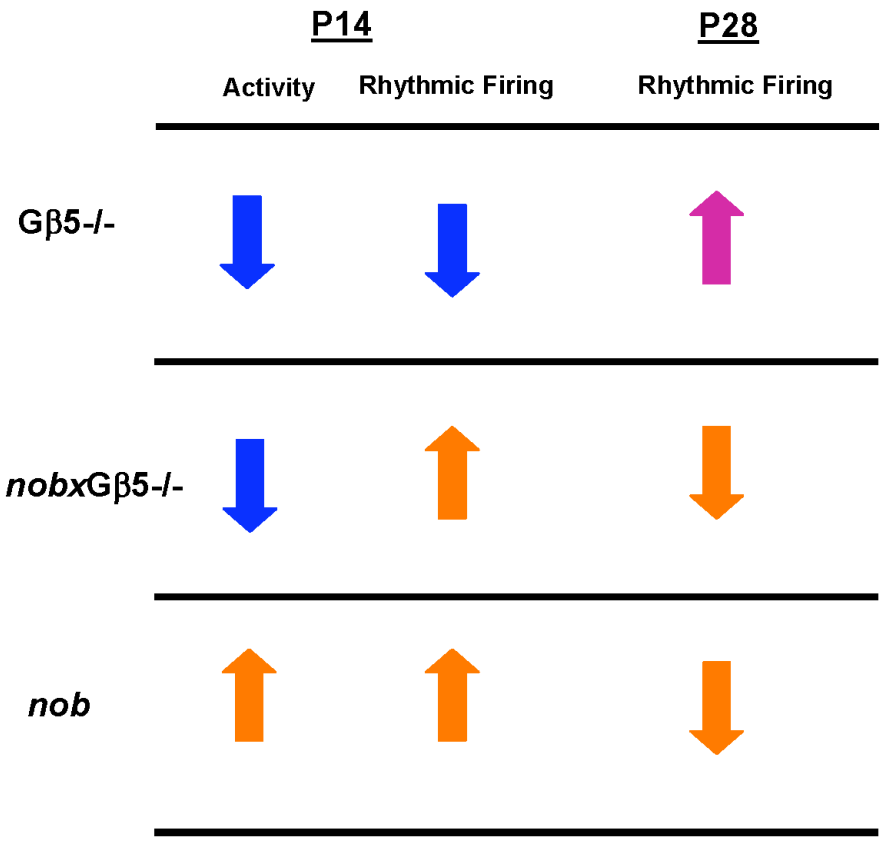
P14
P28
Activity
Rhythmic Firing
Rhythmic Firing
Gβ5-/-
nobxGβ5-/-
nob

Figure 2.18

rhythmicity (Figure 2.18). Given that the *nob* allele retinas only have their rhythmicity in common at P14, it follows that *nob* rhythmicity at P14 predicts *nob*-like RGC activity at P28 (Figure 2.18). In contrast, Gβ5-/- retinas display similar activity to *nobx*Gβ5-/- at P14, with the exception of bold rhythmicity. Yet by P28 they develop unique rhythmic activity. Mechanisms to reconcile this phenomenon are speculative. It is conceivable that *nob* rhythmicity, reinforcing the development of one circuit arrangement through a homeostatic network (Maffei and Fontanini, 2009), precludes Gβ5-/- rhythmicity. Examining the visual responses in the *nobx*Gβ5-/- and Gβ5-/- would be fundamental for exploring underlying differences. Measurement of Gβ5-/- retinal activity at P21 will establish a more thorough time course of these phenotypes and may allow better resolution of Gβ5-/- and *nob* spontaneous activity. Furthermore, pharmacological studies abolish the rhythmicity, perhaps glutamate or GABA receptor subtype specific antagonists, may also provide useful insights into this distinctive activity.

In conclusion, these data provide broad evidence that Gβ5 is necessary for normal retinal function during development. The surprising finding that Gβ5+/- mice also exhibit phenotypes should prompt re-examination of Gβ5+/- phenotypes. Regions where proper circuitry may be altered during adolescence are of particular importance. The ventral tegmental area in addiction reward (Rahman et al., 2003) and diseases like schizophrenia (Kovoor et al., 2005; Bolbekcer, 2009; Puri, 2010) offer clinical motivation to understand Gβ5 function. These encourage the production of reagents that can titrate Gβ5 over development and in a cell-specific manner. These data also provide the launching point for understanding the roles of Gβ5 in developmental retinal signaling, spontaneous neuronal activity, and G-protein *in vivo* regulation.

CHAPTER 3

Gβ5 is required for normal retinogeniculate refinement

Introduction

The development of neural circuits is a monumental task and specific circuit formation is necessary for proper function. In the developing retinogeniculate system, retinal ganglion cells (RGCs) send axons into the lateral geniculate nucleus (LGN) and synapse on geniculate relay cells (Huberman et al., 2007). RGC axons must then arrange themselves to faithfully report a precise map of the visual world and other information to geniculate relay cells. Geniculate relay cells then report on to the cortex (Sherman and Guillery, 2002).

In the visual system, correct map formation within the brain is facilitated by spontaneous retinal activity in the form of spatially and temporally correlated waves (Huberman et al., 2007). Stage I retinal waves are gap junction mediated and appear before birth (Syed et al., 2004). Stage I waves become stage II waves when acetylcholine emerges as the dominant retinal neurotransmitter after P2. Before eye-opening, glutamate transmission overtakes acetylcholine during stage III waves (Blankenship et al., 2009). Stage III spontaneous retinal waves subside around the time of normal visual activity after P14 (Wong et al., 1993; Demas et al., 2003). These retinal wave stages correspond to stages of coarse map formation in the LGN: ingrowth of axons (I), induction phase of eye-specific segregation (II), and the maintenance phase of segregated afferents (III).

Eye-specific segregation, whereby retinal axons from each eye jockey to occupy specifically designated regions of the LGN, has provided a testing ground to examine the role of activity in synaptic specification. Normal retinogeniculate development begins

with RGC axons growing into the LGN at E18-P0 (Godement et al., 1984). Initially, axon terminals from both eyes overlap (Jaubert-Miazza et al, 2005). From P3 to P8, ipsilateral RGC axon terminals refine to occupy the anterior-medial portion of dLGN. Contralateral RGC axons exclusively occupy the remaining dLGN. By P12, RGC terminal fields have segregated into discrete eye-specific regions (Jaubert-Miazza et al., 2005). Fine synaptic refinement largely mirrors eye-specific segregation and further refinement and strengthening occur after eye opening (Hook and Chen, 2006, 2008; Ziburkus and Guido, 2006). Eye-specific segregation appears to establish a scaffold for proper synaptic connections in the dLGN. Segregation failure is associated with abnormal ON/OFF lamination in nicotinic receptor subunit β2 knockout mice (β2-/-) dLGNs (Grubbs et al., 2003). Similarly, failure to segregate eye-specific afferents is coupled with residual synaptic immaturity in mice without complement proteins C1q and C3 (Stevens, et al. 2007). Consequently, without normal geniculate development cortical organization suffers. Geniculocortical projections improperly wire in β2-/- mice (Cang et al., 2005) and azimuthal plane cortical mapping is compromised in mice in β2-/- /EphrinA3/5 mice (Cang et al., 2008).

Disruption of normal retinal activity during development alters segregation of eye-specific afferents. In ferrets, bilateral epibatidine injection alters normal retinal activity (Sun et al., 2008b) and prevents eye-specific segregation (Penn et al., 1998; Huberman et al., 2003). EphrinAs, which are expressed in a gradient in the dLGN, repel axons that have EphAs (Nicol et al., 2007). Loss of ephrins prevents coarse targeting of retinal axons but does not prevent eye-specific segregation (Pfeiffenberger et al., 2006). This segregated salt-and-pepper organization, where segregated eye-specific domains are

scattered throughout the dLGN, is completely abolished if activity is disrupted by epibatidine. In β2 -/- mice with de-correlated stage II waves (Sun et al., 2008b), induction of eye-specific segregation is limited (Rossi et al., 2001). Even after normal segregation by P12, *nob* mice, in which spontaneous retinal waves do not subside (Demas et al., 2006), fail to maintain eye-specific segregation after eye opening.

The precise role of activity in eye-specific segregation in the dLGN remains controversial. A retinal wave, sweeping across the retina, synchronously excites RGCs from one eye. Because retinal waves are sparse, there is a small probability that waves would be present in both eyes simultaneously (Wong et al., 1993). Hebbian mechanisms rely on synchronous firing of cells to register coincident events (Constantine-Paton et al., 1990; Katz and Shatz, 1996). With spatially and temporally correlated activity, waves help report the positions of adjacent cells. Cells that "fire together, wire together" in a Hebbian-like mechanism and carve out distinct regions of dLGN (Katz and Shatz 1996; Feller 2009). Thus in theory activity, or particular elements of activity, instructs eye-specific segregation. Modeling studies provide evidence that the timing of retinal wave bursts is an appealing substrate for segregation of eye-specific (Feller, Butts et al. 1997; Butts, Feller et al. 1999; Eglen 1999; Butts, Kanold et al. 2007) and ON-OFF pathways (Lee, Eglen et al. 2002; Gjorgjieva, Toyoizumi et al. 2009). Finally, the aforementioned disruptions in activity show a timely correspondence with stages of eye-specific segregation. However, Chalupa (2009)(Chalupa, 2007; Chalupa, 2009) cites that activity does not correlate with eye-specific segregation in the protracted retinogeniculate development of the fetal macaque (Warland et al., 2006). Thus, he argues, tightly coupling of activity with retinogeniculate development seen in ferret and mouse is an

artifact and leads to the erroneous conclusion that these processes are linked. This interpretation suggests that while activity may be a requirement for eye-specific segregation, it is largely permissive for, if not simply coincident with, changes in the dLGN.

Availability of reagents provides of means for testing the role of activity in eye-specific segregation. One approach has been to isolate activity parameters responsible for segregation. Disruption of correlation with immunotoxins to starburst amacrine cells does not interfere with eye-specific segregation in ferrets (Huberman et al, 2003). However, this manipulation may have perturbed other activity parameters. In an effort to resolve this matter, Torborg (2005) crossed two strains of mice with de-correlated retinal activity to ascertain additional parameters responsible for segregation: β2 mice, which fail to segregate, and Cx36-/- mice, which do segregate. By analyzing cellular firing parameters they found that high frequency (>10Hz median burst firing frequency) synchronous firing is required for eye-specific segregation. Though this study compared three mice strains with altered activity, it is difficult to determine whether the activities varied along the same continuum. Another option is to titrate retinal activity within a mouse strain. Pharmacological titration of activity with forskolin increases retinal activity, and increases segregation, but does not identify a particular parameter of activity responsible for segregation (Stellwagen and Shatz 2002). Titration may also be achieved using a haploinsufficient heterozygote of a knockout mouse with altered activity. Unfortunately, β2 +/- mice do not present visual phenotypes (Cang et al., 2005) thus cannot be used for titration. Another mouse model must be introduced to titrate activity.

A second approach determining whether activity is instructive or permissive has been to correlate abnormal activity with disruptions in eye-specific refinement. A successful example of activity-segregation correlation is the *nob* mouse whose abnormal retinal activity emerges in conjunction with desegregation of retinal afferents, but after normal activity and segregation (Demas et al., 2006). It has been shown that improper activity in β2-/- (Muir-Robinson et al., 2002; Torborg et al., 2005) or neuropentraxins -/- mice (Bjartmar, Huberman et al. 2006) correlates with disruption in induction of eye-specific refinement. However, under these conditions activity and any activity-independent processes remain coupled, limiting the strength of conclusions. If eye-specific afferents were to undergo alternating abnormal/normal segregation in the face of corresponding abnormal/normal retinal activity, activity would be decoupled from activity-independent processes over development. This modulation would provide compelling evidence that activity is not a static player in eye-specific refinement, but a directive force.

Gβ5 is the 5th member of the Gβ family and stabilizes R7RGS (RGS6, RGS7, RGS9, RGS11) proteins that accelerate Gαi/o subunit GTP hydrolysis. Gβ5-/- mice have a lower frequency of stage II spontaneous retinal waves (Figure 2.5), normal transition from stage II to stage III waves through P10, and less correlated stage III waves (Figure 2.9). Gβ5-/- mice also exhibit a no b-wave phenotype (Rao et al., 2007), indicative of abnormal visual transmission (Peachey and Ball, 2003), and abnormal retinal activity after P14. Gβ5-/- mice have limited refinement at P7, but catch up by p10. After P10, they fail to refine further and exhibit decreased segregation in the maintenance phase as early as P12. Therefore, the Gβ5-/- mouse segregation pattern closely matches the

alternating activity abnormalities in the retina. Gβ5+/- mice have less frequent stage II waves and de-correlated stage III waves. Gβ5+/- mice also exhibit stage III correlation parameters intermediate to Gβ5-/- and Gβ5+/+. This introduces a titration of Hebbian-like activity. However, Gβ5+/- mice achieve normal eye-specific segregation suggesting either these parameters are not instructive for refinement or that a threshold must be met to achieve instruction. At P21 eye-specific segregation in *nob*xGβ5-/- mice was similar to Gβ5-/- mice suggesting a limit to the degree of desegregation of established afferents soon after P14. The Gβ5-/- mouse presents evidence that eye-specific segregation is directed by activity. This further demonstrates the critical period for eye-specific segregation ends soon after eye opening.

Methods

Animals and Genotyping

Animal protocols were identical to those described in chapter 2.

Anatomical tracing

Many of the following procedures including injections, perfusion, sections, and imaging, were performed with the kind permission of W. Guido in his lab. Mice were anesthetized using age appropriate methods (hypothermia for aged <p7, halothane all older ages). If not already exposed, the eye was accessed by separating the eye-lids (>P12) or carefully cutting the skin above the eye and cleaning away the underlying protective membrane. Filament-containing pulled pipettes of borosilate glass were used to poke a hole into the eye just above the ora serrata. A swab was then used to wick away additional fluid from they eye. Another pipette, without filament, was filled with approximately 2ul of 1% cholera toxin B (CTB)-conjugated fluorescent dye in

water/DMSO (1:1). A different conjugated dye was injected into each eye to distinguish eye-specific projections within the brain. The dye was injected into the eye through the pre-made hole using a picospritzer with nitrogen gas propellant under 10ms bursts of +10mPa. Animals then recovered quickly and were housed with parents for 2 days to allow CTB dye transport.

Images and Analysis

Animals were euthanized with halothane and transcardially perfused with 5-10ml of cold PBS followed by 20-50mL of 4% PFA/PBS. Brains were removed and postfixed in 4% PFA/PBS for two days. Brains were then sectioned though the LGN at 70µm and mounted on subbed slides. Coverslips were mounted using Prolong Gold. Serial images of LGN were captured with a Spot *SuperCool* camera onto Metamorph (Molecular Devices) software on an Olympus E600 Fluorescent microscope at 200x magnification. Images were captured with histogram assistance to ensure fluorescence was linearly quantifiable. After imaging through the bulk of the LGN, the 5 largest adjacent sections (3 for ages younger than P12), based on the number of pixels, were used for quantification. The unit of measurement was hemisphere. Individual images were then cut to the borders of the dLGN for either threshold analysis or R-analysis. Single color images were processed with the threshold function in Photoshop (Adobe, San Jose, CA) to include all pixels, usually at pixel intensity between 30-50. Images were then combined. Pixels representing ipsilateral, contralateral, and overlapping terminals where counted by custom software (courtesy of W. Guido Lab). R-analysis takes representative images and calculates the intensity log ratio of ipsilateral channel intensity to contralateral color intensity for each pixel. Pixels were the contralateral signal is 100x the

intensity of the ipsilateral signal gets a value of -2, the converse gets a value of 2, and pixels with relatively equal red and green contributions get a value of 0. A distribution of pixel intensities is then plotted. The variance of this distribution, or R-variance, reflects the degree of segregation between ipsilateral and contralateral pixels.

Statistics

Results from experiments were tested for differences based on experimental condition. JMP7 statistical analysis package executed nonparametric tests (Wilkoxen rank-sum and Kruskal-Wallis) and post hoc pair-wise comparisons (Tukey HSD test). Differences were considered significant at $p>0.05$.

Results

Anatomical tracing with fluorophores tagged cholera toxin B experiments provide a means to assess axonal transport and track eye-specific segregation. Gβ5-/- RGCs transport CTB to all retinofugal targets (dLGN, IGL and vLGN shown, Figure 3.1). RGC terminal fields demonstrate normal gross anatomical barriers and morphology based on axonal field spatial extent in Gβ5+/+ and Gβ5-/- mice throughout development (Figure 3.1). During initial refinement at P7, Gβ5-/- ipsilateral and overlapping projections are elevated (31.9±2.11%, mean ±S.E.M and 28.5±1.9% of LGN, respectively, n = 8 hemispheres) compared to Gβ5+/+ (22.0±2.3% and 15.3±2.79%, respectively, n = 6). Gβ5-/- refinement (11.0±1.1% and 17.05±1.8%, respectively, n = 10) catches up to Gβ5+/+ by P10 (9.33±1.1% and 14.1±1.6%, respectively, n =8). Similarly, contralateral projection areas are increased in Gβ5-/- mice (89.2±0.7%) compared to +/+ at P7 (78.9±3.4%), but appear normal by P10 (75.8±4.3% versus 70.7±4.6%). At P12, whereas Gβ5+/+ continue to refine, ipsilateral projections areas in the Gβ5-/- mice are again

Figure 3.1- Gβ5-/- retinogeniculate projections have limited refinement and an impaired maintenance phase. A. Representative coronal sections of Gβ5-/- and Gβ5 +/+ dLGNs. (Outlining Gβ5-/- P7, left to right) Anterograde tracing with CTB-conjugated fluorescent dyes allow simultaneous visualization of contralateral eye RGC axonal fields (in green) and ipsilateral eye RGC fields (in red). Overlaid red and green channels displays overlap of each eye's respective fields and can be better visualized as yellow in binarized images (far right). Retinogeniculate projections over development at P7, P10, P14, and P21 (top to bottom) in Gβ5-/- illustrate abnormal profiles during refinement, at P7, and during the maintenance phase at P14 and P21. Scale bar is 100 μm. B. *left to right* Ipsilateral, Contralateral and Overlap projection spatial extent as a function of time are normalized to total LGN area. Each data point reflects the mean ± S.E.M of hemispheres at that age and were calculated over five 70 μm-thick sections (three sections before P12) from the middle of dLGN. C. Rvar analysis assesses the degree of overlap in retinogeniculate projections by calculating the ipsilateral and contralateral signal intensity for each pixel and taken the log of that ratio, i.e. yielding a value of -2 for pixels in which the contralateral signal is 100 times more intense than the ipsilateral signal. When pixel log ratios are plotted as a distribution by percent area of dLGN, separation of peaks in example traces (shown at P7, P10, P14, and P21) indicate increased segregation of projections. D. Variance of R-analysis is proportional to segregation and plotted as a function of time. Measurements are represented as mean ± S.E.M (*, Wilkoxen rank-sum, $p<0.05$). Number of hemispheres used from Gβ5-/-[number of animals] and (Gβ5+/+[number of animals]) at each age are: P7, 6[3] (8[4]); P10, 10[5] (8[4]); P12, 6[3] (8[4]); P14, 10[5] (10[5]); P18, (6[3] (6[3]); P21, 6[3] (8[4]). Asterisks indicate significant differences between groups (Wilkoxen rank-sum, $p<0.05$).

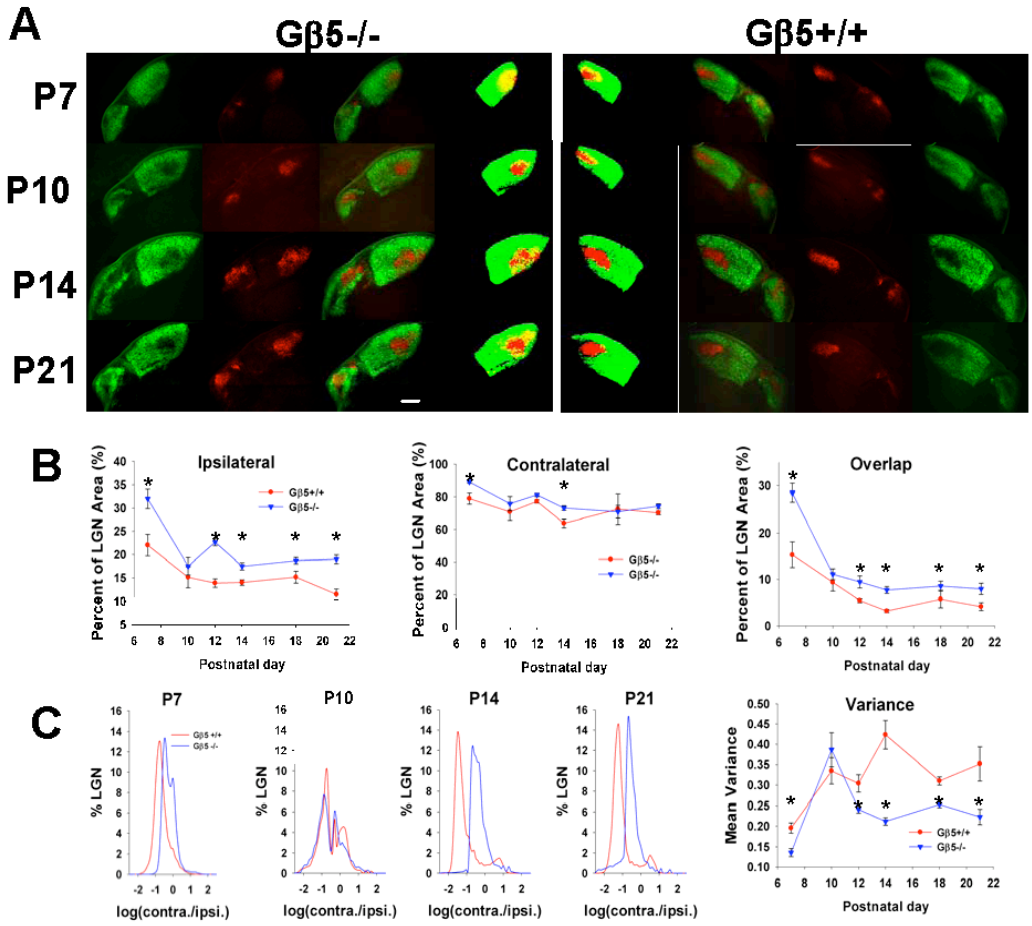
A
Gβ5-/-
Gβ5+/+
P7
P10
P14
P21
B
Ipsilateral
Contralateral
Overlap
Percent of LGN Area (%)
Postnatal day
Gβ5+/+
Gβ5-/-
C
P7
P10
P14
P21
Variance
% LGN
log(contra./ipsi.)
Mean Variance

Figure 3.1

larger than Gβ5+/+ (22.6±0.7%, n = 6, versus 13.88±1.08%, n = 8). These projections contribute to increases in overlapping territories (9.44±1.2% versus 5.45±0.4%). Ipsilateral and overlap of projections areas in Gβ5-/- mice remain high at P14 (17.4±0.7% and 7.69±0.7%, respectively, n = 10) compared to Gβ5+/+ (14.01±0.5% and 3.21±0.3%, respectively, n = 8). At P14, contralateral areas in Gβ5-/- (73.12±4.3) are also large compared to Gβ5+/+ (63.72±2.6%) but return to normal levels by P18 (70.8±3.4% in Gβ5-/-, n = 6, versus 72.4±9.4, n = 6). Gβ5-/- dLGNs exhibit larger ipsilateral and overlapping areas as late as P21 (19.00±0.9 and 7.9±1.2%, respectively, in Gβ5-/-, n = 6, versus 11.46±1.1% and 4.15±0.8%, respectively, n = 8). These results demonstrate that Gβ5-/- mice have slow early segregation, achieve normal segregation by P10, but stop refining by P12.

We also employed R-variance analysis, which measures the contralateral and ipsilateral intensities of each pixel. R-variance verifies our threshold-based results. R variance analysis indicates Gβ5-/- mice decreased segregation at P7 (0.13±0.01, mean ±S.E.M, n = 3 LGNs for all groups) versus Gβ5+/+ (0.19±0.1) and roughly corrects by P10 (Figure 3.1C, 0.38±0.4 for -/- and 0.33±0.3 for +/+). During maintenance, mean variance plots (Figure 1C, right) reveal a reduction in segregation in Gβ5-/- mice through P21 (ranging 0.21-0.25) relative to Gβ5+/+ (ranging 0.31-0.42), confirming threshold analysis results. Plots used to visualized R-analysis show a right-shifted distribution at P7, indicating a greater proportion of unsegregated pixels, yet similar distributions at P10 (Figure 3.1C, left). R-variance plots at P14 and P21 remain unsegregated in Gβ5-/- mice. We conclude from these results that Gβ5-/- mice have eye-specific segregation phenotypes in both induction and maintenance phases but temporarily normalize at P10.

Figure 3.2- Gβ5 and RGS7 are reduced in Gβ5+/- dLGNs at P7. A. *above,* Representative immunoblot of dissected and homogenized dLGN at five and thirteen days after enucleation (2 hemispheres per lane) were probed with antibodies specific for Gβ5 (Gβ5S). *B. above,* Immunoblots of dissected and homogenized dLGN (2 hemispheres per lane, Gβ5+/- n = 5 animals, Gβ5+/+ n = 5 animals) were probed (by C-K. Chen) with antibodies specific for Gβ5 (Gβ5S) and RGS6/7 (7C-1) epitopes. Loading control is GAPDH and genotypes are indicated above Gβ5S band. *Below* Quantification of Gβ5S, RGS6, and RGS7 amounts in dLGN (also kindly by C-K. Chen) are normalized to GAPDH loading control. Asterisks indicate significant difference between groups (Wilkoxen rank-sum, $p<0.05$).

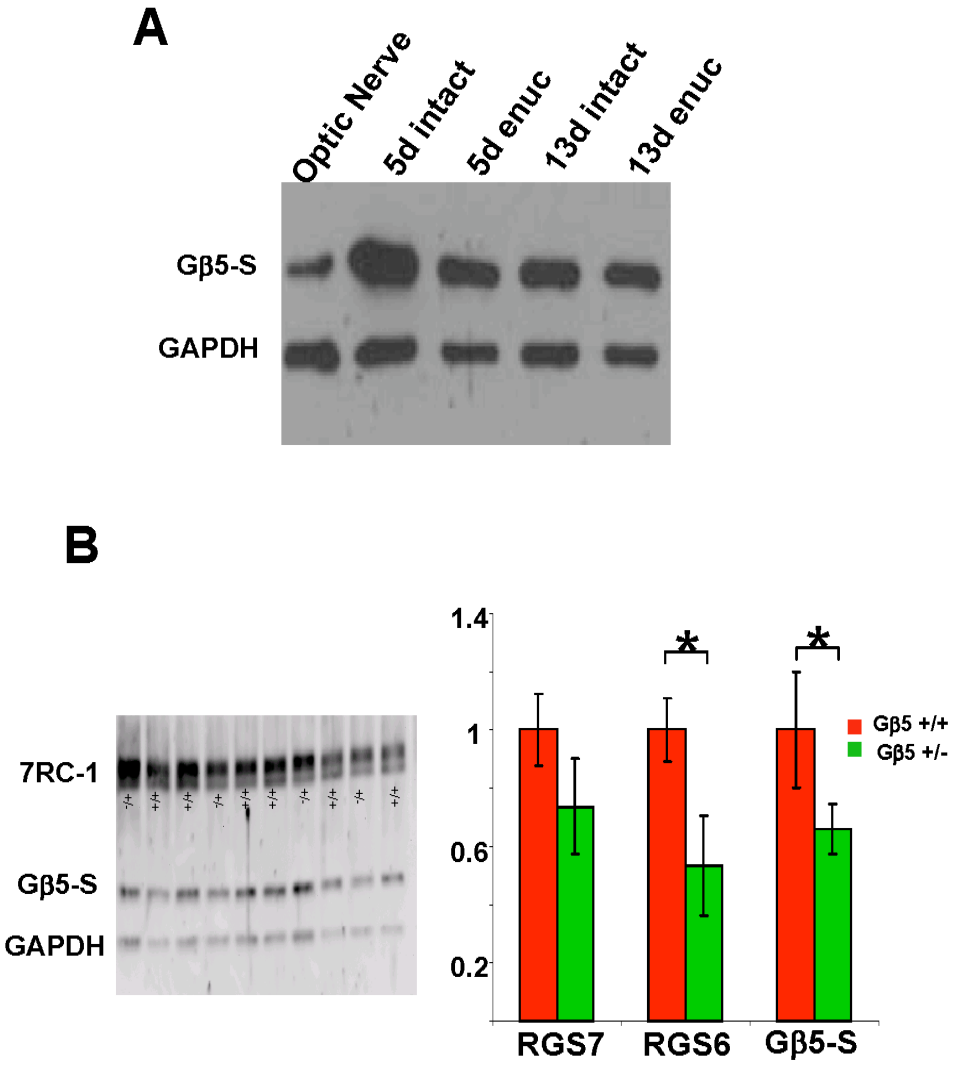
A
Optic Nerve
5d intact
5d enuc
13d intact
13d enuc
Gβ5-S
GAPDH
B
7RC-1
Gβ5-S
GAPDH
1.4
1
0.6
0.2
*
*
Gβ5 +/+
Gβ5 +/-
RGS7
RGS6
Gβ5-S

Figure 3.2

In the retina at P7, Gβ5 protein levels in the Gβ5+/-, but not R7RGS protein levels, are lower than Gβ5+/+ (Figure 2.3B). If levels were significantly decreased in the dLGN, it may be used for comparison to identify the source of the Gβ5-/- refinement phenotype. To ensure that Gβ5 was in dLGN and not contaminated by Gβ5 in the optic nerve, we performed enucleation experiments and analyzed dLGNs after 5 and 13 days (Figure 3.2A, dissections performed by T. Seabrooke and blots performed by C.K. Chen). After 5 and 13 days, we expect Gβ5 would be gone if it was only in the axonal terminals. Gβ5 is clearly present in the dLGN at both timepoints in the absence of an optic nerve where Gβ5 resides. Second, immunoblots of carefully dissected Gβ5+/- and +/+ dLGN were probed with antibodies for Gβ5 or RGS6/7 and quantified for protein levels (Figure 3.2B, probing and quantification by C.K. Chen). Like retina, Gβ5+/- dLGNs have decreased levels of Gβ5 compared to dLGN (65% ± 0.08 of Gβ5 +/+, mean± S.E.M, n = 10 hemispheres, 5 animals, $p<0.005$). Surprisingly, Gβ5+/- RGS7 amounts (76% ± 0.07 of +/+) are not different from Gβ5+/+, whereas RGS6 amounts are (53% ± 0.17, $p<0.05$).

Utilizing the Gβ5 +/- mouse to titrate Gβ5 and RGS7, we then examined the projections of Gβ5 +/- dLGNs. Morphological and eye-specific patterning appeared normal in Gβ5+/- dLGNs (Figure 3.3A). Quantification of Gβ5+/- ipsilateral (23.82±3.4%), contralateral (84.35±3.5%), and overlapping projections (19.78±4.11%) revealed no differences from Gβ5+/+ at P7, where the Gβ5-/- has a significantly increased spatial extent and overlap of ipsilateral and contralateral areas (Figure 3.1B). Similarly, Gβ5+/- ipsilateral, contralateral, and overlapping projections are not different from Gβ5+/+ as late as P21 (Figure 3.3B). The number of Gβ5+/- hemispheres [and animals] at each age are: P7, 6[3]; P10, 8[4]; P12,6[3]; P14, 6[3]; P18, 6[3]; P21, 6[3].

Figure 3.3- Retinogeniculate refinement in Gβ5+/- mice is similar to Gβ5+/+ A. Representative coronal sections of Gβ5+/-(left) and Gβ5+/+ (Chang et al.) over development were obtained by anterograde tracing experiments as described in Figure 1. Central images are binarized and reveal overlap of ipsilateral and contralateral projections (in yellow) in Gβ5+/- and Gβ5+/+. B. Axonal terminal areas of ipsilateral, contralateral, and their respective overlap are plotted as a function of age. C. Examples of R-analysis traces over development show the distribution of log (ipsilateral intensity/contralateral intensity) for each pixel within an image. Traces that largely overlap represent similar degrees of segregation. D. Variance of R-analysis is plotted as a function of age and illustrates the degree of refinement at each age. Gβ5+/+ numbers are the same as in figure 1. Number of Gβ5+/- hemispheres [animals] at each age are: P7, 6[3]; P10, 8[4]; P12,6[3]; P14, 6[3]; P18, 6[3]; P21, 6[3]. Differences were not found between groups (Wilkoxen rank-sum, $p<0.05$).

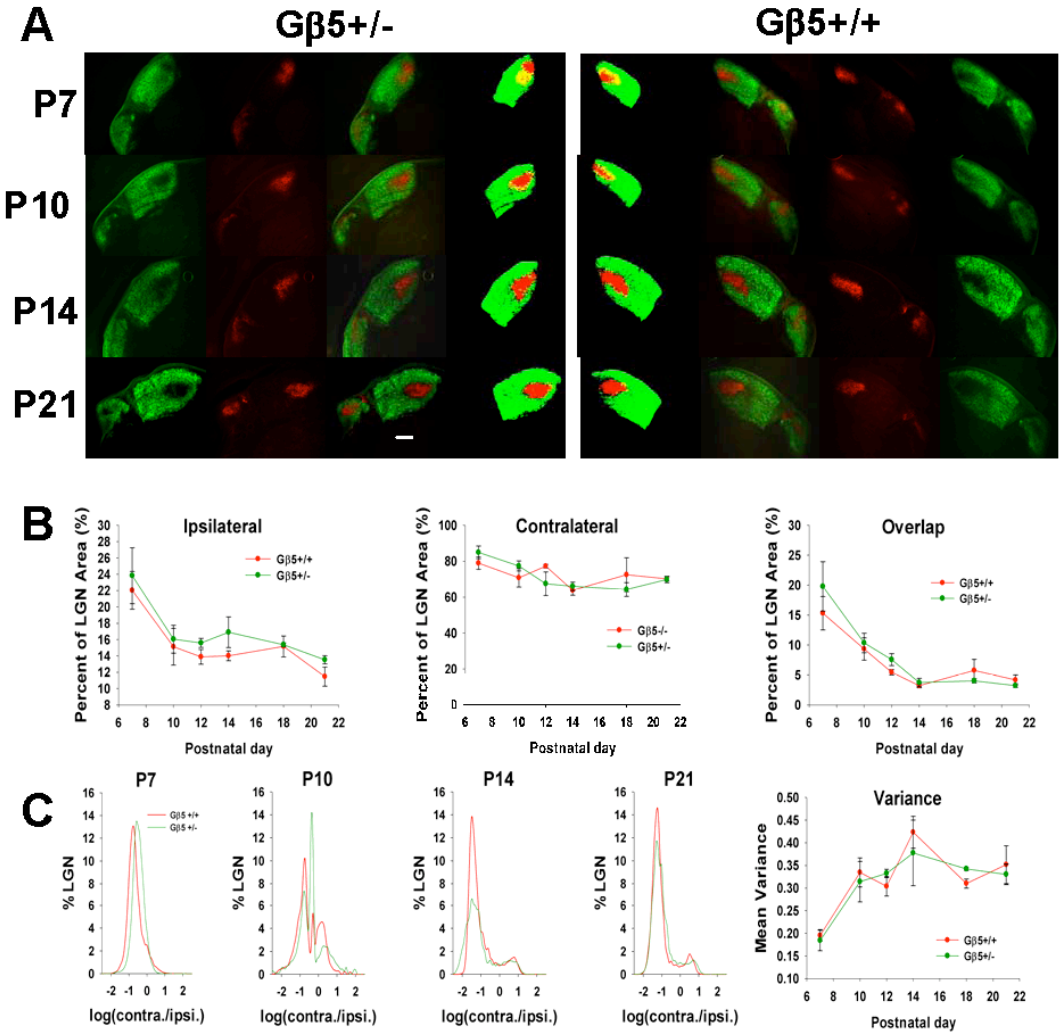
A
Gβ5+/-
Gβ5+/+
P7
P10
P14
P21
B
Ipsilateral
Percent of LGN Area (%)
Postnatal day
Gβ5+/+
Gβ5+/-
Contralateral
Gβ5-/-
Overlap
C
P7
P10
P14
P21
% LGN
log(contra./ipsi.)
Variance
Mean Variance

Figure 3.3

R-analysis and R-variance quantification (Figure 3.3 B and C, R-variance values: P7, 0.18±0.2; P10, 0.31±0.4; P12-21, range 0.33-0.37, n = 3 LGNs per age) confirm our threshold-based findings that Gβ5+/- dLGNs have a similar degree of segregation to Gβ5+/+ from P7-P21. We conclude that Gβ5+/- mice segregate normally.

To elaborate on the course of Gβ5-/- segregation, we examined the retinogeniculate development of earlier (P3) and later (P28) ages in Gβ5-/- dLGNs. At P3, we see both ipsilateral and contralateral projections have targeted the dLGN and overlapping in a similar manner to Gβ5+/+ (Figure 3.4A). Ipsilateral and overlapping Gβ5 -/- projections (49.2±4.5% and 41.5±4.3%, respectively, n = 10) are similar to Gβ5+/+ measures (53±3.8% and 41.16±5.5%, n = 6) at P3. Gβ5-/- contralateral projections are somewhat elevated (79.1±4.1% versus 66.4±5.9% in Gβ5+/+, $P<0.05$), but still indicate RGC targeting in the dLGN. At P28, long after the failure of eye-specific segregation maintenance, we continue to see increased ipsilateral, overlapping, and even contralateral projection areas in Gβ5-/- mice (17.7±0.4% 7.3±0.3%, and 75.7±2.11%, respectively, n = 6, compared to 12.12±1.2%, 5.3±0.7%, and 69.4± 1.18%, respectively, in Gβ5+/+, n = 6). From these results we conclude that Gβ5-/- mice begin retinogeniculate refinement like Gβ5+/+, have limited refinement through P7, rapidly refine through P10, and fail to recover from their segregation pause in the maintenance phase as late as P28.

Because Gβ5 is in the dLGN, we asked whether a normal R7RGS complex was required in dLGN for the refinement seen at P7. Previous reports (Gold et al., 1997) suggest that RGS7 is the sole R7RGS in adult dLGN, even though our western results suggest RGS6 may be present as well (Figure 3.2). We obtained a mouse with a mutant

Figure 3.4- Assessment of retinal projections at extreme ages in Gβ5-/- and early eye-specific segregation in SG7 and *nobx*Gβ5-/- mice. A. Gβ5-/- LGNs begin with normal segregation at P3 and have impaired maintenance as late as P28. Ipsilateral, contralateral and overlapping projections areas are plotted as a function of age from P3 to P28. Data for P7-P21 is the same a data in figure 1 and is presented for comparison. Number of hemispheres used from Gβ5-/-[number of animals] and (Gβ5+/+[number of animals]) are: P3, 13[7] (4[2]); P28, 6[3] (6[3]). Asterisks indicate differences between groups (Wilkoxen rank-sum, $p<0.05$). B. Animals lacking normal RGS7 have normal overlapping projections at P7. Bar graph compares contralateral and ipsilateral projection overlap in SG7 mutant mice (6 hemispheres, 3 animals) with Gβ5+/+, Gβ5+/-, and Gβ5-/- areas presented for reference. Asterisks indicate differences from WT (Kruskal-Wallis, Tukey HSD, $p<0.05$). C. Gβ5-/- and *nob*xGβ5-/- mice have similar maintenance phenotypes at P21. Bar graph compares contralateral and ipsilateral projection overlap in *nob*xGβ5-/- mice (4 hemispheres, 2 animals) with Gβ5+/+, Gβ5+/-, and Gβ5-/- areas presented for reference. Asterisks indicate differences from WT (Kruskal-Wallis, Tukey HSD, $p<0.05$).

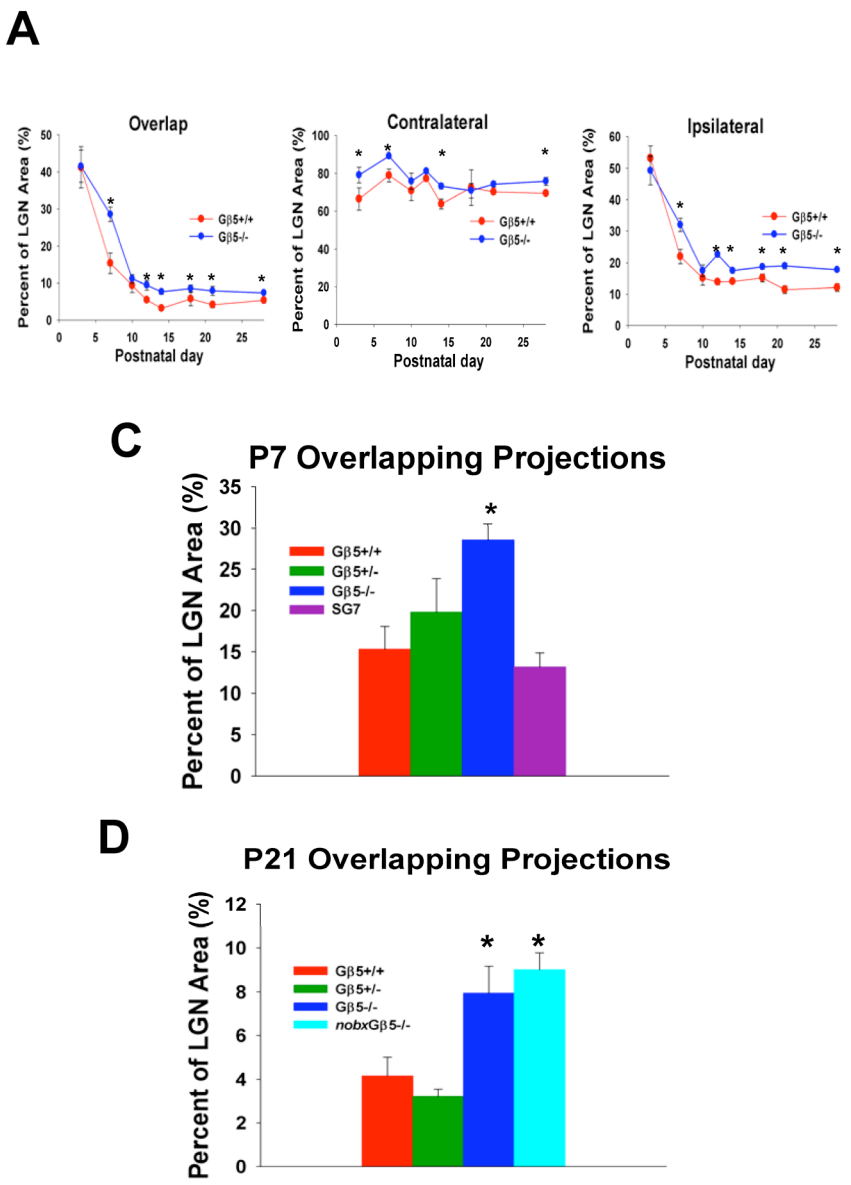
A
Overlap
Contralateral
Ipsilateral
Percent of LGN Area (%)
Postnatal day
Gβ5+/+
Gβ5-/-
C
P7 Overlapping Projections
Percent of LGN Area (%)
Gβ5+/+
Gβ5+/-
Gβ5-/-
SG7
D
P21 Overlapping Projections
Percent of LGN Area (%)
Gβ5+/+
Gβ5+/-
Gβ5-/-
nobxGβ5-/-

Figure 3.4

RGS7, SG7, which is incapable of compensating for loss of RGS11 in the OPL (Chen et al., 2010; Zhang et al., 2010). SG7 mice do not exhibit the decreased interburst interval seen in Gβ5-/- mice (Figure 2.6), making them good candidates for testing R7RGS activity in the dLGN alone. At P7, overlapping projections in SG7 dLGNs (13.3±1.6%, n=4, 2 animals, Figure 3.4B) were similar to Gβ5+/+ dLGNs, suggesting that a normal RGS7 complex is not required in the dLGN for the normal induction of RGC afferent segregation.

Both Gβ5-/- and *nob* mice fail to maintain established segregation (Figure 3.1; Demas et al., 2006). In an effort to understand the underlying mechanism of maintenance loss, we asked how Gβ5-/- and *nob* maintenance phenotypes might interact. To this end, we examined the overlap of retinogeniculate projections of *nob*xGβ5-/- mice at a stable time point of maintenance, P21 (Demas et al., 2006). *nob* animals were crossed with Gβ5+/- and offspring were mated to generate *nob*xGβ5-/- mice. We find that overlap of ipsilateral and contralateral projections in *nob*xGβ5-/- mice (8.99±0.7%, n=4, 2 animals, Figure 3.4D) were similar to single Gβ5-/-, yet still different from both Gβ5+/+ and Gβ5+/-. We conclude that *nob*xGβ5-/-, Gβ5-/-, and likely *nob* mice, exhibit similar maintenance failure phenocopies.

Conclusions

In this study, we investigated the retinogeniculate projections of mice with diminished R7RGS activity and arrived at five conclusions. 1) After targeting the dLGN (Figure 3.4A), retinal afferents in Gβ5-/- exhibit slower induction of refinement (Figures 3.1), but eventually refine to Gβ5+/+ levels by P10. 2) As Gβ5+/+ continue to refine, at P12 there is a sudden loss of established refinements. 3) RGS6 and Gβ5 are decreased in

the dLGNs of Gβ5+/- mice. 4) Gβ5+/- animals do not exhibit a retinogeniculate refinement phenotype (Figure 3.3), although they have less Gβ5 and RGS7 in the dLGN (Figure 3.2B), and that normal RGS7 is not necessary for refinement (Figure 3.4B). 5) *nob*xGβ5-/- mice dLGN (de-) segregation levels are similar to Gβ5-/- mice (Figure 3.4C).

Eye-specific refinement of Gβ5-/- mice and the onset of maintenance

The initial refinement of retinogeniculate afferents has been extensively described in ferret and several mouse models (Muir-Robinson et al., 2002; Torborg et al., 2004; Torborg and Feller 2005; Torborg et al., 2005; Bjartmar et al., 2006; Stevens et al., 2007; Huberman et al., 2008). Of particular interest, especially regarding activity-dependant mechanisms of refinement, is the ACh β2-/- mouse in which activity is de-correlated (Torborg et al., 2005; Sun et al., 2008) and eye-specific segregation fails (Rossi et al., 2001; Muir-Robinson et al., 2002). β2-/- mice eventually segregate after onset glutamatergic activity, though with a persistently abnormal pattern. We find Gβ5-/- mice also have limited initial eye-specific refinement but subsequently refine by P10 with a normal eye-specific patterning, much sooner than β2-/- mice. This suggests the respective segregation phenotypes in the two mouse lines may have different sources of impairment. Identifying the dominant phenotype by crossing the two animals may provide insight into the exact differences between β2-/- and Gβ5-/- segregation.

Because maintenance of eye-specific segregation is normally static process, maintenance is observed indirectly by disruption (Chapman, 2000; Demas et al., 2006). Therefore, plastic anomalies during the maintenance phase are an indication of an underlying maintenance process. Gβ5-/- afferents exhibit a relative cessation of their refinement at P12, even as Gβ5+/+ eye-specific afferents continue to refine. This

refinement halt is a combination of a dramatic increase in ipsilateral area, an abnormal plastic event, in the presence of continued refinements in contralateral area (Figure 3.1). The ipsilateral territories then remain high. The contralateral area is similar to Gβ5+/+ at several points save P14 and P28 where it is abnormal, but not drastically different like ipsilateral projections (Figure 3.4A). Overall, these data suggest that Gβ5-/- afferents have a loss of segregation during the maintenance phase and that ipsilateral projections are the main source of the significantly increased overlapping afferents.

Loss of established segregation provides a means to understand when the maintenance phase begins. Demas, et al (2006) could only determine plastic events starting at P12. At that age both Gβ5-/- and *nob* show increased ipsilateral areas, however, only Gβ5-/- have decreased segregation compared to Gβ5+/+. The addition of the P10 time point in this study suggests the onset of the maintenance phase as sometime after P10 but before P12. This adjusts the beginning of the maintenance phase to an earlier point than previously described. However, determining the precise timing of retinogeniculate phases may be better clarified using pharmacological means, such as APB (Chapman, 2000), over a staggered timeline, thus bypassing any questionable development or intrinsic dLGN confounders.

Source of LGN phenotype and retinal activity in Gβ5-/-

We performed several experiments in an attempt to identify the source of the Gβ5 refinement phenotype at P7. RGS7 was previously thought to be the only R7RGS in the dLGN based on *in situ* hybridization (Gold et al., 1997). Following this assumption, we employed SG7 mice, with a hypomorphic RGS7, to determine if RGS7 has a role in the dLGN. SG7 mice are suitable because do not exhibit the increased IWI phenotype seen in

Gβ5 -/- mice (Figure 2.6). We found no differences in the segregation of SG7 and Gβ5 +/+ or Gβ5+/- dLGNs. We also performed immunoblots indicating that Gβ5 is in the LGN. If Gβ5 were acting at the dLGN, animals with reduced Gβ5 would have a similarly reduced segregation (Figure 3.2). However, Gβ5+/- mice have a decrease in Gβ5 but do not have a segregation phenotype. Surprisingly, Gβ5 +/- mice also have diminished levels of RGS6 in the dLGN, identifying previously unsuspected R7RGS in the dLGN (Gold et al., 1997). Our data initially suggests Gβ5 does not play a role in the LGN during refinement at P7. However, firmer conclusions could be reached by P7 tracing experiments with a proper RGS7-/-, the RGS6-/-, and even the RGS6/7-/-.

We argue that Gβ5 is not involved in the dLGN at P7 for two reasons. First, at P7, Gβ5 +/+ dLGNs have very low expression of Gβ5 that may be below critical levels (Figure A13B). Second, activity dependant refinement is likely to operate by sufficiently depolarizing postsynaptic cells (Guido, 2008). $GABA_B$, a GPCR coupled to Gαi/o, delivers the slow inhibitory component of postsynaptic relay cell responses. However, $GABA_B$ currents not emerge as a significant influence until P10 (Ziburkus et al., 2003) long after we see the refinement phenotype. Therefore, though Gβ5 is in the dLGN, it does not likely play a role until later stages of development. Unfortunately, Gβ5 levels in Gβ5+/- mice are similar to Gβ5+/+ by P14, at least in retina, rendering the Gβ5+/- less useful as a Gβ5 titrating agent during the maintenance phase. Ideally, either an LGN-specific knockout of Gβ5 or RGS7 and 6 would give a conclusive result. To date, however, the absence of an effective LGN-specific Cre driver makes this experiment impossible. However, an RGS7/6 -/- could be useful to clarify the role R7RGS activity in the dLGN , but only if the waves are not also abnormal.

Comparison of *nob* and Gβ5-/- phenotypes in maintenance

Gβ5 -/- and *nob*xGβ5-/- exhibit similar phenotypes (Figure 3.4D): decreased segregation of projections at P21. Are the maintenance phenotypes seen in Gβ5-/- mice the same problem as those in *nob*? Though a direct comparison was not performed segregation levels of *nob* mice, when overlaid with Gβ5-/- and *nob*xGβ5-/- all are similar. Additionally, *nob*xGβ5-/- cross mice do not desegregate beyond the individual genotypes. These results suggest Gβ5-/- and *nob* phenotypes have the same source, OPL lack of transmission in the retina (Pardue et al., 1998; Rao et al., 2007). For the purposes of this discussion, we will consider the phenotypes "phenocopies" that appear similar but may have different underlying causes (electrical or organic). For instance, Gβ5 -/- mice may have increased inhibitory drive after P12, thereby limiting any further refinement. Or *nob*xGβ5-/- mice may have some combination of activity anomalies. An alternative possibility is that there is a ceiling for refinement. With that addition of the Gβ5 -/- and *nob*xGβ5 -/-, it is clear that all three loss-of-maintenance mouse strains possess similar segregation levels, regardless of the source. Such a consistent finding suggests that once axons have arrived and segregated through P12 in the dLGN, they remain in a scaffold that limits coarse rearrangement.

Maintenance program does not require a normal eye-specific segregation program

Development often relies on a sequence of successful steps. In a nihilist scheme, if an early step is incorrect, like in abnormal eye-specific refinement in the β2 -/- mouse (Muir-Robinson et al., 2002), future steps are similarly anomalous or aborted. Alternatively, in vision, survivalist schemes are also observed. For example, cortical plasticity may be capable of salvaging an improper image from that same β2 -/- dLGN

(Grubbs et al., 2003; Cang et al., 2005) because some sight is better than none. In retinogeniculate development, two phases have been defined: refinement and maintenance. It is clear that both phases can be observed independently as with the β2 -/- mouse (Muir-Robinson et al., 2002) and the *nob* (Demas et al., 2006) mouse models.

Do these two phases constitute a single continuous process, one with the same rules throughout, or more than one process, where induction of refinement and maintenance are not a continuous processes? Decoupling events in retinogeniculate refinement has been a useful approach to such questions (Huberman et al., 2002). Ideally, a model that uncouples both phases would be suitable to ask this question, where maintenance can occur in the presence of an altered induction process. The difficulties lie in 1) detecting the maintenance phase (indirectly) and 2) achieving a suitable degree of refinement to reveal any changes in the maintenance phase. Gβ5 -/- mice satisfy both of these criteria. Induction of refinement in Gβ5 -/- mice is disrupted and briefly recovers, though not far enough to see a distinct "loss" of maintenance. Gβ5 -/- mice then have maintenance segregation levels similar to *nob (*Figure 3.1, Demas et al., 2006). If plasticity is all that is needed to determine a maintenance process, in Gβ5 -/- mice we observe a decoupling of refinement and maintenance. This interpretation suggests that normal refinement is dispensable for the plasticity during maintenance phase. An alternative explanation lies within the dLGN itself. Gβ5 may dampen geniculate plasticity during maintenance by prolonging inhibitory processes like $GABA_B$ (Crunelli and Leresche, 1991). Temporarily suspending this possibility, however, our findings offer the possibility that problems seen in maintenance phases will be independent of earlier developmental detours.

Discussion of retinogeniculate development

Retinal activity and retinogeniculate refinement

As mentioned in the introduction, the role of retinal activity in retinogeniculate refinement is hotly contested (Chalupa 2009; Feller 2009). Gβ5-/- mice have abnormal stage II and stage III retinal activity as well as coincident refinement and maintenance phenotypes. At P7, Gβ5-/- retinas have an increased interwave interval, increased interburst interval, and decreased overall activity (Figures 2.4B and 2.5). Decreased activity and increased interwave interval are seen in P7 Gβ5+/- as well. Gβ5-/- mice, but not Gβ5+/- mice, have a significantly decreased eye-specific segregation at P7. This implies that the interburst interval, the only unique feature of Gβ5-/- retinal activity, is responsible for the phenotype. The magnitude and frequency of depolarization is critical to proposed intracellular mechanisms of refinement in relay cells (Guido, 2008). The interburst interval parameter fits well with that hypothesis. Indeed, the bursting dynamics alone, collectively called burst timing dependant plasticity (BTDP), could reasonably drive eye-segregation based on modeling studies (Butts et al., 2007). Another option is that the Gβ5-/- phenotype is the result of Gβ5 loss in the dLGN. This cannot be ruled out completely but we conclude it is not the case based on the discussion above. At P7 Gβ5+/- mice have normal segregation, however still exhibit altered retinal activity. We propose that Gβ5+/- increased peak burst activity may rescue the refinement phenotype even in the face of low IWI. Such a process would be similar to forskolin altering the IWI (Stellwagen and Shatz 2002) but retaining the critical >10Hz synchronous firing (Torborg et al., 2005) that is lacking in β2 retinas. A similar case can be made for low Gβ5 in the

Gβ5+/- dLGN. Another possibility is that some aspect of Gβ5+/- activity is above an "instructive" threshold.

Interestingly, Gβ5-/- dLGNs recover to wild-type levels by P10, during the transition from cholinergic to glutamatergic activity. Gβ5-/- mice do undergo a normal transition from stage II to stage III (Figure 2.6), suggesting that the transition itself may provide a "reset" on activity and rectify refinement phenotypes. Indeed, β2-/- mice have an early transition (Bansal et al., 2000). But there is no P10 timepoint to match. Given the P7 and P14 phenotypes, it is likely P10 is also de-segregated. This suggests stage transitions that occur within the normal window constitute normal activity.

At P12, both Gβ5-/- and Gβ5+/- mice have a reduced ST correlation of retinal activity in stage III (Figure 2.7), however, only Gβ5-/- exhibit the decreased segregation (Figure 3.1). Correlated activity, synonymous with synchronous activity, is a critical element in the Hebbian hypothesis (Constantine-Paton et al., 1990) but its utility for eye-specific segregation has been challenged (Huberman et al., 2003). Superficially, these results appear to confirm the Huberman finding. However, closer examination reveals two dose-dependant RGC burst parameters, the percent of spikes in bursts and the mean spikes per burst (both related to the measurement of ST correlation). Thus retinal afferents may have to achieve a threshold of correlated/interburst activity in order to refine further or avoid desegregation.

At P14 (and P28), Gβ5-/- retinas display persistent wave activity at a higher frequency than Gβ5+/+ and Gβ5+/- (Figure 2.11). Gβ5-/- mice also have impaired OPL transmission that constitutes abnormal patterned vision. Consistent with activity-driven

refinement, Gβ5-/- dLGNs remain less segregated than Gβ5+/+ as late as P28, similar to *nob*.

No b-wave phenotype correlates with maintenance failure

Previous compelling evidence supporting an instructive role for activity came from studying *nob* mice (Demas et al., 2006). Persistent abnormal activity, even in the dark, prevented maintenance of eye-specific afferents after eye opening. Demas et al concluded that the abnormal activity, and not merely a disruption of normal patterned vision, drives maintenance failure. While Gβ5-/- mice have slightly perturbed activity at P14 (Figures 2.11, 2.12, and 2.13), their disruption pales in comparison to the *nob* mouse. Yet both Gβ5-/- and *nob* dLGNs have maintenance failure. In combination, *nob*xGβ5-/- mice possess RGC firing traits of Gβ5-/- *and* rhythmic harmonic firing and still exhibit a similar phenotype as Gβ5-/-. We assume that the *nob*xGβ5-/- also has a no b-wave phenotype. In short, the activities of both Gβ5-/-, *nob*xGβ5-/-, and *nob* retinas are vastly different yet associate the same dLGN phenocopy. The salient common feature among all these animals is a no b-wave phenotype. Therefore, maintenance may simply require normal OPL signaling whose fine parameters have not yet been observed.

To make firm conclusions, three critical sets of data must be obtained. First, the activity of the P21 *nobx*Gβ5-/- and Gβ5-/- retinas must be assessed for a direct comparison with P21 dLGNs. Second, the dLGN phenotypes of *nobx*Gβ5-/- appear stable because both *nob* and Gβ5-/- are stable at P21. However, a more comprehensive timeline that includes P14 and P28 would allow a better comparison of activity to eye-specific segregation. Third, though Gβ5+/+ can be used as a reference, the measurements of *nob* dLGNs should be directly compared with *nob*xGβ5-/-. Together, these experiments will

Figure 3.5 – Gβ5-/- mice have an abnormal-normal-abnormal activity-segregation profile. Chart shows activity-segregation profiles for Gβ5-/- and two seminal segregation models: β2-/- and *nob*. "X" indicates improper activity or refinement. A green "check" indicates normal activity or segregation. In the case of β2-/- mice, ensemble activity has only been assessed before P12 and normal retinal activity is assumed between P14-28. In *nob* mice, segregation has not been assessed at P10.

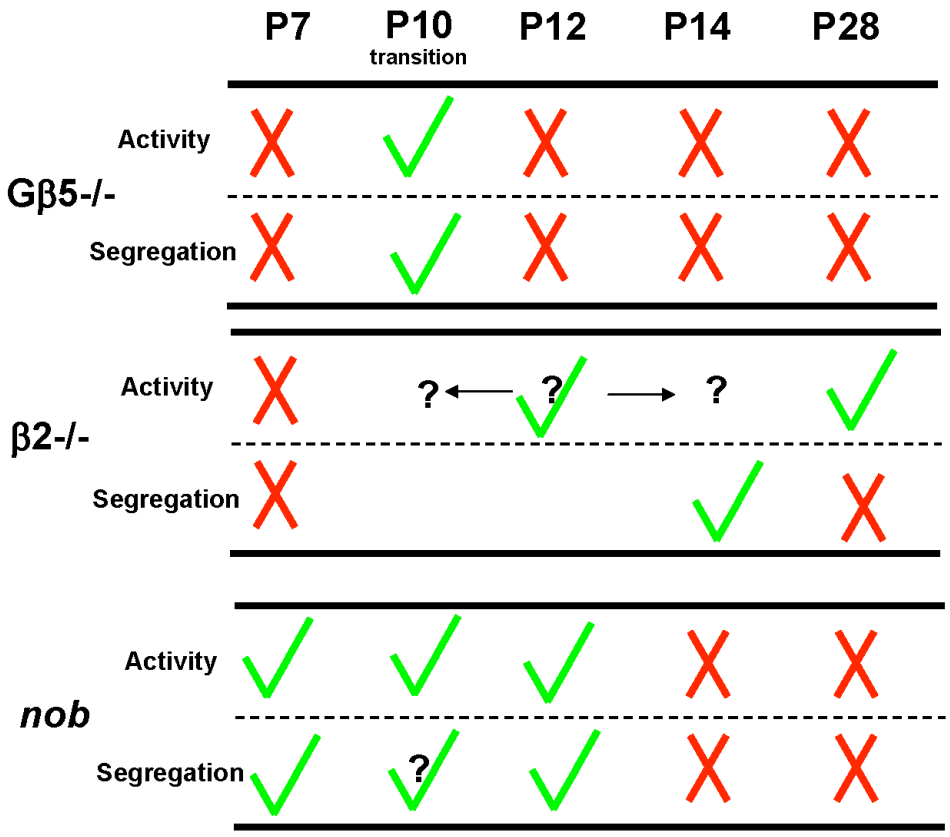
P7
P10
transition
P12
P14
P28
Activity
Gβ5-/-
Segregation
Activity
β2-/-
Segregation
Activity
nob
Segregation

Figure 3.5

help titrate the relative activity of no b-wave animals and eye-specific segregation during the maintenance phase, a thereby clarifying the elements of activity that drive de-segregation (Demas et al., 2006). Finally, if a "no b-wave" phenotypes does indicate a maintenance failure, testing other *nob* animals may provide further support for this conclusion.

Abnormal-normal-abnormal retinal activity correlates with eye-specific segregation in dLGN

Much of the debate regarding activity's role in eye-specific segregation hinges upon whether activity is instructive (necessary and sufficient where activity levels correspond directly to degree of segregation; Feller, 2009) or permissive (activity is only necessary; Chalupa, 2009). In many cases, the evidence in favor of an instructive role suffer from the inability to isolate activity from organic mechanisms. Previous experimental designs did not titrate activity parameters to show a dose-response (Penn et al., 1998; Stellwagen and Shatz 2002; Torborg, Hansen et al. 2005). This study has similar pitfalls but emerges with one clear finding. In Gβ5-/- mice, abnormal stage II retinal activity, a timely stage II-III transition, and abnormal stage III waves correspond with abnormal induction of refinement, relative recovery at P10, and decreased segregation during the maintenance phase. This abnormal-normal-abnormal profile in Gβ5-/- mice presents a tight correlation of activity with eye-specific refinement. The types of activity that are critical may vary depending on the stage of retinogeniculate refinement and require further study. Salient differences in Gβ5-/- activity, the interburst interval and correlative firing within a burst, appeal to a Hebbian mechanism of

reinforcement. Ultimately, this activity-segregation correlation provides more solid evidence in favor of instructive roles than titration alone.

CHAPTER 4

State of retinofugal projections in mice with retinal remodeling after photoreceptor degeneration

Abstract

Photoreceptor degeneration (PD) is a common cause of blindness. Recent studies demonstrate that degeneration of photoreceptors triggers retinal remodeling in which neuronal glial, and vascular elements are reorganize in the retina. To understand the impact retinal remodeling after PD on the structure and function of central visual targets, we compared two mouse models of photoreceptor degeneration with different degrees of retinal remodeling. We used two aged mouse models: the ΔCT mice with little remodeling and the TG9N mice with aggressive remodeling. We made intravitreal injections of Alexafluor-conjugated cholera toxin B (CTB) to anterograde label targets of retinal projections in the brain. We also measured consensual pupillary light reflex (PLR) and recorded evoked synaptic responses of relay cells in the dorsal lateral geniculate nucleus (dLGN) to examine whether retinal projections make functional connections with their central visual targets. In ΔCT and TG9N models after photoreceptor degeneration, we found that retinal innervation, topography, and eye-specific patterning are greatly preserved in all recipient targets including suprachiasmatic nucleus, dLGN, pretectal nucleus and superior colliculus. In dLGN, the pattern of innervation and the degree of segregation of ipsilateral and contralateral retinal projections were indistinguishable from age-matched controls. All animals displayed PLRs at 12,000 cd/m^2 light intensity, however, degenerated mice had a significantly reduced constriction after 30 seconds, consistent with a decrease in melanopsin positive cells. Evidence of a functional

retinogeniculate synapse was also found in all animals by *in vitro* recordings of dLGN relay cells in brain slices. We conclude that retinal remodeling does not grossly affect the structural and functional state of retinofugal projections.

Introduction

One of the worst clinical conditions, and certainly the worst visual condition, is blindness. In a survey of Americans, blindness was considered a fate comparable to death (Saaddine et al., 2003). Sadly, almost two-thirds of Americans over seventy have some form of major visual impairment. While some of these conditions are treatable, like cataracts and myopia, some, like macular degeneration or retinitis pigmentosa (RP)(Rattner and Nathans, 2006), are progressive and irreversible: dooming many to a slow loss of facilities and independence.

Animal models of retinal degeneration and mechanisms of photoreceptor death

The effort to fight blindness has lead to several animal models of photoreceptors degeneration (Chang et al., 2002; Rakoczy et al., 2006). *rd*1 (rodless) mice, with an autosomal recessive nonsense mutation in the PDE6β subunit (Farber and Lolley 1974; Pittler and Baehr 1991), are the oldest commonly used mouse model of RP (Sidman and Green, 1965); Pittler et al., 1993). The *rd10* mouse is another spontaneous mutant with a missense mutation in rod PDEβ (Chang et al., 2007) and has provided useful insights into degeneration (Chang et al., 2007; Gargini et al., 2007; Mazzoni et al., 2008). Experimentally generated mice, like the ΔCT mouse with transgenic expression of a truncated rhodopsin (Chen et al., 1995; Jones et al., 2003), provide a means to study both normal processes and degeneration. The resulting time course and severity of photoreceptor degeneration (PD) varies from model to model.

In AIPL-/- mice (Ramamurthy et al., 2004), which models the early onset retinopathy Lebers Congenital Amaurosis (LCA), photoreceptors develop but completely degenerate before P30. *rd2* mice *(*formerly *rds*) have a mutations in peripherin 2 (Connell et al., 1991) and a slow loss rods and cones over several months (Sanyal et al., 1980). Less is know about primary cone degeneration in mice because murine retinas are rod-dominated (Lewis et al., 2010; Carter-Dawson and LaVail 1979). However, there are some models that are thought to mimic cone-rod dystrophies because they remodel extensively after degeneration, such as the TG9N mouse (Marc and Jones 2003). TG9N mice express a truncated N-terminus of RGS9 in rods and will be discussed later in more detail. Altogether, the variety of mouse models provides variable time courses and phenotypes for investigation of PD pathology.

Much work has emphasized the events that herald cell death after PD (Wenzel et al., 2005; Sancho-Pelluz et al., 2008). Models of phototransduction signaling have yielded insights into the degenerative mechanisms. For example, metabolic imbalance of cGMP, the substrate for PDEαβ, in *rd1* (Farber and Lolley, 1974) or prolonged rhodopsin activation in ΔCT (Chen et al., 1995) are the most likely instigators of degeneration in those respective models. After rhodopsin is phosphorylated on its C-terminal by rhodopsin kinase, a target missing in ΔCT mice, arrestin binds phosphorylated rhodopsin (Wilden et al., 1986; Wilden et al., 1986; Xu et al., 1997). Under normal conditions, this does not lead to photoreceptor degeneration. However, if the Schiff base linkage at L296 is to a glutamate, the arrestin/rhodopsin complex is greatly favored over dissociation. This arrestin/rhodopsin complex accumulates in the inner segment of photoreceptors and does trigger degeneration (Chen, Shi et al. 2006).

Not all degeneration models are the result of visual signaling malfunction. Accumulation of toxic N-retinyl-N- retinylidene ethanolamine in the RPE of ABCA4 transporter knockout mice, a model for Stargardts macular dystrophy (Weng et al., 1999), poisons the RPE. Without RPE support, photoreceptor degeneration naturally ensues.

The penultimate steps in cell death may be as variable as the insult (Wenzel et al., 2005). Mechanisms of phototransduction-related photoreceptor death have been explored with light-induced photoreceptor death. Bright-light triggers transcription factor AP-1 mediated-apoptosis whereas low-light apoptosis requires transducin (Hao et al., 2002). There is evidence that retinitis pigmentosa eventually converges onto a final common pathway involving XIAP, an inhibitor caspases 3, 7 and 9 (Leonard et al., 2007). Cone photoreceptor death can follow early rod death of peripheral through a "bystander effect" via gap junctions (Ripps, 2002) or absence of exogenous rod derived cone viability factor (RdCVF; Leveillard et al., 2004). Knowledge of these pathways may lead to valuable interventions. Until such treatments are consistently successful, however, methods to restore vision after degeneration present realistic alternatives.

Photoreceptor degeneration can be detected physiologically by a diminishing a-wave on electroretinogram in both humans and animal models (Heckenlively et al., 1989; Chang et al., 2007). However, other aspects involving non-image forming functions are not immediately affected after complete photoreceptor degeneration. *rd*1 mice have been instrumental for studying retinal function in the absence of photoreceptors. The pupillary light response (PLR) measures pupillary constriction of the contralateral eye after light exposure. In young *rd1* mice (<P100), PLRs are virtually indistinguishable from wild-type in both magnitude and latency (Lucas et al., 2001). Accounting for this light

sensitivity are intrinsically photosensitive retinal ganglion cells (ipRGCs) that project to image and non-image forming centers in the brain (Dacey et al., 2005; Hatta et al., 2006). Melanopsin, a divergent photopigment found in ipRGCs (Yau and Hardie, 2009), is capable of transducing light signals directly, perhaps via an invertebrate-like signal transduction mechanism involving Gαq and PLC (Hankins et al., 2008). Therefore, even without photoreceptors ipRGCs mediate non-image forming functions in mammals such as PLR (Hattar et al., 2003; Panda et al., 2003). Similarly, at adult ages (P200) circadian rhythm entrainment, the non-image visual function that sets biological internal clocks, is also largely unchanged because of remaining ipRGC input (Foster et al., 1991; Provencio et al., 1994). These are evident shortly after photoreceptor loss but do not constitute the full.

Photoreceptor loss is a model of deafferentation

Deafferentation, the loss or detachment of sensory inputs, provokes changes in neural connectivity and function (Baekelandt et al., 1994; Milam et al., 1998; Rubel and Fritzsch 2002; Strettoi et al., 2003). Deafferentation is seen in human glaucoma, where RGCs die after crushing interocular pressure (Gupta et al., 2006; Yucel and Gupta 2008), auditory hair cell injury (Kong et al., 2010), and hippocampal-enterorinal lesions rodent models (Hamori, 1990). Though systemic responses vary, each model elicits downstream changes in target tissues. For example, cochlear hair cell death initiates spiral ganglion and auditory nerve degeneration and sprouting. This insult also leads to upregulation of GAP-43 in the cochlear nucleus (Kraus et al., 2009). In hippocampus, treatment ibotenic acid leads to cell death in the enterorinal cortex, degeneration along the perforant path and denervation. After 4 weeks, sprouting of cells in the dentate gyrus is evident (Kadish

and Van Groen, 2003). Somatosensory changes, like the 'phantom limb' of amputees described by Ramachandran (Ramachandran et al., 1992), have also been documented and represent rewiring after input loss.

Photoreceptors represent the sensory input into the retina as well as the downstream visual system. Massive photoreceptor death represents drastic insult to the retina: an intricate network of homeostatic, immunological, and protoplasmic components (Rattner and Nathans 2006; Chalupa and Williams 2008). Over time, elements within the retina react to loss of their primary input, photoreceptors, as well as reacting to each other (Marc et al., 2003, Figure 4.1). At the OPL, loss of photoreceptors alters bipolar cell synapses in *rd1* (Strettoi and Pignatelli, 2000) and *rd10* mice (Gargini et al., 2007). Ectopic projections in bipolar cells (Strettoi et al., 2003) and aberrant spontaneous activity in *rd1* mice (Stasheff, 2008) also follow prolonged loss photoreceptors. In excitatory light injury of photoreceptors, ionotropic glutamate signaling is altered (Marc et al., 2007). These events are accompanied by waves of apoptosis in several models (Marc et al., 2003). Gliosis, the infiltration and migration of glia, precedes glial seal formation above the INL. Vascular pathology from vessel infiltration to angiogenesis is also evident. Collectively, these changes are call "retinal remodeling" and have been documented in both human (Jones et al., 2003; Aleman et al., 2007) and animal photoreceptor degeneration (Strettoi and Pignatelli 2000; Marc et al., 2003; Strettoi et al., 2003). In mouse models, these changes can range from mild, as seen in ΔCT mice, to severe, epitomized by the TG9N mouse (Jones et al., 2003; Marc,

Figure 4.1- Retinal Degeneration leads to retinal remodeling. A. Normal retina exhibits photoreceptors and regular lamination. B. Remodeling of retinal neural components and follows photoreceptor degeneration. *Left to right, noted changes marked by red circles.* In rod degeneration models, photoreceptor degeneration begins with shortening of rod outer segments and extension of rod pedicles. After photoreceptor death, tropic support loss, and an initial wave of apoptosis, early remodeling neurite remodeling is evident. In advanced remodeling, bipolar and amacrine cells somas can migrate and microneuromas, abnormal clusters of cell bodies can be seen. Not shown are the extensive vascular and glial changes that accompany retina remodeling.

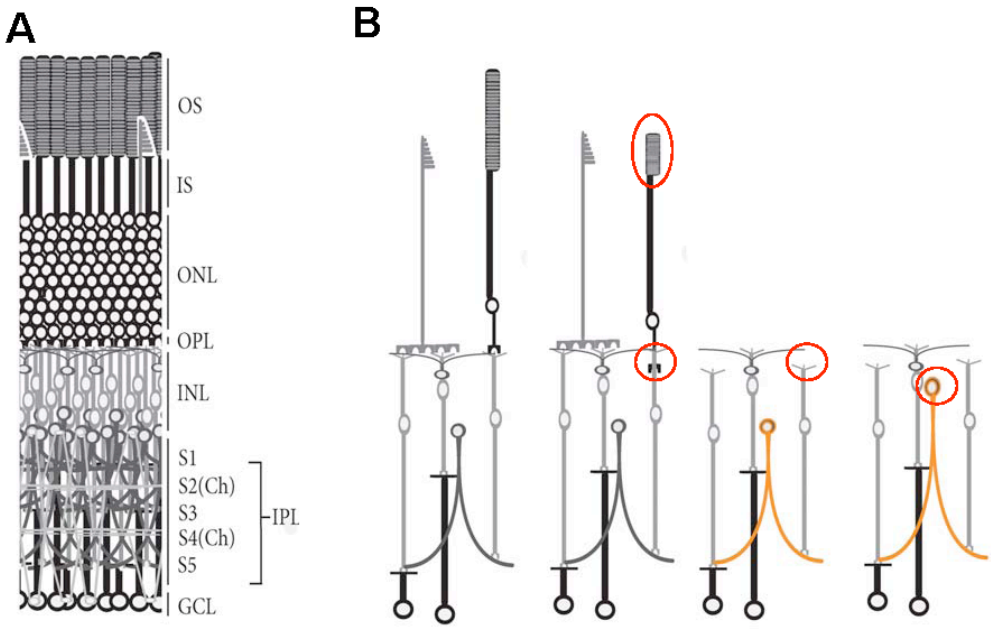

Figure 4.1

Jones et al. 2003). The mechanisms of retinal remodeling are likely as variable as their sources and it is hypothesized that the timing of photoreceptor death plays a role in subsequent changes (Marc and Jones 2003).

These changes represent an obstacle for the treatment of PD in the retina. Epiretinal prostheses consist of stimulating electrodes implanted along the GCL that transmit visual information from a remote device (Humayun et al., 2003; Weiland et al., 2005). Glial proliferation can interfere with bio-electric device interfaces and function (Butterwick et al., 2009), as would spontaneous activity (Stasheff, 2008). Stem cell (Lamba et al., 2009) and embryonic retinal epithelium transplantation (Sagdullaev et al., 2003) are promising treatments designed to regenerate integrated photoreceptors. However, these treatments ultimately rely on the entire retinal circuitry, which may be compromised in the face of retinal remodeling. The glial seal below the RPE may displace transplanted tissues (Marc and Jones 2003). Availability of intrinsic factors in the degenerated retina like RdCVF (Leveillard, Mohand-Said et al. 2004) may alter cell survivability. Another option is to bypass aberrant retinal circuitry integration of transplanted tissues. Targeting channelrhodopsin-2 (ChOP2) (Lagali, Balya et al. 2008) to ON-bipolar cells or melanopsin to RGCs (Lin et al., 2008a) has shown promising results. Even with a variety of treatments and varying degrees of retinal remodeling, it is surprising to learn that no studies have directly addressed the impact of remodeling on clinical interventions.

Central retinal projections have not been compared in mice with differing degrees of retinal remodeling

What happens to the central projections in retinal injury? Chemical exposure (Ito et al., 2008), genetic manipulations in RGCs (Weimer et al., 2006), and optic nerve-crush (Schwartz, 2004) directly damage RGCs. Central projection loss predictably follows. Studies that have examined the function of retinofugal projections in animals with PD usually did so after a prospective treatment with visually evoked potentials (Bi et al., 2006; Lin et al., 2008) or behavioral studies (Lagali et al., 2008). Functional evidence of PD retinal projections was selective for retinal treatment responsiveness, long after interventions, and could not assess naïve RGC function. Other studies in naïve (untreated) photoreceptor degenerated animals either reported anatomically intact connections (Mazzoni et al., 2008), without functional data, or functional data without anatomical correlates (Provencio et al., 1994). One recent study (Lupi et al., 2010) has assessed activation of central circadian nuclei in *rd1* mice but not image forming pathways.

The retinotopically-ordered superior colliculus (SC) and dorsal lateral geniculate nucleus (dLGN) in mice constitute the major image forming pathways. The dLGN is the major conduit for image forming information to the cortex (Sherman and Guillery, 2002). In mammals, eye-specific projections occupy discrete territories in the dLGN. Ipsilateral eye RGCs project within an anteriodorsal tube and contralateral eye projections fill the remaining dLGN (Guido, 2008). Eye-specific patterning in dLGN has not been fully assessed (Torborg and Feller, 2004) in degenerated animals. Retinal activity is thought to maintain these eye-specific projections in young mice up to P14 (Demas et al., 2006), but has not been assessed in aged mice. Mice that degenerate at different times permit the titration of visual activity as photoreceptors disappear. Eye-specific patterning also

reflects synaptic specificity and maturity (Chapter 1, Ziburkus and Guido 2006; Stevens et al., 2007) that may determine the effectiveness of retina-based treatments for PD. Therefore, examination of the eye-specific patterning in the dLGN of PD mice would provide critical information regarding (Gargini et al., 2007). Central retinal projections have not been studied in light of retinal remodeling. Addressing these concerns would advance our knowledge visual system injury, especially if framed as a comparison of remodeling mouse strains. Animals with differing degrees of retinal remodeling represent additional, unique insults to the system that could drive the retinal states further from normal (Marc and Jones 2003; Jones et al., 2005; Jones et al., 2006).

A comparison of the retinofugal projections in PD models with varying degrees of retinal remodeling would simultaneously address lingering concerns of projection stability across animal models, eye-specific patterning, and the impact of retinal remodeling on central projections. Jones (2003) used computerized molecular phenotyping (CMP)(Marc and Jones, 2002) to identify retinal cells by amino acid signatures in degenerating retinas. Following cell subtypes with CMP, they reported a spectrum of retinal remodeling across animal models and humans. Remodeling was consistent within strains and groupings (Jones et al., 2003). Flanking the spectrum of remodeling are the ΔCT and TG9N mice. The ΔCT transgenic mice, which overexpress a C-terminal truncated rhodopsin, exhibit early PD during postnatal development and little subsequent retinal remodeling. In ΔCT mice, photoreceptor degeneration is largely complete by P30 yet remodeling is mild as late as P500 (Jones et al., 2003). By comparison, the degeneration patterns of TG9N transgenic mice, which express an N-terminal fragment of regulator of g-protein signaling 9 (RGS9) in rods, have rapid and

aggressive progression. Photoreceptors in the TG9N mouse develop normally. However, they degenerate to 50% by P30 and are completely degenerated by P60. Aggressive retinal remodeling follows TG9N PD as early as P160 (Jones et al., 2003; Marc and Jones 2003). Therefore, ΔCT and TG9N animals represent the mild and severe PD-related retinal remodeling conditions, respectively (Jones et al., 2003).

We examined RGC targets within the brain of ΔCT and TG9N mice by anterograde tracing, assessing pupillary light responses (PLR), and recording evoked postsynaptic potentials in the dLGN relay cells. Anatomically, we found that IF and NIF retinofugal projections among ΔCT, TG9N, and age-matched control mice are indistinguishable. Eye-specific projections were normal across all conditions. Similarly, optic tract stimulation elicits postsynaptic responses in dLGN in all conditions suggesting intact synaptic connectivity after both PD and remodeling. Interestingly, magnitudes of PLR constriction were diminished in degenerated mice. Flat-mount retinal cell counts revealed a decrease in melanopsin cells. Because other components of the PLR were intact, reduced melanopsin cell input explains the PLR phenotype in degenerated mice. This limits pathological sequella to the retina. We conclude that retinal remodeling does not grossly affect the state of retinofugal projections.

Methods

Animals and Genotyping

The genotyping methods are detailed in chapter 2. Two transgenic strains, TG9N and ΔCT, aged P200-500 with age-matched siblings were used in this study. The RhoΔCTA (ΔCT) mice, overexpressing a C-terminal truncated rhodopsin mutant, were genotyped by the presence of a 250 bp PCR product with primers: Rh2 5'-tgg gag atg acg

acg cct aa and Rh3 5'-tga ggg agg ggg tac aga tcc. The TG9N mice, expressing the N-terminal domain of mouse RGS9-1, were genotyped by the presence of a 250 bp PCR product with primers: RGS9-1 5'- acg atc cga cac caa ggc cag and 3ms9 5'- ggc gtc tga aat cgg tag aga ctg. At the time of experiments, both TG9N and ΔCT had complete photoreceptor degeneration as previously described (Jones et al, 2003, Arvo Abstract, 2003). Animals were kept in 12 hour light-dark cycles until experiments. All animal experiments were conducted according to the ARVO Statement for the Use of Animals in Ophthalmic and Vision Research, with approval from the Institutional Animal Use and Care Committee of Virginia Commonwealth University.

Histology

Enucleated mouse eyeballs were fixed overnight in 2% paraformaldehyde/2% glutaraldehyde in 0.1 M PB (pH=7.4), immediately following euthanasia. The eyecup, which is without the cornea and the lens, was then fixed in 1% osmium tetroxide in 0.1 M calcodylic acid (pH =7.4) at room temperature for 2 h, followed by dehydration in ethanol. The eye cup was then impregnated with Spurr reagent (Electron Microscopy Sciences, Hatfield, PA) and cured at 70°C for at least 48 hours. Retinas were sectioned on a Sorvall MT 6000 Ultra-microtome at 1 μm thickness and stained with 0.15% Toluidine Blue in 0.5% sodium borate. Images were taken under bright field illumination using an Olympus ES600 microscope.

Immunohistochemistry was performed as previously described (Rao et al., 2007). Mice were deeply anesthetized and their enucleated eye balls were fixed in 4% PFA/PBS for 45 minutes at room temperature. An eye cup was made from the eye ball and transferred to 30% sucrose for cryoprotection at 4°C. After embedding eye cups in TBS

(Triangle Biomedical Company, Durham, NC), frozen blocks were sectioned at 14-16 μm on a Vibratome © Compro 3000 cryostat and dried. Sections were probed using one of the following primary antibodies at the given dilution: Sox9 (Chemicon, Temecula, CA, 1:100) or ChAT (Chemicon, 1:50). Fluorophore conjugated-secondary antibodies (Chemicon, Temecula, CA, 1:1000 for all types) were used to visualize the presence of bound primary antibodies and counterstained for DAPI (0.5 μg / ml, Anaspec, San Jose, CA) and mounted in ProLong Gold (Invitrogen, Carlsbad, CA). Flatmount retinas were stained before flattening to preserve integrity of the retina. Fluorescent images were then captured under mercury light with appropriate light filters on an Olympus ES600 microscope using Metamorph software (Molecular Devices, Sunnyvale, CA).

Flatmount retinal preparations fixed and stained, similarly described above, with primary antibodies against SMI-32 (labeling projection neurons) and OPN4 (homemade, VCU0013, labeling melanopsin). RPE was then removed; retinas were laid flat and mounted in ProLong (Invitrogen, Carlsbad, CA). Retinas were imaged piecemeal and a composite image was constructed to prevent double counting of cells. Cells were counted using NIH ImageJ (NIH, Bethesda, MD) cell counter plugin.

Anterograde tracing studies

To visualize eye-specific projections in central visual targets, Alexa Fuor 488 (green) or Alexa Fluor 594 (red) conjugated CTB (Invitrogen, Calsbad, CA, 1% in distilled water) was injected intravitreally using pulled glass pipettes into the eyes. Each eye was injected with different fluorescent conjugates so that the retinal projections from both eyes could be viewed simultaneously in a single section (Jaubet-Miazza et al., 2005). Two days post injection, animals were anesthetized and transcardially perfused

with cold PBS, followed by 4% PFA/PBS. The brain was removed, post-fixed at least 48 hours in 4% PFA/PBS and sectioned in the coronal axis at 70 μm thickness. Serial sections were collected on glass slides beginning just before the optic chiasm and through the superior colliculus. Sections were briefly dried and then sealed in ProLong Gold (Invitrogen). Sections were imaged separately using green and red filters on a Nikon E600 fluorescent microscope with Spot SuperCool *fx* camera using Metamorph software. Alexa dyes and microscope filters sufficiently isolate red and green channels to minimize signal bleed-through. To ensure valid quantifications, we adjusted the histogram intensity function until all (~99%) pixels fell within the linear range of fluorescent dye intensity.

Quantification of Retinogeniculate Projections

The spatial extent in retinogeniculate projections was measured from captured images as previously described (Jaubert-Miazza et al., 2005). Captured images were exported as a 24-bit TIFF to Photoshop CS3 for processing. Threshold analysis, which used the threshold function to set the baseline intensity of each fluorophores (between 40-70), was performed to generate tricolor images. RGC axon terminals were identified by respective red or green pixels and where yellow represents the co-localization of both red and green pixels. Five adjacent sections in the middle third of each dLGN, identified as those with the most pixels, were selected for quantification. Pixels were then counted using custom software (Jaubert-Miazza et al., 2005). Contralateral, ipsilateral, and overlap percent areas were calculated relative to total area of dLGN, which is the sum of contralateral and ipsilateral pixels in an image. A threshold independent method for analyzing the degree of eye specific segregation was employed (Torborg and Feller, 2005) to confirm threshold results. For each pixel in analyzed sections of dLGN, the

logarithim of the intensity ratio (R= log10 Fi/Fc) was calculated with custom software (Jaubert-Miazza et al., 2005), where F_C is the contralateral fluorescent intensity and F_I is the ipsilateral fluorescent intensity of a given pixel. Using representative images, the ratios were then plotted as a frequency histogram (bin size 0.1 log units) and these subsequent distributions (R-distributions) are compared across strains. R-distributions with greater variances between the two eye-specific inputs correspond to a greater degree of eye-specific segregation.

Consensual pupillary light responses

All experiments were performed under dim red light and animals were dark adapted at least 30 minutes. Light from a variable-wattage halogen light source, filtered through various neutral density filters and transmitted through fiber optic cable, was focused through a condensing lens onto the left eye of unanesthetized mice. An electronic shutter controlled the onset and time of light exposure. The light intensity was measured by a light meter (Control Company, Friendswood, TX). Each mouse was tested for PLR three times. Each trial was 60 seconds long with >5 minutes between trials. Pupillary light responses were recorded in the dark using a Sony DSC-96 video camera under night vision with +1, +2, and +4 diopter lenses. Recordings were converted to video files and analyzed with custom Matlab software (Mathworks, Natick, MA). Images were analyzed with a program that identified the oval pupil and tracked its size over time. A threshold approach was also used to identify the pupillary area under less ideal light conditions. Sudden movements of the animal could lead to erroneous measurements for particular frames and those frames were discarded. After PLRs were plotted, stable and consistent trials were visually examined and selected for the analysis. Stimulus onset was

determined by auditory click on video and registered as time 0 in analysis. Constriction plateau was measured 30 seconds after light exposure.

Electrophysiology

To examine the synaptic responses evoked by optic tract stimulations, an acute thalamic slice preparation was adopted in which the retinal connections to the LGN remain intact (Chen and Regehr, 2000). Mice were anesthetized with isoflurane and perfused with cold saline, then decapitated. The brain was removed from the skull and the two hemispheres were separated by cutting along the midline at an angle of 10-20°. The medial aspect of the brain was then glued onto an angled wedge (15-25°) of a vibratome cutting stage and submerged in a 4˚C oxygenated (95%O_2 / 5% CO_2) solution of artificial cerebral spinal fluid (ACSF, in mM: 124 NaCl, 2.5 KCl, 1.25 NaH_2PO_4, 0.1 $MgSO_4$, 26 $NaHCO_3$, 10 Dextrose, 2 $CaCl_2$, saturated with 95% O_2/ 5% CO_2, pH=7.4). Using a vibratome (Lieca 2000), 250-300 μm thick sections were cut in the parasagittal plane. Slices containing LGN were placed in a holding chamber and incubated in oxygenated ACSF at 30° C for 1 hr. Individual slices were then transferred to a recording chamber maintained at 32°C and perfused continuously at a rate of 2.0 ml/min with oxygenated ACSF.

In vitro recordings: intracellular recordings were typically done in the whole cell configuration (Blanton) with the aid of a fixed-stage microscope (Olympus EX51WI) equipped with differential interference contrast optics and a water-immersion objectives to view individual neurons within the slice. Electrodes were pulled in two stages from borosilicate glass and filled with a solution containing (in mM) 140 K Gluconate, 10

HEPES, 1.1 EGTA-Na, 0.1 $CaCl_2$, 2 $MgCl_2$, 2 ATP-Mg, 0.2 GTP-Na (pH=7.2). The final tip resistance of filled electrodes is 3-5 MΩ.

Whole cell recordings were done in current clamp mode using an Axoclamp 2B amplifier. To achieve a high impedance seal, the electrode was brought into close proximity of a cell by monitoring the voltage responses to small current pulses (0.1-0.3 nA 100-200 msec) delivered through the recording electrode and noting an increase (20-50 MΩ) in electrode resistance. Once contact was made, a slight negative pressure was applied to form a gigaohm seal. Additional suction or a brief electrical pulse was then applied to rupture the membrane and obtain whole cell access. Whole cell configuration was indicated by a sudden DC drop of ≥60 mV, the appearance of large action potentials, and an input resistance >300 MΩ. Whole cell recording was done in digital current clamp or single electrode voltage clamp mode using the Axoclamp 2B amplifier. Pipette capacitance, series resistance and whole cell capacitance were carefully monitored and compensated electronically during the recording. Current-voltage relations were examined at different membrane potentials by injecting a series of square wave current pulses (0.1nA-1A, 0.01-0.1 nA steps, 300-700 msec) to reach steady state. The voltage responses to these current steps were used to determine the presence and operating range of voltage-gated conductances and to explore the repetitive firing characteristics of thalamic cells. Because it is very difficult to achieve and maintain stable Giga ohm seals in aged tissue (Tanaka et al., 2008), we also resorted to a loose patch configuration which enabled us to record either extracellular single unit response or a small evoked field response (Moyer and Brown, 1998).

To evoke synaptic activity in LGN, square-wave pulses (0.1-0.3 ms. 0.1- 1 mA) were delivered at variable rates (0.2-3.33 Hz) through a pair of thin-gauged Ir wires (0.5MΩ) positioned in the optic tract. In some instances, Tetrodotoxin (TTX, 2-4 μm) or 6,7-dinitroquinoxaline-2,3-dione (DNQX. 10-20 μm), and bicuculline (10-20 μm) were bath applied. Neuronal activity was digitized (10-20 KHz) through an interface unit, acquired and stored directly on computer, and analyzed using a variety of custom made or commercial software (Strathclyde Electrophysology Software, Whole Cell Analysis Program V3.8.2.)

Statistics

Statistical analysis was performed on JMP8 software (Cary, NC) and SPSS (Chicago, IL). Non-parametric comparisons of spatial extent first identified differences among the groups (Kruskal-Wallis) and then identified group differences (Tukey HSD). Pupillary responses were tested as repeated values (generalized linear model (GLM) for repeated values with Tamhane P2 pair-wise comparisons). P values less than 0.05 were considered significant.

Results

The degeneration of photoreceptors in TG9N and ΔCT retinas was previously reported (Jones et al., 2003; Chen et al., 1995). ONL and OS layers are absent by 2 months in both strains, indicating loss of retinal photoreceptors (seen in Figure 4.2). Retinal remodeling has not been verified with immunohistochemistry in either TG9N or ΔCT mice. (Figure 4.2B). Y.L. Chen performed all immunohistochemistry in this section, including retinal flatmounts.

Figure 4.2-ΔCT and TG9N retinas remodel to a different degree after photoreceptor death. Immunohistochemistry was performed by Y-L. Chen on control and degenerated retinas to assess degeneration and neuronal remodeling. A. Inner nuclear layer (Clancy et al.), or the presumptive INL, is identify with bars for each image i. Calbindin immunostaining (red fluorescence) identifies horizontal cells, amacrine cells and three distinct strata in the inner nuclear layer(Clancy et al.). Recoverin positive cells (green fluorescence) synapse with horizontal cells and their contact demarcates the OPL, when present. ii. Chx10 immunostaining identifies cone bipolar cells (red fluorescence). iii. Rod bipolar cells stain positive for PKCa. *left* Fluorescent images of retinal cross sections were immunostained for ChAT to identify cholinergic amacrine cells and strata. *Right* Light microscopic images show the retina is physically intact. B. *left* Fluorescent images of retinal cross sections were immunostained for ChAT to identify cholinergic amacrine cells and strata. *Right* Light microscopic images show the retina is physically intact. C. Quantification of RGC cell counts in each condition (n = 2 retinas and 2 animals per condition) D. Whole mount retinas have been stained to identify projecting retinal ganglion cells (SMI-32) and melanopsin containing cells (OPN4). Sites of positive staining are marked by black dots. Orientation of retinas is identified in the nasal (N) and superior directions (S) with the arrow legend. Scale Bar: 500 μm.

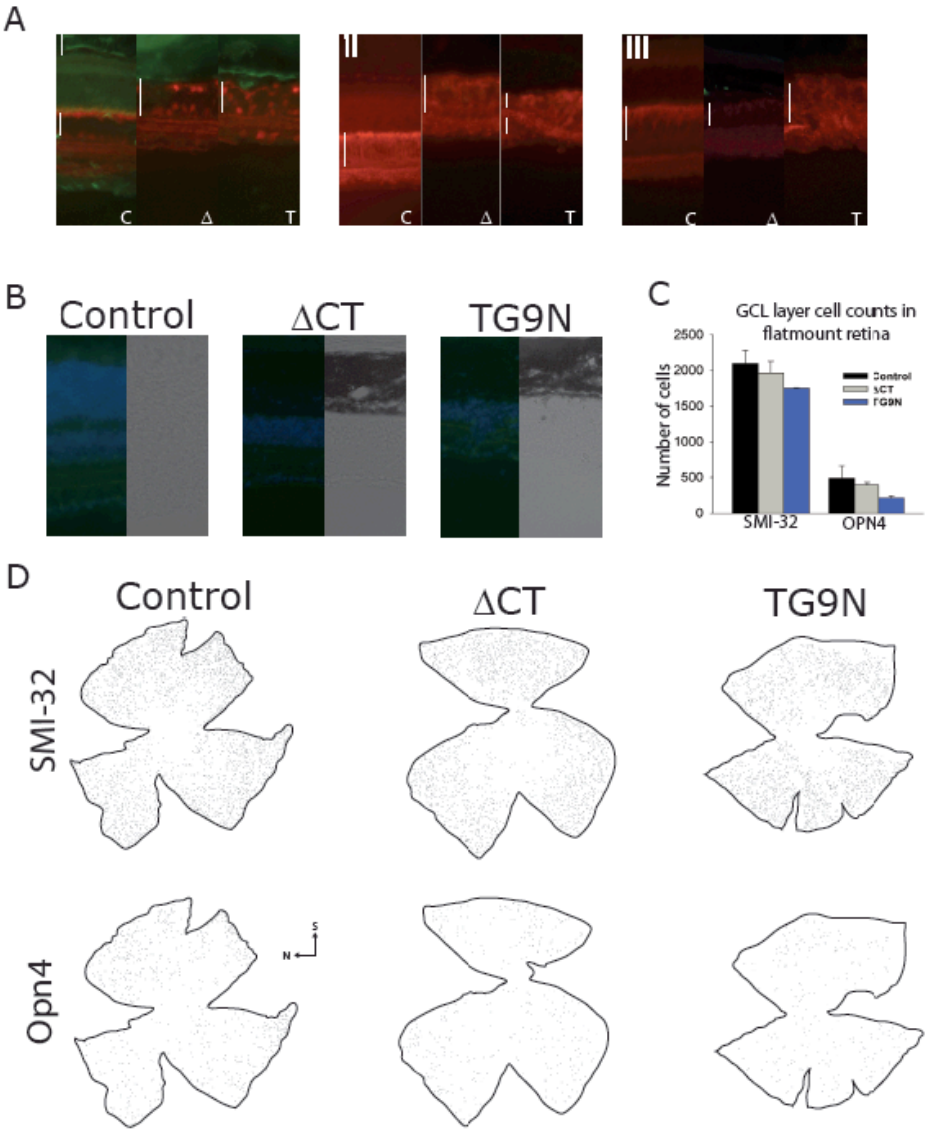
A
I
II
III
C
Δ
T
B
Control
ΔCT
TG9N
C
GCL layer cell counts in flatmount retina
Number of cells
2500
2000
1500
1000
500
0
Control
ΔCT
TG9N
SMI-32
OPN4
D
Control
ΔCT
TG9N
SMI-32
Opn4
N
S

Figure 4.2

Figure 4.3-Gross morphology of retinofugal projections is intact in ΔCT and TG9N mice. Intravitreal injections of CTB conjugated-Alexa dyes trace to central targets via retinal ganglion cells. Coronal sections are displayed. *From top to bottom:* Dorsal lateral geniculate nucleus (dLGN) at 10x: All conditions show normal eye-specific organization, green for contralateral terminals and red for ipsilateral terminals, and morphology. Ventral LGN (vLGN) and intergeniculate leaflet (IGL) at 10x: IGL is located dorsal to vLGN. All conditions show similar eye-specific patterning and terminal field bulk. Suprachiasmatic nucleus (SCN) at 20x: all three conditions show bilateral RGC targeting. Olivary pretectal nucleus (OPN) at 20x: Nuclei shows ipsilateral core in red and contralateral "chevron" in green. Superior Colliculus (SC) at 10x: Tracings in all conditions show robust contralateral projections and barely detectable ipsilateral projections. Scale bars: 20μm at 10x magnifications and 10μm at 20x magnifications.

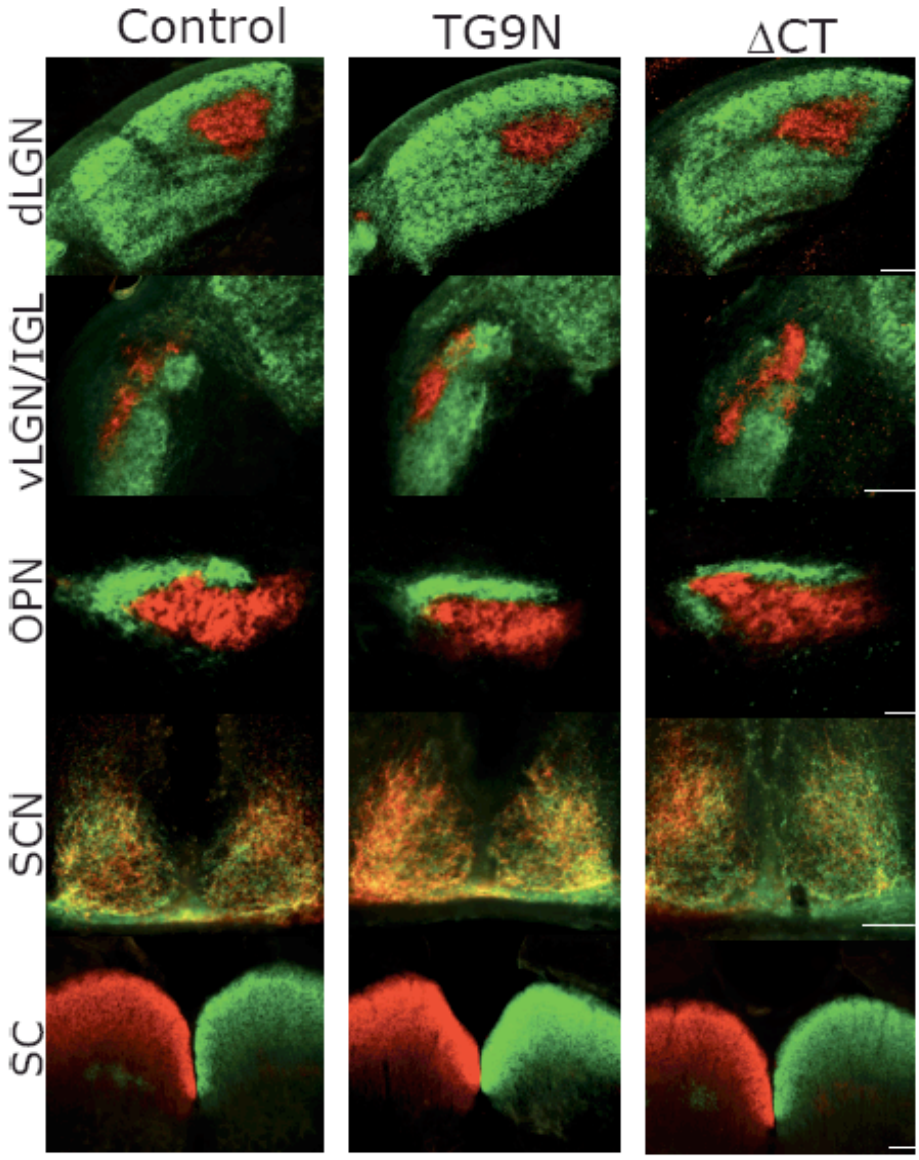

Figure 4.3

In control retinas, calbindin, labeling amacrine cells and their processes as well as horizontal cells, labels three parallel strata in the IPL. Cell bodies neatly align along the upper GCL, lower INL, and upper INL (horizontal cells) (Figure 4.2A,I; Wassle, 2004). In TG9N retinas, soma are seen migrating across the presumptive INL and occasionally breaking the three IPL strata (Figure 4.2A,i). Such changes appear to demonstrate remodeling "in action" because they illustrate somatic migration along the apparent trajectory of ectopic processes. Calbindin positive processes are also found penetrating the INL, accompanied by displaced cells bodies, as well as in the clustering in the GCL. When calbindin is co-stained with recoverin, labeling cone bipolar cells and photoreceptors, the OPL is clearly delineated at the intersection of horizontal cells and photoreceptor terminals. TG9N retina staining confirmed the absence of photoreceptors and abnormal bipolar cell morphology. In ΔCT retinas (Figure 4.2A,i), calbindin staining was slightly perturbed, occasionally displaying clusters of cells at the periphery of the INL, but somatic migration was tame compared to TG9N.

In control retinas, Gγ13 labeling, which identifies ON bipolar cells, display rows of soma filling the upper 3rd of the INL and distinct terminals puncta in the IPL (Figure 4.2A,ii). In TG9N retinas, Gγ13 labeling illustrates changes in ON bipolar cell morphology, projections, and location (Figure 4.2A, ii). Most striking is the disorganization of IPL strata sometimes traversing the bulk of the vertical retina. Gγ13 terminals are preserved within the strata. However, displaced cells bodies now occupy virtually all the space between the remnant OPL and the reorganized INL. In ΔCT retinas (Figure 4.2A, ii), Gγ13 reveals slightly more advanced remodeling than calbindin, as processes concentrate at the INL-OPL margin, but is mild compared to TG9N.

Rod bipolar cells, stained with PKCα, exhibit sprouting as early as 13 months even in control mice (Liets, et al., 2006; Terzibasi et al., 2007). We asked whether this sprouting would be accelerated remodel retinas. Control retinas at this age (>P200) barely show hints of sprouting, if any (Figure 4.2A, iii). Unfortunately, remodeling in TG9N retinas is so severe that sprouting was not evident above the noise of remodeling (Figure 4.2A, iii). Rather we see globular somas and diagonal IPL strata. In contrast, ΔCT retinas appeared normal, though some mild sprouting may be evident (Figure 4.2A, iii). In summary, our results indicate ΔCT do have some modest remodeling at older ages. However, these changes pale in comparison the severe remodeling in TG9N retinas.

In control retinas (Figure 4.2B), ChAT staining demonstrates the two characteristically parallel bands at two fifths (2/5, S2) and four fifths (4/5, S4) of the IPL. Similar to our structural observations in TG9N, ChAT staining is discontinuous in regions below the described breaks in the INL. Counterstaining with DAPI emphasizes the overall disorder in TG9N retinas, with massive nuclei invasion into the INL. ΔCT retinas retain the distinctive lamina morphology (INL, GCL) (Figure 4.2B). We considered the possibility that the changes we see in the TG9N animals are the result of sectioning artifact. Therefore, we compared bright-field images of the exact same visual fields we see morphological changes in the retina. TG9N retinas, as well as ΔCT and control retinas, were intact, verifying the changes are due to cellular events (Figure 4.2B).

To further quantify the degree of remodeling and cell loss of RGCs, we prepared flatmount retinas stained for projection RGCs and melanopsin-containing cells (Figure 4.2D). In no condition did we observe marked redistribution of cell bodies or regional cell loss. When compared to control mice (Figure 1C, 2097 ± 181 mean (± SEM) cells

per retina, n = 2 retina, 2 mice), SMI-32 counts were lower in ΔCT retinas (1964 ± 164, n = 2, 2) and further diminished in TG9N mice (1750 ± 10, n = 2, 2). In the same retinas, cell counts also indicate a pronounced loss of melanopsin cells in TG9N retinas (214 ± 31) compared to control (488 ± 177). ΔCT retinas had intermediate melanopsin counts closer to control (394 ± 38). When we calculated OPN4/SMI-32 ratios for each animal condition, the proportion of OPN4 positive cells is reduced in both PD conditions. However, TG9N (0.12) retinas had the most conspicuous reduction of OPN4 cells compared to both ΔCT (0.20) and control (0.23).

Having confirmed the differences in remodeling between TG9N and ΔCT mice using immunohistochemical techniques, we next used anterograde tracing to label retinal ganglion cell (RGC) axons and visualize their innervated targets in the brain. After intravitreal eye injection, the Alexa-dye conjugated CTB tracers (Angelucci et al., 1996) were readily taken up by RGCs and transported from retinas to central structures in both ΔCT and TG9N mice. We observed robust terminal labeling in a number of central visual targets including suprachiasmatic nucleus (SCN), lateral geniculate nuclei (comprised of the dorsal lateral geniculate nucleus, dLGN, the intergeniculate leaflet, IGL, and the ventral LGN, vLGN), the olivary prectal nucleus (OPN), and the superior colliculus (SC) (Figure 4.3). RGC projections appear to arborize and maintain the boundaries of their respective nuclei. Because we injected different Alexa dyes conjugated to CTB (488nm and 593nm emission spectra) into one or the other eye, we were able to address whether eye specific patterns of RGC projections were perturbed after PD. Overall, we found that eye-specific patterning is maintained and indistinguishable from controls, suggesting that visual topography is preserved at all retinofugal targets.

Hallmark identifying morphology of central structures, delimited by terminal axonal arbors of RGCs (Figure 4.3), was similar in all groups. For example, SCN were bilaterally innervated (Hattar et al., 2006) and similar to findings in hamster (Muscat et al., 2003) with projections from each eye showing extensive overlap in each nucleus. In dorsal (d) and ventral (v)LGN, retinal projections form distinct non-overlapping modules (Jaubert-Miazza et al., 2005). For dLGN, contralateral retinal terminals fill the majority of the structure and the characteristic dorsomedial patch of ipsilateral terminals occupies the remainder. For vLGN, contralateral projections reside in the lateral half of vLGN (Harrington, 1997) and ipsilateral projections lay in 2-3 semi-lobular patches in regions absent of contralateral projections (Jaubert-Miazza et al., 2005). In the OPN, contralateral RGC axons formed a "chevron"- shaped shell around a dense ipsilateral core similar to previous reports (Hattar et al., 2006). In the SC, all animals displayed robust contralateral projections to the superficial layers. Similarly, weak projections could be seen in the stratum opticum (Huberman et al., 2008). Together, these tracing studies found no coarse differences in anatomical projections, target innervation, and eye-specific patterning of the retinofugal projections of TG9N and ΔCT mice when compared to control.

Quantification of CTB labeled projections in dLGN is a well-established means for computing spatial extent of retinofugal projections and degree of eye-specific segregation in the IF pathway (Jaubert-Miazza et al., 2005; Torborg and Feller 2004). We employed this method to further evaluate whether there are differences undetected by qualitative examination of tracing data. To measure the RGC terminal fields, we first quantified pixels in binarized images (Fig. 4.4A) with red and green pixel color

Figure 4.4-Fine retinogeniculate terminal patterning is intact in ΔCT and TG9N mice. After anterograde tracing with CTB conjugated Alexafluor dyes, Coronal sections of dLGN were imaged and analyzed by pixel counts and pixel analysis. *A, Images of dLGN:* (from left to right) Individual contralateral, ipsilateral, superimposed, and binarized images. Binarized images represent ipsilateral projections in green, contralateral projections in red, and overlapping ipsilateral and contralateral projections as yellow. *B, Spatial extent analysis of images*: (from left to right) Areas are reported as a percentage of total LGN area. Contralateral, Ipsilateral, and Overlapping area comparisons show that both TG9N (blue) and ΔCT (gray) are not significantly different from controls (black) ($p<0.05$). Far right, segregation comparison of representative dLGN sections show similar distributions of eye-specific pixel intensity for all conditions and confirms similarities in the spatial extent data for overlapping projections.

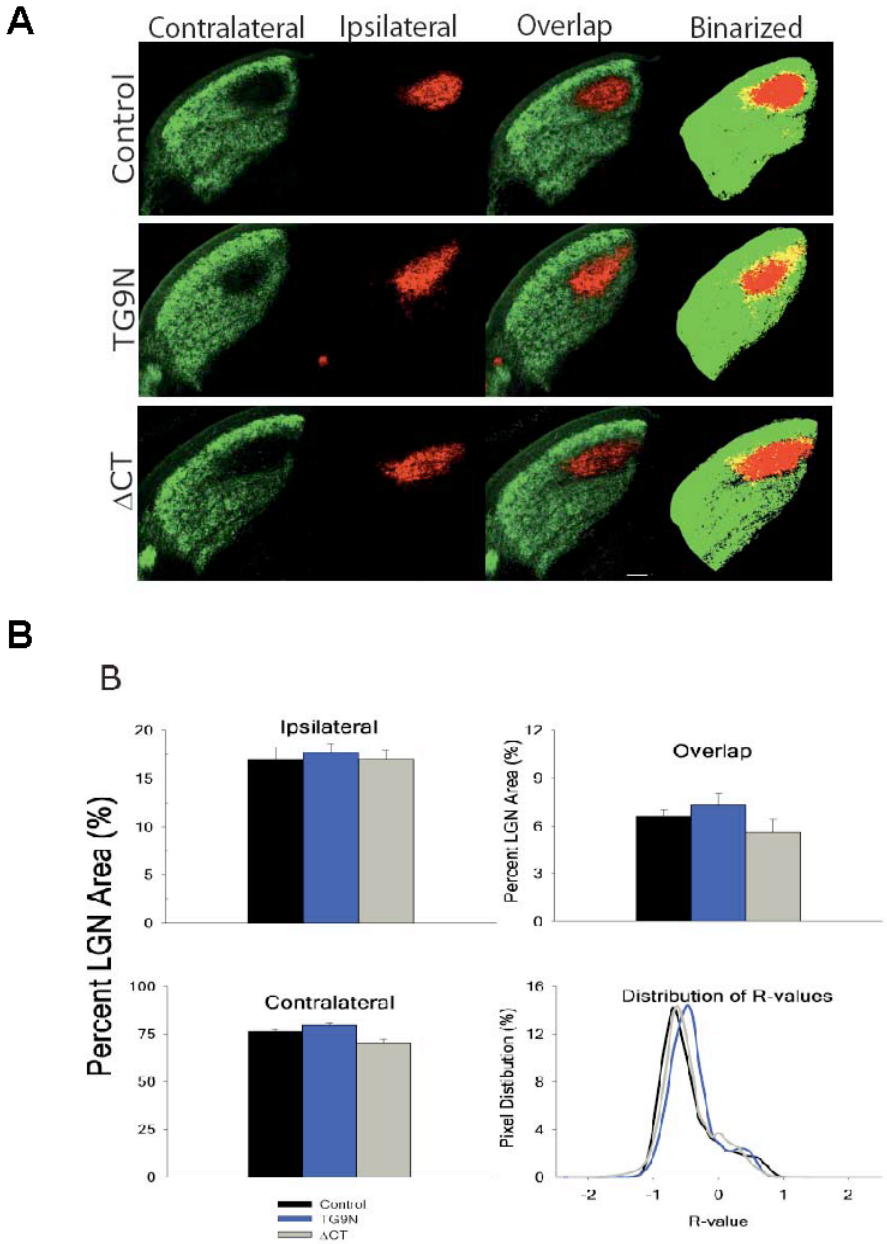
A
Contralateral
Ipsilateral
Overlap
Binarized
Control
TG9N
ΔCT
B
B
Ipsilateral
Overlap
Contralateral
Distribution of R-values
Percent LGN Area (%)
Pixel Distribution (%)
R-value
Control
TG9N
ΔCT

Figure 4.4

representing the respective eye-specific projection and yellow representing overlapping fields, and then calculated each as a percent of total dLGN area (Figure 4.4B). Contralateral projections areas of both ΔCT (mean ± S.E.M, 70.16 ± 2.30%, n=6 LGNs) and TG9N (79.67 ± 0.96%, n=6 LGNs) animals were not statistically different from control (76.41 ± 1.22%, n=4 LGNs, Tukey HSD, $p>0.05$). Ipsilateral projections areas of ΔCT (17.25 ± 0.91%, n=6 LGNs) and TG9N (17.71 ± 0.86%, n=6 LGNs) mice were also not significantly different from control animals (17.00 ± 1.23%, n=4 LGNs). The spatial extent of overlapping contralateral and ipsilateral projections are a coarse assessment of eye-specific segregation and used here to reveal potential plastic events that may take place as the result of axonal remodeling in the dLGN. Spatial extent of overlapping projections (Figure 4.4B) for ΔCT (5.61 ± 0.8%, n=6 LGNs) and TG9N (7.3 ± 0.72%, n=6 LGNs) animals were not significantly different from control (6.64 ± 0.38%, n=4 LGNs), suggesting that RGC terminal field remodeling had not taken place in the IF pathway. Interestingly, TG9N mice do have statistically significant larger contralateral projections areas than ΔCT mice ($p<0.05$, Tukey HSD), although both have contralateral projections similar to that of control. The lack of differences across all other measurements and retention of eye-specific patterning greatly outweigh the minor difference in contralateral area. Therefore, collectively our threshold data show no differences in the spatial extent of projections to dLGN among TG9N, ΔCT, and control animals.

We also performed a separate threshold-independent R-variance (R_{var}) analysis on representative LGN sections to confirm the binarized image results because

Figure 4.5-Whole-cell Current clamp intracellular recordings identify physiologically intact retinogeniculate synapses in TG9N dLGNs. Figure 4 and 5 recordings and figures generated by T. Krahe and figure legends written by W. Guido. *A:* Retinogeniculate in vitro preparation arrangement shows optic tract (OT), dLGN, recording electrode (RE) and stimulating electrode (SE). *B: Excitatory postsynaptic potentials:* Representative examples of excitatory postsynaptic potentials (EPSPs) evoked by suprathreshold optic tract (OT) stimulation. Postsynaptic activity evoked in TG9N (Chang et al.) slices was similar to control (left) activity (average of 5 traces). Membrane potentials for control and TG9N animals were –61mV and –63mV, respectively. For all panels, black arrows indicate stimulus artifact. Insets above averaged traces are plots of postsynaptic responses amplitudes after OT stimulation versus time. Values are in percent of change relative to baseline. Each open circle represents the amplitude of a single trace, before and after OT stimulation (control, 5 traces; TG9N, 10 traces). Note that OT stimulation in TG9N animals (right plot) reliably evoked postsynaptic potentials. *C:* EPSPs evoked by pairs of stimuli at 300ms time intervals for control (left) and TG9N (Chang et al.) animals. Plots above paired-pulse traces depict the average percentage change in EPSP amplitude between the first and second pulses for control (Chang et al.) and TG9N (left) animals. Average values are from the traces shown. Note that TG9N animals presented paired-pulse depression similar to control animals, which is characteristic of retinogeniculate synaptic connectivity. *D*: Superimposed TG9N averaged traces (left) showing the response to OT stimulation (same shock strength) before (5 traces) and after (5 traces) bath application of the quisqualate/kainate receptor antagonist 6,7-dinitroquinoxaline-2,3-dione (DNQX, 100μM). Graph to the right depicts the EPSPs amplitudes of the same relay cell plotted against time. Values are in percent of change relative to baseline values. Bath application of 100μM DNQX caused a reduction in EPSP amplitude that could be reversed during washout. Dashed line indicates baseline levels. *E:* Examples of voltage responses evoked by injection of hyperpolarizing and depolarizing current steps (0.1 pA) for control (left) and TG9N (Chang et al.) animals. Note that similar to control, membrane hyperpolarization in TG9N dLGN relay cells activates a strong inward rectifying response while membrane depolarization triggers low-threshold spikes. Insets depict that for TG9N and WT cells there is a substantial delay in firing in response to a depolarizing current pulse.

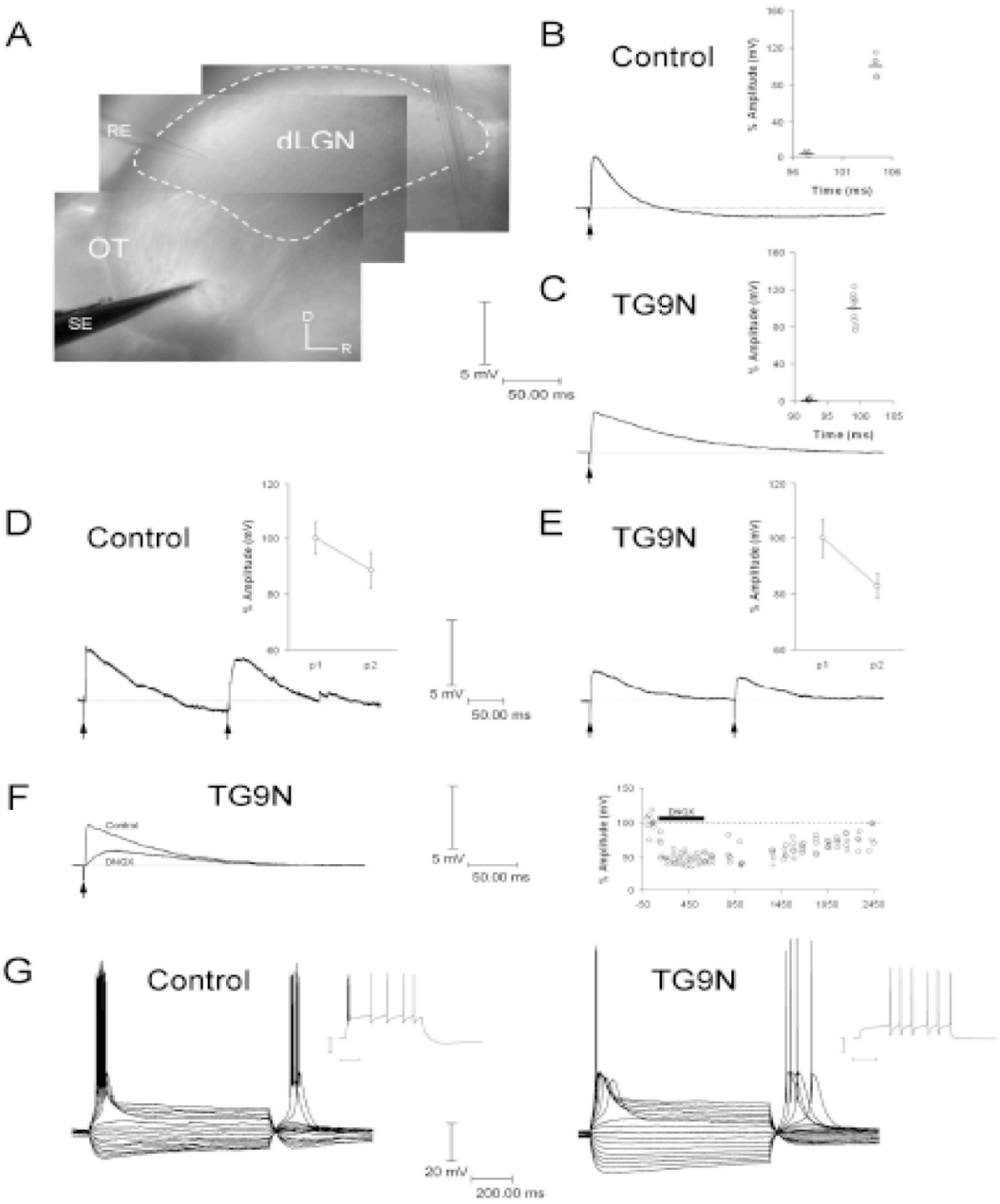
A
RE
dLGN
OT
SE
D
R
B
Control
% Amplitude (mV)
Time (ms)
C
TG9N
% Amplitude (mV)
Time (ms)
5 mV
50.00 ms
D
Control
% Amplitude (mV)
p1
p2
5 mV
50.00 ms
E
TG9N
% Amplitude (mV)
p1
p2
F
TG9N
Control
DNQX
5 mV
50.00 ms
DNQX
% Amplitude (mV)
G
Control
TG9N
20 mV
200.00 ms

Figure 4.5

quantification of eye-specific segregation may be subject to threshold bias. Plots of R_{var} are closely overlapping, suggesting comparable levels of eye-specific segregation (Figure 4.4B, bottom right). These data support the conclusion that IF pathways are morphologically intact in TG9N and ΔCT animals and maintain eye-specific segregation similar to control.

The following describes physiological assessment at the retinogeniculate synapse. Though several animals were attempted for each experimental condition (TG9N = 5, ΔCT = 4, control = 4), due to the age of the dLGNs it was difficult to obtain data consistently (TG9N = 1, ΔCT= 2, control=1). Nevertheless, these results elaborate on functional state of image-forming retinal projections in PD animals. Therefore, they are included in this dissertation. This section (along with the related methods) was written by W. Guido and experiments heroically performed by T. Krahe.

Retinogeniculate connections are the conduits of IF information. To investigate whether TG9N and ΔCT animals maintain functional retinogeniculate synapses after PD, we looked for evidence of excitatory post-synaptic potential (EPSP) in dLGN using a thalamic slice preparation that preserves the connections between RGC axons and dLGN neurons (Chen and Regehr, 2000). Because of the difficulties associated with obtaining viable whole cell recordings in aged tissue (as mentioned in the methods, Tanaka et al., 2008), we also made use of extracellular recordings in the form of loose patch and field potentials. In both TG9N and ΔCT animals, optic tract (OT) stimulation leads to postsynaptic activity in dLGN. Averaged EPSPs evoked by OT stimulation in control and TG9N animals are shown in Figure 4.5A. Bath application of 6,7,-dintroquinoaxaline-2,3-dione (DNQX, 10μM) led to a reduction in EPSP amplitude, confirming the

Figure 4.6-Cell-attached and Field Potential Extracellular Recordings survey Excitatory Postsynaptic Activity in ΔCT and TG9N LGNs *A, Cell-attached current-clamp recording from an LGN relay cell in a control slice:* Averaged action potentials evoked by suprathreshold optic tract (OT) stimulation, before (5 traces), during (5 traces), and after (5 traces) bath application of DNQX (15μM). For all panels, black arrows point to stimulus artifact. Graph to the right depicts the amplitudes of the evoked response (negative slope) of the same relay cell plotted against time. Values are in percent of change relative to baseline values. Bath application of 15μM DNQX caused a reduction in amplitude that could be reversed during washout. The great attenuation of responses by the AMPA antagonist indicates that the extracellular potentials are postsynaptic in origin and mediated by glutamatergic transmission. Dashed line indicates baseline levels. *B, Cell-attached current-clamp recording from an LGN relay cell in a ΔCT slice:* Cell-attached action potentials evoked by suprathreshold optic tract (OT) stimulation (left). Insets above averaged traces show response amplitudes (negative slope) after OT stimulation plotted against time. Values are in percent of change relative to baseline values. Each open circle represents the amplitude of a single trace, before and after OT stimulation (5 traces). OT stimulation in the ΔCT slice evoked reliable postsynaptic potentials. Traces on the right depict evoked postsynaptic responses by pairs of stimuli at 300ms time interval for the ΔCT slice (average of 5 traces). Plots above paired-pulse traces illustrate the average percentage change in amplitude (negative slope) between the first and second pulses for the ΔCT slice recording. Average values are from the traces shown. Note that ΔCT animals presented paired-pulse depression. *C, Extracellular field potentials*: Traces in dLGN after electrical stimulation of the OT at suprathreshold levels of stimulus intensity for control (left) and TG9N (Chang et al.) slices. In both cases, a large (negative in polarity) amplitude response is evoked (average of 5 traces for control and TG9N recordings). Insets above traces depict the postsynaptic response amplitudes (negative slope) plotted against time. Values are in percent of change relative to baseline values. Each open circle represents the amplitude of a single trace, before and after OT stimulation (control, 5 traces; TG9N, 5 traces). Note that OT stimulation in TG9N animals (right plot) reliably evoked postsynaptic potentials. *D, Extracellular field potentials evoked by OT stimulation at suprathreshold levels of stimulus intensity for a dLGN rely cell in a ΔCT slice*: Averaged of traces before (5 traces), during (5 traces), and after (5 traces) bath application of DNQX (15μM). Graph to the right depicts the amplitudes of the evoked response (negative slope) of the same relay cell plotted against time. Values are in percent of change relative to baseline values. Bath application of 15μM DNQX caused a reduction in amplitude that could be reversed during washout. Dashed line indicates baseline levels. Attenuation of responses by DNQX indicates that the extracellular potentials are of postsynaptic origin.

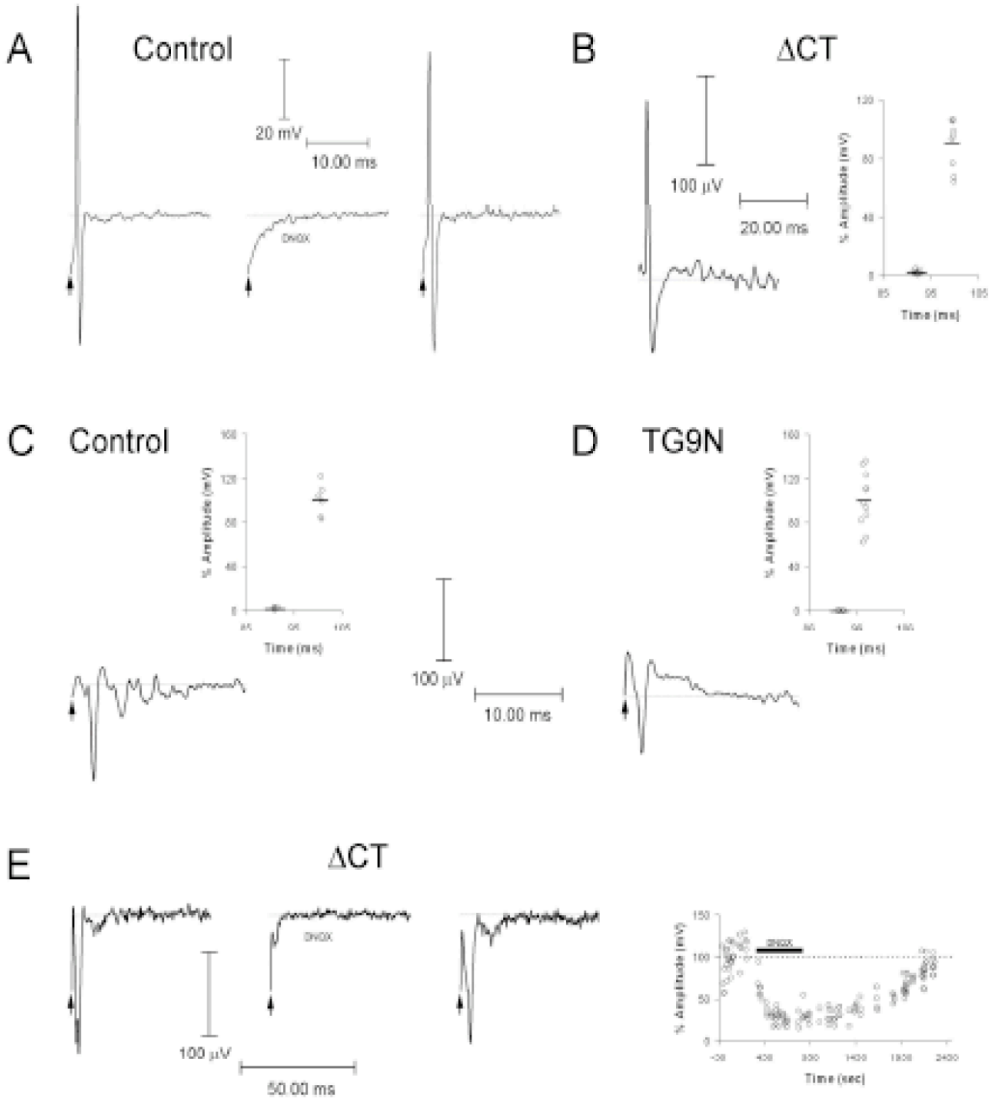
A
Control
20 mV
10.00 ms
DNOX
B
ΔCT
100 µV
20.00 ms
% Amplitude (mV)
Time (ms)
C
Control
% Amplitude (mV)
Time (ms)
100 µV
10.00 ms
D
TG9N
% Amplitude (mV)
Time (ms)
E
ΔCT
DNOX
100 µV
50.00 ms
% Amplitude (mV)
Time (sec)

Figure 4.6

postsynaptic origin of the evoked responses. The retinogeniculate EPSP can be further characterized by the using paired pulse stimulation of OT. When suprathreshold stimuli are delivered in succession, the postsynaptic response shows a pronounced frequency-dependent depression (Turner and Salt 1998; Kielland and Heggelund 2002; Chen and Regehr 2003). Paired-pulse stimulation of the OT in a TG9N slice resulted in a smaller EPSP response of the second pulse (conditioned) compared to the first (suprathreshold-conditioning) EPSP (Figure 4.5C), with a mean (±SEM) depression of 17.09 ± 10.19% (n=4 pulses) at an inter-stimulus interval of 300 ms. Similarly, paired-pulse stimulation in the control slice showed a mean depression of 11.46 ± 6.17% (n=4). These findings suggest that the retinogeniculate presynaptic function appears to be normal in TG9N animals, reflecting the decrease of neurotransmitter release due to depletion of a "release-ready" pool of vesicles (Zucker and Regehr 2002; Chen and Regehr 2003).

Because attempts to record whole cell intracellular responses in ΔCT animals were not successful, we examined synaptic responses using extracellular recording techniques. Figure 4.6A-B presents examples of cell attached extracellular responses to OT stimulation in a control and ΔCT mice. Postsynaptic action potentials were reliably evoked in both control and ΔCT cells by OT stimulation (Figures 4.6A-B). As shown in figure 4.6A, these responses were also blocked by DNQX, indicating that responses were postsynaptic. Stimulation of OT fibers in TG9N, ΔCT and control slices also evoked large amplitude extracellular field potentials (Figs. 4.6C and D). These responses are postsynaptic in origin (Lo et al., 2002) and sensitive to glutamatergic antagonists. Figure 4.6D shows that bath application of DNQX (10μM) abolished the evoked extracellular responses in a ΔCT cell, and upon washout the response returned to baseline values.

In conclusion, using a combination of whole cell and extracellular recordings we found clear evidence that TG9N and ΔCT animals preserve functional retinogeniculate connections after PD. Moreover, the pre- and post-synaptic characteristics of the responses were similar to what was observed in control animals.

Accessory visual functions are mediated through the NIF pathways. Previous reports have shown that *rd1* mice display a pupillary light reflex (PLR) (Provencio et al., 1994; Lucas et al., 2001), demonstrating intact connections through the OPN, to the Edinger-Westphal Nucleus, the ciliary ganglion, and ultimately to the constrictor muscle of the iris (Figure 4.7C). To test whether this simple reflex is intact in TG9N and ΔCT mice, we examined the strength and kinetics of the consensual light reflexes on dark-adapted animals at 12,000 cd/m^2 (~1.7mW/cm^2) intensity. We measured pupil constriction for 60 seconds as the percent pupil area normalized to baseline pupil area before light onset (custom software written and raw analysis also performed by K. Fu.). Both TG9N and ΔCT mice have PLRs (Figures 4.7A and B) that reach a plateau in approximately 15 seconds, thus displaying scaled PLR features similar to control. However, PLR kinetics in PD mice visibly slower and constriction plateau averages are significantly higher in TG9N mice (44.5 ± 11.0%, mean ± SEM) and ΔCT mice (32.5 ± 8.6%) compared to control (5.8 ± 0.6% SEM, Figure 6B, inset). Interestingly, the constriction appeared to relax toward the end of the trials in PD animals, and is seen in the averages traces presented (Figure 4.7B). Interestingly, this feature has been reported in *rd1* mice as well (Lucas et al., 2001).

It is possible that abnormal PLR could be explained by the impairment of downstream components in the reflex pathway. Previous reports have tested constriction

capacity of the iris as a control for this possibility (Hattar et al., 2002; Guler et al., 2008). When we applied 500mM of a cholinergic agonist, carbochol, to each condition (Figure 4.7A) we observed normal similar degrees of intense constriction. Combined with intact anatomical data, these data suggest the source of the PLR deficit in degenerated mice is not in downstream relays or the ultimate effecter.

Conclusions

Retinal remodeling and retinal degeneration does not grossly affect retinofugal projections

Retinal remodeling has been reported in ΔCT and TG9N mice using computational molecular phenotyping (CMP) that identifies retinal cells by amino acid signature (Marc and Jones 2002; Jones et al., 2003). Though useful as a quantitative method, CMP approach does not specify known protein markers for cell subtypes nor can it appreciate fine neurite processes, both of which help identify retinal remodeling changes. To paint a more complete picture, we reexamined ΔCT and TG9N mice and largely confirmed CMP results. As expected, TG9N mice exhibited drastic remodeling of ON and rod bipolar cells processes and as well as calbindin-positive and cholinergic interneurons. Immunohistochemical methods were more sensitive to changes in ΔCT retinas, particularly following bipolar cell processes (Figure 4.2A). These data indicate ΔCT mice have more extensive retinal remodeling than previously proposed.

We employed cell number counts as a secondary barometer of remodeling in the retina (Figure 4.2C). Reduced RGC cell counts in flatmount retina confirmed the degree of remodeling is most severe in TG9N mice and less so in ΔCT mice. Both OPN4, for melanopsin cells, and SMI-32 staining, for large projecting RGCs (Fuentes-Santamaria et

Figure 4.7-ΔCT and TG9N mice exhibit pupillary light responses. *A, Images of PLR time course:* Images of pupils taken in dark under infrared light (left) and after 30 seconds of light exposure (Chang et al.) show examples of PLR in each condition. 500mM Carbachol was applied to eye as a control for iris constrictor function. *B, Quantification of PLR time course:* Quantified with MATLAB by Kevin Fu. Pupillary area as percent of baseline is plotted as a function of time. Each point represents the means ± S.E.M for each genotype. *Inset* Medians ± 1st and 3rd quartiles of percent pupil constriction after 30 seconds for each condition, where lower numbers indicate greater constriction. Asterisks indicate significant differences from control for entire time course (Tamhane T2, unequal variances reflected in inset, repeated measures, $P<0.05$). *C.* Consensual pupillary light response begins with light incident on the retina. Melanopsin-containing RGCs project to the olivary pretectal nucleus (OPN). OPN sends bilateral afferents to the Edinger-Westphal Nucleus (EWN). EWN cells send axons along the oculomotor nerve (III) to the ciliary ganglion. The ciliary ganglion axon releases acetylcholine and innervates the iris constrictor.

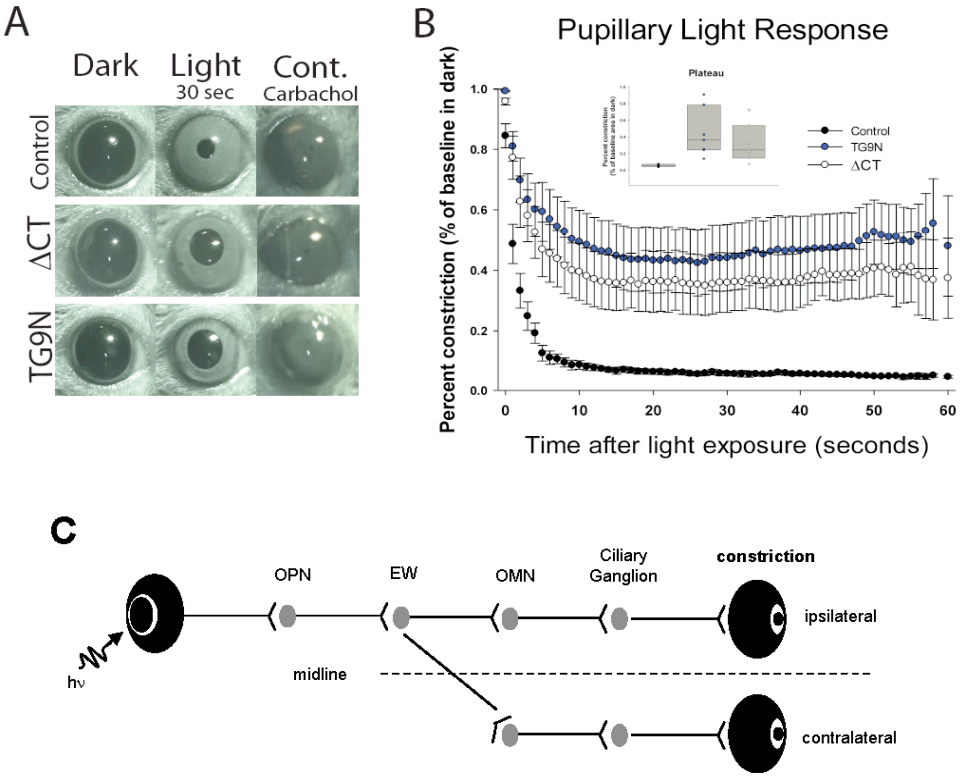
A
Dark
Light
30 sec
Cont.
Carbachol
Control
ΔCT
TG9N
B
Pupillary Light Response
Plateau
Control
TG9N
ΔCT
Percent constriction (% of baseline in dark)
Time after light exposure (seconds)
C
OPN
EW
OMN
Ciliary Ganglion
constriction
ipsilateral
midline
contralateral
hν

Figure 4.7

al., 2006) were decreased in TG9N retinas relative to ΔCT and control. Mazzoni (2008) detected no RGC loss in the *rd10*. Thus we were surprised to see reductions in both the SMI-32 and melanopsin cell counts. Using SMI-32 for normalization, melanopsin:SMI-32 ratios, which approximate the density of melanopsin cells, indicate both TG9N and ΔCT have a disproportionate decrease in melanopsin, a finding reflected in the PLR (Figure 1.6A and B). This drop could be from overall loss of melanopsin cells or simply a reduction in expression of melanopsin (Vugler et al., 2008). Additional time course studies that compare and quantify these remodeling changes may provide insights into the differing anomalous events in TG9N and ΔCT mice, as well as establish the progression of melanopsin loss. Altogether, our results in TG9N mice agree with Jones, et al, who ranked TG9N retinas as more aggressive remodellers than ΔCT. We utilized these differences throughout this study. Several studies have examined retinofugal projections of mice with PD. However, none have asked whether how retinal remodeling influences to central projection changes.

Previous studies have visualized projections of a few image forming centers in *rd10* or *rd1* mice (Bi et al., 2006; Mazzoni, et al., 2008) or non-image forming centers in *rd1* mice (Lupi et al., 2010). None have assessed eye-specific projections at all retinal targets in the same degenerated animals. This is the first study to use CTB tracing to simultaneously visualize projections from both eyes in all major visual centers of mice with photoreceptor degeneration (Hattar et al., 2006). We made a side-by-side comparison of TG9N and ΔCT retinofugal projections using anatomical tracing (Figure 4.3). The stark differences in the inner retinas of TG9N and ΔCT animals contrast with

surprisingly normal innervation of IF and NIF retinofugal projections in the brain (Figure 4.3).

Eye-specific refinement (Huberman et al., 2008) and early maintenance (Chapman 2000; Demas et al., 2006) of retinogeniculate projections are activity dependant. Eye-specific segregation has not been assessed in mice with altered visual activity beyond P28 using modern CTB tracing methods. During retinogeniculate development, dark-reared mice segregate normally (Demas et al., 2006) because spontaneous activity predominates before there is functional photoreceptor transmission at P14 (Demas et al., 2003).

Complete loss of photoreceptors certainly constitutes a decrement in visual activity. Both TG9N and ΔCT mice lose photoreceptors sometime after P21. It is not known whether this is beyond an age when eye-specific afferents can desegregate from loss of visual activity (Demas et al., 2006). Quantification of eye-specific projections at advanced ages both conditions reveals normal segregation. This is not surprising because TG9N and ΔCT mice have likely completed eye-specific refinement before photoreceptor death. Therefore, given this static appearance, it is likely that retinotopy of connective arrangement (Drager and Olsen, 1980) is also preserved. Similar stability is seen in LGN and cortex in humans with LCA (Aguirre et al., 2007) and underscores the significance of these animal models. Hints of this stability were reported in RGCs of *rd10* (Mazzoni et al., 2008) and circadian projections of *rd1* mice (Lupi et al., 2010). Lupi et al also indicates that extreme age (~P700) can impact these projections but we see no differences nearing these advanced ages in TG9N and ΔCT mice. This study elaborates on Mazzoni

and Lupi by revealing the full extent of retinogeniculate projection stability. Such steadfast connections place retina-based therapies one step closer to viable restoration.

The stability of eye-specific segregation stability may be explained by normal adult geniculate GABAergic circuitry (Ziburkus, Lo et al. 2003; Bickford, Slusarczyk et al. 2010). $GABA_A$ and $GABA_B$ activation can dampen plasticity by preventing calcium-mediated changes (Guido, 2008) and thus maintain the status quo. The maintenance of eye-specific segregation has not been extensively studied (Chapman 2000; Demas et al., 2006). But from these studies it is clear that aberrant activity can lead to a failure in segregation maintenance. The precise parameter of activity is not known, thus any activity must be considered. With melanopsin cells modest light responses may still exist in degenerated retinas. Though it is not known whether TG9N and ΔCT retinas have additional alterations in retinal activity, as reported in *rd1* mice (Stasheff, 2008), any changes cannot drive loss of eye-specific segregation at this age and the connections remain anatomically stable. We conclude that neither PD nor subsequent remodeling grossly affect the anatomical state of central projections.

We also compared the functional states of ΔCT and TG9N visual systems. PLRs were present in both PD mice, but kinetics were slower and the overall percent constriction diminished (Figure 4.7). Kinetics of *rd1* mice have been examined at a younger ages (<P100; Lucas et al., 2001). At those ages, responses are similar to control with two exceptions: 1) that loss of photoreceptors contributes to the small delay (<1 second) after light exposure and 2) a relaxing of constriction amplitude at exposures past 30 seconds (Lucas et al., 2001). In our system, the trigger for the onset of light has a margin of error of approximately 1 second, which may account our not detecting the brief

delay. At longer timescales we can reproduce the relaxing of constriction in degenerated retinas (Lucas et al., 2001; Figure 4.7), suggesting the global mechanisms for this phenomenon may be common among degenerated retinas. Testing of PLR and retinal remodeling in other models may provide insights into this unexplained phenotype.

Alterations in ΔCT and TG9N mice are restricted to the retina

The weakened PLRs in aged degenerated retinas may be the result of reduced melanopsin (Figure 1C). Indeed, both TG9N and DCT retinas have fewer melanopsin cells, or expression, and a predictably weakened PLR. Here we titrate the relative amounts of melanopsin, instead of the complete loss in OPN4-/- mice (Hattar et al., 2002), and report an intermediate PLR strength. This dose response reiterates melanopsin's role in PLR kinetics at the retinal level and suggests downstream components are relatively normal. Naturally, carbachol sensitivity experiments verify constrictor muscle responsiveness (Figure 4.7A) and confirm the normal function of other elements contributing to the PLR. Collectively, these changes in are restricted to the retina and do not appear to venture toward retinofugal targets

Previous reports test IF pathway function after delivery of light-sensitive pigments (Bi et al., 2006; Lagali et al., 2008). These treatments could partially restore sensitivity of the IF pathway in *rd1* and *rd10* animals, manifested by enhanced VEP (Bi et al., 2006) and optokinetic responses (Lagal et al., 2008). Over time, these treatments may not only rescue some retinal function but may also restore downstream synaptic connections in the IF that are lost after PD. We tested the retinogeniculate synapse directly (Figures 4.5 and 4.6) via optic tract stimulation and found normal responses in TG9N and ΔCT animals, consistent with anatomical findings. These results suggest that

the improvements after treatment were largely due to modality assimilation. These studies did not exclude the possibility that changes would occur as the result of treatment, contributing to the improvement. Our results suggest de-afferented retinofugal projections in TG9N and ΔCT mice are immediately ready for treatment and are limited by retinal, not central, acclimatization. Apart from overall efficacy, restorative measures for blindness differ in retinal integration, timing of intervention, and effectiveness (Mahadevappa et al., 2005; Shah et al., 2007). TG9N and ΔCT mice may be used to directly compare treatment modalities and optimize treatment conditions for retina-based therapies.

Retinal remodeling in retina based therapies

Many PD animal models that exhibit retinal remodeling are used to test retina-based therapies (Woch et al., 2001; Guven et al., 2005; Sagdullaev and McCall 2005; Sekirnjak et al., 2009). Retinal remodeling may differentially impact their efficacy. It has already been demonstrated that glial infiltration can interfere with subretinal implant interfaces (Butterwick et al., 2009). How does retinal remodeling affect therapeutic interventions in the retina? Some studies suggest that remodeling is not a factor (O'Hearn et al., 2006; Shah et al., 2007; Yanai et al., 2007), however, a direct test has never been performed.

Differing degrees of retinal remodeling may complicate the interpretation of experimental improvements, or lack thereof. Previous studies have demonstrated the usefulness of *rd1* mice in testing retina-based therapies. *rd1* mice also have evidence of intact projections (Lu et al., 2004) and remodeling (Strettoi et al., 2000, 2003). The *rd10* mouse, which exhibits remodeling, is another excellent model for interventional

improvements because the RGC number is unchanged (Mazzoni et al., 2008). However, these two models alone cannot address the manifold changes see in humans. Other models that present considerable retinal changes and remodeling are required to paint a complete picture of retinal substrate for therapy.

We show that TG9N and ΔCT animals' retinofugal projections are largely intact regardless of the degree of retinal remodeling. Indeed, the only major functional difference from control we found, PLR (Figure 4.7), can be attributed to loss of retinal melanopsin cells. Thus retinal changes appear to be the most significant obstacles to restoring visual function. Therefore, we predict present and future therapeutic attempts will be limited mainly by the degree of success in the retina. In the future, to address the complications of retinal remodeling and their impact on retina-based therapies efficacy, comparing animals with varying degrees of retinal remodeling, including TG9N and ΔCT, may advance retinal interventions in the face of retinal remodeling. Finally, our study provides encouraging support that retina-based treatments will continue to be fruitful avenue for advances in visual restoration.

CHAPTER 5

Discussion

This work presents data at two phases of visual system lifetime: development and advanced age. In both studies the critical, independent manipulation was the alteration of the retinal activity followed by the observation of a dependant variable: the properties of retinal axons at central visual targets. In the developmental study of Gβ5-/- and +/- mice, we exclusively assessed retinal activity. This manipulation provided many new avenues to investigate normal visual function as it pertains to Gβ5, particularly the need to explore the visual responses of Gβ5-/- retinas. In the study of aged mice with photoreceptor degeneration, we first assessed the impact of retinal remodeling that occurs after PD. We also directly assessed the anatomical and functional states of central projections relative to vision loss. With a primarily clinical slant, the degeneration data provide a basis of comparison and practical testing grounds for visual restoration after blindness. As different as these studies appear, both provide insights into the retinal state's influence on connectivity at central targets.

Eye-specific maintenance of projections may have a critical period

In visual development, the critical period is an important concept that describes a window exists in neural plasticity within which the capacity for change is largest (Hooks and Chen, 2007). First identified in the visual cortex in cats (Hubel and Wiesel, 1970), the critical period for ocular dominance helped establish the notion that the mammalian visual system permits change during development (Issa et al., 1999) and largely stabilizes those connections in adulthood. In the dLGN of mice, the critical period for activity-driven plasticity closely corresponds to development in the cortex and occurs

coincidently with spontaneous retinal activity (Hooks and Chen 2007; Huberman 2007; Huberman et al., 2008). Normal eye-specific refinement in mice (Jaubert-Miazza et al., 2005) can be interrupted or derailed by abnormal activity (Torborg et al., 2005), improper guidance cues (Pfeiffenberger et al., 2006), or a combination of both (Pfeiffenberger et al., 2006). But the maintenance phase is invisible until altered activity disrupts it (Chapman 2000; Demas et al., 2006). While loss of refinement can eventually recover in β2-/- mice from P8 to P28 (Muir-Robinson et al., 2002), there is no evidence of recovery after a failure to maintain segregation (Demas et al., 2006).

Strengthening and refinement of inputs takes place at the synaptic level (Chen and Regehr 2000; Jaubert-Miazza et al., 2005; Hooks and Chen 2006; Ziburkus and Guido 2006) and can be disrupted as late at P25 (Hooks and Chen 2008). Wild type and Gβ5+/- mice do not deviate from their segregation profiles after P14. Like the *nob* mouse, the elevated overlapping territory in the Gβ5-/- mouse during the maintenance phase sees little change after P14. Though no time course was performed on *nob*xGβ5-/- mice, P21 segregation was similar to both *nob* and Gβ5-/-, implying a failure of maintenance that likely occurs between P10 and P14. β2-/- also do not change segregation over P14 to P28. Similarly, ΔCT and TG9N mice, though much older, possess projection areas similar to wild-type. In these eight known assessments of maintenance in mice, none show effective changes in segregation after P14. This suggests critical period for eye-specific segregation ends at P14. Previously, I inferred that the maintenance phase begins sometime between P10 and P12. Together, these hint that the critical period of the maintenance phase is between P10 and P14. However, changes may occur in animals

with maintenance phenotypes after P28. Looking at *nob* mice and Gβ5-/- mice at more extreme ages help resolve this issue.

ΔCT and TG9N animals may see a loss of refinement sometime after P21 and simply recover as they age. A suitable time point to test this would be approximately P45, somewhere after the loss of all rod input in the ΔCT, but before loss of all photoreceptors in TG9N, permitting comparison of vision loss at different times in maintenance. At the fine synaptic level, ΔCT and TG9N geniculate neurons receive retinal input. However, the precise state of connectivity may change after visual decline. Preparations in which the retinogeniculate circuit is intact permit the estimation of retinal inputs onto geniculate cells (Chen and Regehr 2000; Ziburkus and Guido 2006; Guido 2008). Glutamate receptor subtypes change composition from NMDA-2 to AMPA during development (Liu and Chen 2008). Both approaches may provide insights into the state of retinofugal projections in degenerated mice.

Both Gβ5-/- and *nob* mice have elevated overlapping territories. It conceivably follows that the *nobx*Gβ5-/- would have additive overlapping territories. However, the *nobx*Gβ5-/- is again similar to Gβ5-/- and similarly deviates from wild-type. Demas, et al (2006) concluded that activity was the critical feature the lead to the *nob* failure in refinement, but could not address the persistent failure seen as late as P28. As mentioned before, the only evidence changes in the maintenance phase of eye-specific segregation can be seen no later than P14. We also know that *nob* activity changes drastically from P14 to P28, limiting the possibility that a single parameter of *nob* activity preserves the de-segregated state. Yet the desegregation remains. On the surface, the results suggest activity is not the driver of desegregation. However, a more likely

explanation is consistent with the critical period concept. The critical period for maintenance may be over by P14, in which case activity would its impact before eye opening. Indeed, manipulations that jar eye-specific segregation after P28 have not been reported. This differs from the critical period for synaptic refinement and strengthening, which continues as late as P25 (Hook and Chen, 2008)

As the critical period closes, new mechanisms must emerge to stabilize connections. In mature neurons, one means of preventing change is to prevent excitability of a cell. GABA activates a hyperpolarizing current in geniculate relay cells. During depolarization, calcium can traverse the membrane and act as a second messenger from a number of signaling pathways involved in plasticity (Kornhauser et al., 2002; Flavell and Greenberg 2008; Guido 2008). Naturally, hyperpolarization by GABA prevents these calcium influxes. Synapsing cells also activate programs that regulate postsynaptic scaffolds and stability, such as gephryin at GABAergic synapses, thus dampening any drastic structural changes (Tyagarajan and Fritschy, 2010). Evidence for both scenarios is presented in this work.

What is the mechanism for the Gβ5 -/- maintenance phenotype in dLGN if not presynaptic activity? $GABA_B$, responsible for the slow inhibitory component of mature retinogeniculate responses (Jaubert-Miazza et al., 2005), is coupled to Gαi/o is regulated by R7RGS activity. Prolonged $GABA_B$ –GIRK inhibition, which can be mediated by Gβ5 (Xu et al., 2010), may prevent overt activity-driven plasticity. In this case, the closure of the critical period may be more severe, limiting any further activity-driven changes.

If not directly from activity, where else may Gβ5 participate in the refinement and maintenance phenotypes? Lack of Gβ5 may also alter class 1 adenylate cyclase activity (Dunn et al., 2009; Dunn et al., 2006) in RGC via Gαi/o. Oscillating cAMP levels are responsible for proper ephrinA induced growth cone collapse in developing RGCs (Nicol et al., 2007). Improper retraction is activity dependant and would manifest as reduced eye-specific refinement. However, the desegregation is largely restricted to the ipsilateral axons. Gβ5 may regulate ipsilateral projections (Rebsam, Petros et al. 2009) through EphB1 at the intracellular level via MAPK/PKA crosstalk (Cordeaux and Hill, 2002) or activation of ipsilateral-projection specific transcription factor Zic2 (Lee et al., 2008a). Ephrin signaling may be perturbed at chiasmatic crossing (Petros et al., 2008; Petros et al., 2009). However, one would predict the window of impact for these changes is during coarse map formation and refinement. Additional analysis of early pathfinding in Gβ5-/- would rule out these possibilities. Extraneuronal influences, such as oligodendrocytes and astroglia, also play a critical role in axonal stability (Busch et al., 2010) and mature synaptic function (Bolton and Eroglu, 2009). Astroctyes can preserve retinal integrity (Jones and Marc, 2005; Mazzoni et al., 2008; Sofroniew and Vinters, 2010). Glial changes are seen in the retinas of mice with PD (Jones et al., 2003) and should be thoroughly assessed in other regions of their visual systems. It is unclear if Muller cells in retina or other astrocytes contain Gβ5. This question can be answered by observing co-localization of Gβ5 and glial fibrillary acidic protein in neural tissue. However, Gβ5 is not detected in cultured oligodentrocytes (Chen, C.K, personal communication). Gβ5 is scarce beyond nervous tissue (Watson et al, 1994) and not likely found in hematopoetic tissue. While not ruling out a role, this suggests Gβ5 is not likely involved in RGC

terminal clearance, a step critical for eye-specific refinement that is possibly mediated by microglia (Stevens et al., 2007).

It appears ΔCT and TG9N mice maintain normal projections even after early loss of visual patterning (in ΔCT), late changes in retinal activity (in TG9N), and moderate loss of RGCs (Figure 4.1). A decrease in RGCs should be evident the projections to the dLGN and other retinofugal targets, however they appear normal. There are two likely explanations for this. First, the remaining RGCs may sprout, a phenomenon seen in deafferented projections from enterorhinal cortex (Kadish and Van Groen, 2003). Second, relative to the overall number of RGCs, few project to the dLGN and do not effect the quantification of projections at this level (Chalupa, 2009). Both of these questions can be answered with simple experiments. Single axon tracing of RGCs (Sretavan et al., 1988) would show extensive arbors is abnormal ramification was occurring.

A more rigorous approach to the image quantification of eye-specific segregation may better reveal subtle drops in axonal territory. In these studies we employ R-analysis in conjunction with threshold analysis to assess both segregation and spatial extent of retinal projections. There are three methods for the unbiased quantification of projections described in Torborg, 2005. The first is R-analysis (Figure 3.1 and 3.3). The second is multi-thresholding. This determines overlap by holding the contralateral projection area constant and measures the overlap as a function of increasing ipsilateral threshold. The third, confocal analysis of individual projections, utilizes pixel intensity analysis on the overlapping regions of dLGN. However, spatial extent is a useful measurement that none of these methods can effectively assess across several sections or different animals.

Hence our studies must assess it separately. Another tool may be used is multi-thresholding of both the ipsilateral and contralateral projections. The concurrent graphing of both eye-specific threshold ranges produces a surface plot where max-min or inflection saddles represent objective values of overlap, contralateral, and ipsilateral territories. Thus this approach will allow a direct comparison of spatial extents across several sections.

The ceiling of maintenance and preserved projections in degenerated animals underscore the stability of established retinofugal circuits

Considering the *nob,* Gβ5-/-, and *nob*xGβ5-/- projections, it appears that there is a limited degree of de-segregation after retinal axons find their targets. Extending maintenance into more advanced ages, ΔCT and TG9N mice also exhibit maintained projections. Across tested all animals, we observe changes in retinal architecture or activity over time. The truly remarkable feature is that retinofugal projections remain intact. They do not deviate from either observed or assumed territorial distributions seen at P14. What accounts for this stability? As mentioned, many cell types in the visual system find and maintain targets with the help of adhesion molecules (Sanes and Yamagata, 2009). Indeed, DSCAM, DSCAML1, and Sidekicks1 and 2 (Yamagata and Sanes, 2008) employ molecular matching to determine proper lamination of strata in the IPL of chicks and very likely stabilize the connections. N-cadherins link pre- and postsynaptic membranes together via homophilic adhesions to stabilize synapses (Lee et al., 2008b). In degenerated retina, RGC survival is also a factor. Therefore, target derived survival signals are critical for stability. NT3 is retrogradely transported to the nucleus after binding TrkB at the target. This activates transcription factors like MEF2D, and

subsequently upregulates anti-apoptitic bcl-w (bcl-2) (Pazyra-Murphy et al., 2009) in dorsal root ganglion cells. Thus simply making the connection to a postsynaptic target may account for the bulk retinal projection stability.

The end of the critical period may explain β2-/- retinogeniculate patterning as well. Although the developmental program is greatly disrupted, β2-/- projections eventually refine (Muir-Robinson et al., 2002) into multiple patches in the dLGN by P28, presumably due to normal glutamatergic activity. β2-/- animals crossed with Cx36-/- mice show refinement at P14, but their precise timing of refinement is unknown. It is possible that β2-/- dLGNs refine to a degree but get stuck when the physical anchors of maintenance restrict further refinement. This would also explain the segregated ON/OFF patterning in β2-/- mice (Grubb et al., 2003). Respective ON and OFF patches would not distribute throughout the dLGN because adhesion molecules may restrict massive rearrangements.

The structural complexity of the inner retina limits the resolution of our observations and hence any firm conclusions about the exact roles Gβ5. Still, this work indirectly suggests that Gβ5 plays a crucial role in RGCs above other cell types. First, Gβ5 is found in RGCs. Second, loss of Gβ5 in *nob*xGβ5-/- retinas clearly disrupts RGC activity while sparing *nob* rhythmic activity after eye opening. Because *nob* abnormal rhythmic activity is localized to the bipolar cell, and Gβ5 loss does not drastically impair the rhythmic activity, one can conclude Gβ5 does not exert its primary function within the inner retinal elements. Thus Gβ5 is mostly important for RGC function. This is a critical finding because it allows the field to focus on R7RGS function in RGCs and particularly their potential role in retinogeniculate development.

Investigation of the retina and retinofugal projections has revealed several mechanisms and valuable explanations for neural development, G-protein signaling, and biological function. This work emphasizes the tremendous stability of the initial leg of visual system connections in the face of variable retinal insults. For those stricken with major progressive visual impairments, these observations of the visual system provide hope for clinical endeavors to understand and restore vision.

LIST OF REFERENCES

Ackert, J.M., Farajian, R., Volgyi, B., and Bloomfield, S.A. (2009). GABA blockade unmasks an OFF response in ON direction selective ganglion cells in the mammalian retina. J Physiol 587, 4481-4495.

Angelucci, A., Clasca, F., and Sur, M. (1996). Anterograde axonal tracing with the subunit B of cholera toxin: a highly sensitive immunohistochemical protocol for revealing fine axonal morphology in adult and neonatal brains. J Neurosci Methods 65, 101-112.

Anishchenko, A., Greschner, M., Elstrott, J., Sher, A., Litke, A.M., Feller, M.B., and Chichilnisky, E.J. (2010). Receptive field mosaics of retinal ganglion cells are established without visual experience. J Neurophysiol.

Bansal, A., Singer, J.H., Hwang, B.J., Xu, W., Beaudet, A., and Feller, M.B. (2000). Mice lacking specific nicotinic acetylcholine receptor subunits exhibit dramatically altered spontaneous activity patterns and reveal a limited role for retinal waves in forming ON and OFF circuits in the inner retina. J Neurosci 20, 7672-7681.

Barish, M.E. (1998). Intracellular calcium regulation of channel and receptor expression in the plasmalemma: potential sites of sensitivity along the pathways linking transcription, translation, and insertion. J Neurobiol 37, 146-157.

Baylor, D.A., Lamb, T.D., and Yau, K.W. (1979). Responses of retinal rods to single photons. J Physiol 288, 613-634.

Benians A, N.M., Hosny S, Tinker A (2005). Regulators of G-protein signaling form a quarternary complex with the agonist, receptor, and G-protein. A novel explaination for the acceleration of signaling activation kinetics. J Biol Chem 280, 13383-13394.

Bickford, M.E., Slusarczyk, A., Dilger, E.K., Krahe, T.E., Kucuk, C., and Guido, W. (2010). Synaptic development of the mouse dorsal lateral geniculate nucleus. J Comp Neurol 518, 622-635.

Blake, B.L., Wing, M.R., Zhou, J.Y., Lei, Q., Hillmann, J.R., Behe, C.I., Morris, R.A., Harden, T.K., Bayliss, D.A., Miller, R.J., and Siderovski, D.P. (2001). G beta association and effector interaction selectivities of the divergent G gamma subunit G gamma(13). J Biol Chem 276, 49267-49274.

Blankenship, A.G., and Feller, M.B. (2010). Mechanisms underlying spontaneous patterned activity in developing neural circuits. Nat Rev Neurosci 11, 18-29.

Blankenship, A.G., Ford, K.J., Johnson, J., Seal, R.P., Edwards, R.H., Copenhagen, D.R., and Feller, M.B. (2009). Synaptic and extrasynaptic factors governing glutamatergic retinal waves. Neuron 62, 230-241.

Bodnarenko, S.R., and Chalupa, L.M. (1993). Stratification of ON and OFF ganglion cell dendrites depends on glutamate-mediated afferent activity in the developing retina. Nature 364, 144-146.

Bolton, M.M., and Eroglu, C. (2009). Look who is weaving the neural web: glial control of synapse formation. Curr Opin Neurobiol 19, 491-497.

Burns, M.E., and Baylor, D.A. (2001). Activation, deactivation, and adaptation in vertebrate photoreceptor cells. Annu Rev Neurosci 24, 779-805.

Busch, S.A., Horn, K.P., Cuascut, F.X., Hawthorne, A.L., Bai, L., Miller, R.H., and Silver, J. Adult NG2+ cells are permissive to neurite outgrowth and stabilize sensory

axons during macrophage-induced axonal dieback after spinal cord injury. J Neurosci 30, 255-265.
Butts, D.A., Kanold, P.O., and Shatz, C.J. (2007). A burst-based "Hebbian" learning rule at retinogeniculate synapses links retinal waves to activity-dependent refinement. PLoS Biol 5, e61.
Cabrera-Vera, T.M., Hernandez, S., Earls, L.R., Medkova, M., Sundgren-Andersson, A.K., Surmeier, D.J., and Hamm, H.E. (2004). RGS9-2 modulates D2 dopamine receptor-mediated Ca2+ channel inhibition in rat striatal cholinergic interneurons. Proc Natl Acad Sci U S A 101, 16339-16344.
Cang, J., Niell, C.M., Liu, X., Pfeiffenberger, C., Feldheim, D.A., and Stryker, M.P. (2008). Selective disruption of one Cartesian axis of cortical maps and receptive fields by deficiency in ephrin-As and structured activity. Neuron 57, 511-523.
Cang, J., Renteria, R.C., Kaneko, M., Liu, X., Copenhagen, D.R., and Stryker, M.P. (2005). Development of precise maps in visual cortex requires patterned spontaneous activity in the retina. Neuron 48, 797-809.
Cao, Y., Song, H., Okawa, H., Sampath, A.P., Sokolov, M., and Martemyanov, K.A. (2008). Targeting of RGS7/Gbeta5 to the dendritic tips of ON-bipolar cells is independent of its association with membrane anchor R7BP. J Neurosci 28, 10443-10449.
Carter-Dawson, L.D., and LaVail, M.M. (1979). Rods and cones in the mouse retina. I. Structural analysis using light and electron microscopy. J Comp Neurol 188, 245-262.
Chalupa, L.M. (2009). Retinal waves are unlikely to instruct the formation of eye-specific retinogeniculate projections. Neural Dev 4, 25.
Chalupa, L.M., and Gunhan, E. (2004). Development of On and Off retinal pathways and retinogeniculate projections. Prog Retin Eye Res 23, 31-51.
Chang, B., Hawes, N.L., Pardue, M.T., German, A.M., Hurd, R.E., Davisson, M.T., Nusinowitz, S., Rengarajan, K., Boyd, A.P., Sidney, S.S., et al. (2007). Two mouse retinal degenerations caused by missense mutations in the beta-subunit of rod cGMP phosphodiesterase gene. Vision Res 47, 624-633.
Chapman, B. (2000). Necessity for afferent activity to maintain eye-specific segregation in ferret lateral geniculate nucleus. Science 287, 2479-2482.
Cheever, M.L., Snyder, J.T., Gershburg, S., Siderovski, D.P., Harden, T.K., and Sondek, J. (2008). Crystal structure of the multifunctional Gbeta5-RGS9 complex. Nat Struct Mol Biol 15, 155-162.
Chen, C., and Regehr, W.G. (2000). Developmental remodeling of the retinogeniculate synapse. Neuron 28, 955-966.
Chen, C.K. (2005). The vertebrate phototransduction cascade: amplification and termination mechanisms. Rev Physiol Biochem Pharmacol 154, 101-121.
Chen, C.K., Eversole-Cire, P., Zhang, H., Mancino, V., Chen, Y.J., He, W., Wensel, T.G., and Simon, M.I. (2003). Instability of GGL domain-containing RGS proteins in mice lacking the G protein beta-subunit Gbeta5. Proc Natl Acad Sci U S A 100, 6604-6609.
Chen, F.S., Shim, H., Morhardt, D., Dallman, R., Krahn, E., McWhinney, L., Rao, A., Gold, S.J., and Chen, C.K. (2010). Functional redundancy of R7 RGS proteins in ON-bipolar cell dendrites. Invest Ophthalmol Vis Sci 51, 686-693.

Chen, J., Makino, C.L., Peachey, N.S., Baylor, D.A., and Simon, M.I. (1995). Mechanisms of rhodopsin inactivation in vivo as revealed by a COOH-terminal truncation mutant. Science 267, 374-377.
Clancy, S.M., Fowler, C.E., Finley, M., Suen, K.F., Arrabit, C., Berton, F., Kosaza, T., Casey, P.J., and Slesinger, P.A. (2005). Pertussis-toxin-sensitive Galpha subunits selectively bind to C-terminal domain of neuronal GIRK channels: evidence for a heterotrimeric G-protein-channel complex. Mol Cell Neurosci 28, 375-389.
Clapham, D.E., and Neer, E.J. (1997). G protein beta gamma subunits. Annu Rev Pharmacol Toxicol 37, 167-203.
Constantine-Paton, M., Cline, H.T., and Debski, E. (1990). Patterned activity, synaptic convergence, and the NMDA receptor in developing visual pathways. Annu. Rev. Neurosci 13, 129-154.
Cook, P.M., Prusky, G., and Ramoa, A.S. (1999). The role of spontaneous retinal activity before eye opening in the maturation of form and function in the retinogeniculate pathway of the ferret. Vis Neurosci 16, 491-501.
Cordeaux, Y., and Hill, S.J. (2002). Mechanisms of cross-talk between G-protein-coupled receptors. Neurosignals 11, 45-57.
Crowley, J.C., and Katz, L.C. (2000). Early development of ocular dominance columns. Science 290, 1321-1324.
Crunelli, V., and Leresche, N. (1991). A role for GABAB receptors in excitation and inhibition of thalamocortical cells. Trends Neurosci 14, 16-21.
Debski, E.A., and Cline, H.T. (2002). Activity-dependent mapping in the retinotectal projection. Curr Opin Neurobiol 12, 93-99.
Demas, J., Eglen, S.J., and Wong, R.O. (2003). Developmental loss of synchronous spontaneous activity in the mouse retina is independent of visual experience. J Neurosci 23, 2851-2860.
Demas, J., Sagdullaev, B.T., Green, E., Jaubert-Miazza, L., McCall, M.A., Gregg, R.G., Wong, R.O., and Guido, W. (2006). Failure to maintain eye-specific segregation in nob, a mutant with abnormally patterned retinal activity. Neuron 50, 247-259.
DeVries, S.H., and Schwartz, E.A. (1999). Kainate receptors mediate synaptic transmission between cones and 'Off' bipolar cells in a mammalian retina. Nature 397, 157-160.
Drager, U.C., and Olsen, J.F. (1980). Origins of crossed and uncrossed retinal projections in pigmented and albino mice. J Comp Neurol 191, 383-412.
Drenan, R.M., Doupnik, C.A., Boyle, M.P., Muglia, L.J., Huettner, J.E., Linder, M.E., and Blumer, K.J. (2005). Palmitoylation regulates plasma membrane-nuclear shuttling of R7BP, a novel membrane anchor for the RGS7 family. J Cell Biol 169, 623-633.
Drenan, R.M., Doupnik, C.A., Jayaraman, M., Buchwalter, A.L., Kaltenbronn, K.M., Huettner, J.E., Linder, M.E., and Blumer, K.J. (2006). R7BP augments the function of RGS7*Gbeta5 complexes by a plasma membrane-targeting mechanism. J Biol Chem 281, 28222-28231.
Dunn, T.A., Storm, D.R., and Feller, M.B. (2009). Calcium-dependent increases in protein kinase-A activity in mouse retinal ganglion cells are mediated by multiple adenylate cyclases. PLoS One 4, e7877.
Dunn, T.A., Wang, C.T., Colicos, M.A., Zaccolo, M., DiPilato, L.M., Zhang, J., Tsien, R.Y., and Feller, M.B. (2006). Imaging of cAMP levels and protein kinase A activity

reveals that retinal waves drive oscillations in second-messenger cascades. J Neurosci 26, 12807-12815.
Eggers, E.D., McCall, M.A., and Lukasiewicz, P.D. (2007). Presynaptic inhibition differentially shapes transmission in distinct circuits in the mouse retina. J Physiol 582, 569-582.
Elstrott, J., Anishchenko, A., Greschner, M., Sher, A., Litke, A.M., Chichilnisky, E.J., and Feller, M.B. (2008). Direction selectivity in the retina is established independent of visual experience and cholinergic retinal waves. Neuron 58, 499-506.
Famiglietti, E.V., Jr. (1983). 'Starburst' amacrine cells and cholinergic neurons: mirror-symmetric on and off amacrine cells of rabbit retina. Brain Res 261, 138-144.
Farber, D.B., and Lolley, R.N. (1974). Cyclic guanosine monophosphate: elevation in degenerating photoreceptor cells of the C3H mouse retina. Science 186, 449-451.
Feller, M.B. (2009). Retinal waves are likely to instruct the formation of eye-specific retinogeniculate projections. Neural Dev 4, 24.
Feller, M.B., Wellis, D.P., Stellwagen, D., Werblin, F.S., and Shatz, C.J. (1996). Requirement for cholinergic synaptic transmission in the propagation of spontaneous retinal waves. Science 272, 1182-1187.
Ferre, S., Quiroz, C., Woods, A.S., Cunha, R., Popoli, P., Ciruela, F., Lluis, C., Franco, R., Azdad, K., and Schiffmann, S.N. (2008). An update on adenosine A2A-dopamine D2 receptor interactions: implications for the function of G protein-coupled receptors. Curr Pharm Des 14, 1468-1474.
Fischer, K.F., Lukasiewicz, P.D., and Wong, R.O. (1998). Age-dependent and cell class-specific modulation of retinal ganglion cell bursting activity by GABA. J Neurosci 18, 3767-3778.
Fox, M.A., Sanes, J.R., Borza, D.B., Eswarakumar, V.P., Fassler, R., Hudson, B.G., John, S.W., Ninomiya, Y., Pedchenko, V., Pfaff, S.L., et al. (2007). Distinct target-derived signals organize formation, maturation, and maintenance of motor nerve terminals. Cell 129, 179-193.
Fuentes-Santamaria, V., Stein, B.E., and McHaffie, J.G. (2006). Neurofilament proteins are preferentially expressed in descending output neurons of the cat the superior colliculus: a study using SMI-32. Neuroscience 138, 55-68.
Fuerst, P.G., Bruce, F., Tian, M., Wei, W., Elstrott, J., Feller, M.B., Erskine, L., Singer, J.H., and Burgess, R.W. (2009). DSCAM and DSCAML1 function in self-avoidance in multiple cell types in the developing mouse retina. Neuron 64, 484-497.
Godement, P., Salaun, J., and Imbert, M. (1984). Prenatal and postnatal development of retinogeniculate and retinocollicular projections in the mouse. J Comp Neurol 230, 552-575.
Godfrey, K.B., and Swindale, N.V. (2007). Retinal wave behavior through activity-dependent refractory periods. PLoS Comput Biol 3, e245.
Gold, S.J., Ni, Y.G., Dohlman, H.G., and Nestler, E.J. (1997). Regulators of G-protein signaling (RGS) proteins: region-specific expression of nine subtypes in rat brain. J Neurosci 17, 8024-8037.
Gomez-Ospina, N., Tsuruta, F., Barreto-Chang, O., Hu, L., and Dolmetsch, R. (2006). The C terminus of the L-type voltage-gated calcium channel Ca(V)1.2 encodes a transcription factor. Cell 127, 591-606.

Grabowska, D., Jayaraman, M., Kaltenbronn, K.M., Sandiford, S.L., Wang, Q., Jenkins, S., Slepak, V.Z., Smith, Y., and Blumer, K.J. (2008). Postnatal induction and localization of R7BP, a membrane-anchoring protein for regulator of G protein signaling 7 family-Gbeta5 complexes in brain. Neuroscience 151, 969-982.
Gregg, R.G., Kamermans, M., Klooster, J., Lukasiewicz, P.D., Peachey, N.S., Vessey, K.A., and McCall, M.A. (2007). Nyctalopin expression in retinal bipolar cells restores visual function in a mouse model of complete X-linked congenital stationary night blindness. J Neurophysiol 98, 3023-3033.
Gregg, R.G., Mukhopadhyay, S., Candille, S.I., Ball, S.L., Pardue, M.T., McCall, M.A., and Peachey, N.S. (2003). Identification of the gene and the mutation responsible for the mouse nob phenotype. Invest Ophthalmol Vis Sci 44, 378-384.
Grubbs MS, R., FM, Changeux JP, Thompson ID (2003). Abnormal functional organiztion in the dorsal lateral geniculate nucleus of mice lacking the beta 2 subunit of the nicotinic acetylcholine receptor. Neuron 40, 1161-1172.
Guido, W. (2008). Refinement of the retinogeniculate pathway. J Physiol.
Hamori, J. (1990). Morphological plasticity of postsynaptic neurones in reactive synaptogenesis. J Exp Biol 153, 251-260.
Hankins, M.W., Peirson, S.N., and Foster, R.G. (2008). Melanopsin: an exciting photopigment. Trends Neurosci 31, 27-36.
Harrington, M.E. (1997). The ventral lateral geniculate nucleus and the intergeniculate leaflet: interrelated structures in the visual and circadian systems. Neurosci Biobehav Rev 21, 705-727.
Hattar, S., Kumar, M., Park, A., Tong, P., Tung, J., Yau, K.W., and Berson, D.M. (2006). Central projections of melanopsin-expressing retinal ganglion cells in the mouse. J Comp Neurol 497, 326-349.
Hennig, M.H., Adams, C., Willshaw, D., and Sernagor, E. (2009). Early-stage waves in the retinal network emerge close to a critical state transition between local and global functional connectivity. J Neurosci 29, 1077-1086.
Hooks, B.M., and Chen, C. (2006). Distinct roles for spontaneous and visual activity in remodeling of the retinogeniculate synapse. Neuron 52, 281-291.
Hooks, B.M., and Chen, C. (2007). Critical periods in the visual system: changing views for a model of experience-dependent plasticity. Neuron 56, 312-326.
Hooks, B.M., and Chen, C. (2008). Vision triggers an experience-dependent sensitive period at the retinogeniculate synapse. J Neurosci 28, 4807-4817.
Hooks, S.B., Waldo, G.L., Corbitt, J., Bodor, E.T., Krumins, A.M., and Harden, T.K. (2003). RGS6, RGS7, RGS9, and RGS11 stimulate GTPase activity of Gi family G-proteins with differential selectivity and maximal activity. J Biol Chem 278, 10087-10093.
Hubel, D.H., and Wiesel, T.N. (1970). The period of susceptibility to the physiological effects of unilateral eye closure in kittens. J Physiol 206, 419-436.
Hubel, D.H., and Wiesel, T.N. (2009). Republication of The Journal of Physiology (1959) 148, 574-591: Receptive fields of single neurones in the cat's striate cortex. 1959. J Physiol 587, 2721-2732.
Huberman, A.D. (2007). Mechanisms of eye-specific visual circuit development. Curr Opin Neurobiol 17, 73-80.

Huberman, A.D., Feller, M.B., and Chapman, B. (2008). Mechanisms Underlying Development of Visual Maps and Receptive Fields. Annu Rev Neurosci 31, 479-509.
Huberman, A.D., Wang, G.Y., Liets, L.C., Collins, O.A., Chapman, B., and Chalupa, L.M. (2003). Eye-specific retinogeniculate segregation independent of normal neuronal activity. Science 300, 994-998.
Issa, N.P., Trachtenberg, J.T., Chapman, B., Zahs, K.R., and Stryker, M.P. (1999). The critical period for ocular dominance plasticity in the Ferret's visual cortex. J Neurosci 19, 6965-6978.
J. M. BALLESTEROS1, C. SUN1, A. V. GOLOSHCHAPOV2, H.-J. CHENG2, and L. M. CHALUPA1, 3 (2007). Developing nAChR b2-/- mice manifest retinal waves of action potentials as well as altered retinogeniculate projection patterns.
Jaubert-Miazza, L., Green, E., Lo, F.S., Bui, K., Mills, J., and Guido, W. (2005). Structural and functional composition of the developing retinogeniculate pathway in the mouse. Vis Neurosci 22, 661-676.
Jayaraman, M., Zhou, H., Jia, L., Cain, M.D., and Blumer, K.J. (2009). R9AP and R7BP: traffic cops for the RGS7 family in phototransduction and neuronal GPCR signaling. Trends Pharmacol Sci 30, 17-24.
Jones, B.W., and Marc, R.E. (2005). Retinal remodeling during retinal degeneration. Exp Eye Res 81, 123-137.
Jones, B.W., Watt, C.B., Frederick, J.M., Baehr, W., Chen, C.K., Levine, E.M., Milam, A.H., Lavail, M.M., and Marc, R.E. (2003). Retinal remodeling triggered by photoreceptor degenerations. J Comp Neurol 464, 1-16.
Kadish, I., and Van Groen, T. (2003). Differences in lesion-induced hippocampal plasticity between mice and rats. Neuroscience 116, 499-509.
Kandel, E., Jessel, T., and Schwartz, J. (2000). Principles of Neural Science. McGraw Hill Publishing.
Kerschensteiner, D., Morgan, J.L., Parker, E.D., Lewis, R.M., and Wong, R.O. (2009). Neurotransmission selectively regulates synapse formation in parallel circuits in vivo. Nature 460, 1016-1020.
Kerschensteiner, D., and Wong, R.O. (2008). A precisely timed asynchronous pattern of ON and OFF retinal ganglion cell activity during propagation of retinal waves. Neuron 58, 851-858.
Kong, W.J., Yin, Z.D., Fan, G.R., Li, D., and Huang, X. Time sequence of auditory nerve and spiral ganglion cell degeneration following chronic kanamycin-induced deafness in the guinea pig. Brain Res.
Kornhauser, J.M., Cowan, C.W., Shaywitz, A.J., Dolmetsch, R.E., Griffith, E.C., Hu, L.S., Haddad, C., Xia, Z., and Greenberg, M.E. (2002). CREB transcriptional activity in neurons is regulated by multiple, calcium-specific phosphorylation events. Neuron 34, 221-233.
Koulen, P. (1999). Postnatal development of dopamine D1 receptor immunoreactivity in the rat retina. J Neurosci Res 56, 397-404.
Kovoor, A., Chen, C.K., He, W., Wensel, T.G., Simon, M.I., and Lester, H.A. (2000). Co-expression of Gbeta5 enhances the function of two Ggamma subunit-like domain-containing regulators of G protein signaling proteins. J Biol Chem 275, 3397-3402.

Krispel, C.M., Chen, C.K., Simon, M.I., and Burns, M.E. (2003). Prolonged photoresponses and defective adaptation in rods of Gbeta5-/- mice. J Neurosci 23, 6965-6971.
Krispel, C.M., Chen, D., Melling, N., Chen, Y.J., Martemyanov, K.A., Quillinan, N., Arshavsky, V.Y., Wensel, T.G., Chen, C.K., and Burns, M.E. (2006). RGS expression rate-limits recovery of rod photoresponses. Neuron 51, 409-416.
Kvanta, A., Seregard, S., Sejersen, S., Kull, B., and Fredholm, B.B. (1997). Localization of adenosine receptor messenger RNAs in the rat eye. Exp Eye Res 65, 595-602.
Lamba, D.A., Gust, J., and Reh, T.A. (2009). Transplantation of human embryonic stem cell-derived photoreceptors restores some visual function in Crx-deficient mice. Cell Stem Cell 4, 73-79.
Lee, C.C., and Winer, J.A. (2005). Principles governing auditory cortex connections. Cereb Cortex 15, 1804-1814.
Lee, C.W., Eglen, S.J., and Wong, R.O. (2002). Segregation of ON and OFF retinogeniculate connectivity directed by patterned spontaneous activity. J Neurophysiol 88, 2311-2321.
Lee, R., Petros, T.J., and Mason, C.A. (2008a). Zic2 regulates retinal ganglion cell axon avoidance of ephrinB2 through inducing expression of the guidance receptor EphB1. J Neurosci 28, 5910-5919.
Lee, T.W., Tsang, V.W., and Birch, N.P. (2008b). Synaptic plasticity-associated proteases and protease inhibitors in the brain linked to the processing of extracellular matrix and cell adhesion molecules. Neuron Glia Biol 4, 223-234.
Legendy, C.R., and Salcman, M. (1985). Bursts and recurrences of bursts in the spike trains of spontaneously active striate cortex neurons. J Neurophysiol 53, 926-939.
Leonard, K.C., Petrin, D., Coupland, S.G., Baker, A.N., Leonard, B.C., LaCasse, E.C., Hauswirth, W.W., Korneluk, R.G., and Tsilfidis, C. (2007). XIAP protection of photoreceptors in animal models of retinitis pigmentosa. PLoS One 2, e314.
Lin, B., Koizumi, A., Tanaka, N., Panda, S., and Masland, R.H. (2008a). Restoration of visual function in retinal degeneration mice by ectopic expression of melanopsin. Proc Natl Acad Sci U S A.
Lin, Y., Bloodgood, B.L., Hauser, J.L., Lapan, A.D., Koon, A.C., Kim, T.K., Hu, L.S., Malik, A.N., and Greenberg, M.E. (2008b). Activity-dependent regulation of inhibitory synapse development by Npas4. Nature 455, 1198-1204.
Lo, F.S., Ziburkus, J., and Guido, W. (2002). Synaptic mechanisms regulating the activation of a Ca(2+)-mediated plateau potential in developing relay cells of the LGN. J Neurophysiol 87, 1175-1185.
Lu, B., Coffey, P., and Lund, R. (2004). Increased c-fos-like immunoreactivity in the superior colliculus and lateral geniculate nucleus of the rd mouse. Brain Res 1025, 220-225.
Lucas, R.J., Douglas, R.H., and Foster, R.G. (2001). Characterization of an ocular photopigment capable of driving pupillary constriction in mice. Nat Neurosci 4, 621-626.
Luo, D.G., Xue, T., and Yau, K.W. (2008). How vision begins: an odyssey. Proc Natl Acad Sci U S A 105, 9855-9862.
Lupi, D., Semo, M., and Foster, R.G. Impact of age and retinal degeneration on the light input to circadian brain structures. Neurobiol Aging.

Maffei, A., and Fontanini, A. (2009). Network homeostasis: a matter of coordination. Curr Opin Neurobiol 19, 168-173.
Maffei, L., and Galli-Resta, L. (1990). Correlation in the discharges of neighboring rat retinal ganglion cells during prenatal life. Proc Natl Acad Sci U S A 87, 2861-2864.
Marc, R.E., and Jones, B.W. (2002). Molecular phenotyping of retinal ganglion cells. J Neurosci 22, 413-427.
Marc, R.E., Jones, B.W., Watt, C.B., and Strettoi, E. (2003). Neural remodeling in retinal degeneration. Prog Retin Eye Res 22, 607-655.
Mastronarde, D.N. (1983). Correlated firing of cat retinal ganglion cells. I. Spontaneously active inputs to X- and Y-cells. J Neurophysiol 49, 303-324.
Mastronarde, D.N. (1987). Two classes of single-input X-cells in cat lateral geniculate nucleus. II. Retinal inputs and the generation of receptive-field properties. J Neurophysiol 57, 381-413.
Mazzoni, F., Novelli, E., and Strettoi, E. (2008). Retinal ganglion cells survive and maintain normal dendritic morphology in a mouse model of inherited photoreceptor degeneration. J Neurosci 28, 14282-14292.
McCall, M.A., and Gregg, R.G. (2008). Comparisons of structural and functional abnormalities in mouse b-wave mutants. J Physiol 586, 4385-4392.
McLaughlin, T., Torborg, C.L., Feller, M.B., and O'Leary, D.D. (2003). Retinotopic map refinement requires spontaneous retinal waves during a brief critical period of development. Neuron 40, 1147-1160.
Meister, M., Wong, R.O., Baylor, D.A., and Shatz, C.J. (1991). Synchronous bursts of action potentials in ganglion cells of the developing mammalian retina. Science 252, 939-943.
Miyake, Y., Yagasaki, K., Horiguchi, M., Kawase, Y., and Kanda, T. (1986). Congenital stationary night blindness with negative electroretinogram. A new classification. Arch Ophthalmol 104, 1013-1020.
Mojumder, D.K., Qian, Y., and Wensel, T.G. (2009). Two R7 regulator of G-protein signaling proteins shape retinal bipolar cell signaling. J Neurosci 29, 7753-7765.
Mooney, R., Penn, A.A., Gallego, R., and Shatz, C.J. (1996). Thalamic relay of spontaneous retinal activity prior to vision. Neuron 17, 863-874.
Morgan, J.L., Dhingra, A., Vardi, N., and Wong, R.O. (2006). Axons and dendrites originate from neuroepithelial-like processes of retinal bipolar cells. Nat Neurosci 9, 85-92.
Moseley, M.J., Fielder, A.R., and Stewart, C.E. (2009). The optical treatment of amblyopia. Optom Vis Sci 86, 629-633.
Muir-Robinson, G., Hwang, B.J., and Feller, M.B. (2002). Retinogeniculate axons undergo eye-specific segregation in the absence of eye-specific layers. J Neurosci 22, 5259-5264.
Muscat, L., Huberman, A.D., Jordan, C.L., and Morin, L.P. (2003). Crossed and uncrossed retinal projections to the hamster circadian system. J Comp Neurol 466, 513-524.
Myhr, K.L., Lukasiewicz, P.D., and Wong, R.O. (2001). Mechanisms underlying developmental changes in the firing patterns of ON and OFF retinal ganglion cells during refinement of their central projections. J Neurosci 21, 8664-8671.

Nakatani, K., and Yau, K.W. (1988). Guanosine 3',5'-cyclic monophosphate-activated conductance studied in a truncated rod outer segment of the toad. J Physiol 395, 731-753.
Nicol, X., Bennis, M., Ishikawa, Y., Chan, G.C., Reperant, J., Storm, D.R., and Gaspar, P. (2006). Role of the calcium modulated cyclases in the development of the retinal projections. Eur J Neurosci 24, 3401-3414.
Nicol, X., Voyatzis, S., Muzerelle, A., Narboux-Neme, N., Sudhof, T.C., Miles, R., and Gaspar, P. (2007). cAMP oscillations and retinal activity are permissive for ephrin signaling during the establishment of the retinotopic map. Nat Neurosci 10, 340-347.
O'Leary, D.D., and McLaughlin, T. (2005). Mechanisms of retinotopic map development: Ephs, ephrins, and spontaneous correlated retinal activity. Prog Brain Res 147, 43-65.
Ohsawa, R., and Kageyama, R. (2008). Regulation of retinal cell fate specification by multiple transcription factors. Brain Res 1192, 90-98.
Pardue, M.T., McCall, M.A., LaVail, M.M., Gregg, R.G., and Peachey, N.S. (1998). A naturally occurring mouse model of X-linked congenital stationary night blindness. Invest Ophthalmol Vis Sci 39, 2443-2449.
Pazyra-Murphy, M.F., Hans, A., Courchesne, S.L., Karch, C., Cosker, K.E., Heerssen, H.M., Watson, F.L., Kim, T., Greenberg, M.E., and Segal, R.A. (2009). A retrograde neuronal survival response: target-derived neurotrophins regulate MEF2D and bcl-w. J Neurosci 29, 6700-6709.
Peachey, N.S., and Ball, S.L. (2003). Electrophysiological analysis of visual function in mutant mice. Doc Ophthalmol 107, 13-36.
Penn, A.A., Riquelme, P.A., Feller, M.B., and Shatz, C.J. (1998). Competition in retinogeniculate patterning driven by spontaneous activity. Science 279, 2108-2112.
Petersen, C.C. (2007). The functional organization of the barrel cortex. Neuron 56, 339-355.
Petros, T.J., Rebsam, A., and Mason, C.A. (2008). Retinal axon growth at the optic chiasm: to cross or not to cross. Annu Rev Neurosci 31, 295-315.
Petros, T.J., Shrestha, B.R., and Mason, C. (2009). Specificity and sufficiency of EphB1 in driving the ipsilateral retinal projection. J Neurosci 29, 3463-3474.
Pfeiffenberger, C., Yamada, J., and Feldheim, D.A. (2006). Ephrin-As and patterned retinal activity act together in the development of topographic maps in the primary visual system. J Neurosci 26, 12873-12884.
Pham, T.A., Rubenstein, J.L., Silva, A.J., Storm, D.R., and Stryker, M.P. (2001). The CRE/CREB pathway is transiently expressed in thalamic circuit development and contributes to refinement of retinogeniculate axons. Neuron 31, 409-420.
Pillow, J.W., Shlens, J., Paninski, L., Sher, A., Litke, A.M., Chichilnisky, E.J., and Simoncelli, E.P. (2008). Spatio-temporal correlations and visual signalling in a complete neuronal population. Nature 454, 995-999.
Pittler, S.J., Keeler, C.E., Sidman, R.L., and Baehr, W. (1993). PCR analysis of DNA from 70-year-old sections of rodless retina demonstrates identity with the mouse rd defect. Proc Natl Acad Sci U S A 90, 9616-9619.
Poo, M.M., and Zheng, J. (2006). Calcium Signaling and Neuronal Motility. Annu Rev Cell Dev Biol.
Provencio, I., Wong, S., Lederman, A.B., Argamaso, S.M., and Foster, R.G. (1994). Visual and circadian responses to light in aged retinally degenerate mice. Vision Res 34, 1799-1806.

Pugh, E.N., Jr., and Lamb, T.D. (1993). Amplification and kinetics of the activation steps in phototransduction. Biochim Biophys Acta 1141, 111-149.
Puri, B.K. (2010). Progressive structural brain changes in schizophrenia. Expert Rev Neurother 10, 33-42.
Rahman, Z., Schwarz, J., Gold, S.J., Zachariou, V., Wein, M.N., Choi, K.H., Kovoor, A., Chen, C.K., DiLeone, R.J., Schwarz, S.C., et al. (2003). RGS9 modulates dopamine signaling in the basal ganglia. Neuron 38, 941-952.
Ramachandran, V.S., Rogers-Ramachandran, D., and Stewart, M. (1992). Perceptual correlates of massive cortical reorganization. Science 258, 1159-1160.
Ramamurthy, V., Niemi, G.A., Reh, T.A., and Hurley, J.B. (2004). Leber congenital amaurosis linked to AIPL1: a mouse model reveals destabilization of cGMP phosphodiesterase. Proc Natl Acad Sci U S A 101, 13897-13902.
Rao, A., Dallman, R., Henderson, S., and Chen, C.K. (2007). Gbeta5 is required for normal light responses and morphology of retinal ON-bipolar cells. J Neurosci 27, 14199-14204.
Rattner, A., and Nathans, J. (2006). Macular degeneration: recent advances and therapeutic opportunities. Nat Rev Neurosci 7, 860-872.
Reber, M., Hindges, R., and Lemke, G. (2007). Eph receptors and ephrin ligands in axon guidance. Adv Exp Med Biol 621, 32-49.
Renteria, R.C., Tian, N., Cang, J., Nakanishi, S., Stryker, M.P., and Copenhagen, D.R. (2006). Intrinsic ON responses of the retinal OFF pathway are suppressed by the ON pathway. J Neurosci 26, 11857-11869.
Ripps, H. (2002). Cell death in retinitis pigmentosa: gap junctions and the 'bystander' effect. Exp Eye Res 74, 327-336.
Rossi FM, P.T., Porciatti V, Marubio LM, Maffei L, Changeux JP (2001). Requirement of the nicotinic acetylcholine receptor beta 2 subunit for the anatomical and function development of the visual system. Proc Natl Acad Sci U S A 98, 6453-6458.
Saaddine, J.B., Narayan, K.M., and Vinicor, F. (2003). Vision loss: a public health problem? Ophthalmology 110, 253-254.
Sagdullaev, B.T., Aramant, R.B., Seiler, M.J., Woch, G., and McCall, M.A. (2003). Retinal transplantation-induced recovery of retinotectal visual function in a rodent model of retinitis pigmentosa. Invest Ophthalmol Vis Sci 44, 1686-1695.
Sanes, J.R., and Yamagata, M. (2009). Many paths to synaptic specificity. Annu Rev Cell Dev Biol 25, 161-195.
Sanyal, S., De Ruiter, A., and Hawkins, R.K. (1980). Development and degeneration of retina in rds mutant mice: light microscopy. J Comp Neurol 194, 193-207.
Schambra, U.B., Duncan, G.E., Breese, G.R., Fornaretto, M.G., Caron, M.G., and Fremeau, R.T., Jr. (1994). Ontogeny of D1A and D2 dopamine receptor subtypes in rat brain using in situ hybridization and receptor binding. Neuroscience 62, 65-85.
Schwartz, M. (2004). Optic nerve crush: protection and regeneration. Brain Res Bull 62, 467-471.
Sernagor, E., Young, C., and Eglen, S.J. (2003). Developmental modulation of retinal wave dynamics: shedding light on the GABA saga. J Neurosci 23, 7621-7629.
Sherman, S.M., and Guillery, R.W. (2002). The role of the thalamus in the flow of information to the cortex. Philos Trans R Soc Lond B Biol Sci 357, 1695-1708.

Sherry, D.M., Wang, M.M., Bates, J., and Frishman, L.J. (2003). Expression of vesicular glutamate transporter 1 in the mouse retina reveals temporal ordering in development of rod vs. cone and ON vs. OFF circuits. J Comp Neurol 465, 480-498.
Shlens, J., Field, G.D., Gauthier, J.L., Greschner, M., Sher, A., Litke, A.M., and Chichilnisky, E.J. (2009). The structure of large-scale synchronized firing in primate retina. J Neurosci 29, 5022-5031.
Shlens, J., Rieke, F., and Chichilnisky, E. (2008). Synchronized firing in the retina. Curr Opin Neurobiol 18, 396-402.
Sidman, R.L., and Green, M.C. (1965). Retinal Degeneration in the Mouse: Location of the Rd Locus in Linkage Group Xvii. J Hered 56, 23-29.
Sofroniew, M.V., and Vinters, H.V. Astrocytes: biology and pathology. Acta Neuropathol 119, 7-35.
Song, J.H., Song, H., Wensel, T.G., Sokolov, M., and Martemyanov, K.A. (2007). Localization and differential interaction of R7 RGS proteins with their membrane anchors R7BP and R9AP in neurons of vertebrate retina. Mol Cell Neurosci 35, 311-319.
SPEER, C.M., and CHAPMAN, B. (2009). Functional on and off sublaminae in ferrets with abnormal anatomical sublaminar development. 224.218/B275.
Sperry, R.W. (1963). Chemoaffinity in the Orderly Growth of Nerve Fiber Patterns and Connections. Proc Natl Acad Sci U S A 50, 703-710.
Sretavan, D.W., Shatz, C.J., and Stryker, M.P. (1988). Modification of retinal ganglion cell axon morphology by prenatal infusion of tetrodotoxin. Nature 336, 468-471.
Stacy, R.C., Demas, J., Burgess, R.W., Sanes, J.R., and Wong, R.O. (2005). Disruption and recovery of patterned retinal activity in the absence of acetylcholine. J Neurosci 25, 9347-9357.
Stafford, B.K., Sher, A., Litke, A.M., and Feldheim, D.A. (2009). Spatial-temporal patterns of retinal waves underlying activity-dependent refinement of retinofugal projections. Neuron 64, 200-212.
Stasheff, S.F. (2008). Emergence of sustained spontaneous hyperactivity and temporary preservation of OFF responses in ganglion cells of the retinal degeneration (rd1) mouse. J Neurophysiol 99, 1408-1421.
Stellwagen, D., and Shatz, C.J. (2002). An instructive role for retinal waves in the development of retinogeniculate connectivity. Neuron 33, 357-367.
Stellwagen, D., Shatz, C.J., and Feller, M.B. (1999). Dynamics of retinal waves are controlled by cyclic AMP. Neuron 24, 673-685.
Stevens, B., Allen, N.J., Vazquez, L.E., Howell, G.R., Christopherson, K.S., Nouri, N., Micheva, K.D., Mehalow, A.K., Huberman, A.D., Stafford, B., et al. (2007). The classical complement cascade mediates CNS synapse elimination. Cell 131, 1164-1178.
Strettoi, E., and Pignatelli, V. (2000). Modifications of retinal neurons in a mouse model of retinitis pigmentosa. Proc Natl Acad Sci U S A 97, 11020-11025.
Strettoi, E., Pignatelli, V., Rossi, C., Porciatti, V., and Falsini, B. (2003). Remodeling of second-order neurons in the retina of rd/rd mutant mice. Vision Res 43, 867-877.
Sun, C., Speer, C.M., Wang, G.Y., Chapman, B., and Chalupa, L.M. (2008a). Epibatidine application in vitro blocks retinal waves without silencing all retinal ganglion cell action potentials in developing retina of the mouse and ferret. J Neurophysiol 100, 3253-3263.

Sun, C., Warland, D.K., Ballesteros, J.M., van der List, D., and Chalupa, L.M. (2008b). Retinal waves in mice lacking the beta2 subunit of the nicotinic acetylcholine receptor. Proc Natl Acad Sci U S A 105, 13638-13643.
Syed MM, L.S., Zheng J, Zhou ZJ (2004). Stage-Dependent Dynamics and modulation of spontaneous retinal waves in teh developing mouse retina. J Physiol 560, 533-549.
Tian, N. (2008). Synaptic activity, visual experience and the maturation of retinal synaptic circuitry. J Physiol 586, 4347-4355.
Tian, N., and Copenhagen, D.R. (2001). Visual deprivation alters development of synaptic function in inner retina after eye opening. Neuron 32, 439-449.
Tian, N., and Copenhagen, D.R. (2003). Visual stimulation is required for refinement of ON and OFF pathways in postnatal retina. Neuron 39, 85-96.
Torborg, C., Wang, C.T., Muir-Robinson, G., and Feller, M.B. (2004). L-type calcium channel agonist induces correlated depolarizations in mice lacking the beta2 subunit nAChRs. Vision Res 44, 3347-3355.
Torborg, C.L., and Feller, M.B. (2004). Unbiased analysis of bulk axonal segregation patterns. J Neurosci Methods 135, 17-26.
Torborg, C.L., Hansen, K.A., and Feller, M.B. (2005). High frequency, synchronized bursting drives eye-specific segregation of retinogeniculate projections. Nat Neurosci 8, 72-78.
Tran, V.T., and Dickman, M. (1992). Differential localization of dopamine D1 and D2 receptors in rat retina. Invest Ophthalmol Vis Sci 33, 1620-1626.
Triplett, J.W., Owens, M.T., Yamada, J., Lemke, G., Cang, J., Stryker, M.P., and Feldheim, D.A. (2009). Retinal input instructs alignment of visual topographic maps. Cell 139, 175-185.
Tritsch, N.X., Yi, E., Gale, J.E., Glowatzki, E., and Bergles, D.E. (2007). The origin of spontaneous activity in the developing auditory system. Nature 450, 50-55.
Turner, D.L., and Cepko, C.L. (1987). A common progenitor for neurons and glia persists in rat retina late in development. Nature 328, 131-136.
Tyagarajan, S.K., and Fritschy, J.M. GABA(A) receptors, gephyrin and homeostatic synaptic plasticity. J Physiol 588, 101-106.
Vugler, A.A., Semo, M., Joseph, A., and Jeffery, G. (2008). Survival and remodeling of melanopsin cells during retinal dystrophy. Vis Neurosci 25, 125-138.
Wang, C.T., Blankenship, A.G., Anishchenko, A., Elstrott, J., Fikhman, M., Nakanishi, S., and Feller, M.B. (2007). GABA(A) receptor-mediated signaling alters the structure of spontaneous activity in the developing retina. J Neurosci 27, 9130-9140.
Warland, D.K., Huberman, A.D., and Chalupa, L.M. (2006). Dynamics of spontaneous activity in the fetal macaque retina during development of retinogeniculate pathways. J Neurosci 26, 5190-5197.
Wassle, H. (2004). Parallel processing in the mammalian retina. Nat Rev Neurosci 5, 747-757.
Watts, V.J., and Neve, K.A. (2005). Sensitization of adenylate cyclase by Galpha i/o-coupled receptors. Pharmacol Ther 106, 405-421.
Wenzel, A., Grimm, C., Samardzija, M., and Reme, C.E. (2005). Molecular mechanisms of light-induced photoreceptor apoptosis and neuroprotection for retinal degeneration. Prog Retin Eye Res 24, 275-306.

Wickman, K.D., Iniguez-Lluhl, J.A., Davenport, P.A., Taussig, R., Krapivinsky, G.B., Linder, M.E., Gilman, A.G., and Clapham, D.E. (1994). Recombinant G-protein beta gamma-subunits activate the muscarinic-gated atrial potassium channel. Nature 368, 255-257.
Wong, R.O., Meister, M., and Shatz, C.J. (1993). Transient period of correlated bursting activity during development of the mammalian retina. Neuron 11, 923-938.
Wong, R.O., and Oakley, D.M. (1996). Changing patterns of spontaneous bursting activity of on and off retinal ganglion cells during development. Neuron 16, 1087-1095.
Xu, H.P., Chen, H., Ding, Q., Xie, Z.H., Chen, L., Diao, L., Wang, P., Gan, L., Crair, M.C., and Tian, N. (2010). The immune protein CD3zeta is required for normal development of neural circuits in the retina. Neuron 65, 503-515.
Yamagata, M., and Sanes, J.R. (2008). Dscam and Sidekick proteins direct lamina-specific synaptic connections in vertebrate retina. Nature 451, 465-469.
Yau, K.W., and Hardie, R.C. (2009). Phototransduction motifs and variations. Cell 139, 246-264.
Young, R.W. (1985a). Cell differentiation in the retina of the mouse. Anat Rec 212, 199-205.
Young, R.W. (1985b). Cell proliferation during postnatal development of the retina in the mouse. Brain Res 353, 229-239.
Zhang, J., and Diamond, J.S. (2009). Subunit- and pathway-specific localization of NMDA receptors and scaffolding proteins at ganglion cell synapses in rat retina. J Neurosci 29, 4274-4286.
Zhang, J., Jeffrey, B.G., Morgans, C.W., Burke, N.S., Haley, T.L., Duvoisin, R.M., and Brown, R.L. (2010). RGS7 and -11 complexes accelerate the ON-bipolar cell light response. Invest Ophthalmol Vis Sci 51, 1121-1129.
Zheng, J., Lee, S., and Zhou, Z.J. (2006). A transient network of intrinsically bursting starburst cells underlies the generation of retinal waves. Nat Neurosci 9, 363-371.
Zheng JJ, L.S., Zhou ZJ (2004). A dvelopmental swith in the excitability and functionality of the starburst network in the mammalian retina. Neuron 44, 851-864.
Zhou, Z.J. (1998). Direct participation of starburst amacrine cells in spontaneous rhythmic activities in the developing mammalian retina. J Neurosci 18, 4155-4165.
Zhou, Z.J., and Fain, G.L. (1996). Starburst amacrine cells change from spiking to nonspiking neurons during retinal development. Proc Natl Acad Sci U S A 93, 8057-8062.
Ziburkus, J., Dilger, E.K., Lo, F.S., and Guido, W. (2009). LTD and LTP at the developing retinogeniculate synapse. J Neurophysiol 102, 3082-3090.
Ziburkus, J., and Guido, W. (2006). Loss of binocular responses and reduced retinal convergence during the period of retinogeniculate axon segregation. J Neurophysiol 96, 2775-2784.
Ziburkus, J., Lo, F.S., and Guido, W. (2003). Nature of inhibitory postsynaptic activity in developing relay cells of the lateral geniculate nucleus. J Neurophysiol 90, 1063-1070.

APPENDCIES

APPENDIX A- EARLY INTRINSTICALLY PHOTOSENSITIVE RETINAL GANLION CELL ACTIVITY AND PUPILLARY LIGHT RESPONSES OF Gβ5-/- MICE

P7 animal with waves and blue stimulation for melanopsin cells

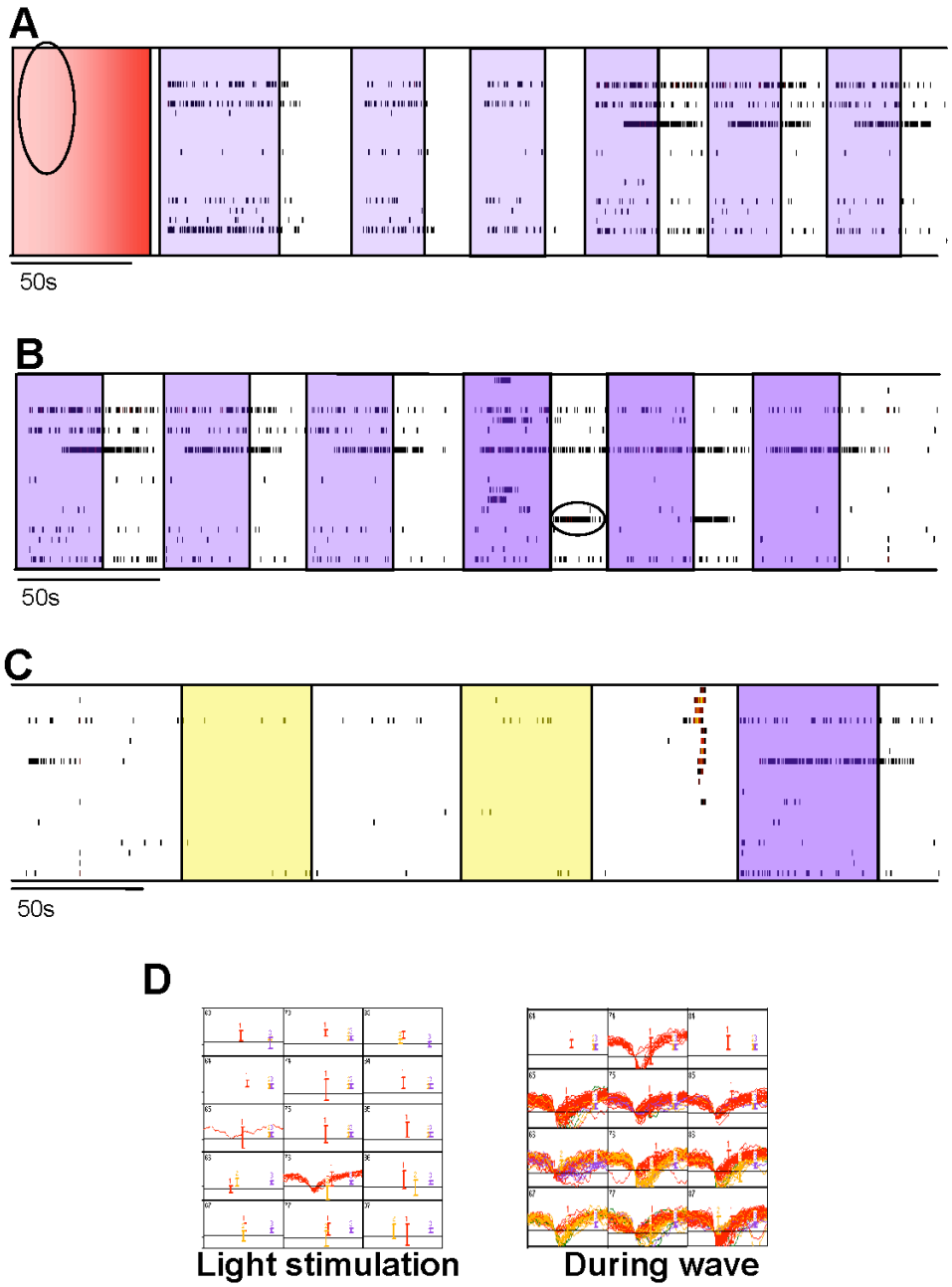

Figure A1

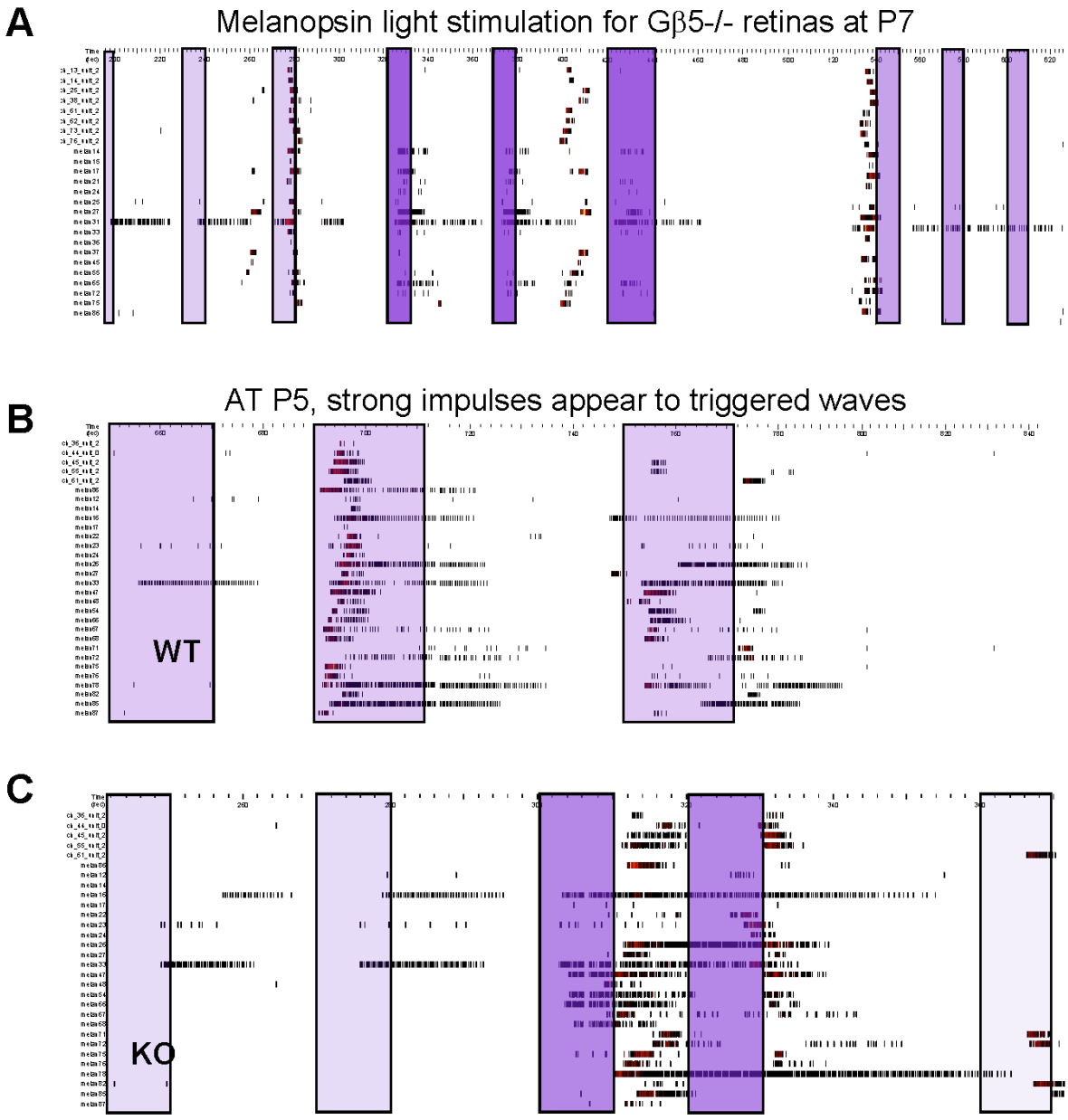
A
Melanopsin light stimulation for Gβ5-/- retinas at P7
B
AT P5, strong impulses appear to triggered waves
WT
C
KO

Figure A2

Extracellular waveforms of Gβ5-/- and +/+ at
P7 exhibit no drastic differences

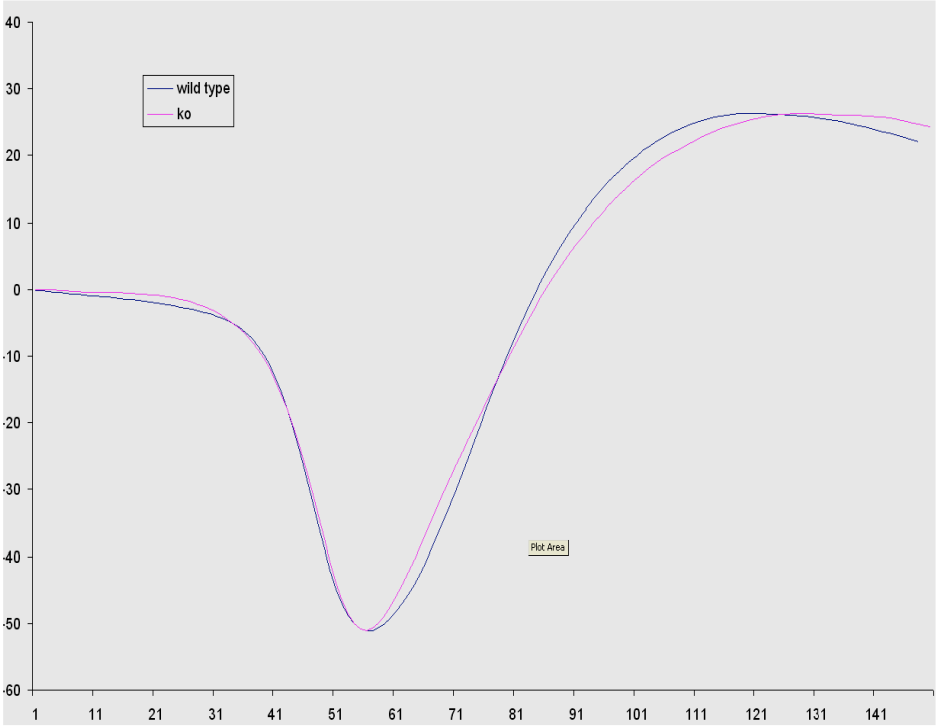

Figure A3

A

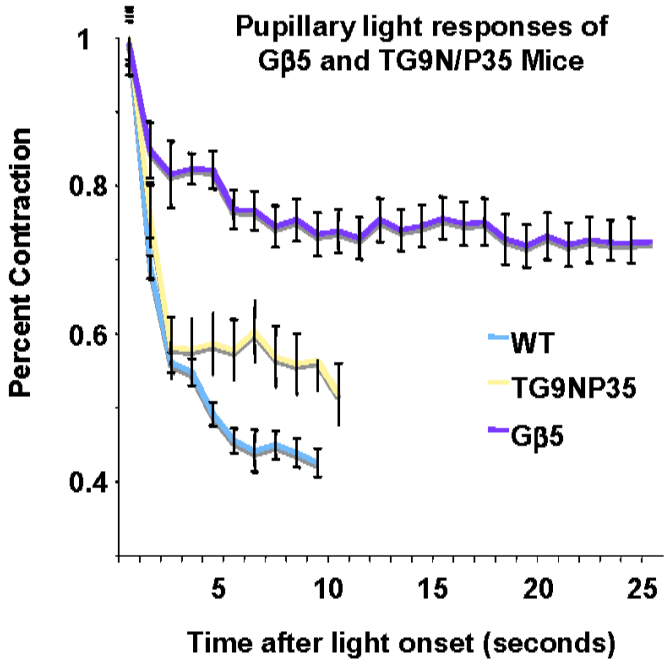
Pupillary light responses of
Gβ5 and TG9N/P35 Mice
Percent Contraction
1
0.8
0.6
0.4
5
10
15
20
25
Time after light onset (seconds)
WT
TG9NP35
Gβ5

B

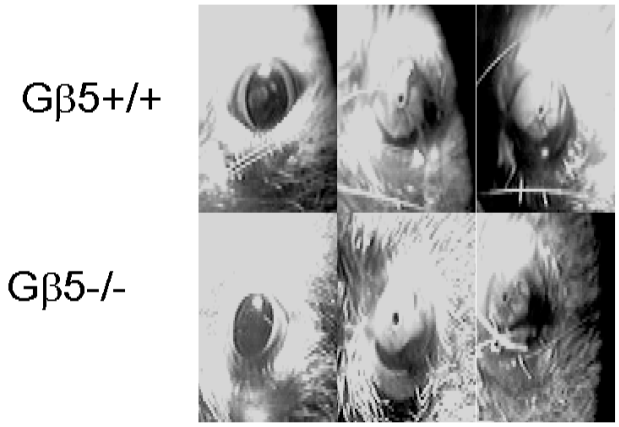
Gβ5+/+
Gβ5-/-

Figure A4

APPENDIX B - MULTIPLE INTENSITY PLRS OF PHOTORECEPTOR DEGENERATION MICE

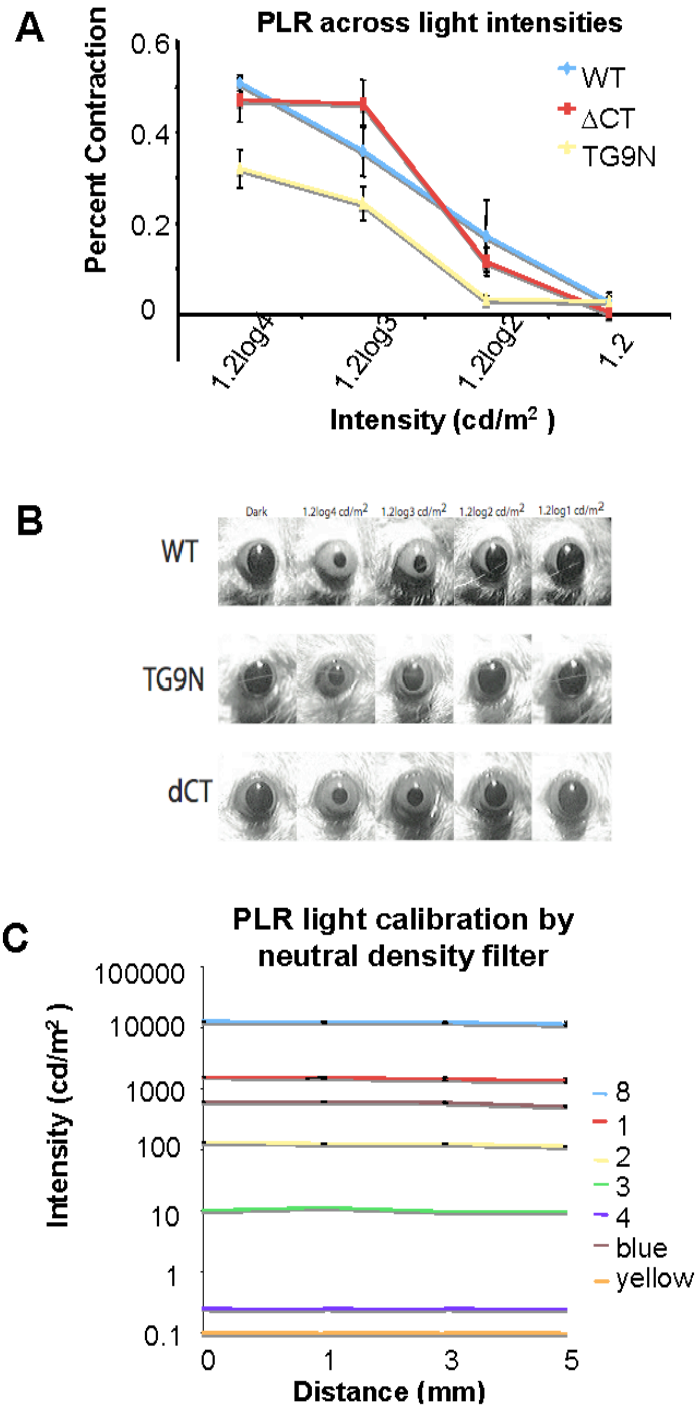
A
PLR across light intensities
Percent Contraction
0.6
0.4
0.2
0
WT
ΔCT
TG9N
1.2log4
1.2log3
1.2log2
1.2
Intensity (cd/m2)
B
Dark
1.2log4 cd/m2
1.2log3 cd/m2
1.2log2 cd/m2
1.2log1 cd/m2
WT
TG9N
dCT
C
PLR light calibration by neutral density filter
Intensity (cd/m2)
100000
10000
1000
100
10
1
0.1
0
1
3
5
Distance (mm)
8
1
2
3
4
blue
yellow

Figure A5

APPENDIX C- BRAINSTEM AUDITORY EVOKED POTENTIALS ARE NORMAL IN Gβ5-/- MICE

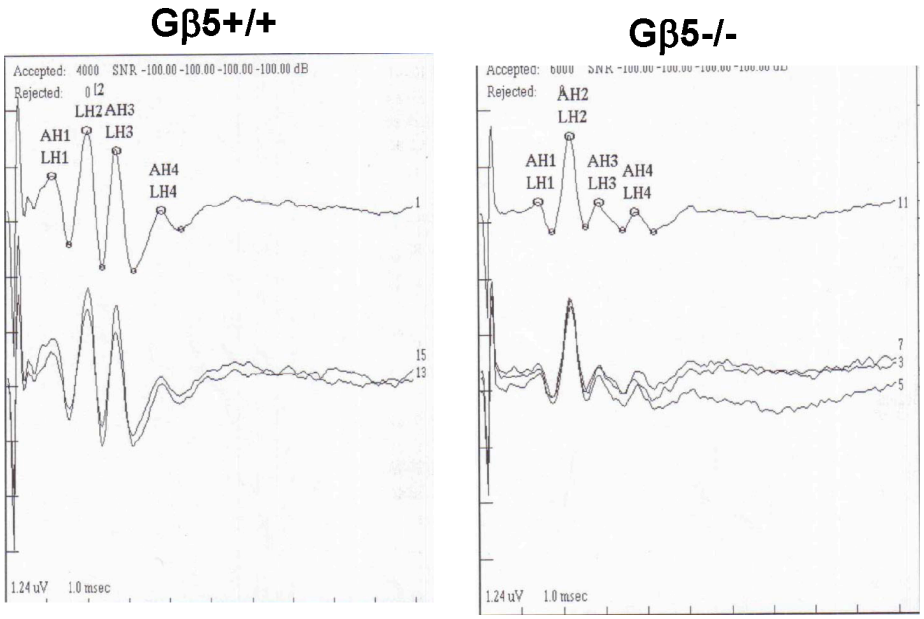

BAEP Waveforms

Waveforms shown are at 70dB from WT and KO animals using a Nicolet BAEP recording device. Temperatures are maintained at 38C or 35C.

Figure A6

A

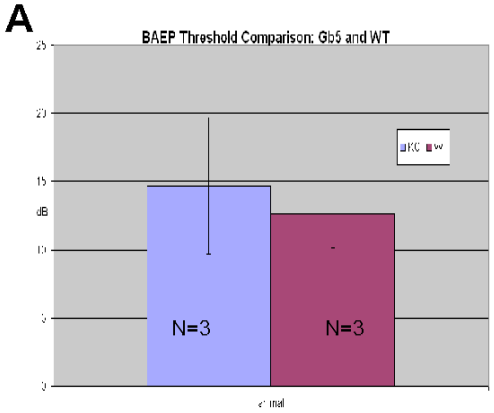

No significant differences in Threshold between KO and WT

B

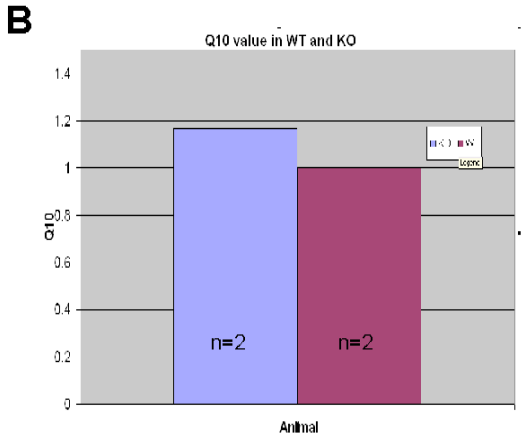

Determined by calculating latency at T=38C and T=35C

- Technical limitations
  - Temperature of animal
  - Accuracy of distance measurement
- Still looks Ion dominated

$$Q_{10} = \left(\frac{R_2}{R_1}\right)^{\left(\frac{10}{T_2 - T_1}\right)}$$

Gβ5 Mouse does not demonstrate a BAEP Phenotype in Threshold or Kinetics

Figure A7

A

Q10

	Gβ5-/-	Gβ5+/+
stim	1.124087	1.129285
LH1	0.594279	0.122714
LH2	1.094551	1.309823
LH3	1.346579	1.460604
LH4	1.471302	1.035823

B

Latencies

T38	KO1	KO2	WT1	WT2	P-value
stim	2.8	2.8	3	2.8	0.25
LH1	10.1	9	9.1	10	0.5
LH2	7	7.5	9.1	6.75	0.359
LH3	5.9	6	5.1	8.5	0.348
LH4	8.5	8.5	9.1	8.1	0.437
T35					P-value
stim	2.9	2.9	3	3	
LH1	8.4	7.9	2.1	6.5	0.360
LH2	7	7.9	8.2	8.2	.344
LH3	6.6	6.4	6.9	5.1	.644
LH4	8.9	10.1	8	9	.063

Analysis of Waveforms

•Designations are Peak-to-peak (from previous peak to labeled peak)

•At 35C, average synaptic latency is slightly longer in the KO at lower temperatures

•At 35C, total BAEP to last peak is longer in KO

•The trend is reversed at 38C

•LH4 latency seems slightly different where the KO is, on average, longer than the WT

Figure A8

APPENDIX D – Gβ5 -/- MOUSE P5 WAVES, P10 ACTIVITY, CHAT IN RETINAS, AND Gβ5 INCREASES IN DLGN OVER AGE

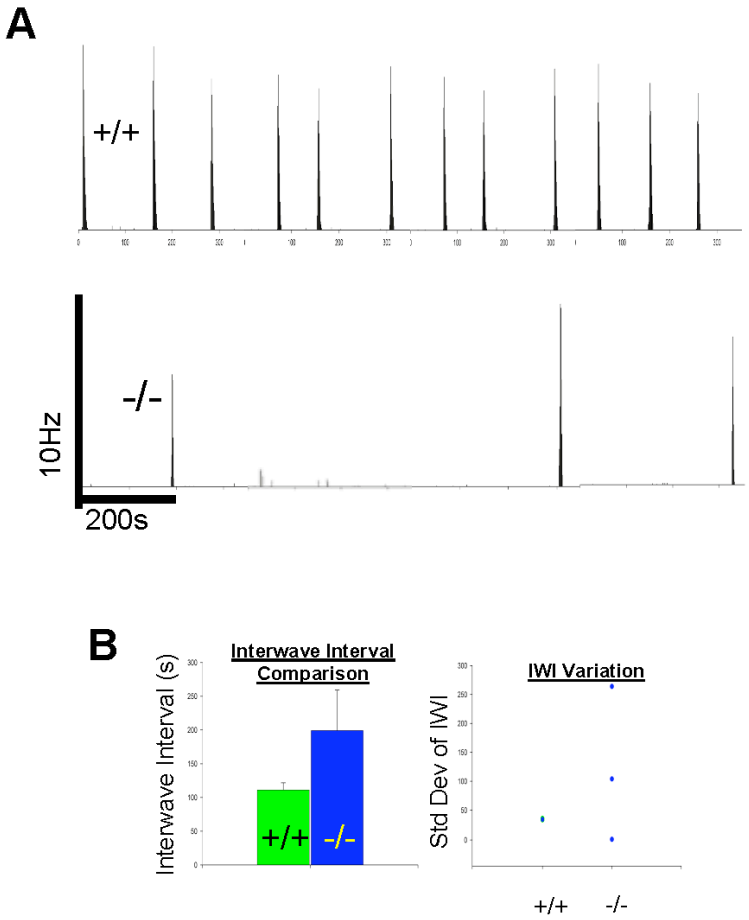

Figure A9

Gβ5-/- mice have low spontaneous retinal wave frequency early in development (p5)

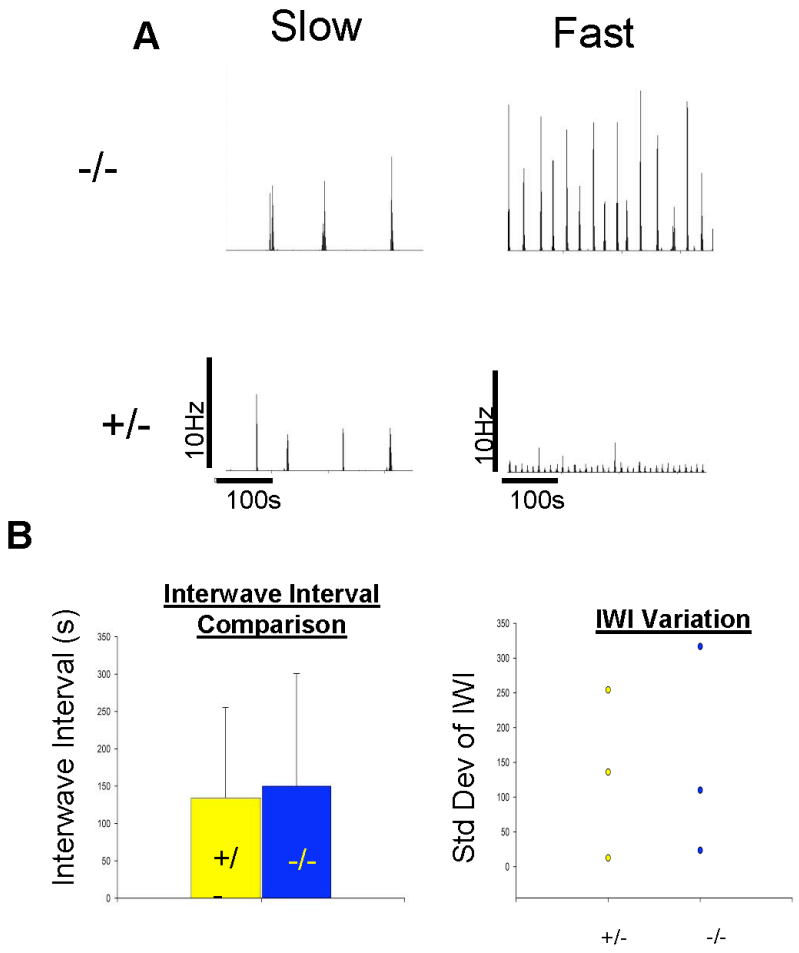

Figure A10

At P10, Gβ5 -/- and +/- mice exhibit transition from cholinergic-like to glutamatergic-like transmission

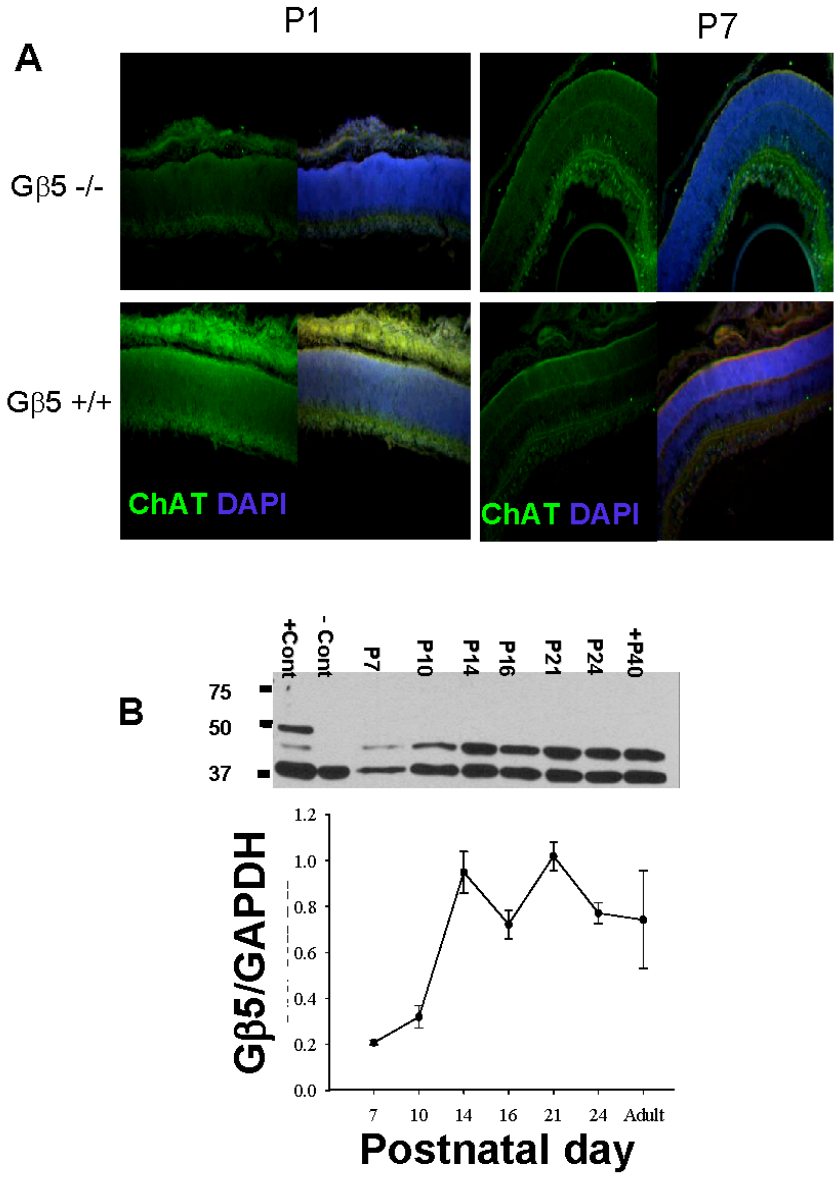
A
P1
P7
Gβ5 -/-
Gβ5 +/+
ChAT DAPI
ChAT DAPI
B
+Cont
- Cont
P7
P10
P14
P16
P21
P24
+P40
75
50
37
Gβ5/GAPDH
1.2
1.0
0.8
0.6
0.4
0.2
0.0
7
10
14
16
21
24
Adult
Postnatal day

Figure A11

APPENDIX E – BURST PARAMETER DISTRIBUTIONS

P7

Distributions Genotype=het

mean freq

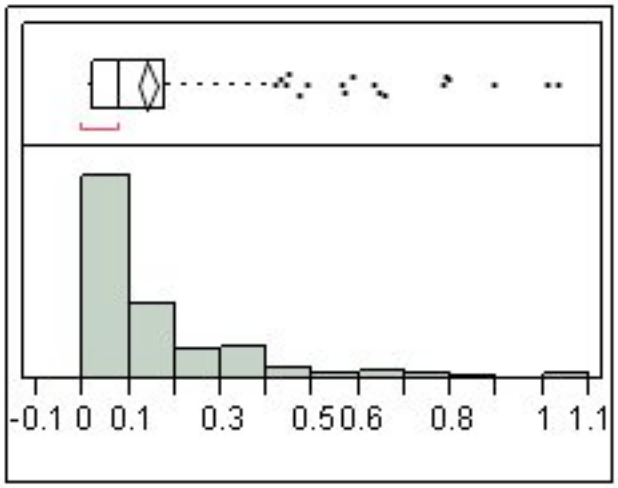

Quantiles

100.0%	maximum	1.02867
99.5%		1.01782
97.5%		0.65225
90.0%		0.36033
75.0%	quartile	0.1775
50.0%	median	0.08183
25.0%	quartile	0.01967
10.0%		0.00333
2.5%		0.00067
0.5%		0.00017
0.0%	minimum	0

Moments

Mean	0.138671
Std Dev	0.1738951
Std Err Mean	0.0099736
Upper 95% Mean	0.1582973
Lower 95% Mean	0.1190448
N	304

numburst

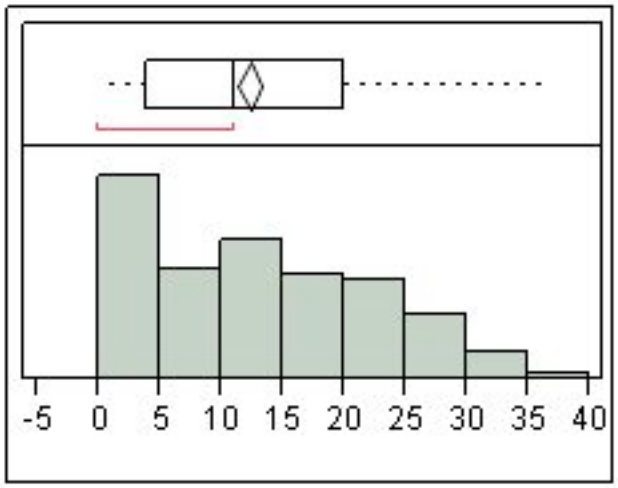

Quantiles

100.0%	maximum	37
99.5%		34.9
97.5%		30
90.0%		25
75.0%	quartile	20
50.0%	median	11
25.0%	quartile	4
10.0%		0
2.5%		0
0.5%		0
0.0%	minimum	0

Moments

Mean	12.296053
Std Dev	9.2217556
Std Err Mean	0.528904
Upper 95% Mean	13.336843
Lower 95% Mean	11.255263
N	304

bursts/sec

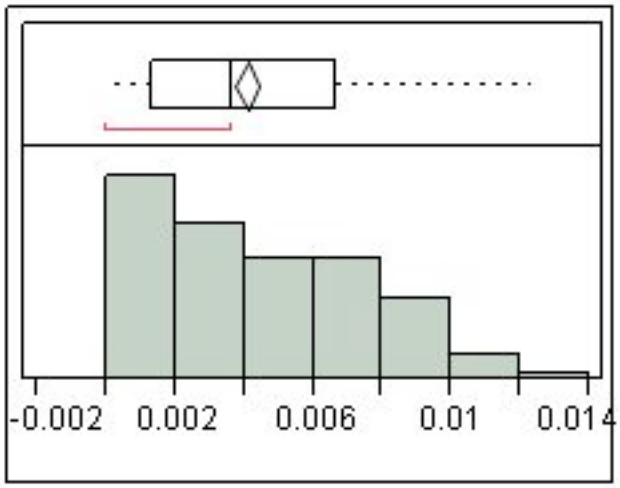

Quantiles

100.0%	maximum	0.01233
99.5%		0.01163
97.5%		0.01
90.0%		0.00833
75.0%	quartile	0.00667
50.0%	median	0.00367
25.0%	quartile	0.00133
10.0%		0
2.5%		0
0.5%		0
0.0%	minimum	0

Moments

Mean	0.0040987
Std Dev	0.0030739
Std Err Mean	0.0001763
Upper 95% Mean	0.0044456
Lower 95% Mean	0.0037517
N	304

%spikes in burst

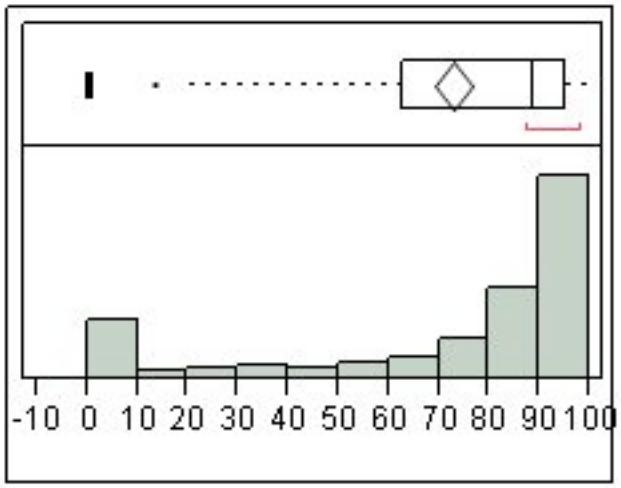

Quantiles

100.0%	maximum	99.3789
99.5%		99.2826
97.5%		98.4923
90.0%		97.0028
75.0%	quartile	95.2844
50.0%	median	88.6775
25.0%	quartile	62.9669
10.0%		0
2.5%		0
0.5%		0
0.0%	minimum	0

Moments

Mean	72.753618
Std Dev	32.849234
Std Err Mean	1.8840328
Upper 95% Mean	76.461063
Lower 95% Mean	69.046173
N	304

mean burst dur

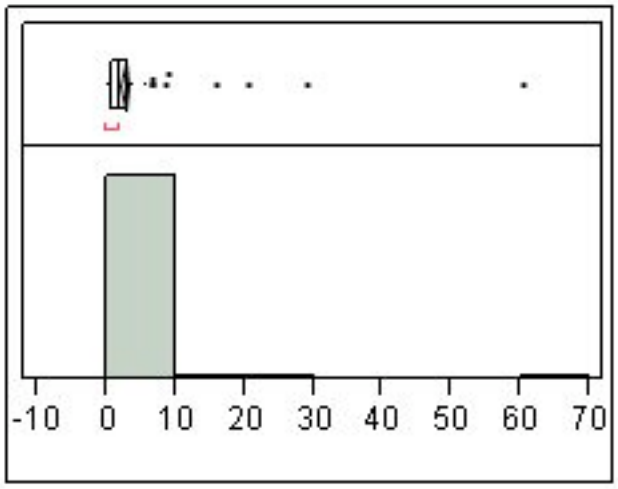

Quantiles

100.0%	maximum	60.3081
99.5%		43.9319
97.5%		6.73293
90.0%		4.32781
75.0%	quartile	3.24991
50.0%	median	2.14386
25.0%	quartile	0.93782
10.0%		0
2.5%		0
0.5%		0
0.0%	minimum	0

Moments

Mean	2.6028046
Std Dev	4.2012073
Std Err Mean	0.2409558
Upper 95% Mean	3.0769632
Lower 95% Mean	2.1286461
N	304

mean spikes/burst

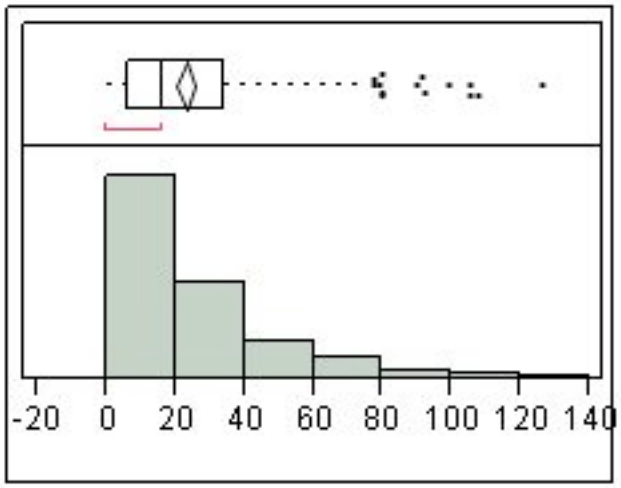

Quantiles

100.0%	maximum	126.261
99.5%		116.368
97.5%		90.1122
90.0%		51.5455
75.0%	quartile	33.8377
50.0%	median	16.0667
25.0%	quartile	6.27841
10.0%		0
2.5%		0
0.5%		0
0.0%	minimum	0

Moments

Mean	23.112476
Std Dev	22.872236
Std Err Mean	1.3118127
Upper 95% Mean	25.693892
Lower 95% Mean	20.531059
N	304

mean ISI

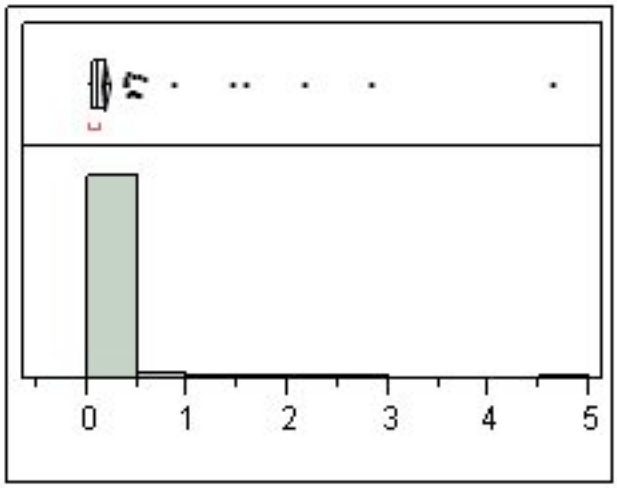

Quantiles

100.0%	maximum	4.63908
99.5%		3.68281
97.5%		0.5366
90.0%		0.28175
75.0%	quartile	0.18026
50.0%	median	0.10041
25.0%	quartile	0.05927
10.0%		0
2.5%		0
0.5%		0
0.0%	minimum	0

Moments

Mean	0.1666213
Std Dev	0.3580734
Std Err Mean	0.0205369
Upper 95% Mean	0.2070343
Lower 95% Mean	0.1262082
N	304

Mean Freq in burst

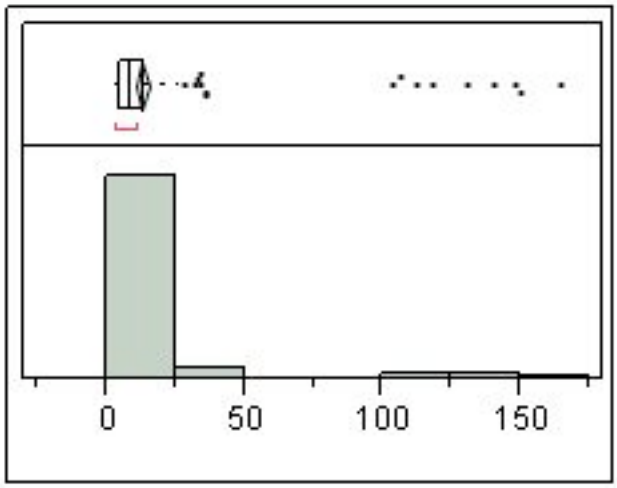

Quantiles

100.0%	maximum	164.724
99.5%		156.856
97.5%		108.582
90.0%		21.0465
75.0%	quartile	13.9899
50.0%	median	8.89653
25.0%	quartile	4.88041
10.0%		0
2.5%		0
0.5%		0
0.0%	minimum	0

Moments

Mean	13.156765
Std Dev	21.982441
Std Err Mean	1.2607795
Upper 95% Mean	15.637757
Lower 95% Mean	10.675773
N	304

Mean Peak Freq

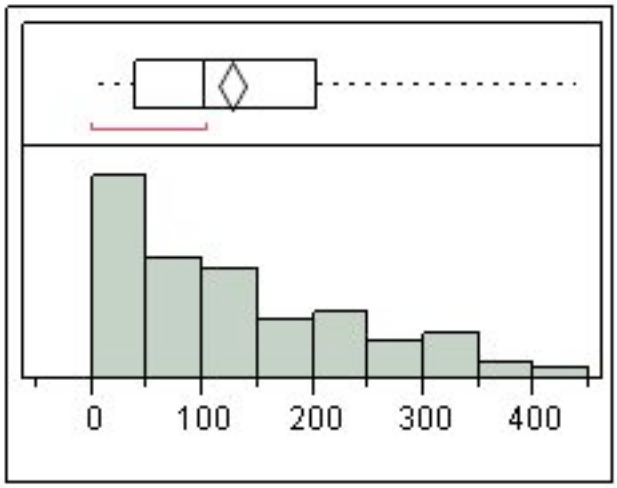

Quantiles

100.0%	maximum	437.177
99.5%		422.703
97.5%		381.287
90.0%		298.641
75.0%	quartile	202.741
50.0%	median	102.461
25.0%	quartile	39.1794
10.0%		0
2.5%		0
0.5%		0
0.0%	minimum	0

Moments

Mean	125.46556
Std Dev	108.72006
Std Err Mean	6.2355233
Upper 95% Mean	137.73597
Lower 95% Mean	113.19514
N	304

mean Interburst Int

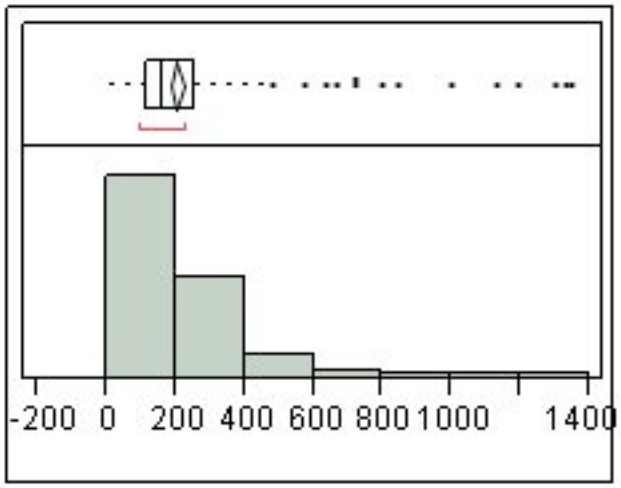

Quantiles

100.0%	maximum	1346.82
99.5%		1337.55
97.5%		813.558
90.0%		410.421
75.0%	quartile	257.668
50.0%	median	164.19
25.0%	quartile	113.895
10.0%		0
2.5%		0
0.5%		0
0.0%	minimum	0

Moments

Mean	205.74414
Std Dev	202.94715
Std Err Mean	11.639817
Upper 95% Mean	228.64926
Lower 95% Mean	182.83903
N	304

Mean Sup

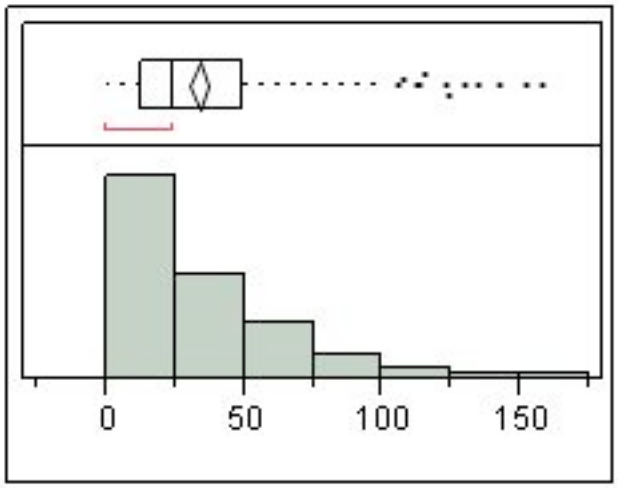

Quantiles

100.0%	maximum	157.767
99.5%		154.684
97.5%		117.901
90.0%		73.9945
75.0%	quartile	48.9367
50.0%	median	24.4702
25.0%	quartile	13.025
10.0%		0
2.5%		0
0.5%		0
0.0%	minimum	0

Moments

Mean	33.619298
Std Dev	30.117141
Std Err Mean	1.7273365
Upper 95% Mean	37.018393
Lower 95% Mean	30.220204
N	304

Distributions Genotype=ko

mean freq

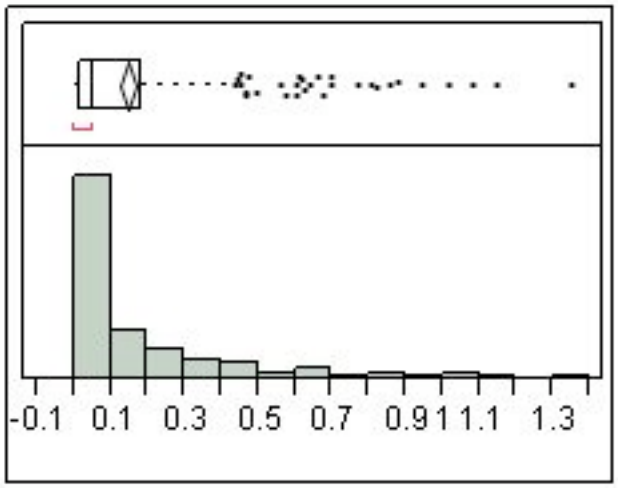

Quantiles

100.0%	maximum	1.34867
99.5%		1.20359
97.5%		0.81278
90.0%		0.4248
75.0%	quartile	0.1835
50.0%	median	0.05133
25.0%	quartile	0.014
10.0%		0.005
2.5%		0.00118
0.5%		0.00033
0.0%	minimum	0.00033

Moments

Mean	0.1437811
Std Dev	0.210627
Std Err Mean	0.0114061
Upper 95% Mean	0.1662164
Lower 95% Mean	0.1213457
N	341

numburst

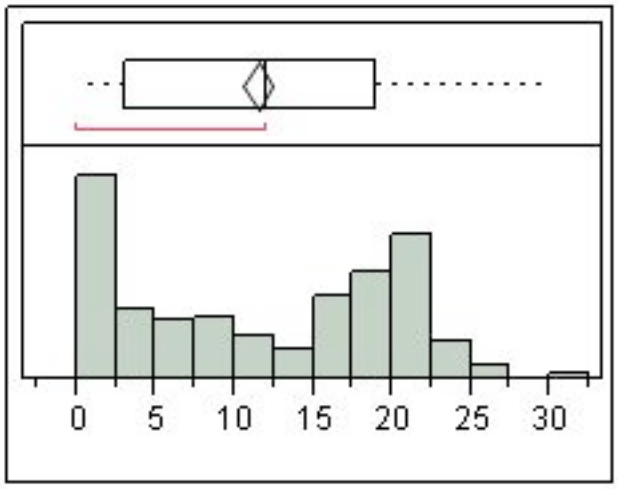

Quantiles

100.0%	maximum	30
99.5%		27.87
97.5%		24
90.0%		22
75.0%	quartile	19
50.0%	median	12
25.0%	quartile	3
10.0%		1
2.5%		0
0.5%		0
0.0%	minimum	0

Moments

Mean	11.454545
Std Dev	8.2872236
Std Err Mean	0.4487783
Upper 95% Mean	12.337277
Lower 95% Mean	10.571814
N	341

bursts/sec

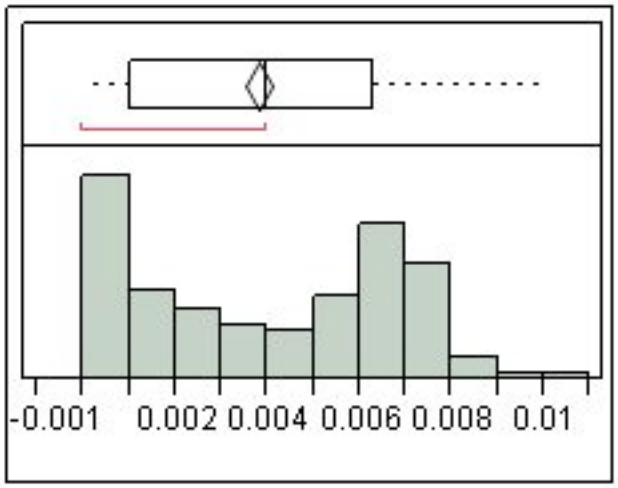

Quantiles

100.0%	maximum	0.01
99.5%		0.00929
97.5%		0.008
90.0%		0.00733
75.0%	quartile	0.00633
50.0%	median	0.004
25.0%	quartile	0.001
10.0%		0.00033
2.5%		0
0.5%		0
0.0%	minimum	0

Moments

Mean	0.0038182
Std Dev	0.0027624
Std Err Mean	0.0001496
Upper 95% Mean	0.0041124
Lower 95% Mean	0.0035239
N	341

%spikes in burst

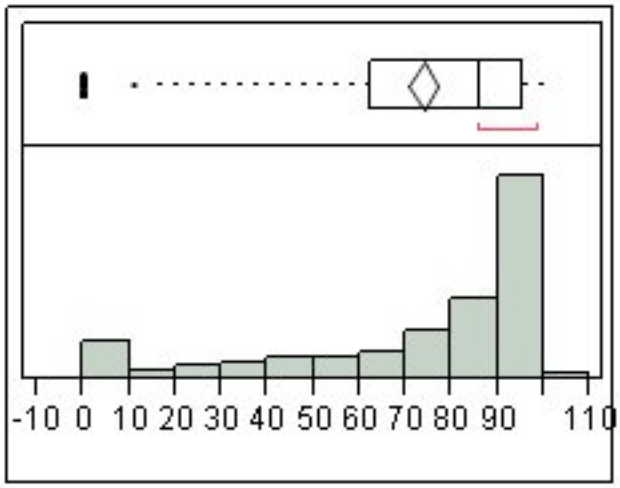

Quantiles

100.0%	maximum	100
99.5%		100
97.5%		98.8952
90.0%		97.5657
75.0%	quartile	95.5287
50.0%	median	86.3636
25.0%	quartile	62.3975
10.0%		22.3492
2.5%		0
0.5%		0
0.0%	minimum	0

Moments

Mean	74.005019
Std Dev	29.615024
Std Err Mean	1.6037435
Upper 95% Mean	77.159528
Lower 95% Mean	70.850511
N	341

mean burst dur

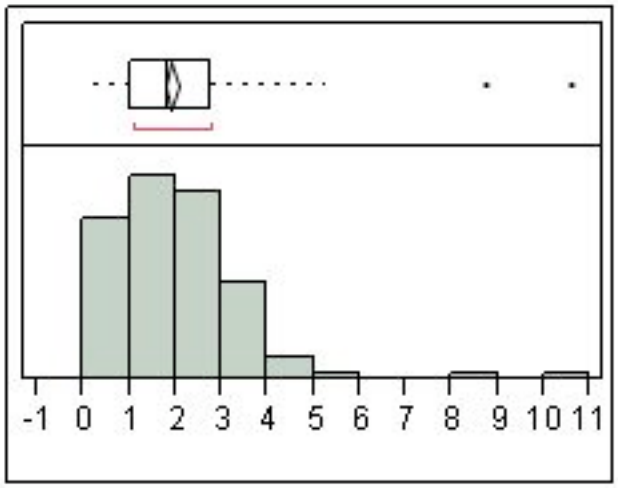

Quantiles

100.0%	maximum	10.5705
99.5%		9.28729
97.5%		4.26984
90.0%		3.3585
75.0%	quartile	2.74745
50.0%	median	1.85445
25.0%	quartile	1.03454
10.0%		0.16886
2.5%		0
0.5%		0
0.0%	minimum	0

Moments

Mean	1.9204383
Std Dev	1.2716175
Std Err Mean	0.0688619
Upper 95% Mean	2.0558874
Lower 95% Mean	1.7849892
N	341

mean spikes/burst

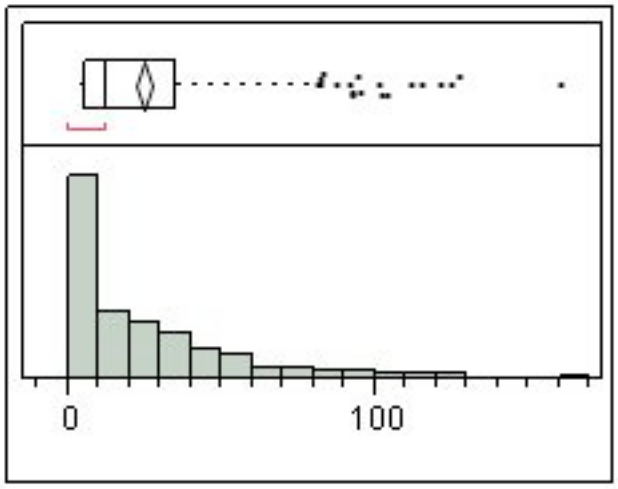

Quantiles

100.0%	maximum	160.792
99.5%		137.155
97.5%		101.328
90.0%		59.7784
75.0%	quartile	35.4839
50.0%	median	12.5714
25.0%	quartile	6
10.0%		4
2.5%		0
0.5%		0
0.0%	minimum	0

Moments

Mean	24.592801
Std Dev	26.76194
Std Err Mean	1.4492403
Upper 95% Mean	27.443407
Lower 95% Mean	21.742195
N	341

mean ISI

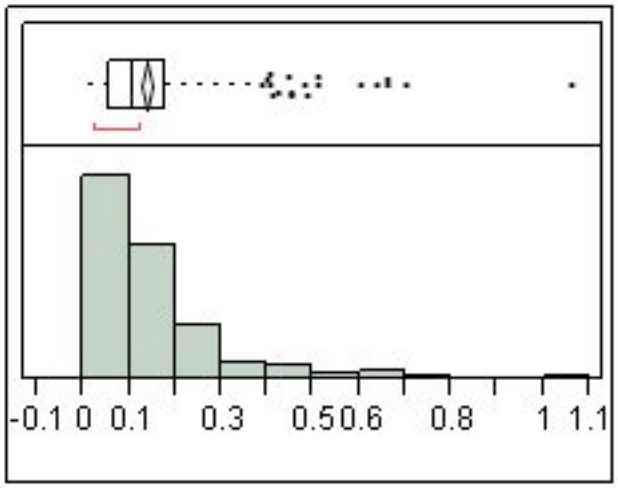

Quantiles

100.0%	maximum	1.0622
99.5%		0.80534
97.5%		0.497
90.0%		0.27927
75.0%	quartile	0.17772
50.0%	median	0.10635
25.0%	quartile	0.05418
10.0%		0.02285
2.5%		0
0.5%		0
0.0%	minimum	0

Moments

Mean	0.1372378
Std Dev	0.129881
Std Err Mean	0.0070335
Upper 95% Mean	0.1510724
Lower 95% Mean	0.1234032
N	341

Mean Freq in burst

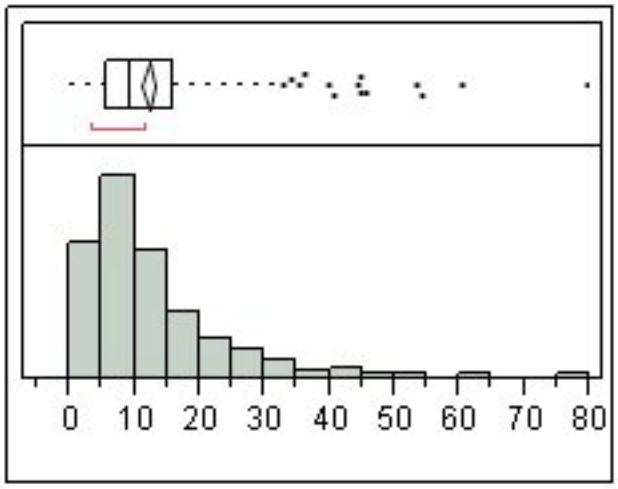

Quantiles

100.0%	maximum	79.7855
99.5%		65.8783
97.5%		42.2962
90.0%		25.733
75.0%	quartile	16.0827
50.0%	median	9.5019
25.0%	quartile	5.6123
10.0%		2.33506
2.5%		0
0.5%		0
0.0%	minimum	0

Moments

Mean	12.152691
Std Dev	10.396597
Std Err Mean	0.5630073
Upper 95% Mean	13.260107
Lower 95% Mean	11.045275
N	341

Mean Peak Freq

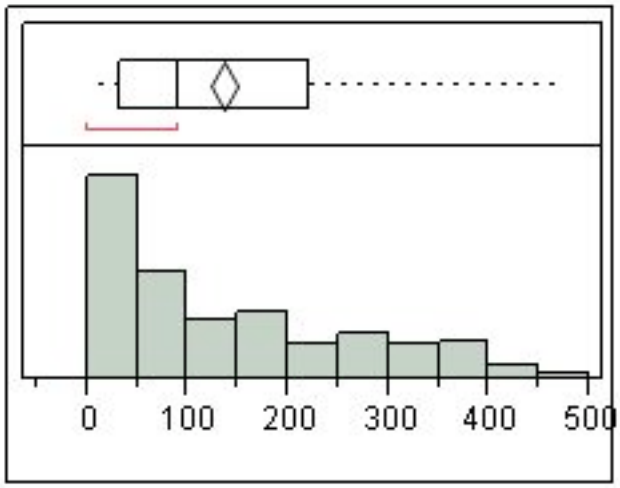

Quantiles

100.0%	maximum	471.698
99.5%		442.856
97.5%		398.282
90.0%		329.513
75.0%	quartile	220.596
50.0%	median	91.9791
25.0%	quartile	31.4448
10.0%		8.17299
2.5%		0
0.5%		0
0.0%	minimum	0

Moments

Mean	135.05844
Std Dev	122.32086
Std Err Mean	6.6240461
Upper 95% Mean	148.08771
Lower 95% Mean	122.02917
N	341

mean Interburst Int

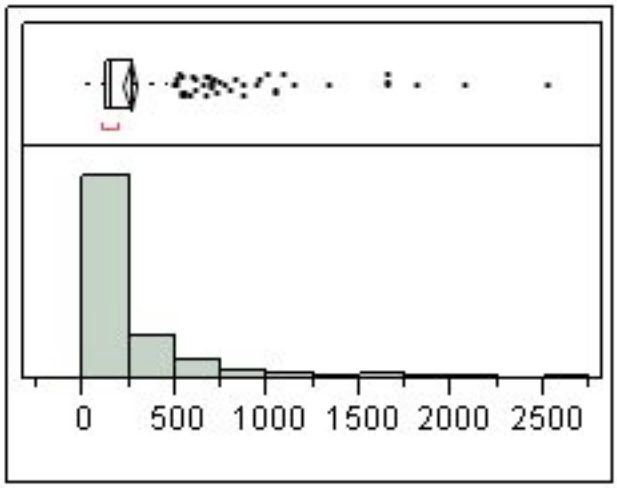

Quantiles

100.0%	maximum	2516.28
99.5%		2199.37
97.5%		1106.67
90.0%		548.85
75.0%	quartile	273.076
50.0%	median	162.482
25.0%	quartile	131.538
10.0%		0
2.5%		0
0.5%		0
0.0%	minimum	0

Moments

Mean	251.32273
Std Dev	310.23774
Std Err Mean	16.800316
Upper 95% Mean	284.36837
Lower 95% Mean	218.27708
N	341

Mean Sup

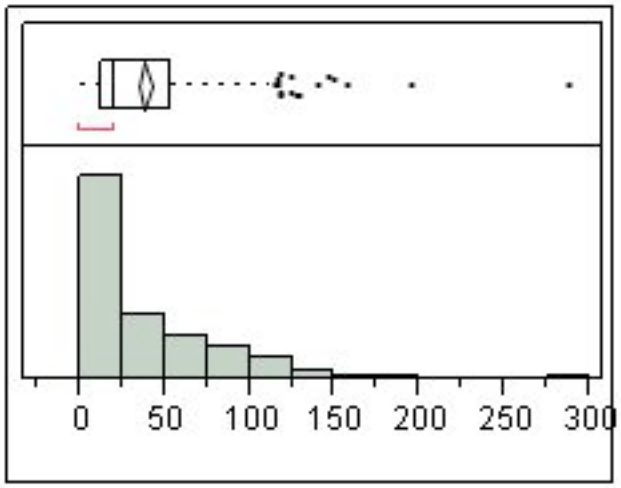

Quantiles

100.0%	maximum	286.811
99.5%		221.242
97.5%		125.645
90.0%		96.7689
75.0%	quartile	53.1106
50.0%	median	20.797
25.0%	quartile	13.2056
10.0%		10.6671
2.5%		0
0.5%		0
0.0%	minimum	0

Moments

Mean	38.191109
Std Dev	37.623195
Std Err Mean	2.0374102
Upper 95% Mean	42.198625
Lower 95% Mean	34.183593
N	341

Distributions Genotype=sg11

mean freq

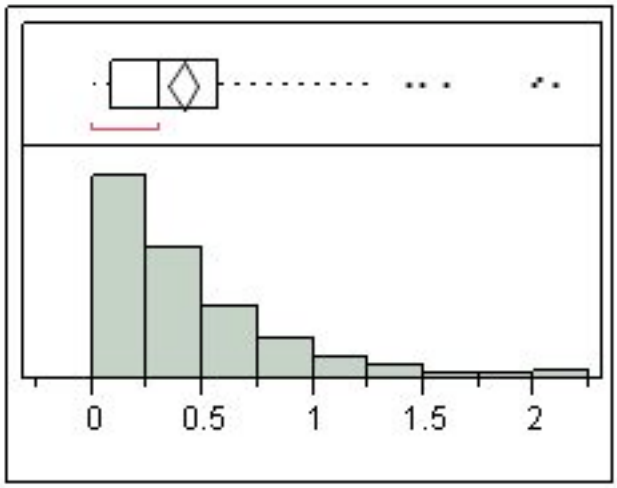

Quantiles

100.0%	maximum	2.09267
99.5%		2.09267
97.5%		1.74842
90.0%		0.952
75.0%	quartile	0.5755
50.0%	median	0.30917
25.0%	quartile	0.08842
10.0%		0.01667
2.5%		0.00196
0.5%		0.00067
0.0%	minimum	0.00067

Moments

Mean	0.4102778
Std Dev	0.4200464
Std Err Mean	0.0350039
Upper 95% Mean	0.4794697
Lower 95% Mean	0.3410859
N	144

numburst

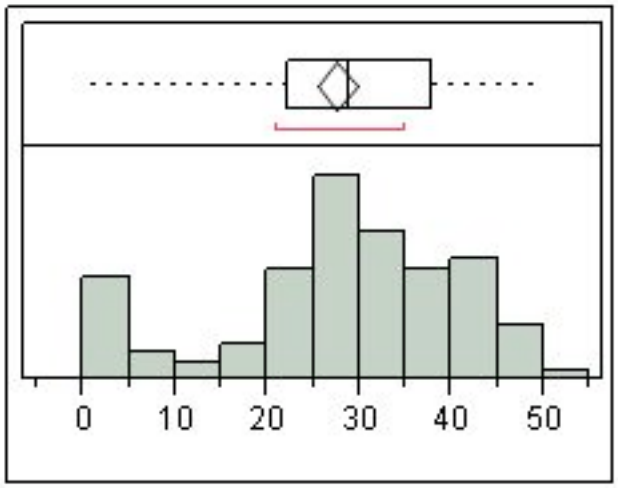

Quantiles

100.0%	maximum	50
99.5%		50
97.5%		47
90.0%		43.5
75.0%	quartile	38
50.0%	median	29
25.0%	quartile	22.25
10.0%		2
2.5%		0
0.5%		0
0.0%	minimum	0

Moments

Mean	27.548611
Std Dev	13.047964
Std Err Mean	1.0873303
Upper 95% Mean	29.697929
Lower 95% Mean	25.399294
N	144

bursts/sec

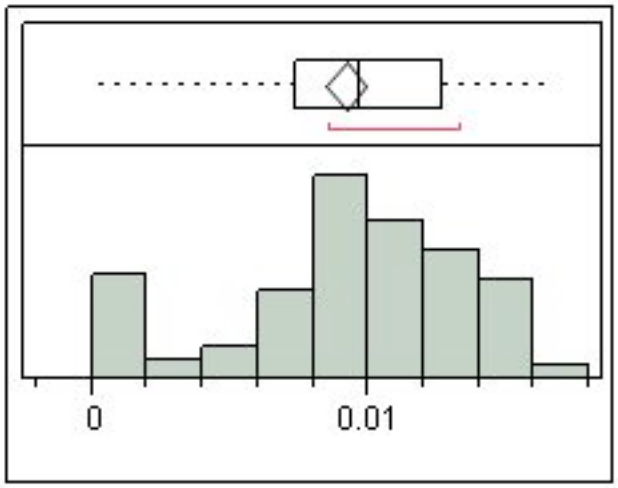

Quantiles

100.0%	maximum	0.01667
99.5%		0.01667
97.5%		0.01567
90.0%		0.0145
75.0%	quartile	0.01267
50.0%	median	0.00967
25.0%	quartile	0.00742
10.0%		0.00067
2.5%		0
0.5%		0
0.0%	minimum	0

Moments

Mean	0.0091829
Std Dev	0.0043493
Std Err Mean	0.0003624
Upper 95% Mean	0.0098993
Lower 95% Mean	0.0084665
N	144

%spikes in burst

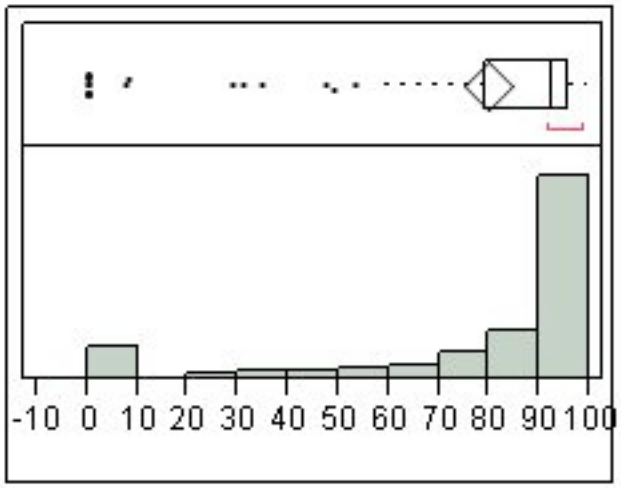

Quantiles

100.0%	maximum	99.4417
99.5%		99.4417
97.5%		98.7119
90.0%		97.3257
75.0%	quartile	95.5395
50.0%	median	92.5013
25.0%	quartile	79.1365
10.0%		29.6703
2.5%		0
0.5%		0
0.0%	minimum	0

Moments

Mean	79.793148
Std Dev	28.181821
Std Err Mean	2.3484851
Upper 95% Mean	84.435381
Lower 95% Mean	75.150916
N	144

mean burst dur

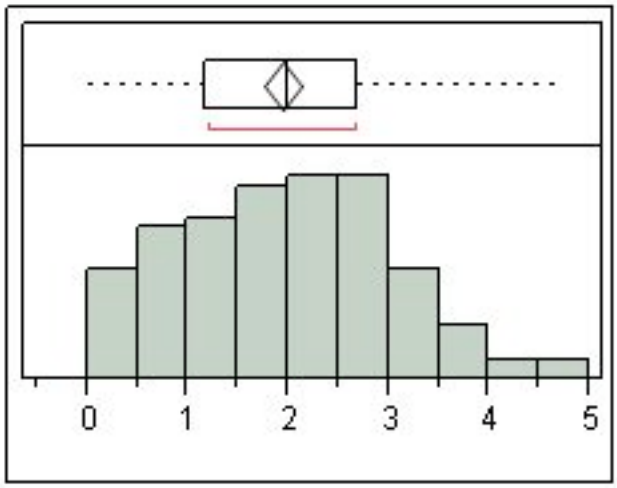

Quantiles

100.0%	maximum	4.72111
99.5%		4.72111
97.5%		4.10426
90.0%		3.31391
75.0%	quartile	2.69165
50.0%	median	1.99358
25.0%	quartile	1.16571
10.0%		0.56095
2.5%		0
0.5%		0
0.0%	minimum	0

Moments

Mean	1.9449816
Std Dev	1.0718023
Std Err Mean	0.0893169
Upper 95% Mean	2.1215335
Lower 95% Mean	1.7684297
N	144

mean spikes/burst

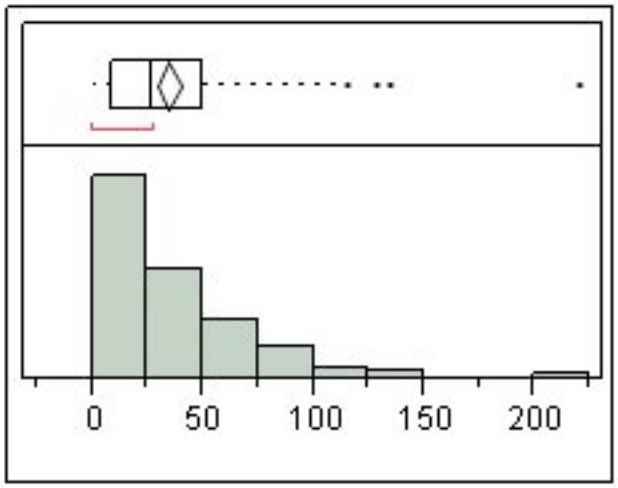

Quantiles

100.0%	maximum	219.846
99.5%		219.846
97.5%		119.912
90.0%		78.845
75.0%	quartile	49.7552
50.0%	median	26.7286
25.0%	quartile	8.27083
10.0%		4.33333
2.5%		0
0.5%		0
0.0%	minimum	0

Moments

Mean	34.504162
Std Dev	33.18565
Std Err Mean	2.7654708
Upper 95% Mean	39.970647
Lower 95% Mean	29.037678
N	144

mean ISI

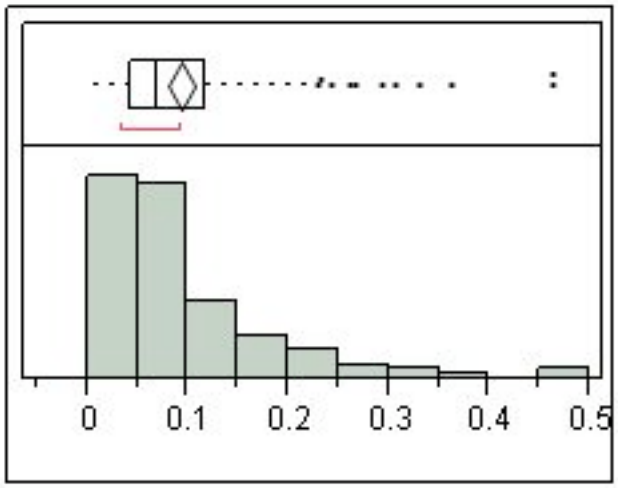

Quantiles

100.0%	maximum	0.46323
99.5%		0.46323
97.5%		0.34135
90.0%		0.21305
75.0%	quartile	0.11615
50.0%	median	0.06877
25.0%	quartile	0.04219
10.0%		0.02117
2.5%		0
0.5%		0
0.0%	minimum	0

Moments

Mean	0.0933447
Std Dev	0.0833992
Std Err Mean	0.0069499
Upper 95% Mean	0.1070826
Lower 95% Mean	0.0796068
N	144

Mean Freq in burst

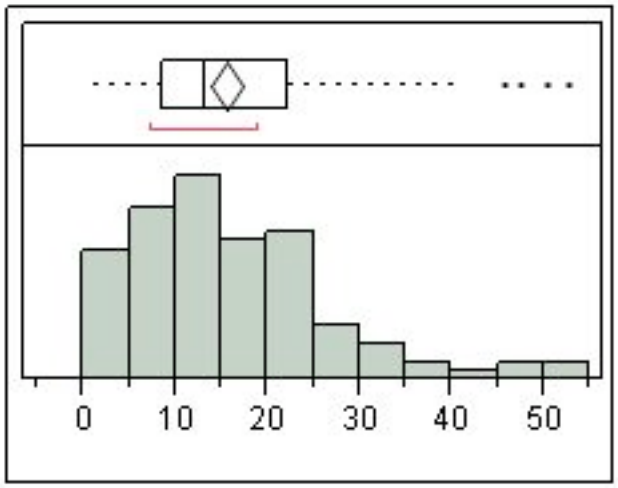

Quantiles

100.0%	maximum	52.5934
99.5%		52.5934
97.5%		46.4047
90.0%		28.7503
75.0%	quartile	22.2139
50.0%	median	13.1369
25.0%	quartile	8.52862
10.0%		3.13962
2.5%		0
0.5%		0
0.0%	minimum	0

Moments

Mean	15.542623
Std Dev	10.527876
Std Err Mean	0.877323
Upper 95% Mean	17.27682
Lower 95% Mean	13.808425
N	144

Mean Peak Freq

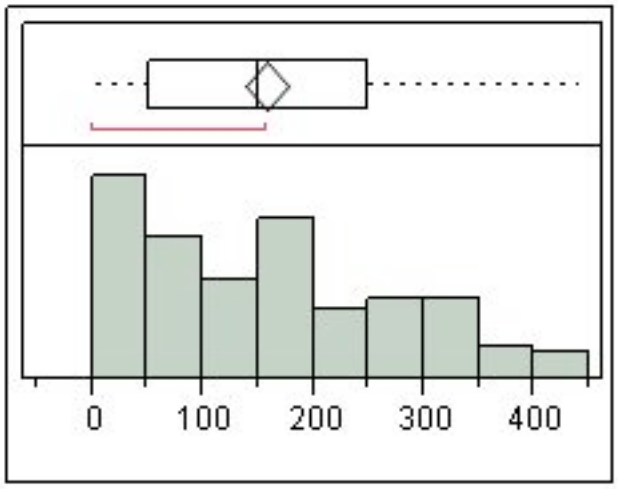

Quantiles

100.0%	maximum	439.996
99.5%		439.996
97.5%		413.519
90.0%		327.688
75.0%	quartile	249.915
50.0%	median	150.502
25.0%	quartile	51.8689
10.0%		11.4291
2.5%		0
0.5%		0
0.0%	minimum	0

Moments

Mean	157.73217
Std Dev	117.35755
Std Err Mean	9.7797956
Upper 95% Mean	177.06381
Lower 95% Mean	138.40052
N	144

mean Interburst Int

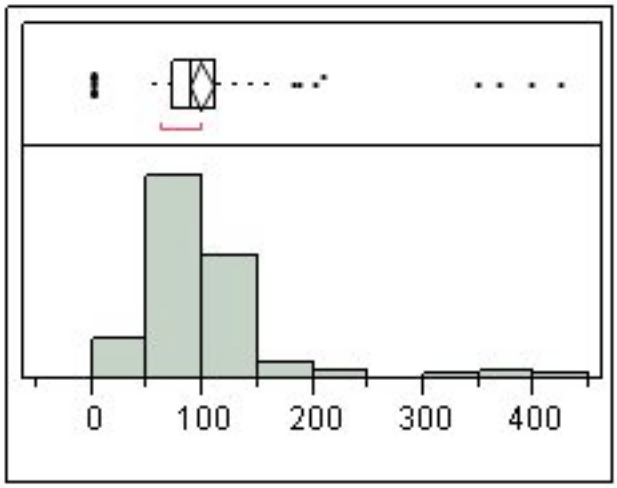

Quantiles

100.0%	maximum	422.872
99.5%		422.872
97.5%		355.299
90.0%		143.3
75.0%	quartile	112.75
50.0%	median	89.7336
25.0%	quartile	72.8578
10.0%		55.1828
2.5%		0
0.5%		0
0.0%	minimum	0

Moments

Mean	97.8491
Std Dev	62.934697
Std Err Mean	5.2445581
Upper 95% Mean	108.21598
Lower 95% Mean	87.482223
N	144

Mean Sup

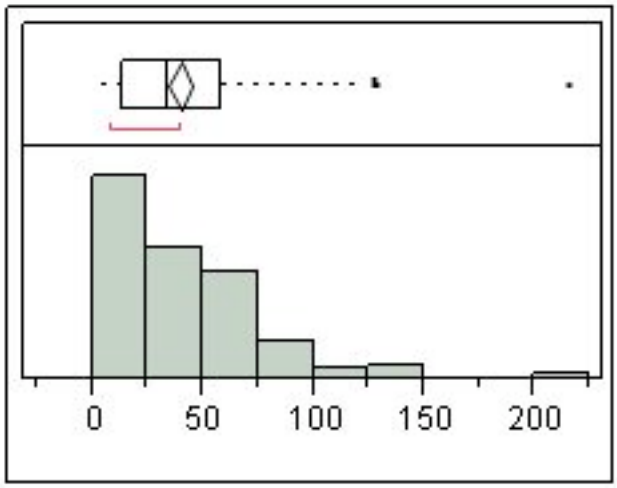

Quantiles

100.0%	maximum	215.441
99.5%		215.441
97.5%		127.195
90.0%		82.0384
75.0%	quartile	58.0579
50.0%	median	33.6331
25.0%	quartile	13.3714
10.0%		9.49012
2.5%		0
0.5%		0
0.0%	minimum	0

Moments

Mean	40.092479
Std Dev	33.520026
Std Err Mean	2.7933355
Upper 95% Mean	45.614044
Lower 95% Mean	34.570915
N	144

Distributions Genotype=sg6

mean freq

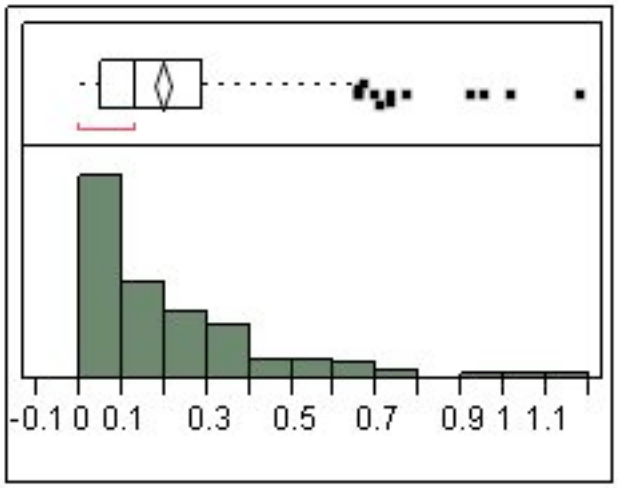

Quantiles

100.0%	maximum	1.172
99.5%		1.05527
97.5%		0.69462
90.0%		0.4535
75.0%	quartile	0.28967
50.0%	median	0.1325
25.0%	quartile	0.05358
10.0%		0.01217
2.5%		0.00354
0.5%		0.00024
0.0%	minimum	0

Moments

Mean	0.1945174
Std Dev	0.1918201
Std Err Mean	0.0103422
Upper 95% Mean	0.2148597
Lower 95% Mean	0.1741752
N	344

numburst

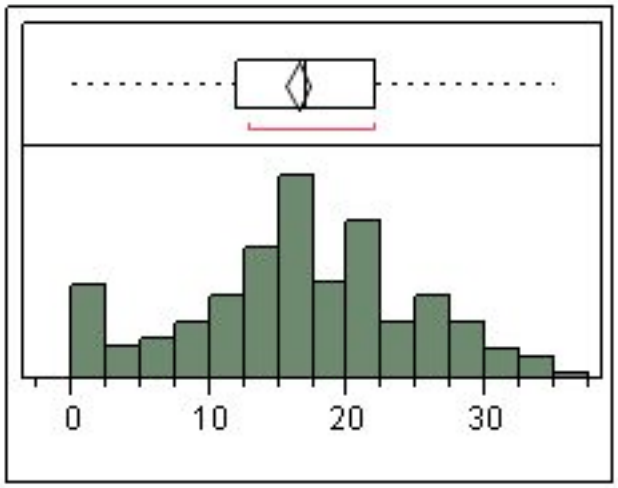

Quantiles

100.0%	maximum	35
99.5%		34.275
97.5%		32
90.0%		27
75.0%	quartile	22
50.0%	median	17
25.0%	quartile	12
10.0%		4
2.5%		0
0.5%		0
0.0%	minimum	0

Moments

Mean	16.395349
Std Dev	8.1505929
Std Err Mean	0.4394505
Upper 95% Mean	17.259706
Lower 95% Mean	15.530992
N	344

bursts/sec

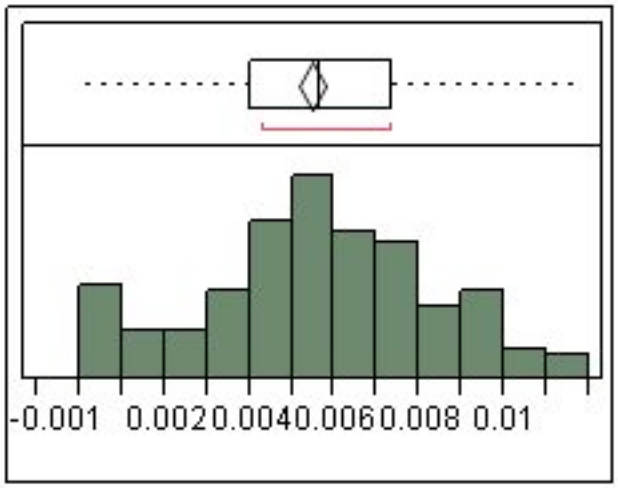

Quantiles

100.0%	maximum	0.01167
99.5%		0.01142
97.5%		0.01067
90.0%		0.009
75.0%	quartile	0.00733
50.0%	median	0.00567
25.0%	quartile	0.004
10.0%		0.00133
2.5%		0
0.5%		0
0.0%	minimum	0

Moments

Mean	0.0054651
Std Dev	0.0027169
Std Err Mean	0.0001465
Upper 95% Mean	0.0057532
Lower 95% Mean	0.005177
N	344

%spikes in burst

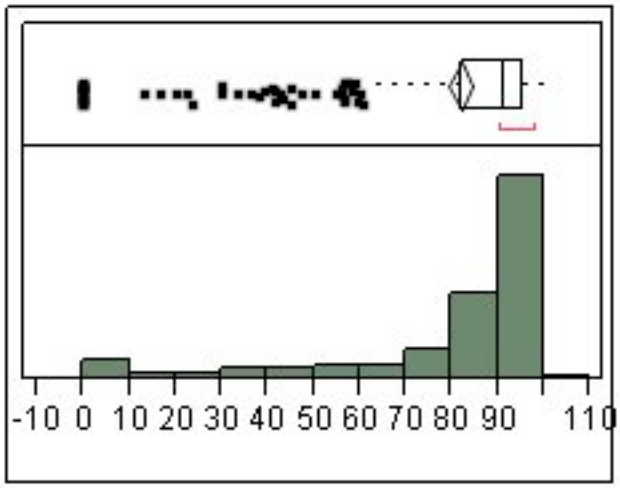

Quantiles

100.0%	maximum	100
99.5%		99.9196
97.5%		98.5669
90.0%		97.5308
75.0%	quartile	95.7081
50.0%	median	91.2019
25.0%	quartile	82.1253
10.0%		46.3095
2.5%		0
0.5%		0
0.0%	minimum	0

Moments

Mean	81.90136
Std Dev	23.829347
Std Err Mean	1.2847923
Upper 95% Mean	84.428424
Lower 95% Mean	79.374297
N	344

mean burst dur

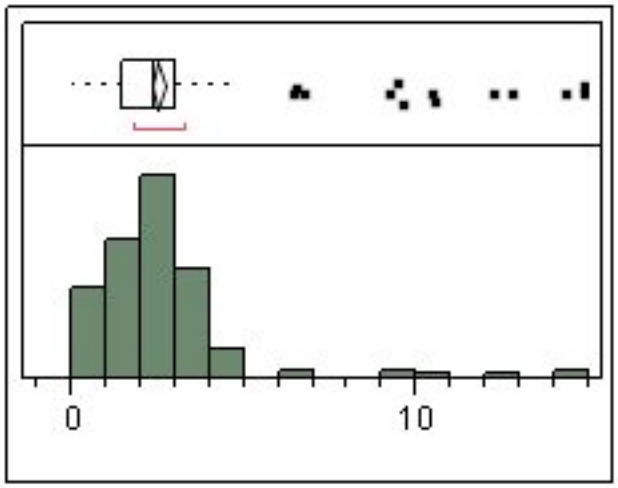

Quantiles

100.0%	maximum	14.8378
99.5%		14.8205
97.5%		9.46495
90.0%		3.87105
75.0%	quartile	3.04856
50.0%	median	2.37373
25.0%	quartile	1.453
10.0%		0.66797
2.5%		0
0.5%		0
0.0%	minimum	0

Moments

Mean	2.5051552
Std Dev	2.0100563
Std Err Mean	0.108375
Upper 95% Mean	2.7183184
Lower 95% Mean	2.291992
N	344

mean spikes/burst

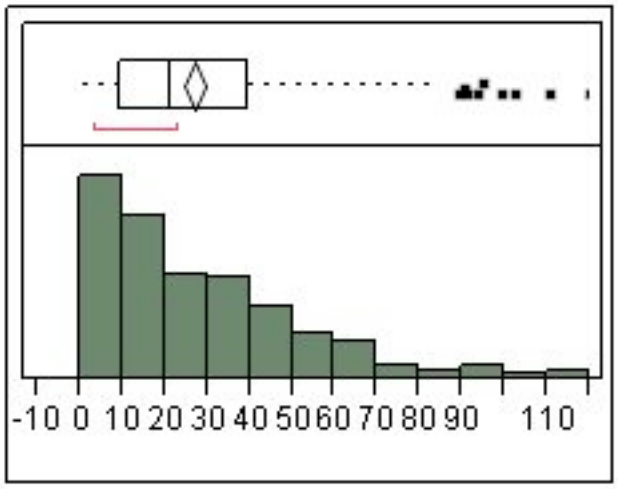

Quantiles

100.0%	maximum	119.75
99.5%		113.285
97.5%		89.7405
90.0%		58.671
75.0%	quartile	39.5016
50.0%	median	21.3234
25.0%	quartile	9.16896
10.0%		5
2.5%		0
0.5%		0
0.0%	minimum	0

Moments

Mean	26.997629
Std Dev	22.314928
Std Err Mean	1.2031403
Upper 95% Mean	29.364091
Lower 95% Mean	24.631168
N	344

mean ISI

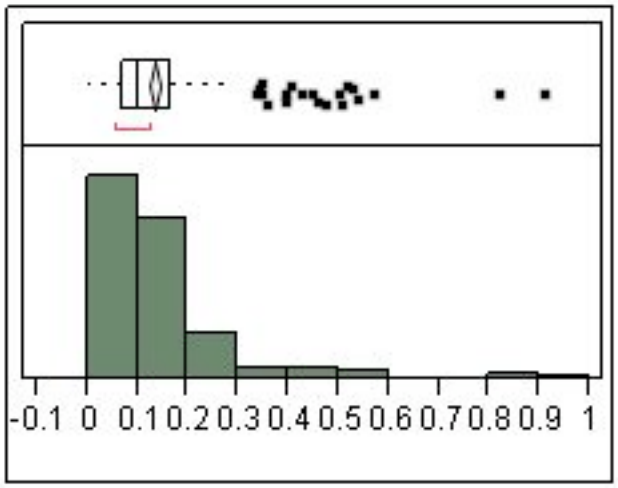

Quantiles

100.0%	maximum	0.9103
99.5%		0.84373
97.5%		0.50014
90.0%		0.23557
75.0%	quartile	0.16371
50.0%	median	0.10402
25.0%	quartile	0.06743
10.0%		0.04403
2.5%		0
0.5%		0
0.0%	minimum	0

Moments

Mean	0.1332787
Std Dev	0.1174594
Std Err Mean	0.006333
Upper 95% Mean	0.1457351
Lower 95% Mean	0.1208224
N	344

Mean Freq in burst

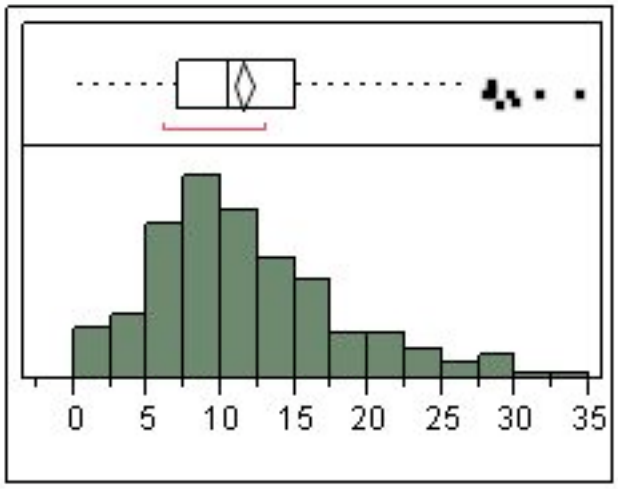

Quantiles

100.0%	maximum	34.1914
99.5%		32.2776
97.5%		28.0397
90.0%		20.3132
75.0%	quartile	15.004
50.0%	median	10.5505
25.0%	quartile	7.11127
10.0%		4.78749
2.5%		0
0.5%		0
0.0%	minimum	0

Moments

Mean	11.516543
Std Dev	6.3541281
Std Err Mean	0.3425916
Upper 95% Mean	12.190388
Lower 95% Mean	10.842698
N	344

Mean Peak Freq

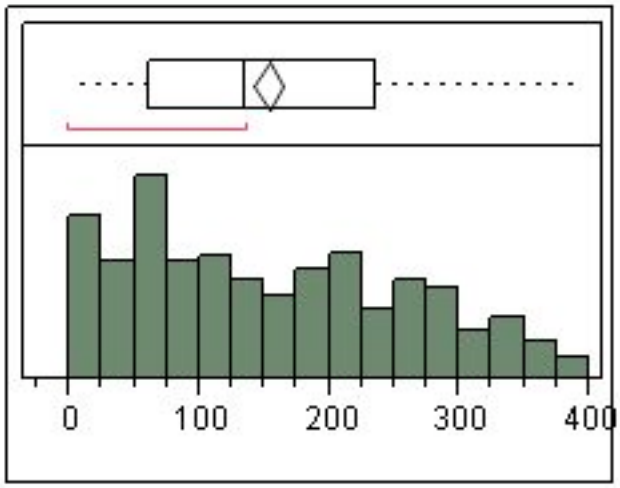

Quantiles

100.0%	maximum	389.756
99.5%		382.925
97.5%		369.879
90.0%		302.666
75.0%	quartile	235.882
50.0%	median	135.026
25.0%	quartile	61.6579
10.0%		23.521
2.5%		0
0.5%		0
0.0%	minimum	0

Moments

Mean	153.34841
Std Dev	104.59711
Std Err Mean	5.6394981
Upper 95% Mean	164.44077
Lower 95% Mean	142.25606
N	344

mean Interburst Int

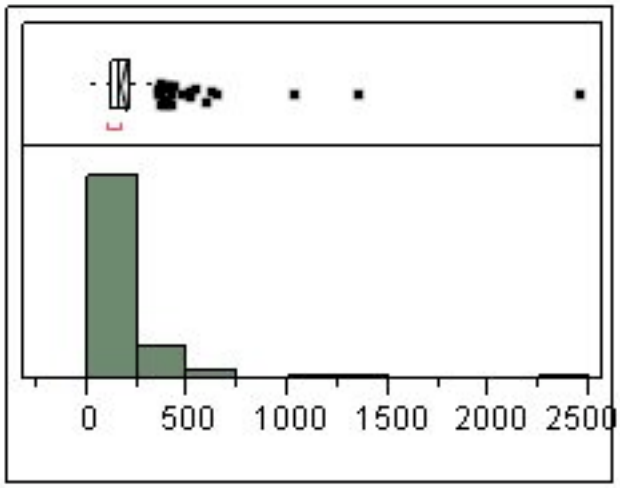

Quantiles

100.0%	maximum	2451.02
99.5%		1650.67
97.5%		504.74
90.0%		298.279
75.0%	quartile	210.31
50.0%	median	157.798
25.0%	quartile	120.258
10.0%		93.668
2.5%		0
0.5%		0
0.0%	minimum	0

Moments

Mean	186.20881
Std Dev	175.74654
Std Err Mean	9.4756182
Upper 95% Mean	204.84644
Lower 95% Mean	167.57117
N	344

Mean Sup

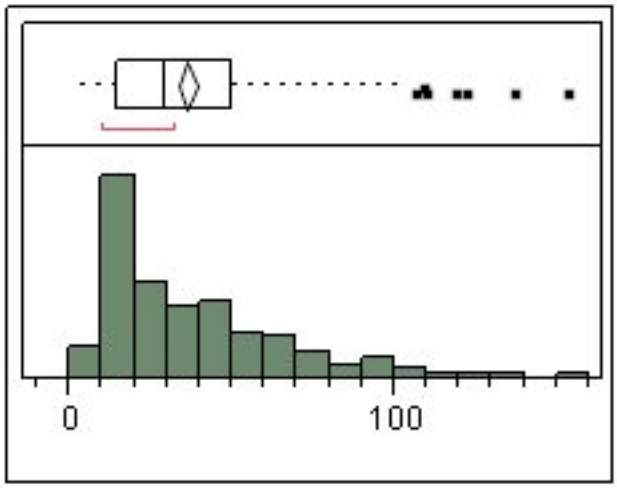

Quantiles

100.0%	maximum	153.457
99.5%		141.393
97.5%		101.224
90.0%		72.2493
75.0%	quartile	50.0727
50.0%	median	29.3293
25.0%	quartile	14.7689
10.0%		12.3361
2.5%		0
0.5%		0
0.0%	minimum	0

Moments

Mean	36.23853
Std Dev	26.668541
Std Err Mean	1.4378714
Upper 95% Mean	39.066685
Lower 95% Mean	33.410375
N	344

Distributions Genotype=sg7

mean freq

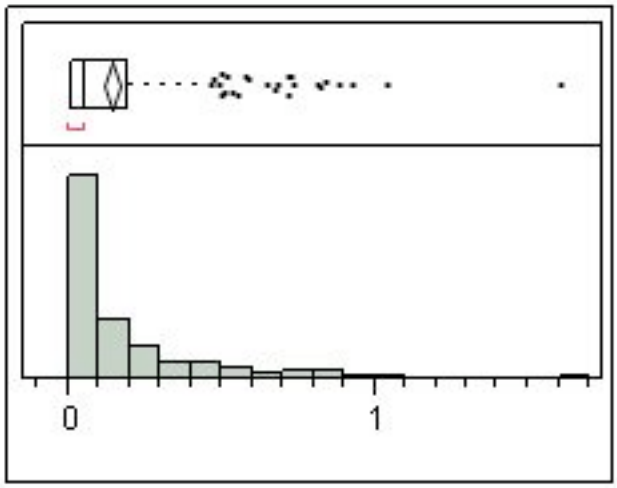

Quantiles

100.0%	maximum	1.60233
99.5%		1.24156
97.5%		0.73445
90.0%		0.40513
75.0%	quartile	0.192
50.0%	median	0.05867
25.0%	quartile	0.01175
10.0%		0.00133
2.5%		0.00033
0.5%		0
0.0%	minimum	0

Moments

Mean	0.1434339
Std Dev	0.2059872
Std Err Mean	0.0113737
Upper 95% Mean	0.1658089
Lower 95% Mean	0.121059
N	328

numburst

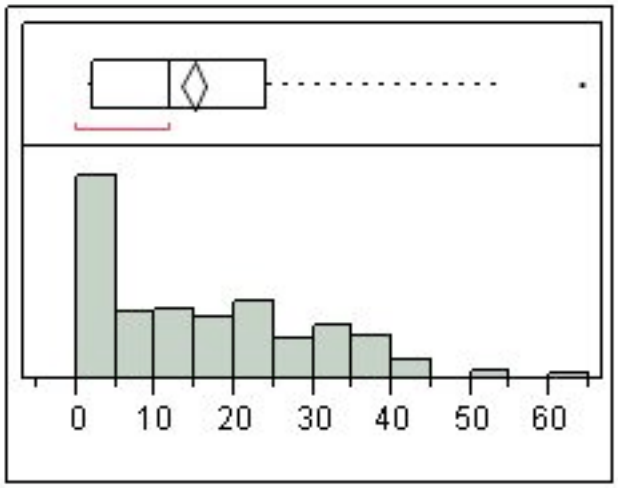

Quantiles

100.0%	maximum	64
99.5%		56.905
97.5%		43
90.0%		35
75.0%	quartile	24
50.0%	median	12
25.0%	quartile	2
10.0%		0
2.5%		0
0.5%		0
0.0%	minimum	0

Moments

Mean	14.841463
Std Dev	13.389
Std Err Mean	0.7392838
Upper 95% Mean	16.295816
Lower 95% Mean	13.387111
N	328

bursts/sec

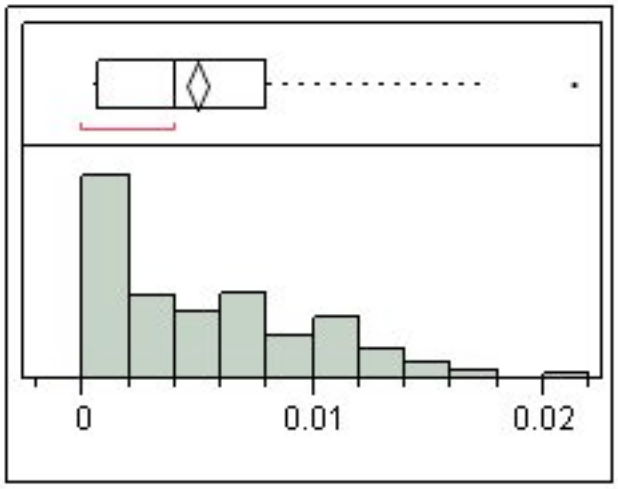

Quantiles

100.0%	maximum	0.02133
99.5%		0.01897
97.5%		0.01433
90.0%		0.01167
75.0%	quartile	0.008
50.0%	median	0.004
25.0%	quartile	0.00067
10.0%		0
2.5%		0
0.5%		0
0.0%	minimum	0

Moments

Mean	0.0049472
Std Dev	0.004463
Std Err Mean	0.0002464
Upper 95% Mean	0.0054319
Lower 95% Mean	0.0044624
N	328

%spikes in burst

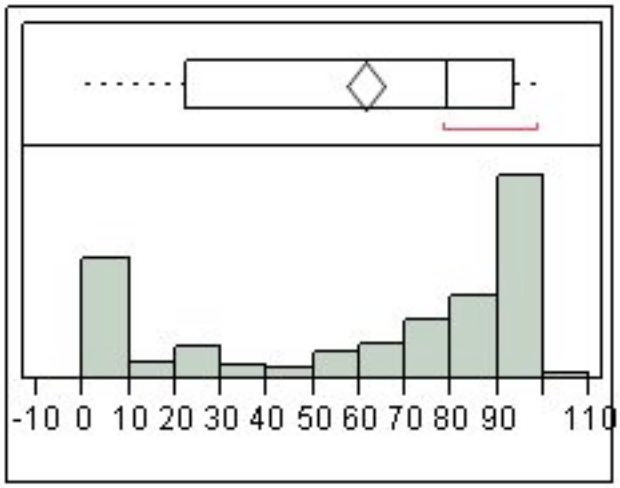

Quantiles

100.0%	maximum	100
99.5%		99.6165
97.5%		98.3349
90.0%		96.2398
75.0%	quartile	93.7442
50.0%	median	79.2789
25.0%	quartile	22.5455
10.0%		0
2.5%		0
0.5%		0
0.0%	minimum	0

Moments

Mean	61.453977
Std Dev	37.794805
Std Err Mean	2.086869
Upper 95% Mean	65.55936
Lower 95% Mean	57.348594
N	328

mean burst dur

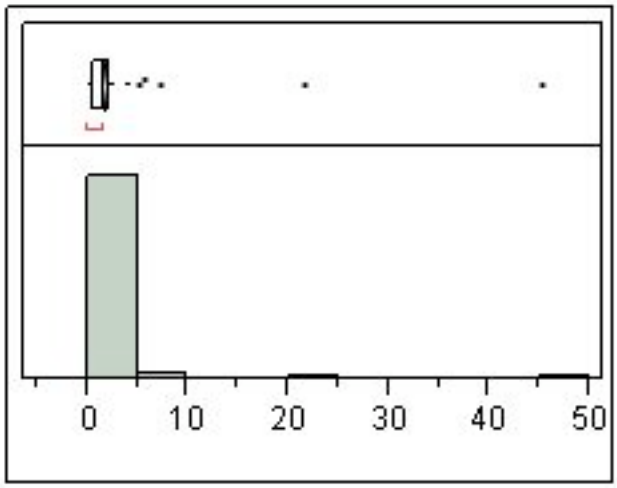

Quantiles

100.0%	maximum	45.2586
99.5%		29.9278
97.5%		4.10038
90.0%		2.85738
75.0%	quartile	2.27416
50.0%	median	1.51026
25.0%	quartile	0.62205
10.0%		0
2.5%		0
0.5%		0
0.0%	minimum	0

Moments

Mean	1.7048581
Std Dev	2.8858262
Std Err Mean	0.1593431
Upper 95% Mean	2.018325
Lower 95% Mean	1.3913911
N	328

mean spikes/burst

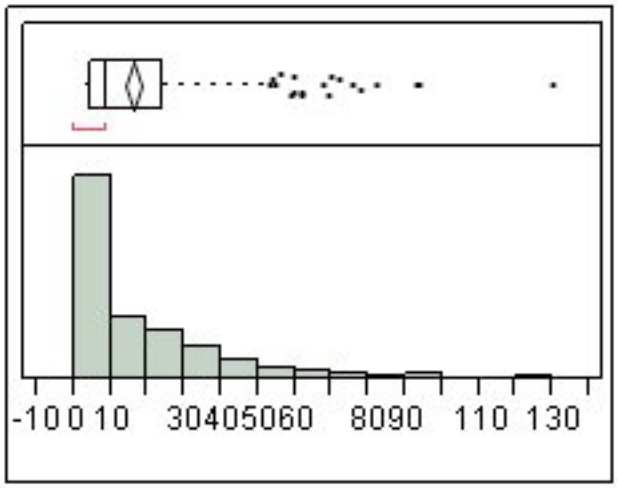

Quantiles

100.0%	maximum	129.762
99.5%		106.575
97.5%		69.5856
90.0%		40.1696
75.0%	quartile	23.8545
50.0%	median	8.97941
25.0%	quartile	4.525
10.0%		0
2.5%		0
0.5%		0
0.0%	minimum	0

Moments

Mean	16.276995
Std Dev	18.878188
Std Err Mean	1.0423736
Upper 95% Mean	18.327599
Lower 95% Mean	14.226391
N	328

mean ISI

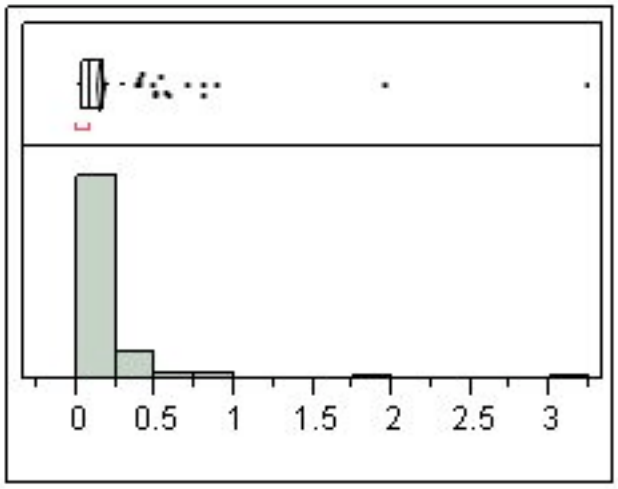

Quantiles

100.0%	maximum	3.23276
99.5%		2.40772
97.5%		0.55344
90.0%		0.29198
75.0%	quartile	0.17937
50.0%	median	0.09652
25.0%	quartile	0.04589
10.0%		0
2.5%		0
0.5%		0
0.0%	minimum	0

Moments

Mean	0.1444271
Std Dev	0.2385328
Std Err Mean	0.0131708
Upper 95% Mean	0.1703372
Lower 95% Mean	0.1185169
N	328

Mean Freq in burst

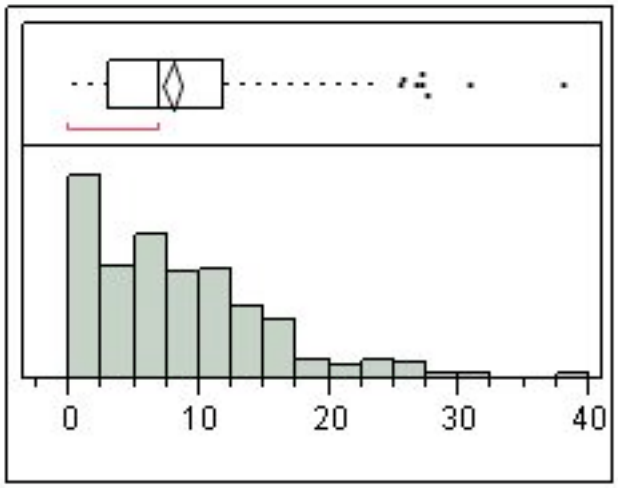

Quantiles

100.0%	maximum	37.9307
99.5%		33.3631
97.5%		25.1062
90.0%		15.808
75.0%	quartile	11.85
50.0%	median	6.97435
25.0%	quartile	2.94423
10.0%		0
2.5%		0
0.5%		0
0.0%	minimum	0

Moments

Mean	7.9604643
Std Dev	6.6591652
Std Err Mean	0.3676909
Upper 95% Mean	8.6838024
Lower 95% Mean	7.2371262
N	328

Mean Peak Freq

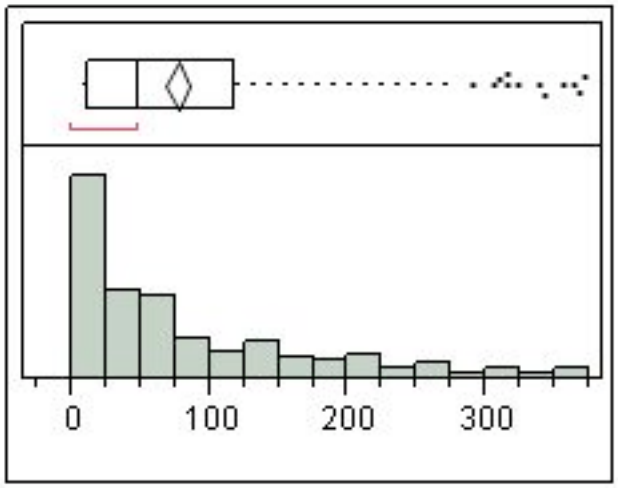

Quantiles

100.0%	maximum	370.527
99.5%		368.552
97.5%		315.399
90.0%		209.5
75.0%	quartile	118.59
50.0%	median	47.8135
25.0%	quartile	10.9003
10.0%		0
2.5%		0
0.5%		0
0.0%	minimum	0

Moments

Mean	76.682833
Std Dev	86.060246
Std Err Mean	4.7518822
Upper 95% Mean	86.03095
Lower 95% Mean	67.334716
N	328

mean Interburst Int

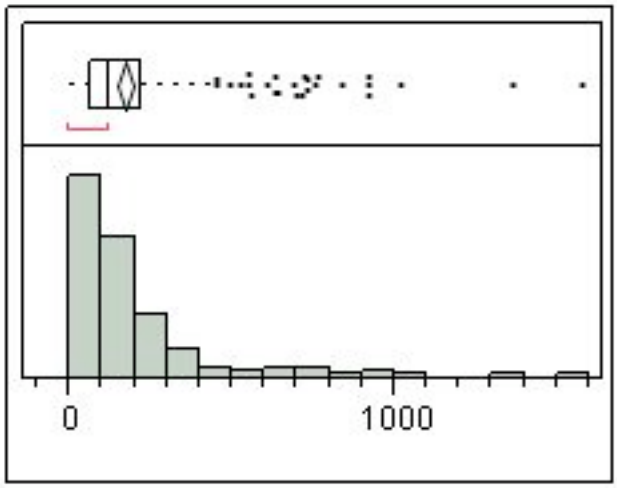

Quantiles

100.0%	maximum	1572.53
99.5%		1439.26
97.5%		762.334
90.0%		345.62
75.0%	quartile	217.133
50.0%	median	118.742
25.0%	quartile	60.9511
10.0%		0
2.5%		0
0.5%		0
0.0%	minimum	0

Moments

Mean	172.18446
Std Dev	208.96029
Std Err Mean	11.537902
Upper 95% Mean	194.88234
Lower 95% Mean	149.48658
N	328

Mean Sup

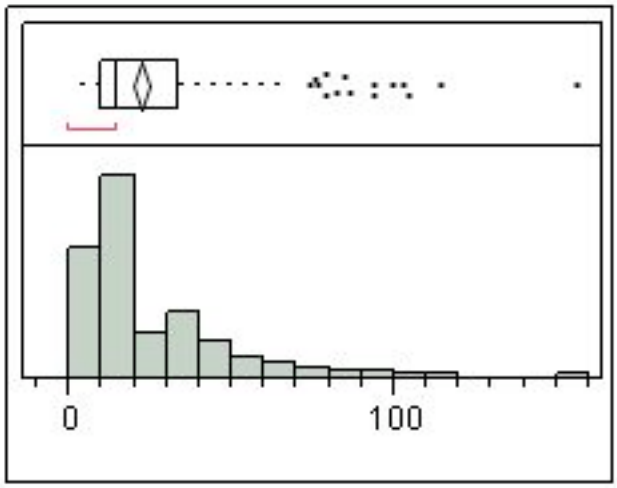

Quantiles

100.0%	maximum	155.919
99.5%		129.045
97.5%		85.7153
90.0%		50.3554
75.0%	quartile	33.4163
50.0%	median	14.2549
25.0%	quartile	10.1017
10.0%		0
2.5%		0
0.5%		0
0.0%	minimum	0

Moments

Mean	22.406106
Std Dev	22.820071
Std Err Mean	1.2600276
Upper 95% Mean	24.88489
Lower 95% Mean	19.927323
N	328

Distributions Genotype=wt

mean freq

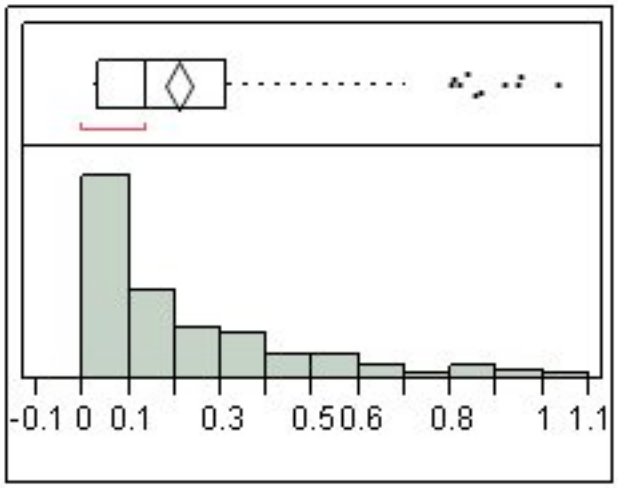

Quantiles

100.0%	maximum	1.03
99.5%		1.02116
97.5%		0.85645
90.0%		0.54167
75.0%	quartile	0.30983
50.0%	median	0.139
25.0%	quartile	0.03433
10.0%		0.00613
2.5%		0.00185
0.5%		3.66e-5
0.0%	minimum	0

Moments

Mean	0.2072685
Std Dev	0.2224006
Std Err Mean	0.0149603
Upper 95% Mean	0.2367523
Lower 95% Mean	0.1777847
N	221

numburst

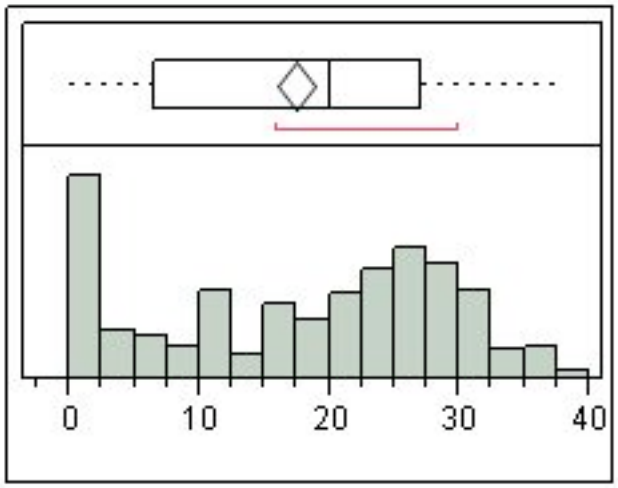

Quantiles

100.0%	maximum	38
99.5%		37.89
97.5%		35
90.0%		30
75.0%	quartile	27
50.0%	median	20
25.0%	quartile	6.5
10.0%		0
2.5%		0
0.5%		0
0.0%	minimum	0

Moments

Mean	17.461538
Std Dev	11.193936
Std Err Mean	0.7529856
Upper 95% Mean	18.945527
Lower 95% Mean	15.97755
N	221

bursts/sec

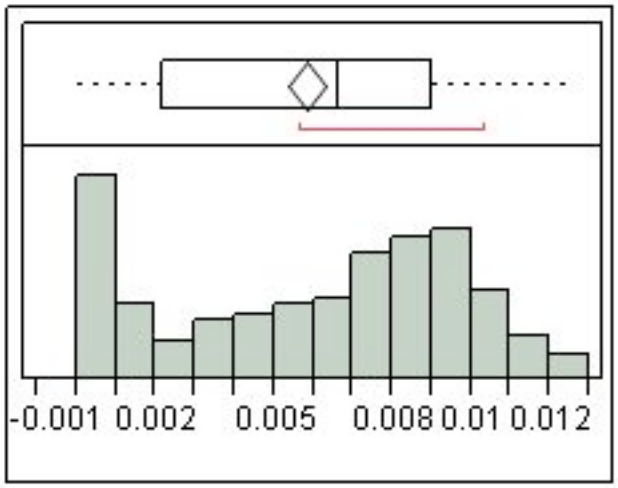

Quantiles

100.0%	maximum	0.01267
99.5%		0.01263
97.5%		0.01167
90.0%		0.01
75.0%	quartile	0.009
50.0%	median	0.00667
25.0%	quartile	0.00217
10.0%		0
2.5%		0
0.5%		0
0.0%	minimum	0

Moments

Mean	0.0058205
Std Dev	0.0037313
Std Err Mean	0.000251
Upper 95% Mean	0.0063152
Lower 95% Mean	0.0053258
N	221

%spikes in burst

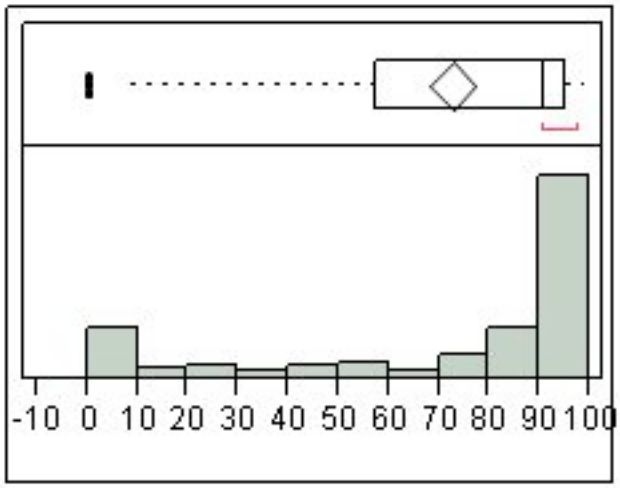

Quantiles

100.0%	maximum	98.9201
99.5%		98.8273
97.5%		97.8559
90.0%		96.8277
75.0%	quartile	95.0769
50.0%	median	90.9804
25.0%	quartile	57.4777
10.0%		0
2.5%		0
0.5%		0
0.0%	minimum	0

Moments

Mean	72.770015
Std Dev	33.701351
Std Err Mean	2.2669982
Upper 95% Mean	77.237827
Lower 95% Mean	68.302202
N	221

mean burst dur

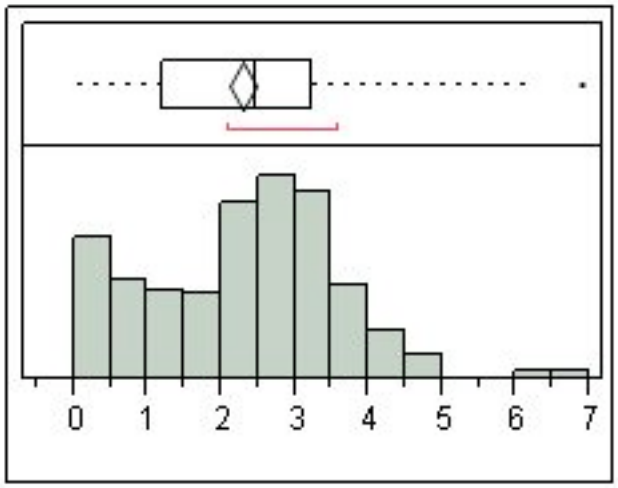

Quantiles

100.0%	maximum	6.90831
99.5%		6.82506
97.5%		4.52318
90.0%		3.73688
75.0%	quartile	3.24519
50.0%	median	2.47937
25.0%	quartile	1.20298
10.0%		0
2.5%		0
0.5%		0
0.0%	minimum	0

Moments

Mean	2.2795285
Std Dev	1.3104383
Std Err Mean	0.0881496
Upper 95% Mean	2.4532543
Lower 95% Mean	2.1058028
N	221

mean spikes/burst

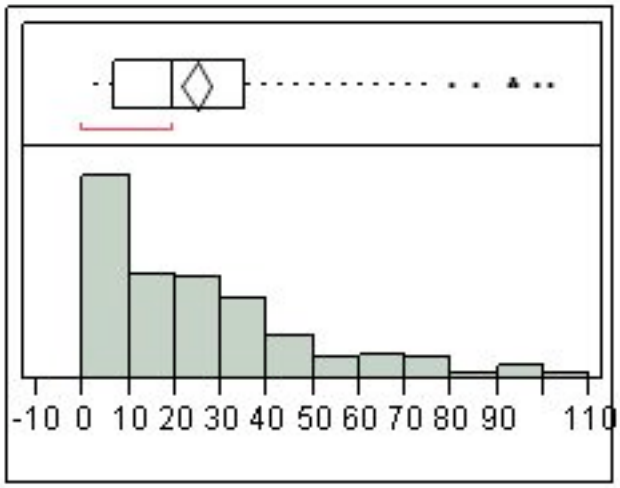

Quantiles

100.0%	maximum	101.308
99.5%		100.977
97.5%		88.4562
90.0%		57.8354
75.0%	quartile	35.1332
50.0%	median	19.5417
25.0%	quartile	6.67262
10.0%		0
2.5%		0
0.5%		0
0.0%	minimum	0

Moments

Mean	24.496046
Std Dev	22.482078
Std Err Mean	1.5123082
Upper 95% Mean	27.476511
Lower 95% Mean	21.51558
N	221

mean ISI

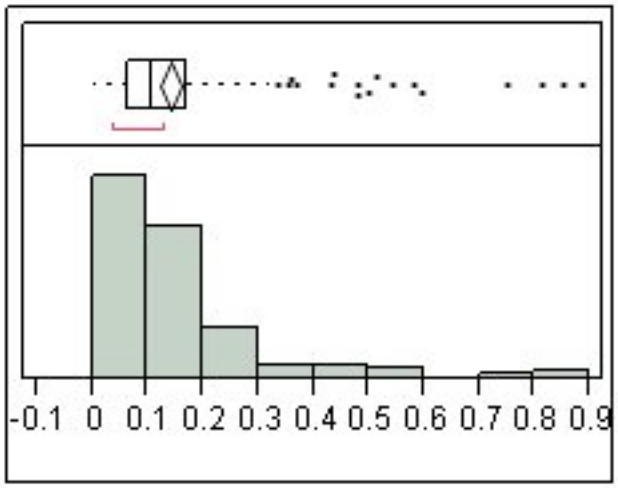

Quantiles

100.0%	maximum	0.88451
99.5%		0.88105
97.5%		0.58768
90.0%		0.26469
75.0%	quartile	0.16934
50.0%	median	0.10815
25.0%	quartile	0.06194
10.0%		0
2.5%		0
0.5%		0
0.0%	minimum	0

Moments

Mean	0.1418247
Std Dev	0.1442072
Std Err Mean	0.0097004
Upper 95% Mean	0.1609423
Lower 95% Mean	0.122707
N	221

Mean Freq in burst

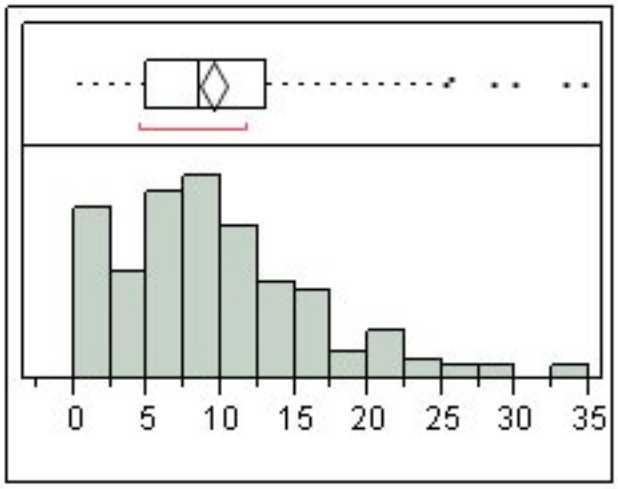

Quantiles

100.0%	maximum	34.6404
99.5%		34.4953
97.5%		25.4454
90.0%		17.8893
75.0%	quartile	13.0592
50.0%	median	8.57238
25.0%	quartile	4.99021
10.0%		0
2.5%		0
0.5%		0
0.0%	minimum	0

Moments

Mean	9.4135934
Std Dev	6.7098906
Std Err Mean	0.4513561
Upper 95% Mean	10.303128
Lower 95% Mean	8.5240583
N	221

Mean Peak Freq

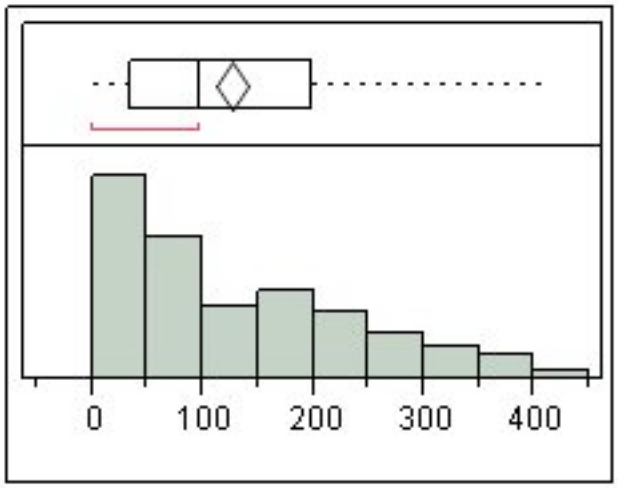

Quantiles

100.0%	maximum	406.172
99.5%		405.769
97.5%		358.115
90.0%		287.72
75.0%	quartile	199.562
50.0%	median	96.5089
25.0%	quartile	35.4175
10.0%		0
2.5%		0
0.5%		0
0.0%	minimum	0

Moments

Mean	125.48147
Std Dev	107.36055
Std Err Mean	7.2218519
Upper 95% Mean	139.71433
Lower 95% Mean	111.2486
N	221

mean Interburst Int

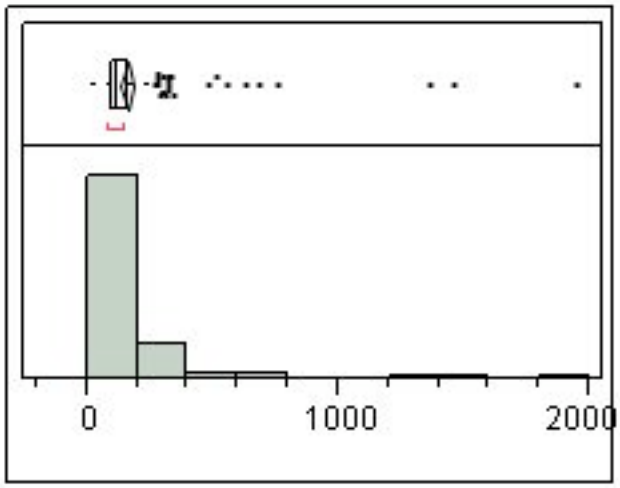

Quantiles

100.0%	maximum	1951.71
99.5%		1897.15
97.5%		652.131
90.0%		281.257
75.0%	quartile	162.966
50.0%	median	118.55
25.0%	quartile	96.3914
10.0%		0
2.5%		0
0.5%		0
0.0%	minimum	0

Moments

Mean	157.95183
Std Dev	204.17635
Std Err Mean	13.734387
Upper 95% Mean	185.01964
Lower 95% Mean	130.88403
N	221

Mean Sup

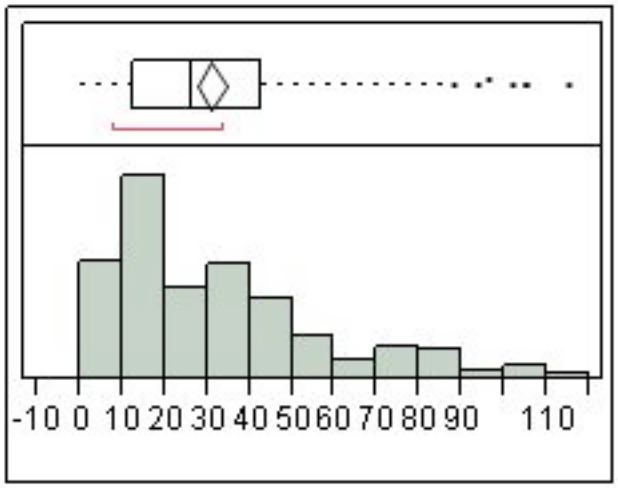

Quantiles

100.0%	maximum	115.027
99.5%		113.948
97.5%		94.8515
90.0%		70.1349
75.0%	quartile	42.7013
50.0%	median	26.4016
25.0%	quartile	12.6356
10.0%		0
2.5%		0
0.5%		0
0.0%	minimum	0

Moments

Mean	31.065642
Std Dev	24.967607
Std Err Mean	1.679503
Upper 95% Mean	34.375616
Lower 95% Mean	27.755669
N	221

P12

Distributions Genotype=het

mean freq

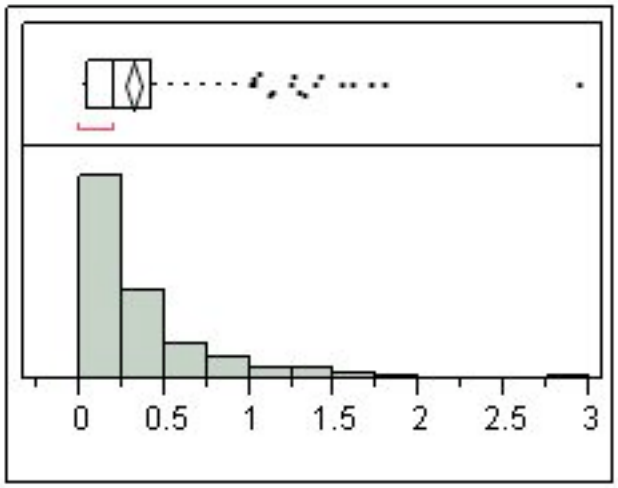

Quantiles

100.0%	maximum	2.9428
99.5%		2.52013
97.5%		1.39368
90.0%		0.79429
75.0%	quartile	0.42169
50.0%	median	0.20506
25.0%	quartile	0.04607
10.0%		0.0068
2.5%		0.00233
0.5%		0.00081
0.0%	minimum	0.0007

Moments

Mean	0.3217066
Std Dev	0.3861668
Std Err Mean	0.0234148
Upper 95% Mean	0.3678047
Lower 95% Mean	0.2756086
N	272

numburst

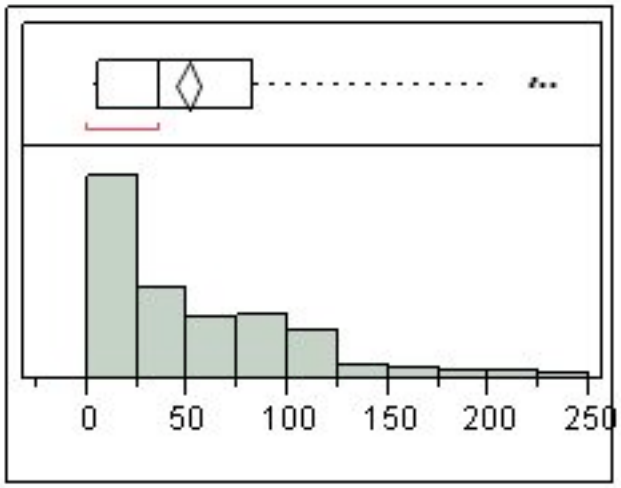

Quantiles

100.0%	maximum	232
99.5%		229.81
97.5%		187.275
90.0%		114.7
75.0%	quartile	83
50.0%	median	36
25.0%	quartile	5
10.0%		1
2.5%		0
0.5%		0
0.0%	minimum	0

Moments

Mean	50.382353
Std Dev	50.671514
Std Err Mean	3.0724118
Upper 95% Mean	56.431183
Lower 95% Mean	44.333523
N	272

bursts/sec

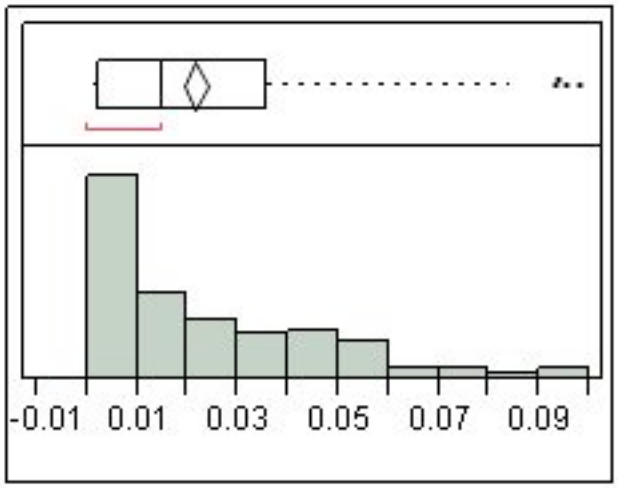

Quantiles

100.0%	maximum	0.09768
99.5%		0.09676
97.5%		0.07885
90.0%		0.05203
75.0%	quartile	0.03544
50.0%	median	0.01497
25.0%	quartile	0.0022
10.0%		0.00034
2.5%		0
0.5%		0
0.0%	minimum	0

Moments

Mean	0.0216171
Std Dev	0.0219447
Std Err Mean	0.0013306
Upper 95% Mean	0.0242367
Lower 95% Mean	0.0189975
N	272

%spikes in burst

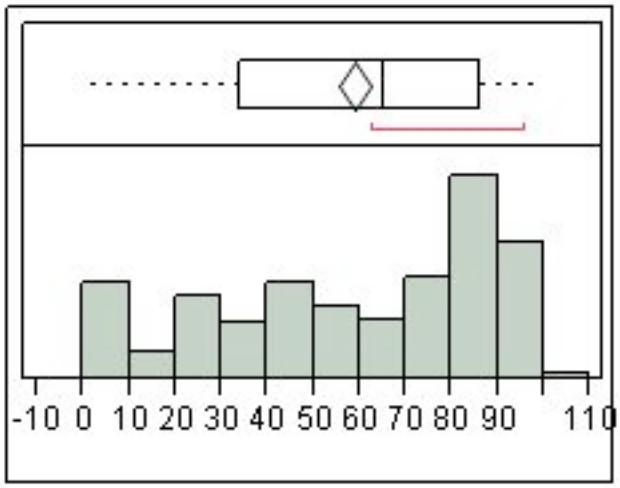

Quantiles

100.0%	maximum	100
99.5%		99.3262
97.5%		95.9272
90.0%		92.3946
75.0%	quartile	86.256
50.0%	median	65.3363
25.0%	quartile	33.8437
10.0%		4.52318
2.5%		0
0.5%		0
0.0%	minimum	0

Moments

Mean	58.904393
Std Dev	30.568043
Std Err Mean	1.8534599
Upper 95% Mean	62.553403
Lower 95% Mean	55.255382
N	272

mean burst dur

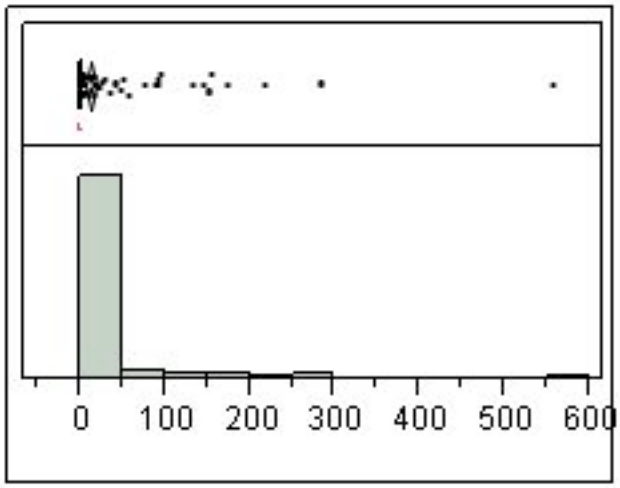

Quantiles

100.0%	maximum	555.465
99.5%		455.821
97.5%		151.221
90.0%		16.195
75.0%	quartile	1.81403
50.0%	median	1.02388
25.0%	quartile	0.68361
10.0%		0.25858
2.5%		0
0.5%		0
0.0%	minimum	0

Moments

Mean	12.663698
Std Dev	49.52956
Std Err Mean	3.0031707
Upper 95% Mean	18.57621
Lower 95% Mean	6.7511872
N	272

mean spikes/burst

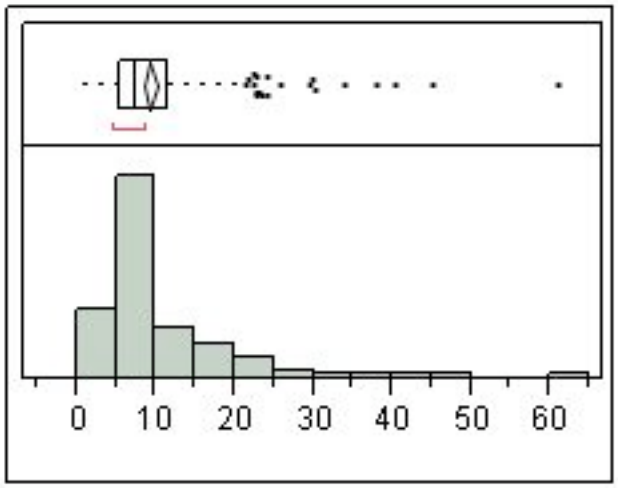

Quantiles

100.0%	maximum	61
99.5%		55.2246
97.5%		29.8419
90.0%		18.5064
75.0%	quartile	11.5799
50.0%	median	7.34633
25.0%	quartile	5.37972
10.0%		4
2.5%		0
0.5%		0
0.0%	minimum	0

Moments

Mean	9.3679402
Std Dev	7.6016697
Std Err Mean	0.4609189
Upper 95% Mean	10.275377
Lower 95% Mean	8.4605032
N	272

mean ISI

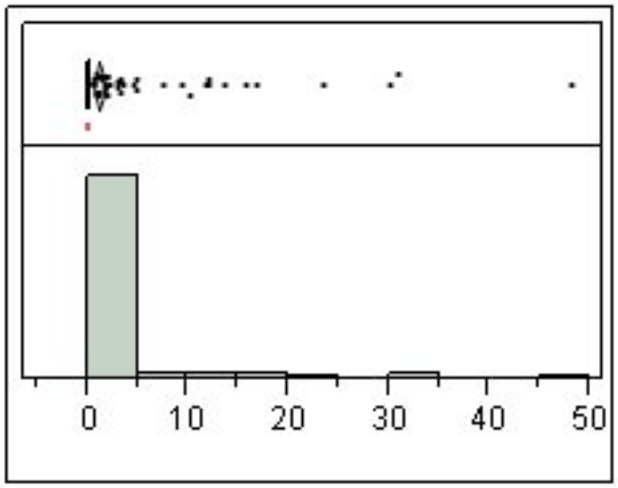

Quantiles

100.0%	maximum	48.1285
99.5%		41.8199
97.5%		14.04
90.0%		1.53095
75.0%	quartile	0.31063
50.0%	median	0.14355
25.0%	quartile	0.08516
10.0%		0.0341
2.5%		0
0.5%		0
0.0%	minimum	0

Moments

Mean	1.2259462
Std Dev	4.6528897
Std Err Mean	0.2821229
Upper 95% Mean	1.7813774
Lower 95% Mean	0.670515
N	272

Mean Freq in burst

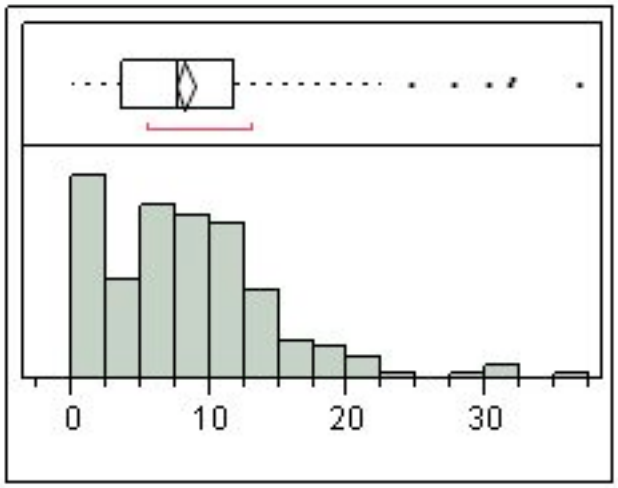

Quantiles

100.0%	maximum	36.6492
99.5%		34.8883
97.5%		22.7961
90.0%		15.4836
75.0%	quartile	11.7488
50.0%	median	7.71248
25.0%	quartile	3.74174
10.0%		0.03268
2.5%		0
0.5%		0
0.0%	minimum	0

Moments

Mean	8.2048391
Std Dev	6.2961909
Std Err Mean	0.3817626
Upper 95% Mean	8.9564368
Lower 95% Mean	7.4532415
N	272

Mean Peak Freq

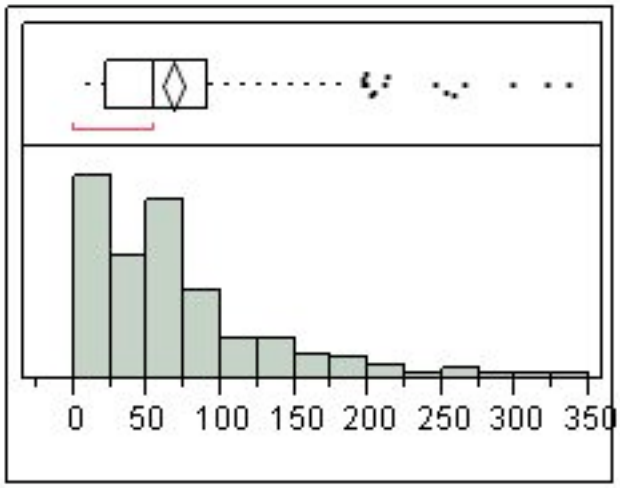

Quantiles

100.0%	maximum	334.784
99.5%		329.68
97.5%		246.639
90.0%		148.995
75.0%	quartile	91.0675
50.0%	median	55.2729
25.0%	quartile	21.7989
10.0%		0.5541
2.5%		0
0.5%		0
0.0%	minimum	0

Moments

Mean	66.795611
Std Dev	61.053951
Std Err Mean	3.7019395
Upper 95% Mean	74.083828
Lower 95% Mean	59.507395
N	272

mean Interburst Int

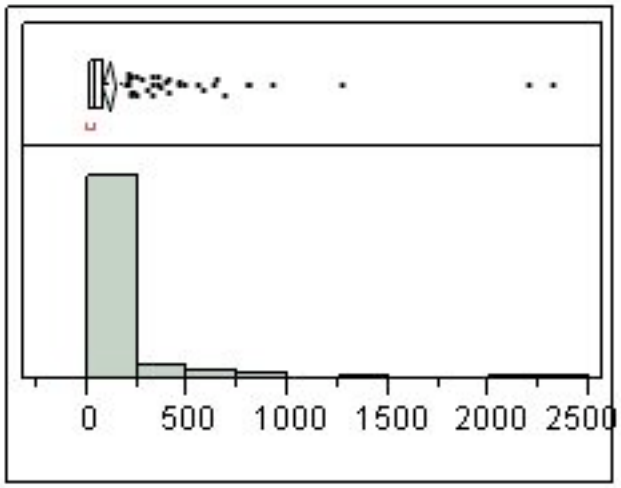

Quantiles

100.0%	maximum	2311.27
99.5%		2269.7
97.5%		697.043
90.0%		245.02
75.0%	quartile	84.2315
50.0%	median	36.3075
25.0%	quartile	18.5034
10.0%		0
2.5%		0
0.5%		0
0.0%	minimum	0

Moments

Mean	104.30988
Std Dev	242.97461
Std Err Mean	14.7325
Upper 95% Mean	133.31458
Lower 95% Mean	75.305175
N	272

Mean Sup

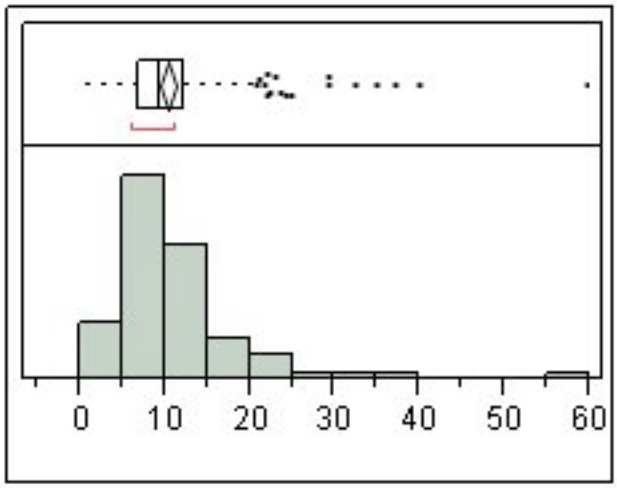

Quantiles

100.0%	maximum	59.8321
99.5%		52.5563
97.5%		29.2275
90.0%		18.0176
75.0%	quartile	12.3857
50.0%	median	9.43074
25.0%	quartile	6.92183
10.0%		4.12054
2.5%		0
0.5%		0
0.0%	minimum	0

Moments

Mean	10.35348
Std Dev	6.9004591
Std Err Mean	0.4184018
Upper 95% Mean	11.177211
Lower 95% Mean	9.5297488
N	272

Distributions Genotype=ko

mean freq

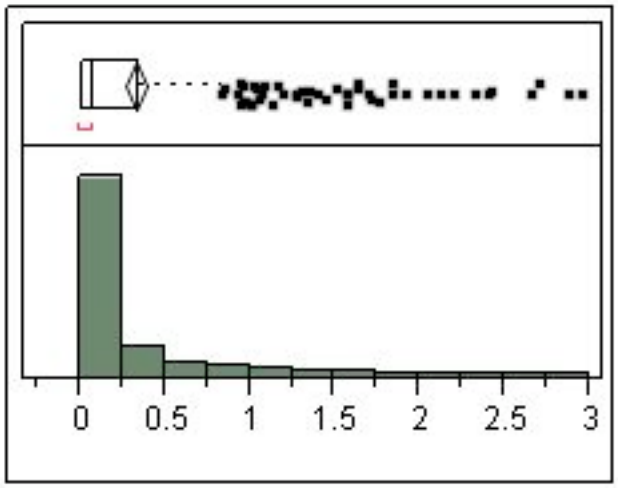

Quantiles

100.0%	maximum	2.95906
99.5%		2.89268
97.5%		2.13213
90.0%		1.07292
75.0%	quartile	0.339
50.0%	median	0.08248
25.0%	quartile	0.00942
10.0%		0.00182
2.5%		0.00035
0.5%		0.00035
0.0%	minimum	0.00035

Moments

Mean	0.3278029
Std Dev	0.5550562
Std Err Mean	0.0296267
Upper 95% Mean	0.3860716
Lower 95% Mean	0.2695341
N	351

numburst

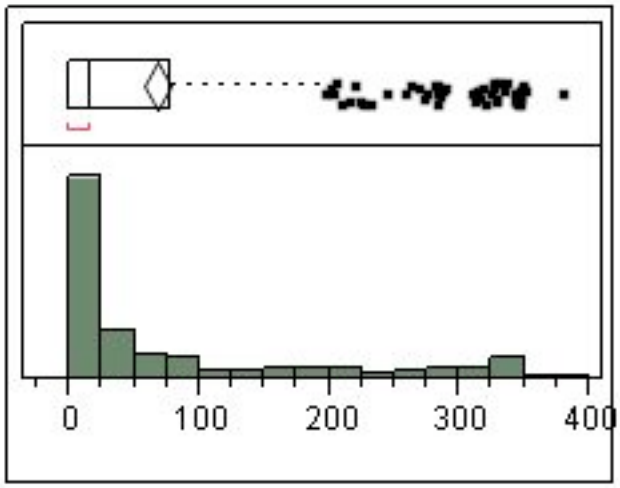

Quantiles

100.0%	maximum	380
99.5%		357.96
97.5%		345.2
90.0%		273.8
75.0%	quartile	78
50.0%	median	16
25.0%	quartile	0
10.0%		0
2.5%		0
0.5%		0
0.0%	minimum	0

Moments

Mean	67.700855
Std Dev	103.31734
Std Err Mean	5.5146717
Upper 95% Mean	78.546918
Lower 95% Mean	56.854791
N	351

bursts/sec

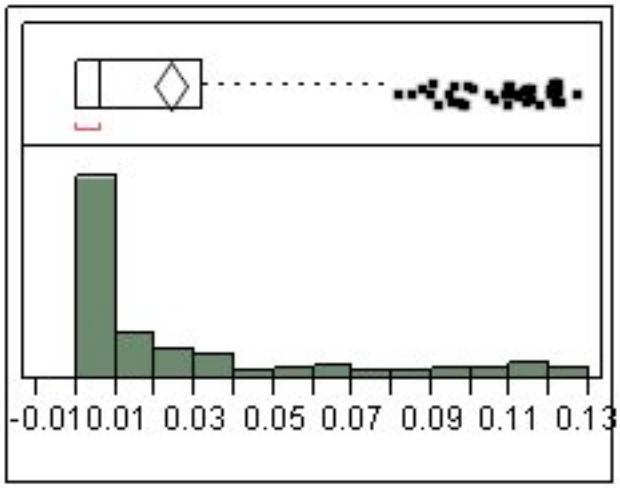

Quantiles

100.0%	maximum	0.12667
99.5%		0.12359
97.5%		0.12025
90.0%		0.09347
75.0%	quartile	0.03167
50.0%	median	0.00594
25.0%	quartile	0
10.0%		0
2.5%		0
0.5%		0
0.0%	minimum	0

Moments

Mean	0.0238237
Std Dev	0.0355275
Std Err Mean	0.0018963
Upper 95% Mean	0.0275533
Lower 95% Mean	0.020094
N	351

%spikes in burst

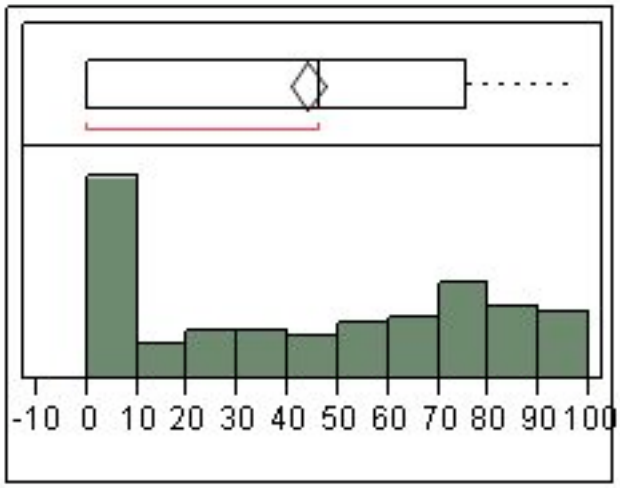

Quantiles

100.0%	maximum	97.7545
99.5%		96.8141
97.5%		94.1453
90.0%		89.0623
75.0%	quartile	75.4484
50.0%	median	46.4286
25.0%	quartile	0
10.0%		0
2.5%		0
0.5%		0
0.0%	minimum	0

Moments

Mean	43.917404
Std Dev	34.238648
Std Err Mean	1.8275238
Upper 95% Mean	47.511713
Lower 95% Mean	40.323094
N	351

mean burst dur

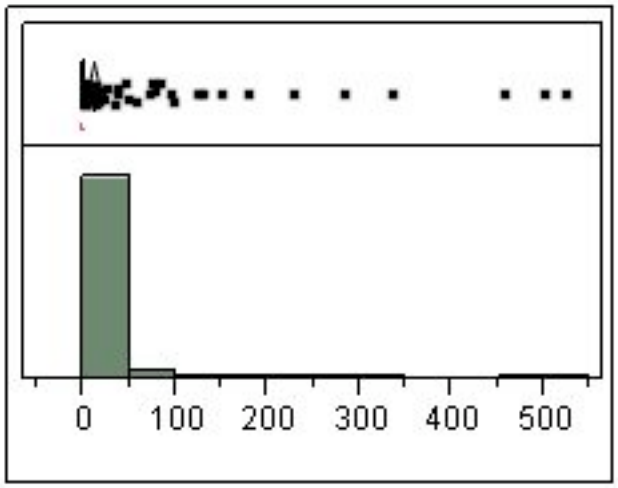

Quantiles

100.0%	maximum	524.213
99.5%		506.303
97.5%		134.623
90.0%		8.50589
75.0%	quartile	0.9958
50.0%	median	0.65359
25.0%	quartile	0
10.0%		0
2.5%		0
0.5%		0
0.0%	minimum	0

Moments

Mean	11.652904
Std Dev	55.456191
Std Err Mean	2.9600325
Upper 95% Mean	17.474593
Lower 95% Mean	5.831216
N	351

mean spikes/burst

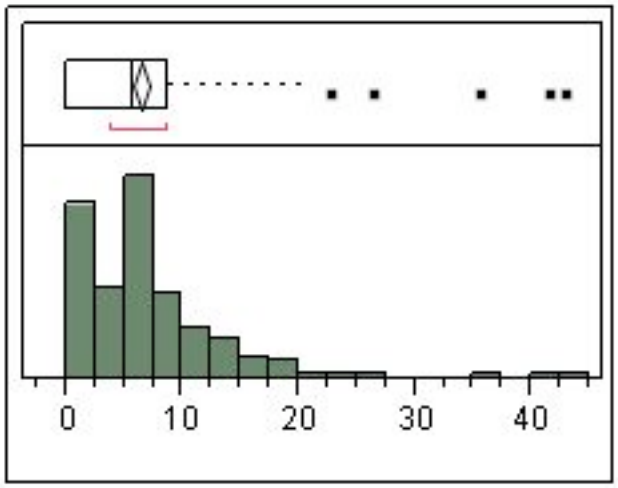

Quantiles

100.0%	maximum	43
99.5%		41.86
97.5%		19.5028
90.0%		13.6771
75.0%	quartile	8.73214
50.0%	median	5.69032
25.0%	quartile	0
10.0%		0
2.5%		0
0.5%		0
0.0%	minimum	0

Moments

Mean	6.4219293
Std Dev	5.939505
Std Err Mean	0.3170273
Upper 95% Mean	7.0454476
Lower 95% Mean	5.7984111
N	351

mean ISI

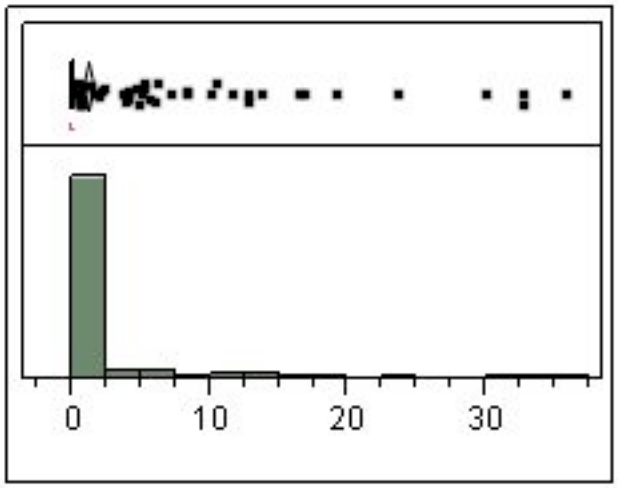

Quantiles

100.0%	maximum	35.7605
99.5%		33.4826
97.5%		14.2658
90.0%		1.1676
75.0%	quartile	0.16511
50.0%	median	0.09059
25.0%	quartile	0
10.0%		0
2.5%		0
0.5%		0
0.0%	minimum	0

Moments

Mean	1.1644375
Std Dev	4.3735547
Std Err Mean	0.2334431
Upper 95% Mean	1.6235652
Lower 95% Mean	0.7053098
N	351

Mean Freq in burst

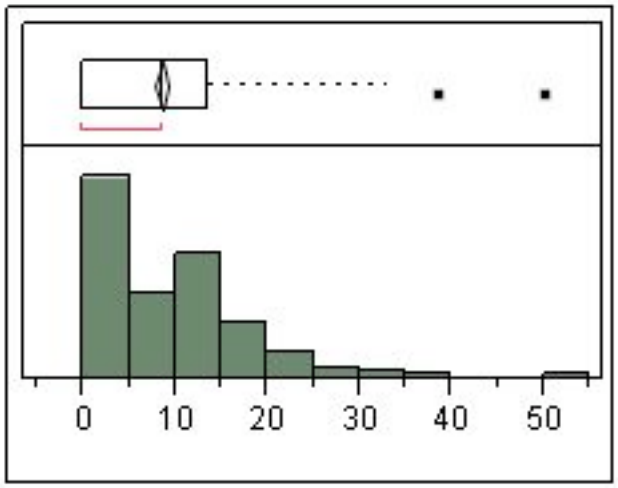

Quantiles

100.0%	maximum	50.0971
99.5%		41.2935
97.5%		26.061
90.0%		18.6722
75.0%	quartile	13.4628
50.0%	median	8.51864
25.0%	quartile	0
10.0%		0
2.5%		0
0.5%		0
0.0%	minimum	0

Moments

Mean	8.4952228
Std Dev	8.0938041
Std Err Mean	0.4320153
Upper 95% Mean	9.3448953
Lower 95% Mean	7.6455502
N	351

Mean Peak Freq

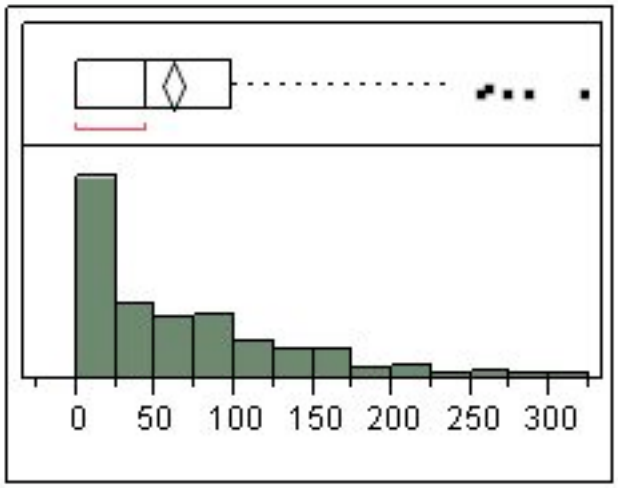

Quantiles

100.0%	maximum	321.05
99.5%		293.858
97.5%		223.595
90.0%		155.11
75.0%	quartile	97.7679
50.0%	median	43.8508
25.0%	quartile	0
10.0%		0
2.5%		0
0.5%		0
0.0%	minimum	0

Moments

Mean	61.540871
Std Dev	64.633549
Std Err Mean	3.4498836
Upper 95% Mean	68.325982
Lower 95% Mean	54.755761
N	351

mean Interburst Int

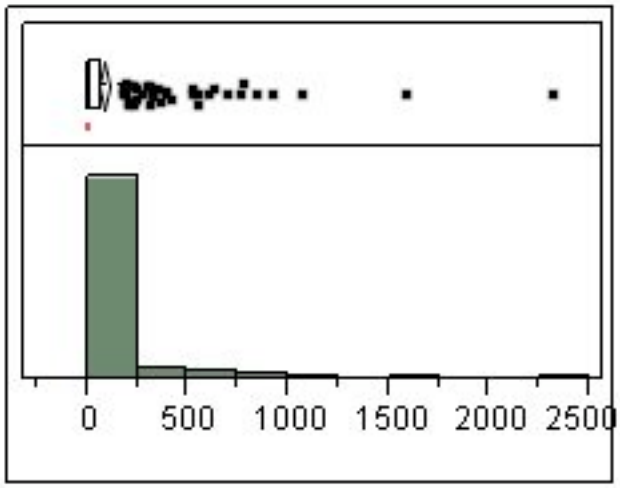

Quantiles

100.0%	maximum	2311.27
99.5%		1760.6
97.5%		644.881
90.0%		202.143
75.0%	quartile	69.2513
50.0%	median	15.8549
25.0%	quartile	0
10.0%		0
2.5%		0
0.5%		0
0.0%	minimum	0

Moments

Mean	81.528635
Std Dev	203.93682
Std Err Mean	10.885342
Upper 95% Mean	102.93755
Lower 95% Mean	60.119726
N	351

Mean Sup

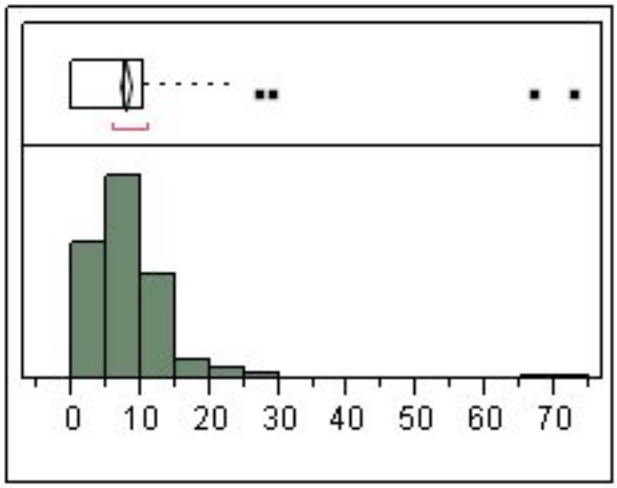

Quantiles

100.0%	maximum	72.6375
99.5%		68.2958
97.5%		20.9411
90.0%		13.4055
75.0%	quartile	10.3149
50.0%	median	7.94637
25.0%	quartile	0
10.0%		0
2.5%		0
0.5%		0
0.0%	minimum	0

Moments

Mean	7.5951892
Std Dev	7.1289545
Std Err Mean	0.3805154
Upper 95% Mean	8.3435737
Lower 95% Mean	6.8468048
N	351

Distributions Genotype=wt

mean freq

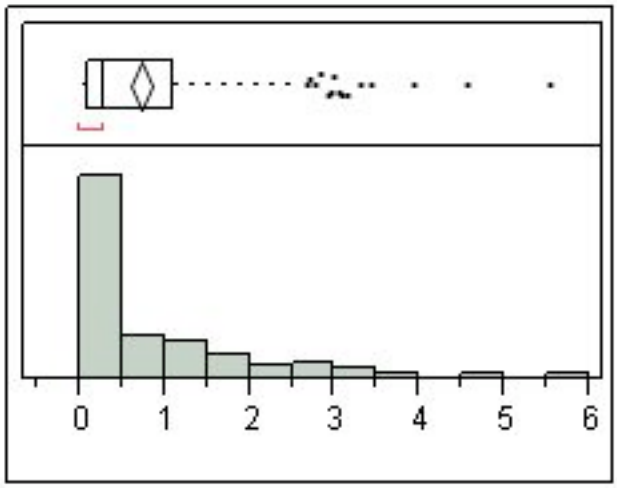

Quantiles

100.0%	maximum	5.54082
99.5%		5.33492
97.5%		3.1273
90.0%		2.04134
75.0%	quartile	1.10972
50.0%	median	0.28267
25.0%	quartile	0.1045
10.0%		0.0334
2.5%		0.00435
0.5%		0.00147
0.0%	minimum	0.00133

Moments

Mean	0.7267291
Std Dev	0.9248098
Std Err Mean	0.0595722
Upper 95% Mean	0.8440803
Lower 95% Mean	0.6093779
N	241

numburst

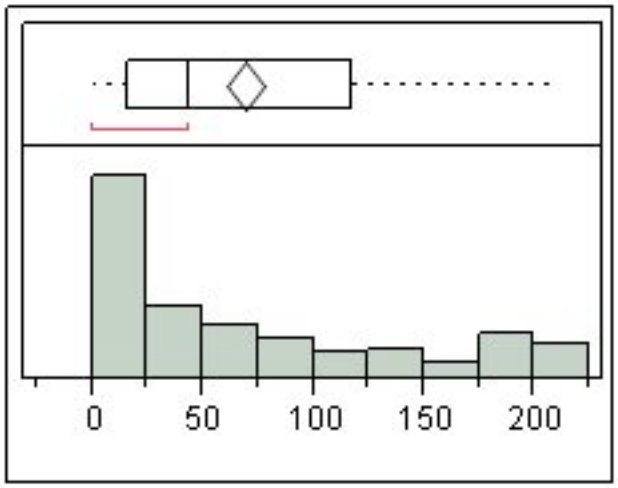

Quantiles

100.0%	maximum	210
99.5%		209.58
97.5%		206.9
90.0%		189.8
75.0%	quartile	117
50.0%	median	44
25.0%	quartile	16
10.0%		9
2.5%		1
0.5%		0
0.0%	minimum	0

Moments

Mean	69.684647
Std Dev	66.531259
Std Err Mean	4.2856552
Upper 95% Mean	78.126949
Lower 95% Mean	61.242345
N	241

bursts/sec

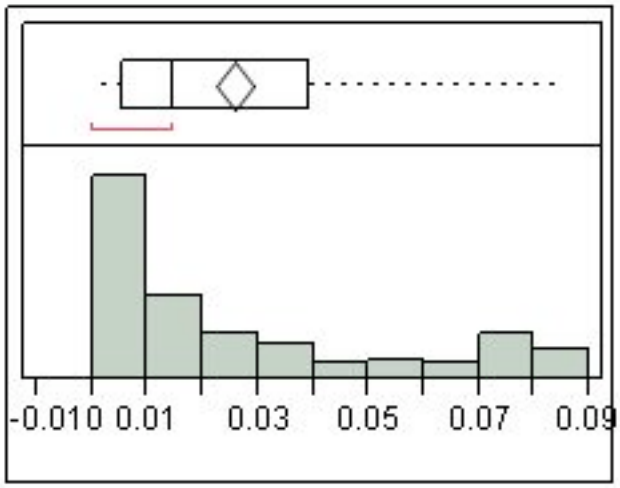

Quantiles

100.0%	maximum	0.08363
99.5%		0.08346
97.5%		0.0824
90.0%		0.07559
75.0%	quartile	0.03917
50.0%	median	0.01467
25.0%	quartile	0.00533
10.0%		0.003
2.5%		0.00033
0.5%		0
0.0%	minimum	0

Moments

Mean	0.0257908
Std Dev	0.026599
Std Err Mean	0.0017134
Upper 95% Mean	0.0291661
Lower 95% Mean	0.0224156
N	241

%spikes in burst

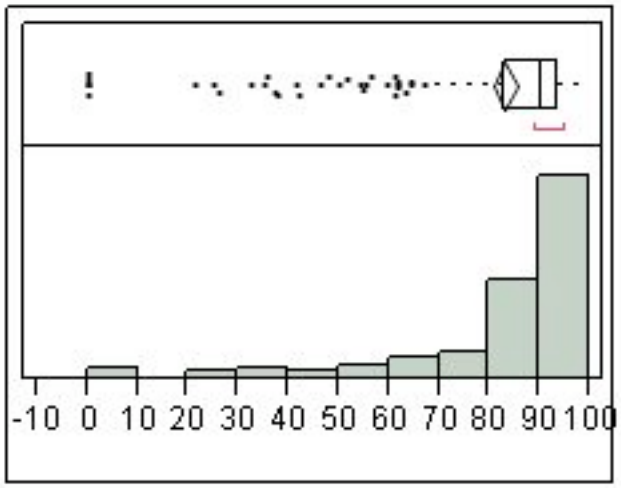

Quantiles

100.0%	maximum	99.2383
99.5%		99.0455
97.5%		97.2939
90.0%		94.9551
75.0%	quartile	93.4017
50.0%	median	90.5724
25.0%	quartile	82.8942
10.0%		59.9372
2.5%		21.693
0.5%		0
0.0%	minimum	0

Moments

Mean	83.066877
Std Dev	19.160309
Std Err Mean	1.234224
Upper 95% Mean	85.498172
Lower 95% Mean	80.635582
N	241

mean burst dur

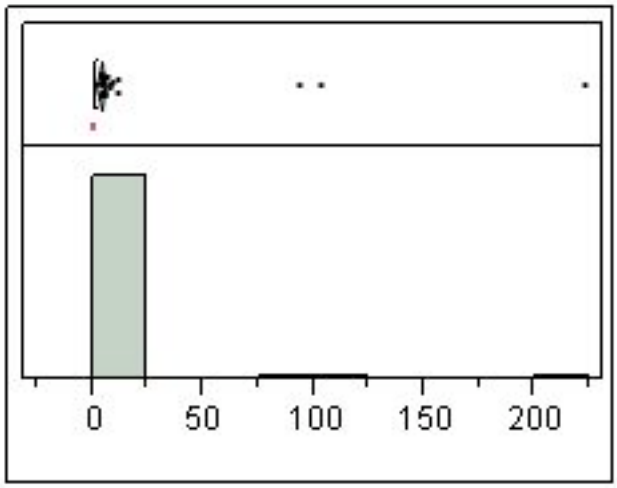

Quantiles

100.0%	maximum	222.571
99.5%		197.485
97.5%		8.46255
90.0%		3.91737
75.0%	quartile	2.1495
50.0%	median	1.43241
25.0%	quartile	1.07521
10.0%		0.80973
2.5%		0.33373
0.5%		0
0.0%	minimum	0

Moments

Mean	3.6445387
Std Dev	16.73586
Std Err Mean	1.0780515
Upper 95% Mean	5.7681898
Lower 95% Mean	1.5208877
N	241

mean spikes/burst

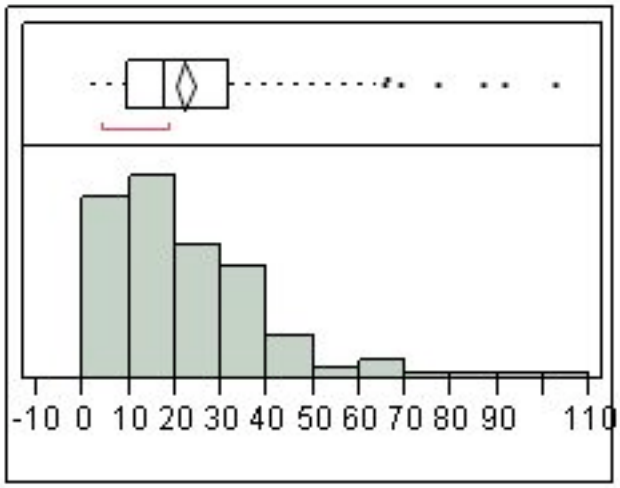

Quantiles

100.0%	maximum	102.458
99.5%		100.129
97.5%		65.7038
90.0%		42.7268
75.0%	quartile	31.5
50.0%	median	17.8302
25.0%	quartile	9.87951
10.0%		6
2.5%		4.01667
0.5%		0
0.0%	minimum	0

Moments

Mean	22.139734
Std Dev	16.630746
Std Err Mean	1.0712805
Upper 95% Mean	24.250047
Lower 95% Mean	20.029421
N	241

mean ISI

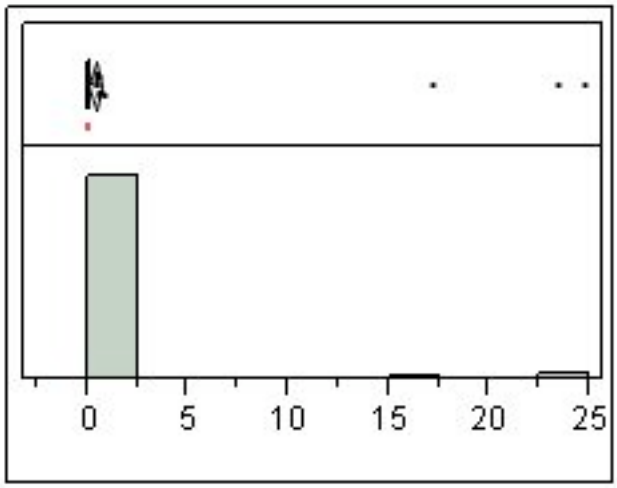

Quantiles

100.0%	maximum	24.7301
99.5%		24.4579
97.5%		0.55552
90.0%		0.26253
75.0%	quartile	0.17331
50.0%	median	0.09114
25.0%	quartile	0.05303
10.0%		0.03647
2.5%		0.02068
0.5%		0
0.0%	minimum	0

Moments

Mean	0.3944242
Std Dev	2.4368624
Std Err Mean	0.1569721
Upper 95% Mean	0.7036432
Lower 95% Mean	0.0852052
N	241

Mean Freq in burst

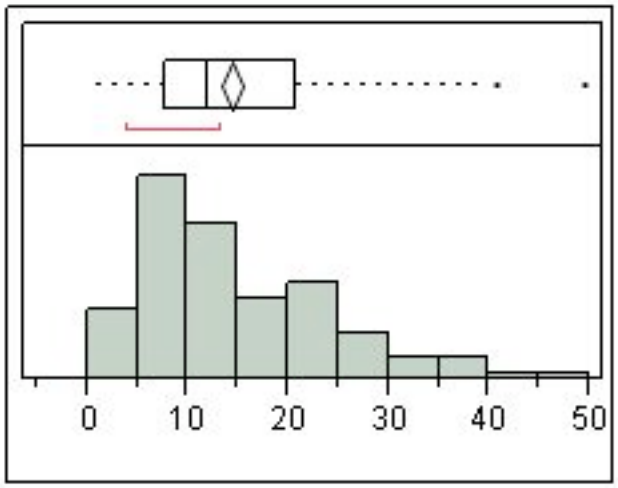

Quantiles

100.0%	maximum	49.5397
99.5%		47.6775
97.5%		36.795
90.0%		26.6944
75.0%	quartile	20.8033
50.0%	median	11.9748
25.0%	quartile	7.75733
10.0%		4.57353
2.5%		0.04055
0.5%		0
0.0%	minimum	0

Moments

Mean	14.391008
Std Dev	9.2214996
Std Err Mean	0.594009
Upper 95% Mean	15.561145
Lower 95% Mean	13.220871
N	241

Mean Peak Freq

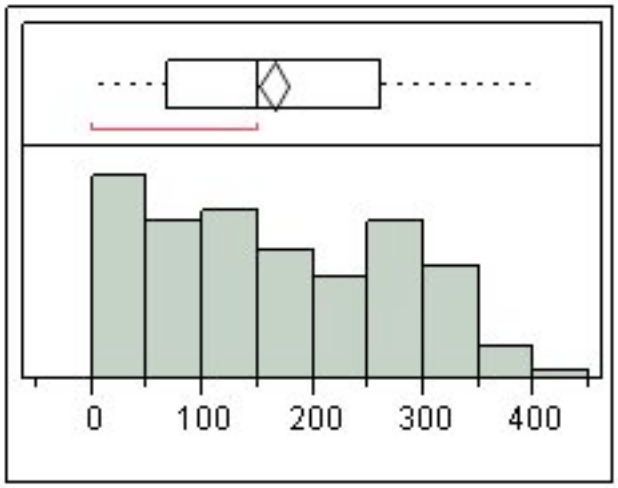

Quantiles

100.0%	maximum	407.159
99.5%		399.213
97.5%		351.769
90.0%		306.336
75.0%	quartile	261.191
50.0%	median	151.004
25.0%	quartile	69.5342
10.0%		21.6552
2.5%		3.88495
0.5%		0
0.0%	minimum	0

Moments

Mean	163.79805
Std Dev	107.17579
Std Err Mean	6.9037996
Upper 95% Mean	177.39782
Lower 95% Mean	150.19827
N	241

mean Interburst Int

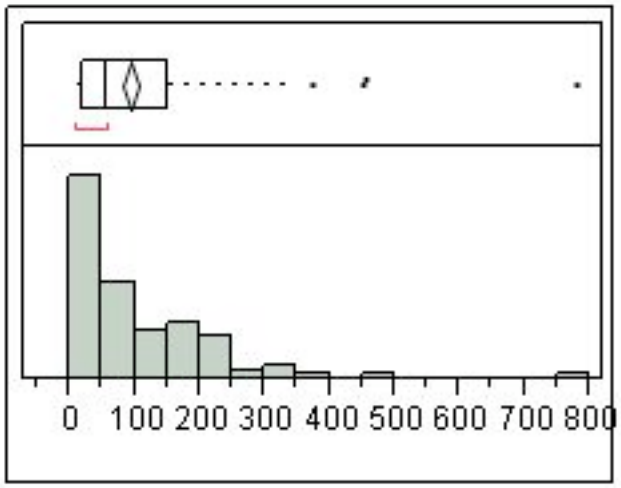

Quantiles

100.0%	maximum	779.975
99.5%		711.428
97.5%		330.035
90.0%		208.703
75.0%	quartile	152.882
50.0%	median	57.1276
25.0%	quartile	18.8938
10.0%		12.531
2.5%		0
0.5%		0
0.0%	minimum	0

Moments

Mean	93.349358
Std Dev	98.714019
Std Err Mean	6.3587289
Upper 95% Mean	105.8754
Lower 95% Mean	80.823313
N	241

Mean Sup

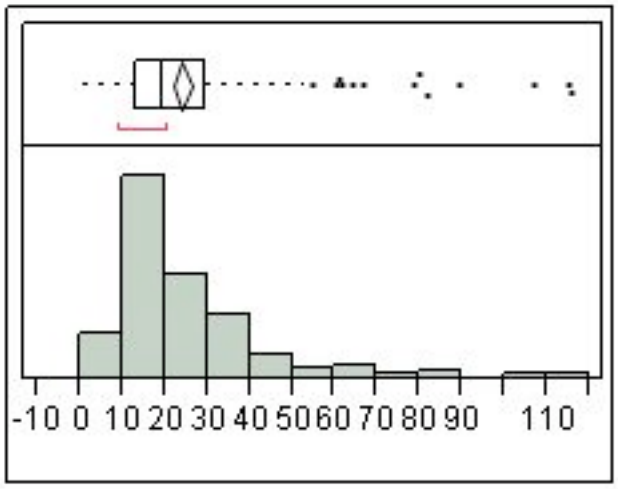

Quantiles

100.0%	maximum	115.68
99.5%		115.488
97.5%		80.0014
90.0%		41.2511
75.0%	quartile	29.3819
50.0%	median	19.2536
25.0%	quartile	13.0313
10.0%		10.0447
2.5%		4.243
0.5%		0
0.0%	minimum	0

Moments

Mean	24.007964
Std Dev	17.508759
Std Err Mean	1.1278383
Upper 95% Mean	26.22969
Lower 95% Mean	21.786238
N	241

P14

Distributions Genotype= WT

mean freq

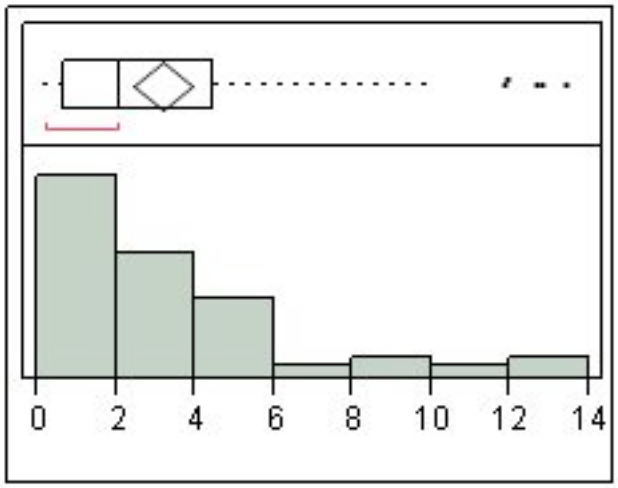

Quantiles

100.0%	maximum	13.4187
99.5%		13.4187
97.5%		12.8226
90.0%		8.30553
75.0%	quartile	4.45958
50.0%	median	2.07817
25.0%	quartile	0.70308
10.0%		0.37893
2.5%		0.03467
0.5%		0.03467
0.0%	minimum	0.03467

Moments

Mean	3.1957436
Std Dev	3.2610372
Std Err Mean	0.3692398
Upper 95% Mean	3.9309939
Lower 95% Mean	2.4604933
N	78

numburst

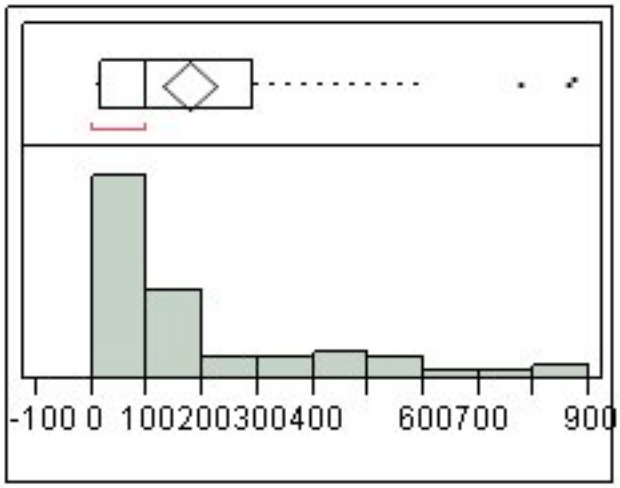

Quantiles

100.0%	maximum	872
99.5%		872
97.5%		862.25
90.0%		506.4
75.0%	quartile	292.75
50.0%	median	97
25.0%	quartile	16.75
10.0%		4
2.5%		0
0.5%		0
0.0%	minimum	0

Moments

Mean	174.88462
Std Dev	211.94853
Std Err Mean	23.998446
Upper 95% Mean	222.67163
Lower 95% Mean	127.0976
N	78

bursts/sec

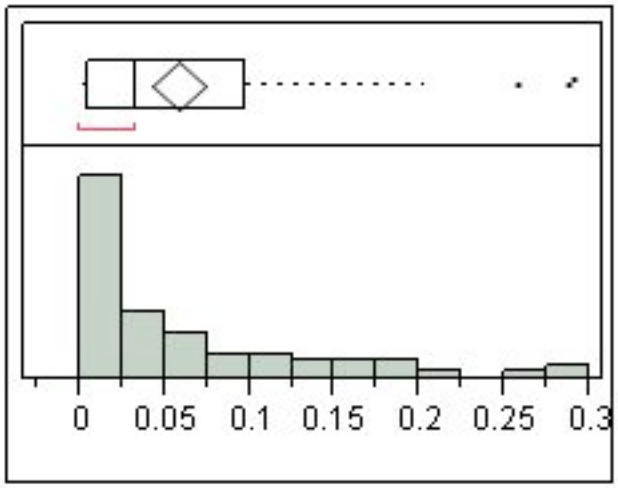

Quantiles

100.0%	maximum	0.29067
99.5%		0.29067
97.5%		0.28742
90.0%		0.1688
75.0%	quartile	0.09758
50.0%	median	0.03233
25.0%	quartile	0.00558
10.0%		0.00133
2.5%		0
0.5%		0
0.0%	minimum	0

Moments

Mean	0.0582948
Std Dev	0.0706495
Std Err Mean	0.0079995
Upper 95% Mean	0.0742238
Lower 95% Mean	0.0423658
N	78

%spikes in burst

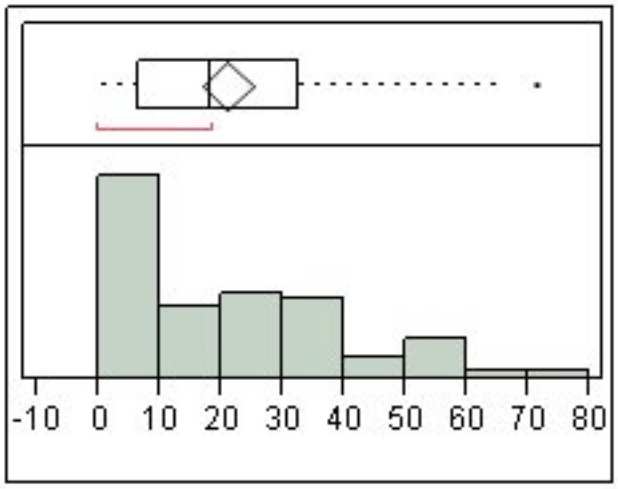

Quantiles

100.0%	maximum	71.2984
99.5%		71.2984
97.5%		66.6402
90.0%		50.403
75.0%	quartile	32.4043
50.0%	median	18.2354
25.0%	quartile	6.61484
10.0%		1.30254
2.5%		0
0.5%		0
0.0%	minimum	0

Moments

Mean	21.082311
Std Dev	17.767623
Std Err Mean	2.0117871
Upper 95% Mean	25.088291
Lower 95% Mean	17.076331
N	78

mean burst dur

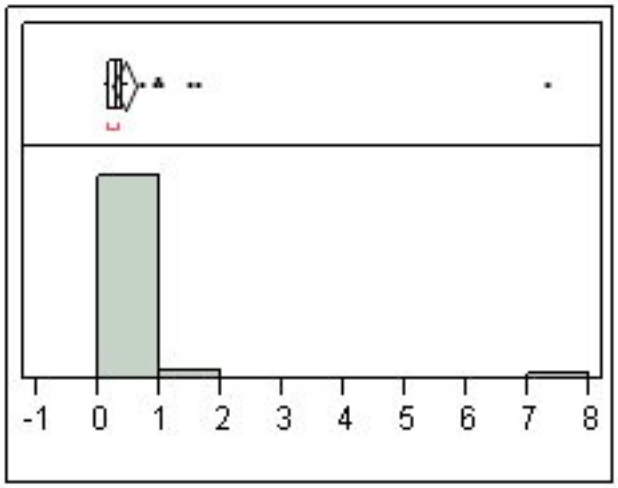

Quantiles

100.0%	maximum	7.30963
99.5%		7.30963
97.5%		1.76628
90.0%		0.58431
75.0%	quartile	0.38871
50.0%	median	0.28785
25.0%	quartile	0.19533
10.0%		0.13238
2.5%		0
0.5%		0
0.0%	minimum	0

Moments

Mean	0.4244457
Std Dev	0.834113
Std Err Mean	0.0944447
Upper 95% Mean	0.6125091
Lower 95% Mean	0.2363823
N	78

mean spikes/burst

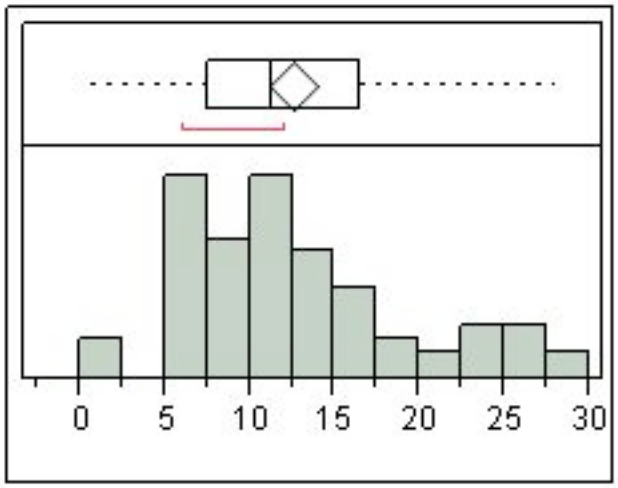

Quantiles

100.0%	maximum	28
99.5%		28
97.5%		27.743
90.0%		23.2577
75.0%	quartile	16.4247
50.0%	median	11.2914
25.0%	quartile	7.54348
10.0%		6.23676
2.5%		0
0.5%		0
0.0%	minimum	0

Moments

Mean	12.566005
Std Dev	6.4702109
Std Err Mean	0.7326071
Upper 95% Mean	14.024812
Lower 95% Mean	11.107198
N	78

mean ISI

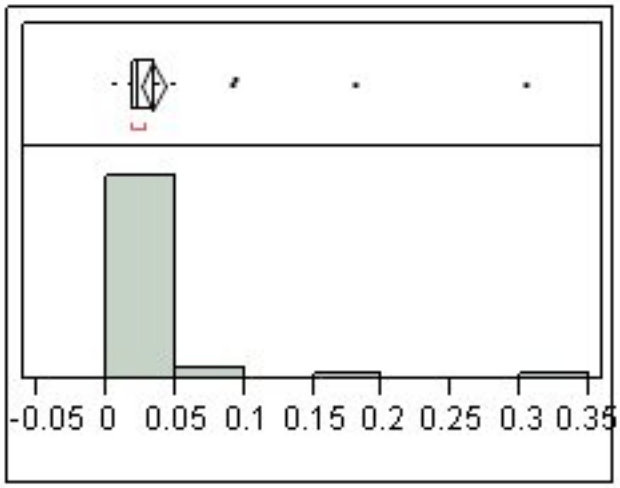

Quantiles

100.0%	maximum	0.30406
99.5%		0.30406
97.5%		0.18355
90.0%		0.04716
75.0%	quartile	0.0355
50.0%	median	0.02401
25.0%	quartile	0.02023
10.0%		0.01437
2.5%		0
0.5%		0
0.0%	minimum	0

Moments

Mean	0.0337551
Std Dev	0.0385221
Std Err Mean	0.0043618
Upper 95% Mean	0.0424405
Lower 95% Mean	0.0250697
N	78

Mean Freq in burst

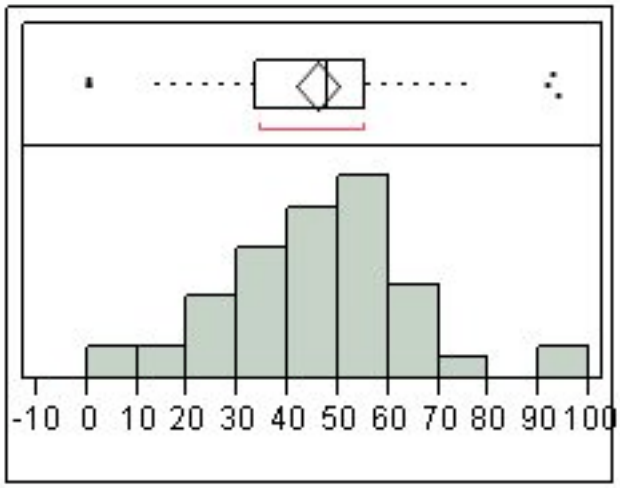

Quantiles

100.0%	maximum	93.4268
99.5%		93.4268
97.5%		92.5706
90.0%		66.7565
75.0%	quartile	55.1168
50.0%	median	47.9723
25.0%	quartile	33.3645
10.0%		21.1851
2.5%		0
0.5%		0
0.0%	minimum	0

Moments

Mean	45.860454
Std Dev	19.06313
Std Err Mean	2.1584744
Upper 95% Mean	50.158526
Lower 95% Mean	41.562383
N	78

Mean Peak Freq

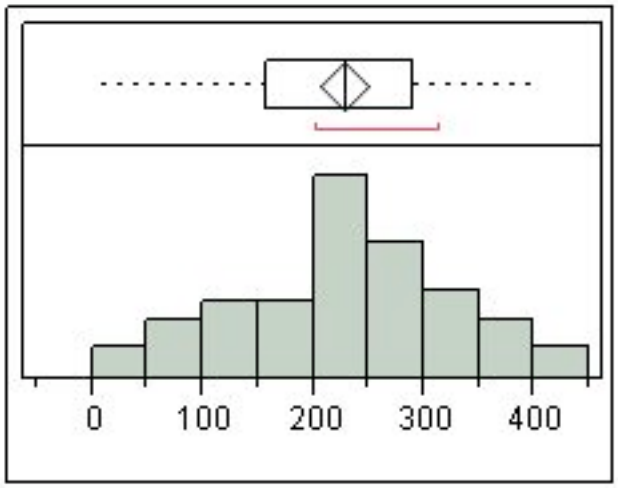

Quantiles

100.0%	maximum	405.577
99.5%		405.577
97.5%		404.533
90.0%		361.032
75.0%	quartile	289.756
50.0%	median	231.26
25.0%	quartile	157.349
10.0%		77.8983
2.5%		0
0.5%		0
0.0%	minimum	0

Moments

Mean	227.04809
Std Dev	96.482434
Std Err Mean	10.924484
Upper 95% Mean	248.80152
Lower 95% Mean	205.29467
N	78

mean Interburst Int

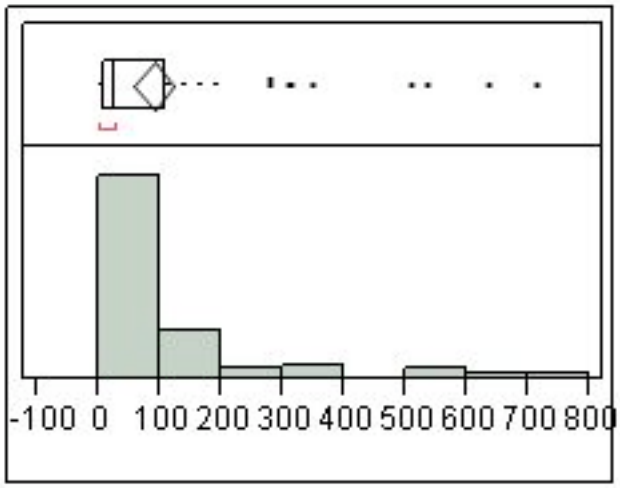

Quantiles

100.0%	maximum	713.706
99.5%		713.706
97.5%		637.941
90.0%		281.23
75.0%	quartile	109.917
50.0%	median	24.6096
25.0%	quartile	9.65398
10.0%		5.27541
2.5%		0
0.5%		0
0.0%	minimum	0

Moments

Mean	90.671946
Std Dev	144.96083
Std Err Mean	16.413582
Upper 95% Mean	123.35556
Lower 95% Mean	57.988329
N	78

Mean Sup

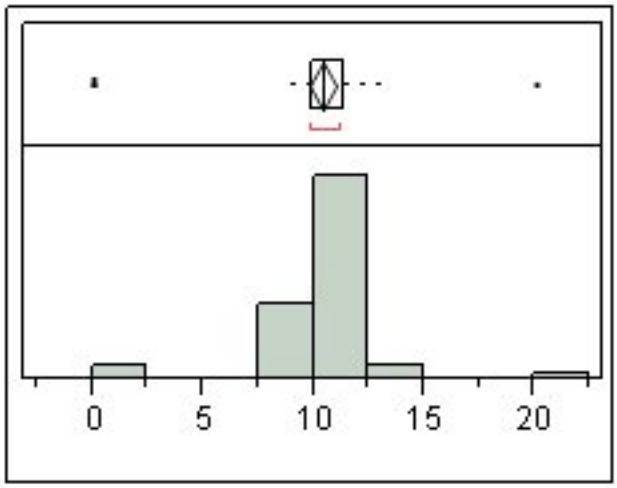

Quantiles

100.0%	maximum	20.0798
99.5%		20.0798
97.5%		13.705
90.0%		12.152
75.0%	quartile	11.4
50.0%	median	10.5836
25.0%	quartile	9.9541
10.0%		9.42572
2.5%		0
0.5%		0
0.0%	minimum	0

Moments

Mean	10.420007
Std Dev	2.5440264
Std Err Mean	0.2880543
Upper 95% Mean	10.993596
Lower 95% Mean	9.8464172
N	78

Distributions Genotype=het

mean freq

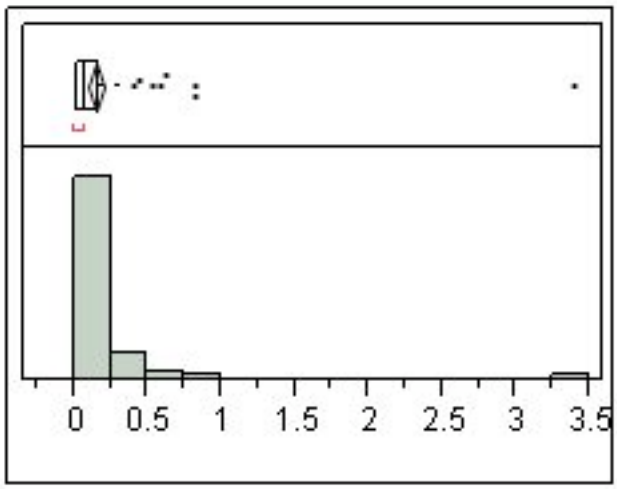

Quantiles

100.0%	maximum	3.38882
99.5%		3.38882
97.5%		0.75038
90.0%		0.31988
75.0%	quartile	0.17473
50.0%	median	0.08365
25.0%	quartile	0.02772
10.0%		0.00512
2.5%		0.00058
0.5%		0.00036
0.0%	minimum	0.00036

Moments

Mean	0.1525206
Std Dev	0.3210483
Std Err Mean	0.0279437
Upper 95% Mean	0.2077999
Lower 95% Mean	0.0972414
N	132

numburst

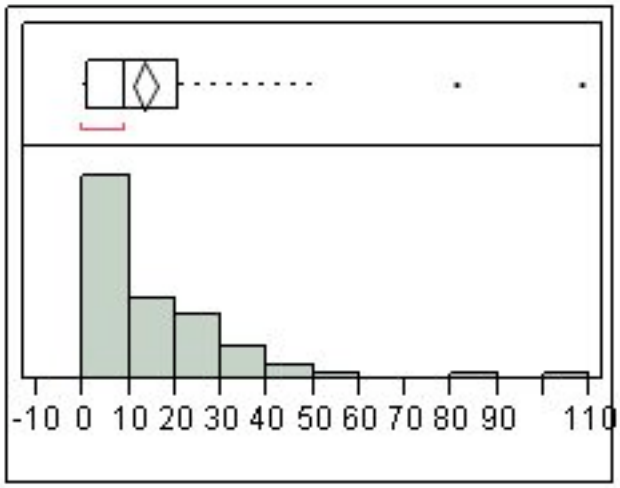

Quantiles

100.0%	maximum	108
99.5%		108
97.5%		48.05
90.0%		31.7
75.0%	quartile	21
50.0%	median	9
25.0%	quartile	1
10.0%		0
2.5%		0
0.5%		0
0.0%	minimum	0

Moments

Mean	13.469697
Std Dev	15.947164
Std Err Mean	1.3880225
Upper 95% Mean	16.215537
Lower 95% Mean	10.723857
N	132

bursts/sec

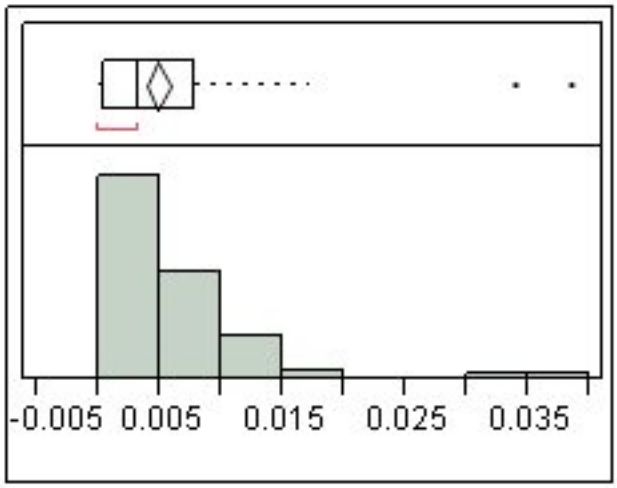

Quantiles

100.0%	maximum	0.03854
99.5%		0.03854
97.5%		0.01706
90.0%		0.01125
75.0%	quartile	0.00791
50.0%	median	0.00321
25.0%	quartile	0.00036
10.0%		0
2.5%		0
0.5%		0
0.0%	minimum	0

Moments

Mean	0.0048457
Std Dev	0.0058483
Std Err Mean	0.000509
Upper 95% Mean	0.0058527
Lower 95% Mean	0.0038388
N	132

%spikes in burst

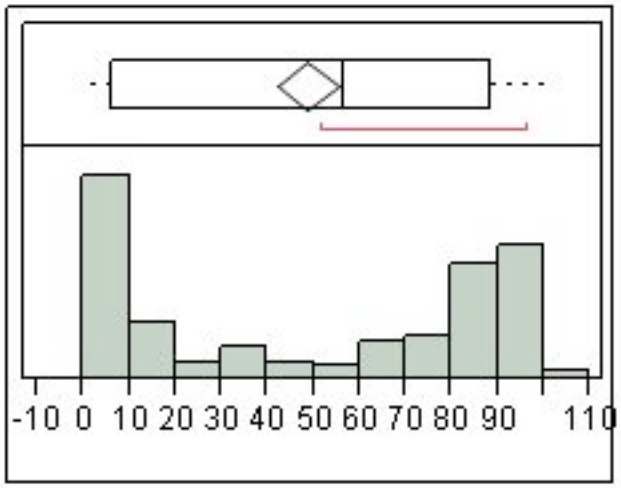

Quantiles

100.0%	maximum	100
99.5%		100
97.5%		96.0499
90.0%		92.7368
75.0%	quartile	88.4589
50.0%	median	56.8648
25.0%	quartile	6.32149
10.0%		0
2.5%		0
0.5%		0
0.0%	minimum	0

Moments

Mean	48.65235
Std Dev	39.012224
Std Err Mean	3.3955783
Upper 95% Mean	55.369613
Lower 95% Mean	41.935086
N	132

mean burst dur

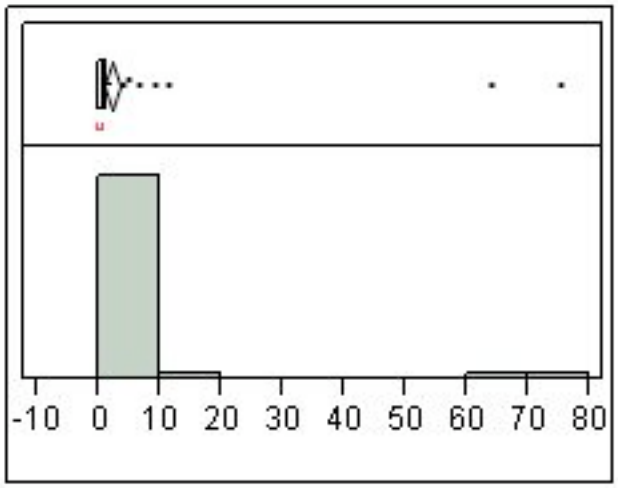

Quantiles

100.0%	maximum	75.2536
99.5%		75.2536
97.5%		10.4208
90.0%		2.63232
75.0%	quartile	1.47827
50.0%	median	0.75538
25.0%	quartile	0.18337
10.0%		0
2.5%		0
0.5%		0
0.0%	minimum	0

Moments

Mean	2.1451866
Std Dev	8.5560421
Std Err Mean	0.7447079
Upper 95% Mean	3.6183964
Lower 95% Mean	0.6719768
N	132

mean spikes/burst

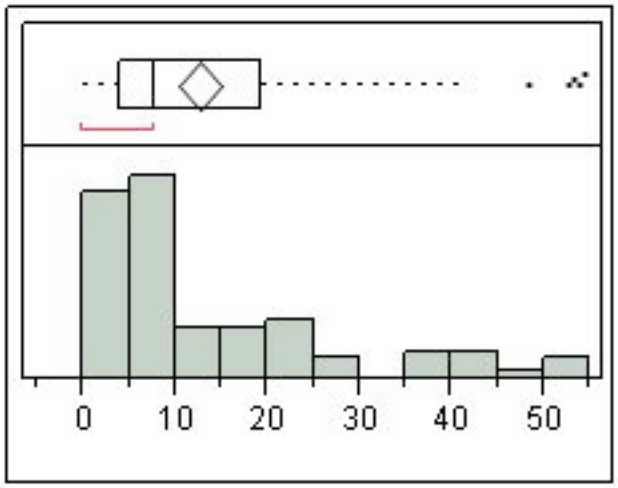

Quantiles

100.0%	maximum	54.3333
99.5%		54.3333
97.5%		53.0363
90.0%		38.9694
75.0%	quartile	19.2756
50.0%	median	7.73333
25.0%	quartile	4
10.0%		0
2.5%		0
0.5%		0
0.0%	minimum	0

Moments

Mean	12.639676
Std Dev	13.601023
Std Err Mean	1.1838171
Upper 95% Mean	14.981549
Lower 95% Mean	10.297803
N	132

mean ISI

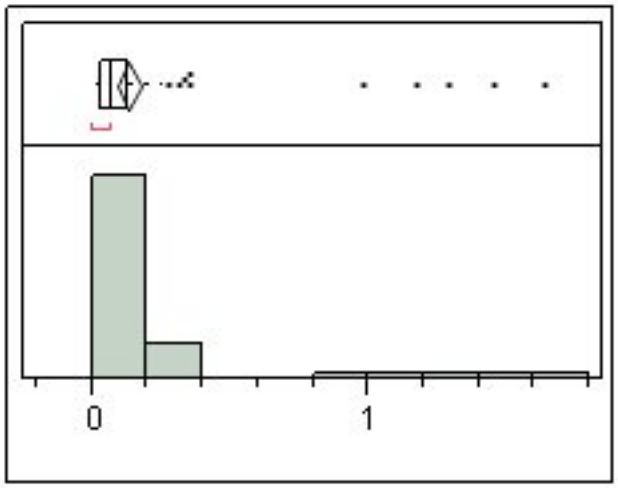

Quantiles

100.0%	maximum	1.63645
99.5%		1.63645
97.5%		1.25044
90.0%		0.24085
75.0%	quartile	0.12586
50.0%	median	0.06725
25.0%	quartile	0.03044
10.0%		0
2.5%		0
0.5%		0
0.0%	minimum	0

Moments

Mean	0.1312987
Std Dev	0.2518069
Std Err Mean	0.021917
Upper 95% Mean	0.1746557
Lower 95% Mean	0.0879416
N	132

Mean Freq in burst

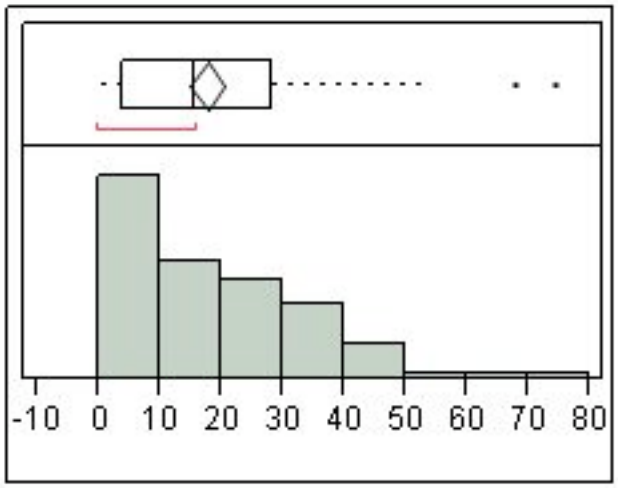

Quantiles

100.0%	maximum	74.2942
99.5%		74.2942
97.5%		52.7184
90.0%		38.928
75.0%	quartile	28.1286
50.0%	median	15.8229
25.0%	quartile	3.78143
10.0%		0
2.5%		0
0.5%		0
0.0%	minimum	0

Moments

Mean	17.661484
Std Dev	15.553425
Std Err Mean	1.3537519
Upper 95% Mean	20.339528
Lower 95% Mean	14.98344
N	132

Mean Peak Freq

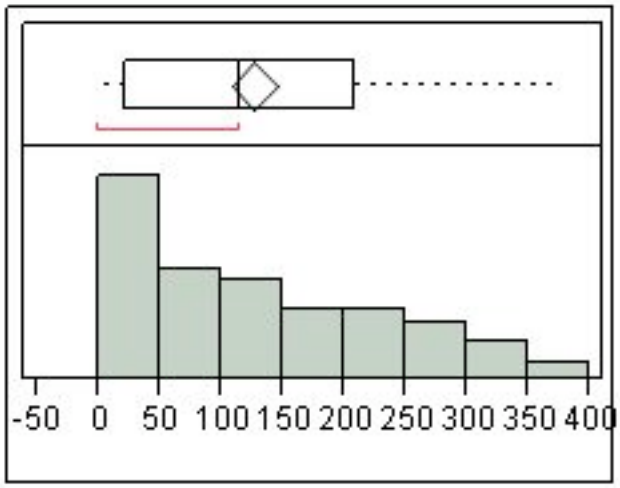

Quantiles

100.0%	maximum	378.861
99.5%		378.861
97.5%		352.548
90.0%		288.546
75.0%	quartile	208.5
50.0%	median	114.535
25.0%	quartile	21.3659
10.0%		0
2.5%		0
0.5%		0
0.0%	minimum	0

Moments

Mean	126.29378
Std Dev	107.94505
Std Err Mean	9.3954106
Upper 95% Mean	144.88015
Lower 95% Mean	107.70742
N	132

mean Interburst Int

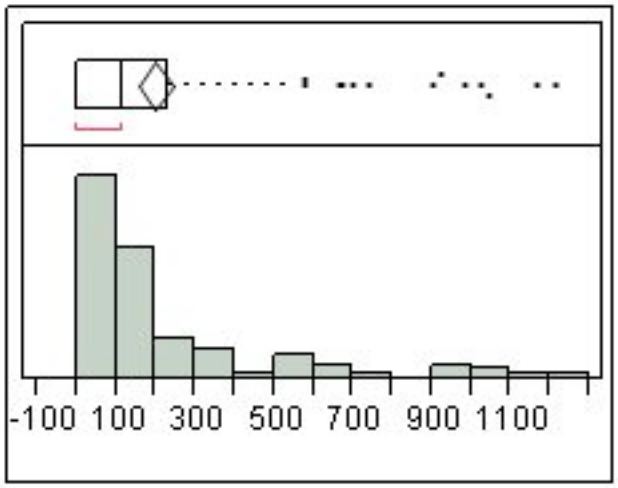

Quantiles

100.0%	maximum	1208.86
99.5%		1208.86
97.5%		1034.99
90.0%		567.686
75.0%	quartile	228.876
50.0%	median	115.023
25.0%	quartile	0
10.0%		0
2.5%		0
0.5%		0
0.0%	minimum	0

Moments

Mean	200.7014
Std Dev	260.35908
Std Err Mean	22.661349
Upper 95% Mean	245.53095
Lower 95% Mean	155.87185
N	132

Mean Sup

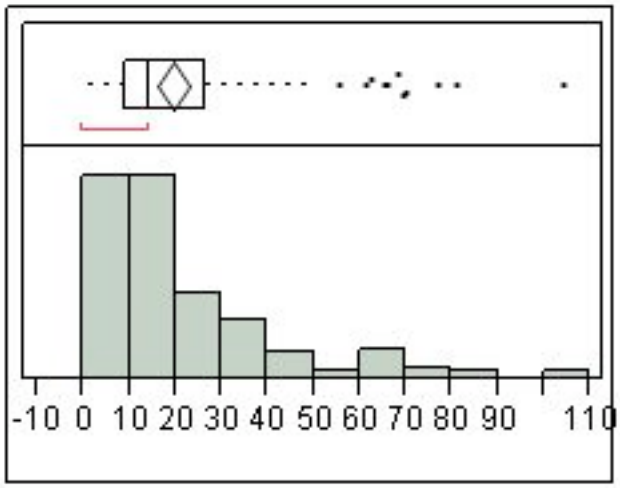

Quantiles

100.0%	maximum	104.309
99.5%		104.309
97.5%		74.7947
90.0%		43.2873
75.0%	quartile	26.4502
50.0%	median	14.4264
25.0%	quartile	9.26576
10.0%		0
2.5%		0
0.5%		0
0.0%	minimum	0

Moments

Mean	19.690421
Std Dev	19.791153
Std Err Mean	1.7225988
Upper 95% Mean	23.098133
Lower 95% Mean	16.28271
N	132

Distributions Genotype=ko

mean freq

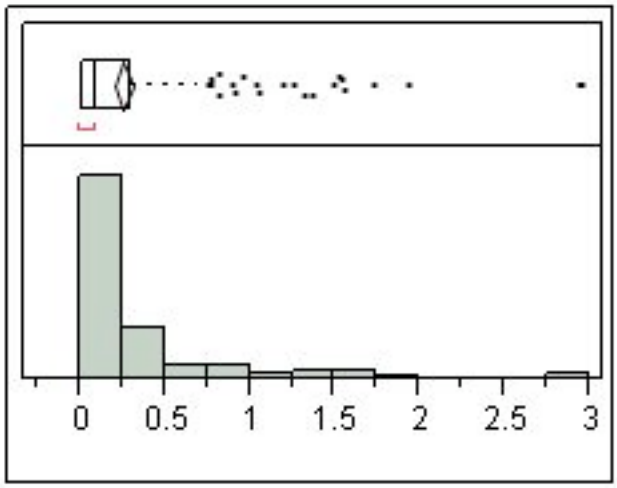

Quantiles

100.0%	maximum	2.94967
99.5%		2.94815
97.5%		1.54603
90.0%		0.76001
75.0%	quartile	0.30667
50.0%	median	0.08867
25.0%	quartile	0.02087
10.0%		0.00391
2.5%		0.00054
0.5%		0
0.0%	minimum	0

Moments

Mean	0.2594594
Std Dev	0.4403844
Std Err Mean	0.0298266
Upper 95% Mean	0.3182463
Lower 95% Mean	0.2006725
N	218

numburst

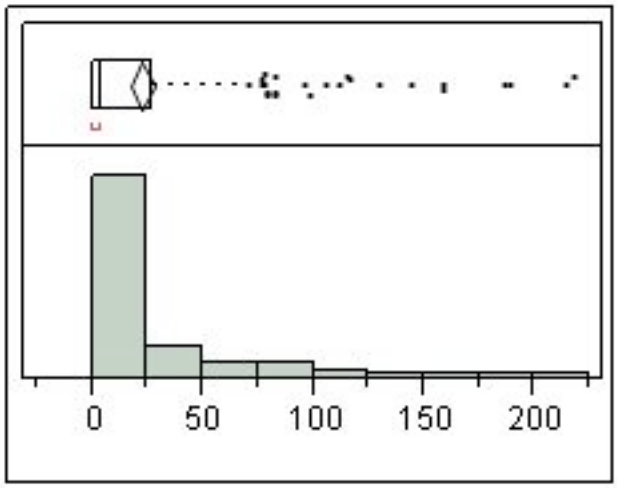

Quantiles

100.0%	maximum	218
99.5%		217.62
97.5%		158.525
90.0%		77.1
75.0%	quartile	27
50.0%	median	4
25.0%	quartile	0
10.0%		0
2.5%		0
0.5%		0
0.0%	minimum	0

Moments

Mean	22.325688
Std Dev	39.831435
Std Err Mean	2.6977252
Upper 95% Mean	27.642787
Lower 95% Mean	17.00859
N	218

bursts/sec

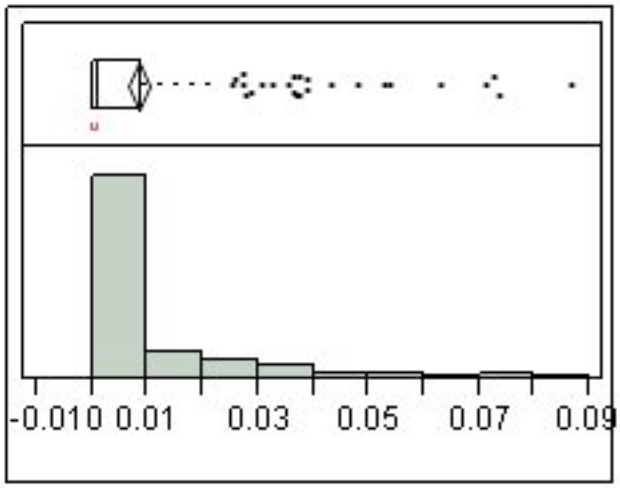

Quantiles

100.0%	maximum	0.08664
99.5%		0.0854
97.5%		0.05852
90.0%		0.02737
75.0%	quartile	0.009
50.0%	median	0.00133
25.0%	quartile	0
10.0%		0
2.5%		0
0.5%		0
0.0%	minimum	0

Moments

Mean	0.0083193
Std Dev	0.0149339
Std Err Mean	0.0010115
Upper 95% Mean	0.0103128
Lower 95% Mean	0.0063258
N	218

%spikes in burst

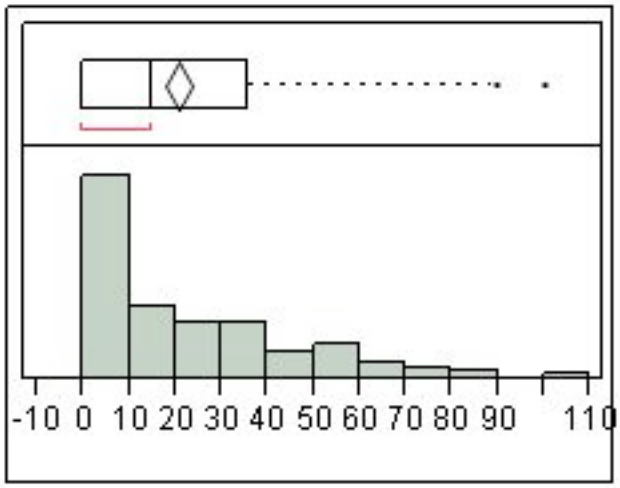

Quantiles

100.0%	maximum	100
99.5%		99.0058
97.5%		74.936
90.0%		54.3588
75.0%	quartile	35.808
50.0%	median	14.8039
25.0%	quartile	0
10.0%		0
2.5%		0
0.5%		0
0.0%	minimum	0

Moments

Mean	20.775547
Std Dev	22.321603
Std Err Mean	1.5118097
Upper 95% Mean	23.755258
Lower 95% Mean	17.795836
N	218

mean burst dur

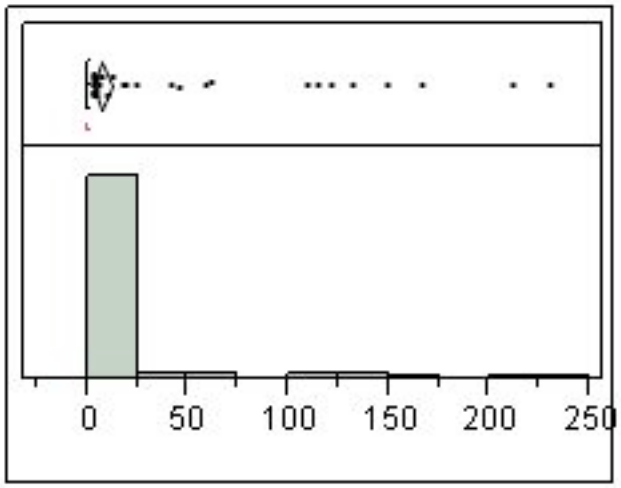

Quantiles

100.0%	maximum	230.178
99.5%		228.396
97.5%		126.939
90.0%		4.46972
75.0%	quartile	0.87539
50.0%	median	0.24247
25.0%	quartile	0
10.0%		0
2.5%		0
0.5%		0
0.0%	minimum	0

Moments

Mean	7.5371973
Std Dev	30.744788
Std Err Mean	2.0822998
Upper 95% Mean	11.641319
Lower 95% Mean	3.4330754
N	218

mean spikes/burst

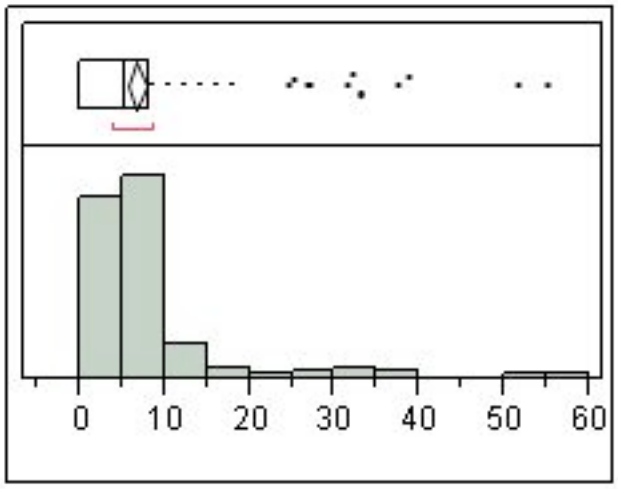

Quantiles

100.0%	maximum	55
99.5%		54.6833
97.5%		33
90.0%		12.3
75.0%	quartile	8.14323
50.0%	median	5.51563
25.0%	quartile	0
10.0%		0
2.5%		0
0.5%		0
0.0%	minimum	0

Moments

Mean	6.684427
Std Dev	8.1527672
Std Err Mean	0.5521751
Upper 95% Mean	7.7727399
Lower 95% Mean	5.596114
N	218

mean ISI

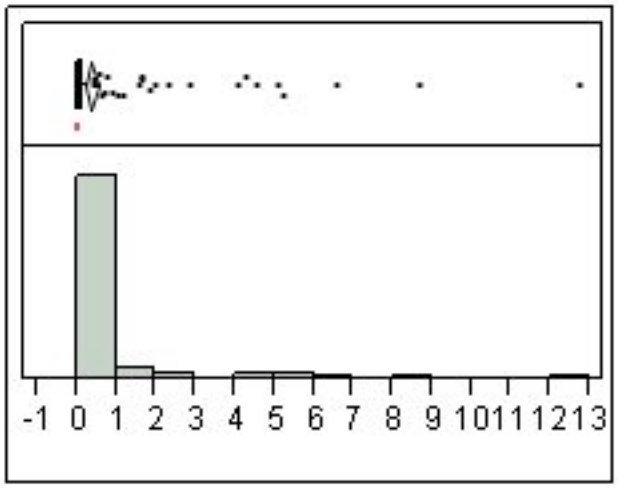

Quantiles

100.0%	maximum	12.7226
99.5%		12.3359
97.5%		4.82642
90.0%		0.55219
75.0%	quartile	0.13776
50.0%	median	0.04845
25.0%	quartile	0
10.0%		0
2.5%		0
0.5%		0
0.0%	minimum	0

Moments

Mean	0.3864688
Std Dev	1.3449503
Std Err Mean	0.0910915
Upper 95% Mean	0.5660063
Lower 95% Mean	0.2069314
N	218

Mean Freq in burst

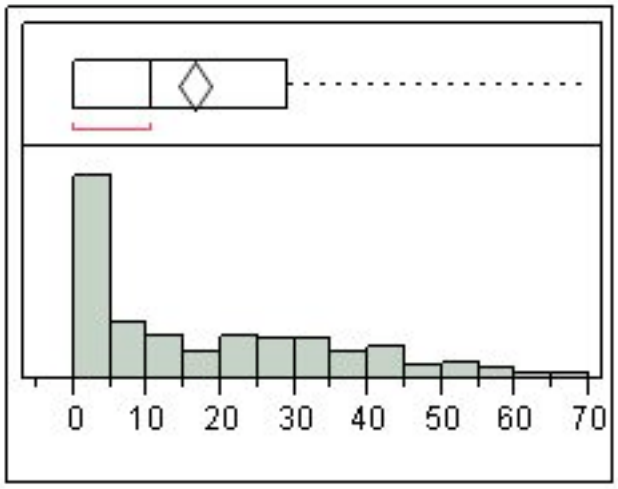

Quantiles

100.0%	maximum	68.993
99.5%		68.1863
97.5%		54.9907
90.0%		41.7944
75.0%	quartile	29.2182
50.0%	median	10.5392
25.0%	quartile	0
10.0%		0
2.5%		0
0.5%		0
0.0%	minimum	0

Moments

Mean	16.368931
Std Dev	17.05862
Std Err Mean	1.1553555
Upper 95% Mean	18.646086
Lower 95% Mean	14.091776
N	218

Mean Peak Freq

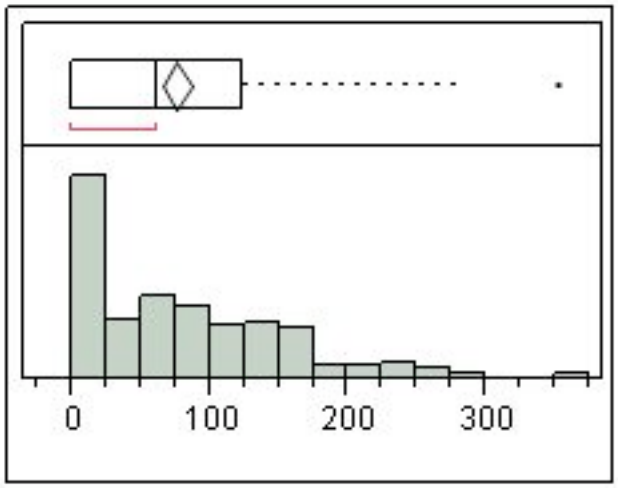

Quantiles

100.0%	maximum	352.113
99.5%		345.651
97.5%		248.549
90.0%		171.234
75.0%	quartile	123.939
50.0%	median	62.7133
25.0%	quartile	0
10.0%		0
2.5%		0
0.5%		0
0.0%	minimum	0

Moments

Mean	76.430491
Std Dev	72.615363
Std Err Mean	4.918133
Upper 95% Mean	86.123916
Lower 95% Mean	66.737066
N	218

mean Interburst Int

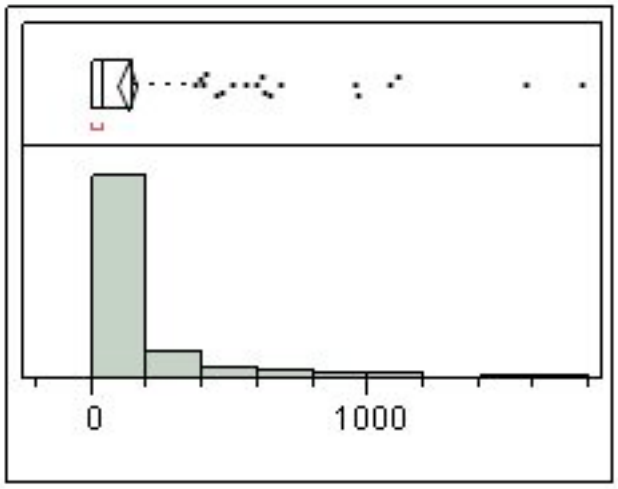

Quantiles

100.0%	maximum	1771.16
99.5%		1752.19
97.5%		955.021
90.0%		314.344
75.0%	quartile	144.931
50.0%	median	40.2563
25.0%	quartile	0
10.0%		0
2.5%		0
0.5%		0
0.0%	minimum	0

Moments

Mean	124.52467
Std Dev	237.72768
Std Err Mean	16.10095
Upper 95% Mean	156.25894
Lower 95% Mean	92.790397
N	218

Mean Sup

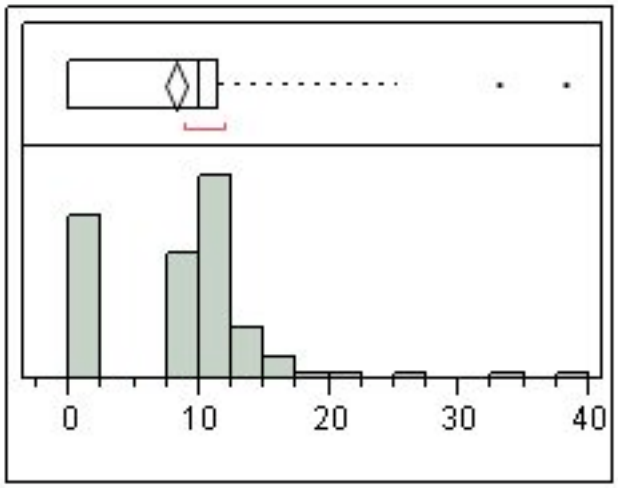

Quantiles

100.0%	maximum	38.1648
99.5%		37.6662
97.5%		17.1087
90.0%		13.2712
75.0%	quartile	11.4636
50.0%	median	9.94886
25.0%	quartile	0
10.0%		0
2.5%		0
0.5%		0
0.0%	minimum	0

Moments

Mean	8.2499749
Std Dev	6.0417683
Std Err Mean	0.4092002
Upper 95% Mean	9.0564905
Lower 95% Mean	7.4434592
N	218

Distributions Genotype=nhet

mean freq

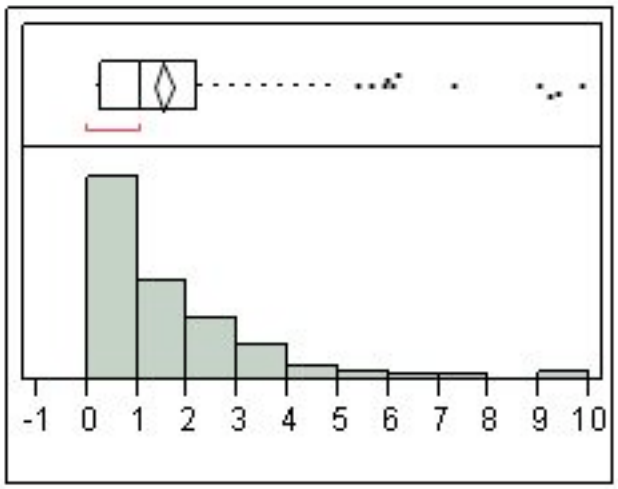

Quantiles

100.0%	maximum	9.82457
99.5%		9.6475
97.5%		6.08238
90.0%		3.68265
75.0%	quartile	2.17666
50.0%	median	1.07488
25.0%	quartile	0.292
10.0%		0.02851
2.5%		0.00308
0.5%		0.00061
0.0%	minimum	0.00044

Moments

Mean	1.5203883
Std Dev	1.6859978
Std Err Mean	0.1007576
Upper 95% Mean	1.71873
Lower 95% Mean	1.3220466
N	280

numburst

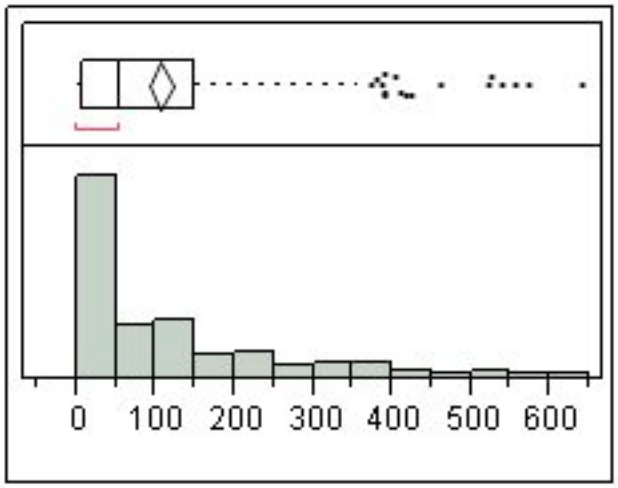

Quantiles

100.0%	maximum	639
99.5%		611.865
97.5%		459.125
90.0%		314.5
75.0%	quartile	149.75
50.0%	median	53.5
25.0%	quartile	7
10.0%		0
2.5%		0
0.5%		0
0.0%	minimum	0

Moments

Mean	106.37857
Std Dev	130.12026
Std Err Mean	7.776173
Upper 95% Mean	121.68599
Lower 95% Mean	91.071151
N	280

bursts/sec

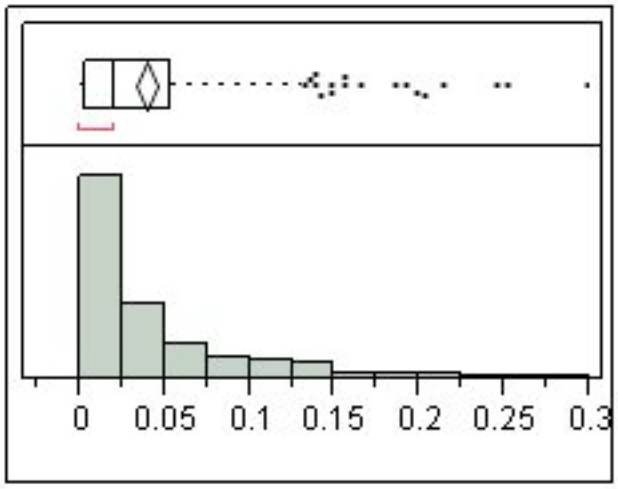

Quantiles

100.0%	maximum	0.29769
99.5%		0.27901
97.5%		0.19132
90.0%		0.11688
75.0%	quartile	0.05419
50.0%	median	0.02075
25.0%	quartile	0.00267
10.0%		0
2.5%		0
0.5%		0
0.0%	minimum	0

Moments

Mean	0.0396271
Std Dev	0.0507996
Std Err Mean	0.0030359
Upper 95% Mean	0.0456032
Lower 95% Mean	0.033651
N	280

%spikes in burst

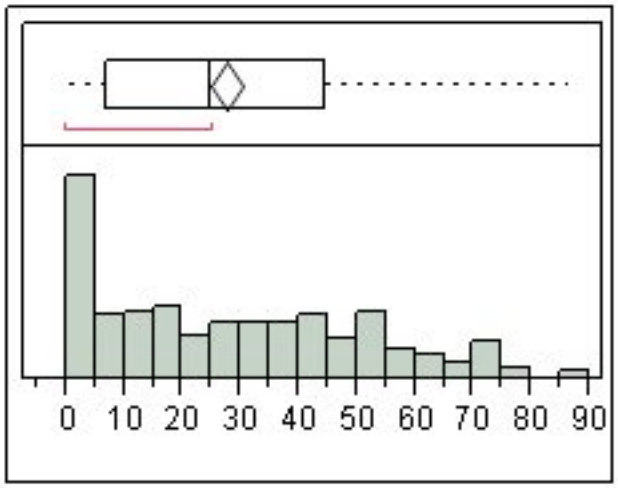

Quantiles

100.0%	maximum	86.3664
99.5%		86.1023
97.5%		74.3716
90.0%		59.4038
75.0%	quartile	44.5414
50.0%	median	24.8441
25.0%	quartile	6.95873
10.0%		0
2.5%		0
0.5%		0
0.0%	minimum	0

Moments

Mean	27.619439
Std Dev	22.618662
Std Err Mean	1.3517236
Upper 95% Mean	30.280311
Lower 95% Mean	24.958567
N	280

mean burst dur

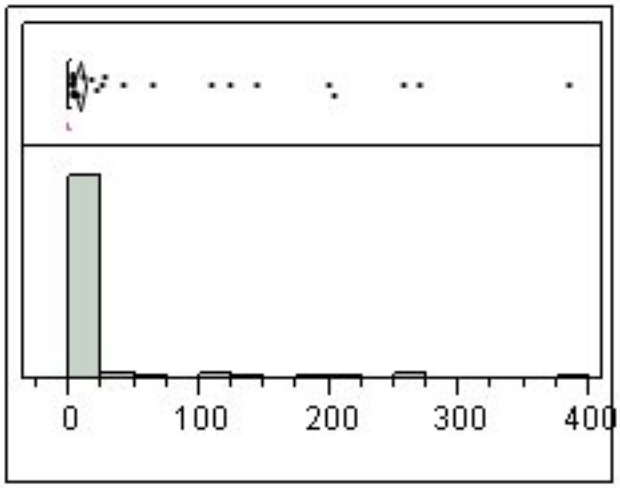

Quantiles

100.0%	maximum	384.493
99.5%		337.727
97.5%		123.463
90.0%		0.79416
75.0%	quartile	0.56734
50.0%	median	0.34388
25.0%	quartile	0.1873
10.0%		0
2.5%		0
0.5%		0
0.0%	minimum	0

Moments

Mean	7.1143856
Std Dev	38.20395
Std Err Mean	2.2831227
Upper 95% Mean	11.60872
Lower 95% Mean	2.6200514
N	280

mean spikes/burst

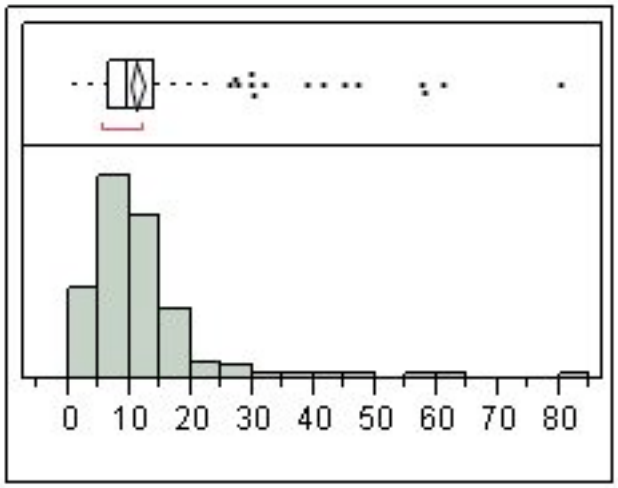

Quantiles

100.0%	maximum	80
99.5%		72.305
97.5%		41.6704
90.0%		18.4613
75.0%	quartile	13.9463
50.0%	median	9.79788
25.0%	quartile	6.59321
10.0%		0
2.5%		0
0.5%		0
0.0%	minimum	0

Moments

Mean	11.291523
Std Dev	9.7078211
Std Err Mean	0.5801533
Upper 95% Mean	12.433557
Lower 95% Mean	10.14949
N	280

mean ISI

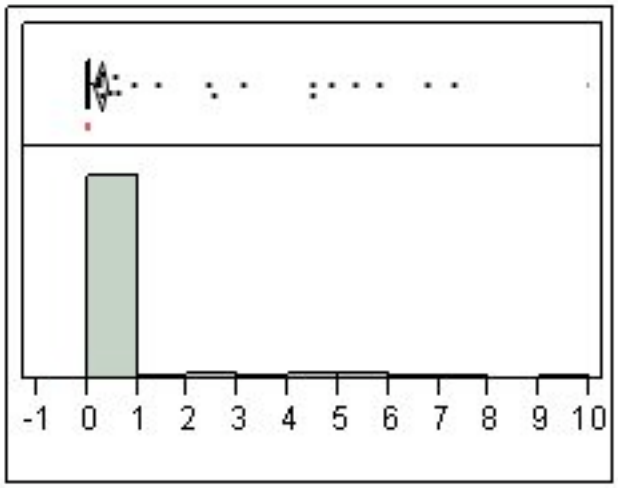

Quantiles

100.0%	maximum	9.97708
99.5%		8.88684
97.5%		4.48285
90.0%		0.07932
75.0%	quartile	0.05299
50.0%	median	0.03545
25.0%	quartile	0.02228
10.0%		0
2.5%		0
0.5%		0
0.0%	minimum	0

Moments

Mean	0.2534702
Std Dev	1.0911699
Std Err Mean	0.0652099
Upper 95% Mean	0.381836
Lower 95% Mean	0.1251043
N	280

Mean Freq in burst

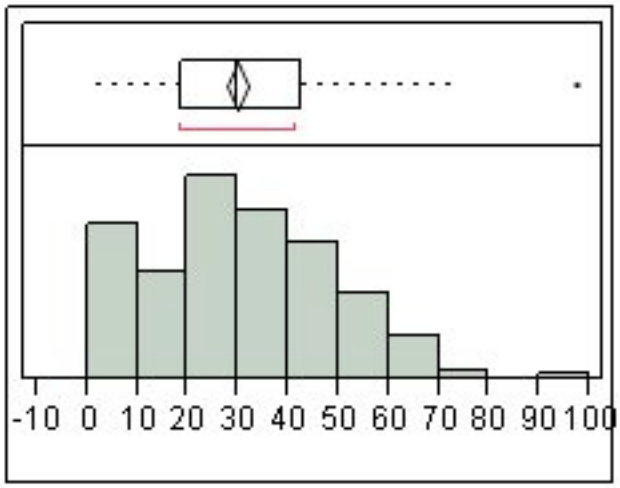

Quantiles

100.0%	maximum	97.2579
99.5%		87.4099
97.5%		65.6151
90.0%		54.2536
75.0%	quartile	42.566
50.0%	median	29.6951
25.0%	quartile	18.929
10.0%		0
2.5%		0
0.5%		0
0.0%	minimum	0

Moments

Mean	29.722082
Std Dev	18.863421
Std Err Mean	1.127305
Upper 95% Mean	31.941185
Lower 95% Mean	27.502979
N	280

Mean Peak Freq

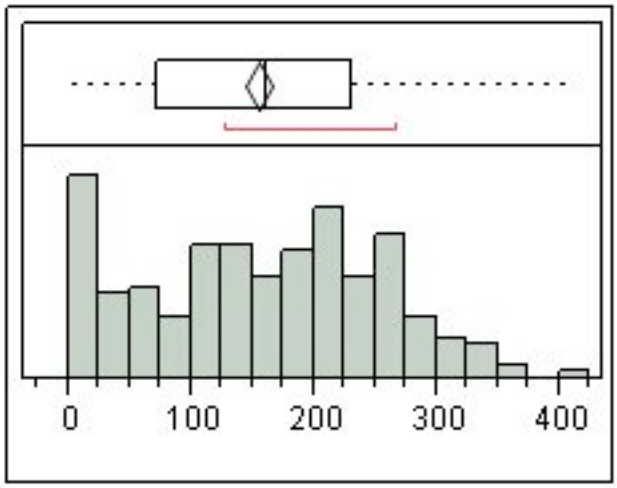

Quantiles

100.0%	maximum	408.298
99.5%		391.573
97.5%		328.935
90.0%		273.011
75.0%	quartile	232.302
50.0%	median	161.493
25.0%	quartile	73.182
10.0%		0
2.5%		0
0.5%		0
0.0%	minimum	0

Moments

Mean	155.31041
Std Dev	96.845791
Std Err Mean	5.787643
Upper 95% Mean	166.70341
Lower 95% Mean	143.91742
N	280

mean Interburst Int

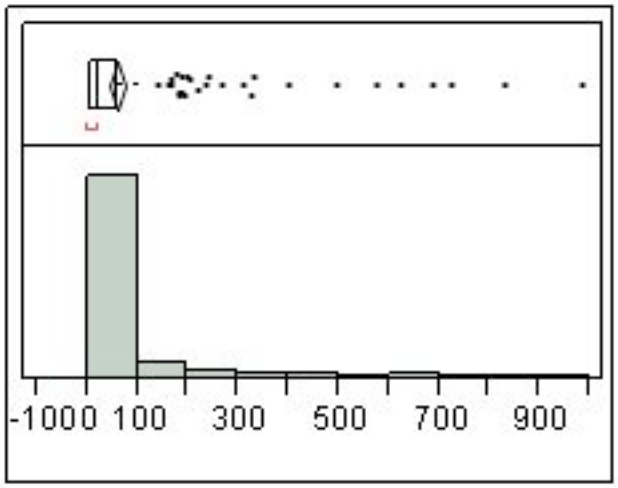

Quantiles

100.0%	maximum	984.412
99.5%		922.067
97.5%		497.871
90.0%		159.072
75.0%	quartile	58.331
50.0%	median	19.8466
25.0%	quartile	7.15356
10.0%		0
2.5%		0
0.5%		0
0.0%	minimum	0

Moments

Mean	60.004164
Std Dev	125.2411
Std Err Mean	7.4845875
Upper 95% Mean	74.737597
Lower 95% Mean	45.27073
N	280

Mean Sup

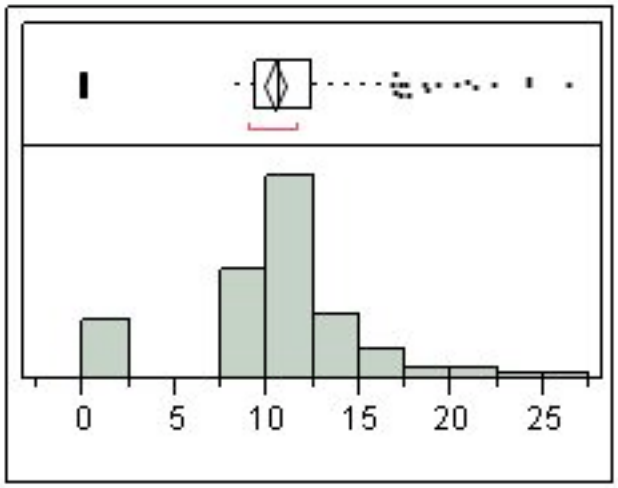

Quantiles

100.0%	maximum	26.2902
99.5%		25.4445
97.5%		20.2754
90.0%		15.0356
75.0%	quartile	12.3649
50.0%	median	10.6761
25.0%	quartile	9.44688
10.0%		0
2.5%		0
0.5%		0
0.0%	minimum	0

Moments

Mean	10.357898
Std Dev	4.7132405
Std Err Mean	0.28167
Upper 95% Mean	10.912367
Lower 95% Mean	9.8034301
N	280

Distributions Genotype=nko

mean freq

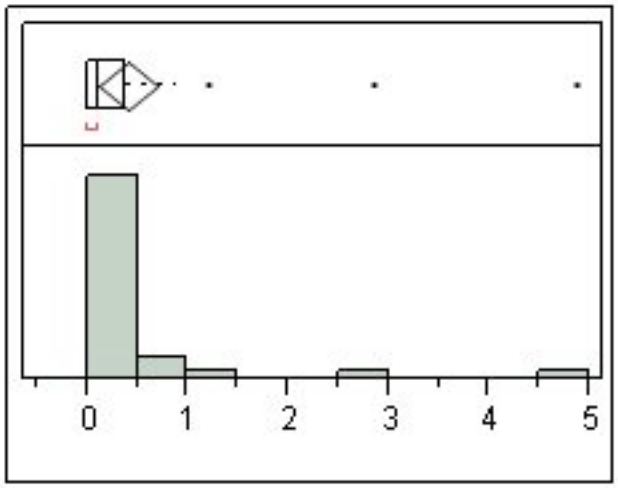

Quantiles

100.0%	maximum	4.87639
99.5%		4.87639
97.5%		4.87639
90.0%		0.91746
75.0%	quartile	0.37788
50.0%	median	0.11104
25.0%	quartile	0.01146
10.0%		0.00143
2.5%		0.00069
0.5%		0.00069
0.0%	minimum	0.00069

Moments

Mean	0.4115501
Std Dev	0.9042021
Std Err Mean	0.146681
Upper 95% Mean	0.7087539
Lower 95% Mean	0.1143462
N	38

numburst

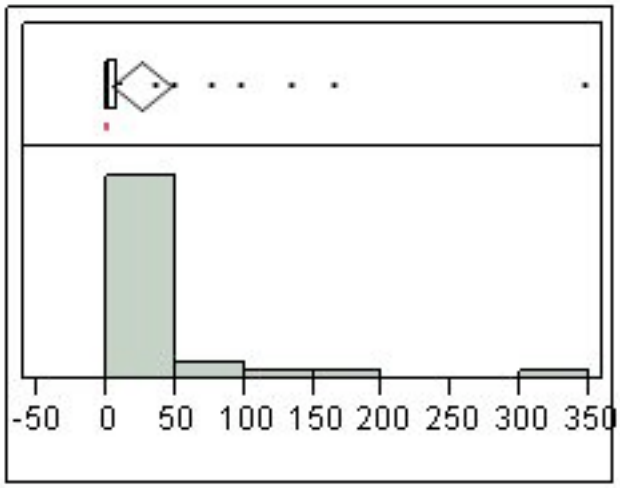

Quantiles

100.0%	maximum	346
99.5%		346
97.5%		346
90.0%		99.7
75.0%	quartile	8.5
50.0%	median	2
25.0%	quartile	0
10.0%		0
2.5%		0
0.5%		0
0.0%	minimum	0

Moments

Mean	25.684211
Std Dev	65.533612
Std Err Mean	10.630956
Upper 95% Mean	47.224573
Lower 95% Mean	4.1438482
N	38

bursts/sec

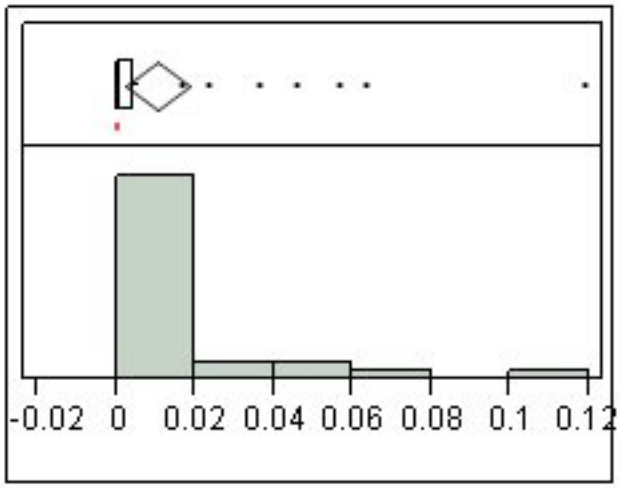

Quantiles

100.0%	maximum	0.1188
99.5%		0.1188
97.5%		0.1188
90.0%		0.04693
75.0%	quartile	0.00406
50.0%	median	0.00082
25.0%	quartile	0
10.0%		0
2.5%		0
0.5%		0
0.0%	minimum	0

Moments

Mean	0.0104401
Std Dev	0.0241761
Std Err Mean	0.0039219
Upper 95% Mean	0.0183866
Lower 95% Mean	0.0024936
N	38

%spikes in burst

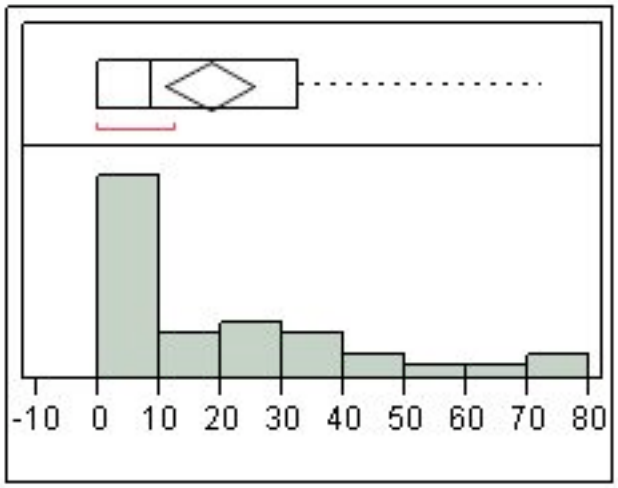

Quantiles

100.0%	maximum	72.2222
99.5%		72.2222
97.5%		72.2222
90.0%		55.0179
75.0%	quartile	32.6679
50.0%	median	8.88158
25.0%	quartile	0
10.0%		0
2.5%		0
0.5%		0
0.0%	minimum	0

Moments

Mean	18.147673
Std Dev	21.833333
Std Err Mean	3.5418343
Upper 95% Mean	25.324111
Lower 95% Mean	10.971235
N	38

mean burst dur

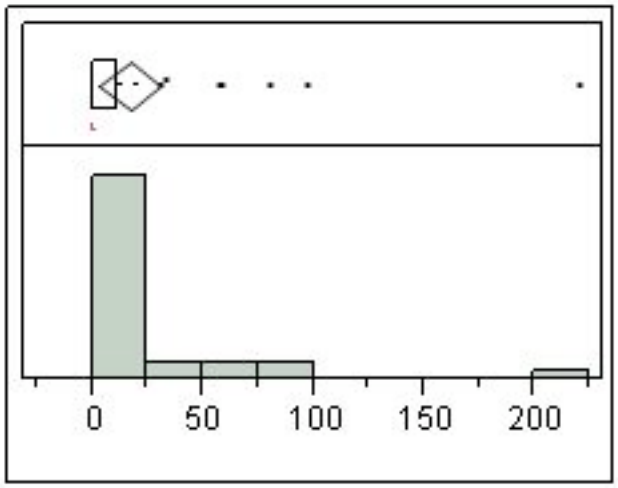

Quantiles

100.0%	maximum	220.398
99.5%		220.398
97.5%		220.398
90.0%		60.5774
75.0%	quartile	10.7187
50.0%	median	0.36364
25.0%	quartile	0
10.0%		0
2.5%		0
0.5%		0
0.0%	minimum	0

Moments

Mean	16.801001
Std Dev	41.373266
Std Err Mean	6.71163
Upper 95% Mean	30.400055
Lower 95% Mean	3.2019468
N	38

mean spikes/burst

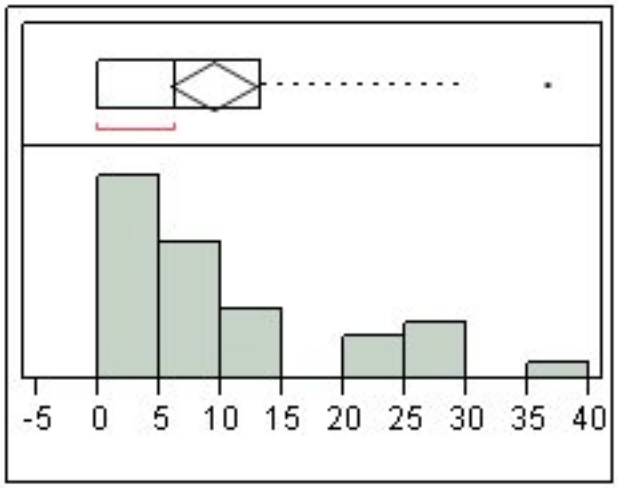

Quantiles

100.0%	maximum	36.5
99.5%		36.5
97.5%		36.5
90.0%		28.5801
75.0%	quartile	13.25
50.0%	median	6.20408
25.0%	quartile	0
10.0%		0
2.5%		0
0.5%		0
0.0%	minimum	0

Moments

Mean	9.3025555
Std Dev	10.429154
Std Err Mean	1.6918323
Upper 95% Mean	12.730533
Lower 95% Mean	5.8745777
N	38

mean ISI

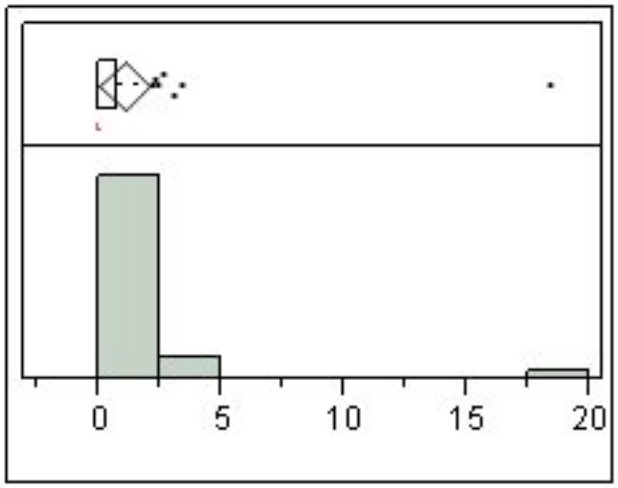

Quantiles

100.0%	maximum	18.3665
99.5%		18.3665
97.5%		18.3665
90.0%		2.6873
75.0%	quartile	0.81502
50.0%	median	0.05316
25.0%	quartile	0
10.0%		0
2.5%		0
0.5%		0
0.0%	minimum	0

Moments

Mean	1.0485989
Std Dev	3.0488902
Std Err Mean	0.4945953
Upper 95% Mean	2.0507441
Lower 95% Mean	0.0464536
N	38

Mean Freq in burst

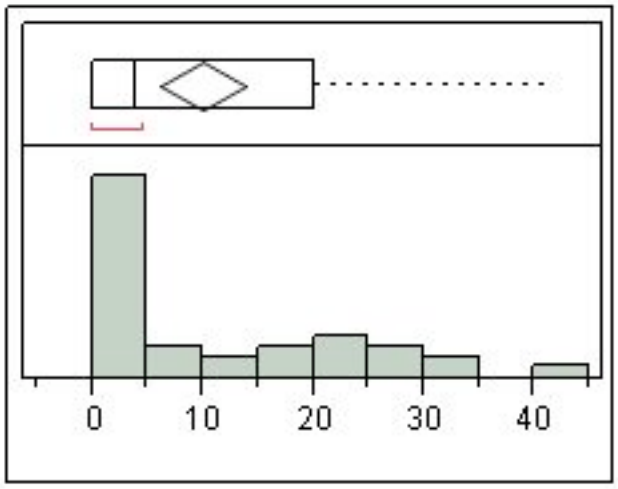

Quantiles

100.0%	maximum	41.713
99.5%		41.713
97.5%		41.713
90.0%		29.1102
75.0%	quartile	20.2385
50.0%	median	3.96036
25.0%	quartile	0
10.0%		0
2.5%		0
0.5%		0
0.0%	minimum	0

Moments

Mean	9.9715888
Std Dev	11.991778
Std Err Mean	1.9453233
Upper 95% Mean	13.913188
Lower 95% Mean	6.0299894
N	38

Mean Peak Freq

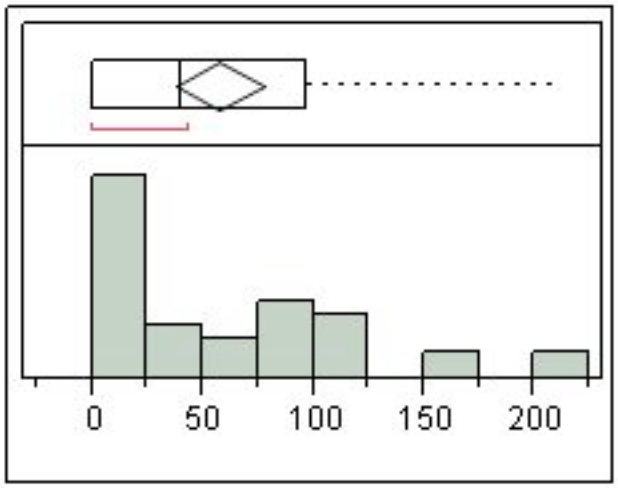

Quantiles

100.0%	maximum	210.835
99.5%		210.835
97.5%		210.835
90.0%		160.706
75.0%	quartile	97.1124
50.0%	median	40.192
25.0%	quartile	0
10.0%		0
2.5%		0
0.5%		0
0.0%	minimum	0

Moments

Mean	57.672436
Std Dev	61.189319
Std Err Mean	9.9262183
Upper 95% Mean	77.784865
Lower 95% Mean	37.560008
N	38

mean Interburst Int

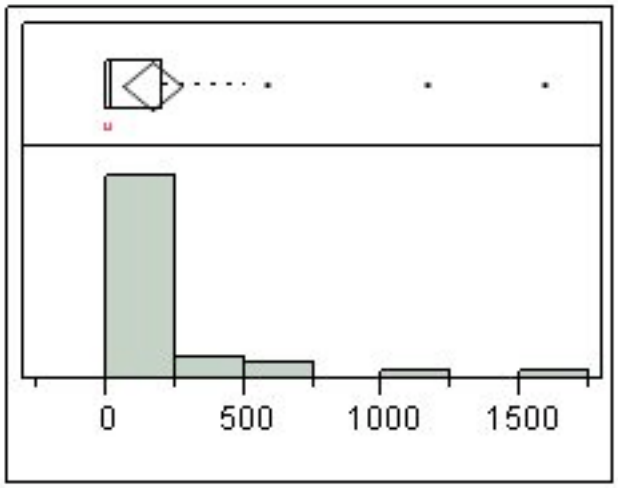

Quantiles

100.0%	maximum	1585.72
99.5%		1585.72
97.5%		1585.72
90.0%		512.339
75.0%	quartile	205.828
50.0%	median	16.7224
25.0%	quartile	0
10.0%		0
2.5%		0
0.5%		0
0.0%	minimum	0

Moments

Mean	165.35432
Std Dev	331.38825
Std Err Mean	53.758273
Upper 95% Mean	274.27892
Lower 95% Mean	56.42971
N	38

Mean Sup

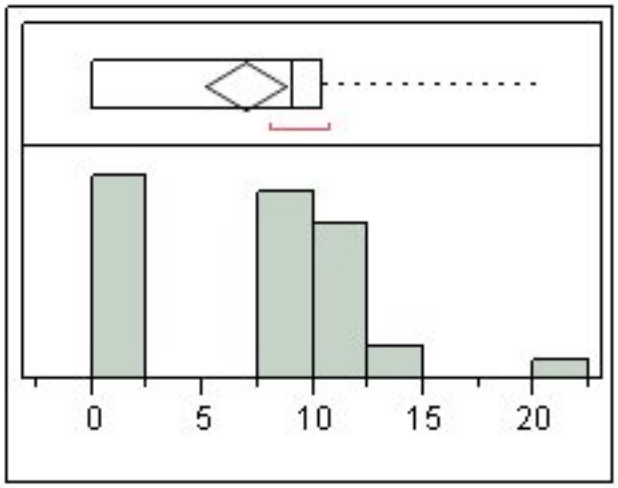

Quantiles

100.0%	maximum	20.0594
99.5%		20.0594
97.5%		20.0594
90.0%		12.2325
75.0%	quartile	10.3828
50.0%	median	9.07302
25.0%	quartile	0
10.0%		0
2.5%		0
0.5%		0
0.0%	minimum	0

Moments

Mean	6.8946394
Std Dev	5.4107342
Std Err Mean	0.877737
Upper 95% Mean	8.6731035
Lower 95% Mean	5.1161754
N	38

Distributions Genotype=nwt

mean freq

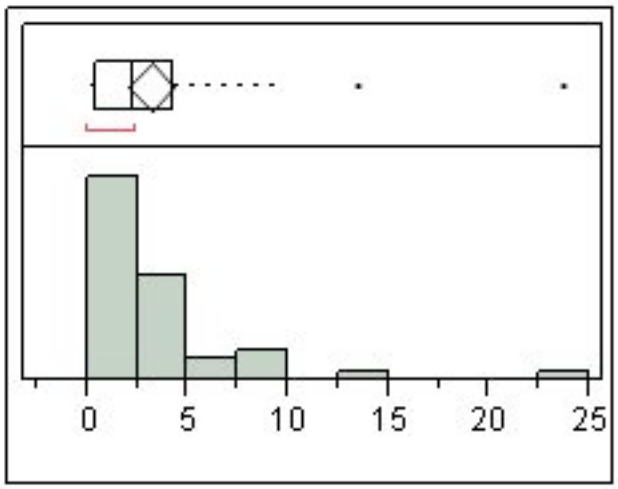

Quantiles

100.0%	maximum	23.669
99.5%		23.669
97.5%		19.3006
90.0%		8.39337
75.0%	quartile	4.2415
50.0%	median	2.32683
25.0%	quartile	0.391
10.0%		0.10007
2.5%		0.00514
0.5%		0.005
0.0%	minimum	0.005

Moments

Mean	3.1539703
Std Dev	4.0100178
Std Err Mean	0.5358612
Upper 95% Mean	4.22786
Lower 95% Mean	2.0800805
N	56

numburst

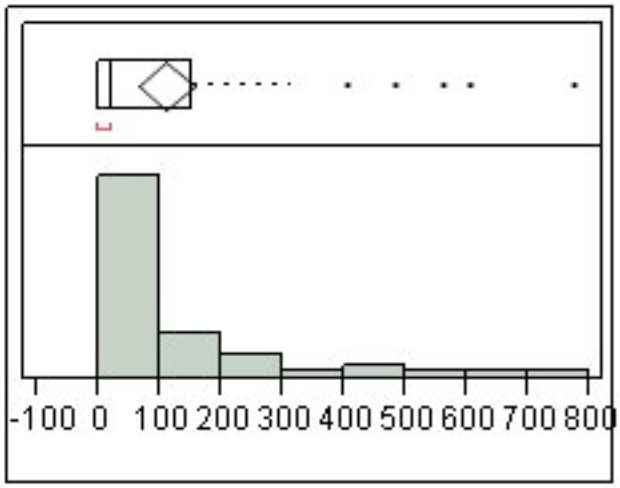

Quantiles

100.0%	maximum	774
99.5%		774
97.5%		702.175
90.0%		340.3
75.0%	quartile	150.75
50.0%	median	22.5
25.0%	quartile	1.25
10.0%		0
2.5%		0
0.5%		0
0.0%	minimum	0

Moments

Mean	110.21429
Std Dev	171.8352
Std Err Mean	22.962444
Upper 95% Mean	156.23205
Lower 95% Mean	64.196519
N	56

bursts/sec

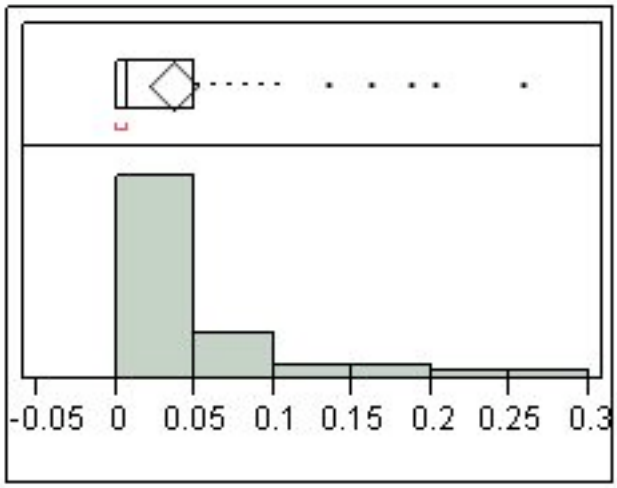

Quantiles

100.0%	maximum	0.258
99.5%		0.258
97.5%		0.23406
90.0%		0.11343
75.0%	quartile	0.05025
50.0%	median	0.0075
25.0%	quartile	0.00042
10.0%		0
2.5%		0
0.5%		0
0.0%	minimum	0

Moments

Mean	0.0367381
Std Dev	0.0572784
Std Err Mean	0.0076542
Upper 95% Mean	0.0520773
Lower 95% Mean	0.0213988
N	56

%spikes in burst

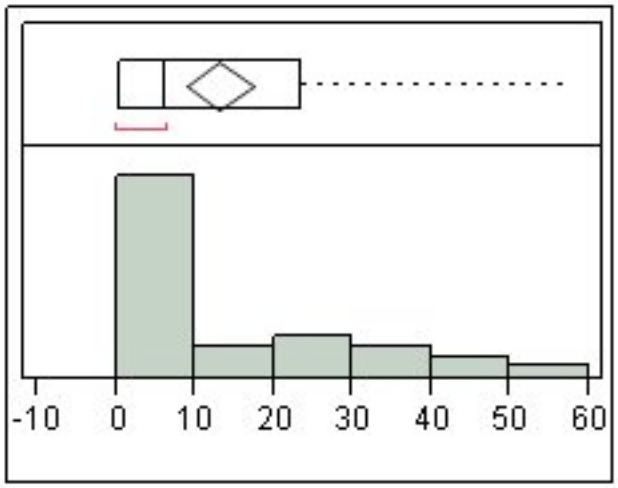

Quantiles

100.0%	maximum	56.4498
99.5%		56.4498
97.5%		53.8001
90.0%		40.2461
75.0%	quartile	23.5344
50.0%	median	6.29933
25.0%	quartile	0.57589
10.0%		0
2.5%		0
0.5%		0
0.0%	minimum	0

Moments

Mean	13.097695
Std Dev	15.681975
Std Err Mean	2.0955921
Upper 95% Mean	17.297356
Lower 95% Mean	8.8980348
N	56

mean burst dur

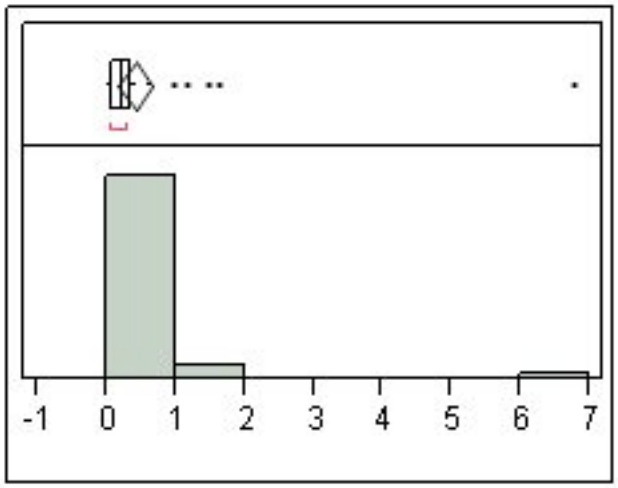

Quantiles

100.0%	maximum	6.78678
99.5%		6.78678
97.5%		4.59266
90.0%		0.79965
75.0%	quartile	0.36989
50.0%	median	0.23522
25.0%	quartile	0.10143
10.0%		0
2.5%		0
0.5%		0
0.0%	minimum	0

Moments

Mean	0.4153431
Std Dev	0.9281558
Std Err Mean	0.12403
Upper 95% Mean	0.6639049
Lower 95% Mean	0.1667814
N	56

mean spikes/burst

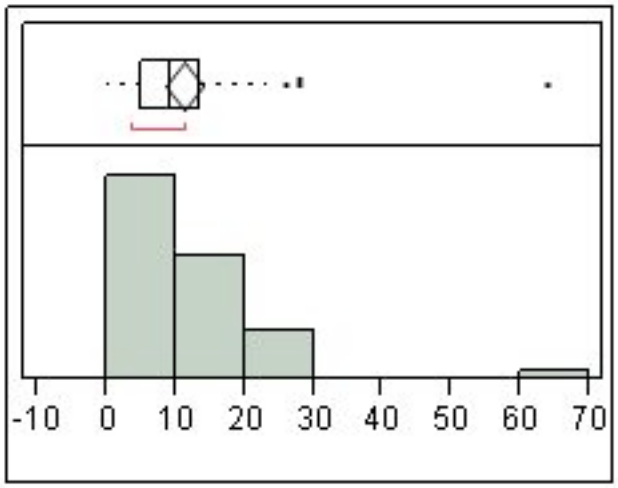

Quantiles

100.0%	maximum	63.8857
99.5%		63.8857
97.5%		48.6343
90.0%		22.6506
75.0%	quartile	13.5104
50.0%	median	9.51169
25.0%	quartile	5.25
10.0%		0
2.5%		0
0.5%		0
0.0%	minimum	0

Moments

Mean	11.185901
Std Dev	10.110404
Std Err Mean	1.3510596
Upper 95% Mean	13.893485
Lower 95% Mean	8.4783172
N	56

mean ISI

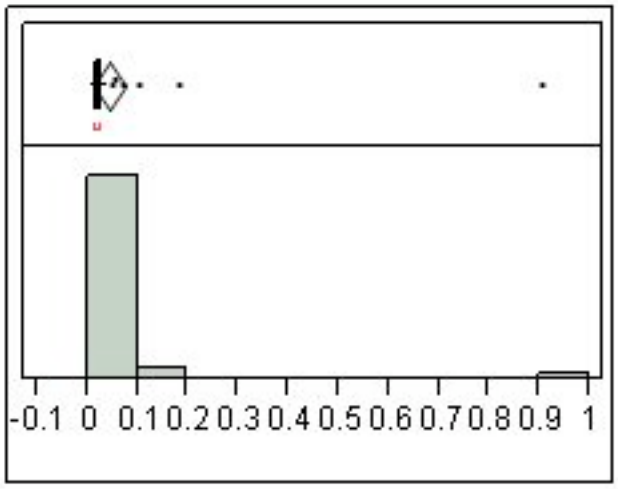

Quantiles

100.0%	maximum	0.9049
99.5%		0.9049
97.5%		0.59702
90.0%		0.05018
75.0%	quartile	0.02856
50.0%	median	0.02092
25.0%	quartile	0.01644
10.0%		0
2.5%		0
0.5%		0
0.0%	minimum	0

Moments

Mean	0.0421353
Std Dev	0.1205462
Std Err Mean	0.0161087
Upper 95% Mean	0.0744178
Lower 95% Mean	0.0098529
N	56

Mean Freq in burst

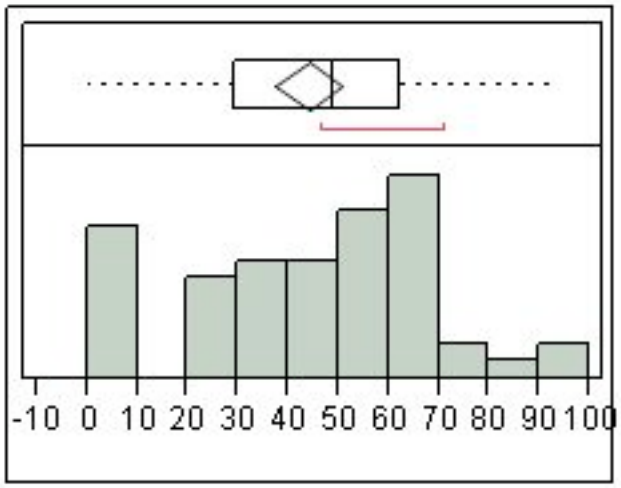

Quantiles

100.0%	maximum	93.0521
99.5%		93.0521
97.5%		92.4102
90.0%		70.2008
75.0%	quartile	62.368
50.0%	median	49.2295
25.0%	quartile	29.2321
10.0%		0
2.5%		0
0.5%		0
0.0%	minimum	0

Moments

Mean	44.188555
Std Dev	24.814702
Std Err Mean	3.3160041
Upper 95% Mean	50.833976
Lower 95% Mean	37.543135
N	56

Mean Peak Freq

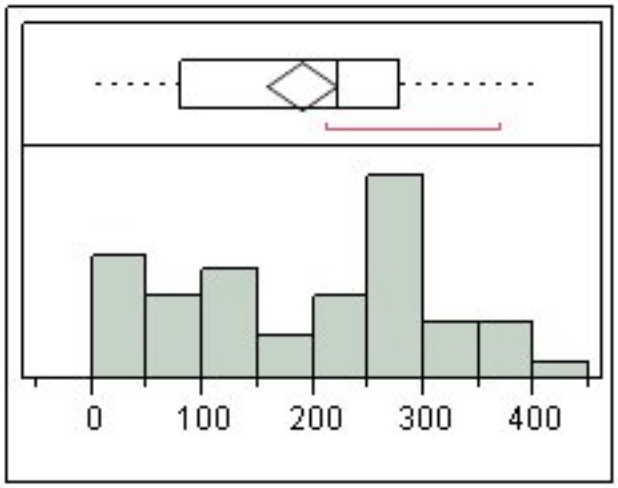

Quantiles

100.0%	maximum	405.616
99.5%		405.616
97.5%		390.161
90.0%		338.417
75.0%		

P28

Distributions Genotype=het

mean freq

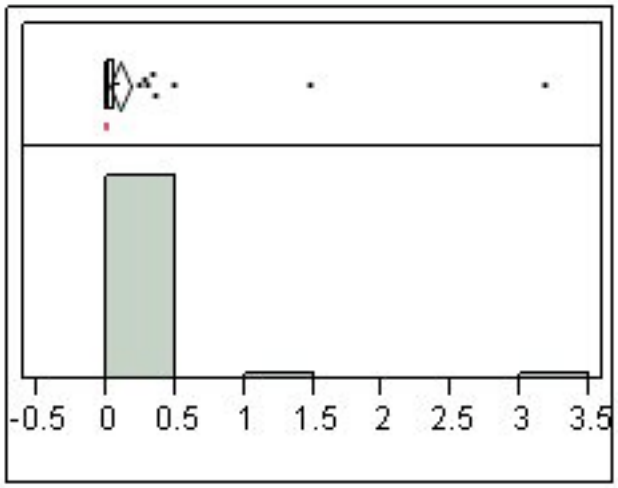

Quantiles

100.0%	maximum	3.16619
99.5%		3.16619
97.5%		1.37406
90.0%		0.18871
75.0%	quartile	0.05686
50.0%	median	0.01221
25.0%	quartile	0.00191
10.0%		0.00043
2.5%		0.00038
0.5%		0.00036
0.0%	minimum	0.00036

Moments

Mean	0.1011958
Std Dev	0.3849421
Std Err Mean	0.0422529
Upper 95% Mean	0.1852503
Lower 95% Mean	0.0171414
N	83

numburst

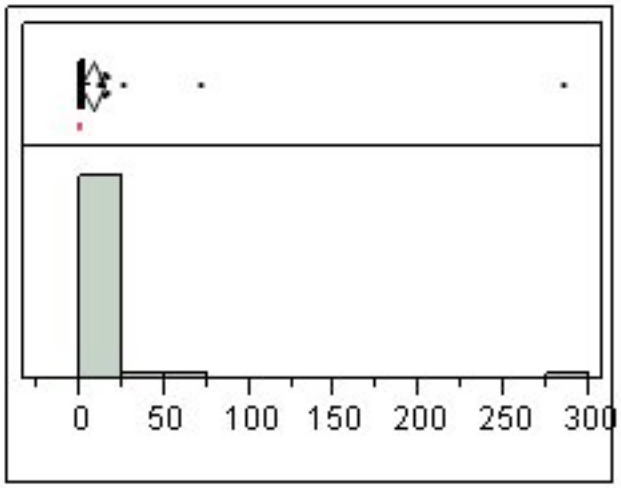

Quantiles

100.0%	maximum	285
99.5%		285
97.5%		66.5
90.0%		13
75.0%	quartile	4
50.0%	median	2
25.0%	quartile	0
10.0%		0
2.5%		0
0.5%		0
0.0%	minimum	0

Moments

Mean	7.4337349
Std Dev	32.084185
Std Err Mean	3.5216969
Upper 95% Mean	14.439512
Lower 95% Mean	0.427958
N	83

bursts/sec

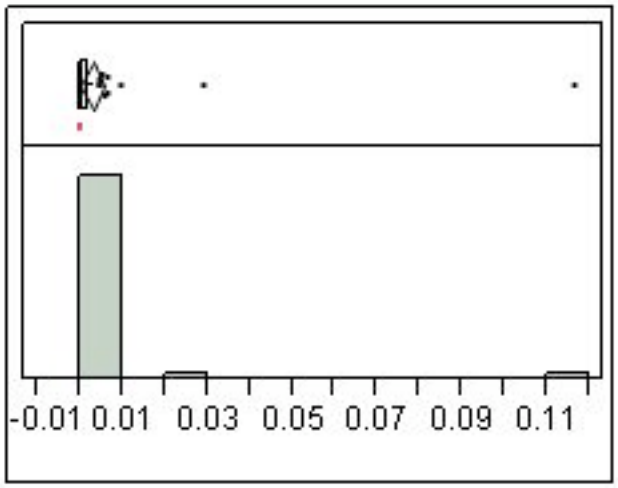

Quantiles

100.0%	maximum	0.1163
99.5%		0.1163
97.5%		0.02702
90.0%		0.00463
75.0%	quartile	0.00163
50.0%	median	0.00067
25.0%	quartile	0
10.0%		0
2.5%		0
0.5%		0
0.0%	minimum	0

Moments

Mean	0.0029315
Std Dev	0.013082
Std Err Mean	0.0014359
Upper 95% Mean	0.005788
Lower 95% Mean	7.4979e-5
N	83

%spikes in burst

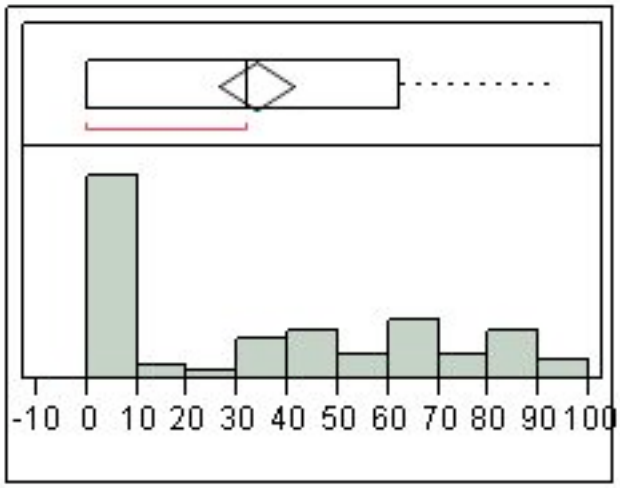

Quantiles

100.0%	maximum	94.1666
99.5%		94.1666
97.5%		92.9787
90.0%		83.2265
75.0%	quartile	62.5
50.0%	median	32.1429
25.0%	quartile	0
10.0%		0
2.5%		0
0.5%		0
0.0%	minimum	0

Moments

Mean	33.510543
Std Dev	33.174329
Std Err Mean	3.6413557
Upper 95% Mean	40.754359
Lower 95% Mean	26.266726
N	83

mean burst dur

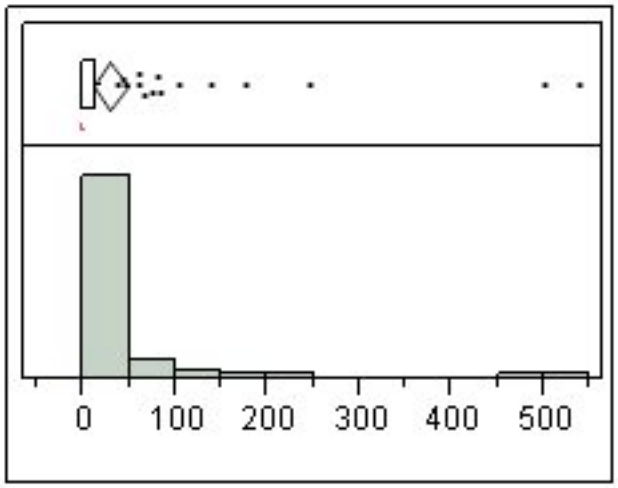

Quantiles

100.0%	maximum	539.708
99.5%		539.708
97.5%		474.108
90.0%		76.8001
75.0%	quartile	13.1615
50.0%	median	0.11492
25.0%	quartile	0
10.0%		0
2.5%		0
0.5%		0
0.0%	minimum	0

Moments

Mean	29.292549
Std Dev	87.67343
Std Err Mean	9.6234092
Upper 95% Mean	48.436575
Lower 95% Mean	10.148522
N	83

mean spikes/burst

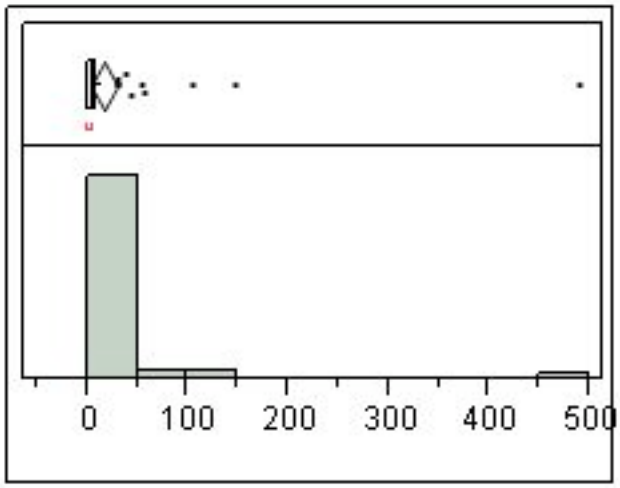

Quantiles

100.0%	maximum	488.313
99.5%		488.313
97.5%		142.45
90.0%		30.6
75.0%	quartile	9.69231
50.0%	median	4.85916
25.0%	quartile	0
10.0%		0
2.5%		0
0.5%		0
0.0%	minimum	0

Moments

Mean	16.509419
Std Dev	56.77985
Std Err Mean	6.2323982
Upper 95% Mean	28.907644
Lower 95% Mean	4.1111932
N	83

mean ISI

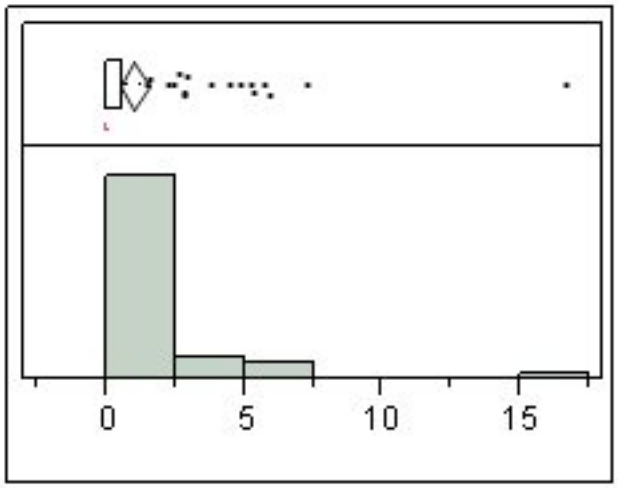

Quantiles

100.0%	maximum	16.6505
99.5%		16.6505
97.5%		7.16187
90.0%		4.19715
75.0%	quartile	0.57539
50.0%	median	0.02673
25.0%	quartile	0
10.0%		0
2.5%		0
0.5%		0
0.0%	minimum	0

Moments

Mean	1.0264635
Std Dev	2.4087052
Std Err Mean	0.2643897
Upper 95% Mean	1.5524189
Lower 95% Mean	0.5005081
N	83

Mean Freq in burst

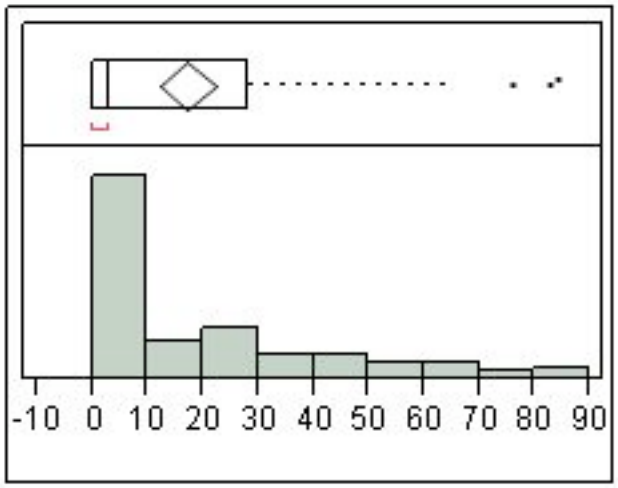

Quantiles

100.0%	maximum	84.3076
99.5%		84.3076
97.5%		82.2428
90.0%		55.1712
75.0%	quartile	28.2428
50.0%	median	3.07964
25.0%	quartile	0
10.0%		0
2.5%		0
0.5%		0
0.0%	minimum	0

Moments

Mean	17.235063
Std Dev	22.52914
Std Err Mean	2.4728944
Upper 95% Mean	22.154437
Lower 95% Mean	12.315688
N	83

Mean Peak Freq

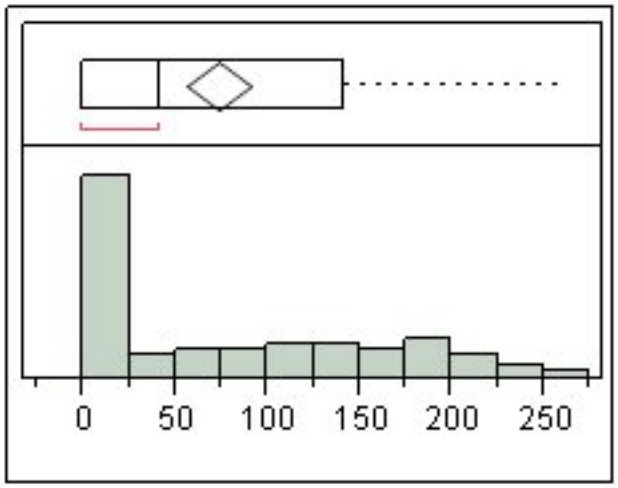

Quantiles

100.0%	maximum	262.887
99.5%		262.887
97.5%		242.857
90.0%		193.982
75.0%	quartile	142.257
50.0%	median	41.5212
25.0%	quartile	0
10.0%		0
2.5%		0
0.5%		0
0.0%	minimum	0

Moments

Mean	74.098941
Std Dev	80.196482
Std Err Mean	8.8027075
Upper 95% Mean	91.610331
Lower 95% Mean	56.587552
N	83

mean Interburst Int

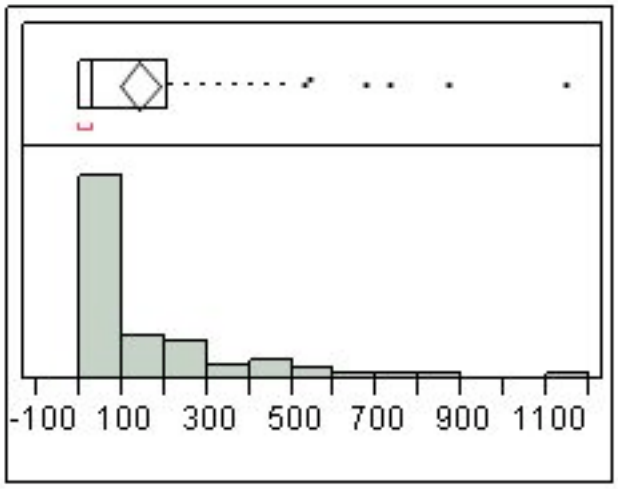

Quantiles

100.0%	maximum	1146.04
99.5%		1146.04
97.5%		855.254
90.0%		465.485
75.0%	quartile	209.367
50.0%	median	31.1271
25.0%	quartile	0
10.0%		0
2.5%		0
0.5%		0
0.0%	minimum	0

Moments

Mean	139.85189
Std Dev	219.92618
Std Err Mean	24.140034
Upper 95% Mean	187.87411
Lower 95% Mean	91.829676
N	83

Mean Sup

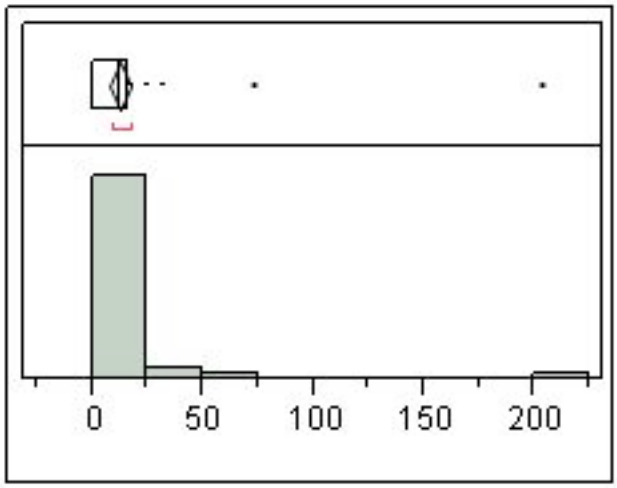

Quantiles

100.0%	maximum	203.685
99.5%		203.685
97.5%		69.104
90.0%		18.008
75.0%	quartile	15.6536
50.0%	median	11.9719
25.0%	quartile	0
10.0%		0
2.5%		0
0.5%		0
0.0%	minimum	0

Moments

Mean	12.323111
Std Dev	23.917703
Std Err Mean	2.625309
Upper 95% Mean	17.545687
Lower 95% Mean	7.1005356
N	83

Distributions Genotype=ko

mean freq

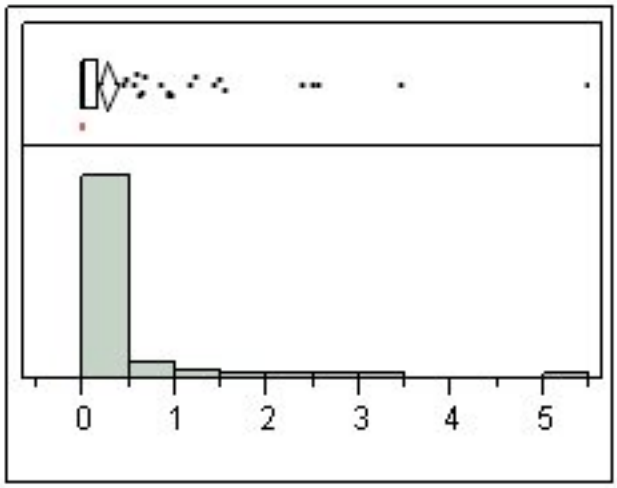

Quantiles

100.0%	maximum	5.48396
99.5%		5.48396
97.5%		2.50708
90.0%		0.78069
75.0%	quartile	0.17192
50.0%	median	0.02533
25.0%	quartile	0.00531
10.0%		0.00137
2.5%		0.00046
0.5%		0.00033
0.0%	minimum	0.00033

Moments

Mean	0.2671725
Std Dev	0.685955
Std Err Mean	0.0575641
Upper 95% Mean	0.3809727
Lower 95% Mean	0.1533722
N	142

numburst

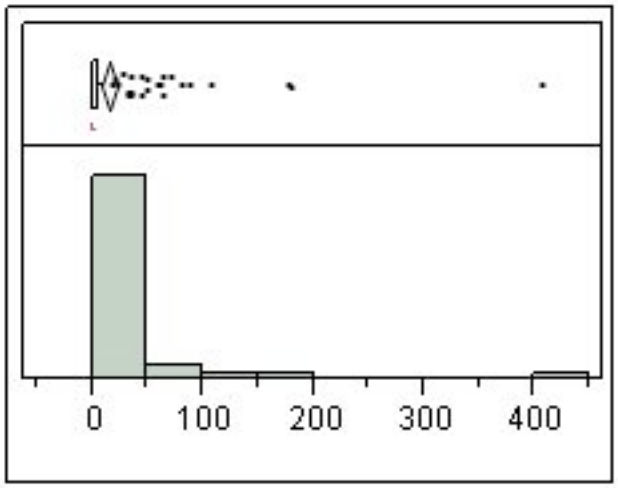

Quantiles

100.0%	maximum	407
99.5%		407
97.5%		136.9
90.0%		43.7
75.0%	quartile	6
50.0%	median	1
25.0%	quartile	0
10.0%		0
2.5%		0
0.5%		0
0.0%	minimum	0

Moments

Mean	14.169014
Std Dev	43.279722
Std Err Mean	3.6319536
Upper 95% Mean	21.349138
Lower 95% Mean	6.9888906
N	142

bursts/sec

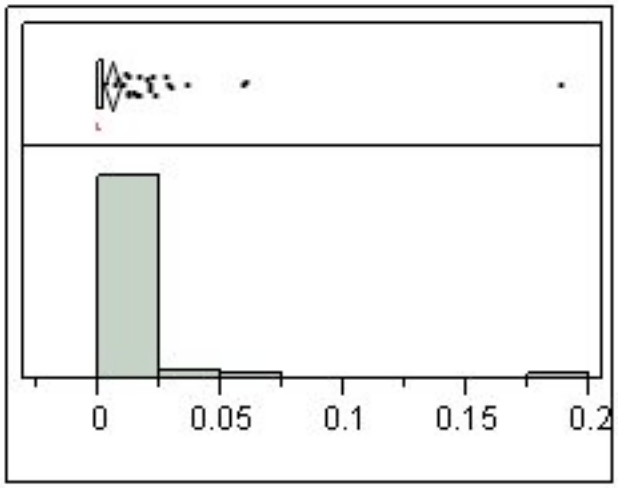

Quantiles

100.0%	maximum	0.18786
99.5%		0.18786
97.5%		0.04563
90.0%		0.01577
75.0%	quartile	0.00251
50.0%	median	0.00046
25.0%	quartile	0
10.0%		0
2.5%		0
0.5%		0
0.0%	minimum	0

Moments

Mean	0.00534
Std Dev	0.0180948
Std Err Mean	0.0015185
Upper 95% Mean	0.008342
Lower 95% Mean	0.0023381
N	142

%spikes in burst

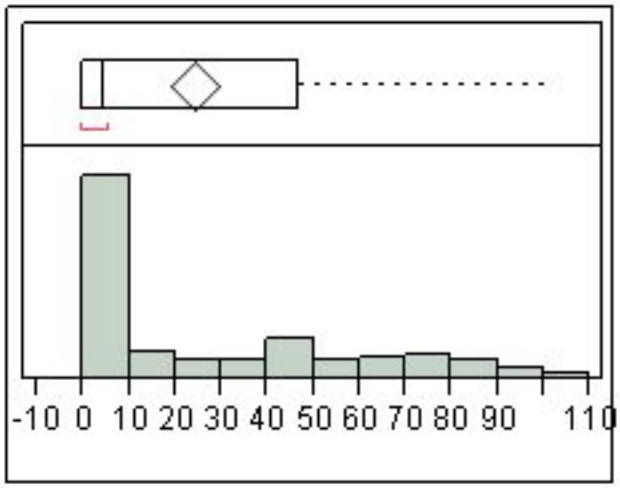

Quantiles

100.0%	maximum	100
99.5%		100
97.5%		91.5952
90.0%		74.0584
75.0%	quartile	46.6846
50.0%	median	4.57272
25.0%	quartile	0
10.0%		0
2.5%		0
0.5%		0
0.0%	minimum	0

Moments

Mean	24.212042
Std Dev	30.476719
Std Err Mean	2.5575495
Upper 95% Mean	29.268142
Lower 95% Mean	19.155942
N	142

mean burst dur

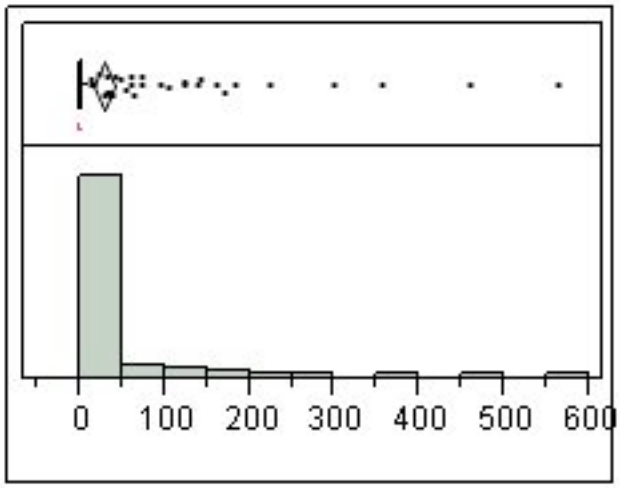

Quantiles

100.0%	maximum	563.488
99.5%		563.488
97.5%		321.844
90.0%		88.0175
75.0%	quartile	4.86532
50.0%	median	0.09583
25.0%	quartile	0
10.0%		0
2.5%		0
0.5%		0
0.0%	minimum	0

Moments

Mean	27.62467
Std Dev	79.705924
Std Err Mean	6.6887726
Upper 95% Mean	40.847915
Lower 95% Mean	14.401424
N	142

mean spikes/burst

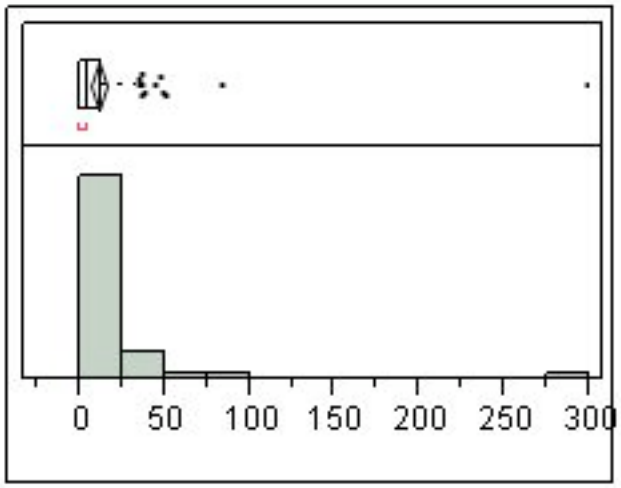

Quantiles

100.0%	maximum	299.167
99.5%		299.167
97.5%		49.7125
90.0%		31.625
75.0%	quartile	13.0324
50.0%	median	5
25.0%	quartile	0
10.0%		0
2.5%		0
0.5%		0
0.0%	minimum	0

Moments

Mean	11.275885
Std Dev	27.846949
Std Err Mean	2.336864
Upper 95% Mean	15.895705
Lower 95% Mean	6.6560651
N	142

mean ISI

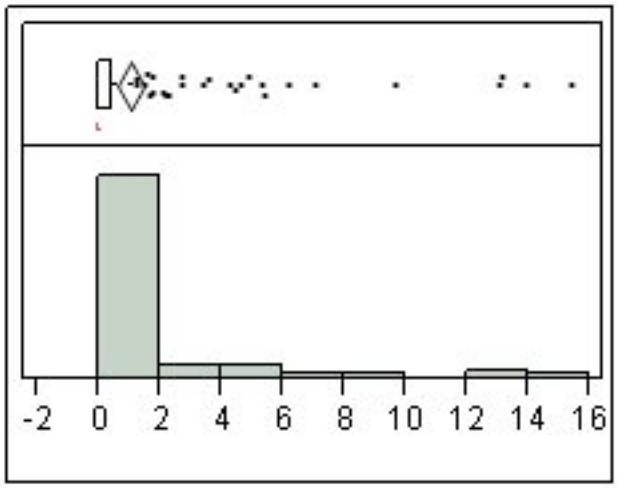

Quantiles

100.0%	maximum	15.3745
99.5%		15.3745
97.5%		13.0734
90.0%		3.50952
75.0%	quartile	0.46805
50.0%	median	0.01924
25.0%	quartile	0
10.0%		0
2.5%		0
0.5%		0
0.0%	minimum	0

Moments

Mean	1.0360313
Std Dev	2.6815061
Std Err Mean	0.225027
Upper 95% Mean	1.4808942
Lower 95% Mean	0.5911683
N	142

Mean Freq in burst

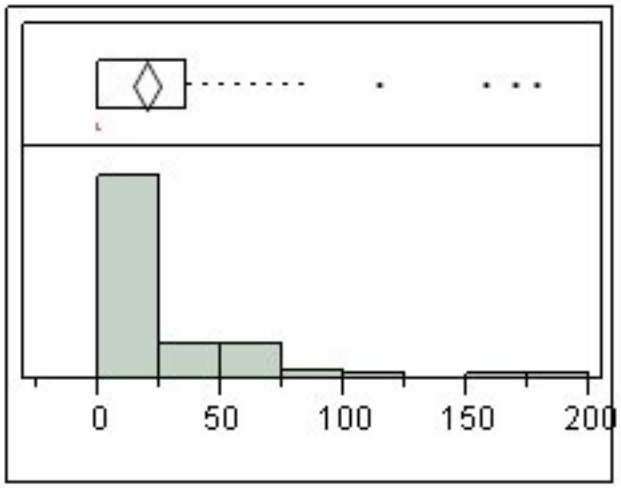

Quantiles

100.0%	maximum	177.895
99.5%		177.895
97.5%		132.779
90.0%		60.8475
75.0%	quartile	36.3319
50.0%	median	0.22584
25.0%	quartile	0
10.0%		0
2.5%		0
0.5%		0
0.0%	minimum	0

Moments

Mean	19.588642
Std Dev	33.075105
Std Err Mean	2.7756012
Upper 95% Mean	25.075816
Lower 95% Mean	14.101469
N	142

Mean Peak Freq

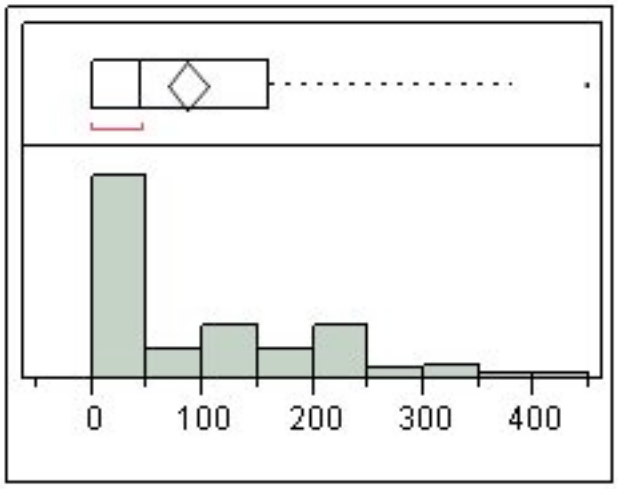

Quantiles

100.0%	maximum	446.429
99.5%		446.429
97.5%		341.668
90.0%		238.042
75.0%	quartile	159.606
50.0%	median	44.8338
25.0%	quartile	0
10.0%		0
2.5%		0
0.5%		0
0.0%	minimum	0

Moments

Mean	86.192464
Std Dev	103.81405
Std Err Mean	8.7118819
Upper 95% Mean	103.41526
Lower 95% Mean	68.969671
N	142

mean Interburst Int

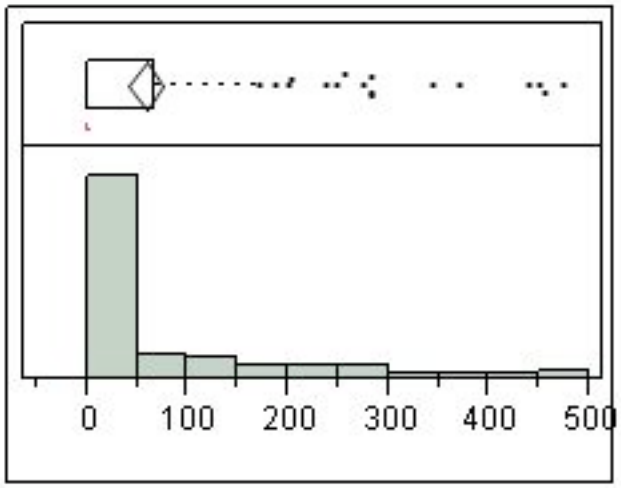

Quantiles

100.0%	maximum	472.288
99.5%		472.288
97.5%		443.179
90.0%		225.926
75.0%	quartile	67.7269
50.0%	median	0
25.0%	quartile	0
10.0%		0
2.5%		0
0.5%		0
0.0%	minimum	0

Moments

Mean	57.86649
Std Dev	106.48042
Std Err Mean	8.9356381
Upper 95% Mean	75.531634
Lower 95% Mean	40.201345
N	142

Mean Sup

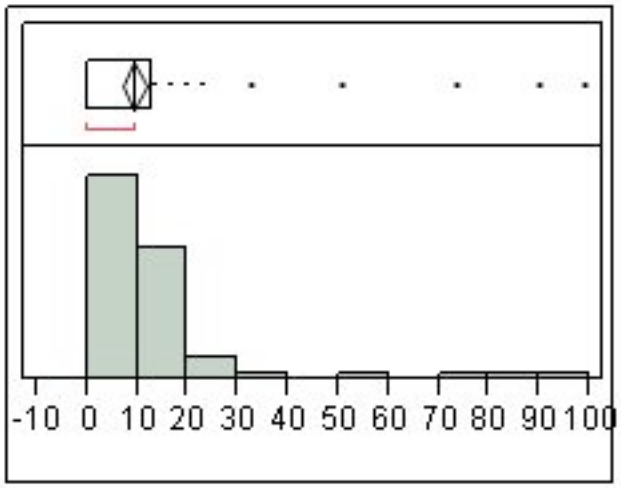

Quantiles

100.0%	maximum	98.9313
99.5%		98.9313
97.5%		60.2031
90.0%		17.1136
75.0%	quartile	12.7692
50.0%	median	9.39994
25.0%	quartile	0
10.0%		0
2.5%		0
0.5%		0
0.0%	minimum	0

Moments

Mean	9.2883172
Std Dev	14.174937
Std Err Mean	1.1895343
Upper 95% Mean	11.639945
Lower 95% Mean	6.9366893
N	142

Distributions Genotype=nhet

mean freq

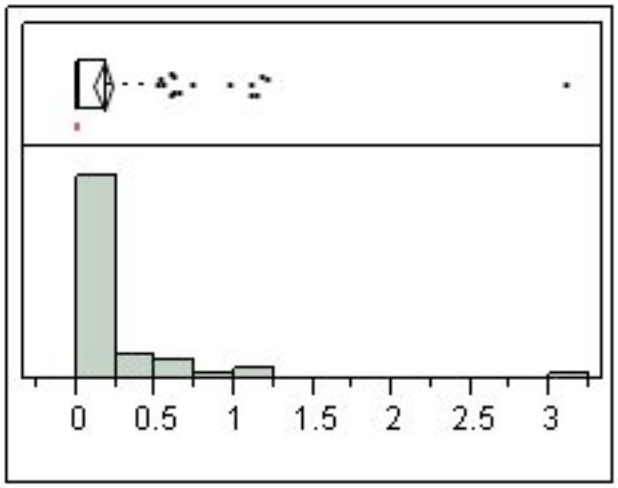

Quantiles

100.0%	maximum	3.09359
99.5%		3.09359
97.5%		1.15253
90.0%		0.56242
75.0%	quartile	0.18259
50.0%	median	0.01581
25.0%	quartile	0.002
10.0%		0.00033
2.5%		0
0.5%		0
0.0%	minimum	0

Moments

Mean	0.1670991
Std Dev	0.3704916
Std Err Mean	0.0317694
Upper 95% Mean	0.2299291
Lower 95% Mean	0.104269
N	136

numburst

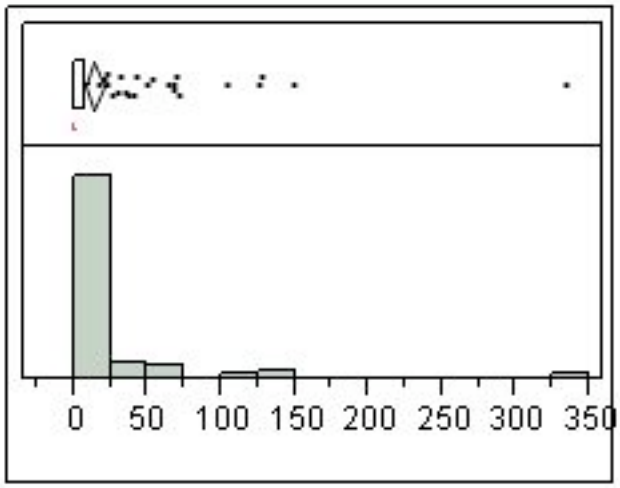

Quantiles

100.0%	maximum	334
99.5%		334
97.5%		126.15
90.0%		41.3
75.0%	quartile	6.75
50.0%	median	0.5
25.0%	quartile	0
10.0%		0
2.5%		0
0.5%		0
0.0%	minimum	0

Moments

Mean	13.257353
Std Dev	37.75496
Std Err Mean	3.2374611
Upper 95% Mean	19.660055
Lower 95% Mean	6.8546512
N	136

bursts/sec

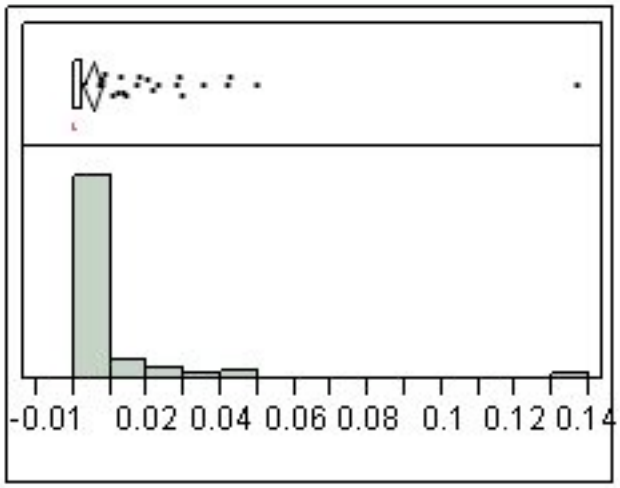

Quantiles

100.0%	maximum	0.13626
99.5%		0.13626
97.5%		0.04205
90.0%		0.01482
75.0%	quartile	0.00247
50.0%	median	0.00017
25.0%	quartile	0
10.0%		0
2.5%		0
0.5%		0
0.0%	minimum	0

Moments

Mean	0.0049063
Std Dev	0.0144658
Std Err Mean	0.0012404
Upper 95% Mean	0.0073595
Lower 95% Mean	0.0024531
N	136

%spikes in burst

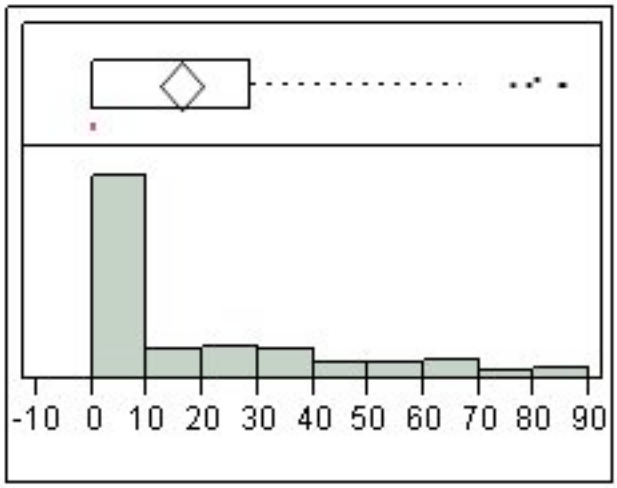

Quantiles

100.0%	maximum	85.1852
99.5%		85.1852
97.5%		79.7781
90.0%		53.2576
75.0%	quartile	28.5714
50.0%	median	0.36496
25.0%	quartile	0
10.0%		0
2.5%		0
0.5%		0
0.0%	minimum	0

Moments

Mean	16.111496
Std Dev	22.817453
Std Err Mean	1.9565804
Upper 95% Mean	19.98101
Lower 95% Mean	12.241982
N	136

mean burst dur

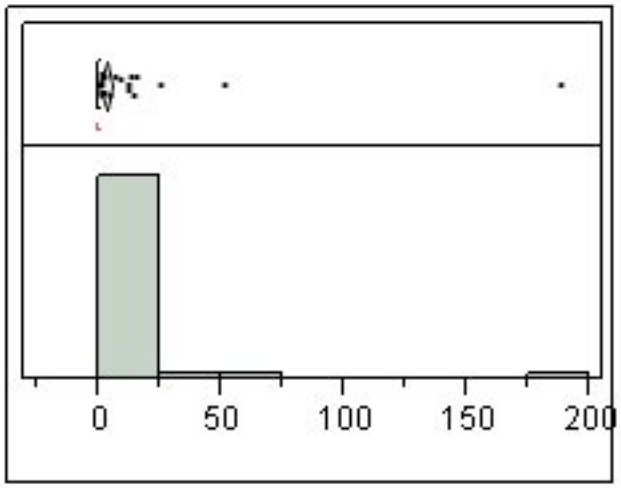

Quantiles

100.0%	maximum	188.03
99.5%		188.03
97.5%		20.7728
90.0%		1.93681
75.0%	quartile	0.1864
50.0%	median	0.01192
25.0%	quartile	0
10.0%		0
2.5%		0
0.5%		0
0.0%	minimum	0

Moments

Mean	2.7286406
Std Dev	16.914416
Std Err Mean	1.4503992
Upper 95% Mean	5.5970839
Lower 95% Mean	-0.139803
N	136

mean spikes/burst

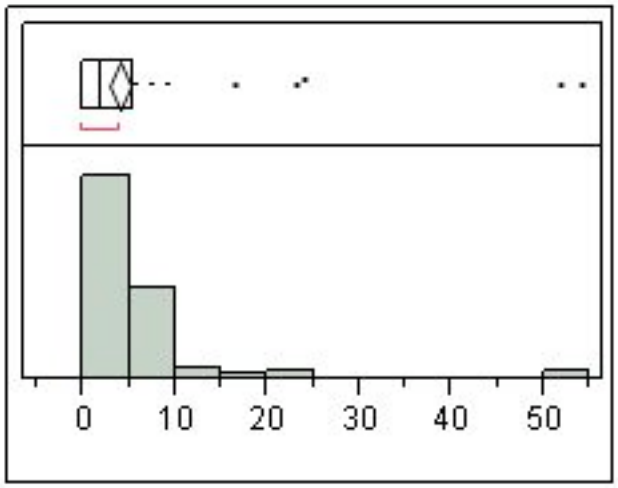

Quantiles

100.0%	maximum	54.2174
99.5%		54.2174
97.5%		23.575
90.0%		8.41951
75.0%	quartile	5.5
50.0%	median	2
25.0%	quartile	0
10.0%		0
2.5%		0
0.5%		0
0.0%	minimum	0

Moments

Mean	4.0037971
Std Dev	7.3384884
Std Err Mean	0.6292702
Upper 95% Mean	5.2482999
Lower 95% Mean	2.7592943
N	136

mean ISI

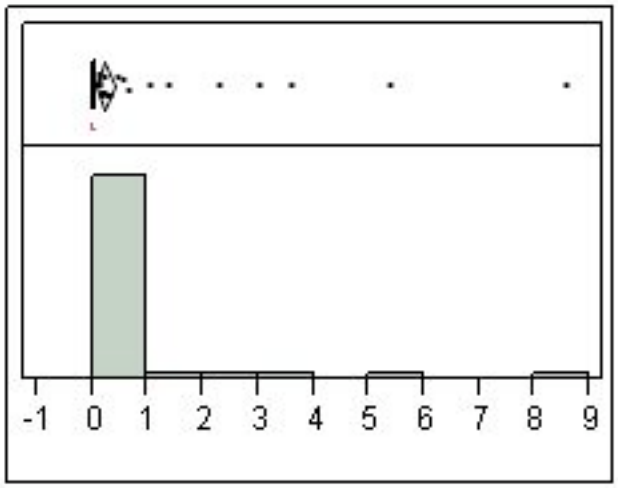

Quantiles

100.0%	maximum	8.54684
99.5%		8.54684
97.5%		3.34117
90.0%		0.22292
75.0%	quartile	0.04153
50.0%	median	0.00397
25.0%	quartile	0
10.0%		0
2.5%		0
0.5%		0
0.0%	minimum	0

Moments

Mean	0.2238637
Std Dev	0.967966
Std Err Mean	0.0830024
Upper 95% Mean	0.3880169
Lower 95% Mean	0.0597105
N	136

Mean Freq in burst

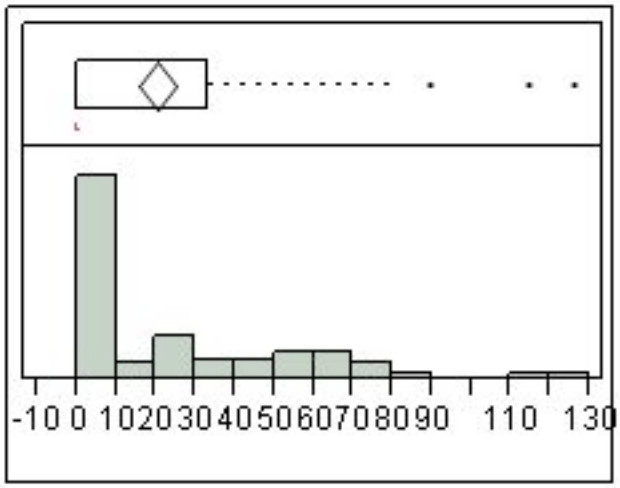

Quantiles

100.0%	maximum	125.839
99.5%		125.839
97.5%		84.8138
90.0%		65.7964
75.0%	quartile	33.364
50.0%	median	0.0585
25.0%	quartile	0
10.0%		0
2.5%		0
0.5%		0
0.0%	minimum	0

Moments

Mean	20.421773
Std Dev	28.004844
Std Err Mean	2.4013956
Upper 95% Mean	25.170994
Lower 95% Mean	15.672551
N	136

Mean Peak Freq

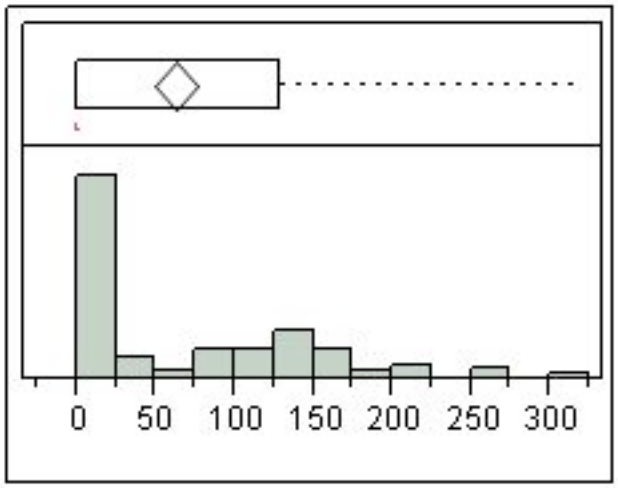

Quantiles

100.0%	maximum	317.494
99.5%		317.494
97.5%		262.996
90.0%		162.429
75.0%	quartile	128.573
50.0%	median	0.17052
25.0%	quartile	0
10.0%		0
2.5%		0
0.5%		0
0.0%	minimum	0

Moments

Mean	63.083929
Std Dev	77.009371
Std Err Mean	6.6034991
Upper 95% Mean	76.143618
Lower 95% Mean	50.02424
N	136

mean Interburst Int

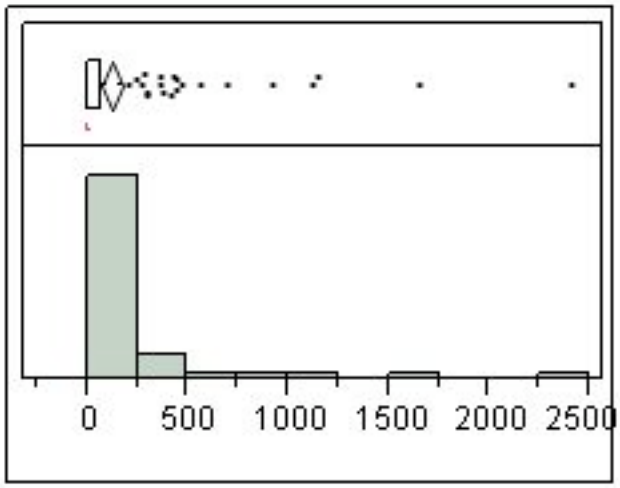

Quantiles

100.0%	maximum	2413.46
99.5%		2413.46
97.5%		1130.78
90.0%		391.756
75.0%	quartile	73.6802
50.0%	median	0
25.0%	quartile	0
10.0%		0
2.5%		0
0.5%		0
0.0%	minimum	0

Moments

Mean	118.70458
Std Dev	310.61398
Std Err Mean	26.634929
Upper 95% Mean	171.38027
Lower 95% Mean	66.028888
N	136

Mean Sup

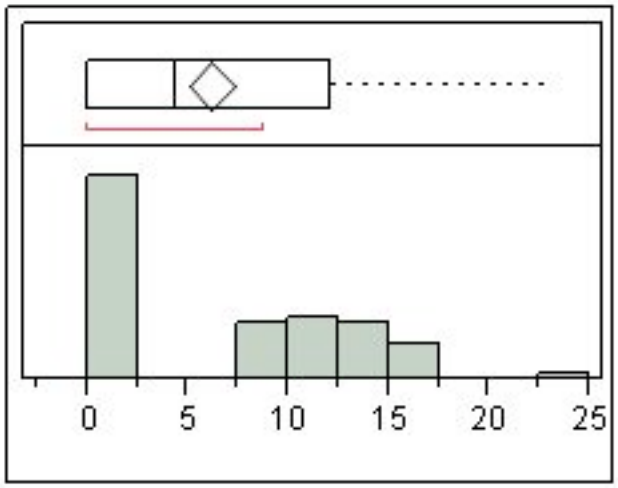

Quantiles

100.0%	maximum	23.0029
99.5%		23.0029
97.5%		16.1457
90.0%		14.916
75.0%	quartile	12.0956
50.0%	median	4.40326
25.0%	quartile	0
10.0%		0
2.5%		0
0.5%		0
0.0%	minimum	0

Moments

Mean	6.1704497
Std Dev	6.4736629
Std Err Mean	0.555112
Upper 95% Mean	7.2682904
Lower 95% Mean	5.0726089
N	136

Distributions Genotype=nko

mean freq

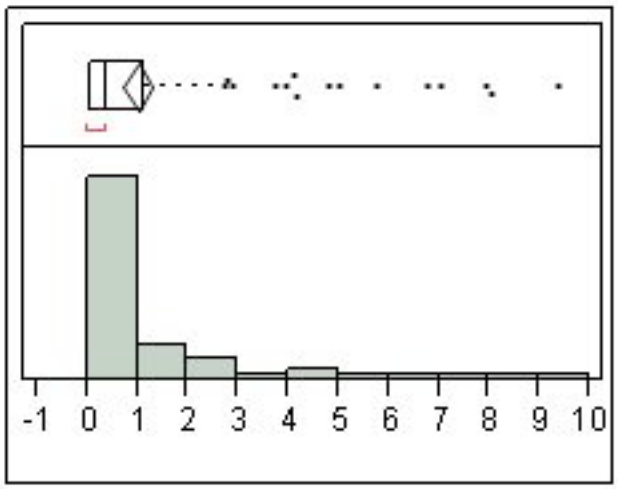

Quantiles

100.0%	maximum	9.38233
99.5%		9.38233
97.5%		7.22503
90.0%		2.71705
75.0%	quartile	1.11292
50.0%	median	0.35951
25.0%	quartile	0.05425
10.0%		0.00657
2.5%		0.00194
0.5%		0.00067
0.0%	minimum	0.00067

Moments

Mean	0.9953521
Std Dev	1.675381
Std Err Mean	0.1367943
Upper 95% Mean	1.2656595
Lower 95% Mean	0.7250448
N	150

numburst

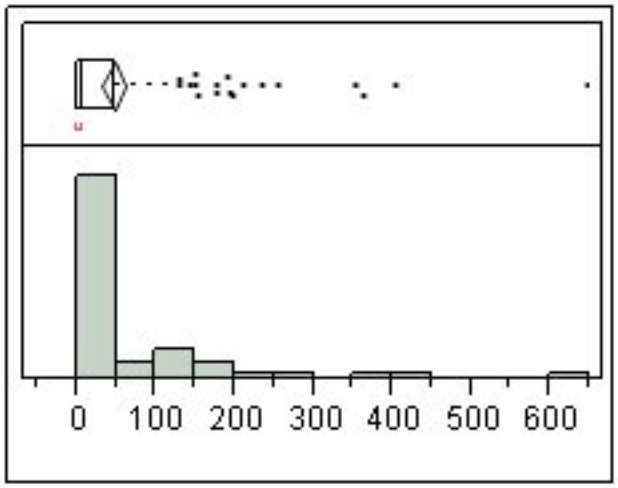

Quantiles

100.0%	maximum	645
99.5%		645
97.5%		353.7
90.0%		147.6
75.0%	quartile	49.75
50.0%	median	9
25.0%	quartile	1
10.0%		0
2.5%		0
0.5%		0
0.0%	minimum	0

Moments

Mean	46.946667
Std Dev	88.180245
Std Err Mean	7.1998868
Upper 95% Mean	61.173738
Lower 95% Mean	32.719595
N	150

bursts/sec

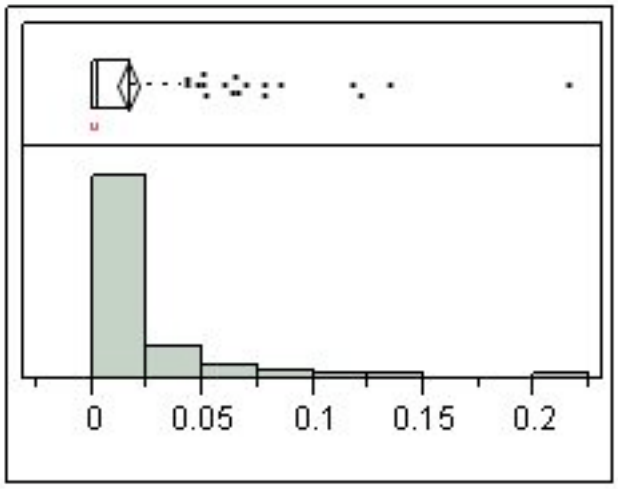

Quantiles

100.0%	maximum	0.215
99.5%		0.215
97.5%		0.1179
90.0%		0.0492
75.0%	quartile	0.01715
50.0%	median	0.003
25.0%	quartile	0.00033
10.0%		0
2.5%		0
0.5%		0
0.0%	minimum	0

Moments

Mean	0.0158194
Std Dev	0.0296088
Std Err Mean	0.0024175
Upper 95% Mean	0.0205965
Lower 95% Mean	0.0110423
N	150

%spikes in burst

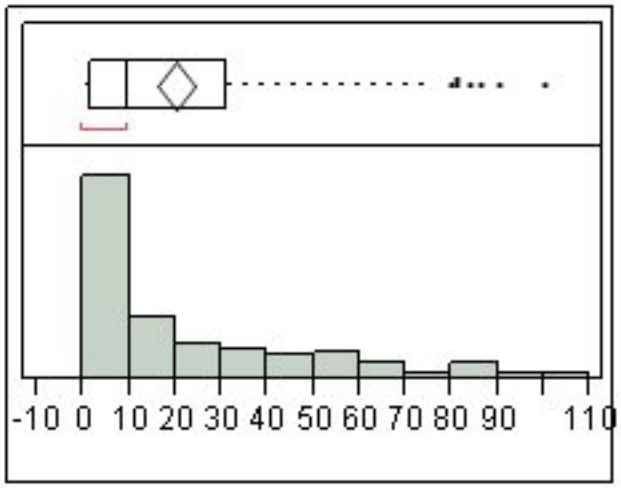

Quantiles

100.0%	maximum	100
99.5%		100
97.5%		84.4583
90.0%		57.5603
75.0%	quartile	30.907
50.0%	median	9.60464
25.0%	quartile	1.4355
10.0%		0
2.5%		0
0.5%		0
0.0%	minimum	0

Moments

Mean	20.256134
Std Dev	24.231896
Std Err Mean	1.978526
Upper 95% Mean	24.165728
Lower 95% Mean	16.346541
N	150

mean burst dur

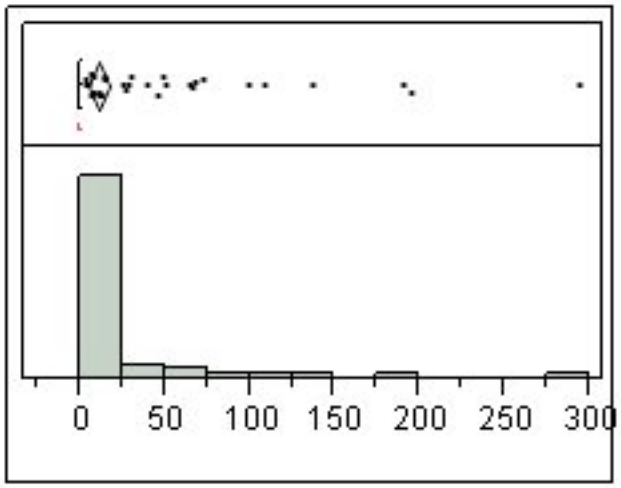

Quantiles

100.0%	maximum	293.081
99.5%		293.081
97.5%		148.453
90.0%		30.0132
75.0%	quartile	0.832
50.0%	median	0.26524
25.0%	quartile	0.0618
10.0%		0
2.5%		0
0.5%		0
0.0%	minimum	0

Moments

Mean	11.474915
Std Dev	37.649918
Std Err Mean	3.0741029
Upper 95% Mean	17.549382
Lower 95% Mean	5.4004466
N	150

mean spikes/burst

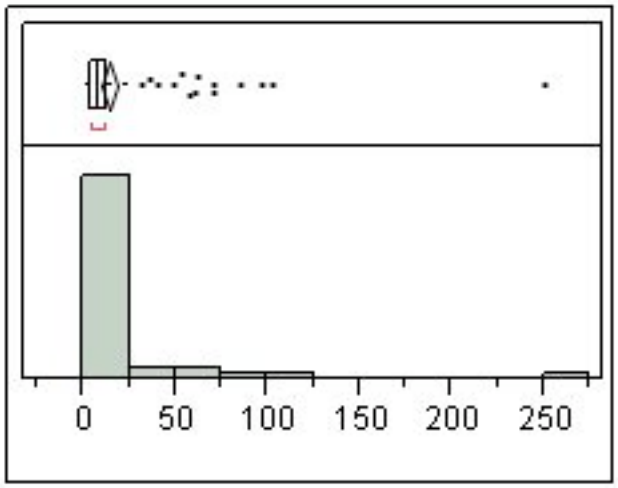

Quantiles

100.0%	maximum	250.5
99.5%		250.5
97.5%		87.4275
90.0%		24.9
75.0%	quartile	12.9559
50.0%	median	7.97927
25.0%	quartile	4.30556
10.0%		0
2.5%		0
0.5%		0
0.0%	minimum	0

Moments

Mean	13.965969
Std Dev	26.229424
Std Err Mean	2.1416235
Upper 95% Mean	18.197845
Lower 95% Mean	9.7340922
N	150

mean ISI

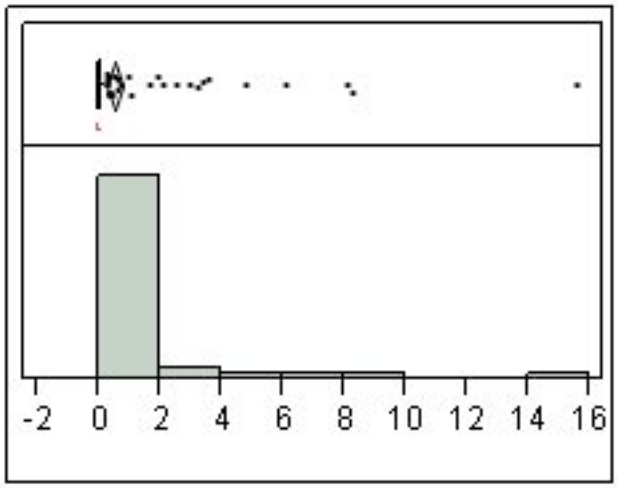

Quantiles

100.0%	maximum	15.5566
99.5%		15.5566
97.5%		6.56829
90.0%		0.92661
75.0%	quartile	0.09502
50.0%	median	0.03753
25.0%	quartile	0.01399
10.0%		0
2.5%		0
0.5%		0
0.0%	minimum	0

Moments

Mean	0.5066384
Std Dev	1.7647409
Std Err Mean	0.1440905
Upper 95% Mean	0.7913631
Lower 95% Mean	0.2219137
N	150

Mean Freq in burst

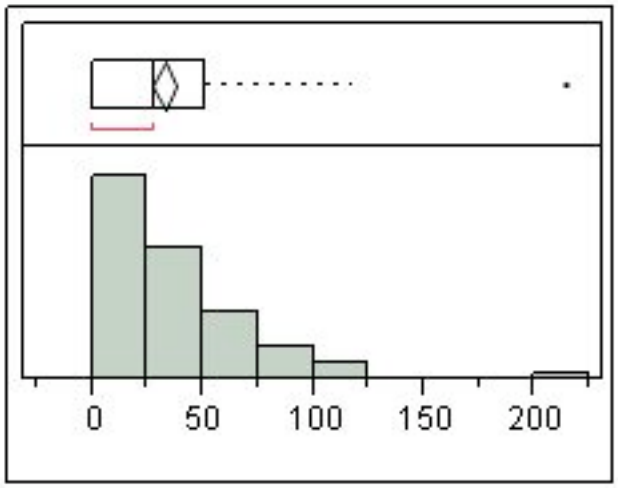

Quantiles

100.0%	maximum	213.802
99.5%		213.802
97.5%		106.778
90.0%		84.6312
75.0%	quartile	50.9397
50.0%	median	28.4448
25.0%	quartile	0.29275
10.0%		0
2.5%		0
0.5%		0
0.0%	minimum	0

Moments

Mean	32.562248
Std Dev	34.306252
Std Err Mean	2.8010937
Upper 95% Mean	38.097246
Lower 95% Mean	27.02725
N	150

Mean Peak Freq

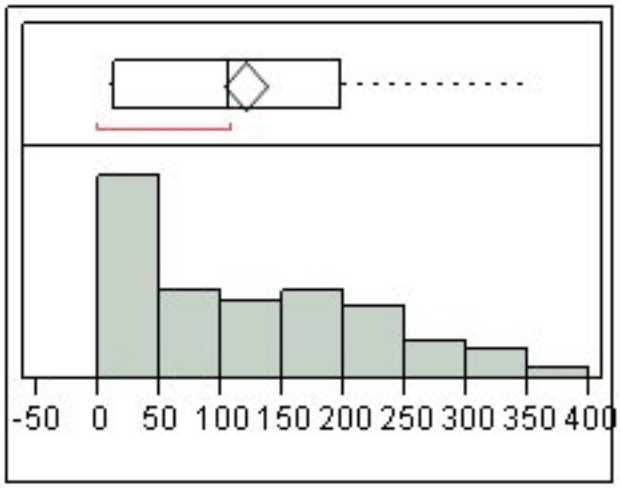

Quantiles

100.0%	maximum	353.471
99.5%		353.471
97.5%		327.604
90.0%		269.524
75.0%	quartile	197.607
50.0%	median	106.12
25.0%	quartile	12.4382
10.0%		0
2.5%		0
0.5%		0
0.0%	minimum	0

Moments

Mean	119.85933
Std Dev	103.29289
Std Err Mean	8.4338288
Upper 95% Mean	136.52468
Lower 95% Mean	103.19397
N	150

mean Interburst Int

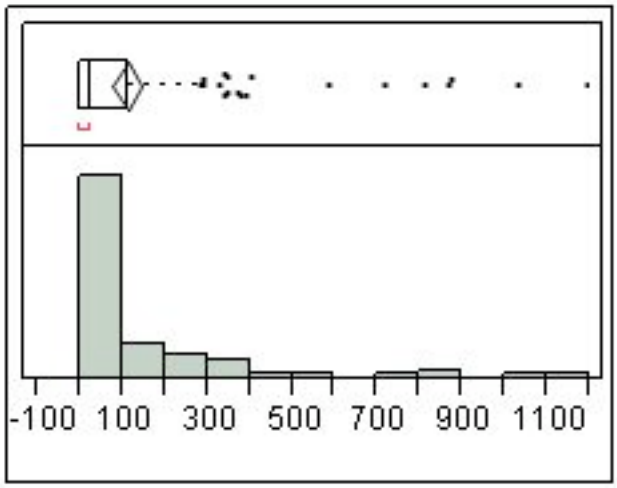

Quantiles

100.0%	maximum	1192.86
99.5%		1192.86
97.5%		869.439
90.0%		336.496
75.0%	quartile	113.671
50.0%	median	25.77
25.0%	quartile	0
10.0%		0
2.5%		0
0.5%		0
0.0%	minimum	0

Moments

Mean	111.06559
Std Dev	200.67254
Std Err Mean	16.384844
Upper 95% Mean	143.44226
Lower 95% Mean	78.688926
N	150

Mean Sup

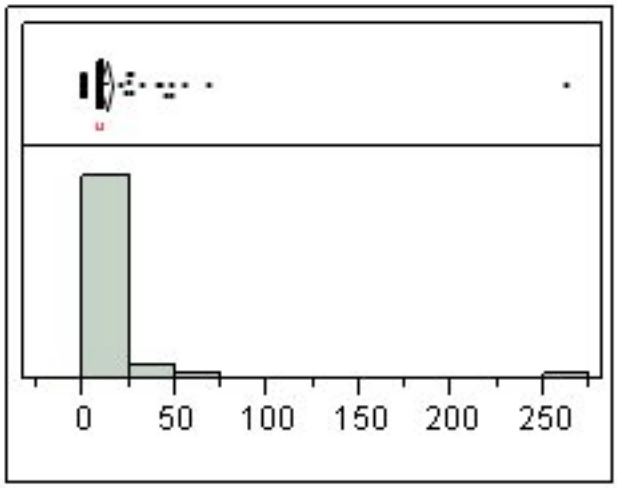

Quantiles

100.0%	maximum	262.041
99.5%		262.041
97.5%		49.4241
90.0%		19.5513
75.0%	quartile	11.6795
50.0%	median	9.81655
25.0%	quartile	8.43799
10.0%		0
2.5%		0
0.5%		0
0.0%	minimum	0

Moments

Mean	12.562467
Std Dev	23.016195
Std Err Mean	1.8792644
Upper 95% Mean	16.275918
Lower 95% Mean	8.8490157
N	150

Distributions Genotype=nwt

mean freq

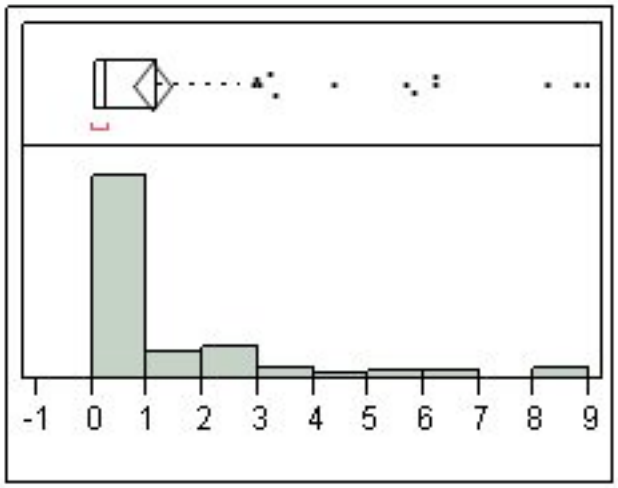

Quantiles

100.0%	maximum	8.96933
99.5%		8.96933
97.5%		8.33839
90.0%		3.00233
75.0%	quartile	1.17088
50.0%	median	0.27722
25.0%	quartile	0.04402
10.0%		0.00434
2.5%		0.0004
0.5%		0
0.0%	minimum	0

Moments

Mean	1.0811275
Std Dev	1.8440898
Std Err Mean	0.1742501
Upper 95% Mean	1.4264157
Lower 95% Mean	0.7358393
N	112

numburst

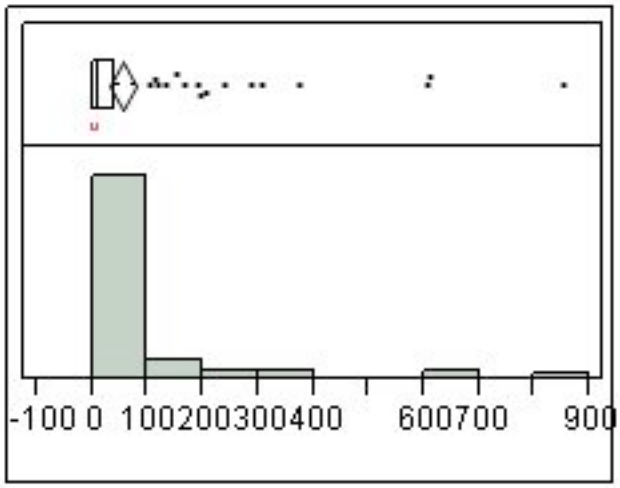

Quantiles

100.0%	maximum	850
99.5%		850
97.5%		605.875
90.0%		161.9
75.0%	quartile	40.75
50.0%	median	9
25.0%	quartile	0.25
10.0%		0
2.5%		0
0.5%		0
0.0%	minimum	0

Moments

Mean	54.232143
Std Dev	126.89884
Std Err Mean	11.990813
Upper 95% Mean	77.992739
Lower 95% Mean	30.471546
N	112

bursts/sec

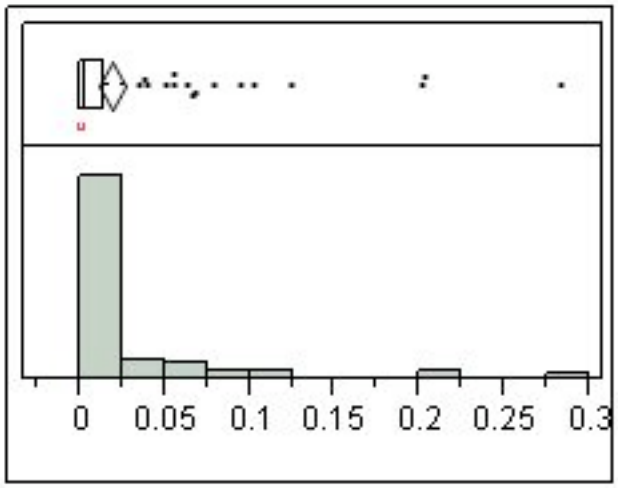

Quantiles

100.0%	maximum	0.28333
99.5%		0.28333
97.5%		0.20196
90.0%		0.05574
75.0%	quartile	0.01367
50.0%	median	0.003
25.0%	quartile	8.33e-5
10.0%		0
2.5%		0
0.5%		0
0.0%	minimum	0

Moments

Mean	0.0183171
Std Dev	0.0423466
Std Err Mean	0.0040014
Upper 95% Mean	0.0262461
Lower 95% Mean	0.0103881
N	112

%spikes in burst

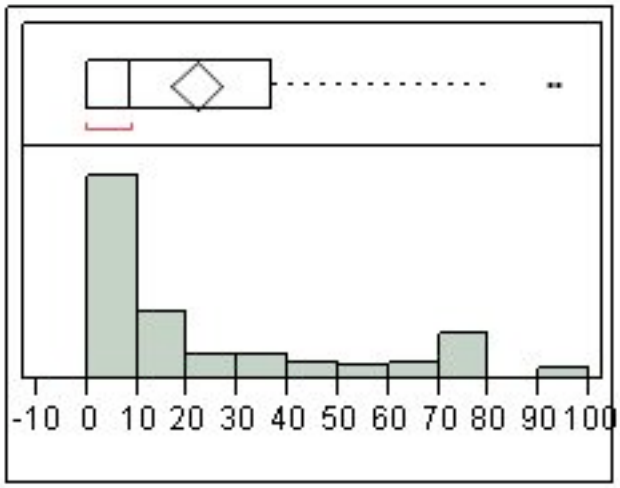

Quantiles

100.0%	maximum	93.7538
99.5%		93.7538
97.5%		81.3397
90.0%		71.2723
75.0%	quartile	36.5859
50.0%	median	8.73608
25.0%	quartile	0.06702
10.0%		0
2.5%		0
0.5%		0
0.0%	minimum	0

Moments

Mean	21.635594
Std Dev	27.06569
Std Err Mean	2.5574673
Upper 95% Mean	26.703386
Lower 95% Mean	16.567801
N	112

mean burst dur

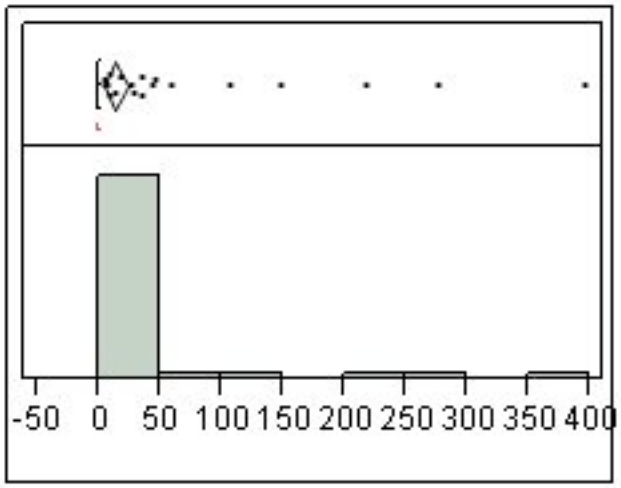

Quantiles

100.0%	maximum	396.692
99.5%		396.692
97.5%		228.309
90.0%		32.361
75.0%	quartile	0.86013
50.0%	median	0.16759
25.0%	quartile	0.0081
10.0%		0
2.5%		0
0.5%		0
0.0%	minimum	0

Moments

Mean	13.731937
Std Dev	52.55516
Std Err Mean	4.9659958
Upper 95% Mean	23.572389
Lower 95% Mean	3.8914845
N	112

mean spikes/burst

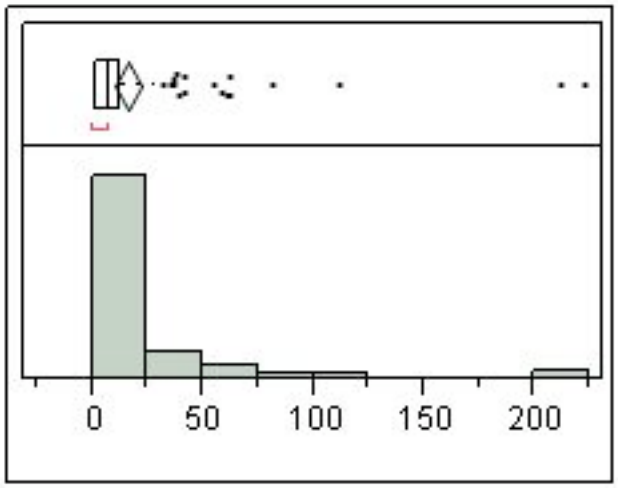

Quantiles

100.0%	maximum	223
99.5%		223
97.5%		129.408
90.0%		41.25
75.0%	quartile	12.3718
50.0%	median	7.27924
25.0%	quartile	1
10.0%		0
2.5%		0
0.5%		0
0.0%	minimum	0

Moments

Mean	16.391117
Std Dev	32.883474
Std Err Mean	3.1071963
Upper 95% Mean	22.548233
Lower 95% Mean	10.234
N	112

mean ISI

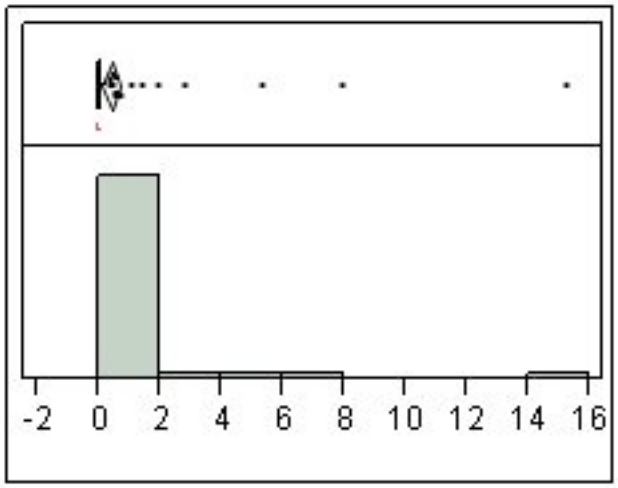

Quantiles

100.0%	maximum	15.2574
99.5%		15.2574
97.5%		5.77068
90.0%		0.48605
75.0%	quartile	0.10082
50.0%	median	0.02445
25.0%	quartile	0.00173
10.0%		0
2.5%		0
0.5%		0
0.0%	minimum	0

Moments

Mean	0.3926141
Std Dev	1.7068686
Std Err Mean	0.1612839
Upper 95% Mean	0.712209
Lower 95% Mean	0.0730193
N	112

Mean Freq in burst

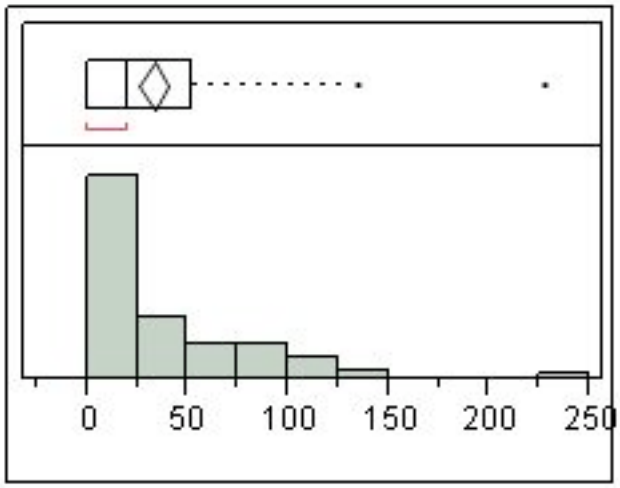

Quantiles

100.0%	maximum	228.03
99.5%		228.03
97.5%		128.745
90.0%		91.1637
75.0%	quartile	51.4696
50.0%	median	19.7996
25.0%	quartile	0.01639
10.0%		0
2.5%		0
0.5%		0
0.0%	minimum	0

Moments

Mean	33.074433
Std Dev	40.859542
Std Err Mean	3.8608638
Upper 95% Mean	40.724992
Lower 95% Mean	25.423873
N	112

Mean Peak Freq

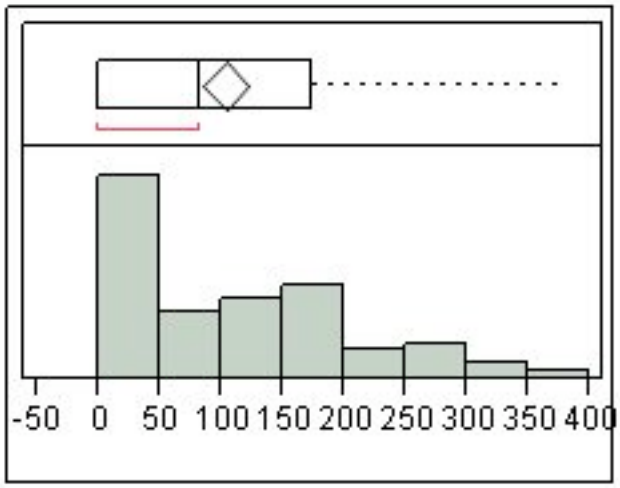

Quantiles

100.0%	maximum	374.946
99.5%		374.946
97.5%		332.065
90.0%		246.917
75.0%	quartile	173.173
50.0%	median	82.2225
25.0%	quartile	0.91562
10.0%		0
2.5%		0
0.5%		0
0.0%	minimum	0

Moments

Mean	103.34146
Std Dev	97.378966
Std Err Mean	9.2014474
Upper 95% Mean	121.57474
Lower 95% Mean	85.10818
N	112

mean Interburst Int

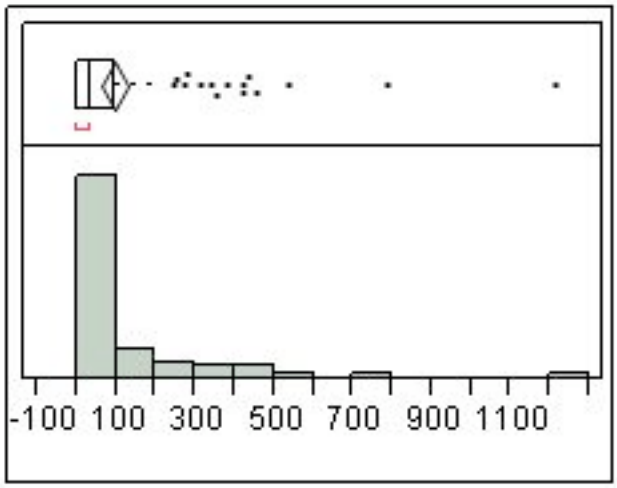

Quantiles

100.0%	maximum	1213.67
99.5%		1213.67
97.5%		580.572
90.0%		301.986
75.0%	quartile	97.3049
50.0%	median	32.8053
25.0%	quartile	0
10.0%		0
2.5%		0
0.5%		0
0.0%	minimum	0

Moments

Mean	95.059022
Std Dev	172.29477
Std Err Mean	16.280325
Upper 95% Mean	127.31957
Lower 95% Mean	62.798471
N	112

Mean Sup

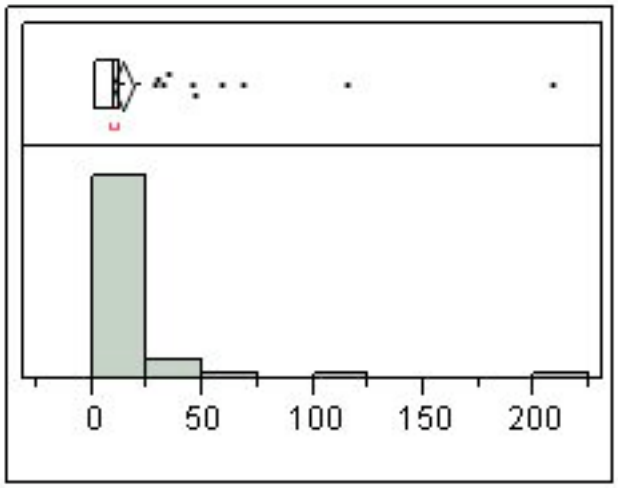

Quantiles

100.0%	maximum	208.247
99.5%		208.247
97.5%		76.2196
90.0%		26.5623
75.0%	quartile	12.2125
50.0%	median	9.79406
25.0%	quartile	2.08063
10.0%		0
2.5%		0
0.5%		0
0.0%	minimum	0

Moments

Mean	13.545382
Std Dev	23.785909
Std Err Mean	2.2475571
Upper 95% Mean	17.999067
Lower 95% Mean	9.0916976
N	112

Distributions Genotype=wt

mean freq

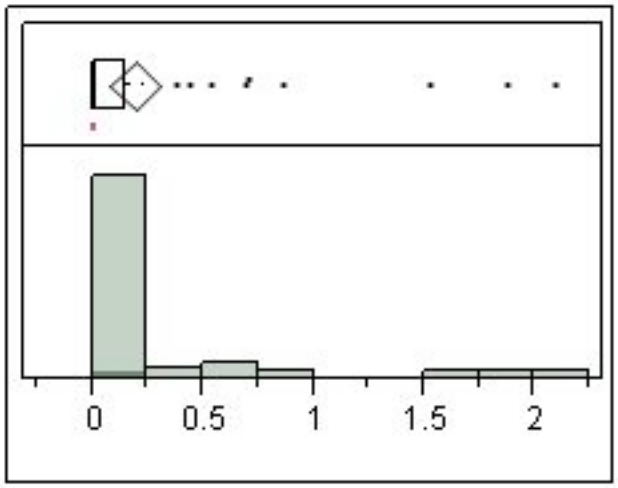

Quantiles

100.0%	maximum	2.09067
99.5%		2.09067
97.5%		1.99915
90.0%		0.69275
75.0%	quartile	0.14444
50.0%	median	0.01333
25.0%	quartile	0.0022
10.0%		0.0009
2.5%		0.00039
0.5%		0.00033
0.0%	minimum	0.00033

Moments

Mean	0.1917324
Std Dev	0.4413948
Std Err Mean	0.0589839
Upper 95% Mean	0.3099387
Lower 95% Mean	0.0735261
N	56

numburst

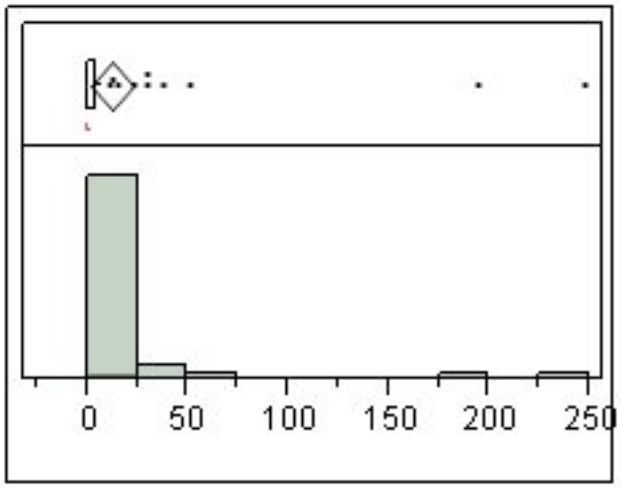

Quantiles

100.0%	maximum	247
99.5%		247
97.5%		224.475
90.0%		29
75.0%	quartile	4
50.0%	median	0
25.0%	quartile	0
10.0%		0
2.5%		0
0.5%		0
0.0%	minimum	0

Moments

Mean	12.196429
Std Dev	42.049071
Std Err Mean	5.6190434
Upper 95% Mean	23.457243
Lower 95% Mean	0.9356139
N	56

bursts/sec

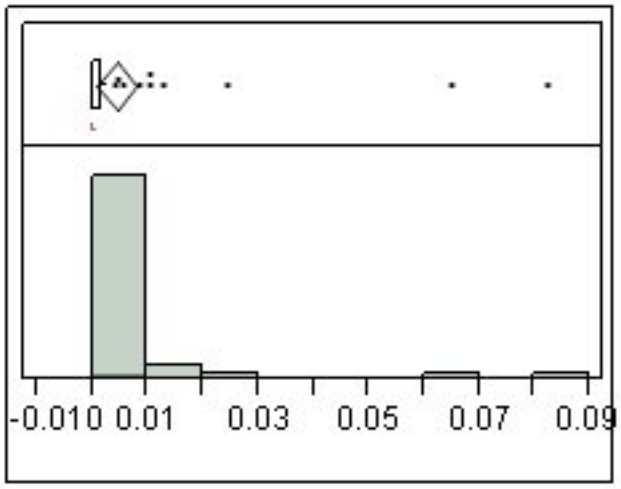

Quantiles

100.0%	maximum	0.08233
99.5%		0.08233
97.5%		0.07482
90.0%		0.01046
75.0%	quartile	0.00144
50.0%	median	0
25.0%	quartile	0
10.0%		0
2.5%		0
0.5%		0
0.0%	minimum	0

Moments

Mean	0.0042799
Std Dev	0.0141835
Std Err Mean	0.0018953
Upper 95% Mean	0.0080782
Lower 95% Mean	0.0004815
N	56

%spikes in burst

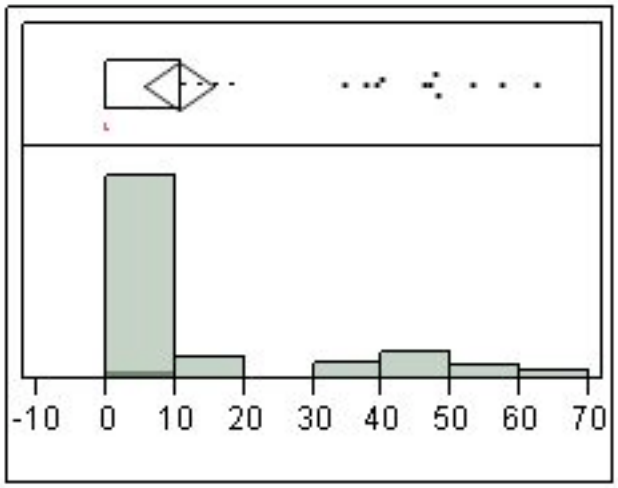

Quantiles

100.0%	maximum	62.4
99.5%		62.4
97.5%		60.1907
90.0%		47.0699
75.0%	quartile	10.9558
50.0%	median	0
25.0%	quartile	0
10.0%		0
2.5%		0
0.5%		0
0.0%	minimum	0

Moments

Mean	10.596224
Std Dev	18.757738
Std Err Mean	2.5066081
Upper 95% Mean	15.619579
Lower 95% Mean	5.5728687
N	56

mean burst dur

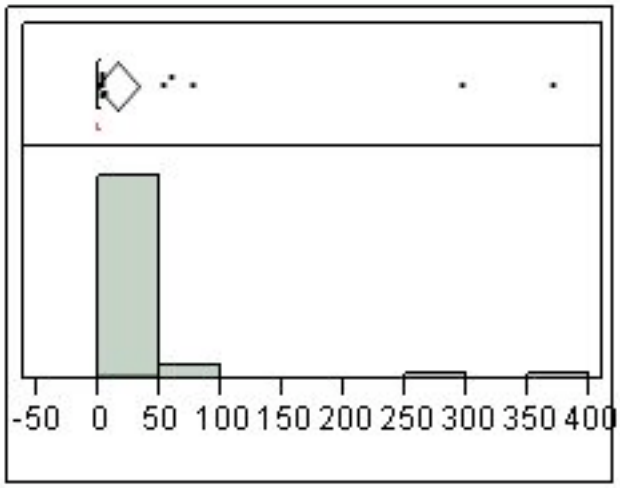

Quantiles

100.0%	maximum	369.771
99.5%		369.771
97.5%		338.053
90.0%		19.1462
75.0%	quartile	0.32027
50.0%	median	0
25.0%	quartile	0
10.0%		0
2.5%		0
0.5%		0
0.0%	minimum	0

Moments

Mean	15.482148
Std Dev	63.601002
Std Err Mean	8.4990414
Upper 95% Mean	32.514608
Lower 95% Mean	-1.550311
N	56

mean spikes/burst

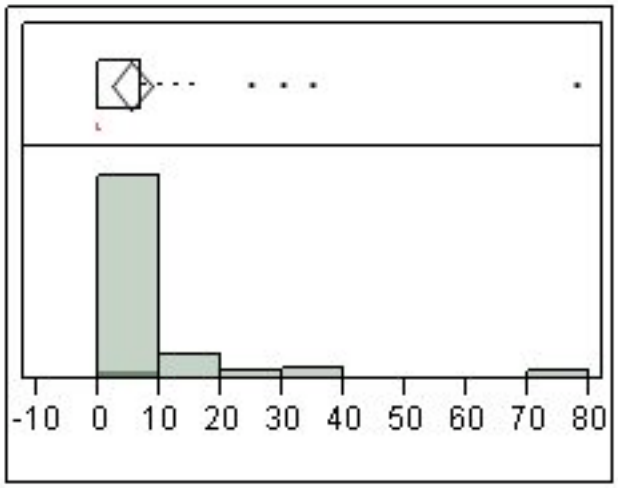

Quantiles

100.0%	maximum	78
99.5%		78
97.5%		59.6187
90.0%		16
75.0%	quartile	6.82282
50.0%	median	0
25.0%	quartile	0
10.0%		0
2.5%		0
0.5%		0
0.0%	minimum	0

Moments

Mean	5.3733943
Std Dev	12.495652
Std Err Mean	1.6698017
Upper 95% Mean	8.7197518
Lower 95% Mean	2.0270369
N	56

mean ISI

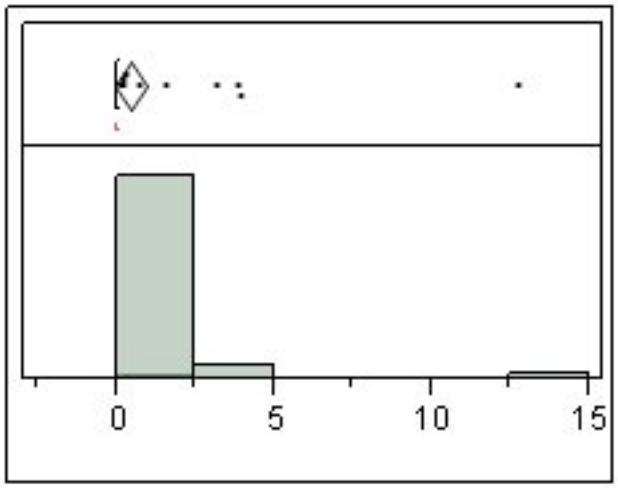

Quantiles

100.0%	maximum	12.7507
99.5%		12.7507
97.5%		9.01099
90.0%		0.9523
75.0%	quartile	0.04189
50.0%	median	0
25.0%	quartile	0
10.0%		0
2.5%		0
0.5%		0
0.0%	minimum	0

Moments

Mean	0.4855427
Std Dev	1.872066
Std Err Mean	0.2501653
Upper 95% Mean	0.9868852
Lower 95% Mean	-0.0158
N	56

Mean Freq in burst

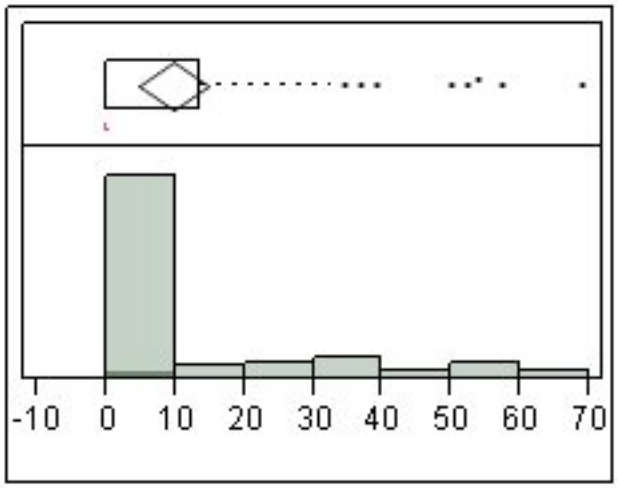

Quantiles

100.0%	maximum	68.8418
99.5%		68.8418
97.5%		63.8343
90.0%		42.41
75.0%	quartile	13.6973
50.0%	median	0
25.0%	quartile	0
10.0%		0
2.5%		0
0.5%		0
0.0%	minimum	0

Moments

Mean	9.6900923
Std Dev	18.314093
Std Err Mean	2.4473236
Upper 95% Mean	14.594638
Lower 95% Mean	4.7855462
N	56

Mean Peak Freq

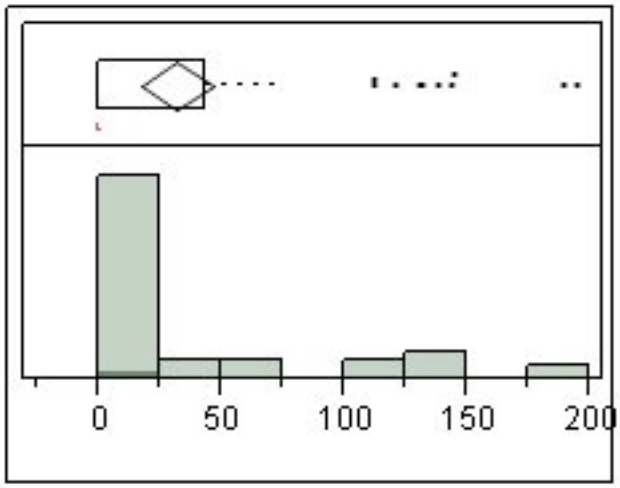

Quantiles

100.0%	maximum	194.69
99.5%		194.69
97.5%		192.36
90.0%		133.338
75.0%	quartile	43.1369
50.0%	median	0
25.0%	quartile	0
10.0%		0
2.5%		0
0.5%		0
0.0%	minimum	0

Moments

Mean	31.80006
Std Dev	55.487143
Std Err Mean	7.4147813
Upper 95% Mean	46.659614
Lower 95% Mean	16.940506
N	56

mean Interburst Int

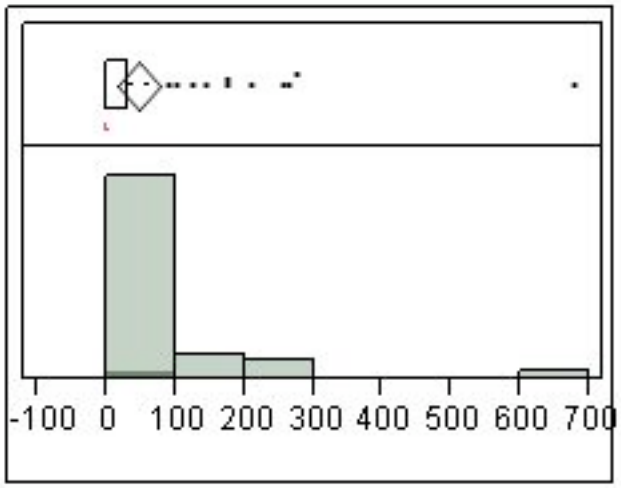

Quantiles

100.0%	maximum	678.169
99.5%		678.169
97.5%		506.814
90.0%		185.603
75.0%	quartile	32.3746
50.0%	median	0
25.0%	quartile	0
10.0%		0
2.5%		0
0.5%		0
0.0%	minimum	0

Moments

Mean	47.922449
Std Dev	113.65439
Std Err Mean	15.187707
Upper 95% Mean	78.359294
Lower 95% Mean	17.485605
N	56

Mean Sup

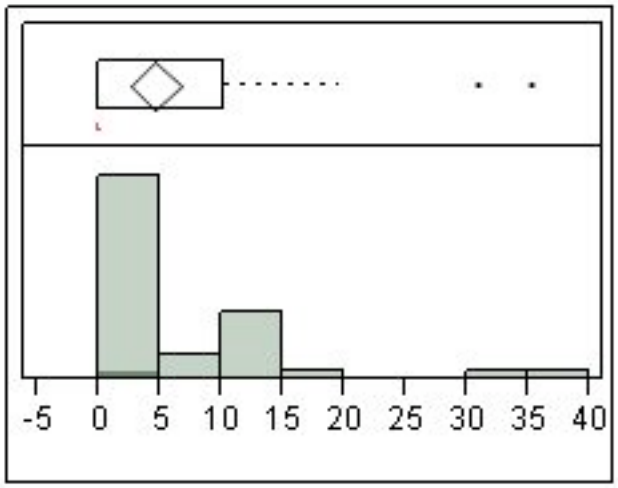

Quantiles

100.0%	maximum	35.3158
99.5%		35.3158
97.5%		33.3818
90.0%		11.5699
75.0%	quartile	10.2271
50.0%	median	0
25.0%	quartile	0
10.0%		0
2.5%		0
0.5%		0
0.0%	minimum	0

Moments

Mean	4.5874997
Std Dev	7.6954486
Std Err Mean	1.0283476
Upper 95% Mean	6.6483543
Lower 95% Mean	2.5266451
N	56

APPENDIX F – MATLAB SUPPLEMENT

This is a transcript of the programs used for MEA analysis. This was performed on Matlab 7.8. This is functional if placed in a single file in matlab. The correlation also requires a lookup table for the positional information.

```
function avesdists = correlater(mati,cellname)
%cells is a 2xn matrix of aves (row1) and dist (row2)
%mati must have averages, cellname is sheet name
targ = mati(1,:);
ref = cellname;
table = evalin('base','lookup');
distlist = [];
refcol = find(table(1,:)==ref);
for i = 1:length(targ);
   refrow = find(table(:,1)==targ(i));
   dist = table(refrow,refcol);
   distlist(i,:) = dist;
end
avesdists(1,:) = mati(size(mati,1),:);
avesdists(2,:) = transpose(distlist);
end

function [mato] = stcorr(cells)
%performs full stcorr on one cell file, mato is a 2xn array of
%corr/position,
r = @(x)x(:,2);
rows = @(x)x(:,1);
colnum = @(x)r(size(x));
rownum = @(x)rows(size(x));
avs = @(x)mean(x(:,(1:colnum(x))));
%files have filename.textdata(cell unitposition) and data(the corr data)
g = fieldnames(cells.textdata);%list of all the worksheets/cells compared
firstfield = g(1);%the first worksheet, to get all the cells compared
unitmat = getunits(cells.textdata.(char(firstfield))(1,:));%to replace cells
corrs = [];
for i = 1:length(g);
   cellsheet = char(g(i));
   cellname = str2num(cellsheet(4:5));% number of cell name for lookup function
   dat = cells.data.(char(cellsheet));%get data from sheet name
   dat((rownum(dat) +1),:) = avs(dat);%get the average of all the columns into last row
   dat(1,:) = unitmat(:,(2:length(unitmat)));%puts cell numbers above column
   corred = correlater(dat,cellname);%places all correlations in a 2xn array
   corrs((1:2),((size(corrs,2)+1):(size(corrs,2)+size(corred,2)))) = corred;
end
mato = corrs;%
end

function [arro] = getunits(chararr)
%makes numbers from cell name array
numcells = length(chararr);
```

```
arr = [];
for i = 1:numcells
   x = chararr{i};
   y = x(4:5);
   if strcmp(y,'e ')
   arr(1,i) = 0;
   else
   arr(1,i) = str2num(y);
   end
end
arro = arr(1,:);

end

function [] = correlationanalysis(age,animal)
%performs correlation analysis
%requires lookup table (mat file) in workspace, all cells must be numbered
%and files may come from NEX crosscorrelation functions
  sheet = importdata(strcat(animal,'.xls'));
  %assignin('base',char(animal), sheet);
datapoints = stcorr(sheet);
sorted = sortrows(transpose(datapoints),2);
g = [];
for i = 1:9
 z = find(sorted(:,2)<=i & sorted(:,2)>(i-1));
 r = mean(sorted(transpose(z),1));
 g(i,1) = r;
end
g(:,2)= [0 ;1; 2; 3; 4; 5; 6; 7; 8];
xlswrite(age,g,animal,'A1');
xlswrite(age,sorted,animal,'D1');
end

function []= meanmedindtoxls(filename,varargin)
%writes inds med and means to xls
evalin('base','clear')%clear variables
getdis_ind(filename)%get animals sheets
%inddelzeros();%clear zeros in animal sheets
for i = 1:(nargin-1)%group genotypes
    var1 = varargin{i};
gtlist2(var1)%normalizes to burst
xlswrite(strcat(filename,'aves'),evalin('base',char(var1)),char(var1)) %only writes the
zeroed means of the
end

for i = 1:(nargin-1)%group genotypes
```

```
    var1 = varargin{i};
gtlist2med(var1)%normalizes to burst
xlswrite(strcat(filename,'aves'),evalin('base',char(var1)),strcat(char(var1),'med')) %only
writes the zeroed means of the
end


function []= mediangraphmaker(filename,varargin)
%makes a graph with medians of individual animals averaged into a genotype
%'mean median stat of individual animals'

evalin('base','clear')%clear variables
getdis_ind(filename)%get animals sheets

for i = 1:(nargin-1)%group genotypes
    var1 = varargin{i};
gtlist2med(var1)
end

for i = [5,7,9,10,12,14,16,18,20]%plot means for all genotypes
v = strcat(filename,titler(i),'m');
x = graphprep(i,varargin);
h = graphfromgt(x,v);
%h = findobj(handle.Name,'Figure 1')
saveas(h,v,'jpg');
close

end

inddelzeros();%clear zeros in animal sheets

for i = [5,7,9,10,12,14,16,18,20]%plot new means without zeros for all genotypes
v = strcat(filename,titler(i),'m','z')
x = graphprep(i,varargin);
h = graphfromgt(x,v);
%h = findobj(handle.Name,'Figure 1')
saveas(h,v,'jpg');
close

end
evalin ('base','clear')
end

function []= mediangraphmakernorm(filename,varargin)
%makes a graph with medians of individual animals averaged into a genotype
%'mean median stat of individual animals'
```

```
evalin('base','clear')%clear variables
getdis_ind(filename)%get animals sheets
inddelzeros();%clear zeros in animal sheets

for i = 1:(nargin-1)%group genotypes
   var1 = varargin{i};
gtlist2mednorm(var1)
xlswrite(strcat(filename,'norm'),evalin('base',char(var1)),char(var1))
end

for i = [5,7,9,10,12,14,16,18,20]%plot means for all genotypes
v = strcat(filename,titler(i),'mn');
x = graphprep(i,varargin);
h = graphfromgt(x,v);
%h = findobj(handle.Name,'Figure 1')
saveas(h,v,'jpg');
close

end


end
evalin ('base','clear')
end
function [mato] = normtoburst(mati)
r = @(x)x(:,2);
colnum = @(x)r(size(x));
normed =[];
sorted = mati;
sorted = delzerosbursts(mati)
bursts = selanadis(sorted,6);
g = colnum(sorted)
for i = 1:g
normed(:,i) = sorted(:,i)./(bursts);
end
mato = normed;
end

function [mato] = normtospikes(mati)
r = @(x)x(:,2);
colnum = @(x)r(size(x));
normed =[];
sorted = delzerosspikes(mati);
spikes = selanadis(sorted,3);
g = colnum(sorted)
```

```
for i = 1:g
normed(:,i) = sorted(:,i)./(spikes);
end
mato = normed;
end

function [] = summartoxls(filename,gtype)
mat = evalin('base',gtype)
xlswrite(filename, mat, gtype)
end

function [outp]= titler (inp);
switch inp
   case  {3}
      outp = 'Spikes'
   case {5}
      outp = 'MF'
   case {6}
      outp = 'NB'
   case {7}
       outp ='BpS'
   case {8}
       outp ='BpM'
   case {23}
       outp ='SDBpM'
   case {10}
       outp ='MBD'
   case {11}
       outp ='SDMBD'
   case {9}
       outp ='PSiB'
   case {12}
       outp ='MSiB'
   case {13}
       outp ='SDMSiB'
   case {14}
       outp = 'ISI'
   case {15}
       outp ='SDISI'
   case {16}
       outp ='MFiB'
   case {17}
       outp ='SDMFiB'
  case {18}
       outp ='MPiB'
  case {19}
```

```
        outp ='SDMPiB'
  case {20}
        outp ='IBI'
   case {21}
        outp ='SDIBI'
   case {22}
       outp ='MSup'
end
end

function []= gtlist2(varargin)%takes 'ind' type data, gets average of each
%animal and combines the averages into a genotype averges.

%!!!When this is run after gtlist2med, it includes the results of
%gtlist2med because the beginning matches the genotype string
    x = evalin('base','who');
    z = []; %will be a numerical summary of all genotypes
   for i = 1:nargin
           var1= varargin{i};
           y = [];
           k = 1;
           vars = size(x,1);
     for r = 1:vars
           varname = x(r);
        if strmatch (var1,varname)%if string matches genotype
              var2 = evalin('base', char(varname));%find that associated matrix
              b = findavsem(summarize(var2));%get the averages and sems
              y(k,:)= b(1,:);%add the averages  to y
              k = k + 1% set k to go to next row
              % when this is done, y will have the averages for the
              % genotype var1
        end

          %z((((2.*i)-1):(2.*i)),:)= findavsem(summarize(y))
     end
        z = summarize(y);%summarize the genotype as two rows
        assignin('base',char(var1),z)
   end

end

 function [] = gtlist2med(varargin)%this should produce the genotype list, from 'ind' type
analysis from
 %which the median stat from individual animals(from cells) are averaged together as a
genotype.
    x = evalin('base','who');
```

```
    z = []; %will be a numerical summary of all genotypes
   for i = 1:nargin
          var1 = varargin{i};
          y = [];
          k = 1;
          vars = size(x,1);
     for r = 1:vars
          varname = x(r);
        if strmatch (var1,varname)%if string matches genotype
              var2 = evalin('base', char(varname));%find that associated matrix
              b = findavsem(summarizemed(var2));%get the medians and sems then take the
median and add it to list for genotype
              y(k,:)= b(1,:);%add the median for the animals to y
              k = k + 1;% set k to go to next row
              % when this is done, y will have the averages for the
              % genotype var1
        end

          %z((((2.*i)-1):(2.*i)),:)= findavsem(summarize(y))
     end
       z = summarize(y) ; %the average of the medians
       assignin('base',strcat(char(var1),'med'),z)
   end

 end

 function [] = gtlist2mednorm(varargin)%this should produce the genotype list, from 'ind'
type analysis from
 %which the median stat from individual animals(from cells) are averaged together as a
genotype.
    x = evalin('base','who');
    z = []; %will be a numerical summary of all genotypes
   for i = 1:nargin
          var1 = varargin{i};
          y = [];
          k = 1;
          vars = size(x,1);
     for r = 1:vars
          varname = x(r);
        if strmatch (var1,varname)%if string matches genotype
              var2 = evalin('base', char(varname));%find that associated matrix
              b = findavsem(summarizemed(normtospikes(var2)));%get the medians and
sems then take the median and add it to list for genotype
              y(k,:)= b(1,:);%add the median for the animals to y
              k = k + 1;% set k to go to next row
              % when this is done, y will have the averages for the
```

```
            % genotype var1
        end
          %z((((2.*i)-1):(2.*i)),:)= findavsem(summarize(y))
    end
      z = summarize(y) ; %the average of the medians
      assignin('base',strcat(char(var1),'med'),z)
  end

end

function []= gtlist2norm2(varargin)%takes 'ind' type data, gets average of each
%animal and combines the averages into a genotype averges.

%!!!When this is run after gtlist2med, it includes the results of
%gtlist2med because the beginning matches the genotype string
   x = evalin('base','who');
   z = []; %will be a numerical summary of all genotypes
  for i = 1:nargin
          var1= varargin{i};
          y = [];
          k = 1;
          vars = size(x,1);
    for r = 1:vars
          varname = x(r);
        if strmatch (var1,varname)%if string matches genotype
              var2 = evalin('base', char(varname));%find that associated matrix
              b = findavsem(summarize(normtoburst(var2)));%get the averages and sems
              y(k,:)= b(1,:);%add the averages  to y
              k = k + 1% set k to go to next row
              % when this is done, y will have the averages for the
              % genotype var1
        end

          %z((((2.*i)-1):(2.*i)),:)= findavsem(summarize(y))
    end
      z = summarize(y);%summarize the genotype as two rows
      assignin('base',char(var1),z)
  end

end

function []= gtlist2norm(varargin)%takes 'ind' type data, gets average of each
%animal and combines the averages into a genotype averges.

%!!!When this is run after gtlist2med, it includes the results of
%gtlist2med because the beginning matches the genotype string
```

```
    x = evalin('base','who');
    z = []; %will be a numerical summary of all genotypes
   for i = 1:nargin
          var1= varargin{i};
          y = [];
          k = 1;
          vars = size(x,1);
     for r = 1:vars
          varname = x(r);
        if strmatch (var1,varname)%if string matches genotype
             var2 = evalin('base', char(varname));%find that associated matrix
             b = findavsem(summarize(normtospikes(var2)));%get the averages and sems
             y(k,:)= b(1,:);%add the averages  to y
             k = k + 1% set k to go to next row
             % when this is done, y will have the averages for the
             % genotype var1
        end

          %z((((2.*i)-1):(2.*i)),:)= findavsem(summarize(y))
     end
       z = summarize(y);%summarize the genotype as two rows
       assignin('base',char(var1),z)
   end

 end

 function [] = gtlist(file,main, varargin)

 gtlister2(main,varargin)
 summartoxls(file,main)
 end


 function [] = gtlister2 (main, varargin);% add, as a row to x, the averages of y
 %main =genotype. creates a matrix. Each row is the average of a single animals burst
stats.
 %Followed by summarize to get the mean and sem for graphing.
 %optargin = size(varargin,2);
 assignin ('base',char(main),[])
 fprintf('Number of inputs = %d\n', nargin)
 psg = []
 r = @(x)x(:,2);
 rows = @(x)x(:,1);
 colnum = @(x)r(size(x));
 rownum = @(x)rows(size(x));
```

```
avs= @(x)mean(x(:,(1:colnum(x))));
%x(((rownum(x) + 1)),:) = mean(x(:,(1:colnum(x))))
%returns a file that has averages in the last row

 %varn = varargin(1,i); %gets the ith variable name (basically the column) in dists, the
animal
 %var1 = evalin('base',varargin);

 for i = 1:(nargin-1)
     var1 = varargin{i}
 if ~isempty(psg)
    psg(((rownum(psg) + 1)),:) = avs(var1)
 else
    psg = avs(var1);
 end

 end
    mat= summarize(psg)
    assignin('base',char(main),mat)
end

function [] =inddelzerosspikes()
list = evalin('base','who')
for i = 1:length(list)
    z = evalin('base',list{i})
    assignin ('base', list{i},delzerosspikes(z))
    list{i}
end
end

function []= gtlist2(varargin)%takes 'ind' type data, gets average of each
%animal and combines the averages into a genotype averges.

%!!!When this is run after gtlist2med, it includes the results of
%gtlist2med because the beginning matches the genotype string
    x = evalin('base','who');
    z = []; %will be a numerical summary of all genotypes
   for i = 1:nargin
            var1= varargin{i};
            y = [];
            k = 1;
            vars = size(x,1);
     for r = 1:vars
            varname = x(r);
         if strmatch (var1,varname)%if string matches genotype
                var2 = evalin('base', char(varname));%find that associated matrix
```

```
            b = findavsem(summarize(var2));%get the averages and sems
            y(k,:)= b(1,:);%add the averages  to y
            k = k + 1% set k to go to next row
            % when this is done, y will have the averages for the
            % genotype var1
        end

          %z((((2.*i)-1):(2.*i)),:)= findavsem(summarize(y))
     end
       z = summarize(y);%summarize the genotype as two rows
       assignin('base',char(var1),z)
   end

 end

 function [] = gtlist2med(varargin)%this should produce the genotype list, from 'ind' type
analysis from
 %which the median stat from individual animals(from cells) are averaged together as a
genotype.
     x = evalin('base','who');
     z = []; %will be a numerical summary of all genotypes
    for i = 1:nargin
            var1 = varargin{i};
            y = [];
            k = 1;
            vars = size(x,1);
      for r = 1:vars
            varname = x(r);
         if strmatch (var1,varname)%if string matches genotype
              var2 = evalin('base', char(varname));%find that associated matrix
              b = findavsem(summarizemed(var2));%get the medians and sems then take the
median and add it to list for genotype
              y(k,:)= b(1,:);%add the median for the animals to y
              k = k + 1;% set k to go to next row
              % when this is done, y will have the averages for the
              % genotype var1
         end

          %z((((2.*i)-1):(2.*i)),:)= findavsem(summarize(y))
     end
       z = summarize(y) ; %the average of the medians
       assignin('base',strcat(char(var1),'med'),z)
   end

 end
```

```
 function [] = gtlist2mednorm(varargin)%this should produce the genotype list, from 'ind'
type analysis from
 %which the median stat from individual animals(from cells) are averaged together as a
genotype.
     x = evalin('base','who');
     z = []; %will be a numerical summary of all genotypes
    for i = 1:nargin
            var1 = varargin{i};
            y = [];
            k = 1;
            vars = size(x,1);
      for r = 1:vars
            varname = x(r);
         if strmatch (var1,varname)%if string matches genotype
                var2 = evalin('base', char(varname));%find that associated matrix
                b = findavsem(summarizemed(normtospikes(var2)));%get the medians and
sems then take the median and add it to list for genotype
                y(k,:)= b(1,:);%add the median for the animals to y
                k = k + 1;% set k to go to next row
                % when this is done, y will have the averages for the
                % genotype var1
         end
           %z((((2.*i)-1):(2.*i)),:)= findavsem(summarize(y))
      end
        z = summarize(y) ; %the average of the medians
        assignin('base',strcat(char(var1),'med'),z)
    end

 end

 function []= gtlist2norm2(varargin)%takes 'ind' type data, gets average of each
 %animal and combines the averages into a genotype averges.

 %!!!When this is run after gtlist2med, it includes the results of
 %gtlist2med because the beginning matches the genotype string
     x = evalin('base','who');
     z = []; %will be a numerical summary of all genotypes
    for i = 1:nargin
            var1= varargin{i};
            y = [];
            k = 1;
            vars = size(x,1);
      for r = 1:vars
            varname = x(r);
         if strmatch (var1,varname)%if string matches genotype
                var2 = evalin('base', char(varname));%find that associated matrix
```

```
            b = findavsem(summarize(normtoburst(var2)));%get the averages and sems
            y(k,:)= b(1,:);%add the averages  to y
            k = k + 1% set k to go to next row
            % when this is done, y will have the averages for the
            % genotype var1
        end

          %z((((2.*i)-1):(2.*i)),:)= findavsem(summarize(y))
    end
      z = summarize(y);%summarize the genotype as two rows
      assignin('base',char(var1),z)
  end

end

function []= gtlist2norm(varargin)%takes 'ind' type data, gets average of each
%animal and combines the averages into a genotype averges.

%!!!When this is run after gtlist2med, it includes the results of
%gtlist2med because the beginning matches the genotype string
   x = evalin('base','who');
   z = []; %will be a numerical summary of all genotypes
  for i = 1:nargin
          var1= varargin{i};
          y = [];
          k = 1;
          vars = size(x,1);
    for r = 1:vars
          varname = x(r);
        if strmatch (var1,varname)%if string matches genotype
            var2 = evalin('base', char(varname));%find that associated matrix
            b = findavsem(summarize(normtospikes(var2)));%get the averages and sems
            y(k,:)= b(1,:);%add the averages  to y
            k = k + 1% set k to go to next row
            % when this is done, y will have the averages for the
            % genotype var1
        end

          %z((((2.*i)-1):(2.*i)),:)= findavsem(summarize(y))
    end
      z = summarize(y);%summarize the genotype as two rows
      assignin('base',char(var1),z)
  end

end
```

```
function [] = gtlist(file,main, varargin)

gtlister2(main,varargin)
summartoxls(file,main)
end


function [] = gtlister2 (main, varargin);% add, as a row to x, the averages of y
%main =genotype. creates a matrix. Each row is the average of a single animals burst
stats.
%Followed by summarize to get the mean and sem for graphing.
%optargin = size(varargin,2);
assignin ('base',char(main),[])
fprintf('Number of inputs = %d\n', nargin)
psg = []
r = @(x)x(:,2);
rows = @(x)x(:,1);
colnum = @(x)r(size(x));
rownum = @(x)rows(size(x));

avs= @(x)mean(x(:,(1:colnum(x))));
%x(((rownum(x) + 1)),:) = mean(x(:,(1:colnum(x))))
%returns a file that has averages in the last row

 %varn = varargin(1,i); %gets the ith variable name (basically the column) in dists, the
animal
 %var1 = evalin('base',varargin);

 for i = 1:(nargin-1)
     var1 = varargin{i}
 if ~isempty(psg)
    psg(((rownum(psg) + 1)),:) = avs(var1)
 else
    psg = avs(var1);
 end

 end
    mat= summarize(psg)
    assignin('base',char(main),mat)
end

function [] =inddelzerosspikes()
list = evalin('base','who')
for i = 1:length(list)
    z = evalin('base',list{i})
    assignin ('base', list{i},delzerosspikes(z))
```

```
    list{i}
 end
 end

 function []= gtlist2(varargin)%takes 'ind' type data, gets average of each
 %animal and combines the averages into a genotype averges.

 %!!!When this is run after gtlist2med, it includes the results of
 %gtlist2med because the beginning matches the genotype string
    x = evalin('base','who');
    z = []; %will be a numerical summary of all genotypes
   for i = 1:nargin
           var1= varargin{i};
           y = [];
           k = 1;
           vars = size(x,1);
     for r = 1:vars
           varname = x(r);
        if strmatch (var1,varname)%if string matches genotype
              var2 = evalin('base', char(varname));%find that associated matrix
              b = findavsem(summarize(var2));%get the averages and sems
              y(k,:)= b(1,:);%add the averages  to y
              k = k + 1% set k to go to next row
              % when this is done, y will have the averages for the
              % genotype var1
        end

           %z((((2.*i)-1):(2.*i)),:)= findavsem(summarize(y))
     end
        z = summarize(y);%summarize the genotype as two rows
        assignin('base',char(var1),z)
   end

 end

 function [] = gtlist2med(varargin)%this should produce the genotype list, from 'ind' type
analysis from
 %which the median stat from individual animals(from cells) are averaged together as a
genotype.
     x = evalin('base','who');
     z = []; %will be a numerical summary of all genotypes
    for i = 1:nargin
           var1 = varargin{i};
           y = [];
           k = 1;
           vars = size(x,1);
```

```
    for r = 1:vars
          varname = x(r);
        if strmatch (var1,varname)%if string matches genotype
              var2 = evalin('base', char(varname));%find that associated matrix
              b = findavsem(summarizemed(var2));%get the medians and sems then take the
median and add it to list for genotype
              y(k,:)= b(1,:);%add the median for the animals to y
              k = k + 1;% set k to go to next row
              % when this is done, y will have the averages for the
              % genotype var1
        end

          %z((((2.*i)-1):(2.*i)),:)= findavsem(summarize(y))
    end
       z = summarize(y) ; %the average of the medians
       assignin('base',strcat(char(var1),'med'),z)
   end

 end

 function [] = gtlist2mednorm(varargin)%this should produce the genotype list, from 'ind'
type analysis from
 %which the median stat from individual animals(from cells) are averaged together as a
genotype.
    x = evalin('base','who');
    z = []; %will be a numerical summary of all genotypes
   for i = 1:nargin
          var1 = varargin{i};
          y = [];
          k = 1;
          vars = size(x,1);
    for r = 1:vars
          varname = x(r);
        if strmatch (var1,varname)%if string matches genotype
              var2 = evalin('base', char(varname));%find that associated matrix
              b = findavsem(summarizemed(normtospikes(var2)));%get the medians and
sems then take the median and add it to list for genotype
              y(k,:)= b(1,:);%add the median for the animals to y
              k = k + 1;% set k to go to next row
              % when this is done, y will have the averages for the
              % genotype var1
        end
          %z((((2.*i)-1):(2.*i)),:)= findavsem(summarize(y))
    end
       z = summarize(y) ; %the average of the medians
       assignin('base',strcat(char(var1),'med'),z)
```

```
  end

end

function []= gtlist2norm2(varargin)%takes 'ind' type data, gets average of each
%animal and combines the averages into a genotype averges.

%!!!When this is run after gtlist2med, it includes the results of
%gtlist2med because the beginning matches the genotype string
   x = evalin('base','who');
   z = []; %will be a numerical summary of all genotypes
  for i = 1:nargin
         var1= varargin{i};
         y = [];
         k = 1;
         vars = size(x,1);
    for r = 1:vars
         varname = x(r);
       if strmatch (var1,varname)%if string matches genotype
            var2 = evalin('base', char(varname));%find that associated matrix
            b = findavsem(summarize(normtoburst(var2)));%get the averages and sems
            y(k,:)= b(1,:);%add the averages  to y
            k = k + 1% set k to go to next row
            % when this is done, y will have the averages for the
            % genotype var1
       end

         %z((((2.*i)-1):(2.*i)),:)= findavsem(summarize(y))
    end
      z = summarize(y);%summarize the genotype as two rows
      assignin('base',char(var1),z)
  end

end

function []= gtlist2norm(varargin)%takes 'ind' type data, gets average of each
%animal and combines the averages into a genotype averges.

%!!!When this is run after gtlist2med, it includes the results of
%gtlist2med because the beginning matches the genotype string
   x = evalin('base','who');
   z = []; %will be a numerical summary of all genotypes
  for i = 1:nargin
         var1= varargin{i};
         y = [];
         k = 1;
```

```
            vars = size(x,1);
      for r = 1:vars
            varname = x(r);
         if strmatch (var1,varname)%if string matches genotype
               var2 = evalin('base', char(varname));%find that associated matrix
               b = findavsem(summarize(normtospikes(var2)));%get the averages and sems
               y(k,:)= b(1,:);%add the averages  to y
               k = k + 1% set k to go to next row
               % when this is done, y will have the averages for the
               % genotype var1
         end

            %z((((2.*i)-1):(2.*i)),:)= findavsem(summarize(y))
      end
         z = summarize(y);%summarize the genotype as two rows
         assignin('base',char(var1),z)
    end

 end

 function [] = gtlist(file,main, varargin)

 gtlister2(main,varargin)
 summartoxls(file,main)
 end


 function [] = gtlister2 (main, varargin);% add, as a row to x, the averages of y
 %main =genotype. creates a matrix. Each row is the average of a single animals burst
stats.
 %Followed by summarize to get the mean and sem for graphing.
 %optargin = size(varargin,2);
 assignin ('base',char(main),[])
 fprintf('Number of inputs = %d\n', nargin)
 psg = []
 r = @(x)x(:,2);
 rows = @(x)x(:,1);
 colnum = @(x)r(size(x));
 rownum = @(x)rows(size(x));

 avs= @(x)mean(x(:,(1:colnum(x))));
 %x(((rownum(x) + 1)),:) = mean(x(:,(1:colnum(x))))
 %returns a file that has averages in the last row

  %varn = varargin(1,i); %gets the ith variable name (basically the column) in dists, the
animal
```

```
 %var1 = evalin('base',varargin);

 for i = 1:(nargin-1)
     var1 = varargin{i}
 if ~isempty(psg)
    psg(((rownum(psg) + 1)),:) = avs(var1)
 else
    psg = avs(var1);
 end

 end
    mat= summarize(psg)
    assignin('base',char(main),mat)
end

function [] =inddelzerosspikes()
list = evalin('base','who')
for i = 1:length(list)
    z = evalin('base',list{i})
    assignin ('base', list{i},delzerosspikes(z))
    list{i}
end
end

function []= gtlist2(varargin)%takes 'ind' type data, gets average of each
%animal and combines the averages into a genotype averges.

%!!!When this is run after gtlist2med, it includes the results of
%gtlist2med because the beginning matches the genotype string
    x = evalin('base','who');
    z = []; %will be a numerical summary of all genotypes
   for i = 1:nargin
           var1= varargin{i};
           y = [];
           k = 1;
           vars = size(x,1);
     for r = 1:vars
           varname = x(r);
        if strmatch (var1,varname)%if string matches genotype
              var2 = evalin('base', char(varname));%find that associated matrix
              b = findavsem(summarize(var2));%get the averages and sems
              y(k,:)= b(1,:);%add the averages  to y
              k = k + 1% set k to go to next row
              % when this is done, y will have the averages for the
              % genotype var1
        end
```

```
            %z((((2.*i)-1):(2.*i)),:)= findavsem(summarize(y))
      end
         z = summarize(y);%summarize the genotype as two rows
         assignin('base',char(var1),z)
    end

 end

 function [] = gtlist2med(varargin)%this should produce the genotype list, from 'ind' type
analysis from
 %which the median stat from individual animals(from cells) are averaged together as a
genotype.
     x = evalin('base','who');
     z = []; %will be a numerical summary of all genotypes
    for i = 1:nargin
            var1 = varargin{i};
            y = [];
            k = 1;
            vars = size(x,1);
      for r = 1:vars
            varname = x(r);
         if strmatch (var1,varname)%if string matches genotype
               var2 = evalin('base', char(varname));%find that associated matrix
               b = findavsem(summarizemed(var2));%get the medians and sems then take the
median and add it to list for genotype
               y(k,:)= b(1,:);%add the median for the animals to y
               k = k + 1;% set k to go to next row
               % when this is done, y will have the averages for the
               % genotype var1
         end

            %z((((2.*i)-1):(2.*i)),:)= findavsem(summarize(y))
      end
         z = summarize(y) ; %the average of the medians
         assignin('base',strcat(char(var1),'med'),z)
    end

 end

 function [] = gtlist2mednorm(varargin)%this should produce the genotype list, from 'ind'
type analysis from
 %which the median stat from individual animals(from cells) are averaged together as a
genotype.
     x = evalin('base','who');
     z = []; %will be a numerical summary of all genotypes
```

```
   for i = 1:nargin
          var1 = varargin{i};
          y = [];
          k = 1;
          vars = size(x,1);
     for r = 1:vars
          varname = x(r);
        if strmatch (var1,varname)%if string matches genotype
              var2 = evalin('base', char(varname));%find that associated matrix
              b = findavsem(summarizemed(normtospikes(var2)));%get the medians and
sems then take the median and add it to list for genotype
              y(k,:)= b(1,:);%add the median for the animals to y
              k = k + 1;% set k to go to next row
              % when this is done, y will have the averages for the
              % genotype var1
        end
          %z((((2.*i)-1):(2.*i)),:)= findavsem(summarize(y))
     end
       z = summarize(y) ; %the average of the medians
       assignin('base',strcat(char(var1),'med'),z)
   end

end

function []= gtlist2norm2(varargin)%takes 'ind' type data, gets average of each
%animal and combines the averages into a genotype averges.

%!!!When this is run after gtlist2med, it includes the results of
%gtlist2med because the beginning matches the genotype string
    x = evalin('base','who');
    z = []; %will be a numerical summary of all genotypes
   for i = 1:nargin
          var1= varargin{i};
          y = [];
          k = 1;
          vars = size(x,1);
     for r = 1:vars
          varname = x(r);
        if strmatch (var1,varname)%if string matches genotype
              var2 = evalin('base', char(varname));%find that associated matrix
              b = findavsem(summarize(normtoburst(var2)));%get the averages and sems
              y(k,:)= b(1,:);%add the averages  to y
              k = k + 1% set k to go to next row
              % when this is done, y will have the averages for the
              % genotype var1
        end
```

```
        %z((((2.*i)-1):(2.*i)),:)= findavsem(summarize(y))
    end
      z = summarize(y);%summarize the genotype as two rows
      assignin('base',char(var1),z)
  end

end

function []= gtlist2norm(varargin)%takes 'ind' type data, gets average of each
%animal and combines the averages into a genotype averges.

%!!!When this is run after gtlist2med, it includes the results of
%gtlist2med because the beginning matches the genotype string
   x = evalin('base','who');
   z = []; %will be a numerical summary of all genotypes
  for i = 1:nargin
        var1= varargin{i};
        y = [];
        k = 1;
        vars = size(x,1);
    for r = 1:vars
        varname = x(r);
      if strmatch (var1,varname)%if string matches genotype
            var2 = evalin('base', char(varname));%find that associated matrix
            b = findavsem(summarize(normtospikes(var2)));%get the averages and sems
            y(k,:)= b(1,:);%add the averages  to y
            k = k + 1% set k to go to next row
            % when this is done, y will have the averages for the
            % genotype var1
      end

        %z((((2.*i)-1):(2.*i)),:)= findavsem(summarize(y))
    end
      z = summarize(y);%summarize the genotype as two rows
      assignin('base',char(var1),z)
  end

end

function [] = gtlist(file,main, varargin)

gtlister2(main,varargin)
summartoxls(file,main)
end
```

```
function [] = gtlister2 (main, varargin);% add, as a row to x, the averages of y
%main =genotype. creates a matrix. Each row is the average of a single animals burst
stats.
%Followed by summarize to get the mean and sem for graphing.
%optargin = size(varargin,2);
assignin ('base',char(main),[])
fprintf('Number of inputs = %d\n', nargin)
psg = []
r = @(x)x(:,2);
rows = @(x)x(:,1);
colnum = @(x)r(size(x));
rownum = @(x)rows(size(x));

avs= @(x)mean(x(:,(1:colnum(x))));
%x(((rownum(x) + 1)),:) = mean(x(:,(1:colnum(x))))
%returns a file that has averages in the last row

 %varn = varargin(1,i); %gets the ith variable name (basically the column) in dists, the
animal
 %var1 = evalin('base',varargin);

 for i = 1:(nargin-1)
    var1 = varargin{i}
 if ~isempty(psg)
   psg(((rownum(psg) + 1)),:) = avs(var1)
 else
   psg = avs(var1);
 end

 end
   mat= summarize(psg)
   assignin('base',char(main),mat)
end

function [] =inddelzerosspikes()
list = evalin('base','who')
for i = 1:length(list)
   z = evalin('base',list{i})
   assignin ('base', list{i},delzerosspikes(z))
   list{i}
end
end

function []= gtlist2(varargin)%takes 'ind' type data, gets average of each
%animal and combines the averages into a genotype averges.
```

```
%!!!When this is run after gtlist2med, it includes the results of
%gtlist2med because the beginning matches the genotype string
    x = evalin('base','who');
    z = []; %will be a numerical summary of all genotypes
   for i = 1:nargin
          var1= varargin{i};
          y = [];
          k = 1;
          vars = size(x,1);
     for r = 1:vars
          varname = x(r);
        if strmatch (var1,varname)%if string matches genotype
             var2 = evalin('base', char(varname));%find that associated matrix
             b = findavsem(summarize(var2));%get the averages and sems
             y(k,:)= b(1,:);%add the averages  to y
             k = k + 1% set k to go to next row
             % when this is done, y will have the averages for the
             % genotype var1
        end

          %z((((2.*i)-1):(2.*i)),:)= findavsem(summarize(y))
     end
       z = summarize(y);%summarize the genotype as two rows
       assignin('base',char(var1),z)
   end

end

 function [] = gtlist2med(varargin)%this should produce the genotype list, from 'ind' type
analysis from
 %which the median stat from individual animals(from cells) are averaged together as a
genotype.
    x = evalin('base','who');
    z = []; %will be a numerical summary of all genotypes
   for i = 1:nargin
          var1 = varargin{i};
          y = [];
          k = 1;
          vars = size(x,1);
     for r = 1:vars
          varname = x(r);
        if strmatch (var1,varname)%if string matches genotype
             var2 = evalin('base', char(varname));%find that associated matrix
             b = findavsem(summarizemed(var2));%get the medians and sems then take the
median and add it to list for genotype
```

```
            y(k,:)= b(1,:);%add the median for the animals to y
            k = k + 1;% set k to go to next row
            % when this is done, y will have the averages for the
            % genotype var1
        end

          %z((((2.*i)-1):(2.*i)),:)= findavsem(summarize(y))
     end
       z = summarize(y) ; %the average of the medians
       assignin('base',strcat(char(var1),'med'),z)
   end

end

function [] = gtlist2mednorm(varargin)%this should produce the genotype list, from 'ind'
type analysis from
%which the median stat from individual animals(from cells) are averaged together as a
genotype.
    x = evalin('base','who');
    z = []; %will be a numerical summary of all genotypes
   for i = 1:nargin
          var1 = varargin{i};
          y = [];
          k = 1;
          vars = size(x,1);
     for r = 1:vars
          varname = x(r);
        if strmatch (var1,varname)%if string matches genotype
            var2 = evalin('base', char(varname));%find that associated matrix
            b = findavsem(summarizemed(normtospikes(var2)));%get the medians and
sems then take the median and add it to list for genotype
            y(k,:)= b(1,:);%add the median for the animals to y
            k = k + 1;% set k to go to next row
            % when this is done, y will have the averages for the
            % genotype var1
        end
          %z((((2.*i)-1):(2.*i)),:)= findavsem(summarize(y))
     end
       z = summarize(y) ; %the average of the medians
       assignin('base',strcat(char(var1),'med'),z)
   end

end

function []= gtlist2norm2(varargin)%takes 'ind' type data, gets average of each
%animal and combines the averages into a genotype averges.
```

```
%!!!When this is run after gtlist2med, it includes the results of
%gtlist2med because the beginning matches the genotype string
   x = evalin('base','who');
   z = []; %will be a numerical summary of all genotypes
  for i = 1:nargin
          var1= varargin{i};
          y = [];
          k = 1;
          vars = size(x,1);
    for r = 1:vars
          varname = x(r);
       if strmatch (var1,varname)%if string matches genotype
             var2 = evalin('base', char(varname));%find that associated matrix
             b = findavsem(summarize(normtoburst(var2)));%get the averages and sems
             y(k,:)= b(1,:);%add the averages  to y
             k = k + 1% set k to go to next row
             % when this is done, y will have the averages for the
             % genotype var1
       end

          %z((((2.*i)-1):(2.*i)),:)= findavsem(summarize(y))
    end
      z = summarize(y);%summarize the genotype as two rows
      assignin('base',char(var1),z)
  end

end

function []= gtlist2norm(varargin)%takes 'ind' type data, gets average of each
%animal and combines the averages into a genotype averges.

%!!!When this is run after gtlist2med, it includes the results of
%gtlist2med because the beginning matches the genotype string
   x = evalin('base','who');
   z = []; %will be a numerical summary of all genotypes
  for i = 1:nargin
          var1= varargin{i};
          y = [];
          k = 1;
          vars = size(x,1);
    for r = 1:vars
          varname = x(r);
       if strmatch (var1,varname)%if string matches genotype
             var2 = evalin('base', char(varname));%find that associated matrix
             b = findavsem(summarize(normtospikes(var2)));%get the averages and sems
```

```
            y(k,:)= b(1,:);%add the averages  to y
            k = k + 1% set k to go to next row
            % when this is done, y will have the averages for the
            % genotype var1
        end

          %z((((2.*i)-1):(2.*i)),:)= findavsem(summarize(y))
     end
       z = summarize(y);%summarize the genotype as two rows
       assignin('base',char(var1),z)
   end

end

function [] = gtlist(file,main, varargin)

gtlister2(main,varargin)
summartoxls(file,main)
end


function [] = gtlister2 (main, varargin);% add, as a row to x, the averages of y
%main =genotype. creates a matrix. Each row is the average of a single animals burst
stats.
%Followed by summarize to get the mean and sem for graphing.
%optargin = size(varargin,2);
assignin ('base',char(main),[])
fprintf('Number of inputs = %d\n', nargin)
psg = []
r = @(x)x(:,2);
rows = @(x)x(:,1);
colnum = @(x)r(size(x));
rownum = @(x)rows(size(x));

avs= @(x)mean(x(:,(1:colnum(x))));
%x(((rownum(x) + 1)),:) = mean(x(:,(1:colnum(x))))
%returns a file that has averages in the last row

 %varn = varargin(1,i); %gets the ith variable name (basically the column) in dists, the
animal
 %var1 = evalin('base',varargin);

 for i = 1:(nargin-1)
     var1 = varargin{i}
 if ~isempty(psg)
    psg(((rownum(psg) + 1)),:) = avs(var1)
```

```
 else
    psg = avs(var1);
 end

 end
    mat= summarize(psg)
    assignin('base',char(main),mat)
end

function [] =inddelzerosspikes()
list = evalin('base','who')
for i = 1:length(list)
    z = evalin('base',list{i})
    assignin ('base', list{i},delzerosspikes(z))
    list{i}
end
end

function [] = cdgrapher2(ana); % plots a cd of the selected parameter

z = input('3Spikes  5Mean Freq. 6Num. Bursts    7Bursts_Per Second\n8Bursts_Per
Minute  23St. Dev. Bursts_Per Minute 9Perc of Spikes_in Bursts\n10Mean
Burst_Duration   11St. Dev. of_Burst Duration\n12Mean Spikes_in Burst    13St. Dev.
of_Spikes In Burst\n14Mean ISI_in Burst  15St. Dev. of_ISI In Burst\n16Mean Freq._in
Burst   17St. Dev. of_Freq. in Burst\n18Mean Peak_Freq. in Burst    19St. Dev. of_Peak
Fr. In Burst \n20Mean Interburst_Interval    21St. Dev. of_Interburst Int.\n22Mean
Burst_Surprise')
lncolors = get(gca,'ColorOrder');
dists = evalin('base', 'who');%gets a list of all genotypes
distsn = size(dists,1);%number of genotypes
%var = evalin('base','delzeros','varn')

for i = 1:distsn

 varn = dists(i,1);
 var = evalin('base',char(varn));
 var2 = delzeros(var);
 [g,plotter] = ecdf(selanadis(var2,z))

 plot(plotter,g,'color',lncolors(i,:));
 hold on
end
legend(dists)
title(strcat(ana, titler(z)))

end
```

```
function [outp]= titler (inp);
switch inp
   case  {3}
      outp = 'spikes'
   case {5}
      outp = 'Mean Freq'
   case {6}
      outp = 'Num Bursts'
   case {7}
       outp ='Bursts/Sec'
   case {8}
       outp ='Bursts/Min'
   case {23}
       outp ='SDBurst/Min'
   case {10}
       outp ='Mean Burst_Duration'
   case {11}
       outp ='SDMean Burst_Duration'
   case {9}
       outp ='% of spikes in burst'
   case {12}
       outp ='Mean Spikes in Burst'
   case {13}
       outp ='SDMean Spikes in Burst'
   case {14}
       outp ='Mean ISI_in Burst'
   case {15}
       outp ='SDMean ISI_in Burst'
   case {16}
       outp ='Mean Freq._in Burst'
   case {17}
       outp ='SDMean Freq._in Burst'
  case {18}
       outp ='Mean Peak_Freq. in Burst'
  case {19}
       outp ='SDMean Peak_Freq. in Burst'
 case {20}
       outp ='Mean Interburst_Interval'
  case {21}
       outp ='SDMean Interburst_Interval'
  case {22}
      outp ='Mean Suprise'
end
end
```

```
function [] = cdgrapher(ana); % plots a cd of the selected parameter

z = input('3Spikes  5Mean Freq. 6Num. Bursts    7Bursts_Per Second\n8Bursts_Per
Minute  23St. Dev. Bursts_Per Minute 9Perc of Spikes_in Bursts\n10Mean
Burst_Duration   11St. Dev. of_Burst Duration\n12Mean Spikes_in Burst    13St. Dev.
of_Spikes In Burst\n14Mean ISI_in Burst  15St. Dev. of_ISI In Burst\n16Mean Freq._in
Burst   17St. Dev. of_Freq. in Burst\n18Mean Peak_Freq. in Burst    19St. Dev. of_Peak
Fr. In Burst \n20Mean Interburst_Interval    21St. Dev. of_Interburst Int.\n22Mean
Burst_Surprise')
lncolors = get(gca,'ColorOrder');
dists = evalin('base', 'who');%gets a list of all genotypes
distsn = size(dists,1);%number of genotypes
%var = evalin('base','delzeros','varn')

for i = 1:distsn

 varn = dists(i,1);
 var = evalin('base',char(varn));
 %var2 = delzeros(var);
 [g,plotter] = ecdf(selanadis(var,z));
 plot(plotter,g,'color',lncolors(i,:));
 hold on
end
legend(dists)
title(strcat(ana, titler(z)))
axis normal

end

function [outp]= titler (inp);
switch inp
   case  {3}
      outp = 'spikes'
   case {5}
      outp = 'Mean Freq'
   case {6}
      outp = 'Num Bursts'
   case {7}
       outp ='Bursts/Sec'
   case {8}
       outp ='Bursts/Min'
   case {23}
       outp ='SDBurst/Min'
   case {10}
       outp ='Mean Burst_Duration'
   case {11}
```

```
        outp ='SDMean Burst_Duration'
    case {9}
        outp ='% of spikes in burst'
    case {12}
        outp ='Mean Spikes in Burst'
    case {13}
        outp ='SDMean Spikes in Burst'
    case {14}
        outp ='Mean ISI_in Burst'
    case {15}
        outp ='SDMean ISI_in Burst'
    case {16}
        outp ='Mean Freq._in Burst'
    case {17}
        outp ='SDMean Freq._in Burst'
   case {18}
        outp ='Mean Peak_Freq. in Burst'
   case {19}
        outp ='SDMean Peak_Freq. in Burst'
  case {20}
        outp ='Mean Interburst_Interval'
   case {21}
        outp ='SDMean Interburst_Interval'
   case {22}
       outp ='Mean Suprise'
end
end

function [graph] = graphfromgt(mat,y)
aves = mat(1,:);
sems = mat(2,:);
%len = length(varargin{1})
graph = barwebwhandle(aves,sems,1,[],y)
% Ex: handles = barweb(my_barvalues, my_errors, [], [], [], [], [], bone, [], bw_legend,
1, 'axis')
% Usage: handles = barweb(barvalues, errors, width, groupnames, bw_title, bw_xlabel,
bw_ylabel, bw_colormap, gridstatus, bw_legend, error_sides, legend_type)
end


function []= graphavs(varargin)%for individuals
avs = []
sems = []
r = @(x)x(:,2);
rows = @(x)x(:,1);
colnum = @(x)r(size(x));
```

```
rownum = @(x)rows(size(x));

for i = 1:nargin
g = varargin{i}
mat = findavsem(g)
avs(i,:) = mat(1,:)
sems(i,:) = mat(2,:)
barweb(avs,sems)
end
end

function [] = getdis_ind(filename)
%take spreadsheets and assigns var names to matlab matrix. workbooks
%should only have sheets with names of each genotype
evalin('base','clear')
[b, y] = xlsfinfo(filename);
nvar= size(y,2);
for i = 1:nvar
   sheet = xlsread(filename,i);
   assignin('base',char(y(:,i)), sheet);
end
evalin('base','clear Sheet1')
end

function [] = getdis(filename)
%take spreadsheets and assigns var names to matlab matrix. workbooks
%should only have sheets with names of each genotype
[b, y] = xlsfinfo(filename)
nvar= size(y,2)
for i = 1:nvar
   sheet = xlsread(filename,i)
   assignin('base',char(y(:,i)), sheet)
end

end

function [matrix] = disavs(matr); %average of columns for burst distibution statistics

%for matrix with all animals grouped under a phenotype, not individual
%animals. %For Individual animals use disavs_ind.

x = matr
%y = input('Analyse
%3Spikes    5Mean Freq. 6Num. Bursts    7Bursts_Per Second
%8Bursts_Per Minute 23St. Dev. Bursts_Per Minute 9Perc of Spikes_in Bursts
%10Mean Burst_Duration  11St. Dev. of_Burst Duration
```

```
%12Mean Spikes_in Burst 13St. Dev. of_Spikes In Burst
%14Mean ISI_in Burst    15St. Dev. of_ISI In Burst
%16Mean Freq._in Burst  17St. Dev. of_Freq. in Burst
%18Mean Peak_Freq. in Burst 19St. Dev. of_Peak Fr. In Burst
%20Mean Interburst_Interval 21St. Dev. of_Interburst Int.
%22Mean Burst_Surprise')

%list of all analyses in the burst files

anList=('Spikes'
'Mean Freq.';
'Num. Bursts';
'Bursts_Per Second';
'Bursts_Per Minute';
'St. Dev. Bursts_Per Minute';
'Perc of Spikes_in Bursts';
'Mean Burst_Duration';
'St. Dev. of_Burst Duration';
'Mean Spikes_in Burst';
'St. Dev. of_Spikes In Burst';
'Mean ISI_in Burst';
'St. Dev. of_ISI In Burst';
'Mean Freq._in Burst';
'St. Dev. of_Freq. in Burst';
'Mean Peak_Freq. in Burst';
'St. Dev. of_Peak Fr. In Burst';
'Mean Interburst_Interval';
'St. Dev. of_Interburst Int.';
'Mean Burst_Surprise')



%plots the cum frequency (hold on after CDF with an order of colors)
%statistics on the CF

%plots the average of those columns in a bar plot (with order of colors)
%statistical comparison of averages.

%%switch
 %   case y = 3
 %
 %   case y = 5
 %
 %   case y = 6
 %
 %   case y = 7
```

```
%
%   case y = 9
%
%   case y = 11
%
%   case y =13
%
%   case y = 15
%
%%   case y = 17
 %
 %  case y = 19
 %
 %  case y = 21


%sortrow(x)
r = @(x)x(:,2)
rows = @(x)x(:,1)
colnum = @(x)r(size(x))
rownum = @(x)rows(size(x))


avs = @(x)mean(1:(colnum(x)))
x(((rownum(x) + 1)),:) = mean(x(:,(1:colnum(x))))
%returns a file that has averages in the last row
matrix = x;

function mat = delzerosspikes(x) %requires a matrix from nex
%sorts rows and deletes selected rows in the distribution that have
%no bursts.

mat = deler (sortrows(x,3))
end
   function r2 = deler(b)
      while b(1,2) ==(0)
         b(1,:) = []
      end
      r2 = b
   end
%  while x(1,2) ==(0) %() ensures that the logic statemtn looks for a number, not a string
%x(1,:) = []

end

function []= cdmaker(ana)
```

```
evalin('base','clear')
getdis(ana)
for i = [5,7,9,10,12,14,16,18,20]
    h = cds1(ana,i);
    saveas(h,strcat(ana,titler(i)),'jpg');
    close
    h = cds2(ana,i);
    saveas(h,strcat(ana,titler(i),'z'),'jpg');
    close
end
end

function [h] = cds1(ana,z); % plots a cd of the selected parameter

%z = input('3Spikes 5Mean Freq. 6Num. Bursts    7Bursts_Per Second\n8Bursts_Per
Minute  23St. Dev. Bursts_Per Minute 9Perc of Spikes_in Bursts\n10Mean
Burst_Duration   11St. Dev. of_Burst Duration\n12Mean Spikes_in Burst    13St. Dev.
of_Spikes In Burst\n14Mean ISI_in Burst  15St. Dev. of_ISI In Burst\n16Mean Freq._in
Burst   17St. Dev. of_Freq. in Burst\n18Mean Peak_Freq. in Burst    19St. Dev. of_Peak
Fr. In Burst \n20Mean Interburst_Interval    21St. Dev. of_Interburst Int.\n22Mean
Burst_Surprise')
lncolors = get(gca,'ColorOrder');
dists = evalin('base', 'who');%gets a list of all genotypes
distsn = size(dists,1);%number of genotypes
%var = evalin('base','delzeros','varn')

for i = 1:distsn

 varn = dists(i,1);
 var = evalin('base',char(varn));
 %var2 = delzeros(var);
 [g,plotter] = ecdf(selanadis(var,z));
 graph = plot(plotter,g,'color',lncolors(i,:));
 hold on
end
legend(dists)
title(strcat(ana, titler(z)))
axis normal
h = graph
end


function [h]= cds2(ana,z);
%z = input('3Spikes 5Mean Freq. 6Num. Bursts    7Bursts_Per Second\n8Bursts_Per
Minute  23St. Dev. Bursts_Per Minute 9Perc of Spikes_in Bursts\n10Mean
Burst_Duration   11St. Dev. of_Burst Duration\n12Mean Spikes_in Burst    13St. Dev.
```

```
of_Spikes In Burst\n14Mean ISI_in Burst  15St. Dev. of_ISI In Burst\n16Mean Freq._in
Burst   17St. Dev. of_Freq. in Burst\n18Mean Peak_Freq. in Burst    19St. Dev. of_Peak
Fr. In Burst \n20Mean Interburst_Interval    21St. Dev. of_Interburst Int.\n22Mean
Burst_Surprise')
 lncolors = get(gca,'ColorOrder');
 dists = evalin('base', 'who');%gets a list of all genotypes
 distsn = size(dists,1);%number of genotypes
 %var = evalin('base','delzeros','varn')

 for i = 1:distsn

  varn = dists(i,1);
  var = evalin('base',char(varn));
  var2 = delzeros(var);
  [g,plotter] = ecdf(selanadis(var2,z))

  graph = plot(plotter,g,'color',lncolors(i,:));
  hold on
 end
 legend(dists)
 title(strcat(ana, titler(z),'z'))
 h = graph
 end

 function [outp]= titler (inp);
 switch inp
    case  {3}
       outp = 'Spikes'
    case {5}
       outp = 'MF'
    case {6}
       outp = 'NB'
    case {7}
        outp ='BpS'
    case {8}
        outp ='BpM'
    case {23}
        outp ='SDBpM'
    case {10}
        outp ='MBD'
    case {11}
        outp ='SDMBD'
    case {9}
        outp ='PSiB'
    case {12}
        outp ='MSiB'
```

```
    case {13}
        outp ='SDMSiB'
    case {14}
        outp = 'ISI'
    case {15}
        outp ='SDISI'
    case {16}
        outp ='MFiB'
    case {17}
        outp ='SDMFiB'
   case {18}
        outp ='MPiB'
   case {19}
        outp ='SDMPiB'
  case {20}
        outp ='IBI'
   case {21}
        outp ='SDIBI'
   case {22}
       outp ='MSup'
end
end

function []= cdmakernorm(ana)%ana is the filename that has the spiking information
evalin('base','clear')
getdis(ana)

list = evalin('base','who')
nvars = size(list,1)

for i = 1:nvars
    var1 = list(i)
z = normtospikes(evalin('base',char(var1)))
assignin('base',char(var1), z)
xlswrite(strcat(ana,'norm'),z,char(var1))
end


for i = [5,7,9,10,12,14,16,18,20]
    h = cds1(ana,i);
    saveas(h,strcat(ana,titler(i)),'jpg');
    close
    h = cds2(ana,i);
    saveas(h,strcat(ana,titler(i),'z'),'jpg');
    close
end
```

```
 end

 function [h] = cds1(ana,z); % plots a cd of the selected parameter

 %z = input('3Spikes 5Mean Freq. 6Num. Bursts    7Bursts_Per Second\n8Bursts_Per
Minute  23St. Dev. Bursts_Per Minute 9Perc of Spikes_in Bursts\n10Mean
Burst_Duration   11St. Dev. of_Burst Duration\n12Mean Spikes_in Burst    13St. Dev.
of_Spikes In Burst\n14Mean ISI_in Burst  15St. Dev. of_ISI In Burst\n16Mean Freq._in
Burst   17St. Dev. of_Freq. in Burst\n18Mean Peak_Freq. in Burst    19St. Dev. of_Peak
Fr. In Burst \n20Mean Interburst_Interval    21St. Dev. of_Interburst Int.\n22Mean
Burst_Surprise')
 lncolors = get(gca,'ColorOrder');
 dists = evalin('base', 'who');%gets a list of all genotypes
 distsn = size(dists,1);%number of genotypes
 %var = evalin('base','delzeros','varn')

 for i = 1:distsn

  varn = dists(i,1);
  var = evalin('base',char(varn));
  %var2 = delzeros(var);
  [g,plotter] = ecdf(selanadis(var,z));
  graph = plot(plotter,g,'color',lncolors(i,:));
  hold on
 end
 legend(dists)
 title(strcat(ana, titler(z)))
 axis normal
 h = graph
 end


 function [h]= cds2(ana,z);
 %z = input('3Spikes 5Mean Freq. 6Num. Bursts    7Bursts_Per Second\n8Bursts_Per
Minute  23St. Dev. Bursts_Per Minute 9Perc of Spikes_in Bursts\n10Mean
Burst_Duration   11St. Dev. of_Burst Duration\n12Mean Spikes_in Burst    13St. Dev.
of_Spikes In Burst\n14Mean ISI_in Burst  15St. Dev. of_ISI In Burst\n16Mean Freq._in
Burst   17St. Dev. of_Freq. in Burst\n18Mean Peak_Freq. in Burst    19St. Dev. of_Peak
Fr. In Burst \n20Mean Interburst_Interval    21St. Dev. of_Interburst Int.\n22Mean
Burst_Surprise')
 lncolors = get(gca,'ColorOrder');
 dists = evalin('base', 'who');%gets a list of all genotypes
 distsn = size(dists,1);%number of genotypes
 %var = evalin('base','delzeros','varn')

 for i = 1:distsn
```

```
 varn = dists(i,1);
 var = evalin('base',char(varn));
 var2 = delzeros(var);
 [g,plotter] = ecdf(selanadis(var2,z))

 graph = plot(plotter,g,'color',lncolors(i,:));
 hold on
end
legend(dists)
title(strcat(ana, titler(z),'z'))
h = graph
end

function [outp]= titler (inp);
switch inp
   case  {3}
      outp = 'Spikes'
   case {5}
      outp = 'MF'
   case {6}
      outp = 'NB'
   case {7}
       outp ='BpS'
   case {8}
       outp ='BpM'
   case {23}
       outp ='SDBpM'
   case {10}
       outp ='MBD'
   case {11}
       outp ='SDMBD'
   case {9}
       outp ='PSiB'
   case {12}
       outp ='MSiB'
   case {13}
       outp ='SDMSiB'
   case {14}
       outp = 'ISI'
   case {15}
       outp ='SDISI'
   case {16}
       outp ='MFiB'
   case {17}
       outp ='SDMFiB'
```

```
   case {18}
        outp ='MPiB'
   case {19}
        outp ='SDMPiB'
  case {20}
        outp ='IBI'
   case {21}
        outp ='SDIBI'
   case {22}
       outp ='MSup'
end
end
```

VITA

Duncan Rogers Morhardt was born on November 27, 1977 in Alexandria, Virginia. He remained in Alexandria until he was 18 and attended TC Williams High School. He attended the University of California, Berkeley, College of Letters and Science and was awarded a Bachelor of Arts in Molecular and Cellular Biology in 2001. In 2004 he was accepted into the Medical and Graduate schools of the Medical College of Virginia at Virginia Commonwealth University.

Duncan enjoys playing piano, the outdoors, and the art of astrological interpretation.